α-Diimine Ferrates and Cobaltates as Highly Reactive Complex Fragments in Synthesis and Catalysis

Dissertation zur Erlangung des

Doktorgrades der Naturwissenschaften

Dr. rer. nat.

am Institut für Anorganische Chemie

an der Fakultät für Chemie und Pharmazie

der Universität Regensburg

vorgelegt von

Thomas M. Maier

aus Kümmersbruck

Regensburg, Mai 2020

Der experimentelle Teil der vorliegenden Arbeit wurde in der Zeit zwischen November 2016 und März 2020 unter Anleitung von Prof. Dr. Robert Wolf am Institut für Anorganische Chemie der Universität Regensburg und unter Anleitung von Dr. Andreas Ehlers (Arbeitskreis Prof. Dr. Moniek Tromp) am van't Hoff Institute for Molecular Sciences der Universiteit van Amsterdam (Januar 2018 - März 2018) angefertigt.

Die Arbeit wurde angeleitet von:		Prof. Dr. Robert Wolf
Promotionsgesuch eingereicht am:		16.03.2020
Tag der mündlichen Prüfung:		28.05.2020
Promotionsausschuss:	Vorsitz	Prof. Dr. Alkwin Slenczka
	Erstgutachter	Prof. Dr. Robert Wolf
	Zweitgutachter	Prof. Dr. Axel Jacobi von Wangelin
	Dritter Prüfer	Prof. Dr. Manfred Scheer

Für meine Familie

Prologue

This thesis reports on the synthesis of low-valent α-diimine iron and cobalt complexes and their application in reductive catalysis. Chapter 1 introduces the versatile chemistry of α-diimine iron and cobalt complexes used in catalysis. Chapter 2 shows the differences between two α-diimine ligands in anionic cobalt complexes and the resulting reactivity towards white phosphorus. Chapter 3 describes the dehydrogenation of amine-boranes catalyzed by an α-diimine cobaltate and subsequent transfer hydrogenation of C=C and C=N bonds. Chapter 4 deals with the hydrogenation of challenging C=C and C=N bonds catalyzed by an *in situ* system of an α-diimine cobalt dibromide and lithium superhydride. Chapter 5 describes the heterogeneous hydrogenation of challenging olefins catalyzed by nickel(0) nanoparticles. The particles are formed under catalytic conditions from a dianionic cyclooctadiene nickel complex. Chapter 6 reports on the synthesis of heteroleptic and homoleptic anionic α-diimine iron complexes and their characterization with various experimental and theoretical methods. Heteroleptic ferrate complexes are efficient pre-catalysts for the homogeneous catalyzed hydroboration of carbonyl compounds. Chapter 7 describes utilization of an α-diimine cobaltate complex for the direct synthesis of an anionic 13-vertex *closo*-cobaltacarborane cluster. Chapter 8 summarizes the results of this thesis.

Prolog

Diese Dissertation handelt von der Synthese niedervalenter α-Diimin-Eisen- und Cobaltkomplexe und deren Anwendung in der reduktiven Katalyse. Kapitel 1 setzt sich mit der Chemie von α-Diimin-Eisen- und Cobaltkomplexen auseinander, wobei der Fokus auf Katalyse liegt. In Kapitel 2 werden die Unterschiede zwischen zwei verschiedenen α-Diimin-Liganden in anionischen Cobaltkomplexen herausgearbeitet. Die unterschiedliche Reaktivität wird exemplarisch in der Aktivierung von weißem Phosphor dargelegt. Kapitel 3 beschreibt die Dehydrierung von Amin-Boranen mit katalytischen Mengen eines α-Diimin-Cobaltats. Der Wasserstoff kann von der aktiven Katalysatorspezies direkt auf C=C- und C=N-Bindungen übertragen werden. Kapitel 4 handelt von der Hydrierung anspruchsvoller C=C- und C=N-Bindungen, die durch ein *in situ* erzeugtes System aus einem α-Diimin(dibromido)cobalt-Komplex und Lithiumsuperhydrid erfolgreich katalysiert wird. Der Fokus dieses Kapitels liegt vor allem auf Vergiftungsstudien und stöchiometrischen Reaktionen. Ein dianionischer Bis(cyclooctadien)nickelkomplex als Präkatalysator in der Hydrierung anspruchsvoller Olefine ist Gegenstand des Kapitels 5. In Kapitel 6 wird die Synthese und Charakterisierung homo- und heteroleptischer anionischer Eisenkomplexe mit verschiedenen experimentellen und theoretischen Methoden besprochen. Die heteroleptischen Komplexe zeigen hierbei eine beachtliche Aktivität in der homogen-katalysierten Hydroborierung von Carbonylverbindungen. In Kapitel 7 wird von der Verwendung eines α-Diimincobaltkomplexes zur direkten Synthese eines anionischen dreizehneckigen *closo*-Cobaltacarboran-Cluster berichtet. Abschließend werden in Kapitel 8 die Ergebnisse dieser Dissertation zusammengefasst.

Table of Contents

1 Heteroleptic *α*-Diimine Fe and Co Complexes in Catalysis

1.1 Introduction

Catalysis is a fundamental principle without which life would not be possible. The term "catalysis" was introduced into science by *Berzelius* in 1835, who described the phenomenon that some compounds are able to initiate reactions at a certain temperature only by their presence. Later, *Ostwald* further defined the concept of a "catalyst" through his development of reaction kinetics around the turn of the 20th century. He received the Nobel prize for chemistry in 1909 for this milestone.[1] According to his explanation a catalyst is a compound which accelerates a chemical reaction without being consumed or influencing the thermodynamic equilibrium. *Eyring* also contributed to this field with his theory of transition states, with which it is possible to understand the catalytic phenomenon as illustrated in Figure 1. With the aid of a catalyst alternative pathways are made possible and transition states are stabilized. The difference in free enthalpy is not influenced.[2]

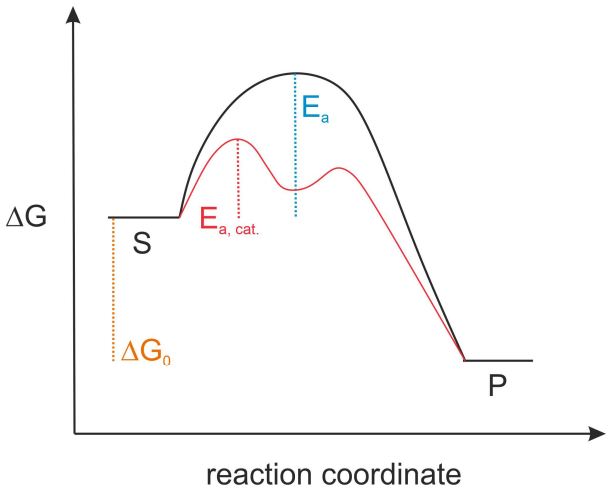

Figure 1. Illustrative reaction energy profile in the absence (black curve) and in the presence (red curve) of a catalyst. E_a = activation energy, ΔG = Gibbs free enthalpy, cat. = catalyzed, S = starting material, P = product.

By minimizing the need for elevated temperatures, industrial catalysis saves a lot of energy. Furthermore, it is not possible to imagine nature without catalytic processes. Transition metals are elemental ingredients of many catalysts in nature, which are called enzymes. These metalloenzymes are uniquely constructed by nature to perform

chemical reactions with high efficiency. For instance, carboanhydrase containing a zinc ion in its active site, catalyzes the reaction of water with carbon dioxide to give carboxylic acid with a turnover frequency of 10^6 molecules per second. Most metalloenzymes contain 3d metals such as iron, zinc, copper, manganese, and cobalt because of their higher availability in nature compared to 4d or 5d metals.[3]

It is challenging for synthetic chemists to mimic nature and find efficient transition metal catalysts, which can be applied in industrial processes. Today, more than 80% of all industrially relevant reactions are catalyzed and generate molecules with a combined value of more than 400 billion euro per year (2007).[2] Unfortunately, complexes based on noble metals such as ruthenium, palladium, rhodium, iridium, and platinum are widely used. Typically, these are extremely efficient. Nonetheless, they suffer from some significant disadvantages compared to the lighter 3d metal complexes. Specifically, they are often scarce, expensive, and toxic, which provides compelling reasons to find alternative catalysts based on benign and more abundant metals such as iron, cobalt or nickel.[4] One important class of reactions are reductive transformations such as hydrogenations of unsaturated bonds (e.g. C=C, C=N, C=O, N≡N) or analogous hydroelementation (hydroboration, hydrosilylation) reactions. Typically, these reactions are catalyzed by transition metals.

Hydrogenations constitute one of the most important reaction classes in the synthesis of bulk- and fine chemicals.[5] Here, homogeneous catalysts generally benefit of a more selective reaction, and milder reaction conditions compared to heterogeneous catalysts. This is particularly evident in the asymmetric hydrogenation of prochiral substrates. Highlighting the importance of such reactions, *Knowles* and *Noyori* received the Nobel prize in 2001 for their work on enantioselective catalytic hydrogenation reactions. For example, for the synthesis of L-DOPA, a Parkinson's drug, a prochiral olefin was hydrogenated using a cationic rhodium(I) complex bearing a C_2-symmetric chiral bis(phosphane) ligand (Scheme 1).[6],[7]

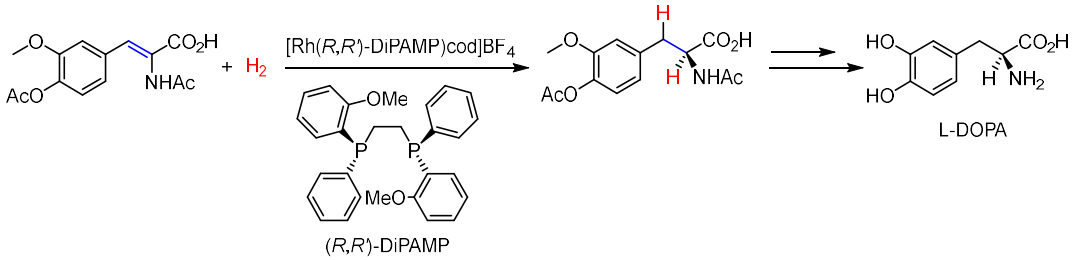

Scheme 1. Synthesis of L-DOPA using an asymmetric hydrogenation step (cod = 1,5-cylooctadiene).

The selectivity and reactivity of a transition metal catalyst strongly depends on its ligand. As mentioned above, it is an important challenge to replace noble metals by earth-abundant metals. Noble metals typically prefer two-electron processes that are well-suited to become steps of a catalytic cycle (oxidative addition, reductive elimination). In contrast, for base metals one-electron redox changes also usually occur and it is hence far more difficult to achieve analogous controlled reactivity and selectivity. One attempt to overcome this limitation is to mimic the reactivity of noble metals, which involves the application of non-innocent/redox-active ligands, which participate in catalytic reactions.[8] This concept was introduced by *Jørgensen* and can be observed in dithiolene, catecholate, and porphyrin complexes, for example.[9] One of the most prominent classes of these ligands is the family of α-diimines. These have excellent acceptor properties and can be easily reduced by metals to their respective radical anions and dianions.[10] As a result, the oxidation state of the bound metal is often complicated to assign. Nevertheless, modern experimental and quantum chemical methods usually allow the oxidation state of the metal and the ligand to be determined quite accurately.[11] For α-diimine ligands, the analysis of C–C and C–N bond lengths by single-crystal X-ray crystallography is crucial. By adding electrons to the neutral α-diimine ligand, the C–C bond gains double bond character and is shortened, whereas the C–N bonds lose double bond character and are stretched (Scheme 2). Thus, experimentally determined bond lengths provide a reliable indicator of the oxidation state of the ligand and, by extension, the metal to which it is bound.

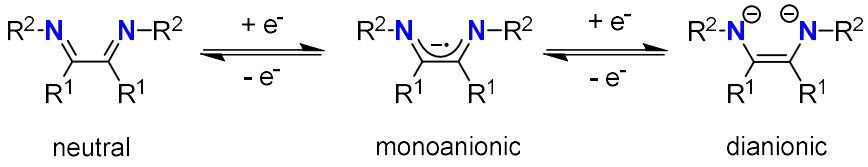

Scheme 2. Reduction of a generic α-diimine ligand to its monoanionic and dianionic states.

α-Diimines are usually synthesized by condensation of a 1,2-dicarbonyl compound and an amine. The reaction is an equilibrium, which is generally acid catalyzed and can be shifted in favor of the desired product by removal of water from the reaction mixture. This can be efficiently achieved by adding water sensitive compounds such as titanium(IV)-tetrachloride, trimethylaluminum or molecular sieves, or through use of a *Dean-Stark* apparatus. The stereoelectronic properties of such α-diimines can conveniently be controlled by varying the groups attached to the nitrogen atoms, as well as the backbone carbons (Scheme 3).

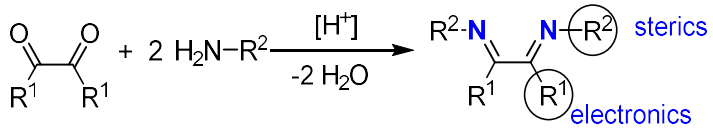

Scheme 3. General synthetic pathway to α-diimines and primary stereoelectronic impact of different substituents.

1.2 Neutral α-Diimine Complexes

α-Diimines as ligands in catalysis were first introduced by *tom Dieck* and co-workers. Their pioneering work described a bis(α-diimine)iron(0) complex, which can be activated by an organoaluminum compound and is then capable of catalyzing selective 1,3-diene dimerization. For instance, the dimerization of 1,3-butadiene led to the formation of 1,5-cyclooctadiene. The equivalent chromium α-diimine complex also catalyzed the dimerization of olefins, e.g. isoprene (Scheme 4).[12]

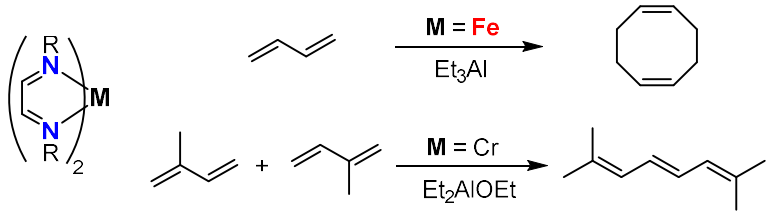

Scheme 4. Bis-1,4-diaza-1,3-diene Fe and Cr complexes in the catalytic olefin dimerization.

As well as the 1,4-diaza-1,3-dienes as used by *tom Dieck* and co-workers the related, 1,3-diiminopyridines (PDIs) are widely used as ligands for transition metal catalysts. In contrast to 1,4-diaza-1,3-diene, which acts as bidentate ligand, PDIs coordinate via three nitrogen donor atoms (Figure 2).[13]

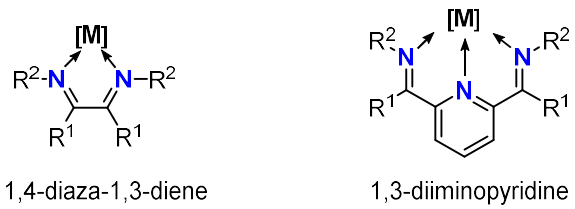

Figure 2. Standard coordination modes of 1,4-diaza-1,3-diene and 1,3-diiminopyridine ligands.

Early on 1,3-diiminopyridine ligands were successfully applied in catalysis in the field of olefin polymerization. The groups of *Brookhart* and *Gibson* contributed significantly with the synthesis of highly active iron and cobalt complexes.[14] *Chirik* and co-workers subsequently used these ligands for the synthesis of low-valent iron and cobalt complexes, which were active in a wide range of reductive transformations such as N_2 activation, hydrogenation of olefins, hydroelementation, and cross-coupling reactions.[15] Scheme 5 displays two examples in the hydrogenation of olefins, which illustrate the efficacy of this ligand system. Catalyst **1** is formed upon reaction of [($^{i\text{Pr}}$PDI)FeBr$_2$] (^{i}Pr = isopropyl) with two equivalents of NaBEt$_3$H under a nitrogen atmosphere. The bis(dinitrogen) iron complex **1** is an effective hydrogenation pre-catalyst for a series of unfunctionalized 1,1- and 1,2-disubstituted olefins under mild conditions (5 mol% **1**, 4 bar H_2, 23 °C).[16] With the aid of a chiral PDI ligand, the similar cobalt methyl complex **2** was also effective in the asymmetric hydrogenation of olefins. Prochiral olefins were hydrogenated with high enantioselectivities up to 96% ee (ee = enantiomeric excess).[17]

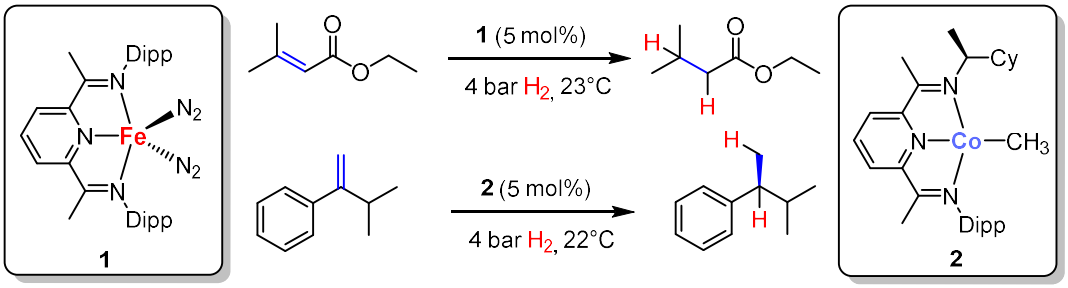

Scheme 5. Selected examples of 1,3-diiminopyridine iron and cobalt complexes developed by *Chirik* for the hydrogenation of C=C bonds. Dipp = 2,6-diisopropylphenyl.

Another important class of diimines are diazadienes bearing a polyarene backbone. Examples are the bis(imino)acenaphthenediimine (BIAN) and phenanthrenediimine (PhDi) families, which are illustrated in Figure 3.

BIAN ligands can be synthesized on a multi gram scale from commercially available acenaphthenequinone and amines. Usually, aniline derivatives are used, which results in bis(aryl)iminoacenaphthene diimines (^{Ar}BIAN).

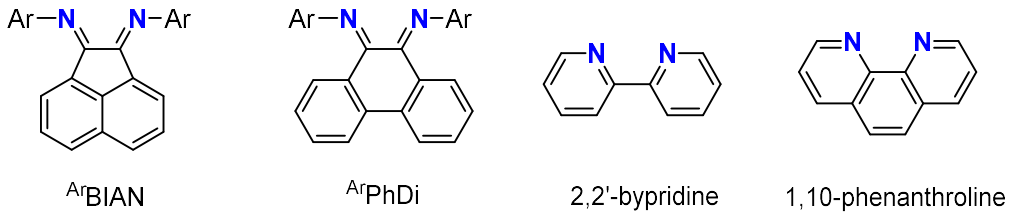

Figure 3. Examples of widely used α-diimine ligands. (^{Ar}BIAN = bis(aryl)acenaphthenediimine; ^{Ar}PhDi = bis(aryl)phenanthrenediimine).

After the first mention of these ligands in the 1960s,[18] the coordination chemistry was established by *Elsevier* and co-workers. Aryl substituted BIAN ligands show noticeably different behavior compared to simple 1,4-diaza-1,3-diene, 2,2'-bypyridine, or 1,10-phenanthroline ligands (Figure 3).[19] Specifically, the two exocyclic imine functionalities lead to better σ-donating and π-accepting properties. Moreover, the rigid backbone allows the nitrogen atoms to endure in the fixed *cis* orientation that is required for metal coordination. This orientation minimizes the cost of reorganization energy upon metal binding. The same behavior also applies for phenanthrenediimine ligands. The examples of catalysis using BIAN transition metal complexes were first described by *Elsevier* and *van Asselt*. A BIAN Pd(0) complex with one weakly-bound alkene ligand was used in the homogeneous hydrogenation of C=C and C=O bonds (Scheme 6).[19a] Many other groups subsequently recognized the potential of this ligand class, and BIAN complexes were extensively studied in the polymerization of olefins as well as in other catalytic transformations.[20]

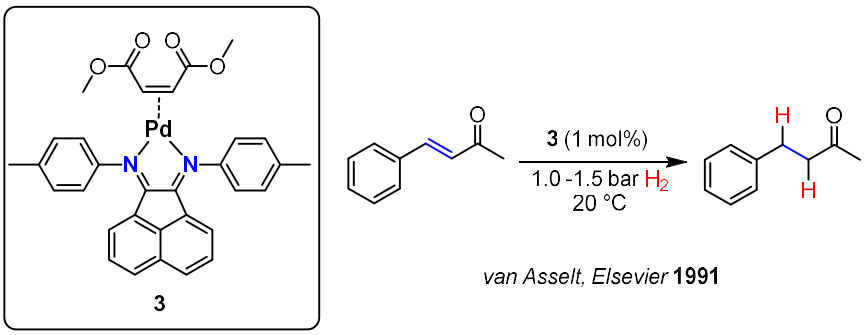

Scheme 6. An [(ArBIAN)Pd(alkene)] complex as a pre-catalyst for the hydrogenation of an α,β-unsaturated carbonyl compound.

Of particular interest to this thesis are the applications of these ligands in base metal (Fe, Co) catalyzed reductive transformations (hydrogenation, hydroboration, hydrosilylation). In the case of iron, there are several reports.[21] *Findlater* and co-workers reported BIAN iron benzene and toluene derivatives, which were used as pre-catalysts in the hydrosilylation of carbonyl compounds and imines as well as in the polymerization of L-lactide (Scheme 7).[21a,f]

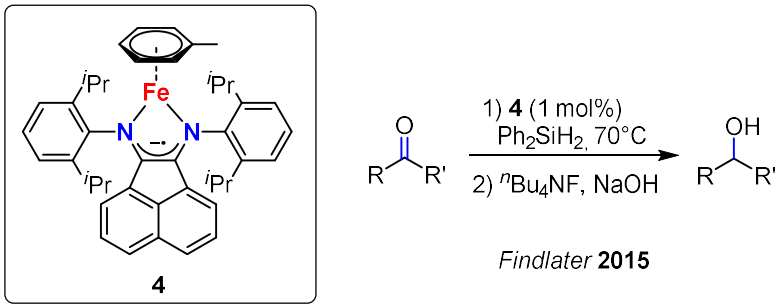

Scheme 7. [(ArBIAN)Fe(toluene)] complex as a pre-catalyst for the hydrosilylation of ketones using diphenylsilane. iPr = isopropyl.

Moreover, the same authors also described the application of [(ArBIAN)$FeCl_2$] (Ar = Dipp = 2,6-diisopropylphenyl, Mes = 2,4,5-trimethylphenyl) in the selective reduction of esters to alcohols via hydrosilylation.[21h] The catalytically active species here is obtained by activation with *n*-butyllithium. With the similar complex [(ArBIAN)$FeBr_2$] (Ar = Dipp, Mes) the hydrosilylation of 1-hexene was possible, which was investigated by *Hoyt* and co-workers.[21] *Jacobi von Wangelin* and co-workers also used [(DippBIAN)$FeCl_2$] as pre-catalyst and were able to hydrogenate sterically hindered

olefins after activation with three equivalents *n*-butyllithium. They proposed an anionic iron complex as the active species (Scheme 8).[21]

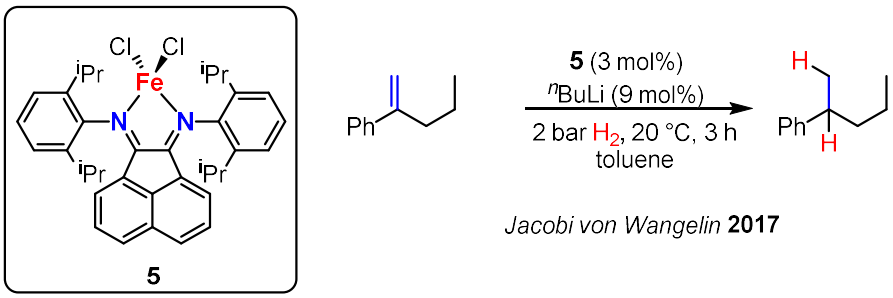

Scheme 8. [(^{Dipp}BIAN)FeCl$_2$] as a potent pre-catalyst for the hydrogenation of sterically hindered olefins.

In contrast to iron, reports of analogous cobalt complexes are scarce.[22] *Ribeiro* and co-workers used [(^{Ar}BIAN)CoCl$_2$] (Ar = Dipp, Mes) in the polymerization of ethylene.[22a] The groups of *Ragaini* and *Beller* synthesized cobalt based heterogeneous catalysts from [(BIAN)$_2$Co]$^{2+}$ precursors. These species displayed high activity in the hydrogenation of aromatic nitro compounds.[22b]

Phenanthrenediimines are not as common as a ligand in transition metal chemistry as BIAN derivatives. This is likely due to the fact that the synthesis of BIAN is simpler and better established. Phenanthrenediimines are typically synthesized in a two-step condensation reaction from phenanthrenquinone.[23] Reactivity studies on metal PhDi complexes are extremely rare. One example is the oxidative addition reaction of dihalogens X$_2$ (X = Cl, Br, I) to a square-planar rhodium complex.[24] Recently, one ^{Ar}PhDi palladium complex was reported which is an active catalyst for the ethylene/methyl acrylate co-polymerization.[25] This is the only described example for a transition metal PhDi catalyst so far.

1.3 Olefin and Polyarene Metalates

Our group has been working intensively in the field of reactive olefin and polyarene metalates.[26] A series of homo and heteroleptic complexes are accessible via straightforward synthetic procedures developed by the groups of *Jonas* and *Ellis*.[27],[28] Selected examples are shown in Figure 4. Emphasis has been on the application of these sources of "naked" metal anions in coordination chemistry. For instance, fascinating

molecules have been synthesized through reaction with alkynes and phosphaalkynes.[26] In cooperation with *Jacobi von Wangelin* the catalytic activity of the bis(anthracene) cobaltate anion has been investigated. This "cobalt(1–) source" is capable of efficiently hydrogenating olefins under mild conditions as shown in Figure 4. The olefin hydrogenation reaction proceeds via a homogeneous mechanism.[29] The stabilization of the "Co⁻" species by coordination of the substrate in solution seems to be crucial for the observed high activity. Under slightly harsher conditions (10 bar H_2, 60 °C) bis(anthracene) cobaltate(1–) is also a potent pre-catalyst for the hydrogenation of ketones and imines (Figure 4). A heterogeneous mechanism is apparently present in this case: the formed products (alcohols, amines) react with the catalyst to effect formation of catalytically active cobalt nanoparticles.

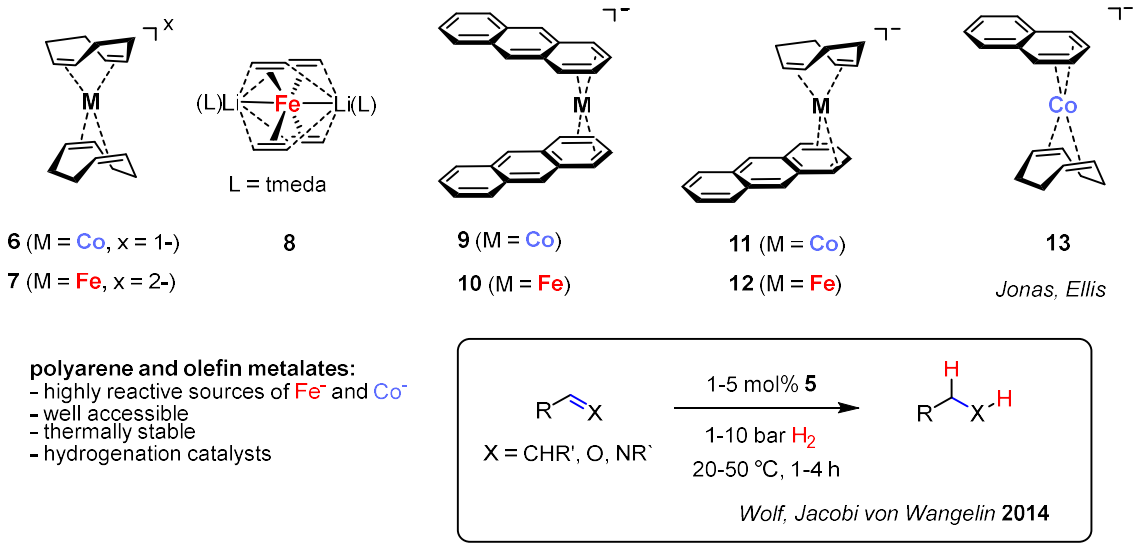

Figure 4. Olefin and polyarene stabilized cobaltate and ferrate anions and the application of bis(anthracene) cobaltate as an efficient pre-catalyst for hydrogenation reactions; tmeda = *N*,*N*′-tetramethylethylenediamine.

1.4 Heteroleptic Anionic α-Diimine Complexes

Redox-active ligands such as α-diimines are well capable of stabilizing highly-reduced anions and as such are a subject of current research. While homoleptic α-diimine complexes are well explored,[30] heteroleptic complexes remain scarce.[21],[31] Metal complexes with one labile olefin or arene ligand in combination with a non-innocent α-diimine ligand are of especially great interest.[21],[32] In particular, anionic complexes in a highly-reduced state are promising pre-catalysts for reductive catalysis. Only a few

such anions have been reported so far. *Uhlig* and co-workers described the complexes **14a,b** and **15a** (Figure 5) which were synthesized from the reaction of [Li(tmeda)][Co(η⁴-cod)₂] (tmeda = *N,N'*-tetramethylethylenediamine) with 1,4-diaza-1,3-dienes and 2,2'-bypryridine (bpy), respectively.[33] However, none of the complexes was fully characterized. Later on, *Ellis* and co-workers showed that **15b** can also be obtained from the reaction of [K([18]c-6)][Co(η⁴-cod)(η⁴-$C_{10}H_8$)] (**9**) with bpy.[27],[28] Recently, *Yang* and co-workers described the synthesis and electronic structures of related dinuclear pyrene complexes (**18**, **19**). So far, no further reactivity studies of these complexes are reported.[34]

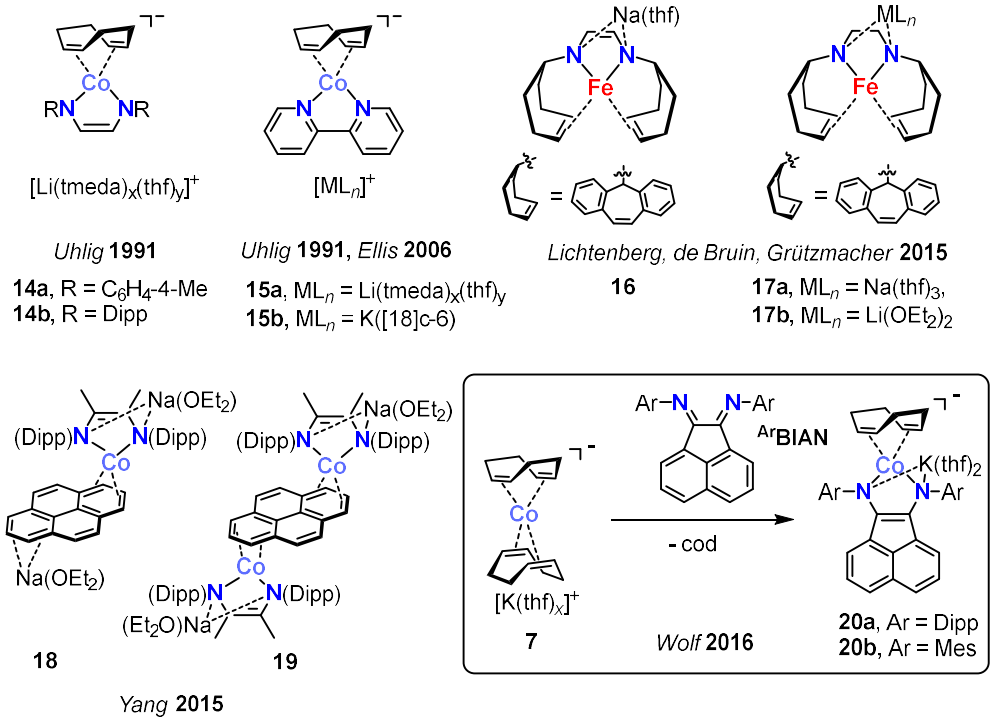

Figure 5. Anionic olefin and polyarene complexes of cobalt and iron with α-diimine ligands.

A number of highly reactive Fe(I) and Fe(II) complexes (**16**, **17a,b**) with chelating amido-olefin ligands and related saturated ligands were synthesized by *Lichtenberg*, *de Bruin* and *Grützmacher*.[35] These complexes show remarkable activities for the iron-catalyzed dehydrogenation of (alkyl)amino boranes and dehydrogenative coupling of silanes.

Our group has also already contributed to this field. The reaction of ^{Ar}BIAN (Ar = Mes, Dipp) with potassium bis(cyclooctadiene) cobaltate led to the formation of **20a,b** in high

yields.[36] These highly-reduced α-diimine cobaltates can activate small molecules including white phosphorus and carbon disulfide, leading to the formation of dinuclear complexes through replacement of the labile 1,5-cyclooctadiene ligand. Preliminary catalytic reactions with **20a,b** were also carried out. The dehydrogenation of dimethylamine-borane with complex **20a** (5 mol%) at room temperature led selectively to the formation of the corresponding 1,3-diaza-2,4-diboretane, with only minor side products (Scheme 9).[37]

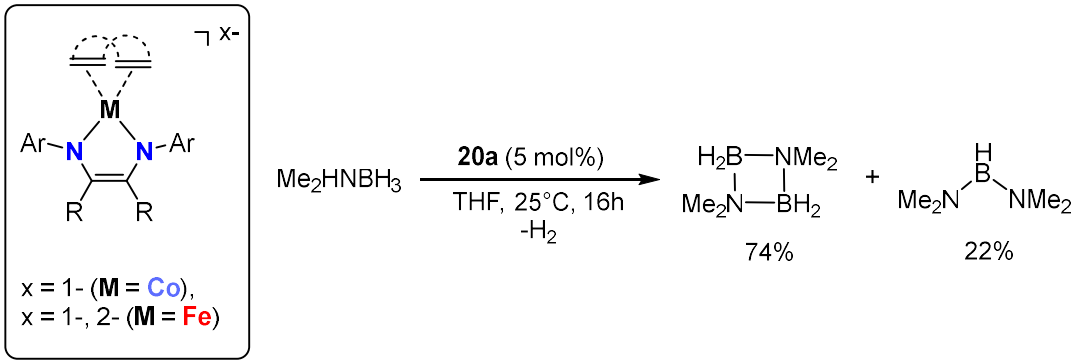

Scheme 9. [(α-diimine)M(olefin/arene)]$^{x-}$ as a key structural motif, and the first catalytic application of [(^{Dipp}BIAN)Co(η^4-cod)]$^-$ (**20a**) in the dehydrogenation of dimethylamine-borane.

1.5 Conclusion

The application of highly-reduced cobaltate and ferrate anions in catalytic reactions is not yet very well investigated. Furthermore, the use of well-defined, pre-formed low-valent metal complexes in catalysis is conceptually different from widely used *in situ* systems, where a ligand metal salt is reduced under the reaction conditions to an unknown low-valent species, which is then catalytically active.

It is of fundamental interest to understand the correlation between structural (metal oxidation state, sterical and electronic properties of the ligands) and catalytic properties. This is necessary for the development of new highly-reactive and selective catalysts for challenging reactions. In particular, the aim of this PhD thesis was to use the properties the BIAN and PhDi α-diimine ligand families for the synthesis of low-valent, heteroleptic complexes of iron and cobalt. These anions can be further applied in catalytic reductive transformations.

1.6 References

[1] "The Nobel Prize in Chemistry 1909" retrieved from the internet on 06.11.2019. http://www.nobelprize.org/prizes/chemistry/1909/summary/

[2] D. Steinborn, *Grundlagen der metallorganischen Komplexkatalyse*, Vieweg + Teubner, **2007**

[3] D. Rehder, *Bioinorganic Chemistry*, Oxford University Press, **2014**

[4] R. Morris Bullock, *Catalysis Without Precious Metals*, Wiley-VCH, Weinheim, **2010**.

[5] a) *Catalytic Hydrogenation* (Ed.: L. Cerveny), Elsevier, Amsterdam, **1986**. b) *The Handbook of Homogeneous Hydrogenations* (Eds.: J. G. de Vries, C. J. Elsevier), Wiley-VCH, Weinheim, **2007**.

[6] a) W. S. Knowles, M. J. Sabacky, B. D. Vineyard, D. J. Weinkauff, *J. Am. Chem. Soc.* **1975**, *97*, 2567-2568. b) H. Doucet, T. Ohkuma, K. Murata, T. Yokozawa, M. Kozawa, E. Katayama, A. F: England, T. Ikariya, R. Noyori, *Angew. Chem. Int. Ed.* **1998**, *37*, 1703-1707. *Angew. Chem.* **1998**, *110*, 1792-1796.

[7] "The Nobel Prize in Chemistry 2001" retrieved from the internet on 06.11.2019. http://www.nobelprize.org/prizes/chemistry/2001/summary/

[8] a) P. J. Chirik, K. Wieghardt, *Science* **2010**, *327*, 794-795. b) V. Lyaskovskyy, B. de Bruin, *ACS Catal.* **2012**, *2*, 270-279. c) V. K. K. Praneeth, M. R. Ringenberg, T. R. Ward *Angew. Chem. Int. Ed.* **2012**, *51*, 10228-10234. *Angew. Chem.* **2012**, *124*, 10374-10380. d) O. R. Luca, R. H. Crabtree, *Chem. Soc. Rev.* **2013**, *42*, 1440-1459.

[9] C. K. Jørgensen, *Coord. Chem. Rev.* **1966**, *1*, 164-178.

[10] BIAN as example: I. L. Fedushkin, A. A. Skatova, V. A. Chudakova, G. K. Fukin, *Angew. Chem. Int. Ed.* **2003**, *42*, 3294-3298. *Angew. Chem.* **2003**, *115*, 3416-3420.

[11] P. J. Chirik, *Inorg. Chem.* **2011**, *50*, 9737-9740.

[12] a) H. tom Dieck, H. Bruder, *J. Chem. Soc. Chem. Commun.* **1977**, 24-25. b) H. tom Dieck, A. Kinzel, *Angew. Chem.* **1979**, *91*, 344.

[13] Z. Flisak, W.-H. Sun, *ACS Catal.* **2015**, *5*, 4713–4724.

[14] a) B. L. Small, M. Brookhart, A. M. A. Bennett, *J. Am. Chem. Soc.* **1998**, *120*, 4049–4050. b) G. J. P. Britovsek, V. C. Gibson, S. J. McTavish, G. A. Solan, A. J. P. White, D. J. Williams, B. S. Kimberley, P. J. Maddox, *Chem. Commun.* **1998**, 849–850. c) G. J. P. Britovsek, M. Bruce, V. C. Gibson, B. S. Kimberley, P. J. Maddox, S. Mastroianni, S. J. McTavish, C. Redshaw, G. A. Solan, S. Strömberg et al., *J. Am. Chem. Soc.* **1999**, *121*, 8728–8740. d) B. L. Small, M. Brookhart, *Macromolecules* **1999**, *32*, 2120–2130. e) C. P. Lenges, P. S. White, W. J. Marshall, M. Brookhart, *Organometallics* **2000**, *19*, 1247–1254.

[15] Recent examples for PDI iron or cobalt complexes in catalysis: a) S. K. Russell, E. Lobkovsky, P. J. Chirik, *J. Am. Chem. Soc.* **2011**, *133*, 8858–8861. b) C. C. Hojilla Atienza, A. M. Tondreau, K. J. Weller, K. M. Lewis, R. W. Cruse, S. A. Nye, J. L. Boyer, J. G. P. Delis, P. J. Chirik, *ACS Catal.* **2012**, *2*, 2169–2172. c) J. M. Darmon, S. C. E. Stieber, K. T. Sylvester, I. Fernández, E. Lobkovsky, S. P. Semproni, E. Bill, K. Wieghardt, S. DeBeer, P. J. Chirik, *J. Am. Chem. Soc.* **2012**, *134*, 17125–17137. d) M. R. Friedfeld, M. Shevlin, G. W. Margulieux, L.-C. Campeau, P. J. Chirik, *J. Am. Chem. Soc.* **2016**, *138*, 3314–3324. e) C. H. Schuster, T. Diao, I. Pappas, P. J. Chirik, *ACS Catal.* **2016**, *6*, 2632–2636. f) N. G. Léonard, M. J. Bezdek, P. J. Chirik, *Organometallics* **2017**, *36*, 142–150. g) S. M. Rummelt, H. Zhong, I. Korobkov, P. J. Chirik, *J. Am. Chem. Soc.* **2018**, *140*, 11589–11593.

[16] S. C. Bart, E. Lobkovsky, P. J. Chirik, *J. Am. Chem. Soc.* **2004**, *126*, 13794–13807.

[17] a) S. Monfette, Z. R. Turner, S. P. Semproni, P. J. Chirik, *J. Am. Chem. Soc.* **2012**, *134*, 4561–4564. b) K. H. Hopmann, *Organometallics* **2013**, *32*, 6388–6399.

[18] a) I. Matei, T. Lixandru, *Bul. Inst. Politeh. Iasi* **1967**, *13*, 245. b) M. Dvolaitzky, *C. R. Acad. Sci. Prais, Ser. C.* **1969**, *268*, 1811.

[19] a) R. van Asselt, C. J. Elsevier, *J. Mol. Catal.* **1991**, *65*, L13-L19. b) R. van Asselt, E. E. C. G. Gielens, R. E. Rülke, C. J. Elsevier *J. Chem. Soc. Chem. Commun.* **1993** 1203-1205. c) R. van Asselt, C. J. Elsevier, W. J. J. Smeets, A. L. Spek, R. Benedix, *Recl. Trav. Chim. Pays-Bays* **1994**, *113*, 88-98. d) R. van Asselt, E. E. C. G. Gielens, R. E. Rülke, K. Vrieze, C. J. Elsevier, *J. Am. Chem. Soc.* **1994**, *116*, 977-985. e) M. W. van Laren, C. J. Elsevier, *Angew. Chem. Int. Ed.* **1999**, *38*, 3715-3717; *Angew. Chem.* **1999**, *111*, 3926-3929.

[20] a) Selected examples: a) L. K. Johnson, C. M. Killian, M. Brookhart, *J. Am. Chem. Soc.* **1995**, *117*, 6414–6415. b) D. P. Gates, S. A. Svejda, E. Onate, C. M. Kilian, L. K. Johnson, P. S. White, M. Brookhart, *Macromolecules* **2000**, *33*, 2320-2334. c) B. L. Small, R. Rios, E. R. Fernandez, D. L. Gerlach, J. A. Halfen, M. J. Carney, *Organometallics* **2010**, *29*, 6723–6731. d) F. Wang, C. Chen, *Polym. Chem.* **2019**, *10*, 2354–2369.

[21] a) F. S. Wekesa, R. Arias-Ugarte, L. Kong, Z. Sumner, G. P. McGovern, M. Findlater, *Organometallics* **2015**, *34*, 5051–5056. b) Y. H. Budnikova, V. V. Khrizanforova, I. L. Fedushkin, A. A. Karasik, *Phosphorus, Sulfur, and Silicon and the Related Elements* **2016**, *191*, 1644–1645. c) M. J. Supej, A. Volkov, L. Darko, R. A. West, J. M. Darmon, C. E. Schulz, K. A. Wheeler, H. M. Hoyt, *Polyhedron* **2016**, *114*, 403–414. d) X. Yu, F. Zhu, D. Bu, H. Lei, *RSC Adv.* **2017**, *7*, 15321–15329. e) M. Villa, D. Miesel, A. Hildebrandt, F. Ragaini, D. Schaarschmidt, A. Jacobi von Wangelin, *ChemCatChem* **2017**, *9*, 3203–3209. f) L. A. Brown, F. S. Wekesa, D. K. Unruh, M. Findlater, B. K. Long, *J. Polym. Sci. Part A: Polym. Chem.* **2017**, *55*, 2824–2830. g) A. Saini, C. R. Smith, F. S. Wekesa, A. K. Helms, M. Findlater, *Org. Biomol. Chem.* **2018**, *16*, 9368–9372. h) S. R: Tamang, A. F. Cozzolino, M. Findlater, *Org. Biomol. Chem.* **2019**, *17*, 1834-1838.

[22] a) V. Rosa, S. A. Carabineiro, T. Avilés, P. T. Gomes, R. Welter, J. M. Campos, M. R. Ribeiro, *J. Organomet. Chem.* **2008**, *693*, 769–775. b) D. Formenti, F. Ferretti, C. Topf, A.-E. Surkus, M.-M. Pohl, J. Radnik, M. Schneider, K. Junge, M. Beller, F. Ragaini, *J. Catal.* **2017**, *351*, 79–89.

[23] V. K. Cherkasov, N. O. Druzhkov, T. N. Kocherova, A. S. Shavyrin, G. K. Fukin, *Tetrahedron* **2012**, *68*, 1422–1426.

[24] D. W. Shaffer, S. A. Ryken, R. A. Zarkesh, A. F. Heyduk, *Inorg. Chem.* **2012**, *51*, 12122–12131.

[25] A. Dall' Anese, V. Rosar, L. Cusin, T. Montini, G. Balducci, I D'Auria, C. Pellecchia, P. Fornasiero, F. Felluga, B. Milani, *Organometallics* **2019**, *38*, 3498-3511.

[26] Selected examples: a) R. Wolf, A. W. Ehlers, J. C. Slootweg, M. Lutz, D. Gudat, M. Hunger, A. L. Spek, K. Lammertsma, *Angew. Chem. Int. Ed.* **2008**, *47*, 4584–4587; *Angew. Chem.* **2008**, *120*, 4660–4663. b) E.-M. Schnöckelborg, R. Wolf, *Chem. Commun.* **2010**, *46*, 2832–2834. c) J. Malberg, E. Lupton, E.-M. Schnöckelborg, B. de Bruin, J. Sutter, K. Meyer, F. Hartl, R. Wolf, *Organometallics* **2013**, *32*, 6040–6052. d) J. Malberg, M. Bodensteiner, D. Paul, T. Wiegand, H. Eckert, R. Wolf, *Angew. Chem. Int. Ed.* **2014**, *53*, 2771–2775; *Angew. Chem.* **2014**, *126*, 2812–2816.

[27] a) K. Jonas, R. Mynott, C. Krüger, J. C. Sekutowski, Y.-H. Tsay, *Angew. Chem. Int. Ed. Engl.* **1976**, *15*, 767–768; *Angew. Chem.* **1976**, *88*, 808–809. b) K. Jonas, US Patent 4169845 **1979**. c) W. W. Brennessel, V. G. Young, J. E. Ellis, *Angew. Chem. Int. Ed.* **2006**, *45*, 7268–7271; *Angew. Chem.* **2006**, *118*, 7426-7429.

[28] W. W. Brennessel, J. E. Ellis, *Inorg. Chem.* **2012**, *51*, 9076–9094.

[29] a) D. Gärtner, A. Welther, B. R. Rad, R. Wolf, A. Jacobi von Wangelin, *Angew. Chem. Int. Ed.* **2014**, *53*, 3722–3726. *Angew. Chem.* **2014**, *126*, 3796-3800. b) P. Büschelberger, D. Gärtner, E. Reyes-Rodriguez, F. Kreyenschmidt, K. Koszinowski, A. Jacobi von Wangelin, R. Wolf, *Chem. Eur. J.* **2017**, *23*, 3139–3151.

[30] Selected examples: a) M. M. Khusniyarov, T. Weyhermüller, E. Bill, K. Wieghardt, *Angew. Chem. Int. Ed.* **2008**, *47*, 1228–1231; *Angew. Chem.* **2008**, *120*, 1248-1251. b) M. M. Khusniyarov, T. Weyhermöller, E. Bill, K. Wieghardt, *J. Am. Chem. Soc.* **2009**, *131*, 1208. c) P. Papanikolaou, P. D. Akrivos, A. Czapik, B. Wicher, M. Gdaniec, N. Tkachenko, *Eur. J. Inorg. Chem.* **2013**, *2013*, 2418–2431.

[31] Selected examples: a) L. Li, P. S. Lopes, V. Rosa, C. A. Figueira, M. A. N. D. A. Lemos, M. T. Duarte, T. Avilés, P. T. Gomes, *Dalton Trans.* **2012**, *41*, 5144–5154. b) A. L. Gottumukkala, J. F. Teichert, D. Heijnen, N. Eisink, S. van Dijk, C. Ferrer, A. van den Hoogenband, A. J. Minnaard, *J. Org. Chem.* **2011**, *76*, 3498–3501. c) P. de Frémont, H. Clavier, V. Rosa, T. Avilés, P. Braunstein, *Organometallics* **2011**, *30*, 2241–2251.

[32] S. C. Bart, E. J. Hawrelak, E. Lobkovsky, P. J. Chirik, *Organometallics* **2005**, *24*, 5518–5527. b) H. Lee, M. G. Campbell, R. Hernández Sánchez, J. Börgel, J. Raynaud, S. E. Parker, T. Ritter, *Organometallics* **2016**, *35*, 2923–2929.

[33] M. Döring, E. Uhlig, T. Taldbach, *Z. Anorg. Allg. Chem.* **1991**, *600*, 163–167.

[34] X. Wang, Y. Zhao, S. Gong, B. Liu, Q.-S. Li, J.-H. Su, B. Wu, X.-J. Yang, *Chem. Eur. J.* **2015**, *21*, 13302–13310.

[35] a) C. Lichtenberg, M. Adelhardt, T. L. Gianetti, K. Meyer, B. de Bruin, H. Grützmacher, *ACS Catal.* **2015**, *5*, 6230–6240. b) C. Lichtenberg, L. Viciu, M. Adelhardt, J. Sutter, K. Meyer, B. de Bruin, H. Grützmacher, *Angew. Chem. Int. Ed.* **2015**, *54*, 5766–5771; *Angew. Chem.* **2015**, *127*, 5858-5863. c) C. Lichtenberg, L. Viciu, M. Vogt, R. E. Rodríguez-Lugo, M. Adelhardt, J. Sutter, M. M. Khusniyarov, K. Meyer, B. de Bruin, E. Bill, H. Grützmacher, *Chem. Commun.* **2015**, *51*, 13890–13893.

[36] S. Pelties, T. M. Maier, D. Herrmann, B. de Bruin, C. Rebreyend, S. Gärtner, I. G. Shenderovich, R. Wolf, *Chem. Eur. J.* **2017**, *23*, 6094–6102.

[37] T. M. Maier, M.Sc. thesis, Regensburg, **2016**.

2 Acenaphthene- and Phenanthrenediimine Ligands in Low-Valent Cobalt Complexes

Thomas M. Maier, Christian M. Hoidn, Karolina Trabitsch, Andreas W. Ehlers, and Robert Wolf

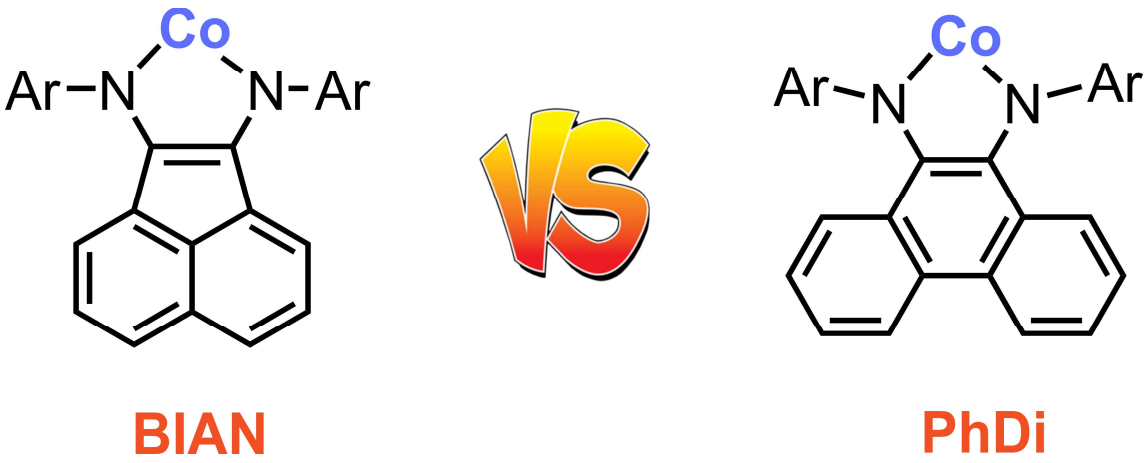

T. M. Maier performed the synthesis and characterization of **3 – 5** as well as the DFT calculations on **7** and **10-^{t}Bu**. T. M. Maier prepared all Figures and Schemes in this chapter except for Figures 8 and 10 and Schemes 4 – 7. A. W. Ehlers assisted with the DFT calculations described in *Chapter 2.2.1.* C. M. Hoidn and K. Trabitsch contributed with the synthesis and characterization of **5 – 9**. Parts of *Chapter 2.2.3* were written by C. M. Hoidn including preparation of Figures 8 and 10 and Schemes 4 – 7. R. Wolf supervised and directed the project.

Parts of *Chapter 2.2.3* were published in *Angewandte Chemie* as a communication: C. M. Hoidn, T. M. Maier, K. Trabitsch, R. Wolf, *Angew. Chem.* **2019**, *131*, 19107-19112; *Angew. Chem. Int. Ed.* **2019**, *58*, 1302-1308.

2.1 Introduction

As mentioned in Chapter 1, low-valent heteroleptic cobaltate complexes with one α-diimine ligand and a π-hydrocarbon as a labile ligand are attractive targets as pre-catalysts in reductive catalysis, or for the activation of small molecules. Specifically, the π-hydrocarbon provides a site for facile ligand exchange, while high reducing power is facilitated by the anionic α-diimine cobalt fragment. There are only a few examples of such complexes known in the literature, which fulfills these requirements (Figure 1). *Uhlig* and co-workers reported the first example of this class by the reaction of [Li(solv){Co(η^4-cod)$_2$}] (cod = 1,5-cyclooctadiene, solv = solvent) with 2,2'-bypridine (bpy) or a glyoxal based α-diimine.[1] The authors analyzed these compounds only by elemental analysis and the measurement of their magnetic moments, however. Later on, *Ellis* and co-workers structurally characterized the [(bpy)Co(cod)]$^-$ anion as lithium salt using single-crystal X-ray crystallography (XRD) and confirmed the work of *Uhlig* and co-workers.[2] *Yang* and co-workers subsequently synthesized anionic cobalt complexes with an α-diimine ligand and pyrene as the π-hydrocarbon.[3] These complexes were intensively characterized by several techniques, including XRD, magnetic susceptibility measurements and DFT calculations. Our group has also recently contributed to this field with the synthesis of [K(thf)$_x${(^{Ar}BIAN)Co(cod)}] [Ar = Dipp (2,6-diisopropylphenyl); Mes (2,4,6-trimethylphenyl); BIAN = bisaryl (imino)acenaphthene], which was successfully used in the activation of small molecules (white phosphorus (P_4), carbon disulfide, phosphaalkynes) and in reductive catalysis [(de)hydrogenation reactions]. These results represent the first synthetic application for those cobaltate anions.[4],[5]

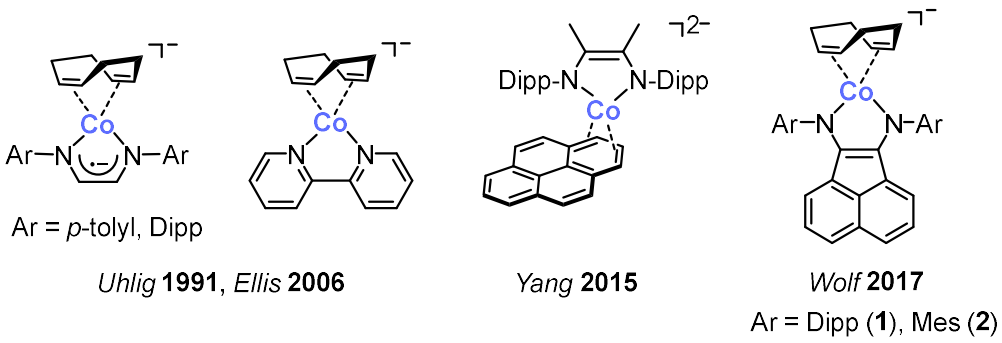

Figure 1. Known heteroleptic α-diimine cobalt anions.[4]

α-Diimine ligands can act synergistically as σ-donors and π-acceptors and are correspondingly able to stabilize low oxidation states.[6] They are also potentially redox-active, which means that they are capable of storing and releasing electrons, which is of special interest in 3d metal catalysis as it is proposed to help facilitate "noble metal-like" 2e⁻ redox processes.[7],[8] There are two ways to control the steric and electronic properties of α-diimines: steric hindrance can be influenced by the choice of the groups which are connected to the nitrogen atoms. Usually, these groups are substituted phenyl rings. The electronic properties can be controlled by the substitution of the ligand backbone, especially in the case of polyaromatic backbones.

Bisaryl(imino)acenapthene (BIAN) and phenanthrenediimine (PhDi) are two examples for this type. Both ligands consist of a polyaromatic backbone and are usually substituted with aryl groups on nitrogen. BIANs have been known since the late 1960s[9] and were introduced as ligands in coordination chemistry by *van Asselt*, *Elsevier* and co-workers.[10] BIAN metal complexes are more popular than the corresponding PhDi complexes, due to the facile synthesis of the ligands at multigram scale and excellent coordination behavior. *Fedushkin* and co-workers also showed that BIAN can store up to four electrons by reduction of ^{Dipp}BIAN using sodium metal.[11] However, in transition metal complexes the formal charge of BIAN usually lies in the range of 0 to –2. The determination of C–C and C–N bond lengths in the α-diimine unit is a sensitive method for the determination of the oxidation state of the ligand (Figure 2). This also applies to the PhDi ligand. In contrast to BIAN, this ligand favors a two-electron reduction in order to achieve an aromatic phenanthrene backbone, which is the case for almost all low-valent metal complexes with PhDi ligands.[12],[13]

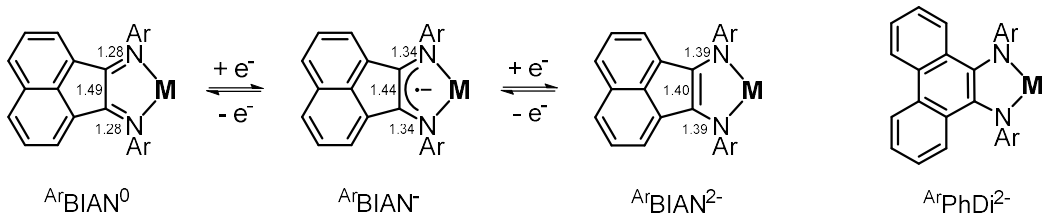

Figure 2. Standard C–C and C–N bond lengths (in Å) for ^{Ar}BIAN transition metal complexes.[4] The same applies to the ^{Ar}PhDi ligand, which is displayed as dianion with an aromatic backbone (right).

The combination of redox-active α-diimines and electron rich 3d metal centers is quite an interesting issue from a theoretical point of view. The electron rich 3d metal center can reduce the α-diimine ligand and the electronic structures of the resulting complexes can be diverse. *Wieghardt* and co-workers and *Grützmacher* and co-workers showed that for iron α-diimine complexes the presence of an antiferromagnetic coupling between the metal center and the α-diimine needs to be considered. Two examples are illustrated schematically in Figure 3.[14],[15] The homoleptic bis(α-diimine) iron complex was synthesized by *Chirik* and co-workers and theoretically investigated by *Wieghardt* and co-workers. The structure contains an Fe(II) high-spin center with two monoanionic α-diimine ligands. Both unpaired electrons from the ligands are coupled antiferromagnetically to two electrons from the Fe(II) center, resulting in a $S = 1$ ground state. A similar behavior is observed in the heteroleptic Fe(I) complex reported by *Grützmacher* and co-workers. One electron of the low-spin Fe(I) center is antiferromagnetically coupled to the electron of the ligand. Thus, an overall $S = 0$ ground state is present, which is supported by DFT calculations.

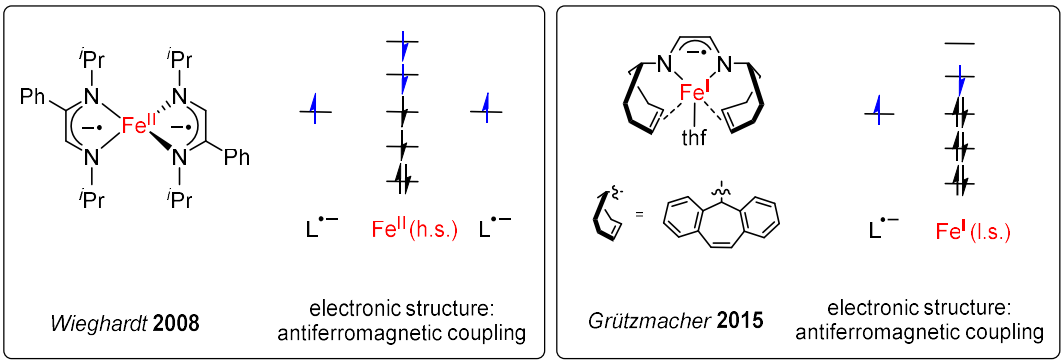

Figure 3. Selected examples of α-diimine complexes with antiferromagnetic coupling between a high-spin (h.s., left) and low-spin (l.s., right) metal center and the π-radical anion(s) of an α-diimine unit.

Herein, a comparison between BIAN and PhDi from a theoretical point of view will be presented. Moreover, the synthesis and characterization of heteroleptic phenanthrenediimine cobaltates with π-hydrocarbons will be reported. These are compared to analogous BIAN complexes in order to identify the differences. Their distinct reactivity is exemplified by the activation of white phosphorus.

2.2 Results and Discussion

2.2.1 Comparison between BIAN and PhDi

At first glance, the generic PhDi and BIAN ligands look quite similar and have only a slight variation in their backbone. Both ligands are excellent π-acceptors and form complexes with electron-rich metal centers. To describe the electronic differences between both ligands more precisely, gas phase DFT calculations at the B3LYP/6-311G(d)[16],[17] level of theory were performed. The geometries of phenyl-substituted BIAN and PhDi ligands with different charges (neutral, monoanionic, dianionic) were optimized (Table 1).

$\Delta E = 0$ kcal mol^{-1} was defined as the neutral ligand with two free electrons. Addition of one electron to the neutral ligand led to a gain of energy in both cases. The monoanionic [^{Ph}BIAN]$^-$ ligand is 28.9 kcal mol^{-1} more stable than the corresponding neutral species. A similar result ($\Delta E = -32.7$ kcal mol^{-1}) was obtained in the case of [^{Ph}PhDi]$^-$. The addition of one more electron is strongly disfavored for both ligands due to the repulsion of negative charges. However, it is experimentally proven that a second reduction is feasible.[11] In case of the second electron, the spin must be taken into account. Theoretically three different spin states are conceivable, which would result either in a closed-shell singlet (c.s.s.), an open-shell singlet (o.s.s), or a triplet ground state. For ^{Ph}BIAN the triplet ground state ($\Delta E = +24.5$ kcal mol^{-1}) is higher in energy compared to the singlet ground states, which are similar in energy [$\Delta E = +20.5$ kcal mol^{-1} (c.s.s) and $\Delta E = +20.9$ kcal mol^{-1} (o.s.s.)]. In contrast to ^{Ph}BIAN, ^{Ph}PhDi shows a slightly different behavior concerning the second reduction. The double-reduced form remains disfavored but the closed-shell singlet spin state is only ($\Delta E = +4.5$ kcal mol^{-1}) higher in energy compared to neutral ^{Ph}PhDi. Calculations for the energy of the open-shell singlet state were attempted in the same way as for ^{Ph}BIAN. Nevertheless, this attempt failed and resulted in the closed-shell singlet solution. The triplet ground state ($\Delta E = +36.6$ kcal mol^{-1}) is much higher in energy. Taken collectively, these results suggest that ^{Ph}PhDi is in principle a better electron acceptor than ^{Ph}BIAN, particularly in the context of two-electron reduction.

Table 1. Properties of optimized aryl substituted BIAN and PhDi ligands.

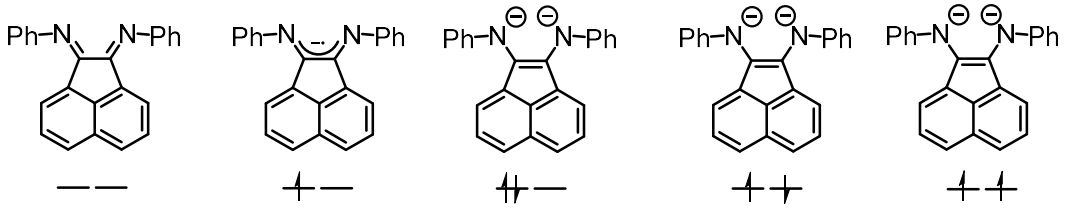

^{Ph}BIAN $[^{Ph}BIAN]^-$ $[^{Ph}BIAN]^{2-}$ c.s.s.[a] $[^{Ph}BIAN]^{2-}$ o.s.s.[b] $[^{Ph}BIAN]^{2-}$ t.[c]

	^{Ph}BIAN	$[^{Ph}BIAN]^-$	$[^{Ph}BIAN]^{2-}$	$[^{Ph}BIAN]^{2-}$	$[^{Ph}BIAN]^{2-}$
Charge	0	-1	-2	-2	-2
Spin		$S = 1$	$S = 0$	$S = 0$	$S = 3/2$
State			c.s.s.	o.s.s	triplet
ΔE/ kcal mol^{-1}	+ 0.0	–28.9	+20.5	+20.9	+24.5

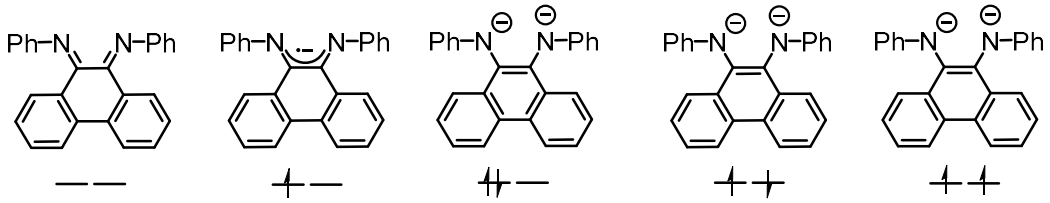

^{Ph}PhDi $[^{Ph}PhDi]^-$ $[^{Ph}PhDi]^{2-}$ c.s.s.[a] $[^{Ph}PhDi]^{2-}$ o.s.s.[b],[d] $[^{Ph}PhDi]^{2-}$ t.[c]

No.	^{Ph}PhDi	$[^{Ph}PhDi]^-$	$[^{Ph}PhDi]^{2-}$	$[^{Ph}PhDi]^{2-}$	$[^{Ph}PhDi]^{2-}$
Charge	0	-1	-2	-2	-2
Spin		$S = 1$	$S = 0$	$S = 0$	$S = 3/2$
State			c.s.s	o.s.s.	triplet
ΔE/ kcal mol^{-1}	+ 0.0	-32.7	+4.5	[e]	+36.6

[a] c.s.s = closed-shell singlet; [b] o.s.s = open-shell singlet; [c] t. = triplet; [d] The same approach as for ^{Ph}BIAN was used.[e] Calculation resulted in the closed-shell singlet solution.

2.2.2 Synthesis of Heteroleptic PhDi Cobaltates with π-Hydrocarbons Ligands

The phenanthrenediimine ligands ^{Ar}PhDi (Ar = Dipp, Mes) were synthesized in a two-step reaction starting from commercially available 1,10-phenanthrenequinone according to modified literature reported procedures.[18] The first condensation step of 1,10-phenanthrenequinone with the corresponding aniline is acid catalyzed, whereas the second condensation requires titanium(IV)-chloride as dehydrating agent to push the equilibrium towards the product (Scheme 1).

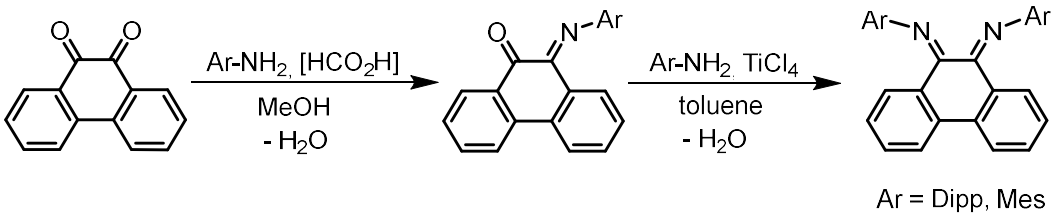

Scheme 1. Synthesis of ^{Ar}PhDi (Ar = Dipp, Mes) ligand in a two-step reaction.

The cobalt complexes [K([18]c-6)][(^{Ar}PhDi)Co(η^4-cod)] [Ar = Dipp (**3**), Mes (**4**)] were synthesized starting from [K([18]c-6)][Co(η^4-cod)] using a ligand exchange reaction and were obtained in moderate yields (up to 54%) (Scheme 2). The complexes were isolated as ion-separated [K([18]c-6)]$^+$ salts.

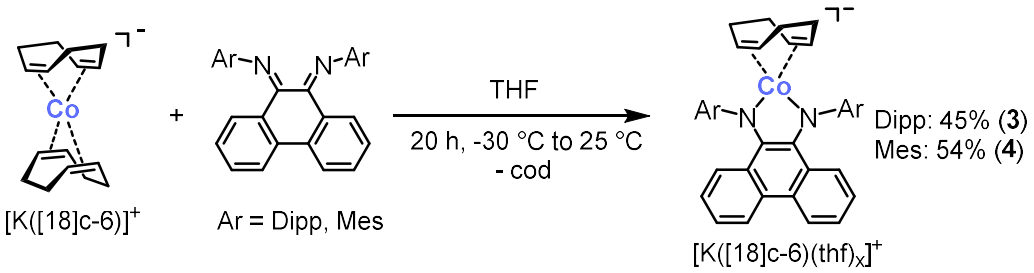

Scheme 2. Synthesis of [K([18]c-6)][(^{Ar}PhDi)Co(η^4-cod)] [Ar = Dipp (**3**), Mes (**4**)].

For the mesityl-substituted complex (**4**), the molecular structure in the solid state could be determined by single-crystal X-ray crystallography. The molecular structure in the solid-state is shown in Figure 4 (right). The analysis reveals a significantly distorted square planar coordination environment for cobalt with a twist angle of 42.6°. As illustrated in Figure 2, PhDi features the same characteristic bond lengths (C–C and C–N) as BIAN, which can be used to determine the formal charge of the ligand. In complex **3** the C–N (1.373(5) Å, 1.3968(4) Å) and C1–C2 (1.406(5) Å) bond lengths indicate a dianionic α-diimine ligand.[12] These bond parameters are similar to those found in [K(dme)$_4${(^{Mes}BIAN)Co(η^4-cod)}] (**2**) (C1–C2: 1.377(5) Å; C–N: 1.378(5) Å, 1.370(4) Å) (Figure 4, left).[19] Consequently, both diamagnetic species are best described as cobalt(I) centers, with a d^8 configuration. Structurally the ^{Mes}BIAN and ^{Mes}PhDi cobaltate complexes differ in the behavior of the mesityl groups. The C1–N1–C15 angle (119.3(3)°) is considerably wider than the equivalent angle C1–N1–C22 in the BIAN cobaltate

(116.1(3)°), which lead to the conclusion that the ^{Mes}PhDi ligand is sterically more demanding.

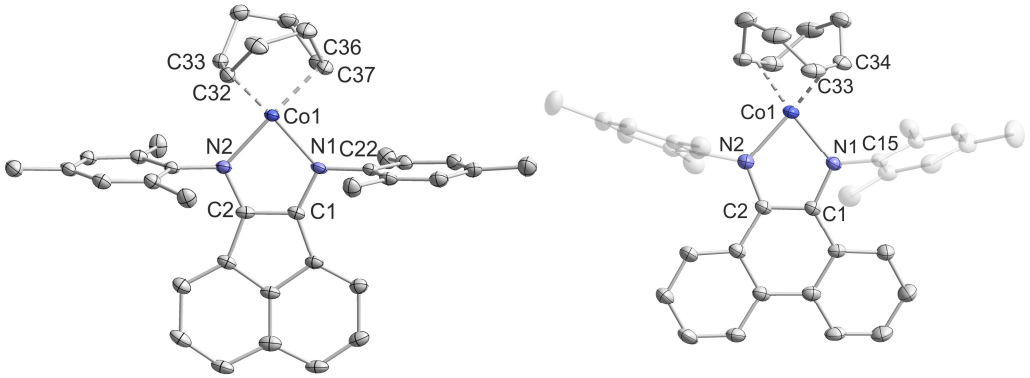

Figure 4. Solid-state molecular structure of [K(dme)$_4${(^{Mes}BIAN)Co(η^4-cod)}] (**2**, left)[19] and [K([18]c-6)(thf)$_2$][(^{Mes}PhDi)Co(η^4-cod)] (**4**, right). The hydrogen atoms and the cation [K([18]c-6)(thf)$_2$]$^+$ for **2** and **4** are omitted for clarity. Thermal ellipsoids are drawn at the 40% probability level. Selected bond lengths [Å] and angles [°]: For **2**: Co1–C32 2.004(4), Co1–C33 2.031(4), Co1–C36 2.027(4), Co1–C37 2.039(4), Co1–N1 1.924(3), Co1–N2 1.936(3), C1–N1 1.378(5), C2–N2 1.370(4), C1–C2 1.377(5), C36–C37 1.387(6), C32–C33 1.400(6); N1–Co1–N2 84.18(1). For **4**: Co1–C33 1.996(4), Co1–C34 2.064(4), Co1–N1 1.921(3), Co1–N2 1.931(3), C1–N1 1.396(4), C2–N2 1.373(5), C1–C2 1.406(5), C33–C44 1.402(7), N1–Co1–N2 81.2(1) C1–N1–C15: 119.3(3).

The ^{1}H NMR spectra of **3** and **4** show sharp signals for the phenanthrenediimine ligand and give rise to three multiplets for the 1,5-cyclooctadiene ligand at 2.80 ppm (cod-CH), 2.30 ppm (cod-CH$_2$), 1.00 ppm (cod-CH) for **3** and 2.54 ppm (cod-CH), 2.30 ppm (cod-CH$_2$) and 0.99 ppm (cod-CH) for **4**. These shifts are similar to the ones reported for **1** and **2**, for which upfield shifted multiplets (in comparison to free cod) were supposed to be caused by the coordination of cod to an electron-rich metal center.[20]

The UV-vis spectra for both compounds (which are colored green in THF) are almost identical and have their main absorption peak at 442 nm [ε = 18500 L mol^{-1} cm^{-1} (**3**)], and 436 nm [ε = 13500 L mol^{-1} cm^{-1} (**4**)], respectively (Figure 5). A sharper band at lower wavelengths [361 nm (ε = 14500 L mol^{-1} cm^{-1} (**2**)), 369 nm (ε = 12000 L mol^{-1} cm^{-1} (**3**))] located next to the main absorption band and a broad shoulder at 600 nm [ε = 3800 L mol^{-1}cm^{-1} (**3**); ε = 3000 L mol^{-1} cm^{-1}(**4**)]. For comparison, the UV-vis spectra of compounds **1** and **2** are displayed in Figure 5 in addition (blue and green curve). The absorption at 441 nm [ε = 12000 L mol^{-1} cm^{-1} (**1**)], 442 nm [ε = 10500 L mol^{-1} cm^{-1} (**2**)], (similar to the main absorption of **3** and **4**), is accompanied by a second absorption (broad shoulder) at 662 nm

[ε = 8500 L mol^{-1} cm^{-1} (**1**)], 645 nm [ε = 6500 L mol^{-1} cm^{-1} (**2**)] is observed for these complexes. In contrast to complexes **3** and **4**, complexes **1** and **2** are solvatochromic.[4]

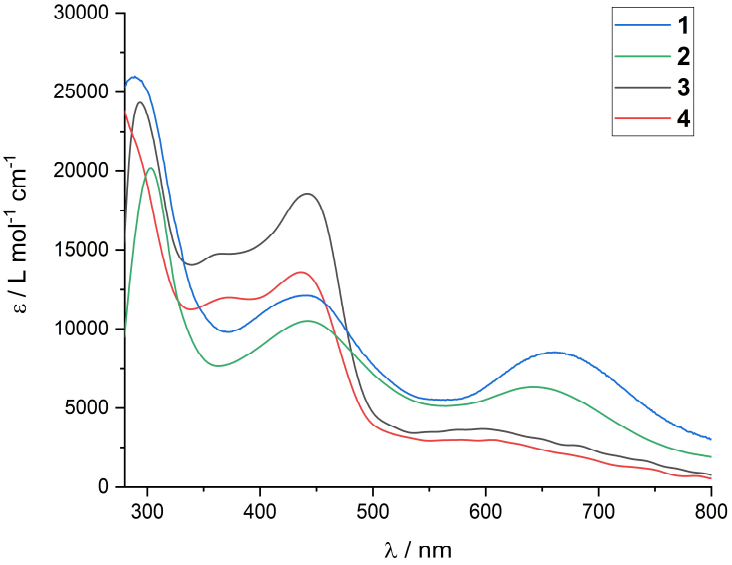

Figure 5 UV-vis spectra of compounds **1**-**4** in THF.

In analogy, the reaction of bis(anthracene) cobaltate(1–) with ^{Dipp}PhDi (Scheme 2) led to the formation of the anthracene containing heteroleptic complex **5** . This is notable as the equivalent reaction with ^{Dipp}BIAN affords the homoleptic bis(α-diimine) complex [(BIAN)$_2$Co]$^-$ as proven by single-crystal X-ray crystallography. This highlights the influence of the ligand and clearly confirms the ability of BIAN and PhDi to mediate divergent reactivity.

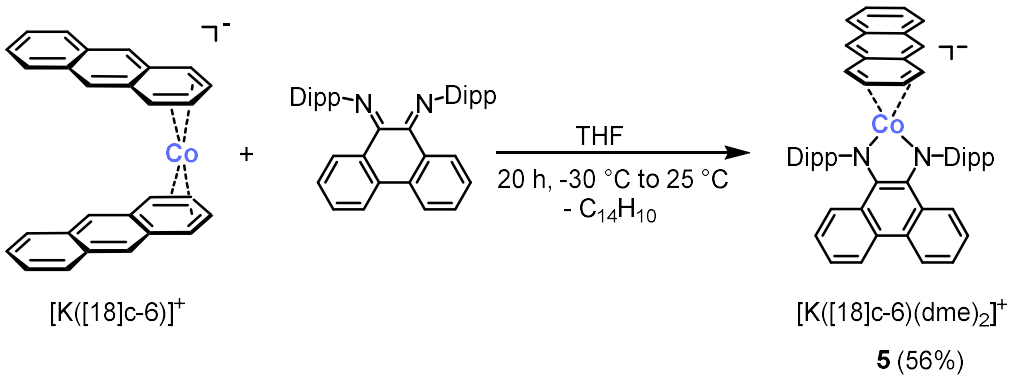

Scheme 2. Synthesis of [K([18]c-6)][(^{Dipp}PhDi)Co(η^4-C$_{14}$H$_{10}$)] (**5**).

Complex **5** was crystallized from DME/*n*-hexane in 56% yield, which directly afforded suitable crystals for single-crystal X-ray crystallography. According to its C–C (C1–C2

1.402(5) Å) and C–N (C1–N1 1.402(5) Å; C2–N2 1.420(7) Å) bond lengths, **5** also contains a dianionic PhDi ligand.[12] The intersection of the planes of the η⁴-diene and the uncoordinated *exo*-naphthalene unit of the anthracene moiety describes its dihedral angle of 26.2° according to the definition by *Ellis* and co-workers for [K[2.2.2]cryptand)(thf)$_x$][Co(η⁴-$C_{14}H_{10}$)$_2$]. This angle is similar to the analogous one found for the parent bis(anthracene) cobaltate(1–) (27.8°)[21] and [Ni(η⁴-$C_{14}H_{10}$)(η²-EtPCH_2CH_2PEt)] (26.2°)[22] but larger than for [K([18]c-6)][Cp*Fe(η⁴-$C_{14}H_{10}$)] (21.8°).[23] This is characteristic for late transition metal complexes, whereas early transition metal complexes typically have larger dihedral angles. By means of electron counting, the anthracene ligand can either be described as neutral ligand with a Co(I) center or as dianionic ligand with a Co(III) center.

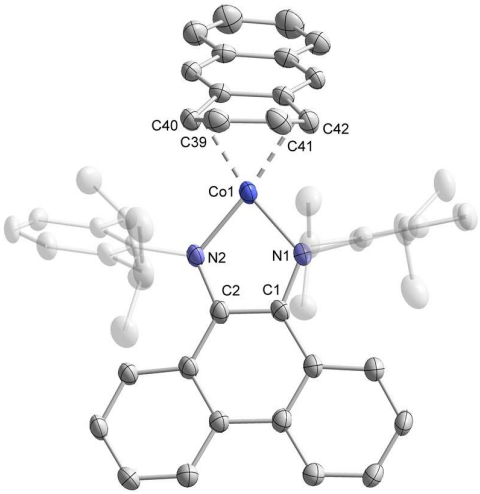

Figure 6. Solid-state molecular structure of [K([18]c-6)(dme)$_2$][(^{Dipp}PhDi)Co(η⁴-$C_{14}H_{10}$)] (**5**). The hydrogen atoms and the cation [K([18]c-6)(dme)$_2$]⁺ are omitted for clarity. Thermal ellipsoids are drawn at the 40% probability level. Selected bond lengths [Å] and angles [°]: C1–C2 1.409(5), N1–C1 1.370(5), N2–C2 1.402(5), N1–Co1 1.880(3), N2–Co1 1.875(3), C39–C40 1.405(7), C41–C42 1.420(7), C39–C41 1.404(7), N1–Co1–N2 82.7(1). Due to a highly disordered cation, the structure could not be refined to a better R_1 value than R_1 = 9.6% with wR_2 = 26.99%.

The ^{1}H NMR spectrum of **5** shows sharp signals and one set of multiplets for the phenanthrenediimine ligand. Of special interest is the chemical shift of the protons bound to those anthracene C atoms (C39–C42) which are directly coordinated to cobalt in η⁴-fashion. These two multiplets are significantly high-field shifted to 5.81 ppm and 1.89 ppm, which experimentally confirm the π-acceptor property of the η⁴-diene unit. The UV-vis spectrum of **5** has two absorption bands at 354 nm (26000 L mol^{-1} cm^{-1}) and 606 nm (13000 L mol^{-1} cm^{-1}) which are also present in **3** and **4** (Figure 7).

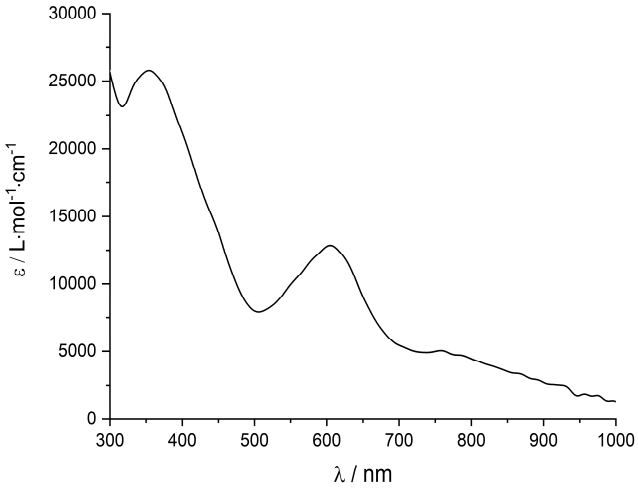

Figure 7. UV-vis spectrum of complex **5** in THF.

2.2.3 Comparison in White Phosphorus Activation

The highly-reduced α-diimine cobalt complexes **1** – **5** are promising starting materials for the activation of small molecules due to the redox non-innocent α-diimine unit and the labile olefin/arene as placeholder. As discussed in section 2.1, complex **1** was successfully applied used for the activation of white phosphorus (P_4).[4] This reaction led to a dinuclear, dianionic dicobalt tetraphosphido complex (**6**) (Scheme 3). Single-crystal X-ray crystallography revealed two P_2^{2-} units bound between two cobalt(II) atoms, two monoanionic BIAN ligands, and two potassium cations which are coordinatively saturated by THF molecules.

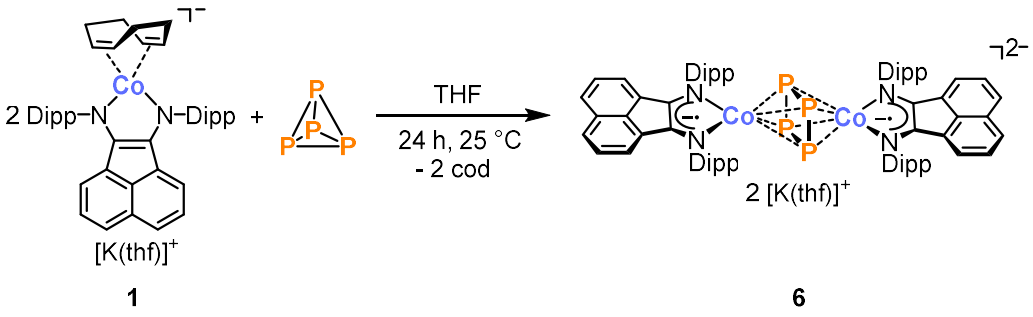

Scheme. 3. Synthesis of the dianionic dicobalt tetraphosphido complex **6**.

Complex **6** was electrochemically investigated by cyclic voltammetry and showed two reversible oxidation processes, as well as one irreversible oxidation. The stability of the

oxidized monoanionic and neutral complexes was experimentally confirmed by oxidation with ferrocenium salts and subsequent isolation as pure compounds.

C. M. Hoidn performed the reaction of **3** and white phosphorus in a 1:1 ratio (Scheme 4). After work-up and subsequent crystallization from a toluene/*n*-hexane mixture, crystals of the newly formed complex **7** were obtained in 80% yield. These crystals were also found to be suitable for single-crystal X-ray crystallography.

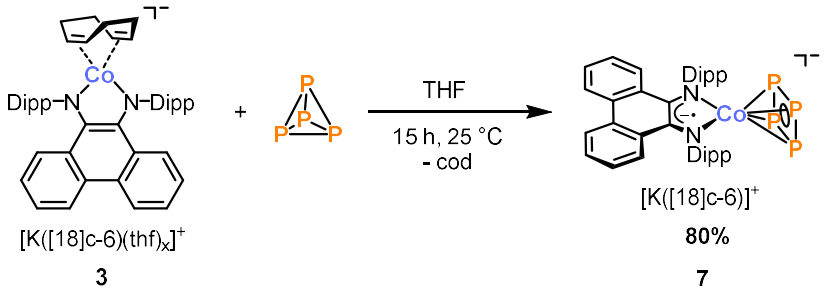

Scheme. 4. Synthesis of the mononuclear cobalt tetraphosphido complex **7**.

The molecular structure of this complex is shown in Figure 8 and confirms the presence of a [(^{Dipp}PhDi)Co(η^4-P_4)]$^-$ anion with a terminally coordinated *cyclo*-P_4 unit and a bidentate PhDi ligand.

The P_4 unit was highly disordered which prevent a detailed interpretation of its structure. Fortunately, the tungsten pentacarbonyl adduct of **7**, [K([18]c-6)] [(^{Dipp}PhDi)Co(μ^2-η^1-η^4-P_4)W(CO)$_5$] (**8**) was quantitatively obtained in the reaction of **7** and [W(CO)$_5$(thf)] and shows an ordered structure, which allows for detailed analysis of the central P_4 unit. The almost square *cyclo*-P_4 unit shows P–P bond lengths of 2.132(4) to 2.173(5) Å (mean: 2.147(7) Å), which are in between the values expected for P–P single (2.22 Å) and double bonds (2.04 Å) and are similar to those found in other *cyclo*-P_4 complexes.[24] The C–C (1.42(1) Å) and C–N (1.36(1) Å) distances of the PhDi backbone indicate the presence of a rare monoanionic PhDi unit.[13] An oxidation state of +III for cobalt and a $[P_4]^{2-}$ unit can be concluded from these data. The same can be assumed for **7**.

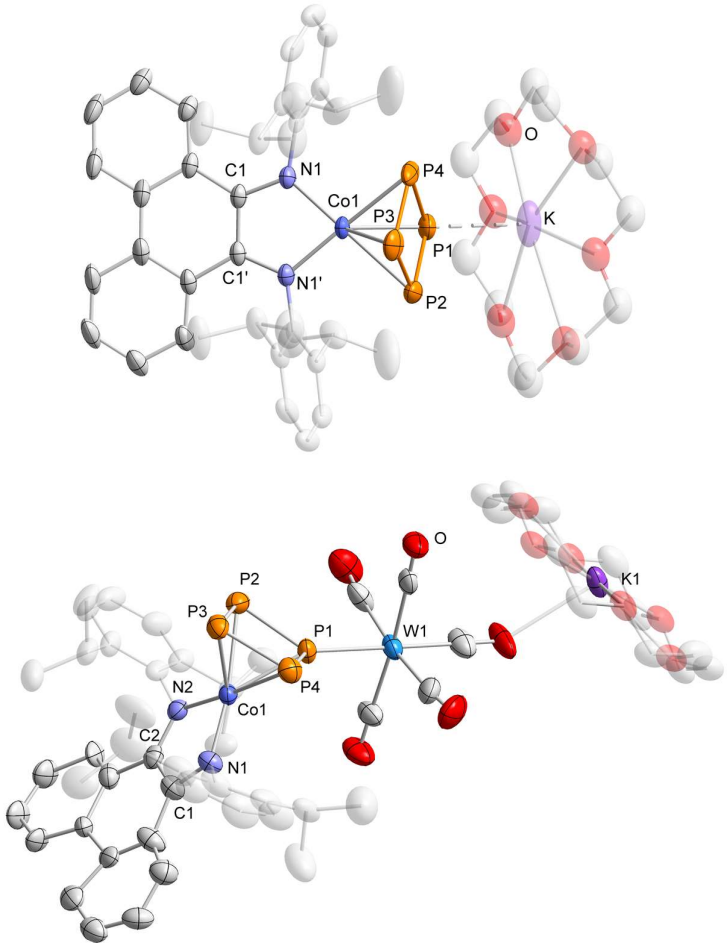

Figure 8. Solid-state molecular structure of [K([18]c-6)][(^{Dipp}PhDi)Co(η^4-P_4)] (**7**, top) and [K([18]c-6)][(^{Dipp}PhDi)Co(μ^2-η^1-η^4-P_4)W(CO)$_5$] (**8**, bottom)**.** Thermal ellipsoids are drawn at the 40% probability level. Hydrogen atoms and disorder of **7** are omitted for clarity. Selected bond lengths [Å] and angles for **8**: W1–P1 2.521(2), 2.527(3), P1–P2 2.151(3), 2.173(5), P1–P4 2.134(3), 2.132(4), P2–P3 2.155(3), 2.133(6), P3–P4 2.153(3), 2.144(7), Co1–P1 2.314(2), 2.297(3), Co1–P2 2.394(2), 2.419(4), Co1–P3 2.313(2), 2.313(4), Co1–P4 2.405(2), 2.392(3), Co1–N1 1.880(6), 1.888(7), Co1–N2 1.888(6), 1.884(8), C1–N1 1.36(1), 1.36(1), C2–N2 1.35(1), 1.36(1), C1–C2 1.42(1), 1.42(1), P1–P2–P3 87.9(1), 87.4(2), P2–P3–P4 91.4(1), 92.5(2), P3–P4–P1 88.4(1), 88.2(2), P2–P1–P4 92.0(1), 91.7(2).

There are only a few examples in the literature about transition metal *end*-deck P_4 complexes and further functionalization with electrophiles.[24] In a single example, *Mezailles* and co-workers investigated the reactivity of an iron *cyclo*-P_4 complex by further coordination with copper(I) chloride or an electron deficient borane.[24f]

Density functional theory (DFT) studies at the OPBE[25]/def2-TZVP[26] level of theory gave further insight into the nature of the *cyclo*-P_4 unit of the anion of **7**. The optimized anionic model compound **7** (^{i}Pr substituted by Me to minimize computational cost) features a square planar *cyclo*-P_4 ligand and P–P distances (2.148-2.152 Å) close to the

crystallographically determined mean value of the *cyclo*-P_4 unit in anion **7** (2.147(7) Å). The aromaticity of the *cyclo*-P_4 ligand was investigated by nucleus independent chemical shift (NICS) DFT calculations (Table 2), where the criterium for aromaticity is a significant value of >0. Conversely, a molecule is anti-aromatic if the NICS value is <0.[27] In comparison to the NICS(0) values of aromatic species (benzene = 8.2, cyclobutadienediide = 10.7) and the anti-aromatic free P_4^{2-} (−5.0),[28] the calculated NICS(0) value for the model complex of **7** (9.4) indicates a substantial aromatic character. Similar observations were also reported by *Mézailles* and co-workers for the P_4^{2-} ligand in $[(PhP(CH_2CH_2PCy_2)_2)Fe(\eta^4\text{-}P_4)]$.[24f]

Table 2. Calculated NICS(0) values.

Compound	NICS value[a]	Character
Benzene (C_6H_6)	8.1	aromatic
Cyclobutadiene dianion $[C_4H_4]^{2-}$	10.4	aromatic
Tetraphosphacylobutadiene dianion $[P_4]^{2-}$	–4.7	anti-aromatic
$[(^{2,6\text{-dmp}}PhDi)Co(\eta^4\text{-}P_4)]^-$	5.1	aromatic

[a] NICS values calculated with the ORCA program package using OPBE/def2-TZVP level of theory. 2,6-dmp = 2,6-dimethylphenyl

Some of the key molecular orbitals (Löwdin population analysis) of $[(^{2,6\text{-dmp}}PhDi)Co(\eta^4\text{-}P_4)]^-$ are shown in Figure 9. The fully occupied orbitals with the highest energies are the orbitals **148**-**153**. Of these, especially **148** (3, and 3), **150** ($3d_{xy}$), and **153** (HOMO) ($3d_{z^2}$, and $3d_{xy}$) exhibit high d-orbital character. Therefore, a d^6-configuration can be concluded. Orbitals **149** and **151** meanwhile show the lone pairs of the P_4 unit. Orbital **152** represents a bonding interaction between the PhDi ligand and cobalt. By contrast, the unoccupied orbitals **154**, and **155** show metal/ligand antibonding character.

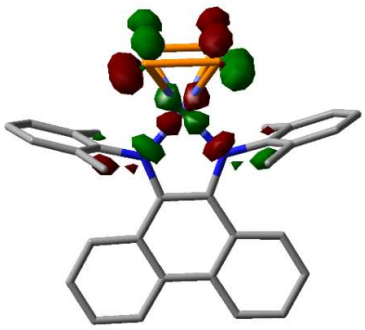

155 (occu.: 0.000, 29% $3d_{yz}$; 0.722 eV)

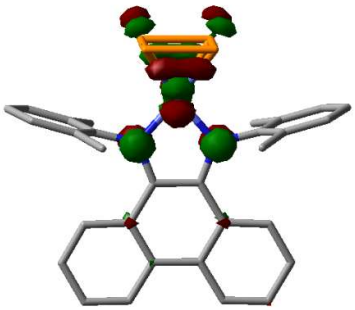

154 (occu.: 0.000, 19% $3d_{xz}$, 7% 3; 0.071 eV)

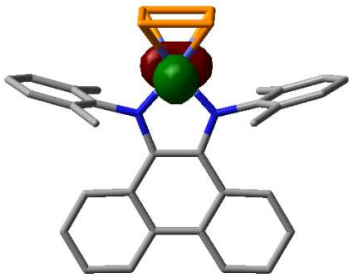

153 (occu.: 2.000, 63% 3, 15% $3d_{xz}$, 4% 3; -1.185 eV)

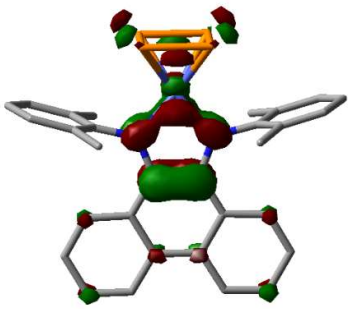

152 (occu.: 2.000 ; -1.455 eV)

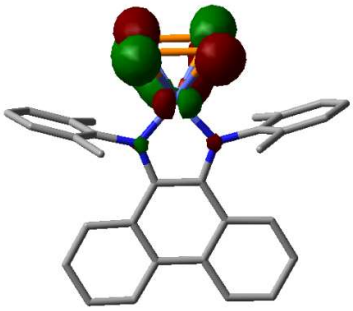

151 (occu.: 2.000 ; -1.657 eV)

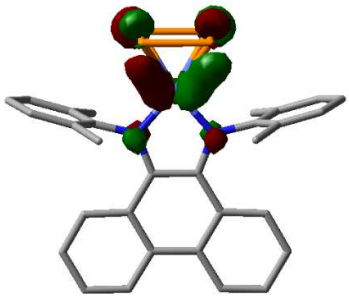

150 (occu.: 2.000, 40% $3d_{xy}$; -1.677 eV)

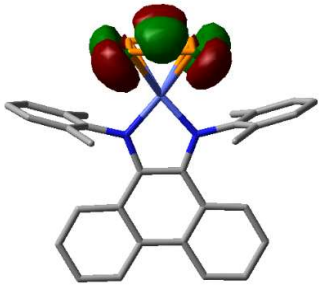

149 (occu.: 2.000 ; -1.715 eV)

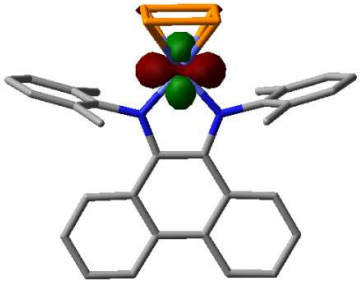

148 (occu.: 2.000, 51% 3, 16% 3, 18% $3d_{xz}$; -1.748 eV)

Figure 9. Frontier molecular orbitals (Löwdin population analysis) of the model compound [($^{2,6\text{-dmp}}$PhDi)Co(η^4-P_4)]$^-$, with an isosurface value = 0.05.

The relatively high energy of the P-centered orbitals **149** and **151** indicates that **7** could be an excellent precursor for P–P bond formation reactions with diorganochloro-phosphanes to produce larger phosphorus cages. Reactions with R_2PCl (R = Cy, ^{t}Bu, Ph, N(^{i}Pr)$_2$) proceeded quantitively in a salt elimination reaction to afford pentaphosphido complexes, which could be isolated in up to 77% yield by a simple work-up procedure (Scheme 3). Similar pentaphosphido cobalt complexes were previously reported by our group derived from a heterobimetallic cobalt-gallium complex.[29] The same reactivity pattern using the BIAN

supported dinuclear dicobalt tetraphosphido complex (**6**) led to a different result. Here, the reaction with diorganochlorophosphanes led to an oxidized neutral dicobalt tetraphosphido complex and diphosphanes.

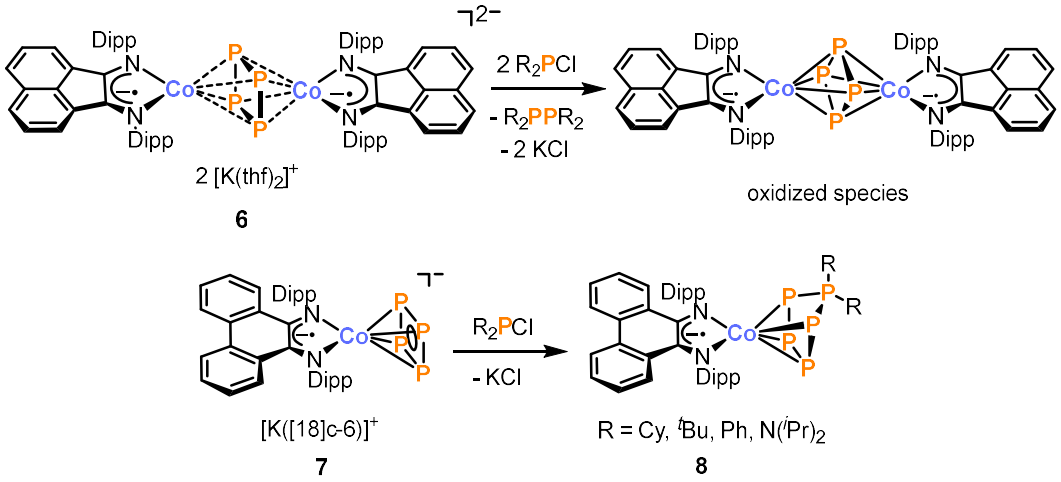

Scheme 5. Different reactivity of **6** and **7** towards diorganochlorophosphanes.

These *cyclo*-P_5R_2 cobalt complexes (**8**) can be further functionalized using cyanides [M]CN (M = $[^nBu_4N]^+$, $[Et_4N]^+$, $[K([18]c\text{-}6)]^+$). Thus, the formation of $[(^{Dipp}PhDi)Co(\eta^3\text{-}P_3)(CN)]^-$ (**9**) was confirmed by $^{31}P\{^1H\}$ NMR spectroscopy and isolated as the tetra-*n*-butylammonium salt ($[^nBu_4N]$-**9**) followed by a reaction with $[^nBu_4N]CN$. In addition, formation of the new cyanodiphosphide anions $[R_2PPCN]^-$ (**10**) (R = Cy, ^{t}Bu, Ph N(^{i}Pr)$_2$) was observed (Scheme 7). The reaction thus results in an unprecedented fragmentation of the polyphosphide ligand into P_3 and P_2 units, the latter one is freed from the coordination sphere of the metal. Only one related reaction involving the [3+2] fragmentation of a P_5 species has been described in literature, which has a completely different outcome. As reported by *Weigand* and co-workers, the reaction of the cation $[P_5DippCl]^+$ with *N,N'*-bis(2,6-diisopropylphenyl)-4,5-dichloro-imidazol-2-ylidene ($IPrCl_2$) affords a triphosphaallyl cation $[(IPrCl_2)P_3(IPrCl_2)]^+$ and an inversely polarized phosphaalkene $[(IPrCl_2)P{=}P(Cl)Dipp]$.[30]

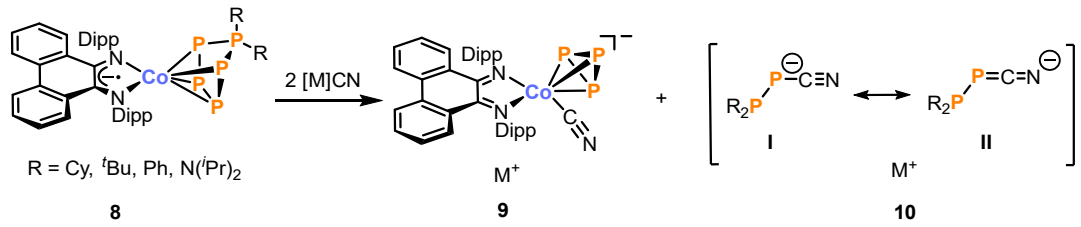

Scheme 6. Fragmentation of the pentaphosphido ligand. ([M] = [^{n}Bu$_4$N]$^+$, [Et$_4$N]$^+$, [K([18]c-6)]$^+$). **I** and **II** are two conceivable resonance structures of the anion in **10**.

Both **9** and **10** were structurally characterized by single-crystal X-ray crystallography as [K([18]c-6)]$^+$ salts [K-([18]c-6)]**[9]** and [K-([18]c-6)]**[10]**. The solid-state molecular structure of the cyanodiphosphide anion [K-([18]c-6)]**[10]** shows an almost linear, phosphanyl-substituted PCN moiety (P1-C1-N1 178.4(1)°) with a P–P distance of 2.1895(4) Å, i.e. close to a typical single bond (Figure 10). The structural motif is reminiscent of *Schmidpeter's* [RPCN]$^-$ (R = CN, Ph) anions.[31] Recently, *Borger* and *Grützmacher* have also described related cyanophosphides [(NHP)PCN]$^-$ with bulky *N*-heterocyclic phosphenium (NHP) substituents, which feature similar bond parameters.[32]

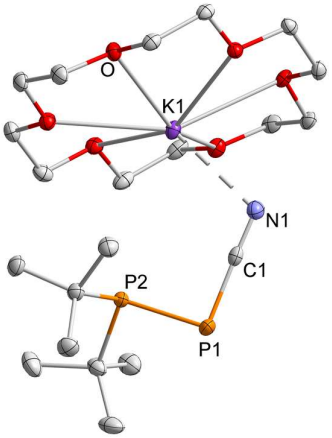

Figure 10. Solid-state molecular structure of [K([18]c-6)][^{t}Bu$_2$PPCN] (**10-^{t}Bu**). Thermal ellipsoids are drawn at the 40% probability level. Hydrogen atoms are omitted for clarity. Selected bond lengths [Å] and angles for: P1–P2 2.1895(4), P1–C1 1.763(1), C1–N1 1.160(2), K1···N1 2.828(1), P1–C1–N1 178.4(1), C1–P1–P2 92.43(4).

Similarly to those compounds, the electronic structure of the anion in salt **10** may be described using either a cyanophosphide ($^-$P–C≡N, **I**) or a phosphaketeneimide (P=C=N$^-$, **II**) resonance structure (Scheme 5). A natural resonance analysis[33] and natural bond analysis at the B3LYP/6-31G+*[34] level of theory shows that the phosphaketeneimide form in fact plays only

a relatively minor role in the electronic ground state of **10-^{t}Bu** (**I**: 69% vs. **II**: 23%). Analogous calculations for related cyanate and phosphaethynolate anions (O^-–C≡X vs. O=C=X^-, X = N, P) gave much higher contributions for the ketene form in NCO^- (33%) and PCO^- (40%).[35]

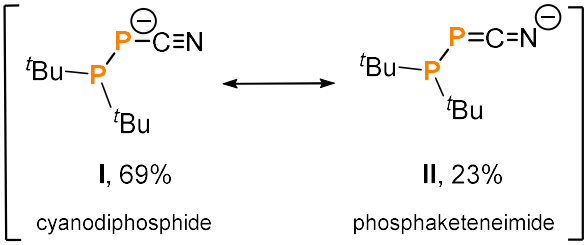

Scheme 7. Result of natural resonance theory analysis of **10-*t*Bu** at the B3LYP/6-31G+* level of theory.

2.3 Conclusion

Within this work, the stereoelectronic properties of two α-diimine ligands (BIAN vs. PhDi) were discussed and compared using DFT calculations. Moreover, three new α-diimine (PhDi) cobaltates **3** – **5** were synthesized and compared to the corresponding BIAN cobaltates **1** and **2**. Interestingly, the differences in their stereoelectronic properties resulted in distinct reactivities in the activation of white phosphorus. In case of ^{Dipp}BIAN a dinuclear dicobalt tetraphosphido complex **6** was formed, whereas the ^{Dipp}PhDi cobaltate led to a *cyclo*-P_4 end deck complex **7**, which was successfully further functionalized with $RPCl_2$ electrophiles. The *cyclo*-P_4 unit of **7** was tested for aromaticity with NICS calculations and indeed shows aromatic character.

2.4 References

[1] M. Döring, E. Uhlig, T. Taldbach, *Z. Anorg. Allg. Chem.* **1991**, *600*, 163–167

[2] W. W. Brennessel, J. E. Ellis, *Inorg. Chem.* **2012**, *51*, 9076–9094.

[3] X. Wang, Y. Zhao, S. Gong, B. Liu, Q.-S. Li, J.-H. Su, B. Wu, X.-J. Yang, *Chem. Eur. J.* **2015**, *21*, 13302–13310.

[4] a) S. Pelties, T. Maier, D. Herrmann, B. de Bruin, C. Rebreyend, S. Gärtner, I. G. Shenderovich, R. Wolf, *Chem. Eur. J.* **2017**, *23*, 6094-6102. b) S. Pelties, *Dissertation: Synthesis, Characterization, and Reactivity Studies on Low-valent 3d Metal Complexes with N-Heterocyclic Carbene and α-Diimine Ligands*, **2016**, Universität Regensburg.

[5] T. M. Maier, S. Sandl, I. G. Shenderovich, A. Jacobi von Wangelin, J. J. Weigand, R. Wolf, *Chem. Eur. J.* **2019**, *25*, 238-245.

[6] J. Reinhold, R. Benedix, P. Birner, H. Henning, *Inorg. Chim. Acta* **1979**, *33*, 209-213.

[7] Concept of redoxactive ligands in catalysis: a) P. J. Chirik, K. Wieghardt, *Science* **2010**, *327*, 794-795. b) W. Kaim, *Inorg. Chem.* **2011**, *50*, 9752-9765. c) P. J. Chirik, *Inorg. Chem.* **2011**, *50*, 9737-9740. d) V. Lyaskovskyy, B. de Bruin *ACS Catal.* **2012**, *2* 270–279. e) O. R. Luca, R. H. Crabtree *Chem. Soc. Rev.* **2013**, *42*, 1440–1459.

[8] Reviews for imine based metal complexes in catalysis: a) P. J. Chirik *Acc. Chem. Res.* **2015**, *48*, 1687–1695. b) T. Zell, R. Langer *ChemCatChem* **2018**, *10*, 1930–1940. c) A. Mukherjee, D. Milstein *ACS Catal.* **2018**, *8*, 11435–11469. d) V. Papa, K. Junge, M. Beller *Chem. Eur. J.* **2019**, *25*, 122–143. e) L. Alig, M. Fritz, S. Schneider *Chem. Rev.* **2019**, *119*, 2681–2751. f) W. Ai, R. Zhong, X. Liu, Q. Liu *Chem. Rev.* **2019**, *119*, 2876–2953.

[9] I. Matei, T. Lixandru, *Bul. Inst. Politeh Iasi* **1967**, *13*, 245. b) M. Dvoilatzky, *Cr. R. Acad. Sci. Prais, Ser. C.* **1969**, *268*, 1811.

[10] a) R. van Asselt, C. J. Elsevier, *Journal of Molecular Catalysis* **1991**, *65*, L13–L19; b) R. van Asselt, E. E. C. G. Gielens, R. E. Rülke, C. J. Elsevier, *J. Chem. Soc., Chem. Commun.* **1993**, 1203–1205; c) R. van Asselt, C. J. Elsevier, W. J. J. Smeets, A. L. Spek, R. Benedix, *Recl. Trav. Chim. Pays-Bas* **1994**, *113*, 88–98; d) R. van Asselt, E. E. C. G. Gielens, R. E. Rulke, K. Vrieze, C. J. Elsevier, *J. Am. Chem. Soc.* **1994**, *116*, 977–985; e) M. W. van Laren, C. J. Elsevier, *Angew. Chem. Int. Ed.* **1999**, *38*, 3715–3717; *Angew. Chem.* **1999**, *111*, 3926-3929.

[11] I. L. Fedushkin, A. A. Skatova, V. A. Chudakova, G. K. Fukin, *Angew. Chem. Int. Ed.* **2003**, *42*, 3294-3298; *Angew. Chem.* **2003**, *115*, 3416-3420.

[12] Selected examples for metal complexes with $[PhDi]^{2-}$ ligands: a) B. Gao, L. Xin, W. Gao, Z.-Q. Hao, X.-Z. Xin, Q-L Wu, Y. Mu, *Polyhedron* **2013**, *63*, 91-95. b) B. Gao, D. Zhao, X. Li, Y. Cui, R. Duan, X. Pang, *RSC Adv.* **2015**, *5*, 440–447. c) G. A. Abakumov, N. O. Druzhkov, T. N. Kocherova, K. A. Kozhanov, A. V. Murugova, E. N. Egorova, *Doklady Chemistry* **2016**, *467*, 109-112. d) N. O. Druzhkov, G. G. Kazakov, A. S. Shavyrin, E. V. Baranov, E. N. Egorova, A. V. Piskunov, G. A. Abakumov, *Inorg. Chem. Commun.* **2018**, *90*, 92–96. e) M. Ma, H. Wang, J. Wang, L. Shen, Y. Zhao, W.-H. Xu, B. Wu, X.-J. Yang, *Dalton Trans.* **2019**, *48*, 2295–2299.

[13] Selected examples for metal complexes with $[PhDi]^{\cdot-}$: B. Gao, X. Luo, W. Gao, L. Huang, S.-M. Gao, X. Liu, Q. Wu, Y. Mu, *Dalton Trans.* **2012**, *41*, 2755–2763. b) Ref.: 12c

[14] a) C. S. Bart, E. J. Hawrelak, E. Lobkovsky, P. J. Chirik, *Organometallics* **2005**, *24*, 5518-5527. b) N.Muresan, C. C. Lu, M. Ghosh, J. C. Peters, M. Abe, L. M. Henling, T. Weyhermöller, E. Bill, K. Wieghardt, *Inorg. Chem.* **2008**, *11*, 4579-4590.

[15] a) C. Lichtenberg, L. Viciu, M. Adelhardt, J. Sutter, K. Meyer, B. de Bruin, H. Grützmacher, *Angew. Chem. Int. Ed.* **2015**, *54*, 5766-5771; *Angew. Chem.* **2015**, *127*, 5858-5863. b) C. Lichtenberg, L. Viciu,

M. Vogt, E. E. Rodriguez,-Lugo, M. Adelhardt, J. Sutter, M. Khusniyarov, K. Meyer, B. de Bruin, E. Bill, H. Grützmacher, *Chem. Commun.* **2015**, *51*, 13890-13893. c) C. Lichtenberg, M. Adelhardt, T. L. Gianetti, K. Meyer, B. de Bruin, H. Grützmacher, *ACS Catal.* **2015**, *5*, 6230-6240.

[16] A. D. Becke, *Phys. Rev. A* **1988**, *38*, 3098–3100.

[17] R. Ditchfield, W. J. Hehre, J. A. Pople, *J. Chem. Phys.* **1971**, *54*, 724.

[18] a) G. A. Abakumov, V. K. Cherkasov, N. O. Druzhkov, Y. A. Kurskii, G. K. Fukin, L. G. Abakumova, T. N. Kocherova, *Synth. Commun.* **2006**, *36*, 3241. b) V. K. Cherkasov, N. O. Druzhkov, T. N. Kocherova, A. S. Shavyrin, G. K. Fukin, *Tetrahedron* **2012**, *68*, 1422.

[19] T. M. Maier, M.Sc. thesis, Regensburg, **2016**

[20] W. W. Brennessel, V. G. Young, J. E. Ellis, *Angew. Chem. Int. Ed.* **2006**, *45*, 7268; *Angew. Chem.* **2006**, *45*, 7268

[21] W. W. Brennessel, V. G. Young, J. E. Ellis, *Angew. Chem. Int. Ed.* **2002**, *114*, 1259-1263; *Angew. Chem.* **2002**, *41*, 1211-1215.

[22] R. Boese, A. Stanger, P. Stellberg, A. Shazar, *Angew. Chem. Int. Ed. Engl.* **1993**, *32*, 1475-1477; *Angew. Chem.* **1993**, *105*, 1500-1502.

[23] E.-M. Schnöckelberg, M. M. Khusniyarov, B. de Bruin, F. Hartl, T. Langer, M. Eul, S. Schulz, R. Pöttgen, R. Wolf, *Inorg. Chem.* **2012**, *51*, 6719-6730.

[24] a) O. J. Scherer, R. Winter, G. Wolmershuser, *Z. Anorg. Allg. Chem.* **1993**, *619*, 827–835. b) O. J. Scherer, J. Vondung, G. Wolmershäuser, *Angew. Chem. Int. Ed.* **1989**, *28*, 1355–1357, *Angew. Chem.* **1989**, *101*, 1395–1397; c) M. Herberhold, G. Frohmader, W. Milius, *J. Organomet. Chem.* **1996**, *522*, 185–196; d) F. Dielmann, A. Timoshkin, M. Piesch, G. Balázs, M. Scheer, *Angew. Chem. Int. Ed.* **2017**, *56*, 1671–1675, *Angew. Chem.* **2017**, *129*, 1693–1698. e) U. Chakraborty, J. Leitl, B. Mühldorf, M. Bodensteiner, S. Pelties, R. Wolf, *Dalton Trans.* **2018**, *47*, 3693–3697. f) A. Cavaillé, N. Saffon-Merceron, N. Nebra, M. Fustier-Boutignon, N. Mézailles, *Angew. Chem. Int. Ed.* **2018**, *57*, 1874–1878 *Angew. Chem.* **2018**, *130*, 1892–1896. g) K. A. Mandla, C. E. Moore, A. L. Rheingold, J. S. Figueroa, *Angew. Chem. Int. Ed.* **2019**, *58*, 1779–1783, *Angew. Chem.* **2018**, *131*, 1793–1797. h) K. A. Mandla, C. E. Moore, A. L. Rheingold, J. S. Figueroa, *Angew. Chem. Int. Ed.* **2019**, *58*, 15329-15333, *Angew. Chem.* **2018**, *131*, 15473-15477.

[25] M. Swart, A. W. Ehlers, K. Lammertsma, *Mol. Phys.* **2004**, *102*, 2467–2474.

[26] F. Weigend, R. Ahlrichs, *Phys. Chem. Chem. Phys.* **2005**, *7*, 3297–3305.

[27] Z. Chen, C. S. Wannere, C. Corminboeuf, R. Puchta, P. v. R. Schleyer, *Chem. Rev.* **2005**, *105*, 3842–3888.

[28] J. O. C. Jiménez-Halla, E. Matito, J. Robles, M. Solà, *J. Organomet. Chem.* **2006**, *691*, 4359–4366.

[29] C. G. P. Ziegler, T. M. Maier, S. Pelties, C. Taube, F. Hennersdorf, A. W. Ehlers, J. J. Weigand, R. Wolf, *Chem. Sci.* **2019**, *10*, 1302-1308.

[30] M. H. Holthausen, S. K. Surmiak, P. Jerabek, G. Frenking, J. J. Weigand, *Angew. Chem. Int. Ed.* **2013**, *52*, 11078–11082, *Angew. Chem.* **2013**, *125*, 11284–11288.

[31] a) W. S. Sheldrick, J. Kroner, F. Zwaschka, A. Schmidpeter, *Angew. Chem. Int. Ed.* **1979**, *18*, 934–935, *Angew. Chem.* **1979**, *91*, 998–1000. b) A. Schmidpeter, K.-H. Zirzow, G. Burget, G. Huttner, I. Jibril, *Chem. Ber.* **1984**, *117*, 1695–1706. c) A. Schmidpeter, G. Burget, F. Zwaschka, W. S. Sheldrick, *Z. Anorg. Allg. Chem.* **1985**, *527*, 17–32.

[32] H. Grützmacher, Z. Li, J. E. Borger, F. Müller, J. R. Harmer, C.-Y. Su, *Angew. Chem. Int. Ed.* **2019**, *58*, 11429-11433; *Angew. Chem.* **2019**, *131*, 11551-11555.

[33] E. D. Glendening, J. K. Badenhoop, A. E. Reed, A. E. Carpenter, J. A. Bohmann, C. M. Morales, C. R. Landis, F. Weinhold, in *NBO 6.0*, Theoretical Chemistry Institute, University of Wisconsin, Madison (WI), **2013**.

[34] a) R. Ditchfield, W. J. Hehre, J. A. Pople, *J. Chem. Phys.***1971**, *54*, 724–728; b) M. J. Frisch, G. W. Trucks, H. B. Schlegel, G. E. Scuseria, M. A. Robb, J. R. Cheeseman, G. Scalmani, V. Barone, B. Mennucci, G. A. Petersson, in *Gaussian 09, Revision A.02*, Gaussian, Inc., Wallingford, CT, **2013**.

[35] S. Alidori, D. Heift, G. Santiso-Quinones, Z. Benkő, H. Grützmacher, M. Caporali, L. Gonsalvi, A. Rossin, M. Peruzzini, *Chem. Eur. J.* **2012**, *18*, 14805-14811.

2.5 Supporting Information

2.5.1 General Procedures

All experiments were performed under an atmosphere of dry Argon (Argon 4.6, Linde) using standard Schlenk techniques or a MBraun UniLab Glovebox.

***Chemicals and Solvents**:* Solvents were dried and degassed with an MBraun SPS800 solvent-purification system. THF, diethyl ether were stored over molecular sieves (3 Å). *n*-hexane was stored over a potassium mirror. 1,2-Dimethoxyethane was stirred over K/benzophenone, distilled and stored over molecular sieves (3 Å). All chemicals were purchased from commercial suppliers and used as received, if not stated otherwise. $[K(dme)_2\{Co(\eta^4\text{-}C_{14}H_{10})_2\}]$ was prepared by *Julia Märsch* and *Marion Till*. Cobaltocene was provided by the inorganic lab course "*Fortgeschrittenenpraktikum Metallorganik"*.

***Computational Details**:* Calculations were carried out with the ORCA[1],[2] (for **6**, NICS) and Gaussian[3] (chapter 2.2.1, **9**, NRT analysis) program package. All geometry optimizations were performed at the B3LYP[4]/6-311G(d)[5] (chapter 2.2.1), OPBE[6]/def2-TZVP[7] (**6**, NICS), B3LYP[4]/6-31G+*[8] level of theory in the gas phase. Frequency calculations were carried out to confirm the nature of stationary points found by geometry optimizations.

Elemental Analyses: CHN analyses were recorded by the analytical department of the University of Regensburg using a Micro Vario Cube (Elementar).

NMR spectroscopy: ^{1}H, ^{13}C{^{1}H}, ^{31}P, and ^{31}P{^{1}H} spectra in solutions were recorded on Bruker Avance 300 (300 MHz) and Bruker Avance 400 (400 MHz) if not stated otherwise. These chemical shifts are given relative to solvents resonances on the tetramethylsilane scale (^{1}H and ^{13}C NMR) and 85% H_3PO_4 in aqueous solution (^{31}P, ^{31}P{^{1}H} NMR). The following abbreviations have been used for multiplicities: s = singlet, d = doublet, t = triplet, q = quartet, sept = septet, m = multiplet, dd = doublet of doublets, dt = doublet of triplets.

Melting point: Melting points were measured on samples in sealed capillaries on a Stuart SMP10 melting point apparatus.

UV-vis spectra: UV-vis spectra were recorded on an Ocean Optics Flame spectrometer (Varian Cary 50 spectrometer) in a Quartz cuvette with a layer thickness of 1 cm at room temperature with a concentration of 10^{-4} to 10^{-6} M.

Single-crystal X-ray crystallography: The single crystal X-ray diffraction (XRD) data were recorded on an Agilent Technologies SuperNova and a GV1000, Titan S2 diffractometer with microfocus Cu K_α radiation (λ = 1.54184 Å), which was used in each measurement. Empirical multi-scan[9] and analytical absorption[10] corrections were applied to the data. The structures were solved with SHELXT[11] and least-square refinements on F^2 were carried out with SHELXL.[12]

2.5.2 Synthesis of Starting Materials

2.5.2.2 Synthesis of Potassium-bis(cyclooctadiene) cobaltate [K(thf)$_{0.2}${Co(η^4-cod)$_2$}]

[K(thf)$_{0.2}${Co(η^4-cod)$_2$}] was synthesized according to *Jonas* and co-workers.[13]

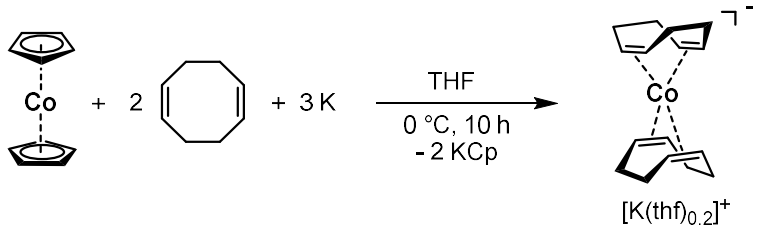

Cobaltocene (9.0 g, 47.8 mmol, 1.0 equiv.) and distilled 1,5-cyclooctadiene (17.7 mL, 144 mmol, 3.0 equiv.) were transferred to potassium metal (7.5 g, 191.8 mmol, 4.0 equiv.) at 0 °C. The reaction mixture was stirred at 0 °C for 10 h with exclution of light. The reaction mixture turned yellow-brown while stirring. The mixture was stored at –80 °C overnight. Subsequently, the suspension was filtered at –80 °C, the filtrate was concentrated and layered with diethyl ether. Dark yellow crystals were isolated after four days at –30°C and dried *in vacuo* (7.5 g, 48.0%). The isolated compound may contain a variable amount of THF. This sample contained 0.2 THF molecules per formula unit based on elemental analysis.

Formula: $CoC_{16}H_{24}\cdot(C_4H_8O)_{0.2}$ (MW = 328.82 g mol^{-1})

Yield: 7.5 g (22.8 mmol, 48%)

^{1}H NMR (300.13 MHz, 300 K, THF-d$_8$) δ[ppm]: 2.20 (s, 16H, cod-CH$_2$), 1.88 (s, 8H, cod-CH)

Elemental analysis calcd. for $C_{16}H_{24}Co\cdot(C_4H_8O)_{0.2}$ (328.82 g mol^{-1}): C: 61.37 H: 7.85; found: C 61.44 H 7.77

2.5.2.2 Synthesis of ^{Dipp}Phenanthrenediimine

^{Dipp}Phenanthrenediimine was synthesized according to *Abakumov* and co-workers (step 1)[14] and *Cherkasov* and co-workers (step 2).[15]

Step 1

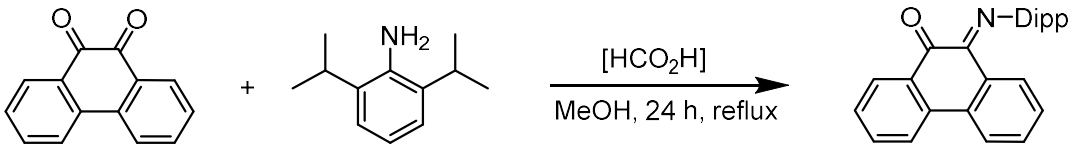

2,6-Diisopropylaniline (4.0 mL, 21.2 mmol, 1.8 equiv.) was added to a solution of 9,10-phenanthrenequinone (2.5 g, 12.0 mmol, 1.0 equiv.) and few drops of formic acid in 80 mL

methanol. The reaction mixture was stirred for 24 h under reflux. The reaction mixture was cooled to 0 °C and the solid collected by filtration and washed with 50 mL cold methanol. The crude product was recrystallized from *n*-heptane. ^{Dipp}Phenanthrene-o-iminoquinone was isolated as green crystals.

Formula: $C_{26}H_{25}NO$ ($M = 367.49\ g{\cdot}mol^{-1}$)

Yield: 2.57 g (7.0 mmol, 58%)

^{1}H NMR (300.13 MHz, 300K, $CDCl_3$): δ [ppm]: 8.40 (d, J = 7.4 Hz, 1H, Phen-H), 8.06 (d, J = 7.7 Hz, 2H, Phen-H), 7.97 (d, J = 7.7 Hz, 1H, Phen-H) 7.67 (m, 2H, Phen-H), 7.51 (t, J = 7.5 Hz, 1H, Phen-H), 7.39 (t, J = 7.5 Hz, 1H, Phen-H), 7.14 (m, 3H, Ar-H), 4.51 (sept, J = 6.8 Hz, 2H, C<u>H</u>$_{Dipp}$), 1.14 (d, J = 6.8 Hz, 12H, C<u>H</u>$_{3\ Dipp}$), 1.03 (d, J = 6.8 Hz, 12H, C<u>H</u>$_{3\ Dipp}$)

Step 2

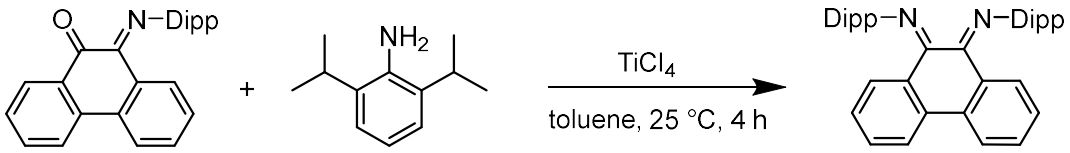

Freshly distilled and dry 2,6-diisopropylaniline (3.5 mL, 18.6 mmol, 2.6 equiv.) was added to a solution of ^{Dipp}Phenanthrene-o-iminoquinone (2.66 g, 7.2 mmol, 1.0 equiv.) in 20 mL dry toluene. Titanium(IV)-chloride (0.85 mL, 7.8 mmol, 1.1 equiv.) was added dropwise. The reaction mixture turned red under formation of titanium(IV)-dioxide and was stirred for 4 h at ambient temperature before 40 mL water was added carefully. The organic phase was separated and the aqueous phase extracted with toluene. Combined organic phases were dried over Na_2SO_4, filtered and concentrated *in vacuo*. The resulting oil was recrystallized from hot acetonitrile. Full crystallization of orange crystals was achieved at 0 °C. ^{Dipp}Phenanthrenediimine was isolated by decanting and drying *in vacuo*.

Formula: $C_{38}H_{42}N_2$ ($M = 526.77\ g{\cdot}mol^{-1}$)

Yield: 1.74 g (3.3 mmol, 46%)

^{1}H NMR (400.13 MHz, 300K, $CDCl_3$): δ [ppm]: 8.37 (d, J = 7.8 Hz, 1H, Phen-H), 7.95 (d, J = 7.7 Hz, 1H, Phen-H), 7.91 (d, J = 7.7 Hz, 1H, Phen-H) 7.65 (t, J = 7.5 Hz, 1H, Phen-H), 7.54 (t, J = 7.5 Hz, 1H, Phen-H), 7.36 (t, J = 7.5 Hz, 1H, Phen-H), 7.10 (m, 3H, Ar-H), 6.91 (m, 4H, Ar-H

and Phen-H), 6.68 (d, J = 7.8 Hz, 1H Phen-H), 2.82 (sept, J = 6.8 Hz, 2H, C<u>H</u>$_{Dipp}$), 1.85 (sept, J = 6.8 Hz, 2H, C<u>H</u>$_{Dipp}$) 1.16 (d, J = 6.8 Hz, 12H, C<u>H</u>$_{3\ Dipp}$), 1.03 (d, J = 6.8 Hz, 12H, C<u>H</u>$_{3\ Dipp}$), 0.75 (d, J = 6.8 Hz, 12H, C<u>H</u>$_{3\ Dipp}$), 0.59 (d, J = 6.8 Hz, 12H, C<u>H</u>$_{3\ Dipp}$)

2.5.2.3 Synthesis of ^{Mes}Phenanthrenediimine

^{Mes}Phenanthrenediimine was synthesized analogous to ^{Dipp}Phenanthrenediimine

Step 1

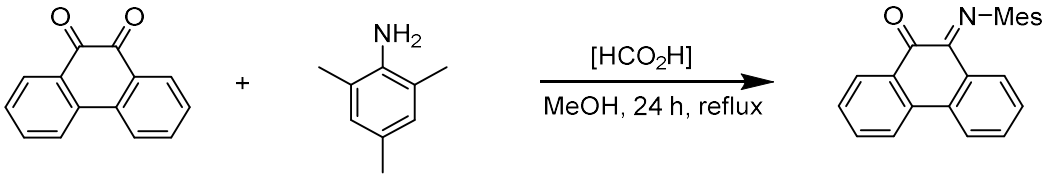

2,4,6-Trimethylaniline (3.0 mL, 21.2 mmol, 1.8 equiv.) was added to a solution of 9,10-phenanthrenequinone (2.5 g, 12.0 mmol, 1.0 equiv.) and few drops of formic acid in 80 mL methanol. The reaction mixture was stirred for 24 h under reflux. The reaction mixture was cooled to –10 °C and the solid collected by filtration and washed with 50 mL cold methanol. The crude product was recrystallized from *n*-heptane. ^{Mes}Phenanthrene-o-iminoquinone was isolated as green-brown powder.

Formula: $C_{23}H_{19}NO$ (M = 325.41 g·mol^{-1})

Yield: 1.38 g (4.2 mmol, 35%)

^{1}H NMR (300.13 MHz, 300K, $CDCl_3$): mixture of two isomers δ [ppm]: 8.45 (d, J = 7.4 Hz, 1H, Phen-H), 8.23 (m, 1H, Phen-H), 8.03 (m, 4H), 7.88 (d, J = 7.4 Hz, 1H, Phen-H), 7.66 (m, 4H), 7.49 (m, 2H), 7.39 (t, J = 7.5 Hz, 1H, Phen-H), 6.97 (d, J = 7.4 Hz, 1H, Phen-H), 6.89 (s, 2H, Ar-H), 2.42 (s, 1.5H, C<u>H</u>$_{3\ para}$), 2.33 (s, 1.5H, C<u>H</u>$_{3\ para}$), 2.30 (s, 3H, C<u>H</u>$_{3\ ortho}$), 1.95 (s, 6H, C<u>H</u>$_{3\ ortho}$)

Step 2

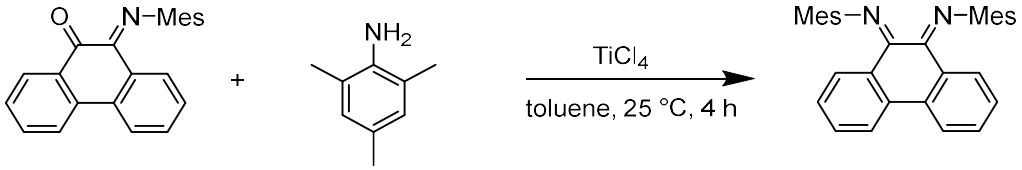

Freshly distilled and dry 2,4,6-trimethylaniline (1.5 mL, 10.4 mmol, 2.5 equiv.) was added to a solution of ^{Mes}Phenanthrene-o-iminoquinone (1.37 g, 4.2 mmol, 1.0 equiv.) in 50 mL dry toluene. Titanium(IV)-chloride (0.85 mL, 7.8 mmol, 1.1 equiv.) was added dropwise. The

reaction mixture turned red under formation of titanium(IV)-dioxide and was stirred for 4 h at ambient temperature before 50 mL water was added carefully. The organic phase was separated and the aqueous phase extracted with toluene. Combined organic phases were dried over Na_2SO_4, filtered and concentrated *in vacuo*. The resulting oil was recrystallized from hot acetonitrile. Full crystallization of orange crystals was achieved at –10 °C. ^{Dipp}Phenanthrenediimine was isolated by decanting and drying *in vacuo*.

Formula: $C_{32}H_{30}N_2$ ($M = 442.61$ g·mol^{-1})

Yield: 0.96 g (2.2 mmol, 52%)

^{1}H NMR (400.13 MHz, 300K, $CDCl_3$) of main isomer: δ [ppm]: 8.31 (d, J = 7.6 Hz, 1H, Phen-H), 7.91 (m, 2H, Phen-H), 7.65 (t, J = 7.5 Hz, 1H, Phen-H), 7.60 (t, J = 7.5 Hz, 1H, Phen-H), 7.50 (t, J = 7.5 Hz, 1H, Phen-H),), 7.39 (t, J = 7.5 Hz, 1H, Phen-H), 6.94 (m, 1H, Phen-H), 6.80 (s, 2H, Ar-H), 6.74 (d, J = 7.8 Hz, Phen-H), 6.64 (s, 2H, Ar-H), 2.26 (s, 3H, C$\underline{H}_{3\ para}$), 2.17 (s, 3H, C$\underline{H}_{3\ para}$), 2.00 (s, 6H, C$\underline{H}_{3\ ortho}$), 1.34 (s, 6H, C$\underline{H}_{3\ ortho}$)

2.5.3 Synthesis of Heteroleptic α-Diimine Cobalt Complexes

2.5.3.1 Synthesis of [K([18]c-6)(thf)$_{1.5}$]{(^{Dipp}PhDi)Co(η^4-cod)}] (3)

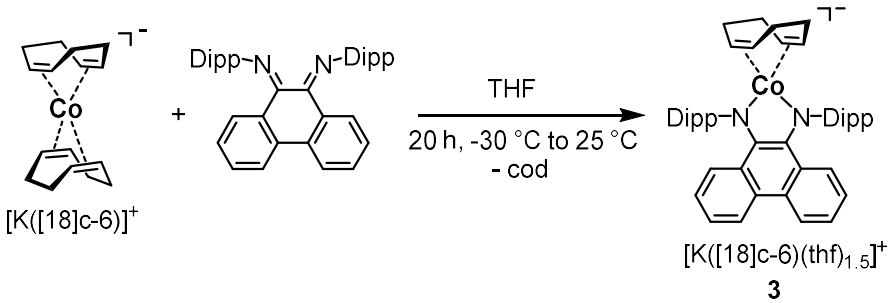

3

$[K(thf)_{0.2}\{Co(\eta^4\text{-cod})_2\}]$ (566 mg, 1.72 mmol, 1.0 equiv.) and 18-crown-6 ([18]c-6) (455 mg, 1.72 mmol, 1.0 equiv.) were dissolved in 20 mL THF. ^{Dipp}Phenanthrenediimine (950 mg, 1.81 mmol, 1.05 equiv.) was dissolved in 20 mL THF and added to the cobaltate at –30 °C. The solution immediately turned deep green, was warmed to ambient temperature and stirred for further 48 h. After filtration, the solution was concentrated to 30 mL THF and layered with 25 mL *n*-hexane. Dark green crystals were obtained by storage at –35 °C within one day. $[K([18]c\text{-}6)(thf)_{1.5})][(^{Dipp}PhDi)Co(\eta^4\text{-cod})\}]$ was isolated by decanting and dried *in vacuo*. Samples for single-crystal X-ray crystallography can be obtained by recrystallization from THF/*n*-hexane. Elemental analysis indicate the presence of 1.5 THF molecules.

Formula: $C_{58}H_{78}CoKN_2O_6 \cdot (C_4H_8O)_{1.5}$ ($M = 1141.5\ g \cdot mol^{-1}$)

Yield: 890 mg (0.78 mmol, 45%)

^{1}H NMR (400.13 MHz, 300K, THF-d_8): δ [ppm]: 8.20 (d, J = 8.1 Hz, 2H, Phen-H), 7.05 (m, 6H, CH_{Ar}), 6.79 (d, J = 9.0 Hz, Phen-H), 6.62 (m, 2H, Phen-H^2), 6.41 (m, 2H, Phen-H), 4.51 (sept, J = 7.0 Hz, 4H, C$\underline{H}_{Dipp}$), 3.34 (br s, 24H, 18c6), 2.80 (m, 4H, cod-CH), 2.30 (m, 4H, cod-CH_2), 1.39 (d, J = 7.1 Hz, 12H, C$\underline{H}_{3\ Dipp}$), 1.00 (m, 4H, cod-CH_2), 0.64 (d, J = 7.1 Hz, 12H, C$\underline{H}_{3\ Dipp}$)

^{13}C{^{1}H} NMR (100.6 MHz, 300K, THF-d_8): δ [ppm]: 157.1 (C_{Ar}), 145.5 (C_{Ar}), 140.0 (C-N), 127.9 (C_{Phen}), 125.8 (C_{Phen}), 124.5 (C_{Phen}), 123.2 (C_{Ar}), 122.7 (C_{Ar}), 122.2 (C_{Phen}), 117.1 (C_{Phen}), 70.8 ([18]c-6), 68.4 (cod-CH), 31.9 (cod-CH_2), 28.2 (CH_{Dipp}), 25.0 ($CH_{3\ Dipp}$);

Elemental analysis calcd. for $C_{58}H_{78}N_2KCoO_6 \cdot (C_4H_8O)_{1.5}$: C 69.54, H 8.21, N 2.53; found: C 68.97, H 8.09, N 2.29

Melting point: T > 180°C: decomposition to a black oil

UV-vis (THF): λ_{max}/nm (ε/L·mol^{-1}·cm^{-1}) = 359 (15000), 442 (18500), 600 (3800)

2.5.3.2 Synthesis of [K([18]c-6)(thf)$_{1.5}$){(^{Mes}PhDi)Co(η^4-cod)}] (4)

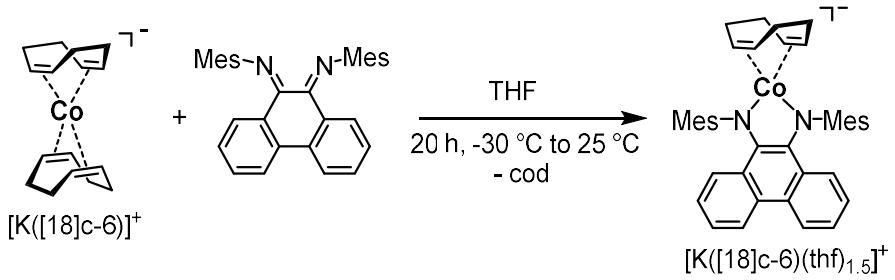

4

^{Mes}Phenanthrenediimine (52 mg, 0.12 mmol, 1.03 equiv.) was dissolved in 2 mL THF and added to a solution of [K(thf)$_{0.2}${Co(η^4-cod)$_2$}] (38 mg, 0.11 mmol, 1.0 equiv.) in 1 mL THF at -30 °C. The color changed to yellow-green and the solution was stirred at ambient temperature for 20 h. [18]c-6 (29 mg, 0.12 mmol, 1.03 equiv.) was added to the reaction mixture. The solvent was evaporated, the residue dissolved in 2 mL THF and filtered. Diffusion of *n*-hexane into the concentrated THF solution afforded dark green crystals, which were suitable for X-ray crystallography. Elemental analysis indicate the presence of 1.5 THF molecules in the bulk material.

Formula: $C_{52}H_{66}CoKN_2O_6 \cdot (C_4H_8O)_{1.5}$ ($M = 1021.30\ g \cdot mol^{-1}$)

Yield: 63 mg (0.062 mmol, 54%)

^{1}H NMR (400.13 MHz, 300K, THF-d_8): δ [ppm]: 8.25 (d, J = 8.1 Hz, Phen-H), 7.25 (d, J = 8.1 Hz 2H, CH_{Ar}), 6.78 (s, 4H, CH_{Ar}) 6.68 (m, 2H, Phen-H), 6.62 (m, 2H, Phen-H^2), 6.54 (m, 2H, Phen-H), 4.51 (sept, J = 7.0 Hz, 4H, C$\underline{H}_{Dipp}$), 3.30 (br s, 24H, 18c6), 2.54 (m, 4H, cod-CH), 2.33 (m, 4H, cod-CH_2), 2.28 (s, 9H, C$\underline{H}_{3\ ortho}$), 2.26 (s, 6H, C$\underline{H}_{3\ para}$), 0.99 (m, 4H, cod-CH_2)

^{13}C{^{1}H} NMR (100.6 MHz, 300K, THF-d_8): δ [ppm]: 156.3 (C_{Ar}), 138.3 (C_{Phen}), 135.0 (C_{Ar}), 129.4 (C_{Ar}), 128.5 (C_{Ar}), 128.0 (C_{Phen}), 124.2 (C_{Phen}), 123.0 (C_{Phen}), 122.9 (C_{Phen}), 122.5 (C_{Phen}), 117.0 (C_{Phen}), 70.4 ([18]c-6), 68.3 (cod-CH), 32.3 (cod-CH_2), 21.3 ($CH_{3\ para}$), 19.9 ($CH_{3\ ortho}$)

Elemental analysis calcd. for $C_{58}H_{78}N_2KCoO_6 \cdot (C_4H_8O)_{1.5}$: C 68.21, H 7.70, N 2.74; found: C 68.15, H 7.27, N 2.79

Melting point: T > 220°C: decomposition to a black oil

UV-vis (THF): λ_{max}/nm (ε/L·mol^{-1}·cm^{-1}) = 366 (12000), 442 (13500), 600 (3000)

2.5.3.3 Synthesis of [K([18]c-6)(dme)$_2$){(^{Dipp}PhDi)Co(η^4-$C_{14}H_{10}$)}] (5)

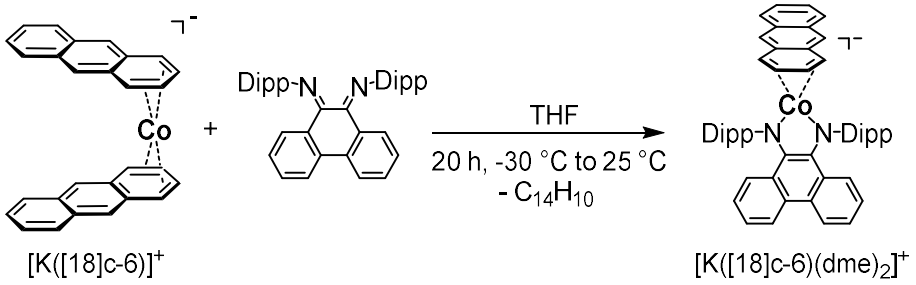

5

18-crown-6 (43 mg, 0.16 mmol, 1.0 equiv) in 1 mL THF was added to a solution of [K(dme)$_2${Co(η^4-$C_{14}H_{10}$)$_2$}] (102 mg, 0.16 mmol, 1.0 equiv.) in 8 mL THF. ^{Dipp}Phenanthrendiimine (85 mg, 0.16 mmol, 1.0 equiv.) was dissolved in 5 mL THF and added to the cobaltate at –30 °C. The reaction mixture turned green, was warmed to ambient temperature and stirred for further 20 h. After evaporation of the solvent, the residue was washed with 15 mL *n*-hexane, dissolved in 4 mL DME, filtered and layered with *n*-hexane. Dark needles were formed by storing the solution at –35 °C. [K([18]c-6)(dme)$_2$)] [(^{Dipp}PhDi)Co(η^4-$C_{14}H_{10}$)}] was isolated by decanting, washing with 20 mL Et_2O and dried *in vacuo*. Elemental analysis indicated the presence of two DME solvent molecules in the bulk material.

Formula: $C_{64}H_{76}CoKN_2O_6 \cdot (C_4H_{10}O_2)_2$ (M = 1247.60 g·mol^{-1})

Yield: 113 mg (0.091 mmol, 56%)

^{1}H NMR (400.13 MHz, 300K, THF-d_8): δ [ppm]: 8.25 (d, J = 7.9 Hz, 2H, CH_{Phen}), 7.18 – 7.09 (m, 8H, CH_{Ar} and CH_{Phen}), 6.91 (m, 2H, $CH_{anthracene}$), 6.75 (m, 2H, $CH_{anthracene}$), 6.71 (m, 2H, CH_{Phen}), 6.53 (m, 2H, CH_{Phen}), 6.15 (s, 2H, $CH_{anthracene}$), 5.81 (m, 2H, $CH_{anthracene\ coordinated}$), 4.10 (sept, J = 6.9 Hz, 4H, $C\underline{H}_{Dipp}$), 3.24 (br s, 24H, [18]c-6), 1.89 (m, 2H, $CH_{anthracene\ coordinated}$), 1.32 (d, J = 6.9 Hz, 4H, $C\underline{H}_3$ $_{Dipp}$), 0.67 (d, J = 6.9 Hz, 4H, $C\underline{H}_3$ $_{Dipp}$)

^{13}C{^{1}H} NMR (100.6 MHz, 300K, THF-d_8): δ [ppm]: 157.8 (C_{Ar}), 144.3 (C_{Ar}), 142.9 ($C_{anthracene}$), 139.9, 132.7, 127.3 (C_{Phen}), 124.8 ($CH_{Anthracen}$), 124.3 (CH_{Phen}), 123.6 (C_{Phen}) , 122.2 (CH_{Ar}), 121.9(CH_{Phen}), 121.8 ($CH_{anthracene}$), 121.7 (CH_{Phen}), 121.6 (CH_{Ar}), 117.2 (CH_{Phen}), 113.6 ($CH_{anthracene}$), 76.6 ($CH_{anthracene\ coordinated}$), 70.0 ([18]c-6), 56.0 ($CH_{anthracene\ coordinated}$), 27.7 ($\underline{C}HDipp$), 24.1 ($\underline{C}H_3$ $_{Dipp}$)

Elemental analysis calcd. for $C_{64}H_{76}CoKN_2O_6 \cdot (C_4H_{10}O_2)_2$: C 69.32, H 7.76, N 2.25; found: C 69.47, H 7.40, N 2.23

Melting point: T > 250°C: decomposition to a black oil

UV-vis (THF): λ_{max}/nm (ε/L·mol^{-1}·cm^{-1}) = 354 (26000), 606 (13000)

2.5.4 Single-Crystal X-ray Crystallography

Table S1. Crystallographic data of **3, 7, 8,** and **10-^{t}Bu**

Compound	**3**	**7**	**8**
Empirical formula	$C_{64}H_{89}CoKN_2O_9$	$C_{50}H_{66}CoKN_2O_6P_4$	$C_{56}H_{68.5}CoKN_2O_{11.25}P_4W$
Formula weight	1128.40	1012.95	1355.38
Temperature [K]	122.9(2)	122.9(2)	122.9(2)
Crystal system	Triclinic	monoclinic	monoclinic
Space group	*P*-1	$P2_1/m$	$C2/c$
a [Å]	10.4494(5)	11.4558(5)	85.6114(9)
b [Å]	12.4133(6)	19.7132(8)	13.0589(2)
c [Å]	25.9192(11)	12.1033(5)	22.4458(3)
α [°]	79.565(4)	90	90
β [°]	87.147(4)	107.690(5)	90.025(1)
γ [°]	67.164(4)	90	90
Volume [Å^3]	3046.5(3)	2604.0(2)	25094.2(6)
Z	2	2	16
ρ_{calc} [g/cm^3]	1.230	1.292	1.435
μ [mm^{-1}]	3.262	4.841	7.426
F(000)	1210.0	1086.0	11016.0
Crystal size [mm^3]	0.3191 × 0.1709 × 0.0708	0.149 × 0.107 × 0.065	0.826 × 0.410 × 0.092
2*Θ* range for data collection [°]	6.938 to 148.5	7.666 – 147.46	6.848 – 149.356
Index ranges	-13 ≤ h ≤ 11, -14 ≤ k ≤ 15, -32 ≤ l ≤ 27	−14 ≤ h ≤ 13, −23 ≤ k ≤ 20 −13 ≤ l ≤ 14	−105 ≤ h ≤ 105, −16 ≤ k ≤ 16, −25 ≤ l ≤ 27
Reflections collected	21864	13745	179882
Independent reflections	11598 [R_{int} = 0.0403, R_{sigma} = 0.0463]	5180 [R_{int} = 0.0364, R_{sigma} = 0.0397]	25277 [R_{int} = 0.0902, R_{sigma} = 0.0395]
Data / restraints / parameters	11598/602/721	5180/132/300	25277/2339/1897
Goodness-of-fit on F^2	1.034	1.086	1.059

Final R indexes [I>=2σ (I)]	R_1 = 0.0818, wR_2 = 0.2343	R_1 = 0.0654, wR_2 = 0.1785	R_1 = 0.0907, wR_2 =
Final R indexes [all data]	R_1 = 0.0976, wR_2 = 0.2527	R_1 = 0.0788, wR_2 = 0.1936	R_1 = 0.0996, wR_2 =
Largest diff. peak/hole [e Å^{-3}]	1.60/-0.59	0.86/−0.56	1.71/−1.47
CCDC-	1944793	1940064	1940071

Compound	**10-^{t}Bu**
Empirical formula	$C_{21}H_{42}KNO_6P_2$
Formula weight	505.59
Temperature [K]	123.0(1)
Crystal system	monoclinic
Space group	$P2_1/n$
a [Å]	16.6663(4)
b [Å]	8.1532(2)
c [Å]	21.7285(5)
α [°]	90
β [°]	112.545(3)
γ [°]	90
Volume [Å^3]	2726.9(1)
Z	4
ρ_{calc} [g/cm^3]	1.232
μ [mm^{-1}]	3.091
F(000)	1088.0
Crystal size [mm^3]	0.402 × 0.319 × 0.228
2Θ range for data collection [°]	8.474 – 147.294
Index ranges	−20 ≤ h ≤ 19, −9 ≤ k ≤ 9 −22 ≤ l ≤ 26
Reflections collected	9240
Independent reflections	5256 [R_{int} = 0.0128, R_{sigma} = 0.0159]
Data / restraints / parameters	5256/0/286
Goodness-of-fit on F^2	1.016
Final R indexes [I>=2σ (I)]	R_1 = 0.0237, wR_2 = 0.0616
Final R indexes [all data]	R_1 = 0.0245, wR_2 = 0.0621
Largest diff. peak/hole [e Å^{-3}]	0.24/−0.19
CCDC-	1940068

2.5.5 NMR Spectra

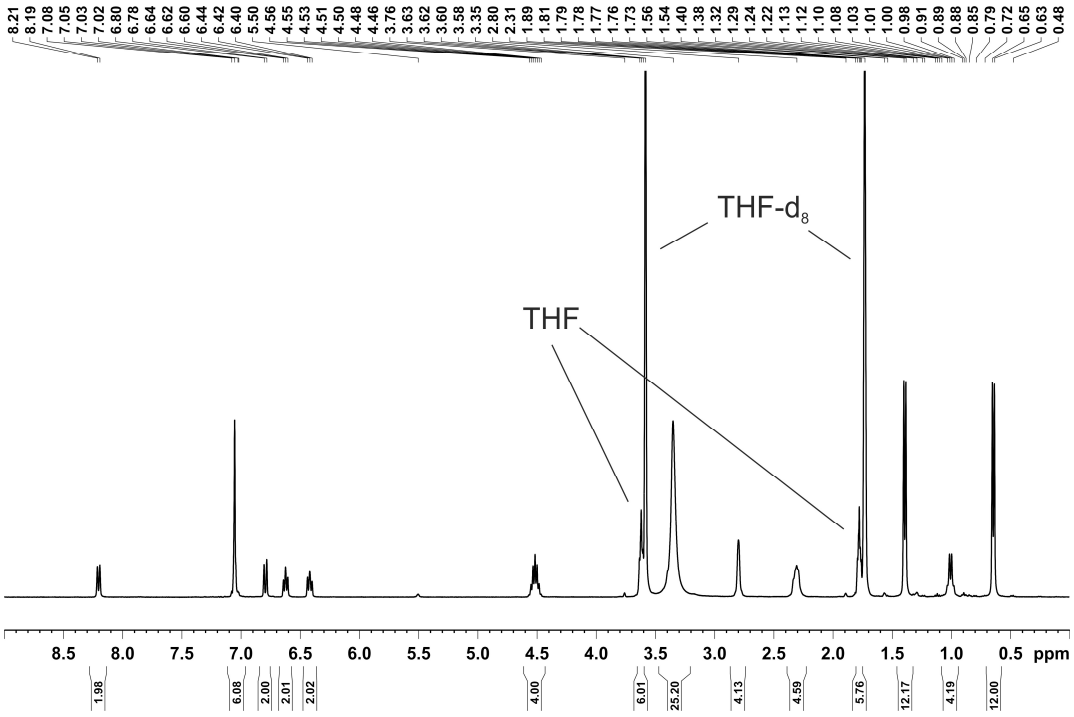

Figure S1. ^{1}H NMR spectrum (400.13 MHz, 300 K, THF-d$_8$) of [K([18]c-6)(thf)$_{1.5}$][(^{Dipp}PhDi)Co(η^4-cod)] (**3**).

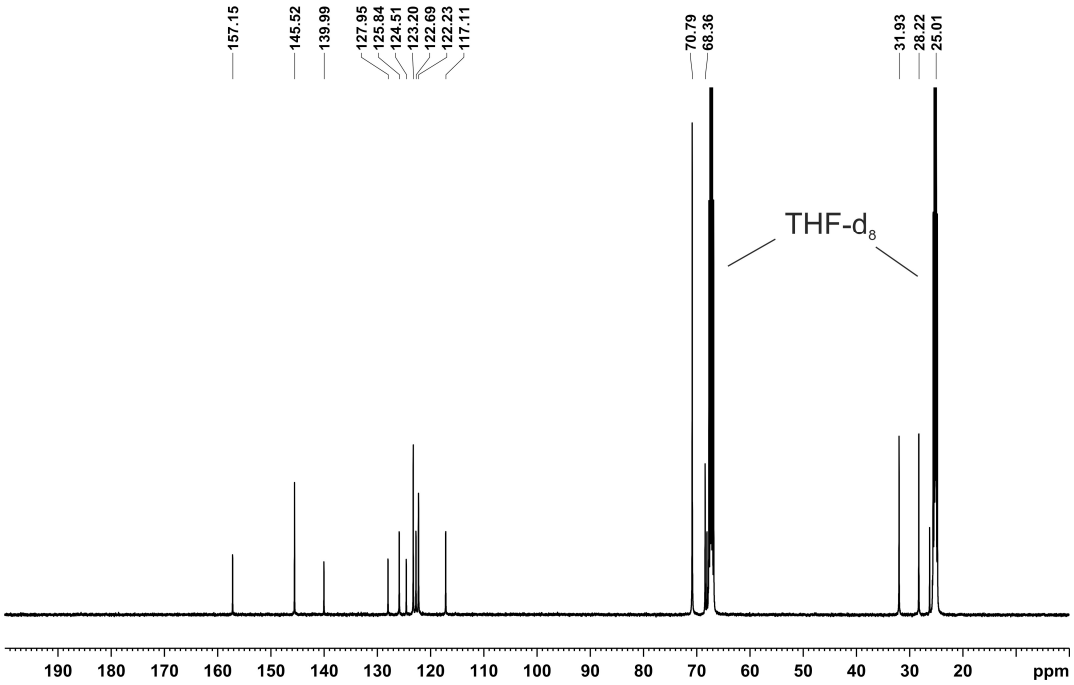

Figure S2. ^{13}C{^{1}H} NMR spectrum (100.6 MHz, 300 K, THF-d$_8$) of [K([18]c-6)(thf)$_{1.5}$][(^{Dipp}PhDi)Co(η^4cod)] (**3**).

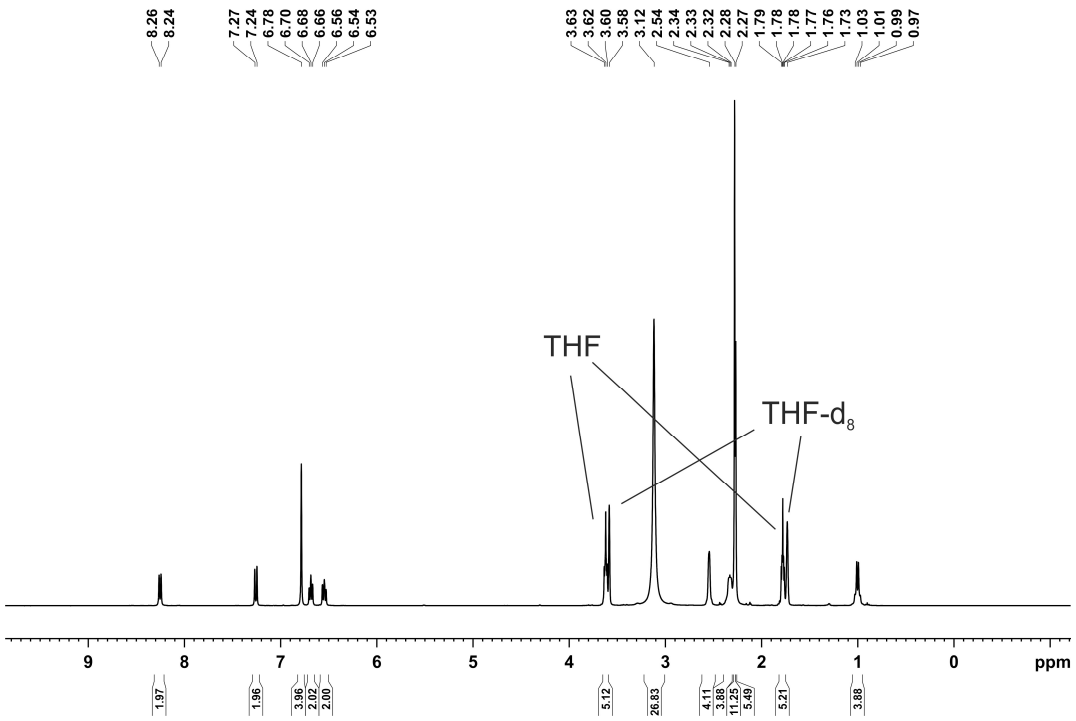

Figure S3. ^{1}H NMR spectrum (400.13 MHz, 300 K, THF-d$_8$) of [K([18]c-6)(thf)$_{1.5}$][(^{Mes}PhDi)Co(η^{4}cod)] (**4**).

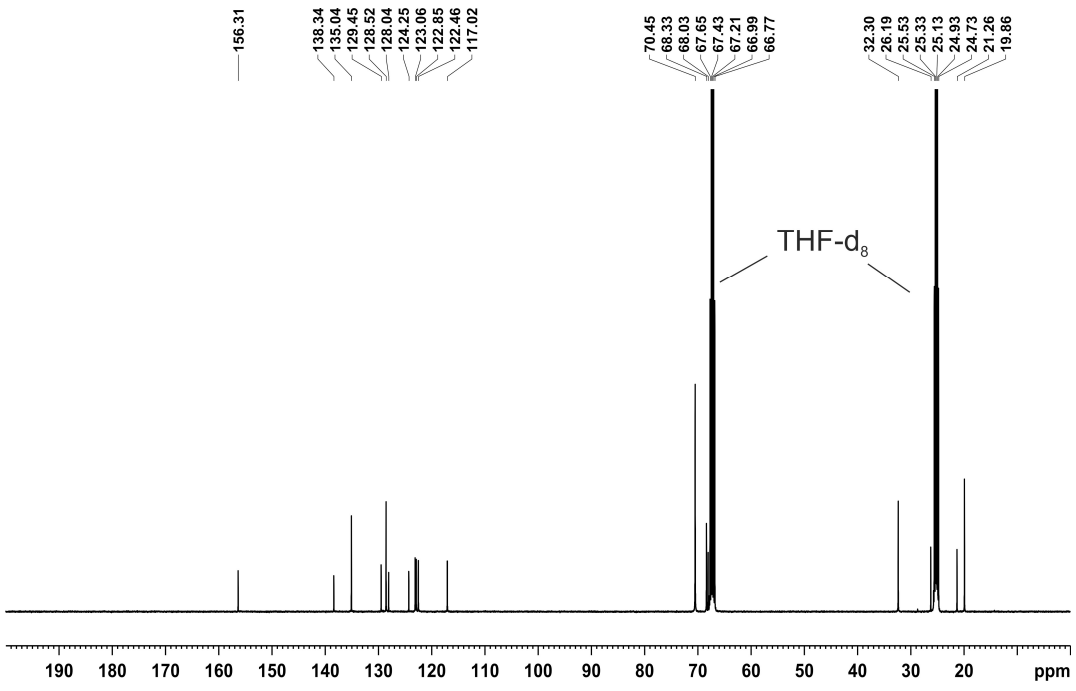

Figure S4. ^{13}C{^{1}H} NMR spectrum (100.6 MHz, 300 K, THF-d$_8$) of [K([18]c-6)(thf)$_{1.5}$][(^{Mes}PhDi)Co(η^4-cod)] (**4**).

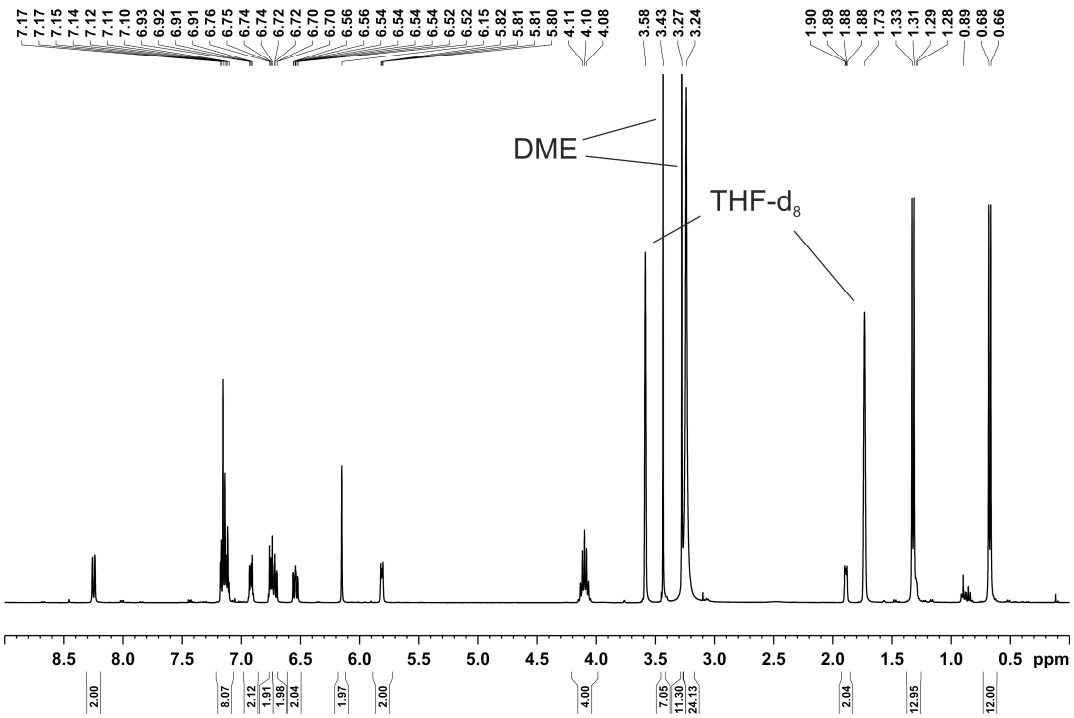

Figure S5. ^{1}H NMR spectrum (400.13 MHz, 300 K, THF-d_8) of [K([18]c-6)(dme)$_2$][(^{Dipp}PhDi)Co(η^4-$C_{14}H_{10}$)] (**5**).

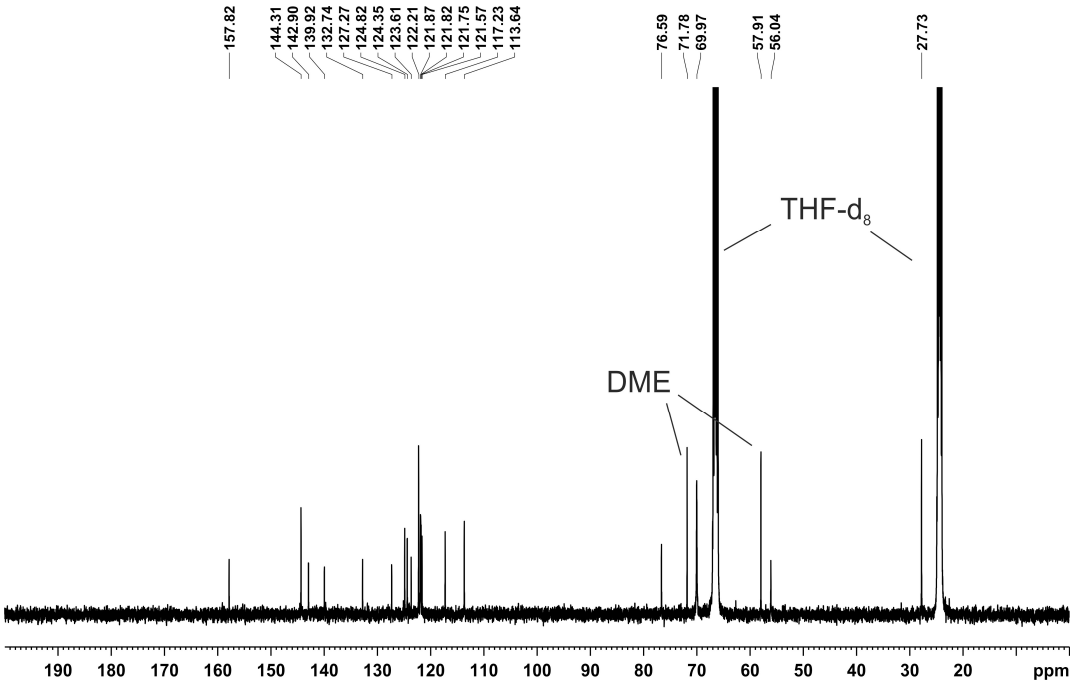

Figure S6. $^{13}C\{^{1}H\}$ NMR spectrum (100.6 MHz, 300 K, THF-d_8) of [K([18]c-6)(dme)$_2$][(^{Dipp}PhDi)Co(η^4-$C_{14}H_{10}$)] (**5**).

2.5.6 DFT Calculations

For experimental details see the General Procedures (Chapter 2.5.1),

2.5.6.1 Optimized coordinates for ^{Ph}BIAN and ^{Ph}PhDi

[^{Ph}BIAN]

N	-1.420500	-1.510600	-0.000000	C	-3.531900	-1.618200	-1.209000
N	1.420500	-1.510700	-0.000000	C	-3.531900	-1.618500	1.209000
C	0.766100	-0.422700	-0.000100	C	-4.920000	-1.722900	-1.202900
C	-0.766100	-0.422700	-0.000000	H	-2.982000	-1.593600	-2.143700
C	-1.184600	1.003100	-0.000000	C	-4.919900	-1.723200	1.202900
C	0.000000	1.779900	-0.000100	H	-2.981900	-1.594100	2.143700
C	1.184600	1.003100	-0.000100	C	-5.622900	-1.770700	-0.000000
C	2.405000	1.648100	-0.000000	H	-5.453900	-1.770800	-2.147000
H	3.336700	1.098000	-0.000100	H	-5.453900	-1.771300	2.146900
C	2.426700	3.065500	0.000000	H	-6.704300	-1.857000	-0.000000
H	3.388400	3.568400	0.000000	C	2.826900	-1.548900	-0.000000
C	1.271100	3.821800	0.000000	C	3.531900	-1.618300	1.209000
H	1.332000	4.906000	0.000100	C	3.531900	-1.618400	-1.209000
C	0.000000	3.189700	0.000000	C	4.919900	-1.723100	1.202900
C	-1.271100	3.821800	0.000100	H	2.981900	-1.593800	2.143700
H	-1.331900	4.906000	0.000100	C	4.919900	-1.723100	-1.202900
C	-2.426700	3.065500	0.000100	H	2.982000	-1.593900	-2.143700
H	-3.388300	3.568400	0.000200	C	5.622900	-1.770700	0.000000
C	-2.405000	1.648100	0.000100	H	5.453900	-1.771000	2.147000
H	-3.336700	1.098100	0.000100	H	5.453900	-1.771100	-2.146900
C	-2.826900	-1.548900	-0.000000	H	6.704300	-1.857000	0.000000

[^{Ph}BIAN]$^{-}$

N	-1.414100	-1.414800	0.242900	C	-3.508200	-0.961400	-0.975900
N	1.414200	-1.414800	-0.243000	C	-3.479500	-2.401500	0.961100
C	0.726900	-0.300700	-0.084300	C	-4.865900	-1.212400	-1.130900
C	-0.726800	-0.300800	0.084100	H	-2.986500	-0.331700	-1.689000
C	-1.160900	1.118300	0.160800	C	-4.838800	-2.632600	0.806100
C	-0.000100	1.921600	-0.000300	H	-2.918700	-2.876500	1.759900
C	1.160900	1.118400	-0.161300	C	-5.553400	-2.039500	-0.239200
C	2.358700	1.770000	-0.397300	H	-5.397000	-0.758000	-1.964900
H	3.281000	1.222200	-0.544500	H	-5.350000	-3.291100	1.505300
C	2.382400	3.191300	-0.428700	H	-6.615300	-2.230600	-0.365400
H	3.334400	3.685300	-0.608100	C	2.768000	-1.539400	-0.088600
C	1.254800	3.959500	-0.225400	C	3.508200	-0.961200	0.975800
H	1.318000	5.044900	-0.238400	C	3.479700	-2.401200	-0.961300
C	-0.000100	3.322100	-0.000100	C	4.865800	-1.212500	1.131100
C	-1.255100	3.959300	0.225600	H	2.986400	-0.331400	1.688600
H	-1.318300	5.044700	0.238700	C	4.839000	-2.632500	-0.805900
C	-2.382600	3.191000	0.429000	H	2.919100	-2.876100	-1.760300
H	-3.334500	3.685000	0.608800	C	5.553300	-2.039600	0.239600
C	-2.358700	1.769800	0.397500	H	5.396800	-0.758100	1.965300
H	-3.280800	1.221800	0.544800	H	5.350300	-3.290900	-1.505100

C	-2.767800	-1.539600	0.088400	H	6.615100	-2.231100	0.366000

[^{Ph}BIAN]$^{2-}$ c.s.s.

N	-1.409200	-1.352600	0.523400	C	-3.419200	-0.850000	-0.855000
N	1.409500	-1.352400	-0.524200	C	-3.433800	-2.581600	0.836200
C	0.685700	-0.243600	-0.182500	C	-4.739700	-1.153300	-1.149100
C	-0.685600	-0.243700	0.182000	H	-2.902600	-0.088100	-1.429800
C	-1.113800	1.167400	0.324600	C	-4.751400	-2.864700	0.529600
C	0.000000	1.991900	0.000000	H	-2.903400	-3.144500	1.600700
C	1.113800	1.167400	-0.324800	C	-5.445600	-2.153800	-0.465600
C	2.269000	1.813900	-0.737100	H	-5.238300	-0.597000	-1.945800
H	3.158400	1.255300	-1.007000	H	-5.260200	-3.662700	1.074400
C	2.296800	3.239900	-0.768000	H	-6.482400	-2.380600	-0.705900
H	3.220600	3.727700	-1.078900	C	2.685200	-1.540100	-0.178600
C	1.218300	4.020400	-0.405000	C	3.419100	-0.849800	0.854700
H	1.288500	5.107300	-0.423400	C	3.433900	-2.581900	-0.836000
C	0.000000	3.383400	0.000100	C	4.739600	-1.153200	1.149100
C	-1.218200	4.020300	0.405300	H	2.902500	-0.087700	1.429300
H	-1.288500	5.107200	0.423800	C	4.751300	-2.865100	-0.529000
C	-2.296700	3.239800	0.768100	H	2.903400	-3.144900	-1.600400
H	-3.220600	3.727600	1.079100	C	5.445400	-2.153900	0.466100
C	-2.269000	1.813800	0.737000	H	5.238000	-0.596700	1.945800
H	-3.158400	1.255200	1.006800	H	5.260200	-3.663300	-1.073500
C	-2.685200	-1.540200	0.178400	H	6.482100	-2.380800	0.706600

[^{Ph}BIAN]$^{2-}$ o.s.s.

N	-1.495500	-1.193800	-0.891500	H	5.358100	-3.548000	-0.974500
N	1.495500	-1.193800	-0.891500	H	6.124600	-2.691800	1.258800
C	0.710100	-0.138300	-0.527200	C	-2.385000	1.900900	-0.239300
C	-0.710100	-0.138200	-0.527300	H	-3.313600	1.353300	-0.354400
C	-1.160400	1.252300	-0.279700	C	-2.651100	-1.507800	-0.303700
C	-0.000000	2.064300	-0.137700	C	-3.531500	-2.441600	-0.960800
C	1.160400	1.252300	-0.279600	C	-3.118300	-1.067300	0.989400
C	2.385000	1.900900	-0.239300	C	-4.736500	-2.843900	-0.417200
H	3.313600	1.353400	-0.354400	H	-3.196500	-2.820700	-1.923500
C	2.420700	3.312200	-0.031700	C	-4.329600	-1.487600	1.517400
H	3.394800	3.799600	0.009400	H	-2.480500	-0.406700	1.567800
C	1.283000	4.078700	0.112900	C	-5.175500	-2.372000	0.833100
H	1.354400	5.155100	0.264000	H	-5.358100	-3.548000	-0.974400
C	-0.000000	3.443600	0.047800	H	-4.624400	-1.121400	2.503200
C	-1.283100	4.078700	0.112900	H	-6.124500	-2.691800	1.258800
H	-1.354400	5.155100	0.263900	C	2.651100	-1.507800	-0.303700
C	-2.420700	3.312200	-0.031700	C	3.118300	-1.067300	0.989400
H	-3.394800	3.799500	0.009400	C	3.531500	-2.441600	-0.960800
H	3.196500	-2.820700	-1.923500	C	4.329600	-1.487600	1.517400
C	5.175500	-2.372000	0.833100	H	2.480500	-0.406700	1.567800
H	4.624500	-1.121400	2.503200	C	4.736600	-2.843900	-0.417200

[^{Ph}BIAN]$^{2-}$ triplet

N	-1.435000	-1.252000	-0.605700	C	-3.437400	-2.522800	-0.891800
N	1.435200	-1.251800	-0.606400	C	-3.335100	-0.981100	0.968700
C	0.746300	-0.126700	-0.382400	C	-4.701300	-2.920800	-0.491400
C	-0.746300	-0.126700	-0.382100	H	-2.958800	-2.968000	-1.760000
C	-1.178600	1.249600	-0.206300	C	-4.595900	-1.402200	1.364100
C	0.000000	2.047600	-0.118600	H	-2.804100	-0.239200	1.554300
C	1.178600	1.249600	-0.206500	C	-5.312900	-2.367900	0.644500
C	2.424500	1.922500	-0.213400	H	-5.225500	-3.683000	-1.069600
H	3.356200	1.375500	-0.305400	H	-5.036800	-0.965500	2.261100
C	2.444600	3.315900	-0.098900	H	-6.304700	-2.684000	0.960800
H	3.410300	3.824000	-0.094500	C	2.689600	-1.520300	-0.193600
C	1.277400	4.089400	0.005200	C	3.334900	-0.981000	0.968500
H	1.344300	5.174900	0.081100	C	3.437500	-2.522700	-0.891900
C	0.000100	3.457600	-0.022100	C	4.595400	-1.402400	1.364400
C	-1.277100	4.089500	0.005400	H	2.803800	-0.238800	1.553700
H	-1.343900	5.175000	0.081300	C	4.701200	-2.921000	-0.491000
C	-2.444300	3.316100	-0.098500	H	2.959300	-2.967900	-1.760400
H	-3.410000	3.824200	-0.094200	C	5.312400	-2.368300	0.645100
C	-2.424400	1.922700	-0.213000	H	5.036100	-0.965700	2.261600
H	-3.356100	1.375700	-0.304900	H	5.225500	-3.683400	-1.069000
C	-2.689600	-1.520400	-0.193200	H	6.303900	-2.684700	0.962000

[^{Ph}PhDi]

N	-1.357500	-1.386200	-0.366200	H	2.974100	-0.033500	-1.620600
N	1.357400	-1.386300	0.365900	C	2.749100	-1.538700	0.460100
C	-0.753600	-0.342500	0.044900	C	3.348800	-2.628100	-0.188700
C	0.753600	-0.342600	-0.045200	H	-6.560700	-2.214500	-0.853000
C	-1.309400	0.906500	0.634800	C	3.535900	-0.716100	1.280000
C	1.309400	0.906500	-0.634900	C	4.715400	-2.853700	-0.062100
C	-2.449500	0.896900	1.446700	H	2.726500	-3.283300	-0.788700
C	-0.605300	2.114700	0.426700	C	4.897300	-0.966300	1.420800
C	2.449600	0.896900	-1.446800	H	3.069700	0.105800	1.812500
C	0.605400	2.114700	-0.426700	C	5.497900	-2.026000	0.742900
H	-2.974000	-0.033600	1.620500	H	5.168400	-3.691500	-0.583000
C	-2.902700	2.064600	2.047500	H	5.492700	-0.325300	2.063800
C	-1.080300	3.281200	1.040600	H	6.560500	-2.214700	0.853200
C	2.902900	2.064700	-2.047400	C	-2.749200	-1.538500	-0.460200
C	1.080500	3.281300	-1.040400	C	-3.348900	-2.627800	0.188900
H	-3.781100	2.039100	2.683500	C	-3.536000	-0.716200	-1.280200
C	-2.217000	3.260000	1.839700	C	-4.715500	-2.853400	0.062400
H	-0.541000	4.213300	0.917800	H	-2.726700	-3.282900	0.789000
H	3.781200	2.039300	-2.683400	C	-4.897400	-0.966300	-1.421000
C	2.217300	3.260100	-1.839500	H	-3.069800	0.105700	-1.813000
H	0.541300	4.213400	-0.917500	C	-5.498000	-2.025700	-0.742700
H	-2.559200	4.175000	2.312400	H	-5.168600	-3.691000	0.583500
H	2.559500	4.175100	-2.312100	H	-5.492900	-0.325400	-2.064000

[^{Ph}PhDi]$^{-}$

N	-1.355000	-1.391500	0.007500	H	3.066900	0.124300	-1.414100
N	1.355100	-1.391500	-0.007600	C	2.682100	-1.608300	0.238100
C	-0.729600	-0.235100	0.092200	C	3.330400	-2.697300	-0.396500
C	0.729600	-0.235100	-0.092300	C	3.437600	-0.891300	1.202600
C	-1.328400	1.038800	0.523800	C	4.649700	-3.022800	-0.111200
C	1.328400	1.038800	-0.523800	H	2.755300	-3.273700	-1.114200
C	-2.553700	1.057800	1.230700	C	4.750500	-1.238000	1.491600
C	-0.643600	2.275000	0.343500	H	2.962800	-0.068900	1.727500
C	2.553600	1.057900	-1.230800	C	5.379700	-2.298500	0.834800
C	0.643600	2.275100	-0.343500	H	5.113700	-3.860500	-0.627600
H	-3.066900	0.124200	1.414000	H	5.294400	-0.669200	2.243000
C	-3.099000	2.230500	1.716500	H	6.408100	-2.562200	1.064500
C	-1.219900	3.454800	0.851900	C	-2.682100	-1.608300	-0.238100
C	3.099000	2.230700	-1.716500	C	-3.330400	-2.697400	0.396400
C	1.219900	3.454800	-0.851800	C	-3.437600	-0.891300	-1.202500
H	-4.036800	2.201200	2.264700	C	-4.649600	-3.022800	0.111200
C	-2.431300	3.447600	1.521000	H	-2.755200	-3.273900	1.114100
H	-0.687400	4.394200	0.748700	C	-4.750600	-1.237900	-1.491400
H	4.036800	2.201400	-2.264700	H	-2.962900	-0.068800	-1.727300
C	2.431300	3.447700	-1.521000	C	-5.379700	-2.298500	-0.834700
H	0.687300	4.394200	-0.748600	H	-5.113600	-3.860600	0.627600
H	-2.845500	4.374000	1.909600	H	-5.294500	-0.669100	-2.242800
H	2.845400	4.374100	-1.909500	H	-6.408100	-2.562200	-1.064400

[^{Ph}PhDi]$^{2-}$ c.s.s.

N	-1.272700	-1.192000	0.594300	H	3.025600	0.334600	-1.426600
N	1.272700	-1.191900	-0.594400	C	2.373700	-1.660700	-0.014600
C	-0.661900	-0.008600	0.253300	C	3.020700	-2.825500	-0.565800
C	0.661900	-0.008600	-0.253400	C	3.015400	-1.130200	1.163900
C	-1.290400	1.264500	0.563500	C	4.166300	-3.371100	-0.017500
C	1.290400	1.264600	-0.563500	H	2.555300	-3.269300	-1.442900
C	-2.559100	1.286000	1.208600	C	4.162600	-1.697200	1.696300
C	-0.652900	2.523100	0.312300	H	2.565000	-0.269100	1.648900
C	2.559200	1.286100	-1.208600	C	4.773900	-2.821800	1.124700
C	0.652900	2.523200	-0.312300	H	4.604300	-4.254900	-0.486400
H	-3.025600	0.334500	1.426600	H	4.597600	-1.250200	2.592800
C	-3.182300	2.461500	1.563500	H	5.673600	-3.258100	1.554000
C	-1.321600	3.710900	0.688600	C	-2.373600	-1.660700	0.014600
C	3.182300	2.461600	-1.563500	C	-3.020600	-2.825500	0.565800
C	1.321500	3.710900	-0.688600	C	-3.015400	-1.130200	-1.163800
H	-4.153500	2.431900	2.054800	C	-4.166300	-3.371200	0.017400
C	-2.561300	3.698000	1.297500	H	-2.555100	-3.269400	1.442800
H	-0.843600	4.670100	0.513000	C	-4.162700	-1.697100	-1.696300
H	4.153500	2.432100	-2.054700	H	-2.565100	-0.269000	-1.648800
C	2.561300	3.698100	-1.297500	C	-4.773900	-2.821800	-1.124700
H	0.843500	4.670200	-0.513000	H	-4.604200	-4.254900	0.486300
H	-3.044700	4.633000	1.575900	H	-4.597700	-1.250100	-2.592700
H	3.044700	4.633100	-1.575800	H	-5.673600	-3.258100	-1.554000

[^{Ph}PhDi]$^{2-}$ o.s.s.

N	1.272800	-1.191500	-0.594600	H	-3.025700	0.334700	1.426200
N	-1.272600	-1.191600	0.594300	C	-2.373600	-1.660600	0.014800
C	0.662000	-0.008300	-0.253500	C	-3.020100	-2.825800	0.565900
C	-0.661900	-0.008400	0.253300	C	-3.015600	-1.130200	-1.163600
C	1.290500	1.264900	-0.563400	C	-4.165600	-3.371800	0.017500
C	-1.290400	1.264700	0.563300	H	-2.554400	-3.269700	1.442800
C	2.559300	1.286500	-1.208400	C	-4.162700	-1.697500	-1.696000
C	0.652900	2.523500	-0.312100	H	-2.565500	-0.268900	-1.648400
C	-2.559300	1.286200	1.208300	C	-4.773500	-2.822400	-1.124500
C	-0.652900	2.523400	0.312200	H	-4.603200	-4.255700	0.486300
H	3.025700	0.335100	-1.426500	H	-4.598000	-1.250500	-2.592400
C	3.182500	2.462000	-1.562900	H	-5.673000	-3.259000	-1.553800
C	1.321800	3.711300	-0.687900	C	2.373700	-1.660600	-0.014900
C	-3.182600	2.461600	1.563000	C	3.020300	-2.825600	-0.566100
C	-1.321900	3.711100	0.688200	C	3.015400	-1.130400	1.163700
H	4.153800	2.432500	-2.054100	C	4.165700	-3.371700	-0.017600
C	2.561600	3.698600	-1.296700	H	2.554800	-3.269300	-1.443200
H	0.843900	4.670500	-0.512000	C	4.162400	-1.697800	1.696200
H	-4.153800	2.432000	2.054100	H	2.565200	-0.269200	1.648700
C	-2.561700	3.698200	1.296900	C	4.773300	-2.822600	1.124600
H	-0.844000	4.670400	0.512400	H	4.603400	-4.255600	-0.486600
H	3.045100	4.633600	-1.574700	H	4.597500	-1.251000	2.592800
H	-3.045200	4.633200	1.575000	H	5.672800	-3.259300	1.554000

[^{Ph}PhDi]$^{2-}$ triplet

N	-1.319500	-1.304700	0.206300	H	3.105800	0.244800	-1.339300
N	1.319500	-1.304700	-0.206300	C	2.582000	-1.636500	0.121700
C	-0.714400	-0.116200	0.142300	C	3.175700	-2.789500	-0.475700
C	0.714400	-0.116200	-0.142200	C	3.363300	-0.995700	1.135700
C	-1.355800	1.161900	0.515700	C	4.434400	-3.243800	-0.110600
C	1.355800	1.161900	-0.515600	H	2.592600	-3.307400	-1.232200
C	-2.603400	1.183100	1.143800	C	4.613800	-1.472700	1.498000
C	-0.646100	2.399400	0.300400	H	2.948100	-0.122700	1.627100
C	2.603400	1.183100	-1.143800	C	5.180100	-2.596400	0.882300
C	0.646100	2.399400	-0.300400	H	4.843000	-4.125600	-0.605200
H	-3.105900	0.244800	1.339400	H	5.167900	-0.951500	2.278900
C	-3.225100	2.385600	1.546700	H	6.164100	-2.958500	1.172100
C	-1.311200	3.611600	0.706500	C	-2.581900	-1.636600	-0.121700
C	3.225000	2.385600	-1.546800	C	-3.175700	-2.789500	0.475700
C	1.311100	3.611600	-0.706600	C	-3.363200	-0.995800	-1.135700
H	-4.203200	2.365800	2.022300	C	-4.434400	-3.243900	0.110600
C	-2.557700	3.591300	1.311500	H	-2.592700	-3.307400	1.232300
H	-0.801100	4.562400	0.594400	C	-4.613700	-1.472800	-1.498100
H	4.203100	2.365800	-2.022300	H	-2.948000	-0.122800	-1.627100
C	2.557600	3.591300	-1.311500	C	-5.180000	-2.596500	-0.882400
H	0.801000	4.562400	-0.594500	H	-4.843000	-4.125600	0.605200
H	-3.015800	4.535000	1.615100	H	-5.167800	-0.951600	-2.279000
H	3.015700	4.534900	-1.615200	H	-6.164000	-2.958600	-1.172200

[(Bis-(2,6-dimethylphenyl)-PhDi)Co(η^4-P_4)]$^-$ (6)

Co	8.242792	4.917323	6.448956	H	10.205862	9.994067	7.404161
P	7.710657	3.827674	4.524113	C	8.171076	10.151381	6.710633
P	9.765875	3.836645	5.149448	H	10.395983	6.432018	7.795664
N	7.829322	6.124645	7.755468	H	6.102778	10.012358	6.120270
N	7.848255	3.713006	7.766403	H	5.691272	6.446698	6.347155
P	9.759175	5.988608	5.136060	H	7.395841	1.500088	9.335431
P	7.704552	5.978815	4.509396	C	6.774176	1.387983	11.361604
C	7.464767	5.633789	8.959481	C	6.408093	3.476531	12.476168
C	7.931926	7.484056	7.436808	H	10.272527	-0.129676	7.445934
C	7.475977	4.210742	8.966144	C	8.236819	-0.320072	6.763741
C	7.967163	2.351827	7.461862	H	10.412229	3.442886	7.808392
C	7.098358	6.372989	10.136357	H	6.164202	-0.213623	6.181735
C	9.156445	8.140973	7.633359	H	5.707792	3.350029	6.376140
C	6.819128	8.151034	6.901822	H	6.712317	9.557979	11.315456
C	7.122239	3.477607	10.150874	C	6.373368	7.766599	12.483537
C	9.200899	1.712656	7.659693	H	6.123296	5.858207	13.372594
C	6.860525	1.665027	6.939374	H	8.267603	11.195485	6.416630
C	7.072280	7.784156	10.183069	H	6.785989	0.299051	11.362673
C	6.745250	5.653370	11.317618	C	6.411926	2.096532	12.510404
C	9.257712	9.478023	7.258642	H	6.122372	4.009649	13.376967
C	10.273266	7.404776	8.285378	H	8.345391	-1.365957	6.480469
C	6.960606	9.488136	6.539577	H	6.092940	8.295187	13.393284
C	5.522026	7.428183	6.803822	H	6.136533	1.572913	13.424556
C	7.119186	2.066767	10.212672	H	4.835009	1.792561	6.252552
C	6.754937	4.203390	11.324170	H	5.139427	2.543980	7.842293
C	9.317299	0.372853	7.299389	H	11.255035	1.921337	8.231952
C	10.310929	2.468938	8.300275	H	10.081832	2.658757	9.356475
C	7.017306	0.325912	6.591131	H	4.798262	7.991520	6.208247
C	5.553442	2.369962	6.841084	H	5.106100	7.256001	7.804593
H	7.337975	8.346012	9.299308	H	10.037363	7.211026	9.339264
C	6.718410	8.469046	11.325670	H	11.208548	7.968281	8.225713
C	6.391206	6.386447	12.463474				

Benzene

C	0.43000000	-1.32420000	0.00000000	H	0.76490000	-2.35560000	0.00000000
C	1.36200000	-0.28970000	0.00000000	H	2.42260000	-0.51570000	0.00000000
C	0.93200000	1.03450000	0.00000000	H	1.65770000	1.84030000	0.00000000
C	-0.43010000	1.32420000	0.00000000	H	-0.76490000	2.35560000	0.00000000
C	-1.36200000	0.28970000	0.00000000	H	-2.42260000	0.51560000	0.00000000
C	-0.93190000	-1.03460000	0.00000000	H	-1.65770000	-1.84020000	0.00000000

Tetraphosphacyclobutadiene dianion [P_4]$^{2-}$

P	-1.15940000	-0.99320000	0.00000000	P	1.15940000	0.99320000	0.00000000
P	0.99320000	-1.15940000	0.00000000	P	-0.99320000	1.15940000	0.00000000

Cyclobutadiene dianion [C_4H_4]$^{2-}$

C	0.73346300	0.73516400	-0.13584900	H	-1.48320600	1.37215200	-0.39917800
C	-0.73166700	0.73619000	0.13516100	H	-1.48677400	-1.36895900	-0.39932000
C	-0.73331800	-0.73472600	0.13517600	H	1.48225600	-1.37006000	0.40361900
C	0.73202100	-0.73672500	-0.13589100	H	1.48472400	1.36744400	0.40329600

[*t*Bu$_2$P(PCN)]$^-$ (10-*t*Bu)

P	-2.25025125563347	1.46192671541032	0.06975734399337

C	-1.48249263244720	2.17594792112246	-1.56153685577599
C	-1.48455801945431	2.42267082026686	1.55794906878339
P	-1.23987848344326	-0.46937869109669	0.34141605861631
C	-2.59131770451527	-1.45482890997712	-0.21938482498852
N	-3.42604970455938	-2.20287040093651	-0.58899826090662
C	-0.00890814923408	2.12996732136812	1.86030248655075
H	0.28850104598841	2.63184716430472	2.80029976826424
H	0.15366163529273	1.04908909600116	1.98500043077861
H	0.65625491822376	2.48697258893101	1.06415267995063
C	-2.32680274775500	1.94512485151463	2.75570272629607
H	-1.97601957428218	2.43592865827684	3.68194320869485
H	-3.39081336451527	2.18570375538604	2.61252911737995
H	-2.23750794117528	0.85520452483224	2.87278103511947
C	-1.68447024536416	3.93477806673562	1.39282391754249
H	-2.71809862051692	4.17335619021589	1.09902122557876
H	-1.47377363019754	4.44789060262598	2.34896223934258
H	-1.00636025142037	4.35701216985181	0.63809689467336
C	0.03978647055547	2.32052627655447	-1.56855263549650
H	0.40353547699629	2.54213205364143	-2.58959894627844
H	0.37794640056983	3.13780513320780	-0.91484395660917
H	0.50912971229198	1.38184548094550	-1.23447331094343
C	-2.16097534408618	3.50889528083265	-1.91222769787168
H	-1.85220039577094	4.32588780613163	-1.24719624440949
H	-1.90351356750635	3.80593909183214	-2.94559699835520
H	-3.25621946739542	3.41634314772173	-1.84843613425414
C	-1.88561511579211	1.14104853897979	-2.62499515855833
H	-2.97421889937842	0.97830770103936	-2.63220213298719
H	-1.57776192081769	1.49722751346534	-3.62481652358444
H	-1.40848810465767	0.17188779081476	-2.42172981054571

2.5.6.2 Natural Theory Analysis

Natural theory analysis for **10-^{t}Bu**

TOPO matrix for the leading resonance structure:

PCN unit: 4P 5C 6N

Atom	1	2	3	4	5	6	7	8	9	10	11	12	13	14	15	16	17
1. P	1	1	1	1	0	0	0	0	0	0	0	0	0	0	0	0	0
2. C	1	0	0	0	0	0	0	0	0	0	0	0	0	0	0	0	0
3. C	1	0	0	0	0	0	1	0	0	0	1	0	0	0	1	0	0
4. P	1	0	0	2	1	0	0	0	0	0	0	0	0	0	0	0	0
5. C	0	0	0	1	0	3	0	0	0	0	0	0	0	0	0	0	0
6. N	0	0	0	0	3	1	0	0	0	0	0	0	0	0	0	0	0
7. C	0	0	1	0	0	0	0	1	1	1	0	0	0	0	0	0	0
8. H	0	0	0	0	0	0	1	0	0	0	0	0	0	0	0	0	0
9. H	0	0	0	0	0	0	1	0	0	0	0	0	0	0	0	0	0
10. H	0	0	0	0	0	0	1	0	0	0	0	0	0	0	0	0	0
11. C	0	0	1	0	0	0	0	0	0	0	0	1	1	1	0	0	0

12.	H	0	0	0	0	0	0	0	0	0	0	1	0	0	0	0	0	0	
13.	H	0	0	0	0	0	0	0	0	0	0	1	0	0	0	0	0	0	
14.	H	0	0	0	0	0	0	0	0	0	0	1	0	0	0	0	0	0	
15.	C	0	0	1	0	0	0	0	0	0	0	0	0	0	0	0	1	1	
16.	H	0	0	0	0	0	0	0	0	0	0	0	0	0	0	1	0	0	
17.	H	0	0	0	0	0	0	0	0	0	0	0	0	0	0	1	0	0	
18.	H	0	0	0	0	0	0	0	0	0	0	0	0	0	0	1	0	0	
19.	C	0	1	0	0	0	0	0	0	0	0	0	0	0	0	0	0	0	
20.	H	0	0	0	0	0	0	0	0	0	0	0	0	0	0	0	0	0	
21.	H	0	0	0	0	0	0	0	0	0	0	0	0	0	0	0	0	0	
22.	H	0	0	0	0	0	0	0	0	0	0	0	0	0	0	0	0	0	
23.	C	0	1	0	0	0	0	0	0	0	0	0	0	0	0	0	0	0	
24.	H	0	0	0	0	0	0	0	0	0	0	0	0	0	0	0	0	0	
25.	H	0	0	0	0	0	0	0	0	0	0	0	0	0	0	0	0	0	
26.	H	0	0	0	0	0	0	0	0	0	0	0	0	0	0	0	0	0	
27.	C	0	1	0	0	0	0	0	0	0	0	0	0	0	0	0	0	0	
28.	H	0	0	0	0	0	0	0	0	0	0	0	0	0	0	0	0	0	
29.	H	0	0	0	0	0	0	0	0	0	0	0	0	0	0	0	0	0	
30.	H	0	0	0	0	0	0	0	0	0	0	0	0	0	0	0	0	0	

Atom	18	19	20	21	22	23	24	25	26	27	28	29	30
1. P	0	0	0	0	0	0	0	0	0	0	0	0	0
2. C	0	1	0	0	0	1	0	0	0	1	0	0	0
3. C	0	0	0	0	0	0	0	0	0	0	0	0	0
4. P	0	0	0	0	0	0	0	0	0	0	0	0	0
5. C	0	0	0	0	0	0	0	0	0	0	0	0	0
6. N	0	0	0	0	0	0	0	0	0	0	0	0	0
7. C	0	0	0	0	0	0	0	0	0	0	0	0	0
8. H	0	0	0	0	0	0	0	0	0	0	0	0	0
9. H	0	0	0	0	0	0	0	0	0	0	0	0	0
10. H	0	0	0	0	0	0	0	0	0	0	0	0	0
11. C	0	0	0	0	0	0	0	0	0	0	0	0	0
12. H	0	0	0	0	0	0	0	0	0	0	0	0	0
13. H	0	0	0	0	0	0	0	0	0	0	0	0	0
14. H	0	0	0	0	0	0	0	0	0	0	0	0	0
15. C	1	0	0	0	0	0	0	0	0	0	0	0	0
16. H	0	0	0	0	0	0	0	0	0	0	0	0	0
17. H	0	0	0	0	0	0	0	0	0	0	0	0	0
18. H	0	0	0	0	0	0	0	0	0	0	0	0	0
19. C	0	0	1	1	1	0	0	0	0	0	0	0	0
20. H	0	1	0	0	0	0	0	0	0	0	0	0	0
21. H	0	1	0	0	0	0	0	0	0	0	0	0	0
22. H	0	1	0	0	0	0	0	0	0	0	0	0	0
23. C	0	0	0	0	0	0	1	1	1	0	0	0	0
24. H	0	0	0	0	0	0	1	0	0	0	0	0	0
25. H	0	0	0	0	0	0	1	0	0	0	0	0	0
26. H	0	0	0	0	0	0	1	0	0	0	0	0	0
27. C	0	0	0	0	0	0	0	0	0	0	1	1	1
28. H	0	0	0	0	0	0	0	0	0	0	1	0	0	0
29. H	0	0	0	0	0	0	0	0	0	0	1	0	0	0
30. H	0	0	0	0	0	0	0	0	0	0	1	0	0	0

Resonance

RS	Weight(%)	Added(Removed)
1*	68.81	
2*(2)	23.37	P 4- C 5, (C 5- N 6), (P 4), N 6
3	4.21	(P 1- C 2), P 1- P 4, C 2, (P 4)
4	2.29	(P 1- P 4), P 4- C 5, (C 5- N 6), N 6
5	1.31	(P 4- C 5), C 5- N 6, P 4, (N 6)
	100.00	* Total * [* = reference structure]

Summary of Natural Population Analysis:

Atom	No	Natural Charge	Natural Population Core	Valence	Rydberg	Total
P	1	0.52853	9.99992	4.43056	0.04099	14.47147
C	2	-0.40171	1.99999	4.37938	0.02233	6.40171
C	3	-0.39640	1.99999	4.37514	0.02126	6.39640
P	4	-0.28387	9.99993	5.24593	0.03801	15.28387
C	5	-0.05061	2.00000	4.00045	0.05016	6.05061
N	6	-0.50036	2.00000	5.47046	0.02990	7.50036
C	7	-0.68031	2.00000	4.66779	0.01253	6.68031
H	8	0.21301	0.00000	0.78594	0.00105	0.78699
H	9	0.25577	0.00000	0.74314	0.00108	0.74423
H	10	0.22940	0.00000	0.76993	0.00066	0.77060
C	11	-0.68540	2.00000	4.67290	0.01251	6.68540
H	12	0.21311	0.00000	0.78596	0.00093	0.78689
H	13	0.23795	0.00000	0.76143	0.00062	0.76205
H	14	0.26053	0.00000	0.73778	0.00169	0.73947
C	15	-0.67318	2.00000	4.66141	0.01177	6.67318
H	16	0.23782	0.00000	0.76128	0.00090	0.76218
H	17	0.22022	0.00000	0.77869	0.00109	0.77978
H	18	0.22567	0.00000	0.77386	0.00047	0.77433
C	19	-0.67967	2.00000	4.66753	0.01215	6.67967
H	20	0.21577	0.00000	0.78310	0.00113	0.78423
H	21	0.21827	0.00000	0.78127	0.00046	0.78173
H	22	0.25453	0.00000	0.74384	0.00163	0.74547
C	23	-0.67488	2.00000	4.66285	0.01203	6.67488
H	24	0.22535	0.00000	0.77397	0.00068	0.77465
H	25	0.21758	0.00000	0.78131	0.00111	0.78242
H	26	0.24050	0.00000	0.75855	0.00095	0.75950
C	27	-0.68781	2.00000	4.67478	0.01303	6.68781
H	28	0.24469	0.00000	0.75459	0.00073	0.75531
H	29	0.21309	0.00000	0.78600	0.00091	0.78691
H	30	0.26240	0.00000	0.73614	0.00146	0.73760
* Total *		-1.00000	39.99980	69.70597	0.29422	110.00000

2.5.7 References

[1] F. Neese, *Wiley Interdiscip. Rev. Comput. Mol. Sci.* **2018**, *8*, e1327.

[2] F. Neese, *Wiley Interdiscip. Rev. Comput. Mol. Sci.* **2012**, *2*, 73–78.

[3] Gaussian 09, Revision A.02, M. J. Frisch, G. W. Trucks, H. B. Schlegel, G. E. Scuseria, M. A. Robb, J. R. Cheeseman, G. Scalmani, V. Barone, G. A. Petersson, H. Nakatsuji, X. Li, M. Caricato, A. Marenich, J. Bloino, B. G. Janesko, R. Gomperts, B. Mennucci, H. P. Hratchian, J. V. Ortiz, A. F. Izmaylov, J. L. Sonnenberg, D. Williams-Young, F. Ding, F. Lipparini, F. Egidi, J. Goings, B. Peng, A. Petrone, T. Henderson, D. Ranasinghe, V. G. Zakrzewski, J. Gao, N. Rega, G. Zheng, W. Liang, M. Hada, M. Ehara, K. Toyota, R. Fukuda, J. Hasegawa, M. Ishida, T. Nakajima, Y. Honda, O. Kitao, H. Nakai, T. Vreven, K. Throssell, J. A. Montgomery, Jr., J. E. Peralta, F. Ogliaro, M. Bearpark, J. J. Heyd, E. Brothers, K. N. Kudin, V. N. Staroverov, T. Keith, R. Kobayashi, J. Normand, K. Raghavachari, A. Rendell, J. C. Burant, S. S. Iyengar, J. Tomasi, M. Cossi, J. M. Millam, M. Klene, C. Adamo, R. Cammi, J. W. Ochterski, R. L. Martin, K. Morokuma, O. Farkas, J. B. Foresman, and D. J. Fox, Gaussian, Inc., Wallingford CT, 2016.

[4] A. D. Becke, *Phys. Rev. A* **1988**, *38*, 3098–3100.

[5] R. Ditchfield, W. J. Hehre, J. A. Pople, *J. Chem. Phys.* **1971**, *54*, 724.

[6] M. Swart, A. W. Ehlers, K. Lammertsma, *Mol. Phys.* **2004**, *102*, 2467–2474.

[7] F. Weigend, R. Ahlrichs, *Phys. Chem. Chem. Phys.* **2005**, *7*, 3297–3305

[8] a) R. Ditchfield, W. J. Hehre, J. A. Pople, *J. Chem. Phys.***1971**, *54*, 724–728; b) M. J. Frisch, G. W. Trucks, H. B. Schlegel, G. E. Scuseria, M. A. Robb, J. R. Cheeseman, G. Scalmani, V. Barone, B. Mennucci, G. A. Petersson, in *Gaussian 09, Revision A.02*, Gaussian, Inc., Wallingford, CT, **2013**.

[9] a) SCALE3ABS, CrysAlisPro, Agilent Technologies Inc. Oxford, GB; b) G. M. Sheldrick, SADABS, Bruker AXS, Madison, USA, **2007**.

[10] a) R. C. Clark and J. S. Reid, *Acta Cryst. A.* **1995**, *51*, 887–597 b) CrysAlisPro, version 40_64.18, Agilent Technologies Inc. Oxford, GB.

[11] G. M. Sheldrick, *Acta Cryst.* **2015**, *A71*, 3–8.

[12] G. M. Sheldrick, *Acta Cryst.* **2015**, *C71*, 3–8.

[13] a) K. Jonas, R. Mynott, C. Krüger, J. C. Sekutowski, Y.-H. Tsay, *Angew. Chem. Int. Ed. Engl.*, **1976**, *15*, 767–768; *Angew. Chem.* **1976**, *88*, 808–809; b) K. Jonas, US Patent 4169845 **1979**.

[14] G. A. Abakumov, V. K. Cherkasov, N. O. Druzhkov, Y. A. Kurskii, G. K. Fukin, L. G. Abakumova, T. N. Kocherova, *Synth. Commun.* **2006**, *36*, 3241.

[15] V. K. Cherkasov, N. O. Druzhkov, T. N. Kocherova, A. S. Shavyrin, G. K. Fukin, *Tetrahedron* **2012**, *68*, 1422.

3 Amine-Borane Dehydrogenation and Transfer Hydrogenation Catalyzed by α-Diimine Cobaltates

Thomas M. Maier, Sebastian Sandl, Ilya G. Shenderovich, Axel Jacobi von Wangelin, Jan J. Weigand, and Robert Wolf

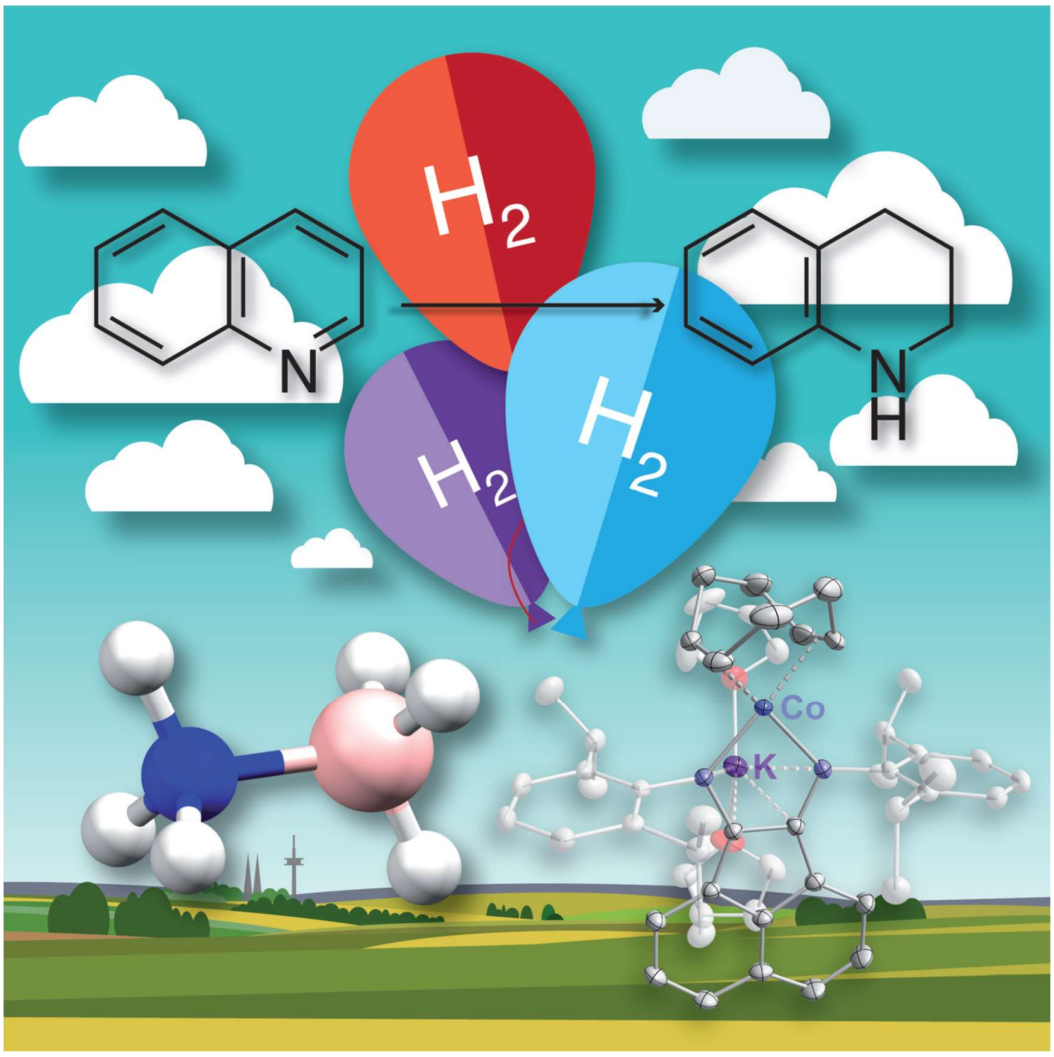

T. M. Maier performed the experimental work and wrote the manuscript. S. Sandl conducted the hydrogenation experiments (Table 2, Figure 10). I. G. Shenderovich recorded and interpreted the ^{11}B MAS NMR spectrum. A few ^{11}B NMR spectra in solution were recorded at the TU Dresden (Figure 2, J. J. Weigand). A. Jacobi von Wangelin and R. Wolf supervised and directed the project.

This chapter was published in *Chemistry – A European Journal* as a full paper: T. M. Maier, S. Sandl, I. G. Shenderovich, A. Jacobi von Wangelin, J. J. Weigand, R. Wolf, *Chem. Eur. J.* **2019**, *25*, 238-245. Reproduced with permission from Wiley-VCH. Schemes, Figures, and text may differ from published version.

3.1 Introduction

Transition metal-catalyzed dehydrogenations of amine-boranes have attracted great attention as a potentially versatile method of hydrogen storage and B-N materials synthesis.[1]-[3] Amine-boranes can serve as solid hydrogen surrogates in transfer hydrogenations.[4] Various dehydrogenation and transfer hydrogenation protocols have been developed with precious metal catalysts, and the underlying mechanisms have been thoroughly studied.[5] By contrast, dehydrogenations are far less advanced with the abundant and cheaper late 3d metals, despite the recent progress with Ti, Mn, Fe, Co, and Ni catalysts.[7]–[13]

While a number of iron catalysts for amine-borane dehydrogenations have been studied recently,[8] effective cobalt catalysts are scarce. [9]-[11] To our knowledge, only four well-defined molecular cobalt catalysts have been reported to date (Figure 1). *Peters* and co-workers reported bis(phosphino)boryl (PBP) cobalt catalysts (Figure 1) for the dehydrogenation of dimethylamine-borane (DMAB)[9] and applications to the transfer hydrogenation of styrene. *Waterman* and co-workers reported that the cyclopentadienylcobalt complexes [Cp^{R}Co(CO)$_2$I] (R= H, Me, Figure 1) catalyze ammonia borane (AB) dehydrogenation at elevated temperatures (65 °C).[10] The authors performed catalytic transfer hydrogenations with styrenes, alkynes, and olefins with an excess (8 equiv.) of AB at 65 °C within 6 h. Tripodal polyphosphine cobalt(I) hydrides (Figure 1) recently reported by *Shubina* and co-workers exhibited similar activity in the AB-dehydrogenation.[11] A mechanism was proposed based on DFT calculations. In 2020, *Weller* and co-workers synthesized a Co(II) pre-catalyst for the dehydrogenation of methylamine-borane.[12]

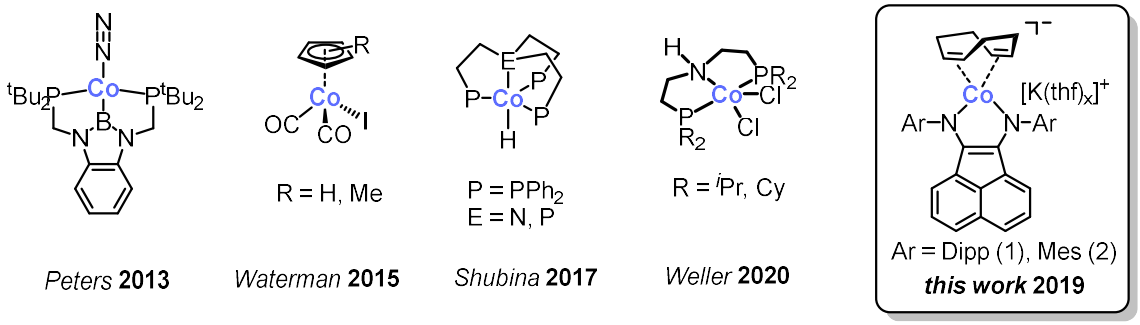

Figure 1. Homogeneous cobalt catalysts for amine-borane dehydrogenation (Dipp = 2,6-diisopropylphenyl, Mes = 2,4,6-trimethylphenyl).

The paucity of cobalt-based amine-borane dehydrogenation and transfer hydrogenation catalysts prompted us to investigate the efficiacy of complexes containing redox-active bisaryl(imino)acenapthene (BIAN) ligands.[14] This ligand class was deemed particularly

suitable because it offers a convenient synthesis from commercial precursors (>60 g scales), redox-activity, modular structure, and a persistent ligand backbone.[14] BIANs have mainly been exploited in noble metal catalysis so far,[15] while applications to 3d metal catalysis have only been reported very sporadically; systematic investigations are still in their infancy.[16]

3.2 Results and Discussion

Key discoveries and model reactions. We previously investigated in our group the catalytic properties of low-valent ferrate and cobaltate anions in the hydrogenation of olefins, ketones, and imines.[17] The pre-catalysts [K([18]c-6)(thf)$_2$][M(η^4–anthracene)$_2$] (M = Fe, Co)[18] and [K(thf)$_x$][Co(η^4–cod)$_2$][19],[20] (cod = 1,5-cyclooctadiene) enabled the hydrogenation of disubstituted alkenes, ketones and imines. Poor activities were observed for the hydrogenation of tri-substituted alkenes and dehydrogenations of amine-boranes.[20] We therefore set out to manipulate the stereoelectronic properties of the catalysts by incorporation of redox-active bis(imino)acenaphthene ligands. The synthesis of [K(thf)$_{1.5}${(^{Dipp}BIAN)Co(η^4-cod)] (**1**) (Dipp = 2,6-diisopropylphenyl; Figure 1) was recently reported.[21] **1** and the closely related mesityl-derivative [K(thf){(^{Mes}BIAN)Co(η^4-cod)] (**2**) (Mes = 2,4,6-trimethylphenyl, see the SI for details) were readily accessible in high yields from a straightforward ligand exchange reaction of [K(thf)$_x${Co(η^4-cod)$_2$}] with ^{Ar}BIAN (Ar = Dipp or Mes). The redox-active BIAN moiety in **1** and **2** may facilitate metal-centered redox processes by its ability to accommodate two electrons, while cod can serve as a placeholder for vacant coordination sites. We commenced our1 studies with dimethylamine-borane (NMe_2HBH_3, DMAB, Scheme 1 and Figure 2) as model substrate and monitored its consumption by ^{11}B NMR spectroscopy. With 5 mol% catalyst loading of **1** at 25 °C, DMAB was completely consumed within 34 h. The formation of two main products, tetramethyl-1,3-diaza-2,4-diboretane (74%) and *N*,*N*′-dimethylaminoborane (22%), and one minor BH_3-containing compound (quartet at -9.5 ppm, $^1J_{BH}$ = 134 Hz) was observed. The less bulky pre-catalyst **2** was far less selective as illustrated by the observation of significant quantities of *N*,*N*′-dimethylaminoborane (19%) and unknown BH_3-containing species (17%). We therefore employed pre-catalyst **1** for further dehydrogenation studies.

A kinetic analysis by ^{11}B NMR spectroscopy showed that the reaction likely proceeded through a stepwise mechanism involving the linear intermediate **B** (Me_2N-BH_2-NMe_2-BH_3) and the unsaturated intermediate **C** (Me_2N=BH_2) (Scheme 1). As proposed by *Schneider* and co-workers

for dehydrogenations catalyzed by a Ru-amido pincer complex and by *Weller* and co-workers with a cationic Rh-phosphine complex,[22] the loss of two molecules dihydrogen operates over two steps when the reaction proceeds through **B**. In case of **C**, both dihydrogen molecules are lost in the first step and a cycloaddition gives the terminal product **D**. We cannot rule out that **B** was also converted into **D** by the loss of one molecule H_2. The side product $HB(NMe)_2$ was reported for many catalytic DMAB hydrogenations in the literature.[5],[8],[9] Monitoring the time-dependent H_2 formation (see the SI) revealed an induction period of approx. 1 min (SI, Figure S2). A comparison of the initial rates indicates that the catalytic dehydrogenation activity of **2** is five times higher than that of **1** (SI, Figure S2).

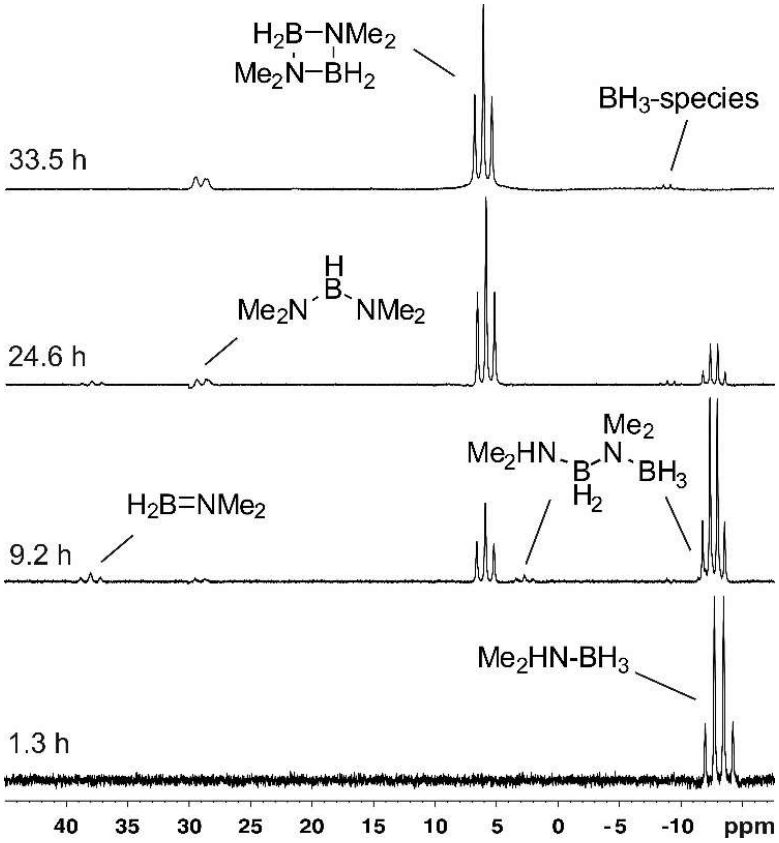

Figure 2. Time-dependent ^{11}B NMR spectra (160.4 MHz, 300 K, C_6D_6 capillary) of the DMAB dehydrogenation with catalyst **1** (0.2 mmol DMAB in 2.5 mL THF).

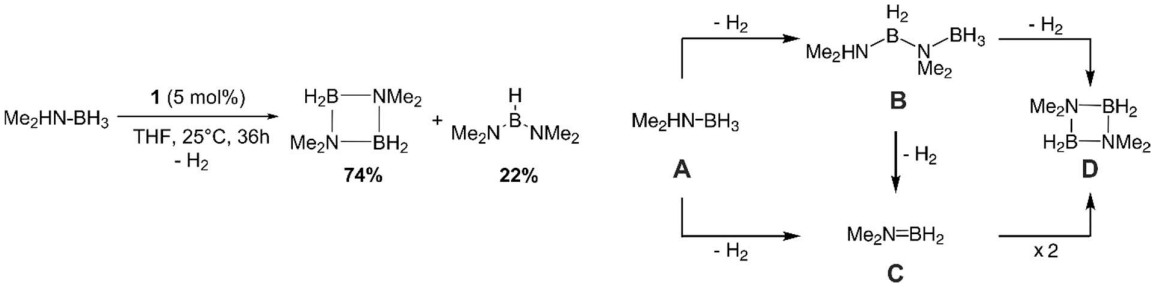

Scheme 1. Dehydrogenation of dimethylamine-borane (NMe_2HBH_3 = DMAB) (left); proposed mechanism based on observed intermediates (bottom).

Furthermore, we studied catalytic dehydrogenations with the sterically more demanding diisopropylamine-borane and the primary *N*-methylamine-borane (Scheme 2). Both reactions were rarely reported under base metal catalysis.[8],[23]

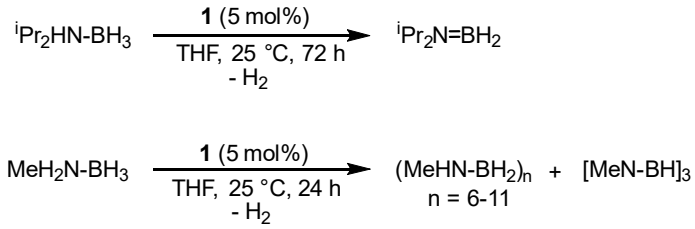

Scheme 2. Dehydrogenation of diisopropylamine-borane (a) and *N*-methylamine-borane (b).

Diisopropylamine-borane exclusively afforded the iminoborane $^{i}Pr_2N{=}BH_2$ after 72 h in THF, which exhibited the characteristic triplet at 34.8 ppm in the ^{11}B NMR spectrum (Figure 3, top). The formation of oligomeric $[MeHN\text{-}BH_2]_n$ (n = 6-11) from *N*-methylamine-borane was corroborated by ESI-MS and ^{11}B NMR spectroscopy. The ESI-MS spectra showed peaks at m/z 186.3 to 443.6 at intervals of 43.1 (corresponding to the monomeric unit H_2B-NMeH, see Figures S8-S9). ^{11}B NMR spectra recorded in THF displayed a broad triplet at –4.8 ppm with the typical line broadening of $^{1}J_{BH}$ = 106 Hz. Significantly broader peaks are expected for a polymer (Figure 3, bottom).[24]

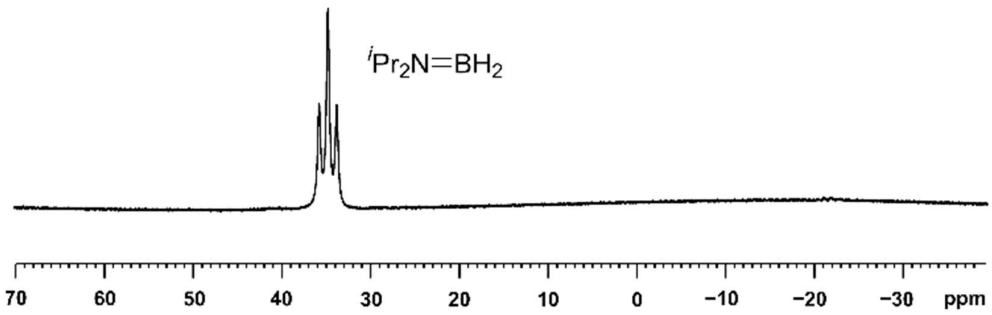

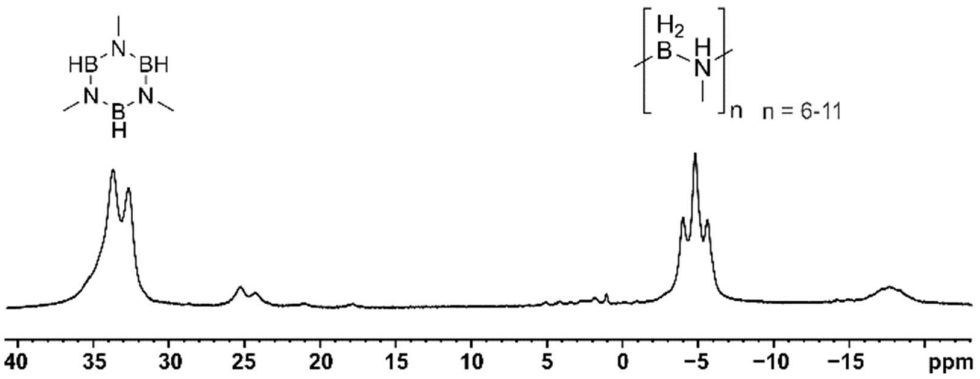

Figure 3 ^{11}B NMR spectra (128.4 MHz, 300 K, C_6D_6) of dehydrogenation products of diisopropylamine-borane (top) and *N*-methylamine-borane (bottom) in THF.

The dehydrogenation of ammonia borane (AB) is of particular interest due its high hydrogen content of 19.6 wt%.[1] The cyclopentadienyl carbonyl cobalt and tripodal phosphine cobalt complexes reported by the groups of *Waterman* and *Shubina*,[8b,c] respectively, are the only previously reported molecular cobalt catalysts for the AB-dehydrogenation (Figure 1).[9] Hence, we sought to compare the properties of pre-catalyst **1** with these benchmark systems that both operate at elevated temperature (65 °C). When **1** (5 mol%) was added to a solution of AB in THF, the evolution of H_2 commenced immediately. This indicates a rapid onset of catalytic dehydrogenation already at ambient temperature. The characterization of reaction intermediates (Scheme 3) was performed by ^{11}B NMR spectroscopy. The starting material AB was completely consumed after 24 h. Borazine (30 ppm) and polyborazine (26 ppm) were identified as the two main soluble products.

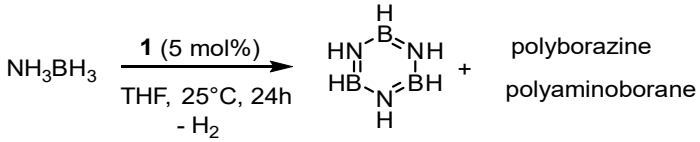

Scheme 3. Dehydrogenation of ammonia borane catalyzed by **1** (5 mol%).

However, it is noteworthy that a white precipitate formed during the reaction in THF. This solid was studied by magic angle spinning (MAS) ^{11}B NMR spectroscopy with proton decoupling and cross-polarization (^{11}B CPMAS NMR) as well as without cross-polarization from protons and with proton coupling. The ^{11}B MAS NMR spectrum of this material showed two signals at 2 ppm and –19 ppm (Figure 4). Proton decoupling (^{11}B{^{1}H} MAS NMR) reduced the linewidth of the –19 ppm resonance while it did not affect the signal at 2 ppm. The intensity

of the former signal was strongly enhanced in the $^{11}B\{^1H\}$ CPMAS spectrum. Thus, this signal should be assigned to a boron atom bonded to hydrogen(s). In contrast, the signal at 2 ppm may be assigned to a boron atom bearing no H atoms. We believe that this solid is polyaminoborane for which similar solid-state NMR data, particularly similar chemical shifts, were reported by *Schneider* and co-workers.[8]

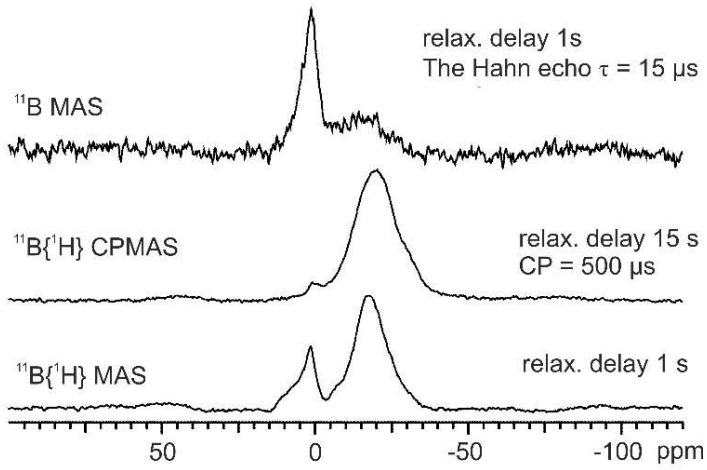

Figure 4. ^{11}B NMR spectra at 300 K of polyaminoborane: MAS at 6 kHz; relax = relaxation.

Mechanistic studies of dehydrogenation. AB dehydrogenation was directly monitored by H_2 evolution at 1–12.5 mol% catalyst loading (Figure 5). An induction period was apparent at low catalyst concentrations, indicating that **1** might act as a pre-catalyst that is converted to the active catalyst species under reaction conditions. The formation of 0.5 equivalents H_2 per AB was observed within the first 2 min with 5 mol% (10 mM) catalyst. Subsequently, the reaction became much slower, indicating catalyst deactivation and possibly a change in the reaction mechanism. A plot of the initial rates *vs.* catalyst concentrations (SI, Figure S3) showed a 2nd order rate in catalyst. A linear relationship between reaction rate and substrate concentration from 50–200 mM was established from dehydrogenations with different AB concentrations and constant catalyst concentration (SI, Figure S4). Higher substrate concentrations afforded no significant enhancement of the initial rate constant. Based on these data, the following rate law can be formulated:

$$d(H_2)/dt = k\cdot[\text{catalyst } \mathbf{1}]^2\cdot[NH_3BH_3] \qquad (1)$$

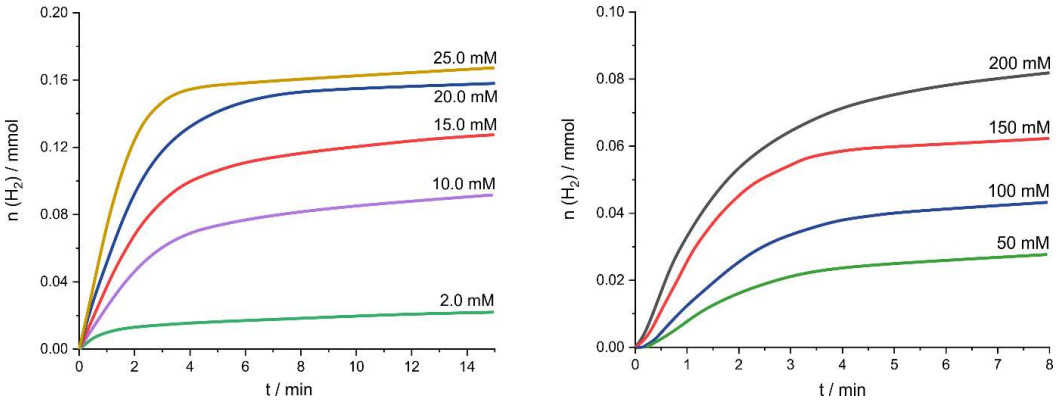

Figure 5. Dehydrogenation of AB catalyzed with different catalyst loading of **1** (Reaction conditions: 0.2 mmol AB in THF (1 mL) at 25 °C, left) and different AB concentration (Reaction conditions: 10 mM **1** in THF (1 mL) at 25 °C, right).

Further mechanistic evidence was gathered from GC-MS investigations of the reaction mixtures, which documented the formation of cyclooctene and cyclooctane arising from (partial) hydrogenation of the 1,5-cyclooctadiene ligand in **1**. No H_2 formation was observed in control experiments with NMe_3BH_3 and NH_3BEt_3. A crossover experiment with a substrate mixture of NMe_3BH_3 and NH_3BEt_3 did not result in any H_2 formation. Consistently, no dehydrogenation products were observed by ^{11}B NMR. These results proved that the presence of H-N *and* H-B entities within one molecule are required to enable dehydrogenation of amine-boranes. To gain more insight into the operating reaction mechanism, we performed dehydrogenations of the deuterated species ND_3BH_3, NH_3BD_3, and ND_3BD_3. Experiments with 5 mol% catalyst **1** and ND_3BH_3 revealed a kinetic isotope effect (KIE) $k(NH_3BH_3)$ / $k(ND_3BH_3)$ = 1.6 (2° KIE), while with NH_3BD_3 a negligible KIE $k(NH_3BH_3)$ / $k(NH_3BD_3)$ of 0.9 was observed. This is strongly indicative of a participation of a protic H-N in the rate determining step. Fully deuterated ammonia borane (ND_3BD_3) showed a strong KIE $k(NH_3BH_3)$ / $k(ND_3BH_3)$ of 2.0 (Figure 6).

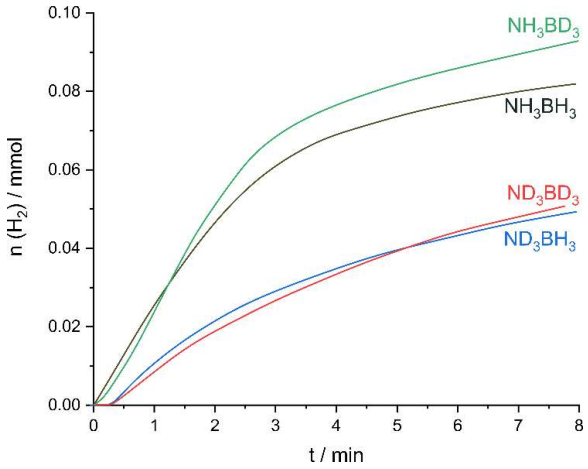

Figure 6. Observation of kinetic isotope effects in the dehydrogenation of ammonia borane. Reaction conditions: 5 mol% **1**, 0.2 mmol AB, THF (1 mL), 25 °C.

Complementing the kinetic studies, we conducted poisoning experiments in order to study the nature of the catalytically active species.[25] The analysis of changes in the catalyst activity by the presence of selective catalyst poisons is an instructive tool for the distinction between homotopic and heterotopic catalysis pathways.[20],[26] Mercury (675 equiv. per [Co]) and $P(OMe)_3$ (0.2 equiv. per catalyst) barely had an influence on the overall reaction rate (5 mol% catalyst, see Figure 7). Both additives are known to selectively poison heterogeneous catalysts.[20],[25],[26] A complementary experiment was performed with the strong π-ligand dibenzo[*a*,*e*]cyclooctatetraene (dct), which selectively deactivates soluble metal complexes in low oxidation states and therefore is a powerful poison of homogeneous catalysts.[20],[25]-[27]

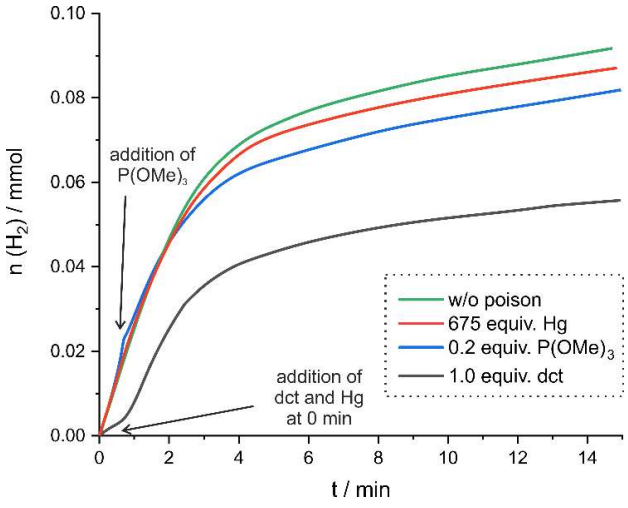

Figure 7. Poisoning experiments in the dehydrogenation of AB. Reaction conditions: 5 mol% **1**, 0.2 mmol AB, THF (1 mL), 25 °C.

Addition of AB to a solution of the catalyst (5 mol% **1**) and dct (2 equiv. per [Co]) significantly slowed down the reaction. The inhibition was not complete as dct underwent partial hydrogenation to *E*/*Z*-dibenzocyclooctene and dibenzocyclooctane (GC-MS). These poisoning studies support the notion of a homotopic reaction mechanism.

The insight gained by these studies can be summarized in a tentative mechanistic scheme (Scheme 4). Catalysis is initiated by the (partial) hydrogenation of the cyclooctadiene ligand. This results in an induction period observed in the reaction-time profiles at low catalyst concentrations. The poisoning studies indicate that a homogeneous (molecular) catalyst is operative, while the 2nd order rate law with respect to cobalt suggests that the rate-determining step involves two cobalt atoms. While the exact structure of the active species still remains obscure presently, it should be noted that numerous transition metal hydrides catalyze amine-borane dehydrogenation,[1] and there is literature precedent for dinuclear cobalt hydride complexes.[33] A dinuclear cobalt hydride species thus might be a plausible on-cycle intermediate. The basic nature of the hydride ligands might explain why N–H transfer appears to be rate determining in this case.

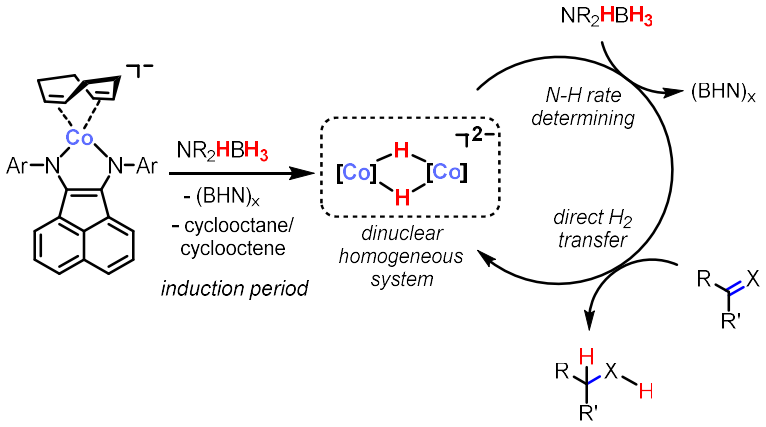

Scheme 4. Summary of the mechanistic information gained for amine-borane dehydrogenation and transfer hydrogenation (X = CR_2; NHR'').

Scope of transfer hydrogenations. Next, we expanded the catalytic applications of **1** and **2** to transfer hydrogenations of C=C and C=N bonds using AB as formal hydrogen donor. Only a few molecular cobalt catalysts are known to be competent in transfer hydrogenations of olefins and imines (Figure 1).[9] We performed initial studies with the combination of NH_3BH_3 and α-methylstyrene (SI, Table S1). Pre-catalysts **1** and **2** gave similar results. Optimizations with **1** showed best activities and full conversion at 5 mol% catalyst loading and equimolar

concentrations of alkene and AB (0.2 mol L^{-1} in THF, see SI: Table S1). Allylbenzene, linear α-olefins, and 4-octene were successfully hydrogenated under these conditions (Figure 8). Complete hydrogenation of 1,1-diphenylethylene proceeded within 40 h at ambient temperature. The reaction conditions were compatible with ethers, esters, amines, CF_3, F, and free alcohols (Figure 8). Minor dehydrohalogenation (3%) was observed for 4-chloro-α-methylstyrene. Alkyl cinnamates underwent competitive carbonyl hydrogenation to give 3-phenyl-1-propanol. Challenging tri-substituted olefins such as 1-phenylcyclopentene, 1-phenyl-1-cyclohexene, and triphenylethylene as well as arene moieties remained untouched even at elevated temperatures and with an excess of AB. Hydrogenation of such unsaturated functions could be realized by applying external H_2 pressure (*vide infra*). The scope of transfer hydrogenations was extended to imines and quinoline derivatives (Figure 8). Hydrogenations of quinolines are of particular interest due to the formation of 1,2,3,4-tetrahydroquinolines, which constitute key motifs of several bioactive compounds.[30],[31] Very few heterogeneous catalysts for the transfer hydrogenation of quinolines and related *N*-heterocycles were described by *Beller* and co-workers,[28] while molecular catalysts are also scarce.[30] Using catalyst **1**, various quinolines were hydrogenated to 1,2,3,4-tetrahydroquinolines at room temperature within 16 h. The equimolar stoichiometry of quinolines and AB underlines the high efficacy of catalyst **1** as 2 equiv. H_2 per AB are being transferred. Quinoxaline containing two C=N bonds was fully hydrogenated.

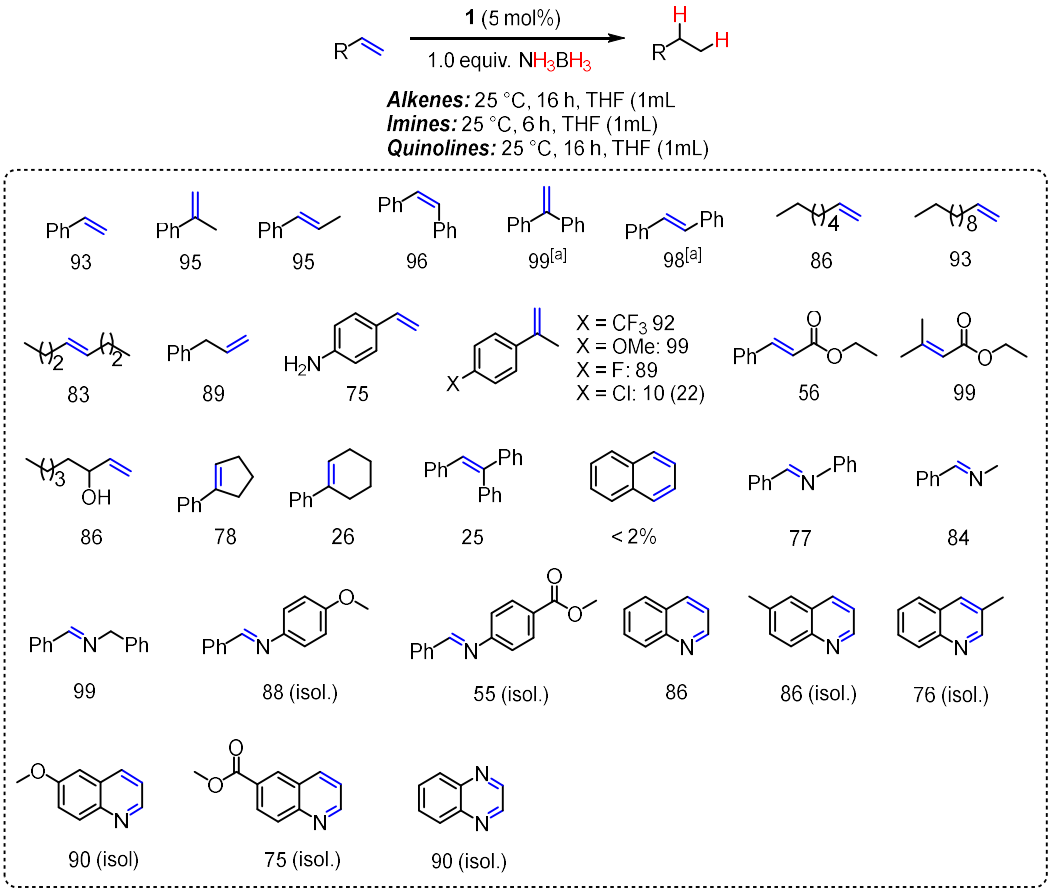

Figure 8. Transfer hydrogenation of alkenes with **1** (5 mol%). Standard conditions: alkene and AB (each 0.2 mmol), THF (1 mL); yields were determined by quantitative GC vs. internal *n*-pentadecane. [a] 40 h.

Mechanistic studies of transfer hydrogenation. We investigated the reaction-time profile of the hydrogenation of α-methyl-styrene (blue curve in Figure 9). The reaction onset is very fast (50% conversion after 3 min) and very similar to the dehydrogenation of AB (Figure 5). The reaction between α-methyl-styrene and AB under an atmosphere of 1 bar D_2 showed no deuterium incorporation after 5 min (GC-MS, see SI: Figure S15). This indicates a direct (i.e. intramolecular) hydrogen transfer from AB to the alkene (see Scheme 4 above) which is orders of magnitude faster than the reduction of the alkene by D_2. Furthermore, this observation argues against a stepwise mechanism involving H_2 formation from AB followed by cobalt-catalyzed hydrogenation of the alkene. Deuterated cumenes (appr. 15-20%, mostly cumene-d_1, little cumene-$d_{2\text{-}7}$) were only observed after long reaction times (16 h, GC-MS, see SI: Figures S14 and S16).[32] Catalyst poisoning studies with dct suggested that the reaction follows a homotopic mechanism. The reaction was immediately inhibited after dct addition at 50% conversion (1.0 equiv. per [Co], Figure 9). The partial hydrogenation of the catalyst poison dct

to a mixture of dibenzocyclooctene and dibenzocyclooctane resulted in the recovery of low catalyst activity after a few minutes (GC-MS).

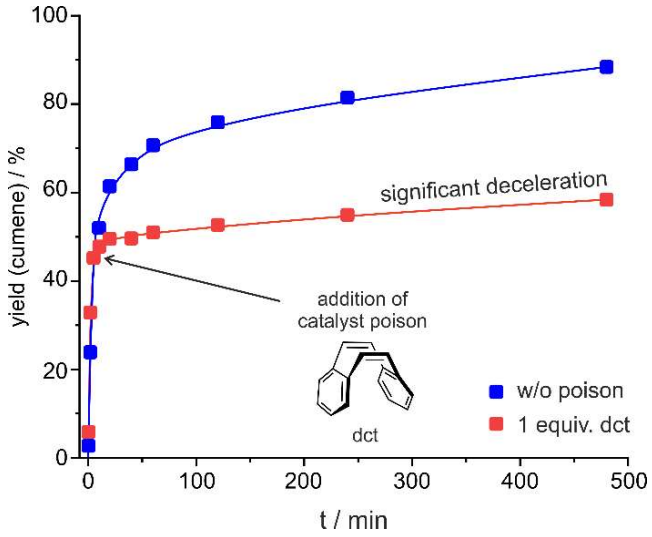

Figure 9. Catalyst poisoning in the transfer hydrogenation with **1**.

Hydrogenation of alkenes. The inefficacy of the transfer hydrogenation protocol for sterically hindered and some functionalized substrates prompted us to develop a hydrogenation protocol that would combine the rapid catalyst activation mechanism by catalytic amounts of AB with a hydrogenation mechanism in the presence of (super)stoichiometric amounts of H_2 gas (Table 1).[34],[35] Pre-catalyst **2** proved slightly higher activity than **1** in the hydrogenation of the model substrate triphenylethylene. With 3 mol% of **2**, the hydrogenation proceeded cleanly at 20 bar H_2 and 60 °C in the presence of several amine-boranes as catalyst activators. Amines and BH_3·THF were unreactive; NMe_2HBH_3 worked poorer than AB.

Table 1. Screening of different additives in the hydrogenation of triphenylethylene with catalyst **2**.[a]

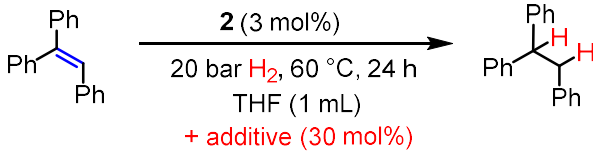

Additive	Yield (conversion) in [%]
w/o	0 (0)
NMe_2HBH_3	**92**
NH_3BH_3	**> 99**
NH_3BH_3 [b]	**> 99**
NEt_3	0 (13)
Pyridine	1 (14)
Piperidine	0 (12)
BH_3·(THF)	2 (52)[c]

[a] Standard conditions: **2** (3 mol%), substrate (0.2 mmol) in THF (1 mL). Yields of hydrogenated products were determined by quantitative GC vs. internal *n*-pentadecane. [b] Catalyst **1** instead of **2**. [c] Possibly due to hydroboration of triphenylethylene.

The general conditions were applied to a series of tri-substituted olefins (Figure 10). It is noteworthy that, unlike the transfer hydrogenation protocol, no dehalogenation was observed for 4-halo-α-methylstyrenes (X = Cl, Br) under these hydrogenation conditions. Naphthalene and pinene were hydrogenated at elevated temperature.

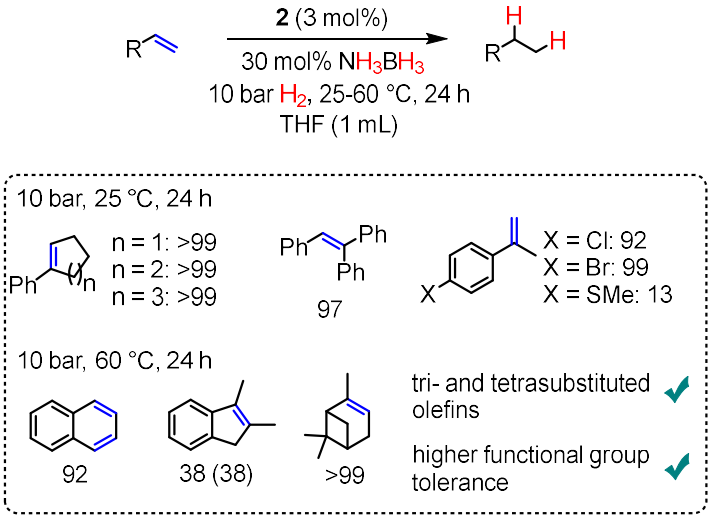

Figure 10. Substrate scope of alkene hydrogenations involving AB-mediated catalyst activation. Bonds in blue indicate sites of π-bond hydrogenation. Standard conditions: 0.2 mmol alkene, THF (1 mL). Yields determined by quantitative GC-FID vs. internal *n*-pentadecane; conversions given in parentheses if <90%.

3.3 Conclusion

We have shown for the first time that highly reduced cobalt anions such as [K(thf)$_{1.5}$\{^{Dipp}BIAN)Co(η^4-cod)\}] (**1**) can be used as active catalysts for the dehydrogenation of ammonia borane (AB) and related amine-boranes under mild conditions. The activitiy of **1** surpasses that of other molecular cobalt catalysts by *Waterman*[10] and *Shubina*[11] (Figure 1), which require elevated temperatures for an effective dehydrogenation reaction. Pre-catalyst **1** displayed a similar activity as *Peter's* PBP pincer complex[9] for the dehydrogenation of DMAB. A mixture of polyaminoborane, borazine, polyborazine was obtained using catalyst **1**, indicating that >1 equiv. H_2 was released from AB. Reaction monitoring and poisoning experiments strongly indicate the operation of a homotopic catalyst. Transfer hydrogenation of olefins, imines, and quinolines have attracted increased interest only recently.[28],[29] Catalyst **1** is also able to catalyze such transformations effectively, which involved the transfer of up to 2 equiv. H_2 from AB. Mechanistic studies documented that the rate-determining step likely involves proton transfer from the amine-borane, while the rate law suggested that more than one Co atom may be involved. Poisoning experiments again supported a homogeneous mechanism. [K(thf)\{^{Mes}BIAN)Co(η^4-cod)\}] (**2**) exhibited similarly good catalytic activity in the transfer hydrogenation reaction between AB and alkenes/imines. A related protocol was used for the hydrogenation of challenging tri-substituted olefins which involved catalyst activation by AB and subsequent hydrogenation under 10 bar H_2. This initial study demonstrates the significant potential of highly reduced α-diimine cobaltates for (de)hydrogenation reactions for the first time. The results have direct ramifications for the development of related reductive transformations and H_2 storage processes under base metal catalysis, which are the subject of on-going investigation in our laboratories.

3.4 References

[1] a) A. Staubitz, A. P. M. Robertson, I. Manners, *Chem. Rev.* **2010**, *110*, 4079–4124. b) A. Rossin, M. Peruzzini, *Chem. Rev.* **2016**, *116*, 8848–8872.

[2] a) F. H. Stephens, V. Pons, R. T. Baker, *Dalton Trans.* **2007**, *0*, 2613–2626. b) N. C. Smythe, J. C. Gordon, *Eur. J. Inorg. Chem.* **2010**, *2010*, 509–521

[3] a) A. Staubitz, A. Presa Soto, I. Manners, *Angew. Chem. Int. Ed.* **2008**, *47*, 6212–6215; *Angew. Chem.* **2008**, *120*, 6308–6311. b) A. Ledoux, P. Larini, C. Boisson, V. Monteil, J. Raynaud, E. Lacôte, *Angew. Chem. Int. Ed.* **2015**, *54*, 15744–15749; *Angew. Chem.* **2015**, *127*, 15970–15975. c) E. M. Leitao, T. Jurca, I. Manners, *Nature Chem.* **2013**, *5*, 817–829.

[4] a) S. Fu, N.-Y. Chen, X. Liu, Z. Shao, S.-P. Luo, Q. Liu, *J. Am. Chem. Soc.* **2016**, *138*, 8588–8594. b) E. Korytiaková, N. O. Thiel, F. Pape, J. F. Teichert, *Chem. Commun.* **2017**, *53*, 732–735.

[5] Selected examples for Ru, Pd, Rh, and Ir: a) C. A. Jaska, K. Temple, A. J. Lough, I. Manners, *Chem. Commun.* **2001**, 962–963. b) A. Staubitz, A. Presa Soto, I. Manners, *Angew. Chem. Int. Ed.* **2008**, *47*, 6212–6215; *Angew. Chem.* **2008**, *120*, 6308–6311. c) N. Blaquiere, S. Diallo-Garcia, S. I. Gorelsky, D. A. Black, K. Fagnou, *J. Am. Chem. Soc.* **2008**, *130*, 14034–14035. d) A. Friedrich, M. Drees, S. Schneider, *Chem. Eur. J.* **2009**, *15*, 10339–10342. e) T. M. Douglas, A. B. Chaplin, A. S. Weller, X. Yang, M. B. Hall, *J. Am. Chem. Soc.* **2009**, *131*, 15440-15456. f) A. Rossin, G. Bottari, A. M. Lozano-Vila, M. Paneque, M. Peruzzini, A. Rossi, F. Zanobini, *Dalton Trans.* **2013**, *42*, 3533–3541. f) E. H. Kwan, H. Ogawa, M. Yamashita, *ChemCatChem* **2017**, *9*, 2457–2462.

[6] a) A. Staubitz, M. E. Sloan, A. P. M. Robertson, A. Friedrich, S. Schneider, P. J. Gates, J. Schmedt auf der Günne, I. Manners, *J. Am. Chem. Soc.* **2010**, *132*, 13332–13345. b) T. Jurca, T. Dellermann, N. E. Stubbs, D. A. Resendiz-Lara, G. R. Whittell, I. Manners, *Chem. Sci.* **2018**, *9*, 3360.

[7] a) T. Kakizawa, Y. Kawano, K. Naganeyama, M. Shimoi, *Chem. Lett.* **2011**, *40*, 171–173. b) S. Muhammad, S. Moncho, E. N. Brothers, A. A. Bengali, *Chem. Commun.* **2014**, *50*, 5874–5877. c) M. Gediga, C. M. Feil, S. H. Schlindwein, J. Bender, M. Nieger, D. Gudat, *Chem. Eur. J.* **2017**, *23*, 11560–11569. d) H. R. Sharpe, A. M. Geer, T. J. Blundell, F. R. Hastings, M. W. Fay, G. A. Rance, W. Lewis, A. J. Blake, D. L. Kays, *Catal. Sci. Technol.* **2018**, *8*, 229–235.

[8] a) J. R. Vance, A. P. M. Robertson, K. Lee, I. Manners, *Chem. Eur. J.* **2011**, *17*, 4099–4103. b) R. T. Baker, J. C. Gordon, C. W. Hamilton, N. J. Henson, P.-H. Lin, S. Maguire, M. Murugesu, B. L. Scott, N. C. Smythe, *J. Am. Chem. Soc.* **2012**, *134*, 5598–5609. c) P. Bhattacharya, J. A. Krause, H. Guan, *J. Am. Chem. Soc.* **2014**, *136*, 11153–11161. d) J. R. Vance, A. Schäfer, A. P. M. Robertson, K. Lee, J. Turner, G. R. Whittell, I. Manners, *J. Am. Chem. Soc.* **2014**, *136*, 3048–3064. e) A. Glüer, M. Förster, V. R. Celinski, J. Schmedt auf der Günne, M. C. Holthausen, S. Schneider, *ACS Catal.* **2015**, *5*, 7214–7217. f) C. Lichtenberg, M. Adelhardt, T. L. Gianetti, K. Meyer, B. de Bruin, H. Grützmacher, *ACS Catal.* **2015**, *5*, 6230–6240. g) C. Lichtenberg, L. Viciu, M. Adelhardt, J. Sutter, K. Meyer, B. de Bruin, H. Grützmacher, *Angew. Chem. Int. Ed.* **2015**, *54*, 5766–5771; *Angew. Chem.* **2015**, *127*, 5858–5863. h) A. M. Lunsford, J. H. Blank, S. Moncho, S. C. Haas, S. Muhammad, E. N. Brothers, M. Y. Darensbourg, A. A. Bengali, *Inorg. Chem.* **2016**, *55*, 964–973. i) N. T. Coles, M. F. Mahon, R. L. Webster, *Organometallics* **2017**, *36*, 2262–2268. j) U. Chakraborty, S. Demeshko, F. Meyer, C. Rebreyend, B. de Bruin, M. Atanasov, F. Neese, B. Mühldorf, R. Wolf, *Angew. Chem. Int. Ed.* **2017**, *56*, 7995–7999; *Angew. Chem.* **2017**, *129*, 8107–8112. k) F. Anke, D. Han, M. Klahn, A. Spannenberg, T. Beweries *Dalton Trans.* **2017**, *46*, 6843–6847, l) J. Turner, N. F. Chilton, A. Kumar, A. L. Colebatch, G. R. Whittell, H. A. Sparkes, A. S. Weller, I. Manners, *Chem. Eur. J.* **2018**, *24*, 14127-14136.

[9] a) T.-P. Lin, J. C. Peters, *J. Am. Chem. Soc.* **2013**, *135*, 15310–15313. b) G. Ganguly, T. Malakar, A. Paul, *ACS Catal.* **2015**, *5*, 2754–2769.

[10] J. K. Pagano, J. P. W. Stelmach, R. Waterman, *Dalton Trans.* **2015**, *44*, 12074–12077.

[11] S. Todisco, L. Luconi, G. Giambastiani, A. Rossin, M. Peruzzini, I. E. Golub, O. A. Filippov, N. V. Belkova, E. S. Shubina, *Inorg. Chem.* **2017**, *56*, 4296–4307.

[12] T. M. Boyd, K. A. Andrea, K. Baston, A. Johnson, D. E. Ryan. A. S. Weller, *Chem. Commun.* **2020**, *56*, 482-485.

[13] a) R. J. Keaton, J. M. Blacquiere, R. T. Baker, *J. Am. Chem. Soc.* **2007**, *129*, 1844–1845. b) M. Vogt, B. de Bruin, H. Berke, M. Trincado, H. Grützmacher, *Chem. Sci.* **2011**, *2*, 723–727. c) A. P. M. Robertson, R. Suter, L. Chabanne, G. R. Whittell, I. Manners, *Inorg. Chem.* **2011**, *50*, 12680–12691. d) S.-K. Kim, S.-A. Hong, H.-J. Son, W.-S. Han, A. Michalak, S.-J. Hwang, S. O. Kang, *Dalton Trans.* **2015**, *44*, 7373–7381.

[14] Reviews on properties of BIAN derivatives and their coordination chemistry with s- and p-block elements: a) N. J. Hill, I. Vargas-Baca, A. H. Cowley, *Dalt. Trans.* **2009**, *9226*, 240; b) I. L. Fedushkin, A. A. Skatova, V. A. Chudakova, G. K. Fukin, *Angew. Chem. Int. Ed.* **2003**, *42*, 3294; *Angew. Chem.* **2003**, *115*, 3416–3420.

[15] Selected examples of (BIAN)Pd(olefin)-catalyzed hydrogenations: a) R. van Asselt, C. J. Elsevier, *J. Mol. Catal. A* **1991**, *65*, L13–L19. b) R. van Asselt, C. J. Elsevier, W. J. J. Smeets, A. L. Spek, R. Benedix, *Recl. Trav. Chim. Pays-Bas* **1994**, *113*, 88–98. c) M. W. Van Laren, C. J. Elsevier, *Angew. Chem. Int. Ed.* **1999**, *38*, 3715–3717; *Angew. Chem.* **1999**, *11*, 3926–3929.

[16] a) F. S. Wekesa, R. Arias-Ugarte, L. Kong, Z. Sumner, G. P. McGovern, M. Findlater, *Organometallics* **2015**, *34*, 5051–5056; b) M. J. Supej, A. Volkov, L. Darko, R. A. West, J. M. Darmon, C. E. Schulz, K. A. Wheeler, H. M. Hoyt, *Polyhedron* **2016**, *114*, 403–414; c) M. Villa, D. Miesel, A. Hildebrandt, F. Ragaini, D. Schaarschmidt, A. Jacobi von Wangelin, *ChemCatChem* **2017**, *9*, 3203–3209.

[17] Review on metalate anions highlighting the pioneering work of Jonas and Ellis: J. E. Ellis, *Inorg. Chem.* **2006**, *45*, 3167–3186.

[18] a) W. W. Brennessel, J. Young Victor G., J. E. Ellis, *Angew. Chem. Int. Ed.* **2002**, *41*, 1211–1215; *Angew. Chem.* **2002**, *114*, 1259–1263. b) W. W. Brennessel, R. E. Jilek, J. E. Ellis, *Angew. Chem. Int. Ed.* **2007**, *46*, 6132–6136; *Angew. Chem.* **2007**, *119*, 6244–6248.

[19] a) K. Jonas, R. Mynott, C. Krüger, J. C. Sekutowski, Y.-H. Tsay, *Angew. Chem. Int. Ed. Engl.* **1976**, *15*, 767–768; *Angew. Chem.* **1976**, *88*, 808–809.

[20] a) D. Gärtner, A. Welther, B. R. Rad, R. Wolf, A. Jacobi von Wangelin, *Angew. Chem. Int. Ed.* **2014**, *53*, 3722–3726; *Angew. Chem.* **2014**, *126*, 3796–3800. b) P. Büschelberger, D. Gärtner, E. Reyes-Rodriguez, F. Kreyenschmidt, K. Koszinowski, A. Jacobi von Wangelin, R. Wolf, *Chem. Eur. J.* **2017**, *23*, 3139–3151.

[21] S. Pelties, T. Maier, D. Herrmann, B. de Bruin, C. Rebreyend, S. Gärtner, I. G. Shenderovich, R. Wolf, *Chem. Eur. J.* **2017**, *23*, 6094–6102.

[22] a) A. Friedrich, M. Drees, S. Schneider, *Chem. Eur. J.* **2009**, *15*, 10339–10342. b) L. J. Sewell, G. C. Lloyd-Jones, A. S. Weller, *J. Am. Chem. Soc* **2012**, *134*, 3598-3610.

[23] Dehydrogenation of diisopropylamino borane: a) C. A. De Albuquerque Pinheiro, C. Roiland, P. Jehan, G. Alcaraz, *Angew. Chem. Int. Ed.* **2018**, *57*, 1519; *Angew. Chem.* **2018**, *130*, 1535. b) ref. [11c].

[24] Selected examples for dehydrogenation of methylamine-borane to poly-*N*-methylaminoborane or $[MeHN\text{-}BH_2]_3$: a) A. Staubitz, A. Presa Soto, I. Manners, *Angew. Chem. Int. Ed.* **2008**, *47*, 6212–6215; *Angew. Chem.* **2008**, *120*, 6308–6311. b) Y. Kawano, M. Uruichi, M. Shimoi, S. Taki, T. Kawaguchi, T. Kakizawa, H. Ogino, *J. Am. Chem. Soc.* **2009**, *131*, 14946–14957. c) T. Kakizawa, Y. Kawano, K. Naganeyama, M. Shimoi, *Chem. Lett.* **2011**, *40*, 171–173. e) G. M. Adams, A. L. Colebatch, J. T. Skornia, A. I. McKay, H. C. Johnson, G. C. Lloyd-Jones, S. A. Macgregor, N. A. Beattie, A. S. Weller, *J. Am. Chem. Soc.* **2018**, *140*, 1481. f) see also ref. [6a], [7k].

[25] Selected reviews on homotopic vs. heterotopic catalysis: a) R. H. Crabtree, *Chem. Rev.* **2012**, *112*, 1536–1554. b) V. Artero, M. Fontecave, *Chem. Soc. Rev.* **2013**, *42*, 2338–2356. c) J. F. Sonnenberg, R. H. Morris, *Catal. Sci. Technol.* **2014**, *4*, 3426–3438

[26] a) P. Büschelberger, E. Reyes-Rodriguez, C. Schöttle, J. Treptow, C. Feldmann, A. Jacobi von Wangelin, R. Wolf, *Catal. Sci. Technol.* **2018**, *8*, 2648–2653. b) S. Sandl, F. Schwarzhuber, S. Pöllath, J. Zweck, A. Jacobi von Wangelin, *Chem. Eur. J.* **2018**, *24*, 3403–3407.

[27] a) D. R. Anton, R. H. Crabtree, *Organometallics* **1983**, *2*, 855–859. b) S. Chaffins, M. Brettreich, F. Wudl, *Synthesis* **2002**, *2002*, 1191–1194. c) G. Franck, M. Brill, G. Helmchen, *Org. Synth.* **2012**, *89*, 55–65.

[28] F. Chen, B. Sahoo, C. Kreyenschulte, H. Lund, M. Zeng, L. He, K. Junge, M. Beller, *Chem. Sci.* **2017**, *8*, 6239–6246.

[29] a) G. Zhang, S. K. Hanson, *Chem. Commun.* **2013**, *49*, 10151–10153. b) G. Zhang, Z. Yin, J. Tan, *RSC Adv.* **2016**, *6*, 22419–22423. c) S. Fu, N.-Y. Chen, X. Liu, Z. Shao, S.-P. Luo, Q. Liu, *J. Am. Chem. Soc.* **2016**, *138*, 8588–8594. d) J. R. Cabrero-Antonino, R. Adam, K. Junge, R. Jackstell, M. Beller, *Catal. Sci. Technol.* **2017**, *7*, 1981–1985. e) V. G. Landge, J. Pitchaimani, S. P. Midya, M. Subaramanian, V. Madhu, E. Balaraman, *Catal. Sci. Technol.* **2018**, *8*, 428–433.

[30] Examples for cobalt-catalyzed imine and quinoline hydrogenation: a) K. Kobayashi, T. Okamoto, T. Oida, S. Tanimoto, *Chem. Lett.* **1986**, *15*, 2031–2034. b) R. Xu, S. Chakraborty, H. Yuan, W. D. Jones, *ACS Catal.* **2015**, *5*, 6350–6354.

[31] Reviews on 1,2,3,4-tetrahydroquinoline chemistry: a) A. R. Katritzky, S. Rachwal, B. Rachwal, *Tetrahedron* **1996**, *52*, 15031–15070. b) V. Sridharan, P. A. Suryavanshi, J. C. Menéndez, *Chem. Rev.* **2011**, *111*, 7157–7259.

[32] ^{2}H NMR spectroscopy of the obtained H/D-cumene mixture showed on average that 20% of the methine positions and 18% of the methyl positions bear D atoms. The higher deuteration level of the methyl positions may indicate the operation of a mono-deuterium atom transfer to the alkene or possibly an H/D-exhange via benzyl radical intermediates.

[33] Selected examples of dinuclear cobalt hydrides: a) M. D. Fryzuk, J. B. Ng, S. J. Rettig, J. C. Huffman, K. Jonas, *Inorg. Chem.* **1991**, *30*, 2437–2441. b) J. L. Kersten, A. L. Rheingold, K. H. Theopold, C. P. Casey. R. A. Widenhoefer, C. E. C. A. Hop, *Angew. Chem.* **1992**, *104*, 1364-1366. c) K. Ding, W. W. Brennessel, P. L. Holland, *J. Am. Chem. Soc.* **2009**, *131*, 10804–10805.

[34] a) *Catalytic Hydrogenation* Ed.: L. Cerveny), Elsevier, Amsterdam, **1986**. b) *The Handbook of Homogeneous Hydrogenation* (Eds.: J. G. de Vries, C. J. Elsevier), Wiley-VCH, Weinheim, **2007**. c) P. J. Chirik, *Acc. Chem. Res.* **2015**, *48*, 1687.

[35] Selected examples of Co-catalyzed alkene hydrogenations: a) Q. Knijenenburg, A. D. Horton, H. van der Heijden, B. de Bruin, P. H. M. Budzelaar, W. A. Gal *J. Mol. Catal. A. Chem.* **2005**, *232*, 151–159. b) G. Zhang, B. L. Scott, S. Hanson, *Angew. Chem. Int. Ed.* **2012**, *51*, 12102-12106; *Angew. Chem.* **2012**, *124*, 12268-12272. c) M. R. Friedfeld, M. Shevlin, J. M. Hoyt, S. W. Krska, M. T. Tudge, P. J. Chirik, *Science* **2013**, *342*, 1076. d) R. P. Yu, J. M. Darmon, C. Milsmann, G. W. Margulieux, S. C. E. Stieber, S. DeBeer, P. J. Chirik, *J. Am. Chem. Soc* **2013**, *135*, 13168–13184. e) M. R. Friedfeld, G. W. Margulieux, B. A. Schäfer, P. J. Chirik, *J. Am. Chem. Soc.* **2014**, *136*, 13178–13181. f) M. R. Friedfeld, H. Zhong, R. T. Ruck, M. Shevlin, P. J. Chirik, *Science* **2018**, *360*, 888.

3.5 Supporting Information

3.5.1 General Procedures

All experiments were performed under an atmosphere of dry Argon (Argon 4.6, Linde) using standard Schlenk techniques or a MBraun UniLab Glovebox.

***Analytical Thin-Layer Chromatography*:** TLC was performed using aluminum plates with silica gel and fluorescent indicator (Macherey-Nagel, 60, UV_{254}). Thin layer chromatography plates were visualized by exposure to UV light (366 or 254 nm).

Chemicals and Solvents: Solvents were dried and degassed with an MBraun SPS800 solvent-purification system. THF, diehtylether were stored over molecular sieves (3 Å). *n*-hexane was stored over a potassium mirror. 1,2-dimethoxyethane was stirred over K/benzophenone, distilled and stored over molecular sieves (3 Å). Commercially available olefins, imines, and quinolines were purified by distillation (Kugelrohr) and in case of liquids dried over molecular sieves (3 Å). Amine-boranes (NH_3BH_3 (60 °C, 10^{-3} mbar, NMe_2HBH_3 (25 °C, 10^{-3} mbar), NMe_3BH_3 (25 °C, 10^{-3} mbar) were sublimed prior to use.

***Column Chromatography**:* Flash column chromatography with silica gel 60 from Sigma Aldrich (63 – 200 μm). Mixture of solvents used are described *vide infra*.

Elemental Analyses: CHN analyses were recorded by the analytical department of the University of Regensburg using a Micro Vario Cube (Elementar)

***ESI-MS*:** ESI-MS spectra were carried out by the analytical department of the University of Regensburg, Agilent Q-TOF 6540 UHD

High Pressure Reactor: Hydrogenation reactions were carried out in 160 and 300 mL high pressure reactors (ParrTM) in 4 mL glass vials. The reactors were loaded under argon, purged with argon, sealed and the internal pressure was adjusted. Hydrogen (99.9992%) was purchased from Linde.

NMR spectroscopy: ^{1}H, ^{2}H, $^{13}C\{^{1}H\}$, $^{11}B\{^{1}H\}$, and ^{11}B NMR spectra in solutions were recorded on Bruker Avance 300 (300 MHz) and BrukerAvance 400 (400 MHz) if not stated otherwise. These chemical shifts are given relative to solvents resonances in the tetramethylsilane scale (^{1}H, $^{13}C\{^{1}H\}$, ^{2}H (TMS-d_{12})) and 15% BF_3-OEt_2 scale ($^{11}B\{^{1}H\}$, ^{11}B). The following abbreviations

have been used for multiplicities: s = singlet, d = doublet, t = triplet, q = quartet, sept = septet, m = multiplet, dd = doublet of doublet, dt = doublet of triplet. Solid-state ^{11}B NMR spectra were recorded on an Infinity$_{plus}$ spectrometer (*Agilent*) operated at 7 Tesla, equipped with a 6 mm pencil CPMAS probe. The spectrum was indirectly referenced to $NaBH_4$ (–42.1 ppm)[1]

Fourier-Transformations-Infrared-Spectroscopy (FT-IR): Spectra were recorded on Agilent Cary 630 FTIR with ATR device. All spectra were recorded at room temperature. Wave numbers are given in cm^{-1}.

Gas chromatography with FID (GC-FID): Shimadzu GC2010plus. Carrier gas: H_2. Colum: Restek Rxi®, (30m x 0.25 mm x 0.25 μm) Carrier gas: H_2. Standard heating procedure: 50°C (2 min), 25°C/min → 280°C (5 min). HP6890 GC-System with injector 7683B and Agilent 7820A System. Column: HP-5, 19091J-413 (30 m × 0.32 mm × 0.25 μm), carrier gas: N_2. Calibration of substrates and products with internal standard *n*-pentadecane and analytically pure samples.

Gas chromatography with mass-selective detector (GC-MS): Agilent 7820A GC system, mass detector 5977B. Carrier gas: H_2. Column: HP-5MS (30m x 0.25 mm x 0.25 μm). Standard heating procedure: 50°C → 300°C. Agilent 6890N Network GC-System, mass detector 5975 MS. Column: HP-5MS (30m × 0.25 mm × 0.25 μm, 5% phenylmethylsiloxane, carrier gas: H_2. Standard heating procedure: 50 °C (2 min), 25 °C/min → 300 °C (5 min).

3.5.1 Synthesis of Starting Materials

3.4.1.1 Synthesis of Bis[*N,N'*-(2,6-diisopropylphenyl)imino]acenaphthene (^{Dipp}BIAN)

^{Dipp}BIAN was synthetized according to a protocol of *Fukuda* and co-workers.[2]

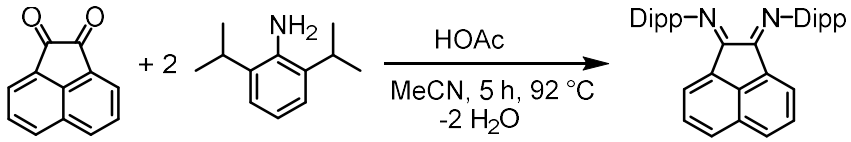

Acenaphthenequinone (7.5 g, 41.2 mmol, 1.0 equiv.) was suspended in 250 mL acetonitrile and heated to reflux for one hour. 65 mL of acetic acid was added to the suspension and reflux was continued for further 30 minutes. 2,6-diisopropylaniline (18.7 mL, 99.1 mmol, 2.7 equiv.) was added dropwise over 30 min. The reaction temperature was kept for additional 4.5 hours. Then the reaction mixture was cooled to room temperature. The crude product was obtained by filtration and washed with *n*-pentane (3 x 50 mL). The solid was dissolved in 300 mL chloroform and filtered. Evaporation of the solvent yielded ^{Dipp}BIAN as yellow-orange powder.

Formula: $C_{36}H_{40}N_2$ ($M = 500.73$ g mol^{-1})

Yield: 17.0 g (34.0 mmol, 83%)

^{1}H NMR (300.13 MHz, 300 K, $CDCl_3$) δ[ppm]: 7.88 (d, J = 8.3 Hz, 2H, CH_{BIAN}), 7.36 (t, J = 7.8 Hz, 2H, CH_{BIAN}), 7.27 (m, 6H, CH_{Dipp}), 6.63 (d, J = 7.2 Hz, 2H, CH_{BIAN}), 3.03 (sept, J = 6.8 Hz, 4H, $CH(CH_3)_2$), 1.23 (d, J = 6.8 Hz, 12H, $CH(CH_3)_2$), 0.97 (d, J = 6.8 Hz, 12H, $CH(CH_3)_2$).

3.4.1.2 Synthesis of Bis[*N,N'*-(2,4,6-trimethylphenyl)imino]acenaphthene (^{Mes}BIAN)

^{Mes}BIAN was synthesized according to a procedure of *Gasperini* and co-workers.[3]

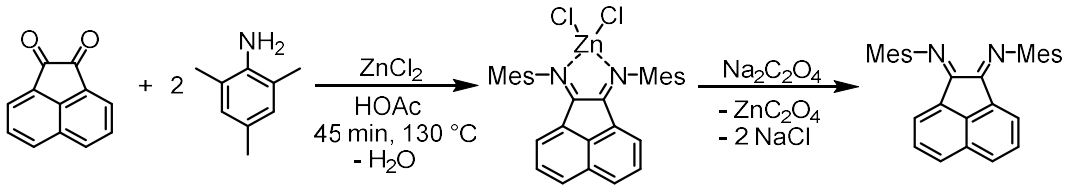

Acenaphthenquinone (5.5 g, 30.0 mmol, 1.0 equiv.) and dry zinc(II)-chloride (10.95 g, 80.3 mmol, 2.7 equiv.) were mixed in 85 mL acetonitrile and stirred for 10 minutes at 60 °C before 2,4,6-trimethylaniline (9.7 mL, 69.2 mmol, 2.3 equiv.) was added to the yellow suspension. The reaction mixture immediately turned orange and was heated to reflux for 45 min. The formed solid was filtered hot and washed with diethyl ether (3 x 50 mL). ^{Mes}BIAN-

$ZnCl_2$ was dried *in vacuo* and dissolved in 500 mL dichloromethane in a separating funnel. After addition of 150 mL saturated sodium oxalate solution, the mixture was shaken for five minutes until white zinc(II)-oxalate complex was formed. The organic phase was separated and dried over magnesium sulfate. After filtration, the solvent was evaporated and ^{Mes}BIAN was obtained as orange powder.

Formula: $C_{30}H_{28}N_2$ (M = 416.57 g mol^{-1})

Yield: 9.1 g (21.8 mmol, 73%)

^{1}H NMR (300.13 MHz, 300 K, $CDCl_3$) δ[ppm]: .89 (d, *J* = 8.2 Hz, 2H, CH_{BIAN}), 7.36 (dd, *J* = 8.2 Hz, 7.2 Hz, 2H, CH_{BIAN}), 6.97 (s, 4H, CH_{Ar}), 6.77 (d, *J* = 7.2 Hz, 2H, CH_{BIAN}), 2.38 (s, 6H, *p*-CH_3), 2.38 (s, 12H, *o*-CH_3)

3.4.1.3 Synthesis of [K(thf)$_{1.5}${(^{Dipp}BIAN)Co (η^4-cod)}]

[K(thf)$_{1.5}${(^{Dipp}BIAN)(Co(η^4-cod)}] was synthesized by a modified procedure from *Wolf* and co-workers.[4]

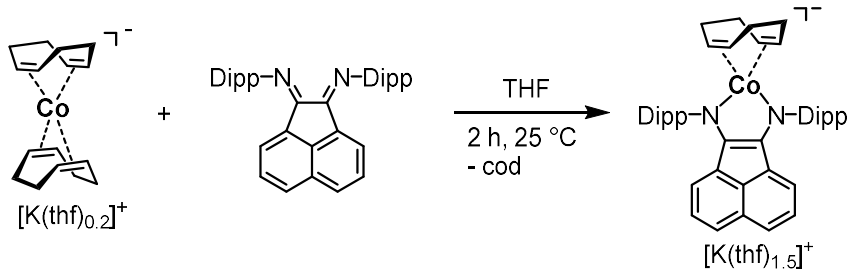

A solution of ^{Dipp}BIAN (2.0 g, 4.0 mmol, 1.0 equiv.) in 200 mL THF was added to a solution of [K(thf)$_{0.2}$Co(η^4-cod)$_2$] (1.3 g, 4.0 mmol, 1.0 equiv.) in 100 mL THF. An immediate color change to dark green was observed. After stirring the reaction mixture for two hours, the solvent was removed and the residue was washed with 100 mL *n*-hexane. The crude product was dissolved in 100 mL THF and filtered. The filtrate was concentrated and layered with *n*-hexane. Dark green crystals were obtained upon storing for one week (1.39 g, 42%). The crystals still contained 0.1 equiv. of *n*-hexane after drying the crystalline solid *in vacuo* according to ^{1}H NMR spectroscopy.

Formula: $C_{44}H_{52}N_2CoK$ $(C_4H_8O)_{1.5}$ $(C_6H_{14})_{0.1}$ (M = 823.7 g mol^{-1})

Yield: 1.39 g (1.68 mmol, 42%)

^{1}H NMR (300.13 MHz, 300 K, THF-d_8) δ[ppm]: 7.04 (overlapping m, 6H, CH_{Ar}), 6.28 (m, 2H, CH_{BIAN}), 6.18 (m, 2H, CH_{BIAN}), 4.88 (m, 2H, CH_{BIAN}), 4.50 (m, 4H, CH_{Dipp}), 2.91 (m, 4H, cod-CH), 2.34 (m, 4H, cod-CH_2), 1.37 (d,12H, CH_3), 1.09 (m, 4H, cod-CH_2), 0.95 (d, 12H, CH_3)

3.4.1.4 Synthesis of [K(thf)$_{1.5}${(^{Mes}BIAN)Co (η^4-cod)}]

[K(thf){(^{Mes}BIAN)Co(η^4-cod)}] was synthesized by a procedure according to *Wolf* and co-workers.[4]

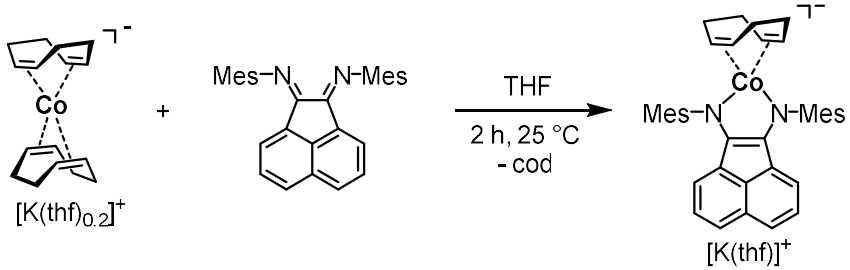

A solution of ^{Mes}BIAN (1.15 g, 2.8 mmol, 1.0 equiv.) in 200 mL THF was added to a solution of [K(thf)$_{0.2}${Co(η^4-cod)$_2$}] (0.9 g, 2.8 mmol, 1.0 equiv.) in 100 mL THF. An immediate color change to dark green was observed. After stirring the reaction mixture for two hours, the solvent was removed and the residue was washed with 100 mL *n*-hexane. The crude product was dissolved in 40 mL THF and filtered. The filtrate was concentrated and layered with *n*-hexane. Dark green crystals were isolated after storage at room temperature upon storing for one week (0.85 g, 43%). The crystals still contained 0.1 equiv. of *n*-hexane after drying the crystalline solid *in vacuo* according to ^{1}H NMR spectroscopy.

Formula: $C_{38}H_{40}N_2CoK$ (C_4H_8O) (C_6H_{14})$_{0.1}$ (M = 703.51 g mol^{-1})

Yield: 0.85 g (1.2 mmol, 43%)

^{1}H NMR (300.13 MHz, 300 K, THF-d_8) δ[ppm]: 6.08 (m, 4H, CH_{Ar}), 6.28 (m, 2H, CH_{BIAN}), 6.37 (m, 4H, CH_{BIAN}), 5.21 (m, 2H, CH_{BIAN}), 2.65 (m, 4H, cod-CH), 2.45 (m, 12H, *o*-CH_3), 2.33 (m, 4H, cod-CH_2), 2.25 (m, 6H, *p*-CH_3), 1.02 (m, 4H, cod-CH_2)

3.4.1.5 Synthesis of NH_2MeBH_3

N-Methylamine-borane was synthesized according to a procedure of *Fagnou* and co-workers.[5]

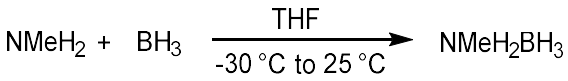

A solution of BH_3 (1 M in THF, 25.0 mL, 25 mmol) was added to a solution of methylamine (2 M in THF, 12.5 mL, 25 mmol) at –30 °C. The reaction mixture was warmed to room temperature and stirred overnight. The solvent was evaporated and the white residue dried *in vacuo*. Sublimation (45 °C, 10^{-3} mbar) afforded a white crystalline solid.

Formula: CH_8BN (M = 44.92 g mol^{-1})

Yield: 0.60 g (13.4 mmol, 54%)

^{1}H NMR (400.13 MHz, 300 K, THF-d_8) δ[ppm]: 4.47 (br s, 2H, NH_2), 2.28 (t, *J* = 6.0 Hz, CH_3), 1.43 (q, *J* = 96 Hz, BH_3)

^{11}B NMR (124.6 MHz, 300 K, THF-d_8) δ[ppm]: –16.2 (s, 1B)

^{11}B{^{1}H} NMR (124.6 MHz, 300 K, THF-d_8) δ[ppm]: –16.2 (q, $^1J_{BH}$= 96 Hz, 1B)

3.4.1.6 Synthesis of NEt_3BH_3

Ammonia-triethylborane was synthesized according to a procedure of *Guan* and co-workers.[6]

$$NH_3 + BEt_3 \xrightarrow[\text{-80 °C to 25 °C}]{\text{THF}} NH_3BEt_3$$

A solution of triethylborane (1 M in THF, 8 mL, 8 mmol) was added to a solution of ammonia (1 M in THF, 8 mL, 8 mmol) at –80 °C. The reaction mixture was warmed up to room temperature and stirred further for two hours. The solvent was evaporated and a colorless oil was obtained.

Formula: $C_6H_{18}BN$ (M = 115.03 g mol^{-1})

Yield: 0.18 g (1.6 mmol, 20%)

^{1}H NMR (400.13 MHz, 300 K, C_6D_6) δ[ppm]: 1.00 (br s, 3H, NH_3), 0.89 (t, *J* = 7.8 Hz, 9H, CH_3), 0.27 (q, *J* = 7.8 Hz, 6H, CH_2)

^{11}B NMR (93.4 MHz, 300 K, C_6D_6) δ[ppm]: –4.1 (s, 1B)

3.4.1.7 Synthesis of ND_3BH_3

N-deuterated ammonia borane (ND_3BH_3) was synthesized according to a procedure of *Baker* and co-workers.[7]

$$NH_3BH_3 \xrightarrow[\text{4 h, 25 °C}]{CD_3OD} ND_3BH_3$$

Ammonia borane (153 mg, 4.96 mmol) was stirred four hours in 10 mL CD_3OD. After evaporation of the solvent, the residue was dried *in vacuo*. The purity of the compound was ascertained by multinuclear NMR spectroscopy (^1H, ^2H, ^{11}B, and $^{11}B\{^1H\}$ NMR). The deuterium content was determined by ^1H NMR spectroscopy using the integrals of residual N**H**$_3$BH_3 (0.23) and comparing this with the integral of N(D/H)$_3$B**H**$_3$ (2.85).

Calculation: 1-(0.23/2.85) = 0.92 = 92% D-content.

Formula: BH_3D_3N ($M = 33.88$ g mol^{-1})

Yield: 0.12 g (3.5 mmol, 71%)

^1H NMR (400.13 MHz, 300 K, THF-d$_8$) δ[ppm]: 1.40 (q, $^1J_{BH}$ = 95 Hz, 3H)

^2H NMR (61.4 MHz, 300 K, THF-d$_8$) δ[ppm]: 3.73 (br s, ND_3)

$^{11}B\{^1H\}$ NMR (124.6 MHz, 300 K, THF-d$_8$) δ[ppm]: –22.4 (q, $^1J_{BH}$ = 95 Hz, 1B)

^{11}B NMR (124.6 MHz, 300 K, THF-d$_8$) δ[ppm]: –22.4 (s, 1B)

3.4.1.8 Synthesis of NH_3BD_3

B-deuterated ammonia borane (NH_3BD_3) was prepared according a procedure of *Ramachandran* and co-workers.[8]

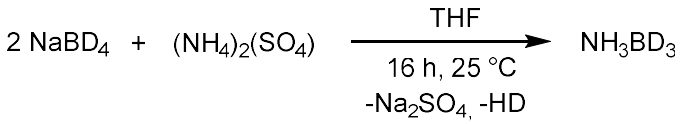

$NaBD_4$ (98%-D-content (abcr), 1.0 g, 23.8 mmol, 1.0 equiv.) and ammonium sulfate (3.2 g, 24.2 mmol, 1.02 equiv.) were mixed as solids and dissolved in THF (200 mL). The solution was stirred for 16 h at 40 °C. After cooling to room temperature, the suspension was filtered and the solvent evaporated. Sublimation (60 °C, 10^{-3} mbar) afforded a white solid. The deuterium content was determined by ^1H NMR spectroscopy using the integrals of residual NH_3B**H**$_3$ (0.38) and N**H**$_3BD_3$ (3.0). Calculation: 1–(0.38/3.0) = 0.87 = 87% NH_3BD_3.

Formula: BH_3D_3N ($M = 33.88$ g mol^{-1})

Yield: 0.30 g (8.9 mmol, 37%)

^1H NMR (400.13 MHz, 300 K, THF-d$_8$) δ[ppm]: 3.95 (m, 3H, NH_3)

^2H NMR (61.4 MHz, 300 K, THF-d$_8$) δ[ppm]: 1.22 (m, BD_3)

^{11}B NMR (126.4 MHz, 300 K, THF-d$_8$) δ[ppm]: –22.6 (s, 1B)

$^{11}B\{^1H\}$ NMR (126.4 MHz, 300 K, THF-d_8) δ[ppm]: –22.5 (s, 1B)

3.4.1.9 Synthesis of ND_3BD_3

Fully deuterated ammonia borane (ND_3BD_3) was synthesized analogously to ND_3BH_3.[7]

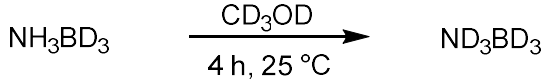

NH_3BD_3 (145 mg, 4.3 mmol, 87%-D-content) was dissolved in 10 mL CD_3OD and stirred for four hours. After evaporation of the solvent the residue was dried *in vacuo*. The purity of the compound was confirmed by multinuclear NMR-spectroscopy (^1H, ^2H, ^{11}B, and $^{11}B\{^1H\}$ NMR). The deuterium content was determined by ^1H NMR spectroscopy using the integral of residual N**H**$_3$B(H/D)$_3$ (1.0), Figure S5 and the integral of N**H**$_3$B(H/D)$_3$ (0.03, Figure S5).

Calculation: [(1–0.1/3) · 0.87] = 0.84 = 84% ND_3BD_3.

Formula: BD_6N (M = 36.90 g mol^{-1})

Yield: 0.30 g (8.9 mmol, 37%)

^1H NMR (400.13 MHz, 300 K, THF-d_8) δ[ppm]: 3.95 (m, 3H, NH_3)

^2H NMR (400.13 MHz, 300 K, THF-d_8) δ[ppm]: 3.73 (br s, ND_3), 1.22 (m, BD_3)

^{11}B NMR (124.6 MHz, 300 K, THF-d_8) δ[ppm]: –22.6 (s, 1B)

$^{11}B\{^1H\}$ NMR (124.6 MHz, 300 K, THF-d_8) δ[ppm]: –22.5 (s, 1B)

3.4.1.10 Synthesis of Poisoning Agents

Mercury (Hg) and trimethylphosphite were received commercially. Trimethylphosphite was distilled prior to use. Both liquids were deaerated by three freeze-pump-thaw cycles. Dibenzo[*a*,*e*]cyclooctatetraene was synthesized in three steps according to procedures of *Wudl* and co-workers,[9] and *Hartwig* and co-workers(step 2 and 3).[10]

Step 1:

5-Dibenzosuberenone (2.91 g, 14.1 mmol, 1.0 equiv.) was dissolved in 20 mL DCM in a 2-necked flask containing a nitrogen bubbler and a dropping funnel. Boron trifluoride etherate complex (2.67 mL, 21.0 mmol, 1.5 equiv.) was added at –10 °C to the solution, which led to an immediate color change to yellow. Trimethylsilyldiazomethane (2.0 M in diethylether, 105 mL, 21.0 mmol, 1.5 equiv.) was dissolved in DCM (25 mL) and added dropwise over 1 h at –10 °C. The reaction mixture was stirred for additional 2 h at –10 °C. The mixture was poured into ice and the organic phase was separated. The aqueous phase was extracted twice with DCM (100 mL) and the organic phases were combined. After washing with brine (80 mL), the organic phase was dried over $MgSO_4$. The solvent was evaporated and a yellow oil was obtained. The crude product was purified by column chromatography (SiO_2 (20 cm); *n*-hexane/ethylacetate 10:1; $R_f = 0.4$). 6*H*-Dibenzo[*a*,*e*]cyclooctatrien-5-on was obtained as white to light yellow solid.

Formula: $C_6H_{12}O$ (M = 220.27 g mol^{-1})

Yield: 1.60 g (7.3 mmol, 52%)

^{1}H NMR (300.13 MHz, 300 K, $CDCl_3$) δ[ppm]: 78.29 (dd, *J* = 8.0 Hz, 1.0 Hz, 1H), 7.53-7.20 (m, 7H, CH_{Ar}), 7.05 (d, *J* = 2.8 Hz, 2H), CH_{alkene}), 4.08 (s, 2H, CH_2)

Step 2:

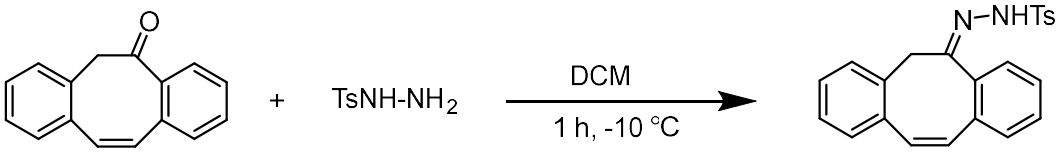

6*H*-Dibenzo[*a*,*e*]cyclooctatrien-5-on (0.55 g, 2.4 mmol, 1.0 equiv.) and tosylhydrazine (0.49 g, 2.6 mmol, 1.1 equiv.) were dissolved in ethanol (15 mL). After addition of three drops of concentrated hydrochloric acid, the suspension was stirred for 22 h. A white solid was received after filtration and dried *in vacuo*. This compound was used in the next step without further purification and analysis.

Formula: $C_{23}H_{12}N_2O_2S$ (M = 388.49 g mol^{-1})

Yield: 0.74 g (7.3 mmol, 80%)

Step 3:

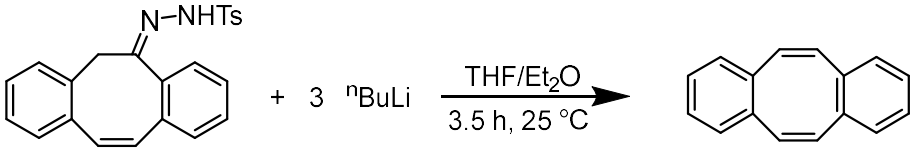

The corresponding hydrazone (1.5 g, 3.9 mmol, 1.0 equiv.) was suspended in a mixture of THF/Et_2O (100 mL, 1:3). ^{n}Butyllithium (2.5 M in hexane; 4.6 mL, 11.6 mmol, 3.0 equiv.) was added dropwise. The reaction mixture turned red and was stirred for 3.5 h (product formation was checked via TLC). A saturated solution of ammonium chloride (15 mL) was added to the solution, which lead to a yellow solution. After phase separation, the aqueous phase was washed with ethylacetate (2x15 mL). The organic phases were combined and dried over Na_2SO_4. A yellow oil was obtained after evaporation of the solvent. The crude product was purified by column chromatography (SiO_2 (20 cm); *n*-hexane; R_f = 0.25). Dibenzo[*a*,*e*]cyclo-octatetraene was obtained as a white solid.

Formula: $C_{16}H_{12}$ ($M = 204.27$ g mol^{-1})

Yield: 380 mg (1.9 mmol, 49%)

^{1}H NMR (300.13 MHz, 300 K, $CDCl_3$) δ[ppm]: 7.17 (m, 4H, CH_{Ar}), 7.08 (m, 1H, CH_{Ar}). 6.77 (s, 1H, CH_{alkene})

3.5.2 Dehydrogenation Reactions

Gas evolution measurements: Gas evolution measurements were done with *Man on the Moon X103*® kit (supplied by Man on the moon Tech, University of Zaragoza, Facultad de Ciencias, C/Pedro Cerbuna 12, 50009 – Zaragoza, Spain; http://www.manonthemoontech.com/). The volume of the reaction apparatus was determined by protic hydrolysis of different amounts of zinc. Evolved hydrogen in mmol was calculated using ideal gas law. Every reaction was done under inert atmosphere.

Figure S1. *Man on the Moon* apparatus for dehydrogenation reactions.

Every 0.3s a datapoint (time, pressure) was generated. Curves were smoothed manually.
In amine-borane dehydrogenation experiments a solution of the catalyst in THF (0.5 mL) was added with a syringe first. The pressure inside the reaction vessel was set to 0 mbar before a solution of amine-borane (0.2 mmol) in THF (0.5 mL) was added with a syringe. The resulting pressure was recorded over time.

1) Dimethylamine-borane (NMe_2HBH_3)

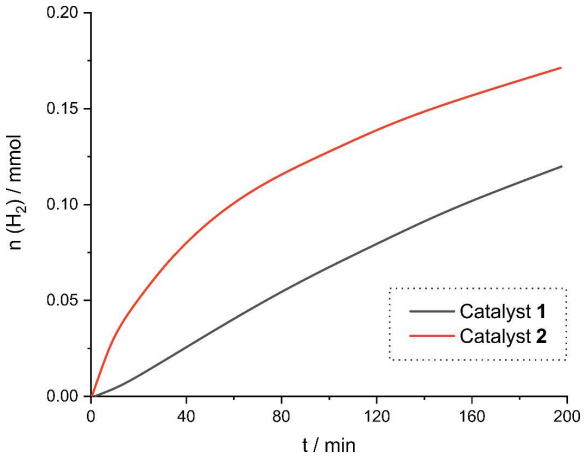

Figure S2. Time-dependent formation of hydrogenation from the dehydrogenation of dimethylamine-borane (200 mM) with catalysts **1** (10 mM, black curve) and **2** (10 mM, red curve).

2) Methylamine-borane ($NMeH_2BH_3$)

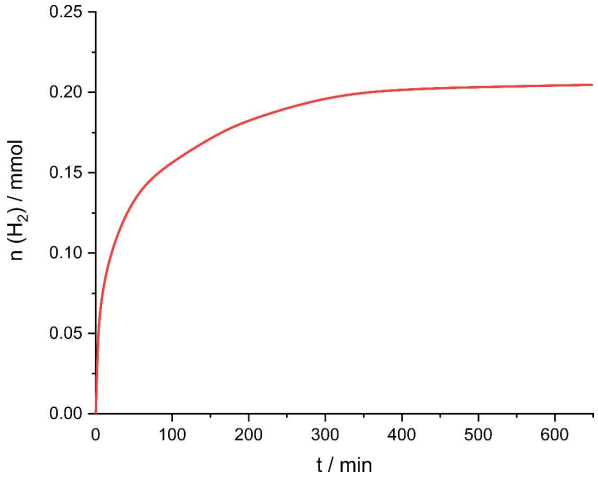

Figure S3. Time-dependent formation of hydrogenation from the dehydrogenation of methylamine-borane (200 mM) with catalyst **1**.

3) Ammonia borane(NH_3BH_3)

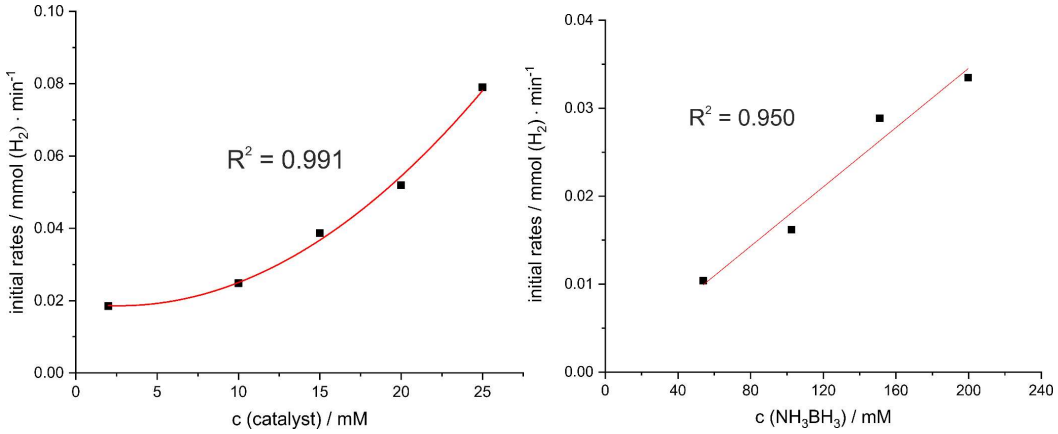

Figure S4. Initial rates of hydrogenation formation from dehydrogenation of ammonia borane(200 mM) vs. catalyst **1** concentration (left) and initial rates of H_2 formation from dehydrogenation of ammonia borane catalyzed by **1** (10 mM) vs. ammonia borane concentration (right).

NMR analysis

Kinetic analysis of NMe_2HBH_3 dehydrogenation

^{11}B NMR spectra for the kinetic analysis of the dehydrogenation of dimethylamine-borane were recorded with a *Bruker 500 MHz Ascend* NMR spectrometer with a *Prodigy CryoProbe*. In an argon-filled glovebox dimethylamine-borane was dissolved in 2,5 mL THF and added dropwise to a solution of the catalyst in 2.5 mL THF. The reaction mixture was stirred at room

temperature. After defined times an aliquot of 0.2 mL was taken, and diluted with 0.4 mL THF, and subsequently analyzed by NMR spectroscopy.

Dehydrogenation of $N^iPr_2HBH_3$

Catalyst **1** (9.7 mg, 0.012 mmol) was dissolved in 0.2 mL THF and $N^iPr_2HBH_3$ (27.0 mg, 0.23 mmol) in 0.5 mL THF. The amine-borane solution was added to the catalyst. The solution was stirred for 72 h at room temperature and after addition of a few drops C_6D_6 transferred in a quartz NMR tube and analyzed by ^{11}B NMR spectroscopy.

Dehydrogenation of $NMeH_2BH_3$

Catalyst **1** (8.2 mg, 0.01 mmol) was dissolved in 0.2 mL THF and $NMeH_2BH_3$ (9.0 mg, 0.2 mmol) in 0.6 mL THF. The amine-borane solution was added to the catalyst. The solution was stirred for 30 h at room temperature and after addition of a few drops C_6D_6 transferred in a quartz NMR tube and analyzed by ^{11}B NMR spectroscopy.

Dehydrogenation of NH_3BH_3

Catalyst **1** (13.3 mg, 0.016 mmol) was dissolved in 0.3 mL THF and NH_3BH_3 (9.6 mg, 0.31 mmol) in 0.3 mL THF. NH_3BH_3 was added to the catalyst. The solution turned dark and was stirred for 40 min. After addition of a few drops of C_6D_6, the reaction mixture was analyzed by ^{11}B NMR spectroscopy. The signals were assigned based on the work of *Schneider* and co-workers.[11]

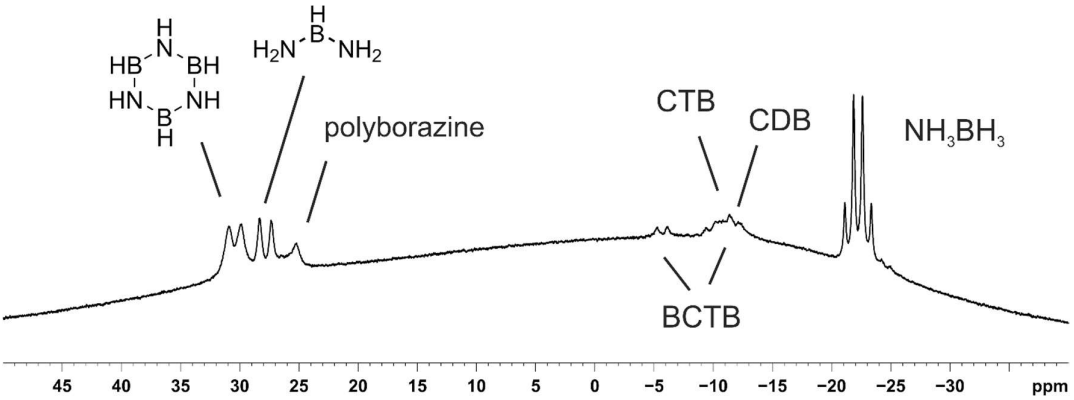

Figure S5. ^{11}B NMR spectrum of NH_3BH_3 dehydrogenation catalyzed by **1** after 40 min (CTB = cyclotriaminoborane, CDB = cyclodiaminoborane, BCTB = H_3NBHNH_2-cyclo-$B_3N_3H_{11}$).

Catalyst **1** (13.8 mg, 0.017 mmol) was dissolved in 0.3 mL THF and NH_3BH_3 (10.6 mg, 0.34 mmol) in 0.3 mL THF. NH_3BH_3 was added to the catalyst. The solution turned dark and

was stirred for 24 h. After addition of a few drops C_6D_6, the reaction mixture was analyzed by ^{11}B NMR spectroscopy.

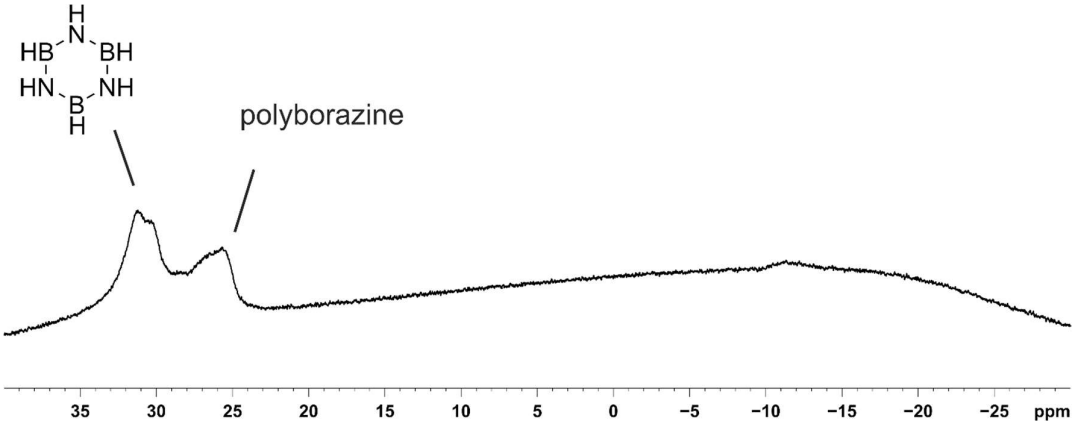

Figure S6. ^{11}B NMR spectrum of NH_3BH_3 dehydrogenation catalyzed by **1** after 24 h.

Isolation of Polyaminoborane from NH_3BH_3 dehydrogenation

NH_3BH_3 (76.5 mg, 2.5 mmol) in 5 mL THF was added to catalyst **1** $[K(Et_2O)_{0.1}\{(^{Dipp}BIAN)Co(cod)\}]$ (96.5 mg, 0.12 mmol) in 5 mL THF. During the reaction, the flask was depressurized briefly by opening the schlenk tube for a moment. After 24 h, the reaction was filtered and the black residue washed with THF, *n*-hexane, and DME. Addition of aqueous HCl led to a color change to white. The white residue (25 mg) was washed several times with Et_2O and dried *in vacuo*. The resulting powder was analyzed by IR-spectroscopy and ^{11}B MAS.

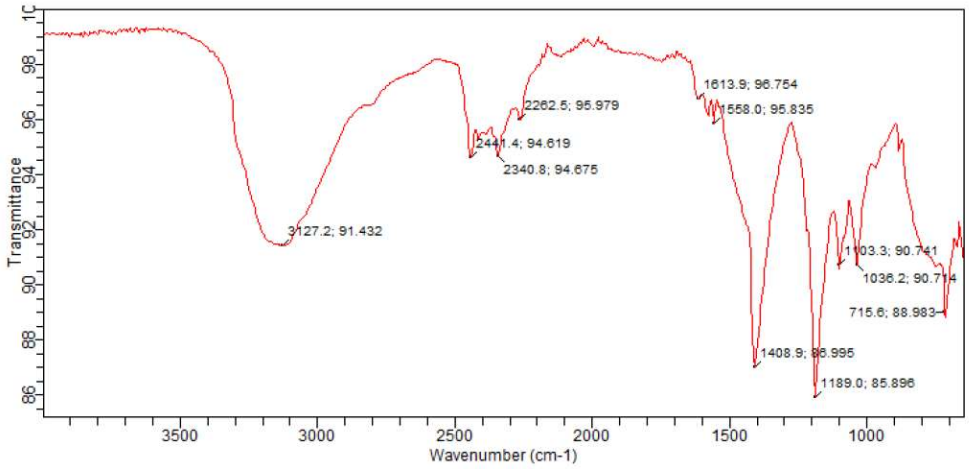

Figure S7. IR-spectra of obtained polyaminoborane.

ESI-MS analysis of $NMeH_2BH_3$ dehydrogenation

Catalyst **1** (8.2 mg, 0.01 mmol) was dissolved in 0.2 mL DME and $NMeH_2BH_3$ (9.0 mg, 0.2 mmol) in 0.6 mL DME. The amine-borane solution was added to the catalyst. The solution was stirred for 24 h at room temperature. After that the solution was filtered two times, diluted with DME, and subsequently analyzed by ESI-MS.

Units of $[-BH_2\text{-}NHMe-]_n$ from n=4 to n=11 can be observed (negative fragmentator potential -120 V). Using a positive fragmentator potential (120 V), ^{Dipp}BIAN (exact mass = 500.32 Da) could be identified as the main species. Addition of formic acid led to the observation of oligomer peaks (Δ m/z = 43).

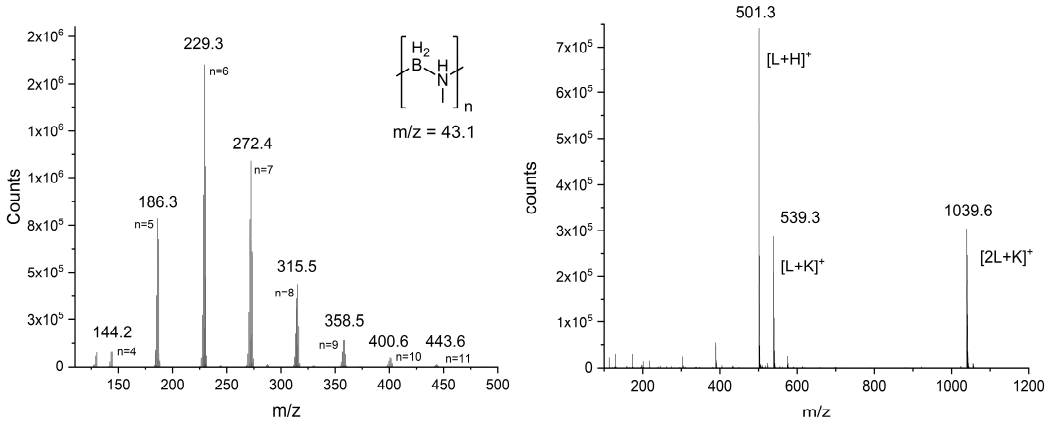

Figure S8. ESI-Scan (rt: 0.445-0.669 min, 28 scans) Frag=-120.0V (left). and ESI-Scan (retention time: 0.907-1.389 min, 59 scans) Frag=+120.0V; L=ligand ^{Dipp}BIAN (exact mass = 500.32 Da), K = potassium (right).

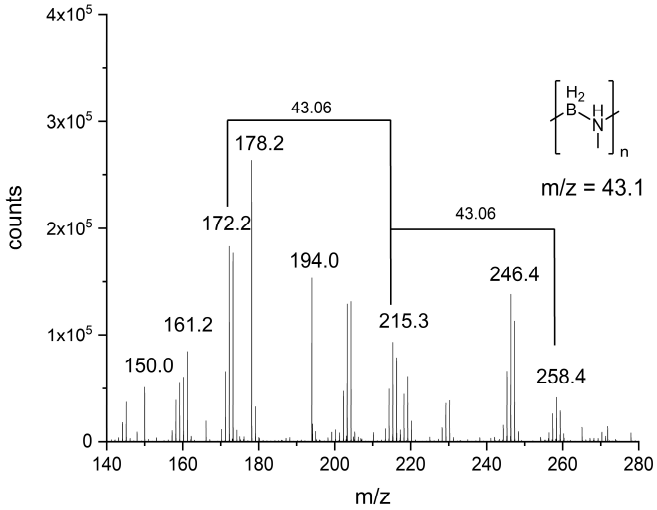

Figure S9. ESI-Scan (rt: 0.188-0.536 min, 22 scans) Frag=+120.0V, add. of 0.1% HCOOH.

Reaction of NMe_3BH_3 with catalyst 1 [K(thf)$_{1.5}${(^{Dipp}BIAN)Co(η^4-cod)}]

Catalyst **1** (12.4 mg, 0.015 mmol) in 0.5 mL THF was added to NMe_3BH_3 (21.9 mg, 0.3 mmol) in 0.3 mL THF. No color change was observed. After stirring for 19 h, and addition of a few drops C_6D_6, the reaction mixture was analyzed by ^{11}B NMR spectroscopy.

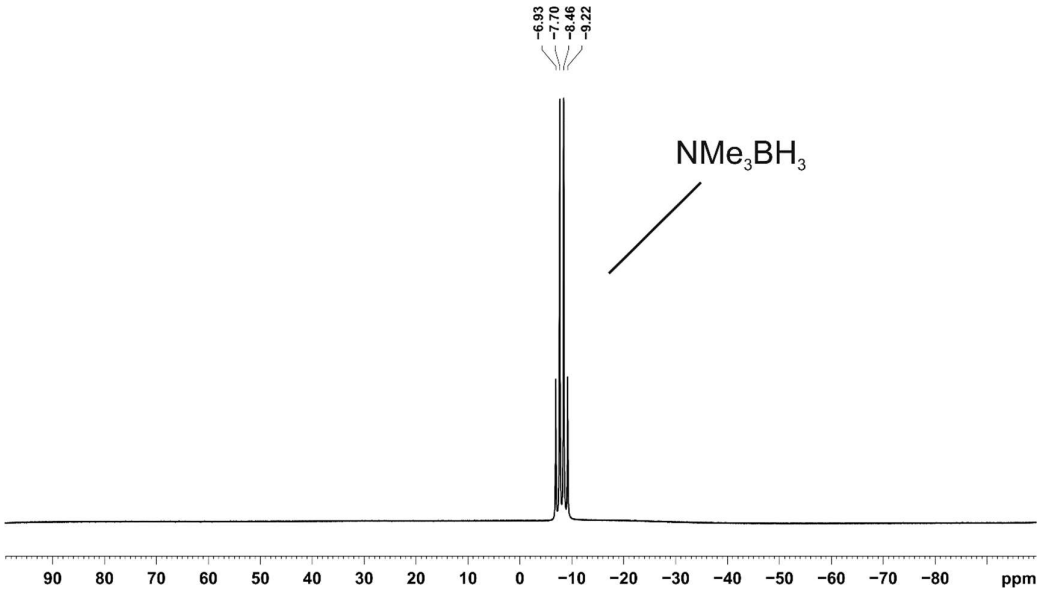

Figure S10. ^{11}B NMR spectrum of a reaction mixture of NMe_3BH_3 and **1**.

Reaction of NH_3BEt_3 with catalyst 1 [K(thf)$_{1.5}${(^{Dipp}BIAN)Co(η^4-cod)}]

Catalyst **1** (6.2 mg, 0.008 mmol) in 0.3 mL THF was added to NH_3BEt_3 (15.2 mg, 0.13 mmol) in 0.3 mL THF. The reaction mixture slightly brownish and was stirred for further 20 h. After addition of a few drops C_6D_6, the solution was analyzed by ^{11}B NMR spectroscopy.

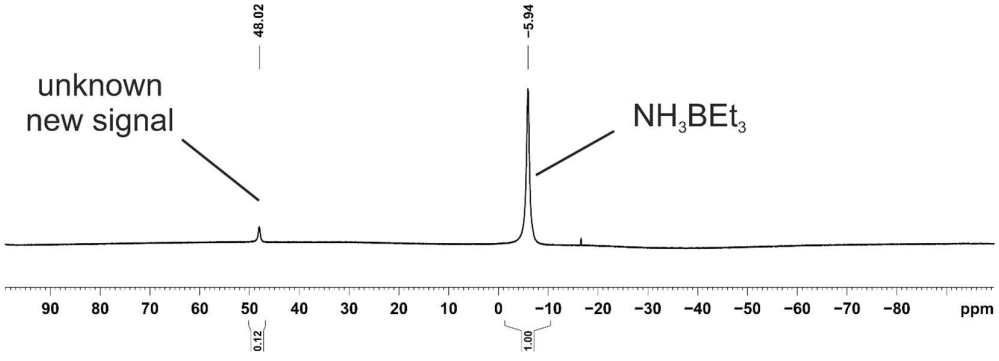

Figure S11. ^{11}B NMR spectrum of a reaction mixture of NH_3BEt_3 and **1**.

Dehydrogenation cross experiment with NH_3BEt_3 and NMe_3BH_3

Catalyst **1** (12.4 mg, 0.015 mmol) in 0.5 mL THF was added to a solution of NMe_3BH_3 (22.1 mg, 0.3 mmol) and NH_3BEt_3 (39.0 mg, 0.34 mmol) in 0.3 mL THF. The color of the reaction turned

slightly lighter. The mixture was stirred for 19 h. After addition of a few drops C_6D_6, the solution was analyzed by ^{11}B NMR spectroscopy.

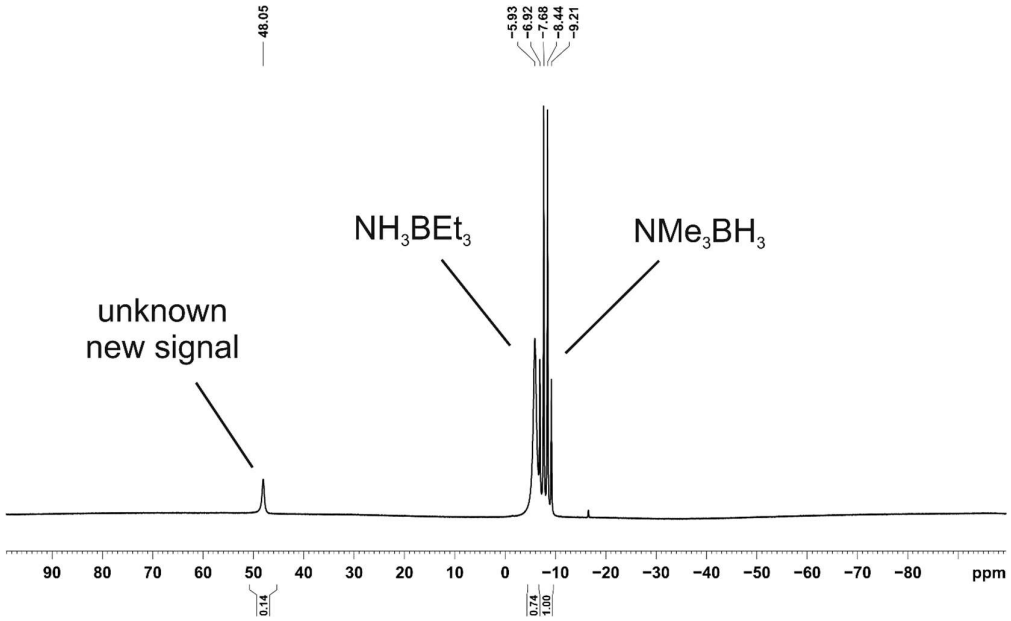

Figure S12. ^{11}B NMR spectrum of a reaction mixture of NMe_3BH_3, NH_3BEt_3 and **1**.

3.5.3 Transferhydrogenation Reactions

General procedure

Under an atmosphere of argon, a 5 mL screw cap vial with a PTFE septum and magnetic stir bar was charged with the catalyst (n = 0.01 mmol) in THF (0.5 mL), *n*-pentadecane (20 μL) as internal standard, and the substrate (n = 0.2 mmol). The ammonia borane solution (n = 0.2 mmol) in THF (0.5 mL) was added with a syringe through the septum. After a certain reaction time, the reaction was quenched with saturated aqueous NH_4Cl or $NaHCO_3$ (in case of imines or quinolines). The mixture was extracted with ethyl acetate and the combined organic layers were dried (Na_2SO_4) and filtered over a pad of silica. The pad of silica was washed with ethyl acetate for one time. The reaction mixture was analyzed by quantitative GC-FID analysis.

Some representative products (0.4 mmol, 2-fold approach) were isolated, in particular 1,2,3,4-tetrahydroquinolines. After the reaction, the solution was quenched with saturated aqueous $NaHCO_3$. The crude product was purified by column chromatography (SiO_2).

Optimization of Reaction Conditions

Table S1. Optimization of NH_3BH_3 dehydrogenation by modifying different parameters (catalyst, concentration, solvent, time).

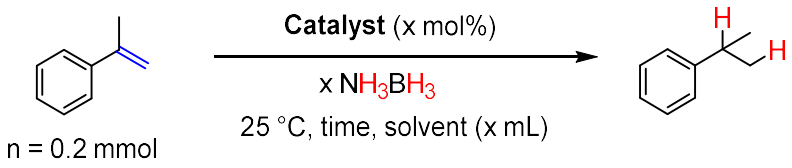

Entry	Catalyst / mol%	NH_3BH_3 / equiv.	Time / h	Solvent / mL	Yield (Conversion) / %
1	**1** (5)	0.4	16	THF (1)	57 (71)
2	**1** (5)	0.65	16	THF (1)	77 (89)
3	**1** (5)	1.0	16	THF (1)	91 (100)
4	**1** (5)	1.0	18	THF (1)	93 (100)*
5	**2** (5)	1.0	18	THF (1)	92 (100)*
6	**1** (5)	1.0	16	DME (1)	93 (100)
7	**1** (5)	1.5	16	THF (1)	84 (94)
8	**1** (5)	1.0	2	THF (1)	71 (76)
9	**1** (5)	1.0	4	THF (1)	77 (81)
10	**1** (5)	1.0	6	THF (1)	81 (86)
11	**1** (0.1)	1.0	16	THF (1)	2 (9)
12	**1** (1)	1.0	16	THF (1)	10 (19)
13	**1** (3)	1.0	16	THF (1)	36 (45)
14	**1** (5)	1.0	16	THF (0.5)	83 (90)
15	**1** (5)	1.0	16	THF (2)	81 (89)
16	-	1.0	16	THF (1)	0 (22)
17	**1** (5)	NMe_2HBH_3 1.0	16	THF (1)	58 (70)

* 0.34 mmol substrate

Isolated products of transfer hydrogenation

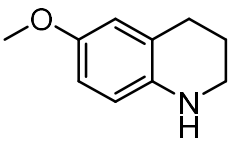

6-methoxy-1,2,3,4-tetrahydroquinoline

$C_{11}H_{15}NO$ 163.22 g mol^{-1}

slightly brownish liquid

Yield 58.4 mg (0.36 mmol, 90 %)

Solvent From Pent:EtOAc:NEt_3 (100:20:1) to Pent:EtOAc:NEt_3 (100:40:1)

^{1}H NMR	(400.13 MHz, 300 K, CD_2Cl_2) δ[ppm]: 6.57 (m, 2H_{Ar}), 6.41 (m, 1H_{Ar}), 3.71 (s, 3H, OCH_3), 3.64 (br s, 1H, NH), 3.24 (t, J = 5.6 Hz, 2H, CH_2), 2.75 (t, J = 6.5 Hz, 2H, CH_2), 1.91 (m, 2H, CH_2)
^{13}C{^{1}H} NMR	(101.4 MHz, 300 K, CD_2Cl_2) δ[ppm]: 152.1, 139.5, 123.1, 115.6, 115,1, 113.1, 56.0, 42.7, 27.6, 22.9
GC-MS	t_R = 9.80 min , (EI, 70 eV): *m*/*z* = 163 [M^+] , 148, 130, 118, 103, 91, 77, 65, 51

Analytical data were in full agreement with *Beller* and co-workers.[12]

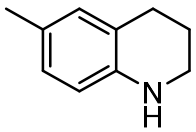

6-methyl-1,2,3,4-tetrahydroquinoline

$C_{10}H_{13}N$ 147.22 g mol^{-1}

slightly brownish liquid

Yield	50.8 mg (0.35 mmol, 86 %)
Solvent	Pent:EtOAc:NEt_3 (100:2:1)
^{1}H NMR	(400.13 MHz, 300 K, CD_2Cl_2) δ[ppm]: 6.71 (m, 2H_{Ar}), 6.37 (m, 1H_{Ar}), 3.70 (br s, 1H, NH), 3.27 (t, J = 5.6 Hz, 2H, CH_2), 2.73 (t, J = 6.4 Hz, 2H, CH_2), 2.02 (s, 3H, CH_3), 1.92 (m, 2H, CH_2)
^{13}C{^{1}H} NMR	(101.4 MHz, 300 K, CD_2Cl_2) δ[ppm]: 143.0 130.3, 127.5, 126.2, 121.8, 114.5, 42.5, 27.3. 22.9, 20.5
GC-MS	t_R = 8.54 min, (EI, 70 eV): *m*/*z* = 146 [M^+], 132, 117, 103, 91, 77, 65, 51

Analytical data were in full agreement with *Beller* and co-workers.[12]

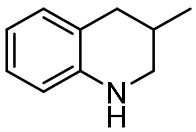

2-methyl-1,2,3,4-tetrahydroquinoline

$C_{10}H_{13}N$ 147.22 g mol^{-1}

slightly yellow liquid

Yield	44.9 mg (0.31 mmol, 76 %)
Solvent	Pent:EtOAc:Net_3 (100:1:1)
^{1}H NMR	(400.13 MHz, 300 K, CD_2Cl_2) δ[ppm]: 6.94 (m, 2H_{Ar}), 6.58 (m, 2H_{Ar}), 6.46 (m, 2H_{Ar}) 3.93 (br s, 1H, NH), 3.28 (dq, J = 11.1 Hz. 2.0 Hz, 1H, CH), 2.78 (m, 1H, CH_2), 2.45 (m, 1H, CH_2), 2.04 (m, 1H, CH_2) 1.07 (d, J = 6.6 Hz, 3H, CH_3)

$^{13}C\{^{1}H\}$ NMR	(101.4 MHz, 300 K, CD_2Cl_2) δ[ppm]: 145.0, 130.0, 127.0, 121.4, 117.0, 114.0, 49.2, 35.9, 27.7, 19.2
GC-MS	t_R = 7.98 min, (EI, 70 eV): *m*/*z* = 143 [M^+], 132, 115, 104, 89, 77, 71, 63, 51

Analytical data were in full agreement with *Beller* and co-workers.[12]

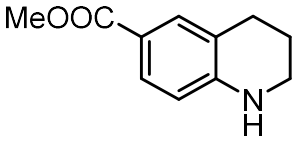

6-methylester-1,2,3,4-tetrahydroquinoline

$C_{11}H_{13}NO_2$ 191.23 g mol^{-1}

almost colorless liquid

Yield	57.0 mg (0.30 mmol, 75 %)
Solvent	From Pent:EtOAc:Net_3 (100:20:1) to EtOAc:Net_3 (100:1)
^{1}H NMR	(400.13 MHz, 300 K, CD_2Cl_2) δ[ppm]: 7.59 (m, $2H_{Ar}$), 6.40 (m, $1H_{Ar}$), 4.50 (br s, 1H, NH), 3.80 (s, 3H, $COOCH_3$), 3.33 (t, J = 5.6 Hz, 2H, CH_2), 2.76 (t, J = 6.3 Hz, 2H, CH_2), 1.90 (m, 2H, CH_2)
$^{13}C\{^{1}H\}$ NMR	(101.4 MHz, 300 K, CD_2Cl_2) δ[ppm]: 167.6, 149.4, 131.4, 129.3, 120.3, 117.5, 112.9, 51.6, 42.0, 27.3, 21.8
GC-MS	t_R = 12.25 min, (EI, 70 eV): *m*/*z* = 191 [M^+], 176, 160, 144, 132, 117, 104, 89, 77, 65, 51

Analytical data were in full agreement with *Beller* and co-workers.[12]

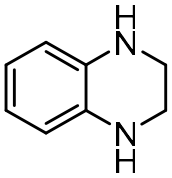

1,2,3,4-tetrahydroquinoxaline

$C_8H_{10}N_2$ 134.18 g mol^{-1}

slightly reddish liquid

Yield	47.8 mg (0.36 mmol, 90 %)
Solvent	From Pent:EtOAc:Net_3 (100:1:1) to EtOAc:Net_3 (100:1)
^{1}H NMR	400.13 MHz, 300 K, CD_2Cl_2) δ[ppm]: 6.50 (m, 4H, CH_{Ar}), 3.54 (br s, 2H, NH), 3.37 (s, 4H, CH_2)
$^{13}C\{^{1}H\}$ NMR	(101.4 MHz, 300 K, CD_2Cl_2) δ[ppm]: 134.2, 118.7, 114.7, 41.7
GC-MS	t_R = 9.12 min, (EI, 70 eV): *m*/*z* = 133 [M^+], 119, 104, 92, 77, 66, 51

Analytical data were in full agreement with *Beller* and co-workers[12]

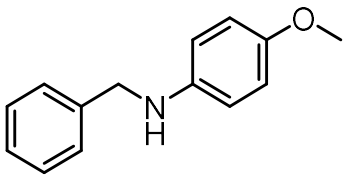

N-benzyl-4-methoxyaniline

$C_{14}H_{15}NO$ 213.28 g mol^{-1}

orange oil

Yield	74.7 mg (0.35 mmol, 88 %)
Solvent	Pent/EA: 95:5 to 90:5 (Alumina N)
^{1}H NMR	(300.13 MHz, 300 K, $CDCl_3$) δ[ppm]: 7.35 – 7.29 (m, 2H, CH_{Ar}), 7.24 – 7.15 (m, 2H, CH_{Ar}), 6.94 – 6.84 (m, 2H, CH_{Ar}), 6.78 – 6.70 (m, 1H, CH_{Ar}), 6.68 – 6.62 (m, 2H, CH_{Ar}), 4.27 (s, 2H, CH_2), 4.20 – 4.00 (br s, 1H, NH), 3.82 (s, 3H, CH_3).
^{13}C{^{1}H}-NMR	(75.5 MHz, 300 K, $CDCl_3$) δ[ppm]: 159.0, 148.2, 131.4, 129.4, 129.0, 117.7, 114.1, 113.0, 55.4, 48.0.
GC-MS	t_R = 10.12 min, (EI, 70 eV): *m*/*z* = 213.1

Analytical data were in full agreement with *Bhanage* and co-workers.[13]

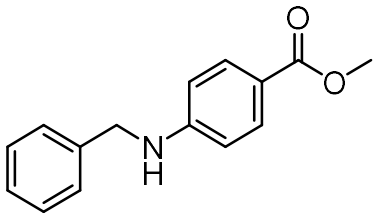

N-benzyl-4-methylesteraniline

$C_{15}H_{15}NO_2$ 241.29 g mol^{-1}

beige powder

Yield	52.3 mg (0.22 mmol, 55 %)
Solvent	Pent/EA: 95:5 to 90:5 (Alumina N).
^{1}H NMR	(300.13 MHz, 300 K, $CDCl_3$) δ[ppm]: 7.91 – 7.84 (m, 2H, CH_{Ar}), 7.40 – 7.28 (m, 5H, CH_{Ar}), 7.65 – 7.56 (m, 2H, CH_{Ar}), 5.20 – 4.60 (br s, 1H, NH), 4.39 (s, 2H, CH_2), 3.85 (s, 3H, CH_3).
GC-MS	t_R = 11.7 min, (EI, 70 eV): *m*/*z* = 241.1

Analytical data were in full agreement with *Yamaguchi* and co-workers.[14]

Monitoring Reaction Progress of TH (α-methylstyrene) with Catalyst 1

Under an atmosphere of argon, a 5 mL screw cap vial with a PTFE septum and magnetic stir bar was charged with catalyst **1** (20.5 mg, n = 0.05 mmol) in THF (2.5 mL), *n*-pentadecane (50 μL) as internal standard, and α-methylstyrene (65 μL, n = 0.5 mmol). The ammonia borane

solution (15.5 mg, n = 0.5 mmol) in THF (2.5 mL) was added with a syringe through the septum. After certain times, an aliquot (0.1 mL) was taken, quenched with saturated aqueous NH_4Cl, filtered over silica, and extracted with ethyl acetate. The sample was analyzed by GC-FID.

TH (α-methylstyrene) with catalyst 1 in a D_2 atmosphere

Under an atmosphere of deuterium gas (99.5% deuterium content, *Sigma-Aldrich*, 1.1 bar, 0.44 mmol), a 10 mL Schlenk flask with a magnetic stir bar was charged with catalyst **1** (8.2 mg, n = 0.01 mmol), α-methylstyrene (26 µL, n = 0.2 mmol) and C_6D_6 (8.3 µL, n = 0.094 mmol) in THF (0.5 mL). The ammonia borane solution (6.2 mg, n = 0.2 mmol) in THF (0.5 mL) was added with a syringe through the septum. After 5 minutes an aliquot (0.1 mL) was taken and analyzed by GC-MS. Subsequently, the septum was removed and the Schlenk flask closed with a glass stopper. After 16 h the reaction mixture was filtered in order to remove polyaminoborane. The solution was analyzed by ^2H NMR spectroscopy. Remaining solution (0.5 mL) was quenched with saturated aqueous NH_4Cl and the organic phase was extracted with ethyl acetate and dried over Na_2SO_4. The sample was analyzed by GC-MS. Deuterium signals of cumene-d_x were assigned according to *Jacobi von Wangelin* and co-workers.[15]

The amount of formed cumene-d (δ = 2.64 ppm) was calculated by comparing the integral with the internal standard C_6D_6 (0.094 mmol) added before starting the reaction.

<u>relative amount of deuterium incorporated into the methine position of the ^{i}Pr group of cumene:</u>

n (cumene-d) = 0.43*0.094 mmol = 0.04 mmol → 0.04 mmol/0.2 mmol = 20%

<u>relative amount of deuterium incorporated into the methyl position of the ^{i}Pr group of cumene:</u>

n (cumene-d) = 2.38*0.094 mmol / 6 = 0.037 mmol → 0.037 mmol / 0.2 mmol = 18%

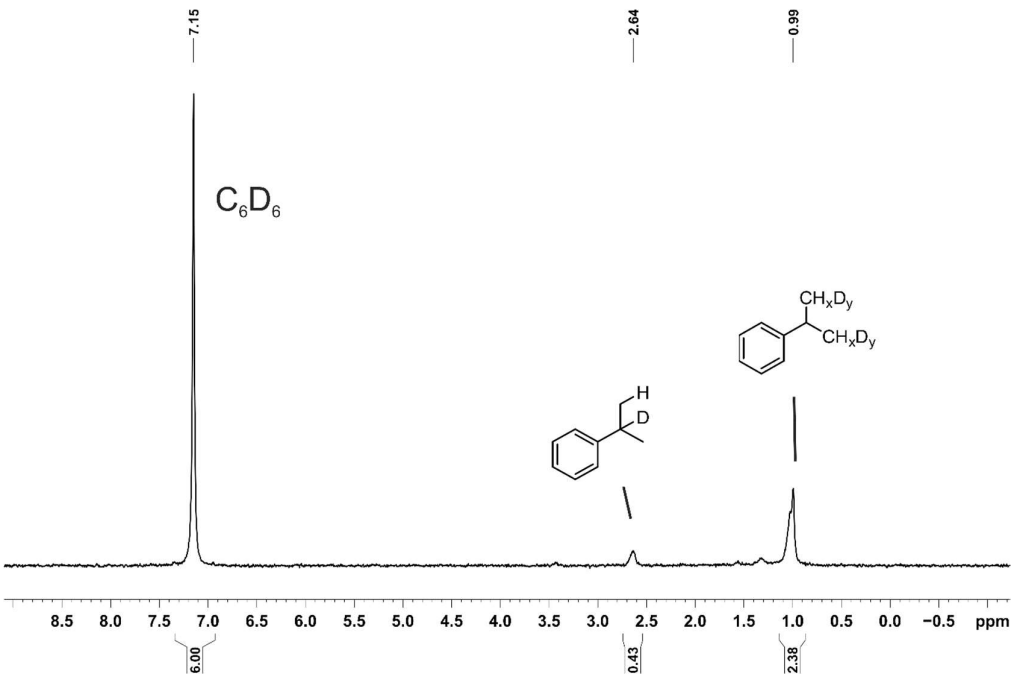

Figure S13. ^{2}H NMR spectrum (61.4 MHz, 300K, THF) of reaction mixture after 16 h.

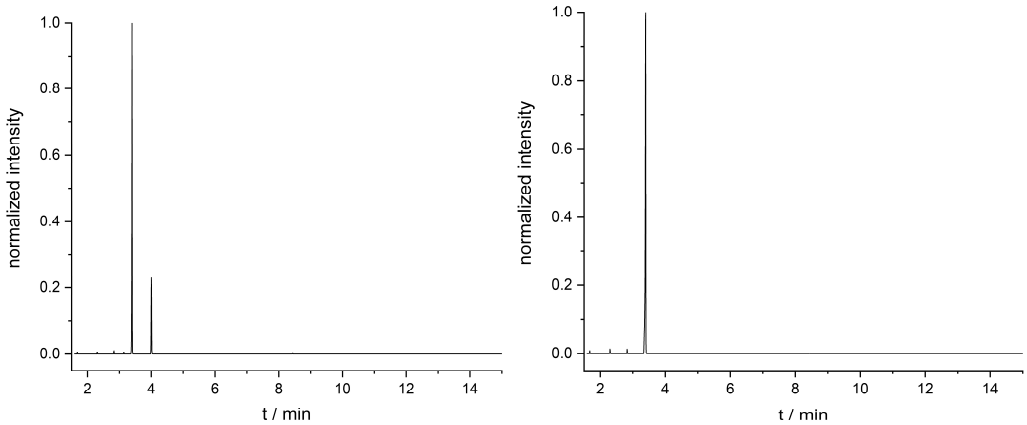

Figure S14. Chromatograms (GC-MS analysis) after 5 min (left) and 16 h (right); 3.39 min (cumene) and 4.00 min (α-methylstyrene).

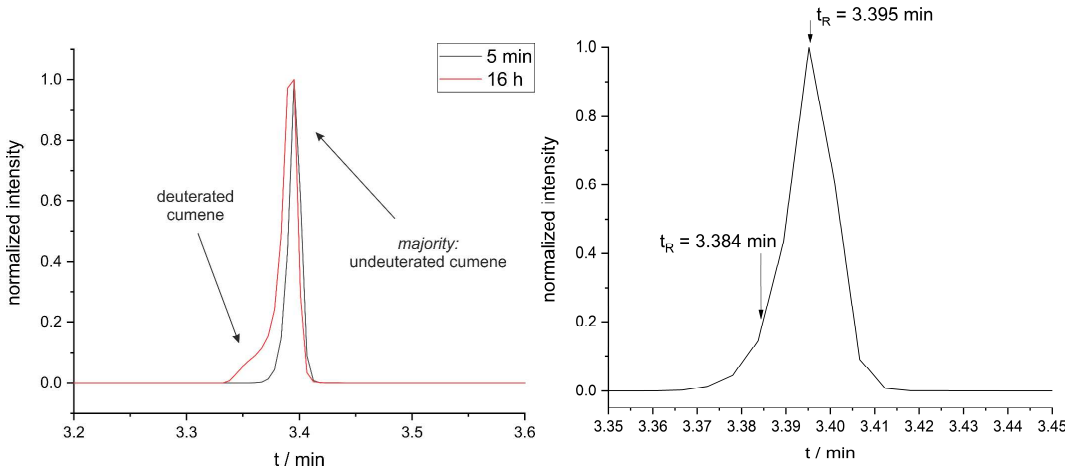

Figure S15. Comparison of cumene peaks in chromatograms after 5 min (black) and 16 h red (left) and zoom of chromatogram after 5 min

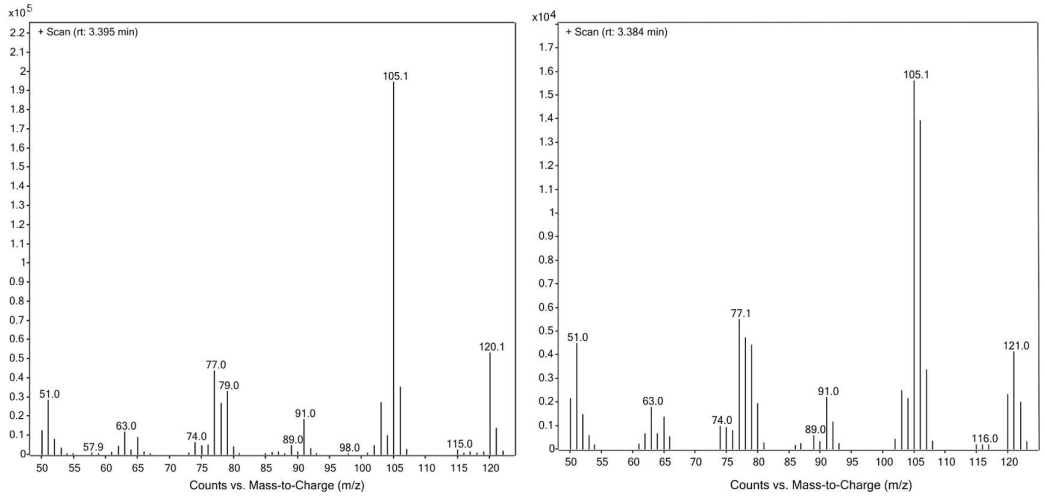

Figure S16. Zoom of chromatogram and m/z data of cumene peak (different retention times) after 5 min.

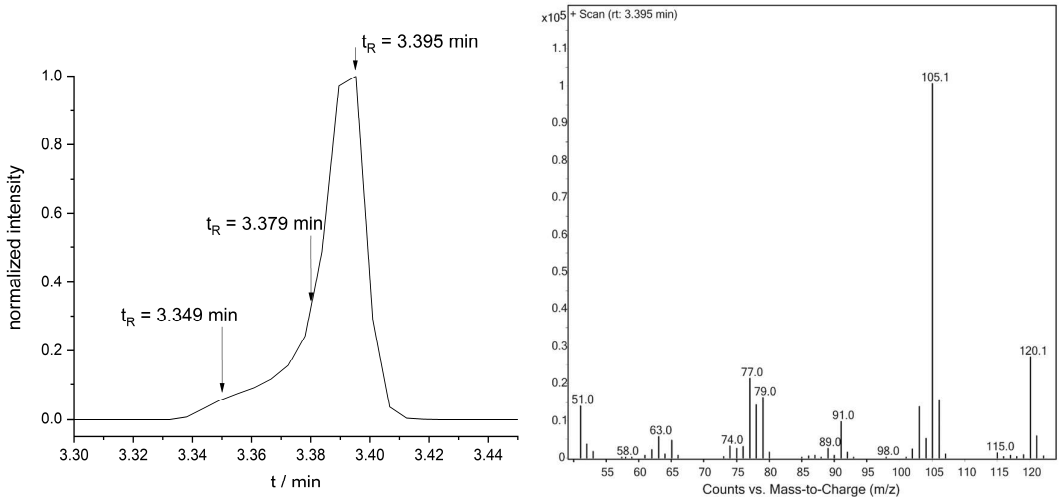

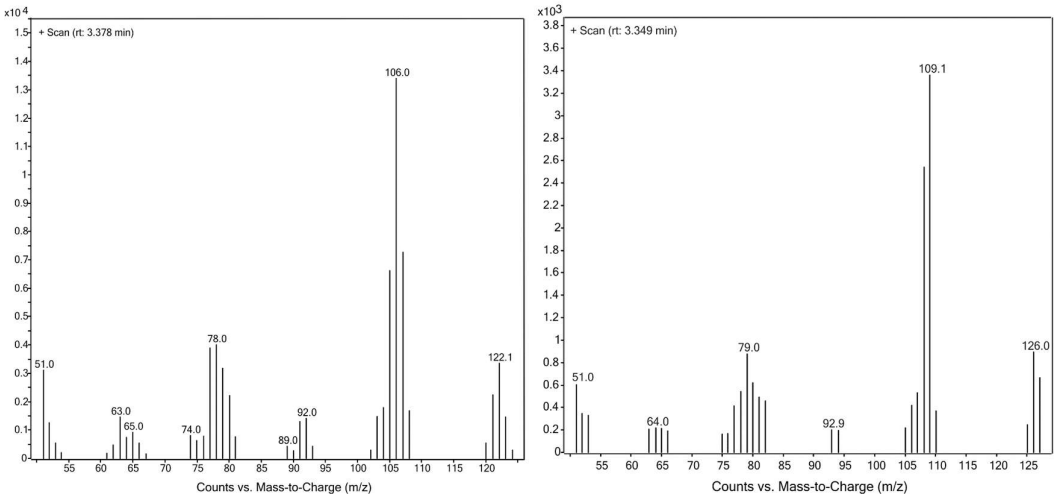

Figure S17. Zoom of chromatogram and m/z data of cumene peak (different retention times) after 16 h.

3.5.4 Hydrogenation Reactions

General procedure

In an argon-filled glovebox, a flame-dried 4 mL reaction vial was charged with the substrate (0.2 mmol), *n*-pentadecane (50 µL) as internal reference for GC-FID quantification and the catalyst (0.006 mmol) in THF (1 mL). A solution of NH_3BH_3 (0.06 mmol) in THF (1 mL) was added during which the color changed to dark violet and hydrogen evolution occurred. The reaction vial was transferred to a high-pressure reactor which was sealed and removed from the glovebox. The reactor was purged with H_2 (3 x 2 bar) and the reaction pressure and temperature were set. After the indicated reaction time, the vial was retrieved and the reaction mixture was hydrolyzed with a saturated aqueous solution of NH_4Cl (1 mL). The reaction mixture was extracted with ethyl acetate (3 x 1 mL), dried over Na_2SO_4 and analyzed by GC-FID and GC-MS. Procedure for substrates, which are not tolerated by the metalate (4-X-alpha-methylstyrene; X=Cl, Br, SMe): The substrate is added after addition of the NH_3BH_3 solution.

Optimization of Reaction Conditions

Table S2. Optimization of reaction conditions by modifying different parameters (catalyst, additive).

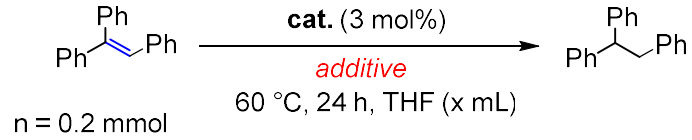

Entry	Catalyst / %	Additive / mol%	Yield (Conversion) / %
1	**1**	-	0 (13)
2	**2**	-	0 (11)
3	**1**	**NH_3BH_3 (30)**	**95** [a]
4	**2**	**NH_3BH_3 (30)**	**>99** [a]
5	**1**	NH_3BH_3 (60)	11 (23) [a]
6	**2**	NH_3BH_3 (60)	10 (19) [a]
7	**1**	NH_3BH_3 (15)	90 [a]
8	**1**	Me_2NHBH_3 (30)	52 (58)
9	**2**	**Me_2NHBH_3 (30)**	**92**
10	**1**	Me_2NHBH_3 (15)	15 (24)
11	**1**	NEt_3 (30)	0 (15)
12	**2**	NEt_3 (30)	1 (13)
13	**2**	Pyrrolidine (30)	1 (13)
14	**2**	Pyridine (30)	1 (14)
15	**2**	Piperidine (30)	0 (12)
16	**2**	BH_3.THF (30)	2 (52)
17	**2**	**NH_3BH_3 (30)**	**14 (27)** [b]

Conditions: 0.2 mmol (0.1 M) alkene in THF, 3 mol% catalyst, 20 bar bar H_2, 25 °C, 24 h. Yields (GC-FID vs. internal *n*-pentadecane); conversions in parentheses if <90%. [a] 10 bar; [b] 3 bar, 3 h.

Optimization of Reaction Conditions

Table S3 Hydrogenation of α-methylstyrene with catalyst **1** and **2** and different temperatures.

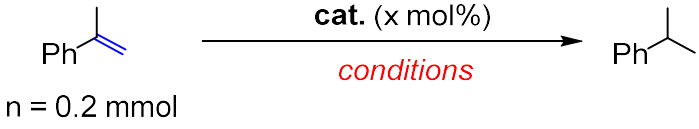

Entry	Catalyst / mol%	Conditions	Yield (Conversion) / %
1	**1** (3 mol%)	60 °C, 20 bar, 24 h	>99 (>99)
2	**2** (3 mol%)	60 °C, 20 bar, 24 h	39 (39)
3	**1** (5 mol%)	25 °C, 20 bar, 13 h	- (<5)
4	**2** (5 mol%)	25 °C, 20 bar, 13 h	- (<5)

Conditions: 0.2 mmol (0.1M) alkene in THF, 3 mol% catalyst. Yields (GC-FID vs. internal *n*-pentadecane); conversions in parentheses if <90%.

Note: The substitution / hydrogenation of 1,5-cyclooctadiene is presumably favored at elevated temperature, which might activate the catalyst precursor for the investigated

3.5.4 References

[1] S. Hayashi, K. Hayamizu, *Bull. Chem. Soc. Jpn.* **1989**, *62*, 2429–2430.

[2] A. Paulovicova, U. El-Ayaan, K. Shibayama, T. Morita, Y. Fukuda, *Eur. J. Inorg. Chem.* **2001**, *2001*, 2641–2646.

[3] M. Gasperini, F. Ragaini, S. Cenini, *Organometallics* **2002**, *21*, 2950–2957.

[4] S. Pelties, T. Maier, D. Herrmann, B. de Bruin, C. Rebreyend, S. Gärtner, I. G. Shenderovich, R. Wolf, *Chem. Eur. J.* **2017**, *23*, 6094–6102.

[5] N. Blaquiere, S. Diallo-Garcia, S. I. Gorelsky, D. A. Black, K. Fagnou, *J. Am. Chem. Soc.* **2008**, *130*, 14034–14035.

[6] P. Bhattacharya, J. A. Krause, H. Guan, *J. Am. Chem. Soc.* **2014**, *136*, 11153–11161.

[7] R. J. Keaton, J. M. Blacquiere, R. T. Baker, *J. Am. Chem. Soc.* **2007**, *129*, 1844–1845.

[8] P. V. Ramachandran, P. D. Gagare, *Inorg. Chem.* **2007**, *46*, 7810–7817.

[9] S. Chaffins, M. Brettreich, F. Wudl, *Synthesis* **2002**, *9*, 1191-1194.

[10] W. Chen, J. F. Hartwig, *J. Am. Chem. Soc.* **2013**, *135*, 2068.

[11] A. Glüer, M. Förster, V. R. Celinski, J. Schmedt auf der Günne, M. C. Holthausen, S. Schneider, *ACS Catal.* **2015**, *5*, 7214–7217.

[12] R. Adam, J. R. Cabrero-Antonino, A. Spannenberg, K. Junge, R. Jackstell, M. Beller, *Angew. Chem. Int. Ed.* **2017**, *56*, 3216. *Angew. Chem.* **2017**, *129*, 3264-3268.

[13] D. B. Bagal, R. A. Watile, M. V. Khedkar, K. P. Dhake, B. M. Bhanage, *Catal. Sci. Technol.* **2012**, *2*, 354.

[14] R. Kawahara, K. I. Fujita, R. Yamaguchi, *Adv. Synth. Catal.* **2011**, *353*, 1161.

[15] T. N. Gieshoff, M. Villa, A. Welther, M. Plois, U. Chakraborty, R. Wolf, A. J. von Wangelin, *Green Chem.* **2015**, *17*, 1408–1413.

4 Cobalt-Catalyzed Hydrogenations via Cobaltate Intermediates

Sebastian Sandl, Thomas M. Maier, Nicolaas P. van Leest, Uttam Chakraborty, Bas de Bruin, Michael Bodensteiner, Robert Wolf, and Axel Jacobi von Wangelin

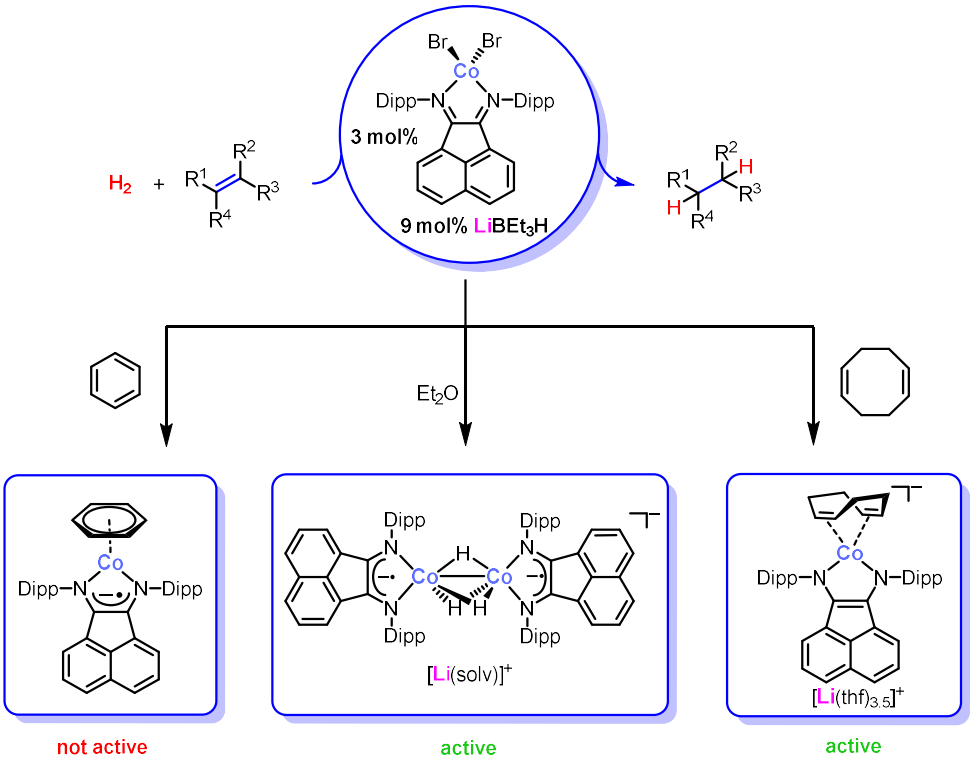

Contributions by T. M. Maier: Synthesis and characterization of [(DippBIAN)CoBr2] and complexes **1**, **2**. M. Bodensteiner assisted with single-crystal X-ray structure analysis of **1**. UV-vis spectroscopy, CV analyses, magnetic moment measurements and elemental analyses on complexes **3**, **4a** and **4b**. DFT calculations on complex **3** including Figure 9. Gas evolution measurement and amine-borane dehydrogenation on complex **4a** (Figures S8 and S9). Poisoning studies (technical assistance of F. Seeberger) and analyses on the *in situ* hydrogenation system including preparation of Figures 4 and 5. Contributions to Tables 1, 2 and Figures 2,3.
Contributions by S. Sandl: Catalytic reactions and mechanistic studies including Tables 1, 2 and S2 – S5, Figures 2 and 3 and Schemes 1 and 3. Synthesis and characterization of complexes **2**, **3**, and **4a,b**.
M. Bodensteiner (for complexes **1**, **4a** and **4b**) and U. Chakraborty (for complex **3**) assisted with the single-crystal X-ray structure analyses.
N. P. van Leest and B. de Bruin recorded and analyzed EPR data.
S. Sandl and A. Jacobi von Wangelin wrote the manuscript with input from all authors. R. Wolf and A. Jacobi von Wangelin supervised and directed the project.

This chapter was published in *ACS Catalysis* as a full paper: S. Sandl, T. M. Maier, N. P. van Leest, S. Kröncke, U. Chakraborty, S. Demeshko, K. Koszinowski, B. de Bruin, F. Meyer, M. Bodensteiner, C. Herrmann, R. Wolf and A. Jacobi von Wangelin, *ACS Catal.* **2019**, *9*, 7596-7606.

4.1 Introduction

Metal-catalyzed hydrogenations of alkenes constitute one of the key chemical transformations with numerous applications ranging from lab-scale syntheses to industrial manufacturing.[1] The elucidation of the underlying catalytic mechanisms by *Eisenberg*, *Halpern*, *Tolman*, and others were major scientific milestones toward the understanding of elementary catalytic reaction steps, and the rational design of more active and selective catalysts. [1],[2] Very recently, the dominance of hydrogenation catalysts based on the noble metals Rh, Ru, Ir, Pd, and Pt has been challenged by the development of highly active 3d transition metal catalysts.[3] While the use of more abundant, cheaper, and often less toxic base metals constitutes an important contribution to a more sustainable chemistry, their distinct reactivity and selectivity has often been plagued by undesirable, destructive side reactions.[4] Nevertheless, recently, elaborate ligand design has enabled the development of highly active cobalt catalysts by the groups of *Beller*, *Budzelaar*, *Chirik*, *Hanson*, *Elsevier*, *de Bruin*, and others (Figure 1).[5][8] In the most recent literature, the implementation of pincer ligands (e.g. *NNN*; *PNP*; *CNC*) has proved crucial to the control of high activity and selectivity.[9]

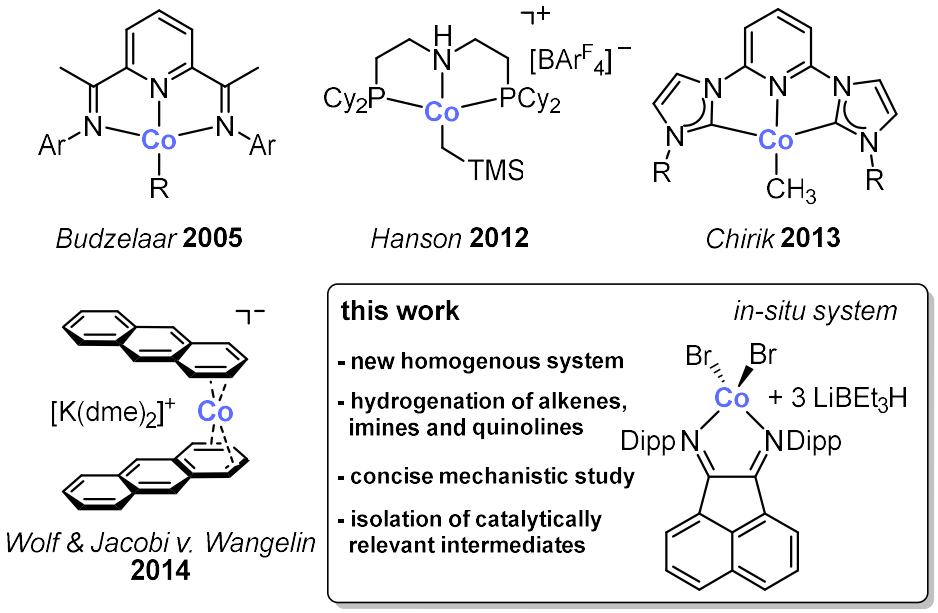

Figure 1. Known homogeneous cobalt catalysts for hydrogenation reactions (Dipp = 2,6-diisopropylphenyl) and catalytic system presented herein.

Following our previous work on the chemistry of 3d metalates containing redox non-innocent arene ligands, such as $[K(dme)_2\{Co(\eta^4\text{-}C_{14}H_{10})_2\}]$ or $[K([18]c\text{-}6)][Fe(\eta^4\text{-}C_{14}H_{10})_2]$,[10] we believed

that an efficient 3d metal catalyst for hydrogenation reactions would fulfil the following criteria: *i*) facilitation of redox steps at the metal by a redox-active ligand; *ii*) modular ligand design that allows convenient synthesis and easy catalyst tuning; *iii*) stabilization of reduced forms of the catalyst by the ligand, and *iv*) broad scope of hydrogenations of unsaturated C=C and C=X bonds. Imine-based ligand architectures constitute a privileged class of ligands as evidenced by the numerous applications in catalysis.[7] Simple α-diimine catalysts were first introduced by *tom Dieck* and co-workers in 1977.[11] Pincer-type motifs such as pyridinediimines[12] (PDIs) have recently received great attention. Bis(imino)acenaphthenes[13],[14] (BIANs) are another class of ligands that fulfils the above mentioned criteria (*i-iii*): BIANs can rapidly synthesized from commercial precursors on multi-gram scales and are highly redox-active, as they are able to accept up to four electrons.[13]b] So far, there are eight reports of BIAN cobalt complexes amongst them five for applications in catalysis.[15] On this basis, we were motivated to investigate combinations of BIAN ligands and cobalt salts for their potential ability to form active hydrogenation pre-catalysts. Herein, we report the benefits of using this simple catalytic system, which presents specific advantages over the current state-of-the-art catalytic system. Using the methodology described herein, clean hydrogenations of challenging sterically hindered alkenes, imines, and heteroarenes proceed under mild conditions. Mechanistic insight into these reactions was gained from the isolation of structurally novel olefin and hydride complexes as potential catalyst intermediates that being distinct from those of traditional noble metal catalysts.

4.2 Results and Discussion

Optimization and Alkene Hydrogenation

Initially, we probed the ability of [(^{Dipp}BIAN)CoBr$_2$] to act as pre-catalyst for the hydrogenation of the model substrate triphenylethylene (TPE) under mild conditions. High conversion was observed using lithium superhydride (LiBEt$_3$H) as activating co-catalyst at 2 bar H_2 and room temperature with only 3 mol% [(^{Dipp}BIAN)CoBr$_2$] (Table 1, procedure A, entry 1). The presence of the olefin substrate during initial pre-catalyst reduction/activation proved crucial for the observed high catalyst activity, possibly due to transient olefin coordination and stabilization of the low-valent catalyst (Table 1, entry 2).[6]d],[16],[17] The significantly lower activity of NaBEt$_3$H relative to LiBEt$_3$H suggests a considerable alkali-cation effect (Table 1, entry 5).[18] Employing other reducing agents in catalytic amounts such as HBpin/KO^{t}Bu instead of

[BEt_3H]$^-$ resulted in almost no activity (Table 1, entry 6). It is also noteworthy that the BIAN cobalt halogenide complex is far more active as pre-catalyst compared to *in situ* formed pre-catalyst from BIAN and the corresponding cobalt halogenide salts (Table 1, entries 7,8).

Table 1. Selected optimization experiments.

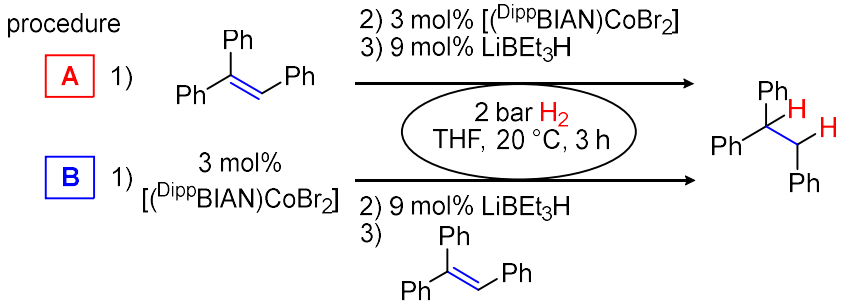

Entry	Deviation from standard conditions	Yield (%) [a]
1	A: reduction in presence of the substrate	92 (93)
2	B: substrate addition after reductant addition	41 (50)
3	A: 6 mol% $LiBEt_3H$	75 (75)
4	A: 6 mol% $NaBEt_3H$ instead of $LiBEt_3H$	23 (33)
5	A: 9 mol% $NaBEt_3H$ instead of $LiBEt_3H$	64 (65)
6	A: 9 mol% HBpin + 9 mol% KO^{t}Bu instead of $LiBEt_3H$	1 (12)
7	A: [(DippBIAN)$CoCl_2$] instead of [(DippBIAN)$CoBr_2$]	72 (72)
8	A: $CoCl_2$ + 2 DippBIAN instead of [(DippBIAN)$CoBr_2$]	25 (35)
9	A: w/o reductant	<1 (9)

Reaction conditions: 0.2 mmol alkene (1 M, THF), 9 mol% $LiBEt_3H$ (1 M, THF), 3 mol% [(DippBIAN)$CoBr_2$], 2 bar H_2; [a] Yields determined by quantitative GC-FID vs. internal *n*-pentadecane; Conversions in parentheses.

After optimization of the reaction conditions, the hydrogenation of other alkenes was investigated. Mono-, di- and tri-substituted alkenes were cleanly hydrogenated at 2-10 bar H_2 pressure at room temperature (Figure 2). The high efficacy of the developed protocol was demonstrated in the hydrogenation of challenging tri- and tetra-substituted alkenes such as myrcene, α-pinene, and α,β,β-trimethylstyrene under mild conditions (Figure 2). Under standard conditions, the hydrogenation of α-methylstyrene exhibited a turnover frequency (TOF) of 780 h^{-1} (see the SI). To the best of our knowledge, this protocol involves one of the most active homogeneous Co catalysts for alkene hydrogenations.[8] The presence of reduction-sensitive functional groups in the alkenes demanded a modified protocol to achieve

satisfactory reactivity, involving addition of the hydride co-catalyst prior to the alkene (procedure B, see Table 1, entry 2 and Figure 2, bottom). This alternative procedure was tolerant to chloride, bromide, ether, and ester functions. In the absence of H_2, 1-octene was rapidly isomerized to a mixture of octene regio- and stereoisomers. For phenylacetylene, slow cyclotrimerization to triphenylbenzene was observed in low yield (see the SI).

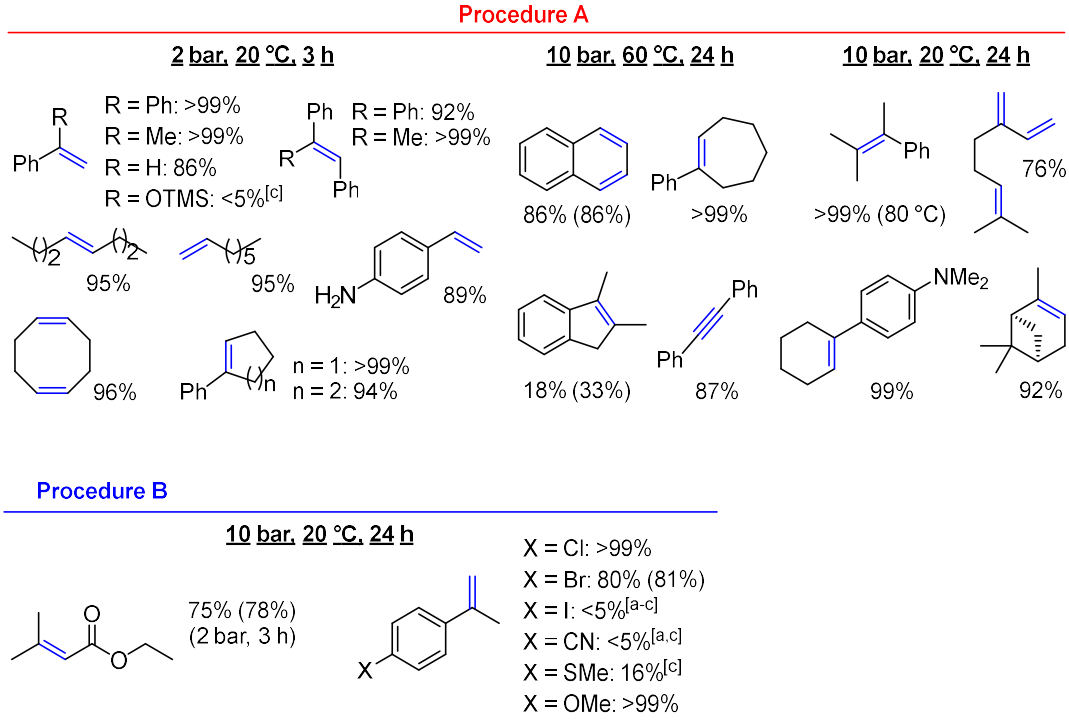

Figure 2. Substrate scope for the hydrogenation of alkenes catalyzed by cobalt BIAN complexes. Bonds in blue indicate the site of complete π-bond hydrogenation. Standard conditions: 0.2 mmol alkene/alkyne (1 M, THF), 3 mol% [(^{Dipp}BIAN)$CoBr_2$], 9 mol% $LiBEt_3H$ (1 M, THF). Yields were determined by quantitative GC-FID vs. *n*-pentadecane. Conversions are given in parentheses if <90%. Procedure A: Pre-catalyst reduction in the presence of substrate. Procedure B: Pre-catalyst reduction in the absence of substrate. [a] Traces of α-methylstyrene formed. [b] Traces of cumene formed. [c] Conversion <20%.

Methodology Extension: Hydrogenation of Imines

The homogeneous Co-catalyzed hydrogenation of imines[8b],[10] and quinolines[8f,h] is still in its infancy, despite being an atom-economic route to amines, which are prevalent in pharmaceutically and bioactively-relevant compounds.[19] Very good conversions were observed using the same cobalt catalyst in hydrogenations of selected electron-deficient as well as electron-rich imines and quinolines (10 bar H_2, 60°C, Figure 3). Potentially reducible ester functionalities were well tolerated, as were other functional groups including amines, fluorines, and ethers.

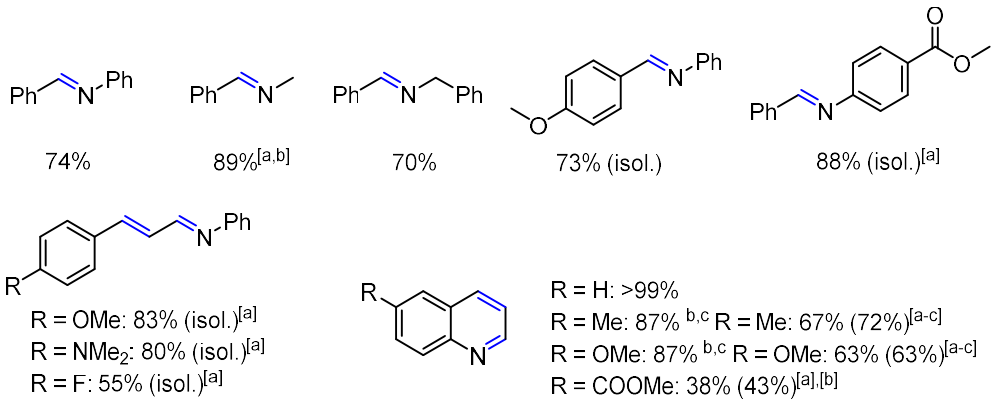

Figure 3. Hydrogenation of imines and quinolines. Blue bonds indicate the site of double bond hydrogenation. Reaction conditions: Procedure A: 0.2 mmol substrate (1 M, THF), 3 mol% [(^{Dipp}BIAN)CoBr$_2$], 9 mol% LiBEt$_3$H (1 M, THF); 10 bar H_2, 60 °C, 24 h. GC-FID yields vs. internal *n*-pentadecane; Conversions in parentheses if <90%. [a] Procedure B. [b] 80 °C. [c] Traces of the 5,6,7,8-tetrahydroquinoline derivative.

Mechanistic Investigations

The advent of 3d transition metal catalysts has gone hand in hand with the utilization of ligands that profoundly influence the electronic properties at the metal ions and enable redox reactivity patterns that are distinct from those of noble metals catalysts.[7] The reaction mechanisms of catalytic alkene hydrogenations with 2nd and 3rd row transition metals (Rh, Ru, Ir, Pd, Pt) are very well understood. For the classical Rh-catalyzed hydrogenation, alkene and hydride complexes have been determined as key catalyst intermediates and the elemental reaction steps involve two electron redox events at the metal.[1]-[3] There is less insight into the hydrogenation mechanisms of first row transition metals and the nature of the key catalyst intermediates is still largely unexplored, although *Chirik* and co-workers reported on a bis(aryl-imidazol-2-ylidene)pyridine cobalt hydride complex and a radical pathway that operates in cobalt-catalyzed alkene hydrogenations.[8]c] We aimed at a concise mechanistic study of Co-BIAN catalysts in alkene hydrogenations that would address the following questions: Is the BIAN ligand redox-active under the reaction conditions? Are radical pathways operating? To what extent are heterogeneous catalyst species involved? Do alkene and hydride intermediates play similarly important roles as 4d and 5d metal catalysts?

We commenced our mechanistic studies with a set of key experiments that address the operation of radical mechanisms and the topicity of the active catalyst species. Initially, radical probes were evaluated. α-Cyclopropylstyrene underwent dual alkene hydrogenation and

hydrogenative ring-opening to give 2-phenylpentane in excellent yields following both procedures A and B, respectively (Scheme 1, A). This might be indicative of a mechanism involving hydrogen atom transfer (HAT).[20] Furthermore, this is in agreement with our observations that non-styrenic alkenes (i.e. alkenes without aryl substituents that could stabilize potential radical intermediates in benzyl positions) are more difficult substrates under the standard conditions. Hydrogen atom transfer from the solvent is rather unlikely as no deuterium incorporation detected for reactions performed in THF-d_8 (Scheme 1, B). The high activity of the catalyst was further demonstrated by the hydrogenation of a C–C–σ–bond in cyclopropylbenzene (Scheme 1, C).

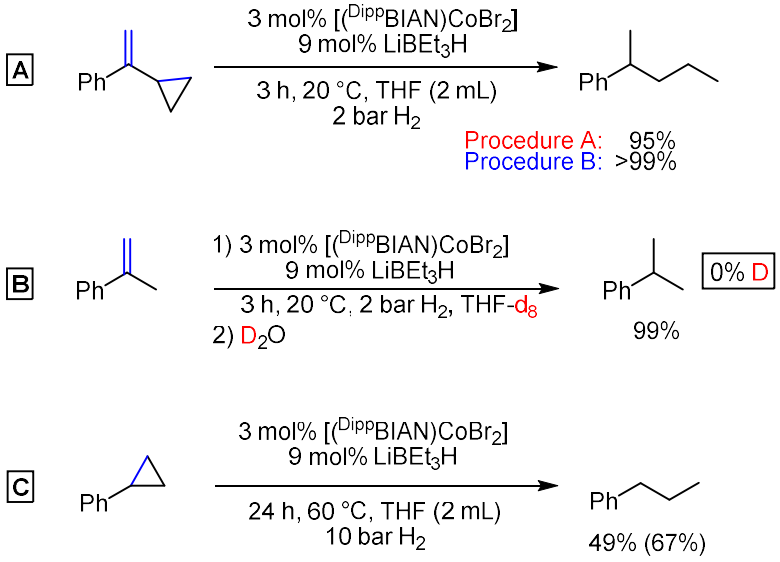

Scheme 1. Key mechanistic experiments.

The clear distinction between homogeneous and heterogeneous catalyst species is complicated,[21] yet our observations are consistent with a homogeneous mechanism. Reaction progress analyses documented an immediate onset of catalytic activity and steady conversion, which indicates a zero order for the substrate in the rate law (Figure 4, green curve). Thus, the rate-determining step presumably does not include olefin coordination. The absence of any sigmoidal curvature clearly argues against initial pre-catalyst nucleation and particle formation.[6] However, an induction period might be invisible due to the experimental setup (Procedure B, substrate conversion determined by gas-uptake; H_2 consumption was recorded after pre-catalyst formation and substrate addition). Kinetic poisoning studies are an useful tool to determine the topicity of the operating catalyst species.[21] The attempted amalgamation

of the catalyst with 300 equiv. mercury (900 mol% vs. substrate) had only a minimal effect on the reaction rate (Figure 4, orange curve). Upon addition of sub-catalytic amounts of trimethylphosphite ($P(OMe)_3$, 0.3 mol%), partial catalyst inhibition was recorded. Complete inhibition was achieved at a catalyst/poison ratio of 1:1 which is consistent with a homotopic catalyst (Figure 4, black curve). The selective homotopic catalyst poison dibenzo[*a*,*e*]cyclooctatetraene[21] (dct, 10 equiv. per Co) resulted in catalyst inhibition which was slightly diminished by the concomitant hydrogenation of dct as a competing substrate (Scheme 4, violet curve, 31% conversion of dct). The lower efficacy of dct as poison is presumably a consequence of the lower stability of 3d olefin complexes vs. their heavier congeners.[17]

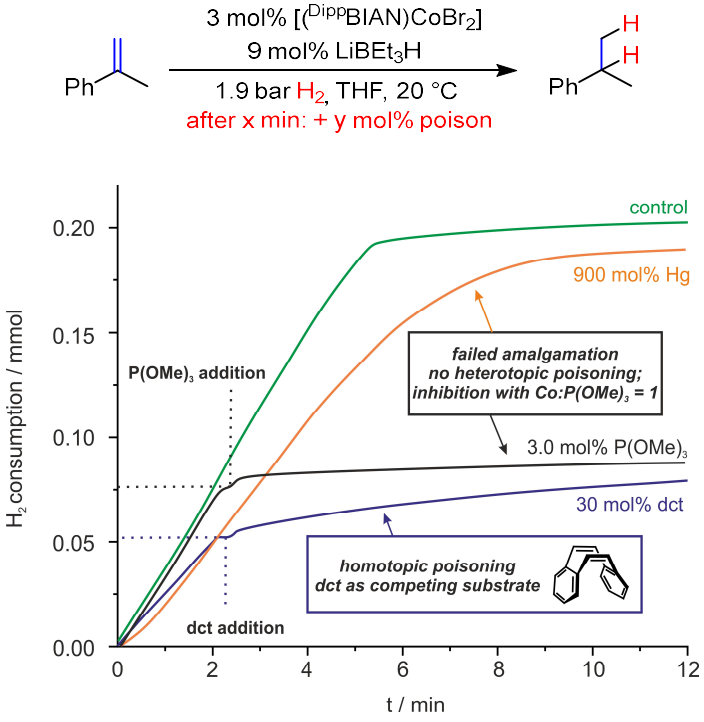

Figure 4. Catalyst poisoning studies with $P(OMe)_3$, Hg, and dct. Procedure B. Substrate conversion determined by gas uptake and quantitative GC-FID vs. internal *n*-pentadecane.

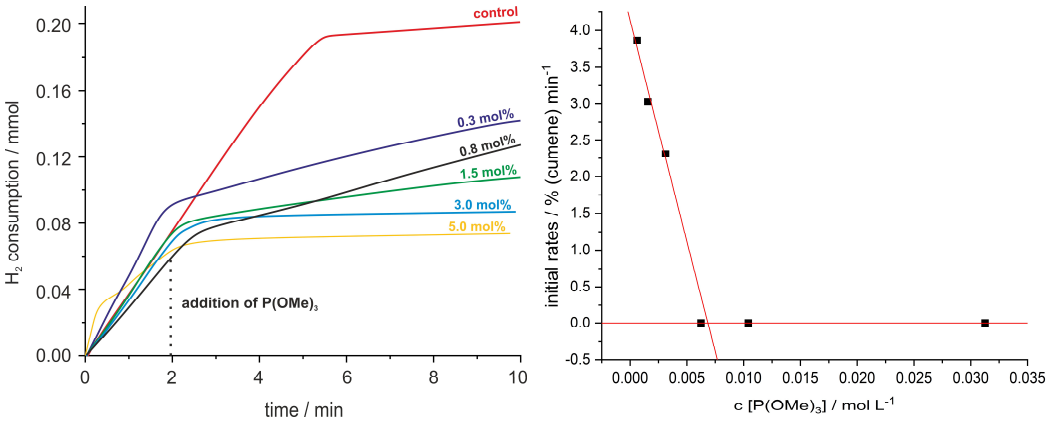

Figure 5. Poisoning experiments with different concentrations of trimethylphosphite (left), and plot of initial rates vs. trimethylphosphite concentration (right).

Complexes and Catalyst Intermediates

Based on the initial mechanistic experiments, we postulate a homotopic mechanism based on molecular cobalt catalysts. However, the distinct electronic properties of 3d transition metals vs. their heavier congeners suggest the participation of intermediate catalyst structures that are distinct from those of the Rh(I) hydrogenation catalysts.

While pathways based on intermediate alkene and hydride complexes have been intensively studied in rhodium-catalyzed hydrogenations, knowledge on related catalyst intermediates with cobalt is still rather rare. To identify potential catalytically-relevant species, we investigated stoichiometric reactions of [(^{Dipp}BIAN)CoBr$_2$] with three equivalents of LiBEt$_3$H, which is the same ratio (1:3) as used in the catalytic hydrogenations in order to isolate such a (^{Dipp}BIAN)Co moiety. We supposed, that the low-valent monomeric unit (^{Dipp}BIAN)Co might exhibit relevant catalytic activity and thus employed several arenes/olefins as labile coordination placeholders during the reductive dehalogenation of [(^{Dipp}BIAN)CoBr$_2$]. Reduction of [(^{Dipp}BIAN)CoBr$_2$] in THF with three equivalents of LiBEt$_3$H and an excess amount of 1,5-cyclooctadiene (cod) led to the formation of [Li(thf)$_{3.5}${(^{Dipp}BIAN)Co(η^4-cod)}] (**1**), which was isolated after recrystallization from a THF/Et$_2$O/*n*-hexane mixture in 17% yield. This complex is the corresponding lithium salt to our previously described potassium cobaltate [K(thf){(^{Dipp}BIAN)Co(η^4-cod)}] (**2**), which showed the same structure in solid-state and similar ^{1}H and ^{13}C{^{1}H} NMR spectra.[15c]

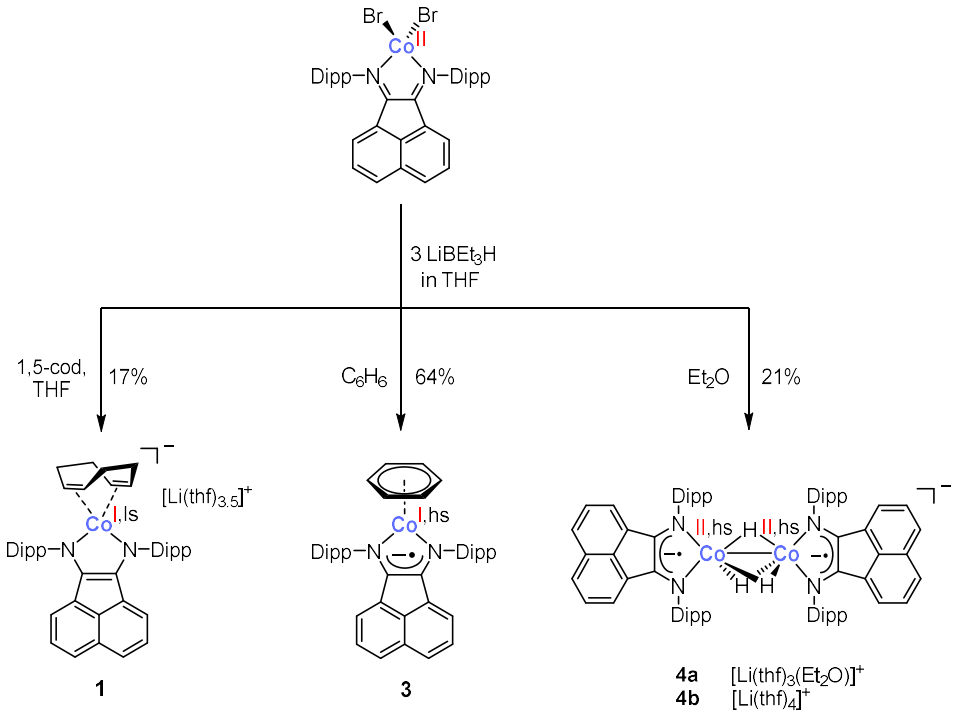

Scheme 2. Cobalt complexes **1**, **3**, and **4**, generated from stoichiometric reductions of [(DippBIAN)CoBr2] with three equivalents of LiBEt3H.

Crystals of **1** suitable for single-crystal X-ray diffraction were grown from THF/*n*-hexane. Complex **1** crystallized in space group $Pmn2_1$ with two molecules per formula unit. From a structural point of view, **1** is essentially identical to the known potassium salt. Based on literature precedents, the BIAN ligand in **1** can be assigned as a dianion based on its key bond distances (C–C: 1.389(4) Å; C–N: 1.383(3) Å; Figure 2).[13],[15c] Consequently, an oxidation state of +I for cobalt is assigned. In comparison, [(DippBIAN)CoBr2] contains a neutral BIAN ligand (C–C: 1.513(7) and 1.521(6) Å; C–N: 1.277(7)–1.286(8) Å) (see the SI).[13b]

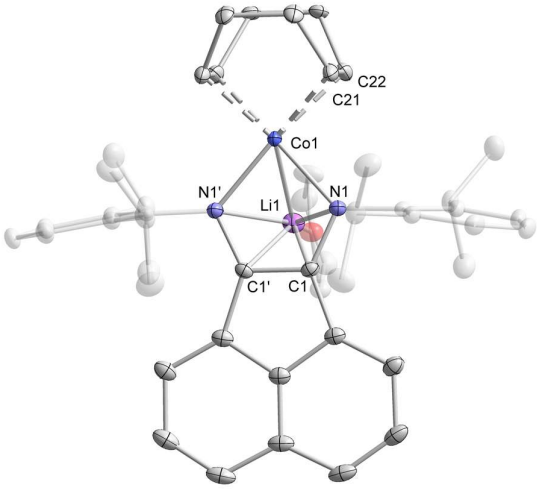

Figure 6. Solid-state molecular structure of [Li(thf){(^{Dipp}BIAN)Co(η^4-cod)}] (**1**) with thermal ellipsoids drawn at the 40% probability level. Selected bond lengths [Å] and angles [°]: C1–C1' 1.389(4), N1–C1 1.383(3), N1–Co1 1.945(1), C21–C22 1.401(4), N1–Co1–N1' 83.0(1). Hydrogen atoms are omitted for clarity.

As a lot of the substrates investigated for hydrogenation are derivatives of styrene and therefore contain potentially-coordinating aryl groups, the reduction of [(^{Dipp}BIAN)CoBr$_2$] was also investigated in benzene. The analogous reduction of [(^{Dipp}BIAN)CoBr$_2$] with three equivalents of LiBEt$_3$H in benzene furnished the neutral complex [(^{Dipp}BIAN)Co(η^6-C$_6$H$_6$)] (**3**) as dark red crystals in 64% yield.[26] The same outcome was observed using a mixture of benzene and cod. The crystals obtained were of sufficient quality to be analyzed by single-crystal X-ray crystallography. Complex **3** crystallized in the triclinic space group *P-1* with two molecules per formula unit. The central cobalt atom is coordinated in η^6-fashion by the benzene ligand and by the two nitrogen donor atoms. Characteristic C–C (1.433(2) Å) and C–N (1.3246(19) Å and 1.3224(19) Å) bond lengths of the α-diimine unit suggest a monoanionic BIAN ligand and a cobalt d^8 configuration, which was also investigated by spectroscopic and theoretical methods. Unfortunately, we were not able to isolate a (BIAN)Co complex analogous to **1** or **3** containing an olefinic substrate as a ligand by the reaction of [(^{Dipp}BIAN)CoBr$_2$] with e.g. styrene.

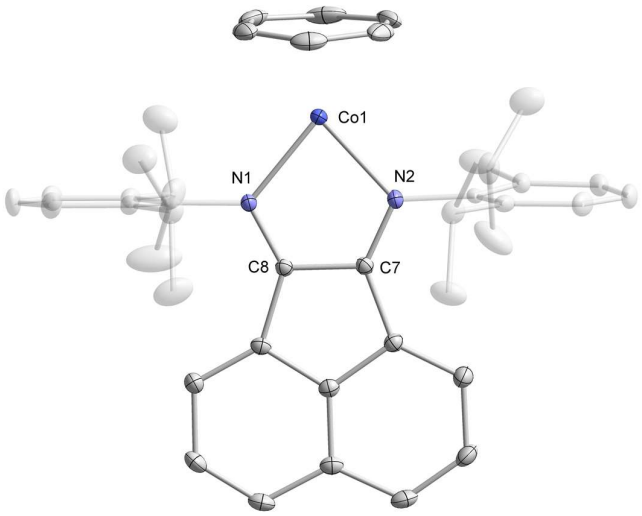

Figure 7. Solid-state molecular structure of [(^{Dipp}BIAN)Co(η^6-C_6H_6)] (**3**) with thermal ellipsoids drawn at the 40% probability level. Selected bond lengths [Å] and angles [°]: C7–C8 1.433(2), N1–C8 1.322(2), N2–C7 1.325(1), N1–Co1 2.000(1), N2–Co1 2.002(1), N1–Co1–N2 81.60(5). Hydrogen atoms and *n*-hexane solvent molecule are omitted for clarity.

Complex **3** is paramagnetic according to ^{1}H NMR spectroscopy and consists of one unpaired electron with an effective magnetic moment (μ_{eff} = 1.9(1) μ_B, C_6D_6) as determined by the Evans NMR method.[27] Therefore, the complex was further characterized by EPR spectroscopy in toluene at room temperature and toluene glass at 20 K. The X-band spectrum of **3** at room temperature features eight lines, which is characteristic for a cobalt-centered radical (nuclear spin of 7/2 for ^{59}Co). At 20 K the EPR spectrum shows rhombic symmetry and was simulated with the assumption of one unpaired electron at cobalt. The simulation is in good agreement with the experimental spectrum. The provided simulation allowed for accurate determination of the *g* and A_{Co} tensors (MHz): [2.013, 2.145, 2.134] and [+185.0, +406.0, 198.4], respectively.

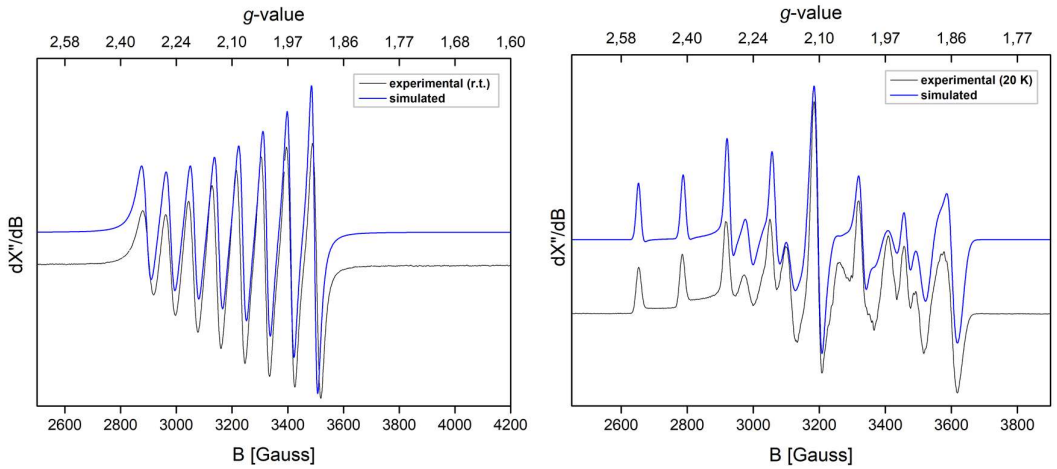

Figure 8. Simulated (blue) and experimental (grey) X-band EPR spectrum of [(^{Dipp}BIAN)Co(η^6-C_6H_6)] in toluene at room temperature (left: ν = 9.389121 GHz, power = 0.6325 mW, mod. amp. = 4.000 G. E = linear A strain) and in a toluene glass at 20 K (right: ν =9. 9.389494 GHz, microwave power = 1.002 mW, mod. amp. = 1.000 G). Inclusion of the Euler angles [–2.0, +90.0, 0] proved to be necessary to align the *g* and A_{Co} tensors and provided a more satisfactory simulation of the measured spectrum. Some linear and quadratic *A*-strain parameters have been included to simulate the final line shape. Some remaining slight deviations in the line shapes between simulation and experiment can be attributed to imperfect glass formation.

Complex **3** shows one absorption in the visible range at 480 nm with an extinction coefficient of 14500 L mol^{-1} cm^{-1} and is correspondingly a red solution in benzene. Due to the presence of two potentially redox-active sites, the redox properties of **3** were of interest. A cyclic voltammogram recorded in THF/^{n}Bu$_4$NPF$_6$ shows a quasi-reversible wave at –2.4 V vs. Fc/Fc^+ (see the SI).

The electronic structure of the complex was also investigated by DFT methods at the B3LYP-D3BJ/def2-TZVP def2/J level of theory using the broken symmetry approach of *Noodleman* and co-workers,[29] which is the method of choice for such open-shell systems. Calculations showed that an antiferromagnetic coupling between a monoanionic ligand and a high-spin cobalt(I) center is present, as illustrated by the spin density plot shown in Figure 9. The broken symmetry solution (S = 1/2) is 5.1 kcal mol^{-1} lower in energy compared to the high-spin solution (S = 3/2).

Analyses of the unrestricted natural orbitals (UNO) also support the assigned high-spin cobalt(I) configuration, and nicely show the interaction between the α-diimine ligand and the metal center (see the SI). Complex **3** is therefore a rare example of a high-spin cobalt(I) center.[30]

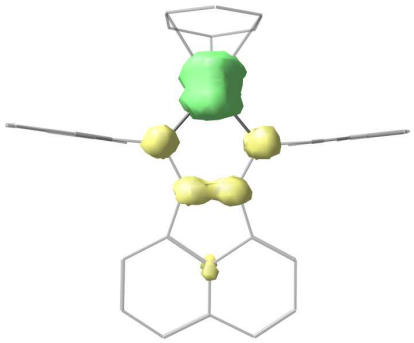

Figure 9. Spin-density plot of **3** according to Mulliken population analysis with an isosurface value of 0.01.

The reduction of [(^{Dipp}BIAN)CoBr$_2$] with LiBEt$_3$H was also investigated in the absence of coordinating olefins or arenes. From the reaction of three equivalents LiBEt$_3$H in Et$_2$O in a closed reaction vessel was isolated the structurally unusual cobalt hydride complex **4a** was isolated. Transition metal hydrides are key intermediates in many synthetic[31] and biological[32] processes. The largest industrial catalytic processes are hydrogenation reactions that operate via metal hydride species. Since the landmark studies of homogeneous Rh-catalyzed hydrogenations,[2] extensive knowledge on hydridorhodium complexes has been collected whereas very little is known about the nature and catalytic role of related intermediates in Co-catalyzed reactions.

The cobalt hydride from our reaction mixture was purified by crystallization from *n*-heptane and Et$_2$O and was isolated in 23% yield as dark green microcrystals and structurally characterized by single-crystal X-ray crystallography. In the solid-state, **4a** is a dimeric species with the molecular formula [Li(thf)$_3$(Et$_2$O){(^{Dipp}BIAN)Co}$_2$(μ–H$_3$)]. The closely related [Li(thf)$_4$]$^+$ solvate (**4b**) can be isolated in an analogous fashion by crystallization from THF/*n*-hexane. The Co–H bond distances are between 1.51(2) and 1.63(5) Å, while the twist angle between the two CoN$_2$ planes is 54.94(7)°. The NCCN bond lengths of BIAN are slightly shorter than in **3** (Figure 7; C–N: 1.333(3)–1.349(3) Å, C–C: 1.412(3)–1.419(3) Å), yet and are in good agreement with those found for the monoanionic BIAN ligand in the complex [(^{Dipp}BIAN)$_2$Fe] (C–N: 1.3367(15) and 1.3393(15) Å, C–C: 1.4234(18) Å) which contains a high-spin Fe^{2+} center antiferromagnetically coupled to BIAN$^{-\bullet}$.[35] Accordingly, the observed bond lengths of the BIAN ligands in **4** suggest a radical anion state of BIAN. The properties of the complex were further studied by ESI-MS (K. Koszinowksi, University of Göttingen), temperature-dependent NMR, SQUID measurements, and theoretical calculations. According to these additional

calculations which are not described in this chapter, trihydridodicobaltate anion of **4a,b** is best described as a [{(^{Dipp}BIAN^{-})Co^{II}}$_2$(μ-H)$_3$] anion.[37]

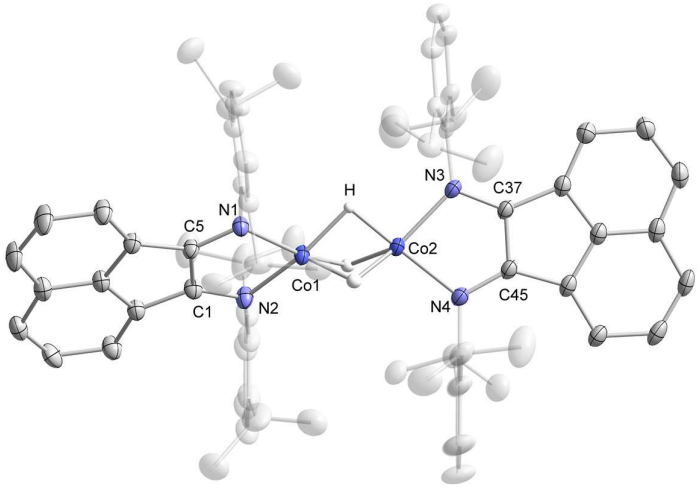

Figure 10. Solid-state molecular structure of [(^{Dipp}BIAN)$_2$Co$_2$(μ-H$_3$)] (**4a**) with thermal ellipsoids drawn at the 40% probability level. Selected bond lengths [Å] and angles [°]: N1–C5 1.339(3), N2–C1 1.333(3), C1–C5 1.412(3), N1–Co1 1.903(2), N2–Co1 1.896(2), N3–C37 1.349(3), N4–C45 1.340(3), C37–C45 1.419(3), N3–Co2 1.909(2), N4–Co2 1.903(2), N1–Co1–N2 83.57(9), N3–Co2–N4 84.02(9). Hydrogen atoms and cation [Li(thf)$_3$(Et$_2$O)]$^+$ are omitted for clarity.

Hydrogenation Activities of Complexes 1-4 and Mechanistic Proposal

We evaluated the catalytic activities of the isolated cobalt complexes **1** – **4** and various pre-catalyst mixtures in a hydrogenation model reaction (Table 2). The cobaltate complex [Li(thf)$_{3.5}${(^{Dipp}BIAN)Co(η^4-cod)}] (**1**) was found to be active for the hydrogenation of cod, albeit exhibiting slightly lower activity than the *in situ* formed catalyst (entry 2). Interestingly, **1** could be further activated by addition of three equivalents of triethylborane (entry 5), which may indicate lewis acid-assisted catalysis.[36] The borane could facilitate the cleavage of H_2 as demonstrated by *Peters* and co-workers with a borylcobalt complex.[36a] The catalytic inactivity of the corresponding potassium derivative [K(thf){(^{Dipp}BIAN)Co(η^4-cod)}] (**2**, Table 2, entry 4) mirrors the observed alkali cation effect during our preliminary optimization experiments (Table 1, entries 1 and 5). One possible explanation for this effect is an attractive non-covalent cation–π interaction. As main electrostatic interaction, the association free enthalpy (ΔH°) for the alkali metals with benzene follows the trend: $Li^+ > Na^+ > K^+$. Hence, the alkali cation can stabilize transition states or bind substrates (i.e. alkenes, arenes) in proximity to the catalyst.[18] Moreover, alkali metals are able to tune the redox activity of the ligand. *Mazzanti* and co-workers reported on the ligand- or metal-based reduction of cobalt salophen complexes,

which is dependent on the alkali metal.[18f] The group of *Holland* reported reduced iron dimers with redox-active formazanate ligands. The dimer, which is stabilized by cation–π interactions, rearranged in THF solution to form a five-membered metallacycle with a reactivity order of $Na^+ > K^+ < Rb^+ < Cs^+$.[18h]

The neutral complex [(^{Dipp}BIAN)Co(η^6-C_6H_6)] (**3**) was only active for cod hydrogenation after additional reduction with $LiBEt_3H$ (Table 2, entry 10). Notably, the related 17 valence electron (VE) complex [(dppe)Co(η^4-cod)] (dppe = 1,2-diphenylphosphinoethane), without a redox-active ligand is indeed an active pre-catalyst for hydrogenations.[7d] The hydridocobaltate [Li(thf)$_3$(Et_2O){(^{Dipp}BIAN)Co}$_2$(μ-H)$_3$] (**4a**) showed moderate hydrogenation activity which was significantly enhanced by further reduction with 0.5 equiv. of $LiBEt_3H$ (entries 8 and 10). It may be speculated that the hydridocobaltate anion present in **4a,b** (or related derivatives) acts as a catalyst reservoir for mononuclear hydrides as indicated by *in situ* NMR studies. Based on the collected synthetic, spectroscopic, and theoretical data, we propose a homotopic reaction mechanism that involves cobaltate complexes as active catalyst species. Rate acceleration by lewis acids and an alkali-cation effect were observed.

Table 2. Hydrogenations with isolated complexes and pre-catalyst mixtures.

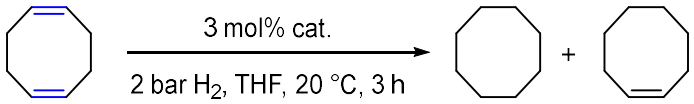

Entry	Catalyst mixture	Yield [%] [a]	
		Cyclooctane	Cyclooctene
1	[(^{Dipp}BIAN)$CoBr_2$] + 9 mol% $LiBEt_3H$	96	1
2	[Li(thf)$_{3.5}${(^{Dipp}BIAN)Co(cod)}] (**1**)	5	61
3	**1** + 9 mol% BEt_3	66	33
4	[K(thf){(^{Dipp}BIAN)Co(cod)}] (**2**)	-	1
5	**2** + 9 mol% BEt_3 + 30 mol% LiBr	3	38
6	**4a**	6	7
7	**4a** + 3 mol% BEt_3	22	22
8	**4a** + 1.5 mol% $LiBEt_3H$	57	43
9	[(^{Dipp}BIAN)Co(η^6-C_6H_6)] **3**	-	-
10	**3** + 9 mol% $LiBEt_3H$	4	29

Reaction conditions: 0.2 mmol alkene, 0.1 M in THF, 3 mol% cat., 2 bar H_2. [a] Yields determined by quantitative GC-FID vs. internal *n*-pentadecane.

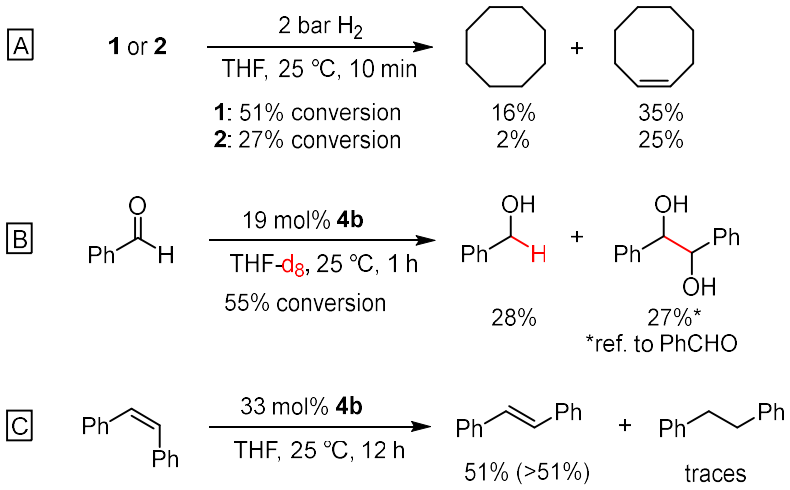

Scheme 3. Related reactivity of **1**, **2**, and **4b**. Yields determined by quantitative GC-FID vs. internal *n*-pentadecane.

The observed alkali cation effect was also evident in the more effective hydrogenation of the cod ligand in complexes **1** and **2** (Scheme 3, A). Preliminary explorations of the reactivity of relevant hydrides were performed with **4b** as model compound: Protolysis occurred with the strong Brønsted acid HCl in dioxane to give H_2 evolution (2.3 ± 0.1 eq. H_2 per dimer, see the SI). In the presence of benzaldehyde, **4b** reacted to give 28% benzyl alcohol and 27% pinacol coupling product (Scheme 3, B). This may indicate the competing operation of hydride transfer and single-electron transfer processes from **4b**. In the absence of dihydrogen, incomplete isomerization of (*Z*)-stilbene to (*E*)-stilbene was observed (51%, Scheme 3, C). Complex **4** also represents a plausible intermediate in our previously described catalytic system for amine-borane dehydrogenation and is indeed a catalyst for this reaction (see the SI).[15]

4.3 Conclusion

In summary, this report has established reduced cobalt complexes as competent catalysts in a user-friendly hydrogenation protocol for challenging alkenes under mild conditions. The obtained reactivity suggests bidentate BIANs as interesting alternatives to well-established pincer-type motifs possessing comparably high activities in cobalt-catalyzed alkene and imine hydrogenations. Mechanistic studies revealed considerable alkali cation and Lewis-acid effects. Synthetic, kinetic, and spectroscopic experiments indicate a mechanism involving homotopic cobaltate catalysts. Catalytically relevant

cobalt complexes were isolated that document the redox non-innocence of the BIAN ligand.

4.4 References

[1] a) S. Nishimura, *Handbook of Heterogeneous Catalytic Hydrogenation for Organic Synthesis*; Wiley: New York, **2001**. b) J. G. de Vries, C. J. Elsevier, *The Handbook of Homogeneous Hydrogenation*, Wiley-VCH, Weinheim **2007**.

[2] a) P. Meakin, J. P. Jesson, C. A. Tolman *J. Am. Chem. Soc.* **1972**, *94*, 3240–3242. b) C. A. Tolman, P. Z. Meakin, D. L. Lindner, J. P. Jesson *J. Am. Chem. Soc.* **1974**, *96*, 2762–2774. c) J. Halpern *Inorg. Chim. Acta* **1981**, *50*, 11–19. d) J. Halpern *Science* **1982**, *217*, 401-407. e) S. B. Duckett, C. L. Newell, R. Eisenberg *J. Am. Chem. Soc.* **1994**, *116*, 10548–10556.

[3] R. M. Bullock, *Catalysis without Precious Metals*, Wiley-VCH, Weinheim, Germany, **2010**.

[4] a) W. Hess, J. Treutwein, G. Hilt *Synthesis* **2008**, 40, 3537–3562. b) M. S. Holzwarth, B. Plietker *ChemCatChem* **2013**, *5*, 1650–1679. c) P. Röse, G. Hilt *Synthesis* **2016**, *48*, 463–492.

[5] R. J. M. Klein Gebbink, M. E. Moret, Wiley-VCH: Weinheim, Germany, **2019**.

[6] a) F. Chen, C. Topf, J. Radnik, C. Kreyenschulte, H. Lund, M. Schneider, A. E. Surkus, L. He, K. Junge, M. Beller *J. Am. Chem. Soc.* **2016**, *138* 8781–8788. b) Z. Wei, Y. Chen, J. Wang, D. Su, M. Tang, S. Mao, Y. Wang *ACS Catal*. **2016**, *6*, 5816–5822. c) R. V. Jagadeesh, K. Murugesan, A. S. Alshammari, H. Neumann, M. M. Pohl, J. Radnik, M. Beller *Science* **2017**, *358*, 326–332. d) S. Sandl, F. Schwarzhuber, S. Pöllath, J. Zweck, A. Jacobi von Wangelin *Chem. Eur. J.* **2018**, *24*, 3403–3407. e) P. Büschelberger, E. Reyes-Rodriguez, C. Schöttle, J. Treptwo, C. Feldmann, A. Jacobi von Wangelin, R. Wolf *Catal. Sci. Technol.* **2018**, *8*, 2648–2653.

[7] Reviews: a) P. J. Chirik *Acc. Chem. Res.* **2015**, *48*, 1687–1695. b) T. Zell, R. Langer *ChemCatChem* **2018**, *10*, 1930–1940. c) A. Mukherjee, D. Milstein *ACS Catal.* **2018**, *8*, 11435–11469. d) V. Papa, K. Junge, M. Beller *Chem. Eur. J.* **2019**, *25*, 122–143. e) L. Alig, M. Fritz, S. Schneider *Chem. Rev.* **2019**, *119*, 2681–2751. f) W. Ai, R. Zhong, X. Liu, Q. Liu *Chem. Rev.* **2019**, *119*, 2876–2953.

[8] Selected examples: a) Q. Knijnenburg, A. D. Horton, H. van der Heijden, T. Kooistra, D. G. H. Hetterscheid, J. M. M. Smits, B. de Bruin, P. H. M. Budzelaar, A. W. Gal *J. Mol. Catal. A Chem.* **2005**, *232,* 151–159. b) G. Zhang, B. L. Scott, S. K. Hanson *Angew. Chem., Int. Ed.* **2012**, *51* 12102–12106; *Angew. Chem.* **2012**, *124*, 12268-12272. c) R. P. Yu, J. M. Darmon, C. Milsmann, G. W. Margulieux, S. C. E. Stieber, S. Debeer, P. J. Chirik *J. Am. Chem. Soc.* **2013**, *135*, 13168–13184. d) M. R. Friedfeld, G. W. Margulieux, B. A. Schaefer, P. J. Chirik *J. Am. Chem. Soc.* **2014**, *136*, 13178–13181. e) S. Rösler, J. Obenauf, R. A. Kempe *J. Am. Chem. Soc.* **2015**, *137*, 7998–8001. f) R. Xu, S. Chakraborty, H. Yuan, W. D. Jones *ACS Catal.* **2015**, *5*, 6350–6354. g) T. J. Korstanje, J. I. van der Vlugt, C. J. Elsevier, B. de Bruin *Science* **2015**, *350 (6258)*, 298-302. h) R. Adam, J. R. Cabrero-Antonino, A. Spannenberg, K. Junge, R. Jackstell, M. Beller *Angew. Chem., Int. Ed.* **2017**, *56*, 3216–3220; *Angew. Chem.* **2017**, *129*, 3264-3268.

[9] a) V. Lyaskovskyy, B. de Bruin *ACS Catal.* **2012**, *2* 270–279. b) O. R. Luca, R. H. Crabtree *Chem. Soc. Rev.* **2013**, *42*, 1440–1459.

[10] a). D. Gärtner, A. Welther, B. R. Rad, R. Wolf, A. Jacobi von Wangelin *Angew. Chem., Int. Ed.* **2014**, *53*, 3722–3726; *Angew. Chem.* **2014**, *126*, 3796-3800. b) P. Büschelberger, D. Gärtner, E. Reyes-Rodriguez, F. Kreyenschmidt, F. Koszinowski, A. Jacobi von Wangelin, R. Wolf *Chem. Eur. J.* **2017**, *23*, 3139–3151.

[11] H. tom Dieck, H. Bruder . *Chem. Soc., Chem. Commun.* **1977**, 24–25.

[12] Z. Flisak, W. H. Sun *ACS Catal.* **2015**, *5*, 4713–4724.

[13] N. J. Hill, I. Vargas-Baca, A. H. Cowley *Dalton Trans.* **2009**, *0*, 240–253. b) I. L. Fedushkin, A. A. Skatova, V. A. Chudakova, G. K. Fukin *Angew. Chem., Int. Ed.* **2003**, *42*, 3294–3298. *Angew. Chem.* **2003**, *115*, 3416-3420.

[14] Selected examples of hydrogenations with BIAN metal complexes: a) R. van Asselt, C. J. Elsevier *J. Mol. Catal.* **1991**, *65,* L13–L19. b) M. W. van Laren, C. J. Elsevier *Angew. Chem., Int. Ed.* **1999**, *38*, 3715–3717; *Angew. Chem.* **1999**, *111*, 3926-3929. c) M. Villa, D. Miesel, A. Hildebrandt, F. Ragaini, D. Schaarschmidt, A. Jacobi von Wangelin *ChemCatChem* **2017**, *9,* 3203–3209.

[15] a) M. M. Khusniyarov, K. Harms, O. Burghaus, J. Sundermeyer *Eur. J. Inorg. Chem.* **2006**, 2985–2996. b) V. Rosa, S. A. Carabineiro, T. Aviles, P. T. Gomes, R. Welter, J. M. Campos, M. R. Ribeiro *J. Organomet. Chem.* **2008**, *693*, 769–775. c) S. Pelties, T. Maier, D. Herrmann, B. de Bruin, C. Rebreyend, S. Gärtner, I. G. Shenderovich, R. Wolf *Chem. Eur. J.* **2017**, *23*, 6094–6102. d) D. Formenti, F. Ferretti, C. Topf, A. E. Surkus, M. M. Pohl, J. Radnik, M. Schneider, K. Junge, M. Beller, F. Ragaini *J. Catal.* **2017**, *351*, 79–89. e) T. M. Maier, S. Sandl, I. G: Shenderovich, A. Jacobi von Wangelin, J. J. Weigand, R. Wolf *Chem. Eur. J.* **2019**, *25*, 238–245. f) C. P. G. Ziegler, T. M. Maier, S. Pelties, C. Taube, F. Hennersdorf, A. W. Ehlers, J. J. Weigand, R. Wolf *Chem. Sci.* **2019**, *10*, 1302–1308.

[16] Recent studies from the Jacobi von Wangelin group showing the beneficial effect of olefins: a) S. Gülak, A. Jacobi von Wangelin *Angew. Chem. Int. Ed.* **2012**, *51,* 1357–1361; *Angew. Chem.* **2011**, *124*, 1386-1390. b) S. Gülak, T. N. Gieshoff, A. Jacobi von Wangelin *Synth. Catal.* **2013**, *355,* 2197–2202. c) S. Gülak, O. Stepanek, J. Malberg, B. R. Rad, M. Kotora, R. Wolf, A. Jacobi von Wangelin *Chem. Sci.* **2013**, *4,* 776–784.

[17] a) J. B. Johnson, T. Rovis *Angew. Chem. Int. Ed.* **2008**, *47,* 840–871; *Angew. Chem.* **2008**, *120*, 852-884. b) C. Defieber, H. J. Grützmacher, E. M. Carreira *Angew. Chem. Int. Ed.* **2008**, *47*, 4482–4502; *Angew. Chem.* **2008**, *120*, 4558-4579.

[18] a) J. P. Collman, R. G. Finke, J. N. Cawse, J. I. Brauman *J. Am. Chem. Soc.* **1978**, *100,* 4766–4772. b) R. Hartmann, P. Chen *Angew. Chem. Int. Ed.* **2001**, *40*, 3581–3585. *Angew. Chem.* **2001**, *113*, 3693-3697. c) A. Macchioni *Chem. Rev.* **2005**, *105,* 2039–2073. d) C. R. Kennedy, S. Lin, E. N. Jacobsen *Angew. Chem. Int. Ed.* **2016**, *55*, 12596–12624; *Angew. Chem.* **2016**, *128*, 12784-12814. e) M. R. Kita, A. J. M. Miller *Angew. Chem., Int. Ed.* **2017**, *56*, 5498–5502; *Angew. Chem.* **2007**, *129*, 5590-5594. f) J. Andrez, V. Guidal, R. Scopelliti, J. Pecaut, S. Gambarelli, M. Mazzanti *J. Am. Chem. Soc.* **2017**, *139*, 8628–8638. g) A. J. Neel, M. J. Hilton M. S. Sigman, F. D. Toste *Nature* **2017**, *543*, 637–646. h) D. L. J. Broere, B. Q. Mercado, E. Bill, K. M. Lancaster *Inorg. Chem.* **2018**, 57, 9580–9591. i) S. Yamada *Chem. Rev.* **2018**, *118*, 11353–11432. j) K. T. Mahmudov, A. V. Gurbanov, F. I. Guseinov M. F. C. Guedes da Silva *Coord. Chem. Rev.* **2019**, *387*, 32–46.

[19] I. Muthukrishnan, V. Sridharan, J. C. Menendez *Chem. Rev.* **2019**, *119*, 5057–5191.

[20] a) Kinetics and mechanism of the hydrogenation of α-cyclopropylstyrene: Rate constant of the ring-opening rearrangement of the corresponding radical: 3.6×10^5 s^{-1} at 22 °C in hexane solution: M. R. Bullock, E. G. Samsel *J. Am. Chem. Soc.* **1990**, *112,* 6886–6898. b) J. Choi, L. Tang, J. R. Norton . *J. Am. Chem. Soc.* **2007**, *129,* 234–240. c) B. de Bruin, W. I. Dzik, S. Li, B. B. Wayland *Chem. Eur. J.* **2009**, *15*, 4312-4320.

[21] a) J. A. Widegren, R. G. Finke *J. Mol. Catal. A* **2003**, *198*, 317–341. b) D. Astruc, F. Lu, J. R. Aranzaes *Angew. Chem. Int. Ed.* **2005**, *44*, 7852–7872; *Angew. Chem.* **2005**, *117*, 8062-8083. c) R. M. Drost, V. Rosar, S. Marta, M. Lutz, N. Demitri, B. Milani, B. de Bruin, C. J. Elsevier *ChemCatChem*, **2015**, *7*, 2095–2107.

[22] a) D. R. Anton, R. H. Crabtree *Organometallics* **1983**, *2*, 855-859. b) G. Franck, M. Brill, G. Helmchen *Org. Synth.* **2012**, *89*, 55-65.

[23] X.-J. Yang, X. Fan, Y. Zhao, X. Wang, B. Liu, J.-H. Su, Q. Dong, M. Xu, B. Wu *Organometallics* **2013**, *32,* 6945–6949.

[24] a) M. Döring, E. Uhlig, T. Taldbach *Z. Anorg. Allg. Chem.* **1991**, *600,* 163–167. b) W. W. Brennessel, J. E. Ellis *Inorg. Chem.* **2012**, *51,* 9076–9094. c) X. Wang, Y. Zhao, S. Gong, B. Liu, Q.-S. Li, J.-H. Su, B. Wu. X.-J. Yang *Chem. Eur. J.* **2015**, *21,* 13302–13310

[25] K. Ray, T. Petrenko, K. Wieghardt, F. Neese *Dalton Trans.* **2007**, 1552–1566.

[26] Similiar cobalt and iron complexes with η^6-arene ligands: a) X.Dai, P. Kapoor, T. H. Warren *J. Am. Chem. Soc.* **2004**, *126,* 4798–4799. b) C. Chen, M. B. Hecht, A. Kavara, W. W. Brennessel, B. Q. Mercado D. J. Weix, P. L. Holland *J. Am. Chem. Soc.* **2015**, *137,* 13244–13247. c) S. C. Bart, E. J. Hawrelak, E. Lobkovsky, P. J. Chirik *Organometallics* **2005**, *24,* 5518–5527. d) see ref.: 23c. e) see ref.: 23d.

[27] D. F. Evans, *J. Chem. Soc.* **1959**, 2003.

[28] a) A. D. Becke *J. Chem. Phys.* **1993**, *98*, 5648. b) F. Weigend *Phys. Chem. Chem. Phys.* **2005**, *7*, 3297. c) F. Weigend *Phys. Chem. Chem. Phys.* **2006**, *8*, 1057.d) S. Grimme, S. Ehrlich, L. Goerigk *J. Comput. Chem.* **2011**, *32*, 1456-1465. e) S. Grimme, J. Antony, S. Ehrlich, H. Krieg *J. Chem. Phys.* **2010**, *132*, 154104.

[29] a) L. Noodleman, J. G. Norman *J. Chem. Phys.* **1979**, *70*, 4903-4906. b) L. Noodleman *J. Chem. Phys.* **1981**, *74*, 5737-5743. c) L. Noodleman, J. G. Norman, J. H. Osborne, A. Aizman, D. A. Case *J. Am. Chem. Soc.* **1985**, *107*, 3418-3426. d) L. Noodleman, E. R. Davidson *Chem. Phys.* **1986**, *109*, 131-143. e) L. Noodleman, C. Y. Peng, D. A. Case, J.-M. Mouesca *Coord. Chem. Rev.* **1995**, *144*, 199-204.

[30] J. Krzystek, A. Ozarowksi, S. A. Zvyagin, J. Telser *Inorg. Chem.*, **2012**, *51*, 4954–4964.

[31] Reviews: a) D. S. Moore, S. D. Robinson *Chem. Soc. Rev.* **1983**, *12,* 415–452. b) M. Y. Darenbourg, C. E. Ash *Adv. Organomet. Chem.* **1987**, 27, 1–50. c) S. J. C. Robinson D. M. Heinekey *Chem. Commun.* **2017**, *53,* 669–676.

[32] Reviews: a) W. Lubitz, H. Ogata, O. Rüdiger, E. Reijerse *Chem. Rev.* **2014**, *114,* 4081–4148. b) D. Schilter, J. M. Camara M. T. Huynh, S. Hammes-Schiffer, T. B. Rauchfuss *Chem. Rev.* **2016**, *116,* 8693–8749.

[33] It is noteworthy that the reaction needs to be performed in a closed reaction vessel as reported by Finke and co-workers. W. W: Laxson, S. Özkar, S. Folkman, R. G. Finke *Inorg. Chim. Acta* **2015**, *432*, 250–257.

[34] a) M. D. Fryzuk, J. B. Ng, S. J. Rettig, J. C. Huffmann, K. Jonas *Inorg. Chem.* **1991**, *30,* 2437–2441. b) J. L. Kersten, A. L. Rheingold, K. H. Theopold, C. P. Casey, R. A. Widenhoefer, C. E. C. A. Hop *Angew. Chem. Int. Ed.* **1992**, *31,* 1341–1343; *Angew. Chem.* **1992**, *104*, 1364-1366. c) K. Ding, W. W: Brennessel, P. L. Holland *J. Am. Chem. Soc.* **2009**, *131,* 10804–10805. d) B. D. Swartz, T. A. Atesin, M. R. Grochowski, S. S. Oster, W. W: Brennessel, W. D. Jones *Inorg. Chim. Acta* **2010**, *363*, 517–522.

[35] I. L. Fedushkin, A. A. Skatova, N. M. Khvoinova, A. N. Lukoyanov, G. K. Fukin, S. Y. Ketkov, M. O. Maslov, A. S. Bogomyakov *Russ. Chem. Bull.* **2013**, *62*, 2122–2131.

[36] Lewis-acid effects in hydrogenation reactions: a) T. P. Lin, J. C. Peters *J. Am. Chem. Soc.* **2013**, *135*, 15310–15313. b) A. Maity, T. S. Teets . *Chem. Rev.* ***2016***, *116,* 8873–8911. c) K. Tokmic, B. J. Jackson, A. Salazar, T. J. Woods, A. R. Fout *J. Am. Chem. Soc.* **2017**, *139,* 13554–13561. d) N. G. Leonard, P. J. Chirik *ACS Catal.* **2018**, *8,* 342–348.

[37] S. Sandl, T. M. Maier, N. P. van Leest, S. Kröncke, U. Chakraborty, S. Demeshko, K. Koszinowski, B. de Bruin, F. Meyer, M. Bodensteiner, C. Herrmann, R. Wolf, A. Jacobi von Wangelin, *ACS Catal.* **2019**, *9*, 7596-7606.

4.5 Supporting Information

4.5.1 General Procedures

All experiments were performed under an atmosphere of dry Argon (Argon 4.6, Linde) using standard Schlenk techniques or a MBraun UniLab Glovebox.

***Analytical Thin-Layer Chromatography*:** TLC was performed using aluminum plates with silica gel and fluorescent indicator (Merck, 60, F254). Thin layer chromatography plates were visualized by exposure to ultraviolet light (366 or 254 nm).

Column Chromatography: Flash column chromatography with silica gel 60 from KMF (0.040-0.063 mm). Mixtures of solvents used are noted in brackets.

Chemicals and Solvents: Solvents were purified, dried, and degassed with an MBraun SPS800 solvent purification system. THF, diethylether were stored over molecular sieves, (3 Å). *n*-Hexane was stored over a potassium mirror. 1,2-dimethoxyethane (DME) was stirred over K/benzophenone and stored over molecular sieves (3 Å). Commercially available olefins were distilled under reduced pressure before use. $LiBEt_3H$ (1 M in THF) was used as received from Sigma-Aldrich or diluted before use.

Computational details: All calculations were carried out with the ORCA program package.[1],[2] All geometry optimizations were performed at the B3LYP-D3BJ/de2-TZVP def2/J[3] level of theory in the gas phase. Frequency calculations were carried out to confirm the nature of stationary points found by geometry optimizations. To save computational cost, all diisopropyl groups were replaced by methyl groups. The broken-symmetry approach of *Noodleman* and co-workers was used.[4]

Cyclic voltammetry: Cyclic voltammetry experiments were performed in a single-compartment cell inside a nitrogen-filled glovebox using a CH Instruments CH1600E potentiostat. The cell was equipped with a platinum disc working electrode (1 mm diameter) polished with 0.05 μm alumina paste, a platinum wire counter electrode and a silver wire as pseudoreference electrode. The supporting electrolyte, tetra-*n*-butylammonium hexafluorophosphate, was dried in vacuo at 110 °C overnight. All redox potentials are reported versus the ferrocenium/ferrocene (Fc^+/Fc) couple. The scan rate is $v = 100$ mV s^{-1} unless stated otherwise.

EPR spectroscopy: The experimental X-band EPR spectrum of **3** was recorded on a Bruker EMX spectrometer (Bruker BioSpin Rheinstetten) equipped with a He temperature-control cryostat system (Oxford Instruments). The *g* values were calculated with the ORCA software package[1],[2] at the B3LYP/def2-TZVP[3] level of theory. The spectrum was analyzed and simulated using the W95EPR program of Prof. Frank Neese.

Gas chromatography with FID (GC-FID): HP6890 GC-System with injector 7683B and Agilent 7820A System. Column: HP-5, 19091J-413 (30 m × 0.32 mm × 0.25 μm), carrier gas: N_2. GC-FID was used for reaction control and catalyst screening. Calibration with internal standard *n*-pentadecane and analytically pure samples. Non-commercial authentic samples were prepared by hydrogenation with palladium on charcoal.

Gas chromatography with mass-selective detector (GC-MS): Agilent 6890N Network GC-System, mass detector 5975 MS. Column: HP-5MS (30m × 0.25 mm × 0.25 μm, 5% phenylmethylsiloxane, carrier gas: H_2. Standard heating procedure: 50 °C (2 min), 25 °C/min -> 300 °C (5 min).

Gas-uptake reaction monitoring: Gas-uptake was monitored with a Man On the Moon X201 kinetic system to maintain a constant reaction pressure. The system was purged with hydrogen prior use. Reservoir pressure was set to about 9 bar H_2. H_2 consumption was related to final yields by GC-FID vs. *n*-pentadecane.

***Gas evolution measurements*:** Gas evolution was monitored with a Man on the Moon X103 kit. Manipulations were performed under inert conditions. The volume of the reaction vessel was determined by protic hydrolysis of different amounts of zinc. The evolved hydrogen amount was calculated using the ideal gas law.

High Pressure Reactor: Hydrogenation reactions were carried out in 160 and 300 mL high pressure reactors (Parr™) in 4 mL glass vials. The reactors were loaded under argon, purged with H_2 (1 min), sealed and the internal pressure was adjusted. Hydrogen (99.9992%) was purchased from Linde.

High resolution mass spectrometry (HRMS): The spectra were recorded by the Central Analytics Lab at the Department of Chemistry, University of Regensburg, on a MAT SSQ 710 A from Finnigan.

^{1}H- and ^{13}C NMR-Spectroscopy: NMR spectra were recorded on Bruker Avance 300 and Avance 400 spectrometers at 300 K and internally referenced to residual solvent resonances.

Magnetic moment: Magnet susceptibility χ_M was determined by performing a NMR experiment following the procedure of *Evans*.[5]

Single-crystal X-ray crystallography: The single crystal X-ray diffraction data were recorded on an Agilent or Rigaku GV 50 with a Titan S2 CCD detector (**1**, **4a**) and on an Agilent SuperNova with an Atlas CCD detector (**3**, [(^{Dipp}BIAN)CoBr$_2$] with microfocus Cu K$_\alpha$ radiation (λ = 1.54184 Å). Empirical multi-scan[6] and analytical absorption[7] corrections were applied to the data.

In case of **4b**, X-ray diffraction data was recorded on a Bruker APEX-II CCD diffractometer with microfocus Mo K$_a$ radiation (λ = 0.71073 Å). Data reduction, scaling and absorption corrections were performed using SAINT (Bruker, V8.34A, after 2013). Multi-scan absorption correction was performed using SADABS-2012/1 (Bruker, 2012).

The structures were solved with SHELXT[8] and least-square refinements on F^2 were carried out with SHELXL.[9]

UV-vis spectroscopy: UV-vis spectra of investigated solutions were recorded on a Varian Cary 50 spectrophotometer in quartz cuvettes with a layer thickness of 1 cm and a concentration of 10^{-4} to 10^{-6} mol·L^{-1} at room temperature.

4.5.2 Synthesis of Starting Materials

^{Dipp}BIAN and [K(thf){(^{Dipp}BIAN)Co(η⁴-cod)}] (**2**) were synthesized according to Chapters 2,3.

4.5.2.1 Synthesis of [(^{Dipp}BIAN)CoBr₂]

[(^{Dipp}BIAN)CoBr₂] was synthetized according to a modified protocol of *Rosa* and co-workers.[10]

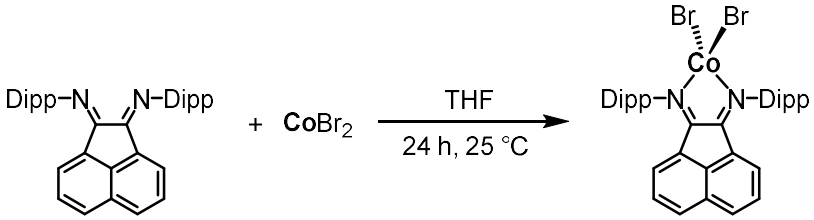

$CoBr_2$ (2.1 g, 9.5 mmol, 1.0 equiv.) and ^{Dipp}BIAN (5.0 g, 10 mmol, 1.1 equiv.) were mixed as solids and dissolved in 120 mL THF. An immediate color change to red occurred. The reaction mixture was stirred for 24 h and the solvent was removed under reduced pressure. The crude product was washed with 40 mL toluene, dissolved in 150 mL DCM and filtered through a P3-frit. After reducing the solvent to 100 mL, the concentrated solution was layered with 70 mL *n*-hexane. Black needles were formed after storing at room temperature in 3 days. They were isolated by decanting the solvent and washing the needles with toluene (3 x 15 mL). These crystals were also suitable for single-crystal X-ray crystallography.

Formula: $C_{36}H_{40}N_2CoBr_2$ ($M = 719.47$ g mol^{-1})

Yield: 7.5 g (1.9 mmol, 49%)

^{1}H NMR (400.13 MHz, 300 K, THF-d_8) δ[ppm]: 7.40 – 6.77 (m), 4.18 (s), 3.99 (s), 3.35 (s), 1.22 (s), 1.06 (s), –2.39 (s), –21.26 (s)

Elemental Analysis calcd. for $C_{36}H_{40}N_2CoBr_2$: C 60.16, H 5.60, N 3.89; found: C 60.16, H 5.48, N 3.77

4.5.3 Synthesis of Catalytically Relevant Cobalt Complexes

4.5.3.1 Synthesis of [Li(thf){(^{Dipp}BIAN)Co(η⁴-cod)}] (1)

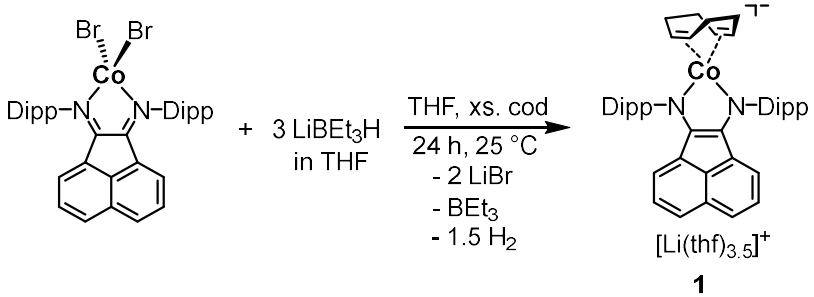

1

A suspension of [(^{Dipp}BIAN)CoBr$_2$] (2.0 g, 2.8 mmol, 1.0 equiv.) was dissolved in 30 mL THF and 1,5-cyclooctadiene (2.0 mL, 16 mmol, 6.0 equiv.) was added to the solution. The reaction mixture was cooled to –30°C and a solution of LiBEt$_3$H (1 M in THF, 8.3 mL, 3.0 equiv.) was added dropwise. The solution was warmed to room temperature and stirred for further 24 h. The solvent was removed under reduced pressure and the residue was washed with 60 mL *n*-hexane. Extraction with 80 mL diethylether and filtration led to a yellow-green solution which was reduced to 1/3 of its original volume and layered with 20 mL *n*-hexane. After a few days, dark crystals of **1** were obtained and isolated by decanting the solution and drying the dark black crystals *in vacuo*. For analytics and catalytic test reactions an aliquot of this product was recrystallized from THF/*n*-hexane (2.5:1) at –30 °C.

Formula: $C_{58}H_{80}N_2CoLiO_{3.5}$ (M = 927.16 g mol^{-1})

Yield: 0.443 g (0.48 mmol, 17%)

^{1}H NMR (400.13 MHz, 300 K, THF-d$_8$) δ[ppm]: 7.06 – 6.99 (m, 6H, CH_{Ar}), 6.24 (m, 4H, CH_{BIAN}), 4.93 (m, 2H, CH_{BIAN}), 4.51 (m, 4H, C*H*$_{Dipp}$), 2.89 (m, 4H, cod-CH), 2.32 (m, 4H, cod-CH_2), 1.37 (d, 12H, $CH_{3(Dipp)}$, 1.03 (m, 4H, cod-CH_2), 0.95 (d, 12H, $CH_{3(Dipp)}$)

^{13}C{^{1}H} NMR (100.6 MHz, 300 K, THF-d$_8$) δ[ppm]: 154.6, 145.7, 127.2 123.0, 122.9, 118.9, 114.5, 64.3, 32.9, 28.2, 26.0 (two quaternary C-atoms could not be detected due to low solubility)

Elemental Analysis calcd. for $C_{58}H_{80}N_2CoLiO_{3.5}$: C 74.82, H 8.70, N 3.02; found: C 74.28, H 8.43, N 2.91

4.5.3.2 Synthesis of [(^{Dipp}BIAN)Co(η^6-C$_6$H$_6$)] (3)

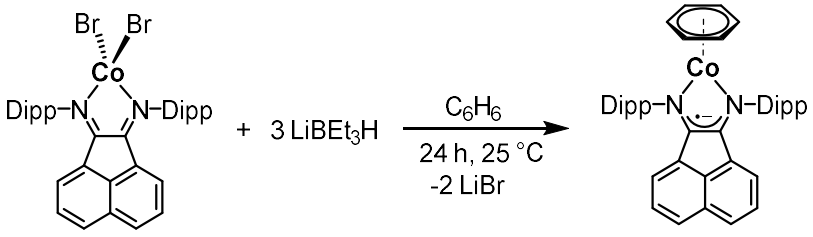

3

A suspension of [(^{Dipp}BIAN)CoBr$_2$] (0.50 g, 0.70 mmol, 1.0 equiv.) in 15 mL benzene was reduced by dropwise addition of LiBEt$_3$H (2.09 mmol, 1.1 M, THF) during which time a color change from pale brown to dark red and concomitant solubilization were observed. After filtration over neutral alumina, the solvent was removed under reduced pressure and

extracted with 30 mL hexane. Dark red crystals of **3** were grown by cooling to –35 °C (3 days), isolated by decanting the solution and dried *in vacuo*. These crystals were also suitable for single-crystal X-ray crystallography.

Formula: $C_{42}H_{46}N_2Co$ (M = 637.78 g mol^{-1})

Yield: 0.282 g (0.44 mmol, 64%)

^{1}H NMR (400.13 MHz, 300 K, THF-d_8) δ[ppm]: 7.40 – 6.77 (m), 4.18 (s), 3.99 (s), 3.35 (s), 1.22 (s), 1.06 (s), –2.39 (s), –21.26 (s)

Cyclic Voltammetry: $E_{1/2}$ = -2.3 V vs. Fc/Fc$^+$ in THF

Elemental Analysis calcd. for $C_{42}H_{46}N_2Co$: C 79.10, H 7.27, N 4.39; found: C 79.20, H 7.36, N 3.77

Magnetic Moment: μ_{eff} (C_6D_6) = 1.9(1) μ_B

Melting point:T > 230°C: decomposition to a black oil

UV-vis (C_6H_6): λ_{max}/nm (ε/L·mol^{-1}·cm^{-1}) = 480 (14500)

4.5.3.3 Synthesis of [(Li(thf)$_3$(Et$_2$O){(^{Dipp}BIAN)$_2$Co(μ-H$_3$)}]

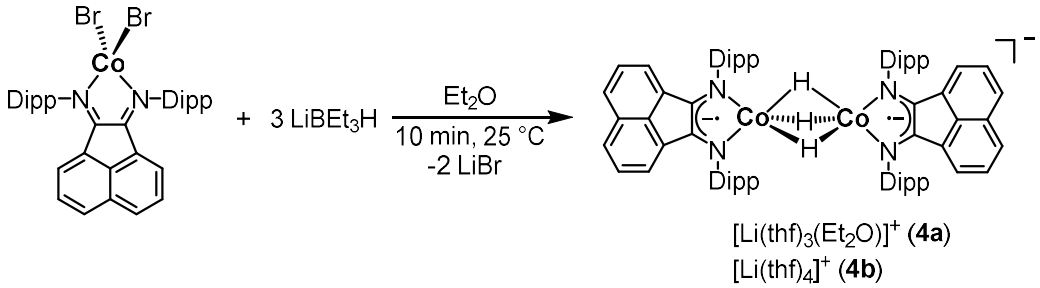

In an argon-filled glovebox, a Schlenk flask was charged with a suspension of [(^{Dipp}BIAN)CoBr$_2$] (1.39 mmol) in 20 mL Et$_2$O and sealed with a septum. After cooling to –35 °C, LiBEt$_3$H (3.0 equiv., 1.1 M, THF) was added dropwise, during which time a color change from pale brown to dark green, effervescence and solubilization was observed. It was found to be very important to create an overpressure in the flask in order to obtain the product. After 10 minutes of stirring, 8 mL *n*-heptane was added and the mixture was filtered through a closed Schlenk frit (P4, gravitation). The filter cake was washed with hexane (3 x 2 mL), and Et$_2$O (4 x 2 mL) to obtain the microcrystalline product in high purity. For the isolation of single crystals, *n*-hexane was used instead of heptane. After filtration, the crystals were grown from the filtrate by slow evaporation at 20 °C. [Li(thf)$_4${(^{Dipp}BIAN)Co}$_2$(μ-H)$_3$] (**4b**) was obtained in

an analogous procedure: The microcrystals were recrystallized from a solution of THF:*n*-hexane = 1:1 at –35°C to obtain crystals, which are suitable for single-crystal X-ray diffraction analysis.

Formula: $C_{88}H_{117}N_2Co_2LiO_4$ (M = 1419.73 g mol^{-1})

Yield: 0.228 g (0.16 mmol, 23%)

^{1}H NMR (400.13 MHz, 300 K, THF-d$_8$) δ[ppm]: 8.37 – 8.32 (d, *J* = 8.2 Hz, 4H), 7.29 – 7.24 (d, *J* = 7.0 Hz, 4H), 6.58 (s, 12H), 6.50 (dd, *J* = 8.1 Hz, *J* = 7.0 Hz, 4H), 3.50 – 3.32 (br, 8H, C*H*$_{Dipp}$), 0.88 (d, *J* = 4.61 Hz, 24H, CH$_{3(Dipp)}$), 0.05 (m, 24H, C*H*$_{3(Dipp)}$), -75.20 (s, 3H, Co*H*Co).

^{13}C{^{1}H} NMR (100.6 MHz, 300 K, THF-d$_8$) δ[ppm]: 169.1, 155.7, 152.4, 139.9, 134.5, 134.3, 133.8, 127.0, 119.8, 116.1, 112.1, 27.5, 24.7

Cyclic Voltammetry: $E_{1/2}$ = –2.4 V vs. Fc/Fc$^+$ in THF

Elemental Analysis calcd. for $C_{88}H_{117}N_2Co_2LiO_4$: C 74.45, H 8.31, N 3.95; found: C 74.66, H 8.29, N 3.82

Magnetic Moment: μ_{eff} (C_6D_6) = 2.1(1) μ_B

Melting point: T > 260°C: decomposition to a black oil

UV-vis (C_6H_6): λ_{max}/nm (ε/L·mol^{-1}·cm^{-1}) = 474 (1200)

4.5.4 Single-Crystal X-ray Crystallography

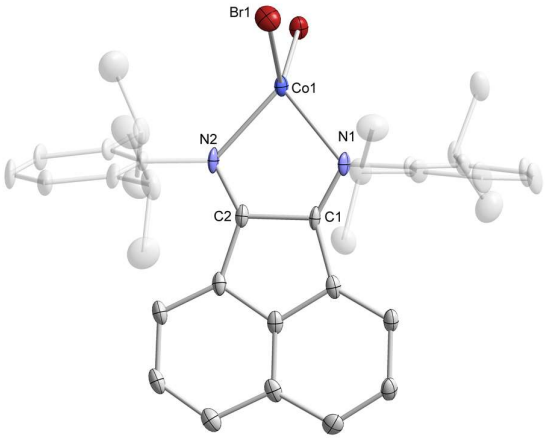

Figure S1. Solid-state molecular structure of [(^{Dipp}BIAN)CoBr$_2$] with thermal ellipsoids drawn at the 40% probability level. Selected bond lengths [Å] and angles [°]: C1–C2 1.513(7), N1–C1 1.278(5), N2–C2 1.277(7), N1–Co1 2.091(4), N2–Co1 2.075(5), Co1–Br1 2.341(1), N1–Co1–N2 82.4(1). Hydrogen atoms are omitted for clarity.

Table S1. Crystallographic data of [(^{Dipp}BIAN)CoBr$_2$], **1**, **3**, **4a**, **4b**

Compound	[(^{Dipp}BIAN)CoBr$_2$]	**1**	**2**
Empirical formula	$C_{36}H_{40}Br_2CoN_2$	$C_{48}H_{60}CoLiN_2O$	$C_{45}H_{53}CoN_2$
Formula weight	719.45	746.85	680.82
Temperature [K]	123.0(10)	123.00(10)	123(1)
Crystal system	monoclinic	orthorhombic	Triclinic
Space group	$P2_1/c$	$Pmn2_1$	P-1
a [Å]	27.0266(7)	17.4715(2)	12.3103(3)
b [Å]	12.0329(2)	10.54720(10)	12.6855(3)
c [Å]	202.8033(6)	10.97630(10)	13.5302(4)
α [°]	90	90	69.519(2)
β [°]	113.047(3)	90	77.844(2)
γ [°]	90	90	79.251(2)
Volume [Å^3]	6823.9(3)	2022.66(4)	1920.22(9)
Z	8	2	2
ρ_{calc} [g/cm^3]	1.401	1.226	1.177
μ [mm^{-1}]	6.871	3.600	3.731
F(000)	2936.0	800	728.0
Crystal size [mm^3]	0.764 × 0.286 × 0.211	0.346 × 0.19 × 0.093	0.291 × 0.197 × 0.073
2Θ range for data collection [°]	7.108 to 147.232	8.384 to 147.308	7.062 to 133.09
Index ranges	-30 ≤ h ≤ 32, -14 ≤ k ≤ 13, -21 ≤ l ≤ 28	-21 ≤ h ≤ 21, -13 ≤ k ≤ 12, -13 ≤ l ≤ 12	-14 ≤ h ≤ 14, -14 ≤ k ≤ 15, -16 ≤ l ≤ 14
Reflections collected	24613	14345	41777
Independent reflections	13116 [R_{int} = 0.0735, R_{sigma} = 0.0749]	3823 [R_{int} = 0.0328, R_{sigma} = 0.0300]	6603 [R_{int} = 0.0613, R_{sigma} = 0.0305]
Data / restraints / parameters	13116/0/755	3823/1/286	6603/0/442
Goodness-of-fit on F^2	1.057	1.057	1.038
Final R indexes [I>=2σ (I)]	R_1 = 0.0857, wR_2 = 0.2360	R_1 = 0.0307, wR_2 = 0.0791	R_1 = 0.0320, wR_2 =
Final R indexes [all data]	R_1 = 0.0892, wR_2 = 0.2404	R_1 = 0.0317, wR_2 = 0.0801	R_1 = 0.0335, wR_2 =
Largest diff. peak/hole [e Å^{-3}]	1.80/-1.56	0.20/-0.41	0.23/-0.51
Flack parameter		-0.021(3)	
CCDC-	1909828	1909827	1909829

.

Compound	**4a**	**4b (**MoK$_\alpha$ radiation)
Empirical formula	$C_{90}Co_2H_{121}LiN_4O_{4.5}$	$C_{92}H_{123}Co_2LiN_4O_5$
Formula weight	1455.70	1489.74
Temperature [K]	138.2(6)	100(1)
Crystal system	orthorhombic	monoclinic
Space group	$Pbca$	$P2_1/n$
a [Å]	25.0102(2)	21.492(1)
b [Å]	21.4146(2)	13.028(1)
c [Å]	30.8908(3)	29.987(2)
α [°]	90	90
β [°]	90	101.086(1)
γ [°]	90	90
Volume [Å^3]	16544.6(3)	8240(1)
Z	8	4

ρ_{calc} [g/cm^3]	1.169	1.201
μ [mm^{-1}]	3.352	0.456
F(000)		
Crystal size [mm^3]	0.31 × 0.24 × 0.16	0.23 × 0.16 × 0.07
1.291 to 2Θ range for data	2.861 to 74.682°	1.291 to 28.906
Index ranges		
Reflections collected	126831	125720
Independent reflections	16725 [R_{int} = 0.0511, R_{sigma} =]	20508 [R_{int} = 0.0433, R_{sigma} =]
Data / restraints / parameters	/686/1175	/1020/1478
Goodness-of-fit on F^2	1.020	1.030
Final R indexes [I>=2σ (I)]	R_1 = 0.0623, wR_2 = 0.1797	R_1 = 0.0432, wR_2 = 0.0994
Final R indexes [all data]	R_1 = 0.0690, wR_2 = 0.1864	R_1 = 0.0650, wR_2 = 0.1100
Largest diff. peak/hole [e Å^{-3}]	1.419/−0.609	0.604/-0.469
CCDC-	1909830	1909831

4.5.5 NMR Spectra

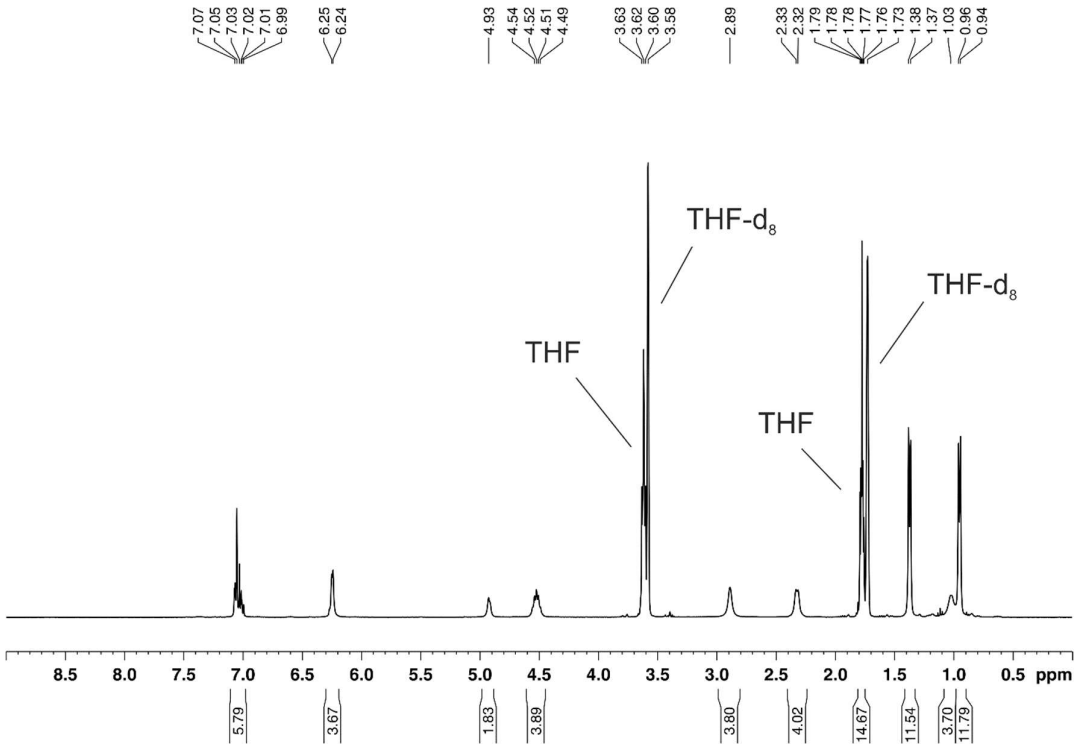

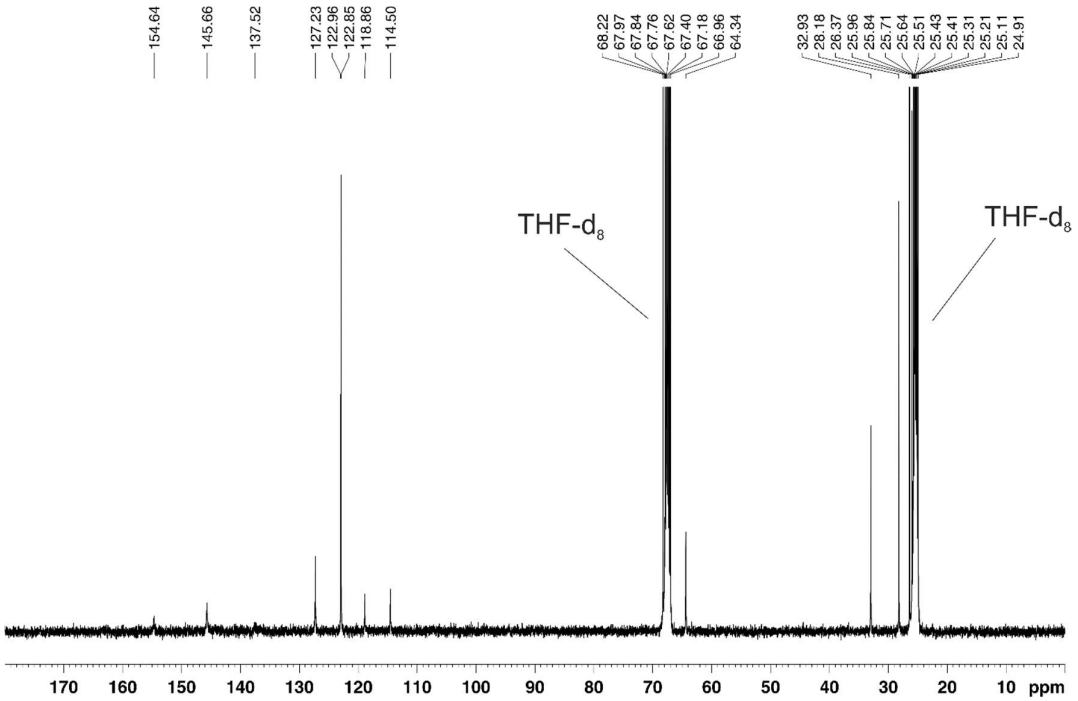

Figure S2. ^{1}H NMR (400.13 MHz, 300K, THF-d$_8$) (top) and ^{13}C{^{1}H} NMR spectra (100.6 MHz, 300K, THF-d$_8$) (bottom) of **1**.

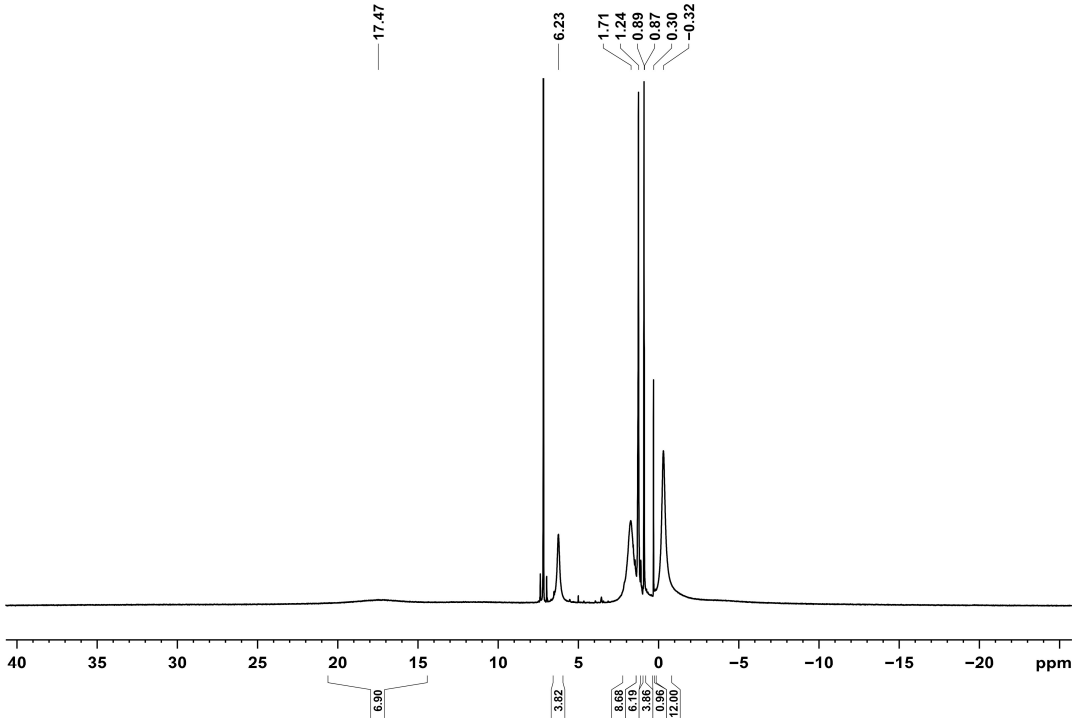

Figure S3. ^{1}H NMR spectrum (400.13 MHz, 300K, THF-d$_8$) of **2.**

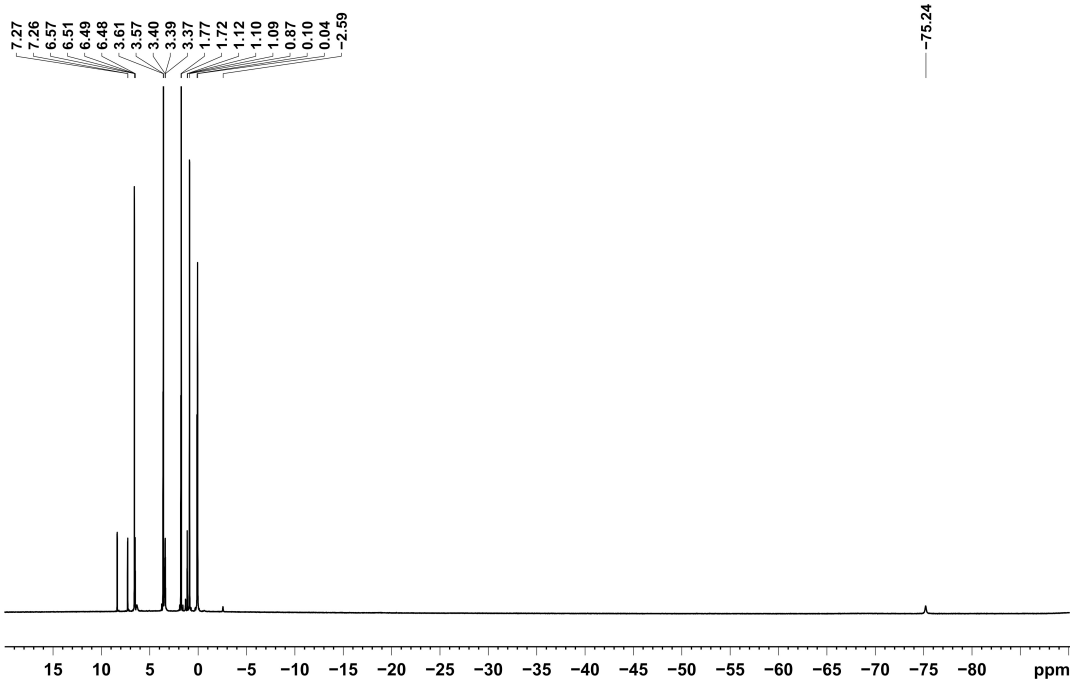

Figure S4. ^{1}H NMR spectrum (400.13 MHz, 300K, THF-d_8) of **4.**

4.5.6 UV-vis Spectra

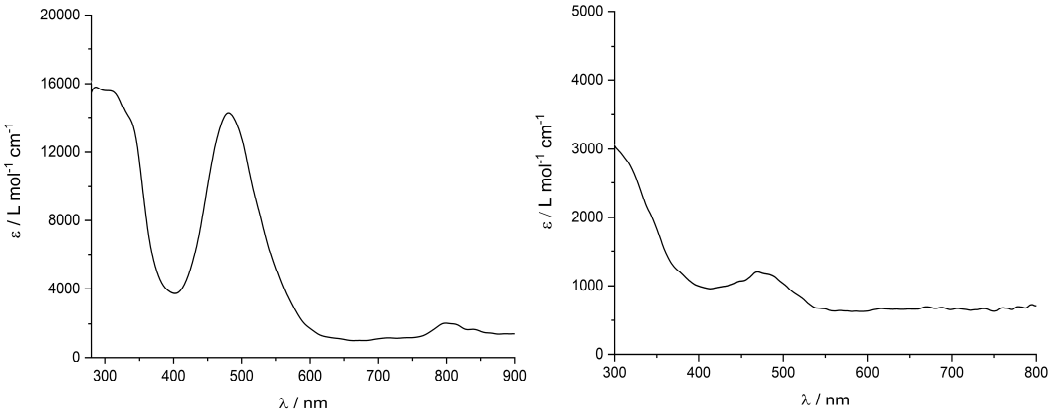

Figure S5. UV-vis spectra of **2** (benzene, left) and **4** (THF, right).

4.5.7 Cyclic Voltammetry

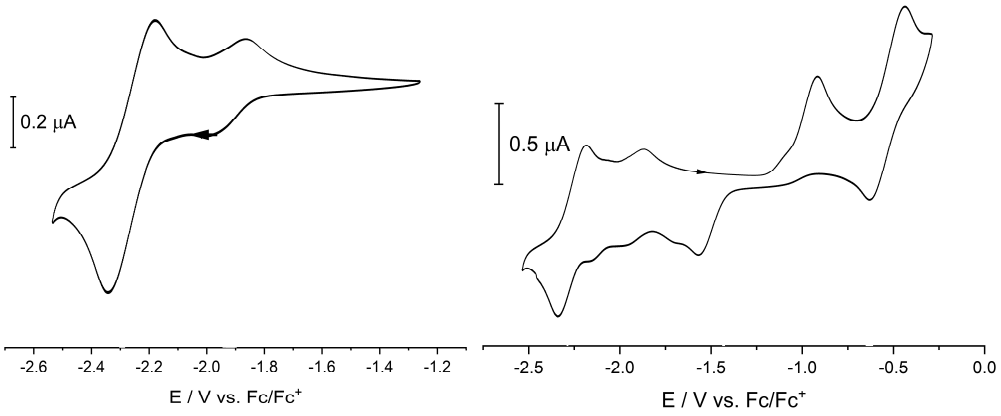

Figure S6. Cyclic voltammogram of **2** in THF/^{n}Bu$_4$NPF$_6$; scan rate: 100 mV s^{-1}.

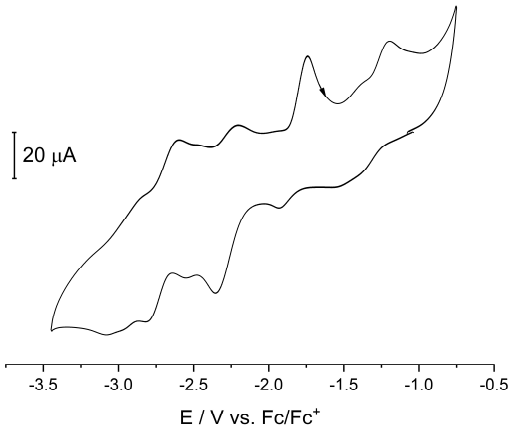

Figure S7. Cyclic voltammogram of **4** in THF/^{n}Bu$_4$NPF$_6$; scan rate: 100 mV s^{-1}.

4.5.8 Catalytic Hydrogenations

4.5.8.1 General Procedure

Procedure A:

In an argon-filled glovebox, a flame-dried 4 mL reaction vial was charged with [(^{Dipp}BIAN)CoBr$_2$] (0.006 mmol), the substrate (0.2 mmol), THF (2 mL) and *n*-pentadecane as internal reference for GC-FID quantification (0.2 mmol). The pale brown solution was reduced by dropwise addition of LiBEt$_3$H (0.018 mmol, 1 M, THF) with a Hamilton syringe, during which time the color changed to red or brown depending on the substrate. After 10 minutes of stirring, the reaction vial was transferred to a high-pressure reactor which was sealed and removed from the glovebox. The reactor was purged with H_2 (3 × 3 bar) and the reaction pressure and temperature were set. After the indicated reaction time, the vial was retrieved

and hydrolyzed with a saturated aqueous solution of NH_4Cl (1 mL). The reaction mixture was extracted with ethyl acetate (3 × 1 mL), dried over sodium sulfate and analyzed by GC-FID and GC-MS.

Procedure B:

In an argon-filled glovebox a flame-dried 4 mL reaction vial was charged with [(^{Dipp}BIAN)$CoBr_2$] (0.006 mmol), THF (1 mL) and *n*-pentadecane as internal reference for GC-FID quantification (0.2 mmol). The resulting pale brown solution was reduced by dropwise addition of $LiBEt_3H$ (0.018 mmol, 1 M, THF) with a Hamilton syringe during which time the color changed to brown. After 10 minutes stirring, the substrate was added and the reaction vial was transferred to a high-pressure reactor which was sealed and removed from the glovebox. See procedure A for hydrogenation and work-up procedure.

Method for kinetic examination in catalytic hydrogenation and poisoning experiments with procedure B:

A flame-dried 10 mL two-necked flask was connected to a *Man on the Moon X201* gas-uptake system with a reservoir pressure of 9 bar H_2 and a constant reaction pressure of 1.9 bar H_2. After purging with H_2, the freshly prepared catalyst solution (reduction of [(^{Dipp}BIAN)$CoBr_2$] (0.006 mmol) with $LiBEt_3H$ (0.018 mmol)) was added via syringe. The recording of the H_2 uptake started with the addition of α-methylstyrene (0.2 mmol). After two minutes, the poisoning agent (for dct and trimethylphosphite) was added by Hamilton syringe. In the case of mercury, the reduced pre-catalyst was stirred over mercury for two or 30 minutes before addition of the substrate. After the reaction, the mixture was treated with a saturated aqueous solution of NH_4Cl and ethyl acetate. The organic phase was separated, filtered through a plug of silica and analyzed by quantitative GC-FID analysis vs. internal standard (*n*-pentadecane). The monitored hydrogen consumption was related to the yield of cumene, which was determined by GC-FID. An induction period may be not detectable since catalyst pre-formation, solvent saturation with H_2, and alkene addition occur prior to the start of the H_2 consumption monitoring. The addition of reagents by syringe through the septum create a temporary leakage that would affect the H_2 pressure recording.

4.5.8.2 Optimization studies

Table S2. Optimization reactions using triphenylethylene as model substrate.

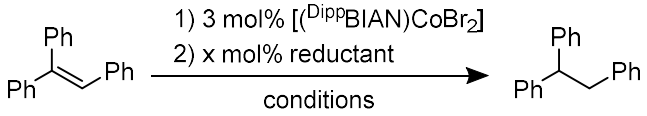

Entry	Reductant (mol%)	Conditions	Yield [%]
1	HBpin (9)	20 bar H_2, 60 °C, 24 h	0 (12)
2	DiBAlH (9)	As entry 1	50 (57)
3	$NaBEt_3H$ (9)	As entry 1	>99
4	$LiBEt_3H$ (9)	As entry 1	>99
5	$LiAlH_4$ (6)	2 bar H_2, 20°C, 3 h	0 (11)
6	HBpin (9) + KO^tBu (9)	As entry 5	<5 (12)
7	K-Selectride (6)	As entry 5	<5 (14)
8	N-Selectride (6)	As entry 5	<5 (14)
9	N-Selectride (9)	As entry 5	8 (15)
10	Li-Selectride (6)	As entry 5	6 (20)
11	Li-Selectride (9)	As entry 5	37 (43)
12	$NaBEt_3H$ (6)	As entry 5	23 (33)
13	$NaBEt_3H$ (9)	As entry 5	64 (65)
14	$LiBEt_3H$ (6)	As entry 5	73 (75)
15	$LiBEt_3H$ (9)	As entry 5	**92**
16	$LiBEt_3H$ (12)	As entry 5	78 (78)

Conditions: 0.2 mmol (0.1 M) alkene in THF, 3 mol% ^{Dipp}BIANCoBr$_2$. Yields were determined by quantitative GC-FID vs. internal *n*-pentadecane. Conversions are given in parentheses if <90%; Reduction in presence of the substrate (protocol A).

Table S3. Hydrogenations with isolated complexes and pre-catalyst mixtures.

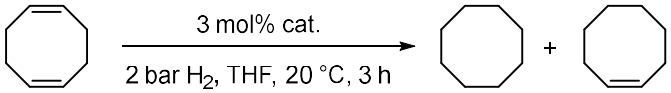

Entry	Catalyst mixture	Yield [%] [a]	
		Cyclooctane	Cyclooctene
1[b]	[(^{Dipp}BIAN)CoBr$_2$] + 9 mol% $LiBEt_3H$	**96**	**1**
2	[Li(thf)$_{3.5}${^{Dipp}BIAN)Co(cod)}] (**1**)	**5**	**61**
3	**1** + 3.5 mol% 12-crown-4	**4**	**44**
4	**1** + 3 mol% [Fc]PF_6	2	17
5	**1** + 9 mol% BEt_3	**66**	**33**
6	[K(thf){(^{Dipp}BIAN)Co(cod)}] (**2**)	**-**	**1**
7	**2** + 3 mol% [Fc]PF_6	1	-
8	**2** + 30 mol% LiBr + [2.2.2]Cryptand	-	2

9	**2** + 30 mol% LiCl + 3 mol% [18]c-6	-	1
10	**2** + 9 mol% BEt_3	1	1
11	**2** + 9 mol% BEt_3+ 30 mol% LiBr	**3**	**38**
12 [b]	(**4a**)	**6**	**7**
13 [b]	**4a** + 3 mol% BEt_3	**22**	**22**
14 [b]	**4a** + 1.5 mol% $LiBEt_3H$	**57**	**43**
15	[(^{Dipp}BIAN)Co(η^6-C_6H_6)] **3**	-	-
16 [c]	**3** + 9 mol% $LiBEt_3H$	4	29

Reaction conditions: 0.2 mmol alkene, 0.1 M in THF, 3 mol% cat., 2 bar H_2. [a] Yields determined by quantitative GC-FID vs. internal *n*-pentadecane.

4.5.8 Other Catalytic Reactions

Isomerization of 1-octene

Table S4. Isomerization of 1-octene

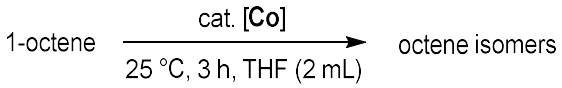

Entry	Procedure	Octene yield [%]				
		1	(*E*)-2	(*E*)-3	(*E*)-4	others
1	A	3	71	22	4	0
2	B	31	39	8	1	20

Conditions: 0.2 mmol (0.1 M) alkene in THF, 3 mol% [(^{Dipp}BIAN)$CoBr_2$]. Yields were determined by rel. peak areas of GC-FID. Procedure A: Reduction in presence of the substrate; Procedure B: Substrate addition after reduction.

Cyclotrimerization of phenylacetylene

Table S5. Cyclotrimerization of 1-phenylacetylene

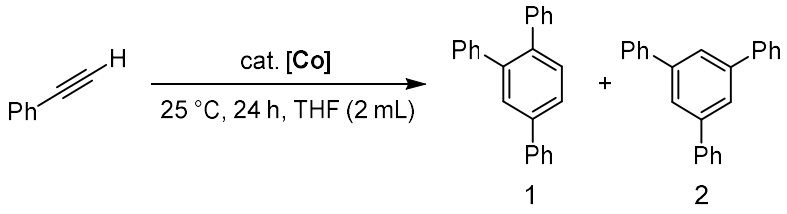

Entry	Procedure	Yield [%]		Conversion [%]
		1	**2**	
1	A	20	9	38
2	B	26	14	54

Conditions: 0.2 mmol (0.1 M) alkene in THF, 3 mol% [(^{Dipp}BIAN)$CoBr_2$]. Yields were determined by rel. peak areas of GC-FID. Procedure A: Reduction in presence of the substrate; Procedure B: Substrate addition after reduction.

Gas evolution measurement

In an argon-filled glovebox, **4a** (16.1 mg, 0.0113 mmol) was dissolved in 1.2 mL THF, transferred outside of the glovebox and added to the Man on the moon gas evolution apparatus by syringe. During the introduction of a solution of HCl in dioxane (4 M) gas evolution was monitored, which corresponds to 2.3 ± 0.1 eq. H_2 per cobalt dimer.

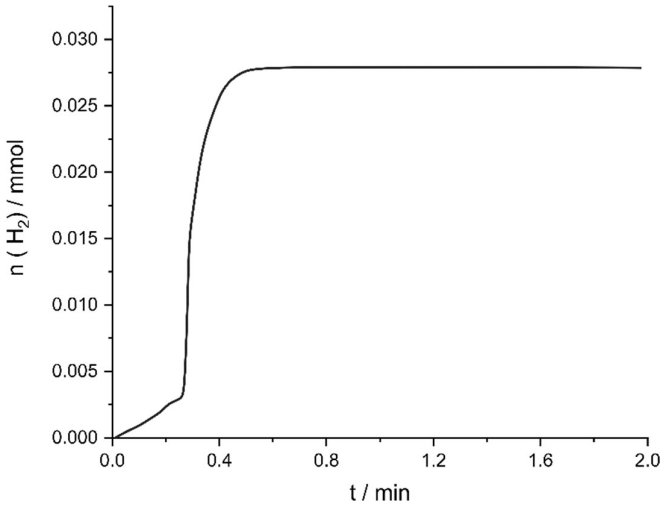

Figure S8. Gas evolution measurement of protolysis of **4a**.

Amine-borane dehydrogenation

In an argon-filled glovebox, **4a** (8.0 mg, 0.006 mmol) was dissolved in THF (0.4 mL). The resulting solution was added dropwise to a solution of NH_3BH_3 (6.4 mg, 0.22 mmol) in THF during which time the color changed from dark green to dark violet. After 17 h, the dark violet solution was filtered from the white precipitate and investigated by ^{11}B NMR.

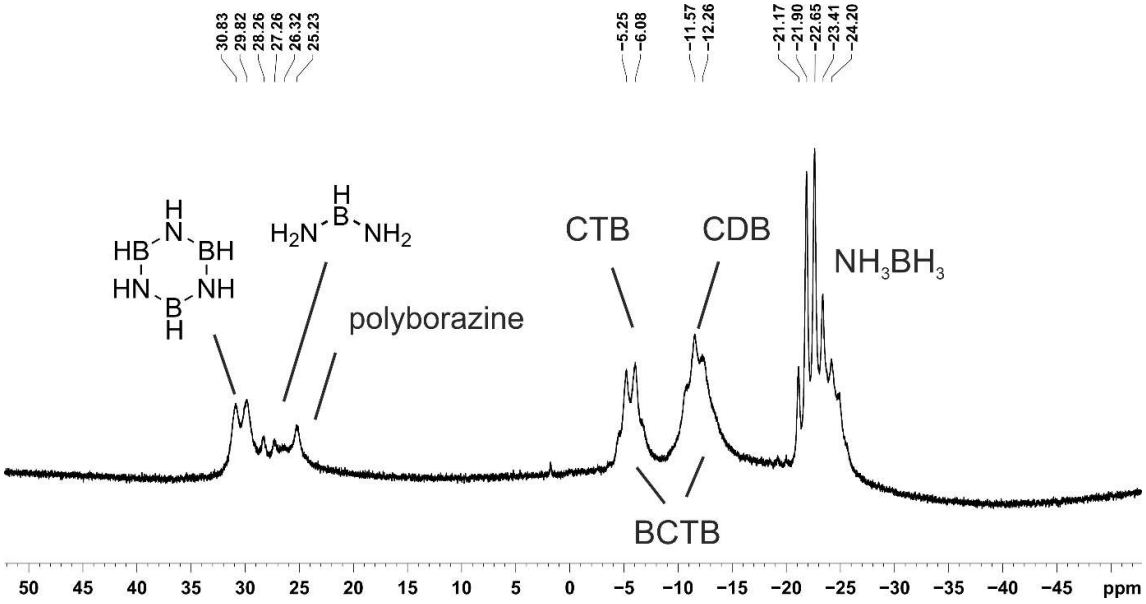

Figure S9. ^{11}B NMR spectrum of NH_3BH_3 dehydrogenation catalyzed by **4a** after 17 h (CTB = cyclotriaminoborane, CDB = cyclodiaminoborane, BCTB = H_3BNH_2-*cyclo*-$B_3N_3H_{11}$).

4.5.9 Computational Details

a) Optimized coordinates for complex **3**

Co	3.373186	4.464605	3.701294	C	4.459853	1.459241	1.492598
N	4.788301	3.658559	2.466997	C	4.163394	0.681467	0.375630
N	5.035374	5.194126	4.637130	H	4.087470	-0.393935	0.487193
C	1.611603	5.654975	3.069253	C	3.968391	1.264503	-0.869735
H	1.611241	6.541621	2.450909	H	3.737827	0.647388	-1.728905
C	1.708954	5.775881	4.471233	C	4.070317	2.642737	-1.008507
H	1.810892	6.750922	4.926119	H	3.921925	3.100769	-1.979535
C	1.763434	4.624384	5.268043	C	4.364942	3.453251	0.085289
H	1.907492	4.714306	6.335380	C	5.067076	5.999106	5.791868
C	1.718913	3.350210	4.664187	C	5.000670	7.394631	5.662088
H	1.800857	2.461795	5.274521	C	4.961442	8.172290	6.817084
C	1.539817	3.230987	3.270110	H	4.913933	9.251150	6.724925
H	1.512644	2.254303	2.808155	C	4.985758	7.584694	8.075339
C	1.486834	4.382560	2.473193	H	4.953751	8.201904	8.964265
H	1.418623	4.291213	1.398474	C	5.051495	6.201994	8.188415
C	6.140244	4.810009	4.027312	H	5.073884	5.740115	9.168647
C	6.006741	3.981392	2.855348	C	5.092564	5.391387	7.056352
C	7.349500	3.680437	2.351920	C	4.692693	0.835868	2.839926
C	8.251381	4.336164	3.235330	H	4.464911	-0.229971	2.820533
C	7.567773	5.035164	4.268763	H	5.732053	0.956374	3.155978
C	8.315752	5.718293	5.201078	H	4.080549	1.315611	3.606677
H	7.850727	6.267110	6.008791	C	4.497527	4.943124	-0.058475
C	9.730341	5.692697	5.087023	H	3.871122	5.465691	0.667696
H	10.314367	6.231564	5.822913	H	5.523829	5.267657	0.130889

C	10.383549	5.012691	4.082292	H	4.218841	5.264274	-1.062194
H	11.465753	5.020635	4.034492	C	4.995320	8.022119	4.296679
C	9.638238	4.297718	3.104560	H	4.206157	7.598791	3.671364
C	10.147410	3.547576	2.008815	H	4.851916	9.100577	4.364375
H	11.217404	3.479880	1.853740	H	5.936063	7.834802	3.773102
C	9.281725	2.909060	1.147751	C	5.184016	3.895703	7.169203
H	9.687495	2.342287	0.318829	H	4.411098	3.407742	6.571457
C	7.871508	2.961593	1.300223	H	6.142081	3.529084	6.791969
H	7.234400	2.442563	0.596997	H	5.082716	3.576768	8.206650
C	4.559912	2.850146	1.337158				

b) Broken-symmetry magnetic coupling analysis

S(High-Spin) = 1.5

<S**2>(High-Spin) = 3.8377

<S**2>(BrokenSym) = 1.6777

E(High-Spin) = -2805.551510 Eh

E(BrokenSym) = -2805.559625 Eh

E(High-Spin)-E(BrokenSym)= 0.2208 eV 1780.893 cm^{-1} (antiferromagnetic coupling)

```
     -------------------------------------------------------
     | Spin-Hamiltonian Analysis based on H(HDvV)= -2J*SA*SB |
-------                                          -----------
| J(1) =   -791.51 cm-1   (from -(E[HS]-E[BS])/Smax**2)          |
| J(2) =   -474.90 cm-1   (from -(E[HS]-E[BS])/(Smax*(Smax+1))   |
| J(3) =   -824.48 cm-1   (from -(E[HS]-E[BS])/(<S**2>HS-<S**2>BS)) |
```

c) Unrestricted natural orbital analysis (UNOs)

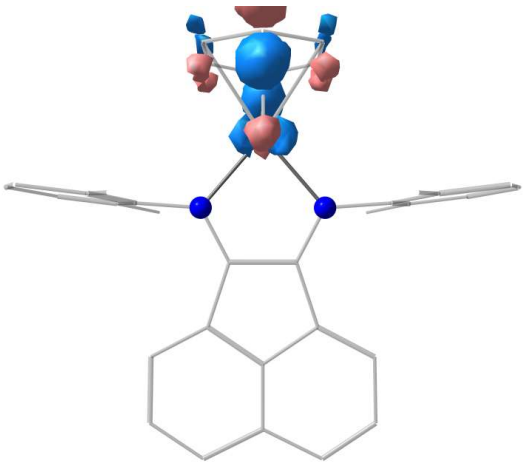

139 (occu.: 0.022, 53% $3d_{yz}$)

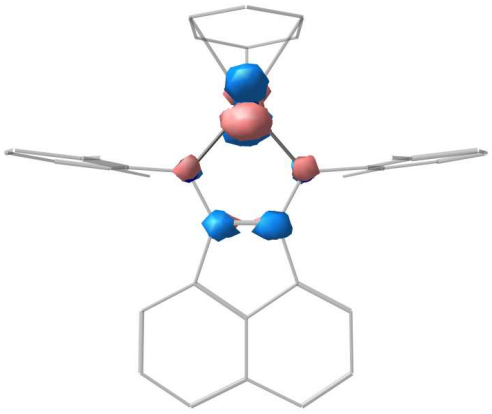

138 (occu.: 0.604, 27% $3d_{xy}$, 13% $3d_{xz}$)

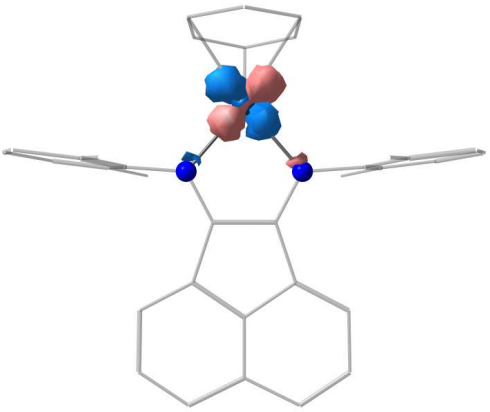

137 (occu.: 1.000, 53% $3d_{xz}$, 27% $3d_{xy}$)

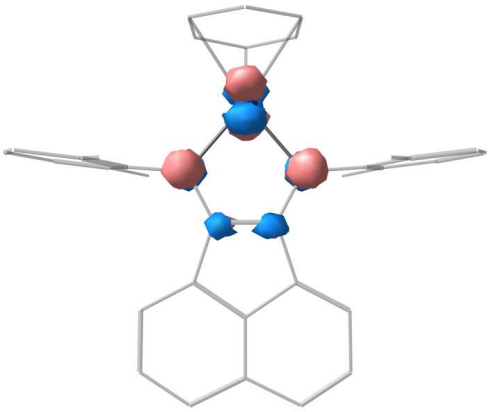

136 (occu.: 1.396, 34% $3d_{xy}$, 17% $3d_{xz}$)

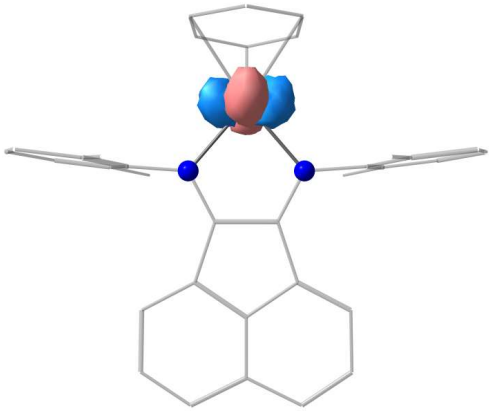

135 (occu.: 1.977, 74% $3d_{yz}$, 7% 3)

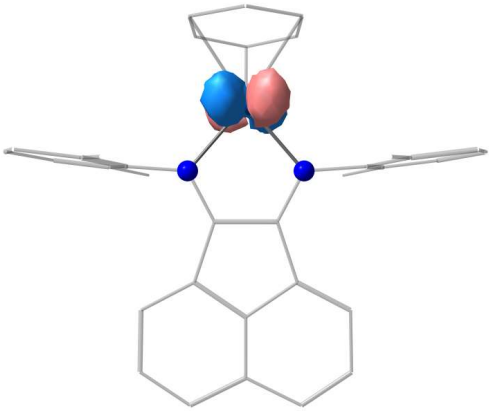

134 (occu.: 1.984, 56% 3, 19%, 3, 11% $3d_{yz}$)

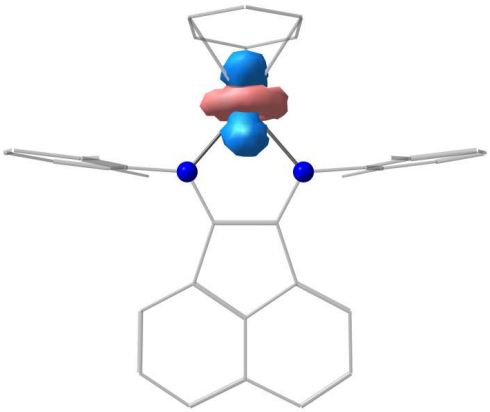

133 (occu.: 1.999, 68% 3 , 23% 3,)

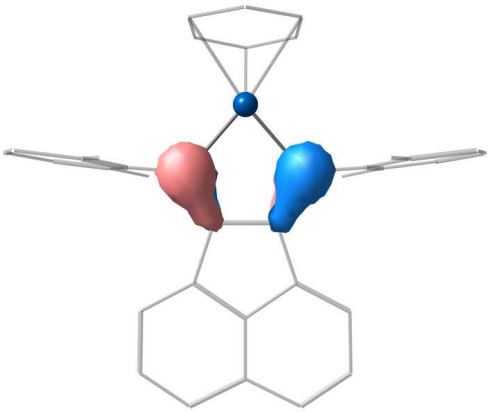

132 (occu.: 1.999)

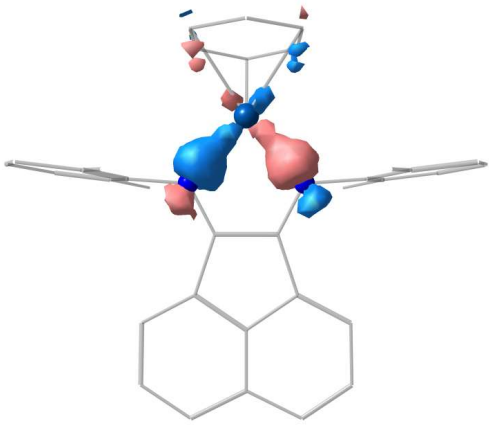

131 (occu.: 1.999, 12% $3d_{xz}$, 6% d_{xy})

d) Löwdin atomic charges and spin populations

0 Co:	-0.067265	1.871502	34 C :	-0.143707	0.000506
1 N :	0.221837	-0.140457	35 C :	-0.129247	-0.001814
2 N :	0.221703	-0.140591	36 H :	0.141671	-0.000312
3 C :	-0.123854	-0.020186	37 C :	-0.153498	0.007065
4 H :	0.151606	0.000039	38 H :	0.139706	0.000022
5 C :	-0.108718	-0.011065	39 C :	-0.129218	-0.001815
6 H :	0.155698	0.000122	40 H :	0.141656	-0.000309
7 C :	-0.108831	-0.011512	41 C :	-0.143634	0.000499
8 H :	0.155742	0.000115	42 C :	-0.142933	-0.014425
9 C :	-0.124110	-0.020486	43 C :	-0.143572	0.000484
10 H :	0.151656	0.000032	44 C :	-0.129250	-0.001813
11 C :	-0.108523	-0.011441	45 H :	0.141645	-0.000308
12 H :	0.155863	0.000118	46 C :	-0.153513	0.007059
13 C :	-0.108930	-0.011397	47 H :	0.139703	0.000022
14 H :	0.155701	0.000119	48 C :	-0.129240	-0.001814
15 C :	-0.149710	-0.146394	49 H :	0.141666	-0.000313
16 C :	-0.149668	-0.146079	50 C :	-0.143592	0.000483
17 C :	-0.061735	-0.007245	51 C :	-0.247110	-0.001232
18 C :	-0.015020	-0.067397	52 H :	0.122049	0.000012
19 C :	-0.061822	-0.007257	53 H :	0.131191	0.000337
20 C :	-0.094820	-0.023417	54 H :	0.128801	-0.000445
21 H :	0.152103	0.000047	55 C :	-0.247142	-0.001264
22 C :	-0.134242	0.006208	56 H :	0.128627	-0.000443
23 H :	0.142641	0.000024	57 H :	0.131210	0.000338
24 C :	-0.098924	-0.031071	58 H :	0.122034	0.000000
25 H :	0.142987	-0.000023	59 C :	-0.247071	-0.001249
26 C :	-0.101963	-0.007892	60 H :	0.128462	-0.000428
27 C :	-0.098886	-0.030885	61 H :	0.122052	-0.000004
28 H :	0.142994	-0.000023	62 H :	0.131226	0.000335
29 C :	-0.134248	0.006194	63 C :	-0.247087	-0.001222

30	H :	0.142642	0.000024	64 H :	0.128682 -0.000435
31	C :	-0.094819	-0.023237	65 H :	0.131188 0.000334
32	H :	0.152113	0.000047	66 H :	0.122073 0.000010
33	C :	-0.143023	-0.014395		

4.5.10 References

[1] F. Neese, *Wiley Interdiscip. Rev. Comput. Mol. Sci.*, DOI:10.1002/wcms.1327

[2] F. Neese, *Wiley Interdiscip. Rev. Comput. Mol. Sci.* **2012**, *2*, 73-78.

[3] a) A. D. Becke *J. Chem. Phys.* **1993**, *98*, 5648. b) F. Weigend *Phys. Chem. Chem. Phys.* **2005**, *7*, 3297. c) F. Weigend *Phys. Chem. Chem. Phys.* **2006**, *8*, 1057.d) S. Grimme, S. Ehrlich, L. Goerigk *J. Comput. Chem.* **2011**, *32*, 1456-1465. e) S. Grimme, J. Antony, S. Ehrlich, H. Krieg *J. Chem. Phys.* **2010**, *132*, 154104.

[4] a) L. Noodleman, J. G. Norman *J. Chem. Phys.* **1979**, *70*, 4903-4906. b) L. Noodleman *J. Chem. Phys.* **1981**, *74*, 5737-5743. c) L. Noodleman, J. G. Norman, J. H. Osborne, A. Aizman, D. A. Case *J. Am. Chem. Soc.* **1985**, *107*, 3418-3426. d) L. Noodleman, E. R. Davidson *Chem. Phys.* **1986**, *109*, 131-143. e) L. Noodleman, C. Y. Peng, D. A. Case, J.-M. Mouesca *Coord. Chem. Rev.* **1995**, *144*, 199-204.

[5] D. F. Evans, *J. Chem. Soc.* **1959**, 2003.

[6] a) SCALE3ABS, CrysAlisPro, Agilent Technologies Inc. Oxford, GB; b) G. M. Sheldrick, SADABS, Bruker AXS, Madison, USA, 2007.

[7] a) R. C. Clark, J. S. Reid, *Acta Crystallogr. A.* **1995**, *51*, 8876; b) CrysAlisPro, version 40_64.18, Agilent Technologies Inc. Oxford, GB.

[8] G. M. Sheldrick, *Acta Cryst.* **2015**, ***A71***, 3.

[9] G. M. Sheldrick, *Acta Cryst.* **2015**, ***C71***, 3.

[10] V. Rosa, R. J. Gonzalez, T. Aviles, P. T. Gomes, R. Welter, A. C: Rizzi, M. C. G. Passeggi, C- D-Brondino *Eur. J. Inorg. Chem.* **2006**, 4761-4769

5 Heterogeneous Olefin Hydrogenation Enabled by a Nickel(–II) Pre-Catalyst

Thomas M. Maier, Sebastian Sandl, Peter Melzl, Josef Zweck, Axel Jacobi von Wangelin, and Robert Wolf

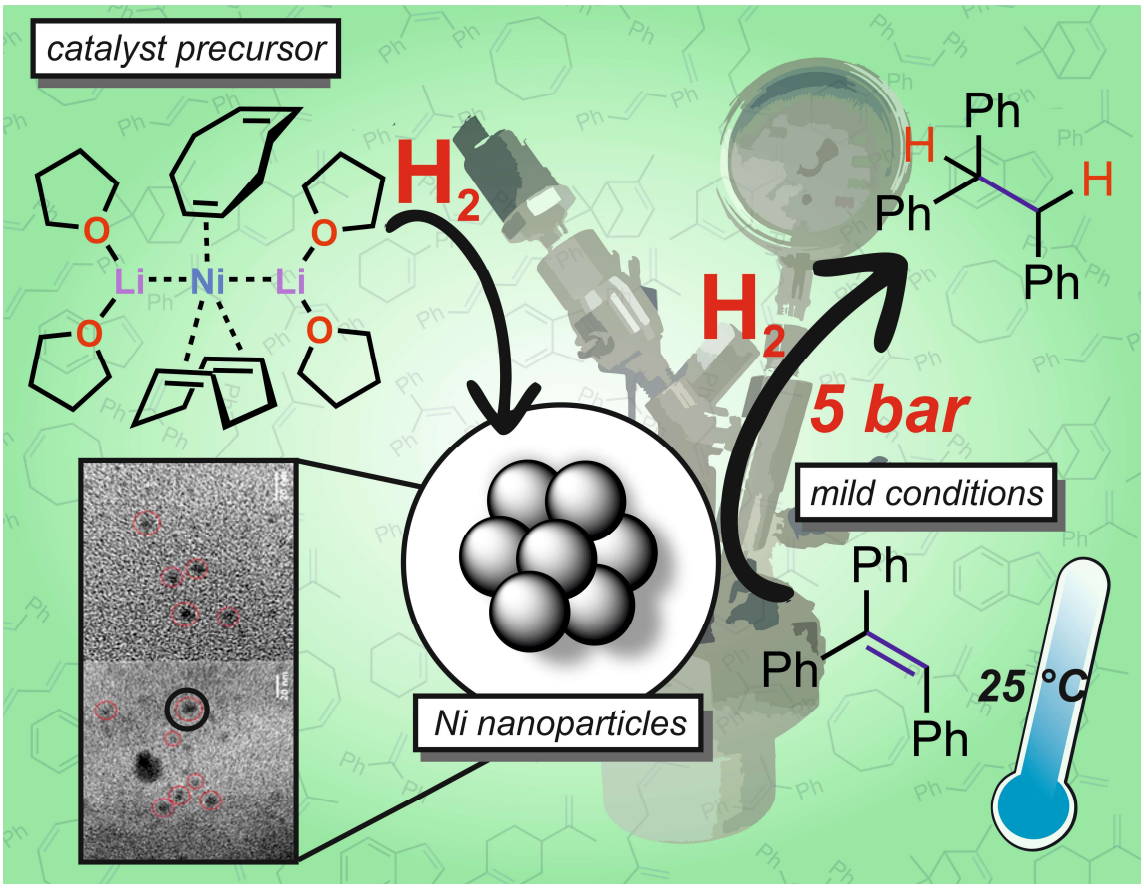

T. M. Maier performed the experimental work and wrote the manuscript. S. Sandl and A. Jacobi von Wangelin conducted and interpreted kinetic investigations including preparation of Figure 4 and some mechanistic experiments (Scheme 2a,b). P. Melzl and J. Zweck recorded and analyzed TEM images (Figure 5). A. Jacobi von Wangelin and R. Wolf supervised and directed the project.

This chapter was published in *Chemistry – A European Journal* as a communication: T. M. Maier, S. Sandl, P. Melzl, J. Zweck, A. Jacobi von Wangelin, J. J. Weigand, R. Wolf, *Chem. Eur. J.* **2020**, *26*, 6113-6117. Reproduced with permission from Wiley-VCH. Schemes, Figures, and text may differ from published version.

5.1 Introduction

Olefin hydrogenation is of high industrial and academic importance as a key step in the synthesis of fine chemicals, agrochemicals, fragrances, and food additives.[1] Precious metal catalysts (Rh, Ir, Pt, Pd, Ru) are most widely applied due to their high activity, selectivity, robustness, and ease of operation.[2] Nevertheless, economic and environmental concern (in particular the poor crustal abundance and high cost of precious metals) have recently stimulated considerable interest in replacing noble metal catalysts by more abundant 3d metal species[3] (e.g. with Mn,[4] Fe,[5] Co[6], Ni[7]-[17]). Over the past decade, major effort has been devoted to the development of iron and cobalt compounds as catalysts for olefin hydrogenation.[5],[6] Especially noteworthy are metal complexes with tridentate pincer ligands.[5d],[6b]

While these developments have been fairly recent, nickel compounds have been applied in technical scale hydrogenations for many decades. Raney nickel was first reported in 1927[7] and is still industrially used in the hardening of vegetable fats, the manufacture of vitamins, fragrances, and food additives as well as various arene functionalizations.[8] Nickel boride (obtained from NiX_2 (X = OAc, Cl) and $NaBH_4$) is an effective catalyst for olefin hydrogenation.[9] The development of more potent heterogeneous nickel catalysts continues to attract significant interest as shown by the groups of *Gómez* and *Philippot*, who reported the use of commercial [Ni(η^4-cod)$_2$] (cod = 1,5-cyclooctadiene) as a catalyst precursor (see Figure 1, **A**).[10],[11] *Zhao* and co-workers demonstrated that Ni(0) nanoparticles (NPs) in ionic liquids hydrogenate α,β-unsaturated carbonyl compounds at 30 bar H_2.[12] In addition, well-defined molecular nickel catalysts have been reported. The groups of *Bouwman* and *Hanson* described the hydrogenation of simple olefins with homogeneous nickel catalysts.[13] *Hazari* and *Driess* prepared heteroleptic carbene/silylene complexes **B** and **C**, which are very active hydrogenation catalysts.[14],[15] Catalyst **D** reported by *Chirik* and co-workers constitutes the current state of the art in catalytic hydrogenations of sterically hindered tri- and tetra-substituted olefins.[16] The active catalyst is assembled from the combination of nickel(II) bis(octanoate), pinacol borane, and an α-diimine ligand. Moreover, recent reports on asymmetric hydrogenations of dehydroamino acids catalyzed by $Ni(OAc)_2$ and the chiral ligand (*S*)-binapine are noteworthy.[17]

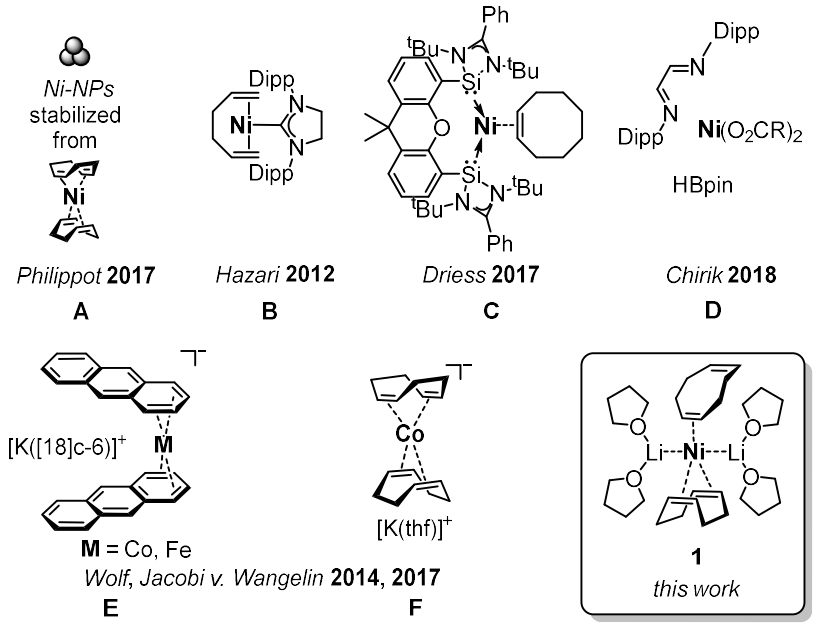

Figure 1. Selected Ni pre-catalysts for C=C bond hydrogenation (top). Low-valent anionic transition metal complexes as hydrogenation catalysts by our group (bottom). Dipp = 2,6-diisopropylphenyl.

We previously investigated low-valent ferrate and cobaltate anions ([K([18]c-6)(thf)$_2$][M(η^4-anthracene)$_2$] (M = Fe, Co), and [K(thf)$_x${Co(η^4-cod)$_2$}] first synthesized by the groups of *Ellis*[18],[19] and *Jonas*[20] as catalysts in the hydrogenation of olefins, ketones, and imines.[6] These "quasi-naked" anionic metal species exhibited high hydrogenation activities for mono/di-substituted C=C bonds but fared poorly for sterically hindered tri/tetra-substituted olefins. Due to the lability of the arene and olefin ligands, both heterogeneous and homogeneous mechanistic pathways are accessible, depending on the nature of the substrate. Following our recent development of effective olefin hydrogenations with anionic iron and cobalt catalysts[6], we were interested to complement these studies with the corresponding nickelate complex [Li$_2$(thf)$_4${Ni(η^2-cod)(η^4-cod)}] (**1**).[21] This compound was first synthesized by *Jonas* and co-workers by reduction of the commercially available [Ni(η^4-cod)$_2$] with Li metal. **1** was only very recently structurally characterized by *Cornella* and co-workers, who also reported that **1** effectively catalyzes Kumada-Corriu cross coupling reactions.[22] Herein, we show that **1** is a pre-catalyst for the hydrogenation of hindered olefins. We provide solid mechanistic evidence that suggests the *in situ* formation of highly-active Ni particles.

5.2 Results and Discussion

Initial optimization experiments were performed using triphenylethylene as model substrate. Most importantly, the ate-complex **1** showed significantly higher activity in comparison with its oxidized counterpart [Ni(η^4-cod)$_2$].[23] With [Ni(η^4-cod)$_2$] only a yield of 36% was achieved within 15 h, whereas full conversion to triphenylethane was observed with **1** (Scheme 1). The same applies for 1-phenyl-1-cyclohexene. No conversion was observed using [Ni(η^4-cod)$_2$], while 74% conversion were observed with **1**. The optimized conditions for triphenylethylene are 1 mol% pre-catalyst **1**, a reaction time of 15 h, and 5 bar H_2 at ambient temperature in 1,2-dimethoxyethane (DME) (Table 1, entries 1-3). The reaction was incomplete after 15 h, when the pressure was decreased to 1.9 bar (Table 1, entry 4).

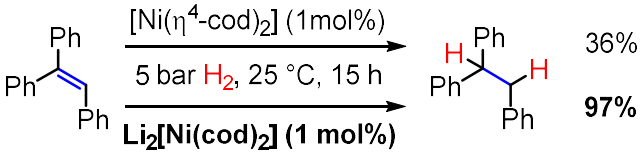

Scheme 1. Comparison of lithium nickelate **1** and [Ni(η^4-cod)$_2$] as pre-catalysts in the hydrogenation of triphenylethylene in DME. Yields were determined by quantitative GC-FID vs. internal *n*-pentadecane.

Table 1. Optimization experiments

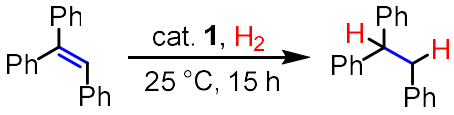

Entry	Catalyst	Solvent [mL]	p (H_2) [bar]	Yield (Conversion) [%]
1	**1**	THF (0.50)	5.0	81 (82)
2	**1**	DME (0.50)	5.0	97 (98)
3	**1**	DME (0.25)	5.0	99 (>99)
4	**1**	DME (0.25)	1.9	72 (74)
5	**1**+ exc. Hg[c]	DME (0.25)	5.0	2 (5)
6	**1**+ dct[d]	DME (0.25)	5.0	92 (>99)

[a] Standard conditions: Substrate (0.2 mmol), 25 °C, 15 h. Yields and conversions were determined by quantitative GC-FID vs. internal *n*-pentadecane. [b] 1 mol%. catalyst. [c] Large excess of Hg (one drop, 50 mg, 0.25 mmol, 125 equiv.). [d] dct (dibenzo[*a*,*e*]cyclooctatetraene; 0.8 mg 0.004 mmol, 2.0 equiv. per [Ni]), 21 h

Under these optimized conditions, linear α-olefins (*trans*-4-octene, allylbenzene) and even sterically hindered olefins such as diphenylethylenes, 1-phenyl-1-cyclohexene, and 1,5-cyclooctadiene were successfully hydrogenated (Figure 2). Myrcene was converted to

2,6-dimethyloctane after 20 h; α-pinene and (*R*)-limonene were hydrogenated under relatively mild conditions (>80% conversion at 50-60 °C). Cinnamic acid (C=C, C=O) and benzonitrile (C≡N) remained untouched under the standard conditions. Note that catalytic amounts of benzonitrile (5 equiv. per [Ni]) also prevented triphenylethylene hydrogenation (*vide infra* and see the SI, Table S9). Pre-catalyst **1** is not competent for the hydrogenation of polyaromatic substrates, e.g. anthracene, naphthalene, and quinolines.

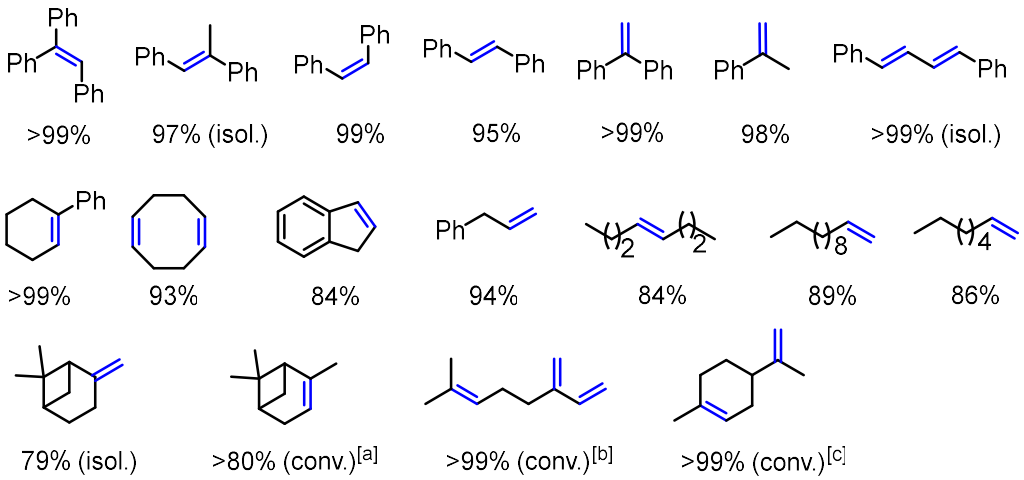

Figure 2. Hydrogenation of olefins with **1** (1 mol%). Standard conditions: 5 bar H_2, 25 °C, 18 h, substrate (0.2 mmol), DME (0.25 mL). Yields and conversions (conv.) were determined by quantitative GC-FID vs. internal *n*-pentadecane Isolated products (isol.) from 1.0 mmol scales (1.25 mL DME). [a] 16 h, 50 °C, 50 bar H_2, DME (0.5 mL). [b] 20 h. [c] 60 °C, 25 bar H_2.

Previous reports on nickel-catalyzed hydrogenation of olefins have barely addressed functional group compatibility.[7]-[16] We extended this protocol to olefinic alcohols, which are often found in bioactive molecules. Gratifyingly, olefins with phenolic as well as primary and secondary aliphatic hydroxyl functions were cleanly hydrogenated. Halogen atoms were partially tolerated. The C=C-hydrogenation of α,β-unsaturated lactones (coumarin) and esters (ethyl cinnamate) exhibited high chemoselectivities. A brief comparison of the catalytic activity of **1** vs. related anionic metalate pre-catalysts revealed that bis(η^4-anthracene) ferrate and bis(η^4-anthracene) cobaltate (**E**, Figure 1) required harsher conditions (60 °C, 2-10 bar H_2, 24 h) than **1** for the hydrogenation of α-methylstyrene and 2-octene.[6] Bis(η^4-cyclooctadiene) cobaltate (**F**) exhibited low functional group tolerance. However, it should be noted that the anions **E** and **F** were effective catalysts in the hydrogenation of ketones and imines.[6g]

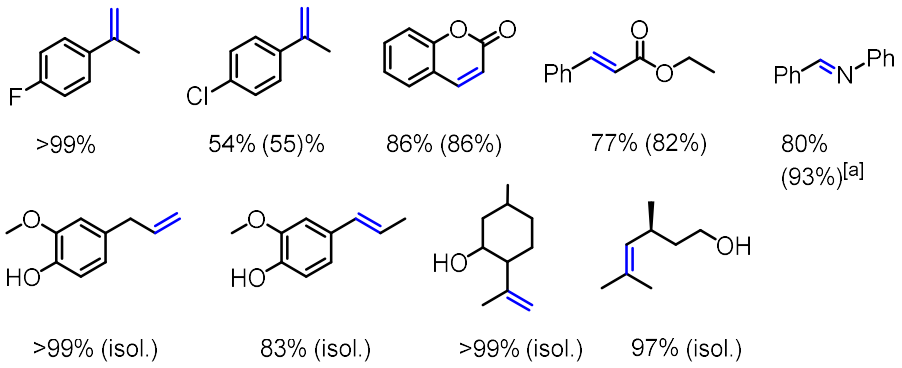

Figure 3. Hydrogenation of functionalized olefins using **1** (1 mol%). Standard conditions: 5 bar H_2, 25 °C, 18 h, substrate 0.2 mmol, DME (0.25 mL). Yields were determined by quantitative GC-FID vs. internal *n*-pentadecane if not stated otherwise. Conversions are given in parentheses. Isolated products (isol.) were obtained from reactions performed on a 1.0 mmol scale in 1.25 mL DME. [a] 5 mol% **1**.

Pre-catalyst **1** is also comparable to related Ni complexes **C** and **D** developed by *Driess* and *Chirik*, respectively (see Figure 1 and additionally Tables S2 and S3 of the SI).[14],[16] It was reported that catalyst **C** enables the complete hydrogenation of 1-octene using 1 bar H_2 and 1.5 mol% catalyst. In comparison, **1** only gives a slightly poorer yield (86%) under the same conditions. Moreover, a similar turnover number and reaction time was observed for **D** and **1** for the hydrogenation of 1-phenyl-1-cyclohexene with H_2 (4 bar) and 0.4 mol% Ni catalyst at 50 °C (see the SI for details). Nonetheless, catalyst **D** inarguably is superior in the hydrogenation of highly challenging substrates such as tetra-substituted alkenes.[16]

In order to study the nature of the catalytic process, simple reaction progress analyses of 1-octene, 2-(*E*)-octene, and α-methylstyrene were performed at 1.9 bar H_2 and ambient temperature using catalyst **1** (1 mol%, see the SI for details). The monitoring experiments revealed significant induction periods and sigmoidal behaviors, which are indicative for slow catalyst formation and nucleation to heterogeneous species (Figure 4).[6] From these experiments, a turnover frequency (TOF) of 601 h^{-1} can be approximated for the hydrogenation of 1-octene at low conversion (see the SI for details), while estimated TOFs are expectedly lower for the secondary olefins 2-octene (103 h^{-1}) and α-methylstyrene (287 h^{-1}). Note that the reported values are inevitably approximate to the presence of an induction period.

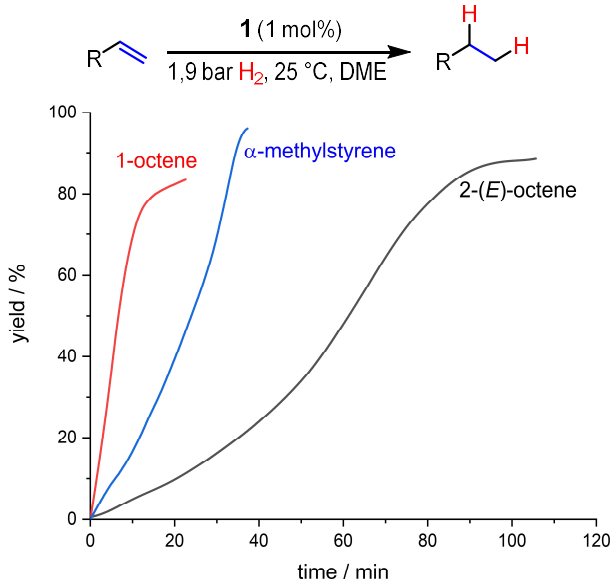

Figure 4. Reaction profiles of the olefin hydrogenations using **1**. Conditions: Substrate (0.2 mmol), DME (0.25 mL), 1.9 bar H_2, 25 °C. Yields determined by H_2 consumption, quantitative GC-FID vs. internal *n*-pentadecane.

The formation of heterogeneous species formed from the reaction of **1** and 1-phenyl-1-cyclohexene under an H_2 atmosphere was investigated by transmission electron microscopy (TEM, Figure 5). Particles of 10-15 nm diameter were observed alongside a few larger particles.

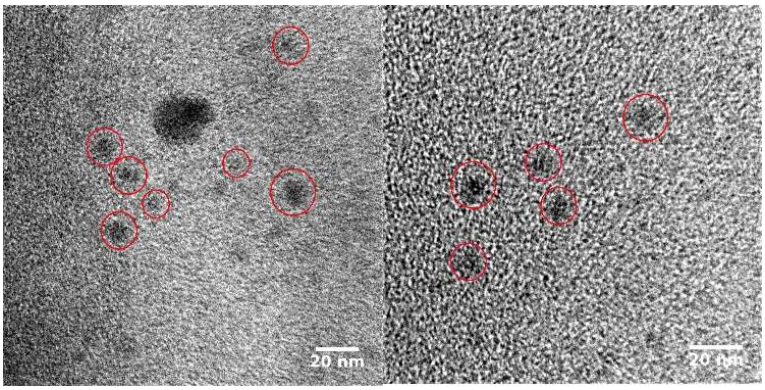

Figure 5. TEM images of particles formed in the hydrogenation of 1-phenyl-1-cyclohexene with **1** (particles highlighted with red circles vs. carbon film support).

Poisoning experiments were performed to corroborate the proposed heterotopic nature of the active catalyst.[25] Addition of excess amounts of mercury led to complete catalyst inhibition in hydrogenations with **1** (Table 1, entry 5).[6],[23] In contrast, the product yield was hardly affected by the presence of two equivalents of dibenzo[*a*,*e*]cyclooctatetraene (dct) per nickel atom (see Table 1, entry 6).[25] In addition, benzonitrile (5 equiv. per Ni atom) is an efficient catalyst

poison, while naphthalene only has a very minor inhibiting effect (see the SI for details). In sum, these results strongly suggest that a heterotopic catalyst is operating.

Further mechanistic experiments were performed with the pre-catalyst **1** under reaction conditions: The rapid color change (orange to black) that was observed when treating a solution of 1-octene in DME with catalytic amounts of **1** under H_2 may indicate nanoparticle formation (Scheme 2a). Isomerization of allylbenzene to 1-propenylbenzene (55%) using **1** (1 mol%) proceeded in the absence of dihydrogen. Minor amounts of the ring-opening product (18%) were detected in the hydrogenation of α-cyclopropylstyrene (Scheme 2b).[26] ^{1}H NMR spectra of **1** and triphenylethylene in the absence of dihydrogen indicated the operation of rapid two-electron transfer from **1**. The resulting deep purple solution (λ_{max} = 511 nm, see the SI, Figure S39) showed the characteristic signals of [Ni(η^4-cod)$_2$] (Scheme 2c). Aqueous work-up afforded significant amounts of triphenylethane (see the SI). The cyclic voltammogram of the postulated triphenylethylene-dianion exhibited one irreversible reduction peak at –2.9 V vs. Fc/Fc$^+$ in THF and DME (see the SI, Figures S35, S36). This species was already detected in literature.[27] Surprisingly, the rate of hydrogenation of triphenylethylene by [Ni(η^4-cod)$_2$] is significantly slower than with **1**. Deuterium experiments were performed to distinguish between H atom transfer (HAT) and ionic reactions (Scheme 2c, 2d). Reaction of **1** and triphenylethylene in THF-d_8 led to no incorporation of D atoms after aqueous work-up. The same reaction in THF and subsequent work-up with D_2O furnished the formation of triphenylethane-d_2 (GC-MS, ^{1}H NMR and ^{2}H NMR spectroscopy). These data strongly support an ionic mechanism. No electron transfer appeared to operate in reactions between **1** and 1-dodecene as no [Ni(η^4-cod)$_2$] was observed but rather olefin isomerization products (Scheme 2e). In summary, the preliminary mechanistic data may suggest an electron-transfer initiation of the catalytic mechanism with reduction-sensitive substrates. Nonetheless, further mechanistic investigations are required to conclusively clarify the catalyst activation mechanism.

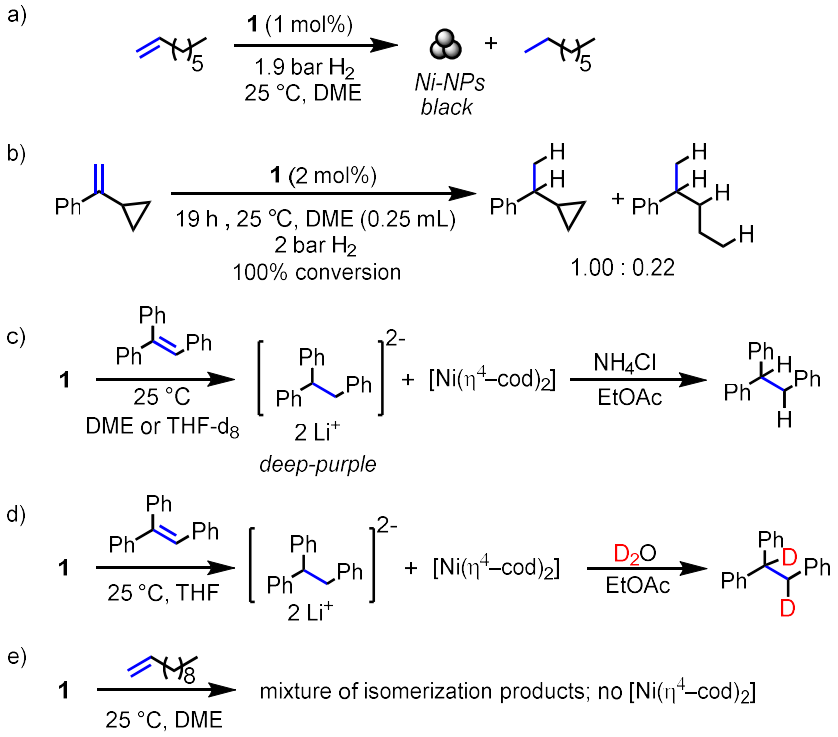

Scheme 2. Mechanistic experiments. a) Nanoparticle formation in the hydrogenation of 1-octene. b) Ring-opening of radical probe. c) Protonation and d) Deuteration of dianionic intermediate from electron transfer with triphenylethylene. e) Catalytic isomerization of 1-dodecene.

5.3 Conclusion

In conclusion, we have shown that dilithiumbis(1,5-cyclooctadiene) nickelate (**1**) is a promising pre-catalyst for the hydrogenation of sterically hindered olefins. The catalytic hydrogenation operates under very mild conditions (5 bar H_2, 25 °C, DME as solvent). This work complements earlier studies of catalytic applications of "quasi-naked" base metal anions to olefin hydrogenations. The nickelate **1** exhibited higher catalytic activities than the related arene metalates (**E** and **F**), yet **1** was compatible with several functional groups (OH, esters, halides). Key mechanistic studies including reaction progress analyses, stoichiometric reactions, poisoning experiments, and transmission electron microscopy were conducted. These investigations support the notion of catalytically active nickel nanoparticles being operative under the reaction conditions. The catalyst formation from **1** is substrate-dependent and involves electron transfer reactions with reducible olefins (e.g. triphenylethylene). This first catalytic application of a stabilized nickelate anion to olefin hydrogenation provides a firm basis for further investigations into the role of highly reduced, anionic metal catalysts as key intermediates in reductive transformations.

5.4 References

[1] a) *Catalytic Hydrogenation* (Ed.: L. Cerveny), Elsevier, Amsterdam, **1986**; b) *The Handbook of Homogeneous Hydrogenation* (Eds.: J. G. de Vries, C. J. Elsevier), Wiley-VCH, Weinheim, **2007**.

[2] a) J. A. Osborn, F. H. Jardine, J. F. Young, G. Wilkinson, *J. Chem. Soc.* **1966**, 1711-1732; b) W. S. Knowles, M. J. Sabacky, B. D. Vineyard, D. J. Weinkauff, *J. Am. Chem. Soc.* **1975**, *97*, 2567–2568; c) H. Doucet, T. Ohkuma, K. Murata, T. Yokozawa, M. Kozawa, E. Katayama, A. F. England, T. Ikariya, R. Noyori, *Angew. Chem. Int. Ed.* **1998**, *37*, 1703–1707; d) Á. Molnár, A. Sárkány, M. Varga, *J. Mol. Catal.* **2001**, *173*, 185–221.

[3] a) *Catalysis without precious metals* (Ed.: R. Morris Bullock), Wiley-VCH, Weinheim, **2010**; b) K. Junge, K. Schröder, M. Beller, *Chem. Commun.* **2011**, *47*, 4849–4859. c) P. J. Chirik, *Acc. Chem. Res.* **2015**, *48*, 1687–1695. d) *Non-Noble Metal Catalysis: Molecular Approaches and Reactions*, (Eds.: R. J. M. Klein Gebbink, M.-E. Moret), Wiley-VCH, Weinheim, **2018**. e) L. Alig, M. Fritz, S. Schneider, *Chem. Rev.* **2019**, *119*, 2681–2751. f) W. Ai, R. Zhong, X. Liu, Q. Liu, *Chem. Rev.* **2018**, *119*, 2876-2953. g) G. A. Filonenko, R. van Putten, E. J. M. Hensen, E. A. Pidko, *Chem. Soc. Rev.* **2018**, *47*, 1459–1483. h) L. Alig, M. Fritz, S. Schneider, *Chem. Rev.* **2019**, *119*, 2681–2751.

[4] Selected examples for Mn a) U. Chakraborty, E. Reyes-Rodriguez, S. Demeshko, F. Meyer, A. Jacobi von Wangelin, *Angew. Chem. Int. Ed.* **2018**, *57*, 4970–4975; *Angew. Chem.* **2018**, *130*, 5064–5069. b) F. Kallmeier, R. Kempe, *Angew. Chem. Int. Ed.* **2018**, *57*, 46–60; *Angew. Chem.* **2018**, *130*, 48–63.

[5] Selected examples for Fe: a) S. C. Bart, E. Lobkovsky, P. J. Chirik, *J. Am. Chem. Soc.* **2004**, *126*, 13794–13807. b) R. J. Trovitch, E. Lobkovsky, E. Bill, P. J. Chirik, *Organometallics* **2008**, *27*, 1470–1478. c) B. A. F. Le Bailly, S. P. Thomas, *RSC Adv.* **2011**, *1*, 1435. d) R. P. Yu, J. M. Darmon, J. M. Hoyt, G. W. Margulieux, Z. R. Turner, P. J. Chirik *ACS Catal.* **2012**, *2*, 1760-1764. e) T. N. Gieshoff, M. Villa, A. Welther, M. Plois, U. Chakraborty, R. Wolf, A. Jacobi von Wangelin, *Green Chemistry* **2015**, *17*, 1408–1413.f) M. Villa, D. Miesel, A. Hildebrandt, F. Ragaini, D. Schaarschmidt, A. Jacobi von Wangelin, *ChemCatChem* **2017**, *9*, 3203–3209. g) J. H. Docherty, J. Peng, A. P. Dominey, S. P. Thomas, *Nat. Chem.* **2017**, *9*, 595-600.

[6] Selected examples for Co: a) Q. Knijnenburg, A. d. Horton, H. van der Heijden, T. M. Kooistra, D. G.H. Hetterscheid, J. M. M. Smits, B. de Bruin, P. H. M. Budzelaar, A. W. Gal, *J. Mol. Catal. A.* **2005**, *232*, 151–159. b) G. Zhang, B. L. Scott, S. K. Hanson, *Angew. Chem. Int. Ed.* **2012**, *51*, 12102–12106; *Angew. Chem.* **2012**, *124*, 12268–12272. c) R. P. Yu, J. M. Darmon, C. Milsmann, G. W. Margulieux, S. C. E. Stieber, S. DeBeer, P. J. Chirik, *J. Am. Chem. Soc.* **2013**, *135*, 13168–13184. d) D. Gärtner, A. Welther, B. R. Rad, R. Wolf, A. Jacobi von Wangelin, *Angew. Chem. Int. Ed.* **2014**, *53*, 3722–3726; *Angew. Chem.* **2014**, *126*, 3796–3800. e) M. R. Friedfeld, G. W. Margulieux, B. A. Schäfer, P. J. Chirik, *J. Am. Chem. Soc.* **2014**, *136*, 13178-13181. f) K. Tokmic, C. R. Markus, L. Zhu, A. R. Fout, *J. Am. Chem. Soc.* **2016**, *138*, 11907–11913. g) P. Büschelberger, D. Gärtner, E. Reyes-Rodriguez, F. Kreyenschmidt, K. Koszinowski, A. Jacobi von Wangelin, R. Wolf, *Chem. Eur. J.* **2017**, *23*, 3139–3151. h) P. Büschelberger, E. Reyes-Rodriguez, C. Schöttle, J. Treptow, C. Feldmann, A. Jacobi von Wangelin, R. Wolf, *Catal. Sci. Technol.* **2018**, *8*, 2648–2653. i) S. Sandl, F. Schwarzhuber, S. Pöllath, J. Zweck, A. Jacobi von Wangelin, *Chem. Eur. J.* **2018**, *24*, 3403–3407. j) F. K. Scharnagl, M. F. Hertrich, F. Ferretti, C. Kreyenschulte, H. Lund, R. Jackstell, M. Beller, *Sci. Adv.* **2018**, *4*, eaau1248. k) S. Sandl, T. M. Maier, N. P. van Leest, S. Kröncke, U. Chakraborty, S. Demeshko, K. Koszinowski, B. de Bruin, F. Meyer, C. Herrmann, R. Wolf, A. Jacobi von Wangein *ACS Catal.* **2019**, *9*, 7596-7606.

[7] M. Raney, *US patent 1628190* **1927**.

[8] a) S. Nishimura, *Handbook of Heterogeneous Catalytic Hydrogenation for Organic Synthesis*, Wiley, New York **2001**. b) T.-K. Yang, D.-S Lee, J. Haas, *Raney Nickel, Encyclopedia of Reagents for Organic Synthesis* **2006**. c) H.-J. Arpe, *Industrial Organic Chemistry*, Wiley-VCH, Weinheim, **2010.**

[9] a) R. Paul, P. Buisson, N. Joseph, *Ind. Eng. Chem.* **1952**, *44*, 1006-1010. b) H. C. Brown, C. A. Brown, *J. Am. Chem. Soc.* **1963**, *85*, 1005–1006. c) C. A. Brown, *J. Org. Chem.* **1970**, *35*, 1900–1904. d) C. A. Brown, V. K. Ahuja, *J. Org. Chem.* **1973**, *38*, 2226–2230. e)

[10] A. Reina, I. Favier, C. Pradel, M. Gómez, *Adv. Synth. Catal.* **2018**, *360*, 3544–3552.

[11] L. Zaramello, B. L. Albuquerque, J. B. Domingos, K. Philippot, *Dalton Trans.* **2017**, *46*, 5082–5090.

[12] Y. Hu, Y. Yu, Z. Hou, H. Yang, B. Feng, H. Li, Y. Qiao, X. Wang, L. Hua, Z. Pan et al., *Chem. Asian J.* **2010**, *5*, 1178–1184.

[13] a) I. M. Angulo, A. M. Kluwer, E. Bouwman, *Chem. Commun.* **1998**, 2689–2690. b) K. V. Vasudevan, B. L. Scott, S. K. Hanson, *Eur. J. Inorg. Chem.* **2012**, *2012*, 4898–4906. c) W. H. Harman, J. C. Peters, *J. Am. Chem. Soc.* **2012**, *134*, 5080–5082.d) T. J. Mooibroek, E. C. M. Wenker, W. Smit, I. Mutikainen, M. Lutz, E. Bouwman, *Inorg. Chem.* **2013**, *52*, 8190–8201.

[14] Y. Wang, A. Kostenko, S. Yao, M. Driess, *J. Am. Chem. Soc.* **2017**, *139*, 13499–13506.

[15] J. Wu, J. W. Faller, N. Hazari, T. J. Schmeier, *Organometallics* **2012**, *31*, 806–809.

[16] N. G. Léonard, P. J. Chirik, *ACS Catal.* **2018**, *8*, 342–348.

[17] a) X. Li, C. You, S. Li, H. Lv, X. Zhang, *Org. Lett.* **2017**, *19*, 5130–5133. b) W. Gao, H. Lv, T. Zhang, Y. Yang, L. W. Chung, Y.-D. Wu, X. Zhang, *Chem. Sci.* **2017**, *8*, 6419-6422.c) J. Long, W. Gao, Y. Guan, H. Lv, X. Zhang, *Org. Lett.* **2018**, *20*, 5914–5917.

[18] Reviews on metalate anions highlighting the pioneering work of Jonas and Ellis: a) J. E. Ellis, *Inorg. Chem.* **2006**, *45*, 3167–3186. b) J. E: Ellis, *Dalton Trans.* **2019**, *48*, 9538-9563.

[19] a) W. W. Brennessel, J. Young, G. Victor, J. E. Ellis, *Angew. Chem. Int. Ed.* **2002**, *41*, 1211–1215; *Angew. Chem.* **2002**, *114*, 1259–1263. b) W. W. Brennessel, R. E. Jilek, J. E. Ellis, *Angew. Chem. Int. Ed.* **2007**, *46*, 6132–6136; *Angew. Chem.* **2007**, *119*, 6244–6248.

[20] K. Jonas, L. Schieferstein, C. Krüger, Y.-H. Tsay, *Angew. Chem. Int. Ed.* **1979**, *18*, 550–551; *Angew. Chem.* **1979**, *91*, 590–591.

[21] K. Jonas, *Angew. Chem. Int. Ed.* **1975**, *14*, 752-753; *Angew. Chem.* **1975**, *87*, 809–810.

[22] L. Nattmann, S. Lutz, P. Ortsack, R. Goddard, J. Cornella, *J. Am. Chem. Soc.* **2018**, *140*, 13628–13633.

[23] For the less challenging substrate 1-dodecene, **1** and [Ni(η^4-cod)$_2$] showed equal activity.

[24] a) J. A. Widegren, R. G. Finke, *J. Mol. Catal. A* **2003**, *198*, 317; b) R. H. Crabtree, *Chem. Rev.* **2012**, *112*, 1536-1554; c) J. F. Sonnenberg, R. H. Morris, *Catal. Sci. Technol.* **2014**, *4*, 3426-3438

[25] a) D. R. Anton, R. H. Crabtree, *Organometallics* **1983**, *2*, 855–859. b) S. Chaffins, M. Brettreich, F. Wudl, *Synthesis* **2002**, 1191–1194. c) G. Franck, M. Brill, G. Helmchen, *Org. Synth.* **2012**, *89*, 55–65.

[26] Kinetics and mechanism of the hydrogenation of α-cyclopropylstyrene: Rate constant of the ring-opening rearrangement of the corresponding radical: 3.6 x 105 s^{-1} at 22°C in hexane solution. a) R. Morris Bullock, E. G. Samsel, *J. Am. Chem. Soc.* **1990**, *112*, 6886-6898. b) J. Choi, L. Tang, J.-R Norton, *J. Am. Chem. Soc.* **2007**, *129*, 234-240.

[27] a) G. Farnia, F. Mran, G. Sandona, M. G. Severin, *J. Chem. Soc.,Perk Trans.* **1982**, *2*, 1153-1158. b) D. Suwatchara, N. V. Rees, R. G: Compton, *J. Electroanal. Chem.* **2012**, *669*, 14-20.

5.5 Supporting Information

5.5.1 General Procedures

All experiments were performed under an atmosphere of dry Argon (Argon 4.6, Linde) using standard Schlenk techniques or a MBraun UniLab Glovebox.

***Analytical Thin-Layer Chromatography*:** TLC was performed using aluminum plates with silica gel and fluorescent indicator (Macherey-Nagel, 60, UV_{254}). Thin layer chromatography plates were visualized by exposure to UV light (366 or 254 nm).

Chemicals and Solvents: Solvents were dried and degassed with an MBraun SPS800 solvent-purification system. THF, diethylether were stored over molecular sieves (3 Å). *n*-hexane was stored over a potassium mirror. 1,2-dimethoxyethane was stirred over K/benzophenone, distilled and stored over molecular sieves (3 Å). Commercially available olefins were purified by distillation (Kugelrohr) and in case of liquids dried over molecular sieves (3 Å). [Ni(η^4-cod)$_2$] was obtained from Sigma-Aldrich and used without further purification.

Cyclic Voltammetry: Cyclic Voltammetry experiments were performed in a single-compartment cell inside a nitrogen-filled glovebox using a CH Instruments CH1600E potentiostat. The cell was equipped with a platinum disc working electrode (2 mm diameter) polished with 0.05 μm alumina paste, a platinum wire counter electrode and an $Ag/AgNO_3$ reference electrode. The supporting electrolyte, tetra-*n*-butylammonium hexafluorophosphate, was dried *in vacuo* at 110°C for three days. All redox potentials are reported vs. the ferrocenium/ferrocene (Fc^+/Fc) couple.

Column Chromatography: Flash column chromatography with silica gel 60 from Sigma Aldrich (63 – 200 μm). Mixture of solvents used are described *vide infra*.

High Pressure Reactor: Hydrogenation reactions were carried out in 160 and 300 mL high pressure reactors (Parr™) in 4 mL glass vials. The reactors were loaded under argon, purged with hydrogen, sealed and the internal pressure was adjusted. Hydrogen (99.9992%) was purchased from Linde.

NMR spectroscopy: ^{1}H and $^{13}C\{^{1}H\}$ NMR spectra in solutions were recorded on Bruker Avance 300 (300 MHz) and BrukerAvance 400 (400 MHz) if not stated otherwise. These chemical shifts are given relative to solvents resonances in the tetramethylsilane scale. The following abbreviations have been used for multiplicities: s = singlet, d = doublet, t = triplet, q = quartet, sept = septet, m = multiplet, dd = doublet of doublet, dt = doublet of triplet.

Gas chromatography with FID (GC-FID): Shimadzu GC2025. Carrier gas: H_2. Colum: Restek Rxi®-5Sil-MS, (30m x 0.25 mm x 0.25 μm) Carrier gas: H_2. Standard heating procedure: 50°C (2 min), 25 °C/min → 280 °C (5 min). Calibration of substrates and products was performed with internal *n*-pentadecane and analytically pure samples.

Gas chromatography with mass-selective detector (GC-MS): Agilent 7820A GC system, mass detector 5977B. Carrier gas: H_2. Column: HP-5MS (30m x 0.25 mm x 0.25 μm). Standard heating procedure: 50 °C → 300 °C.

***Transmission electron microscopy (TEM)*:** The particles were imaged in a FEI Tecnai F30 ST Regensburg special transmission electron microscope, equipped with a field emission gun operated at 300 kV and a super twin lens, capable of a resolution of 0.19 nm.

***UV-vis spectroscopy*:** UV-vis spectra were recorded on an Ocean Optics Flame spectrometer (Varian Cary 50 Spectrophometer) in a Quartz cuvette with a layer thickness of 1 cm at room temperature with a concentration of 10^{-4} to 10^{-6} M.

5.5.2 Synthesis of Pre-catalyst

The procedure for the synthesis of $[Li_2(thf)_4\{Ni(\eta^4\text{-cod})(\eta^2\text{-cod})\}]$ (**1**) was adapted from *Jonas* and co-workers[21] and *Cornella* and co-workers.[2]

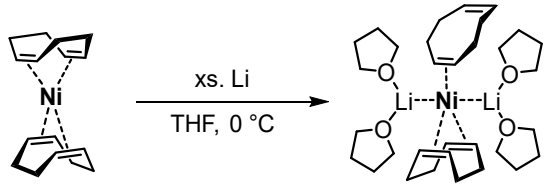

1

$[Ni(\eta^4\text{-cod})_2]$ (1.0 g, 3.6 mmol, 1.0 equiv.) was mixed with lithium metal (0.09 mg, 13.0 mmol, 3.6 equiv.). A cooled (0 °C) THF solution was added and the suspension was stirred for seven hours under exclusion of light until no solid $[Ni(\eta^4\text{-cod})_2]$ was left. After filtration, the orange solution was concentrated to 8 mL and layered with diethylether in a 1:2 ratio. Dark-orange crystals of $[Li_2(thf)_4\{Ni(\eta^4\text{-cod})(\eta^2\text{-cod})\}]$ formed after storage of the solution at –35 °C overnight. The crystals were isolated by decantation and dried *in vacuo* at –30 °C. The complex was stored under argon at –35°C. The ^{1}H NMR spectrum in THF-d_8 at room temperature is in accordance with the spectrum described in literature.[2]

Yield: 1.12 g, (1.94 mmol, 53%)

Chemical formula: $Li_2NiC_{16}H_{24} \cdot (C_4H_8O)_4$ (M = 577.37 g mol^{-1})

^{1}H NMR (400.13 MHz, 300 K, THF-d_8) δ[ppm]: 2.28 (br s), 2.05 (br d), 2.03 (br s), 1.68 (br s).

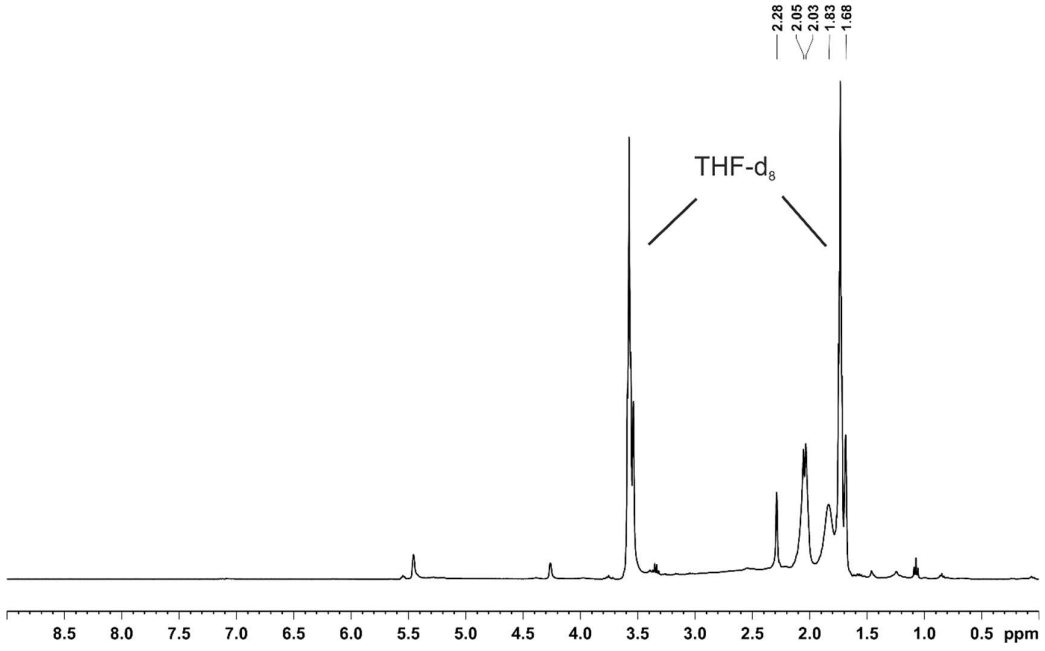

Figure S1. ^{1}H NMR spectrum (400.13 MHz, 300 K, THF-d_8) of **1**.

5.5.3 Hydrogenation Reactions

5.5.3.1 General Procedure

In an argon-filled glovebox, a flame-dried 4 mL reaction vial was charged with the substrate (0.2 mmol) and *n*-pentadecane (20 μL) as internal reference for GC-FID quantification. The catalyst was added as a solution in DME, if not stated otherwise. The reaction vessel was transferred to a high-pressure reactor, which was sealed and removed from the glovebox. The reactor was purged with hydrogen gas (three times) and the reaction pressure and temperature were set. After the indicated reaction time, the vial was retrieved, and the reaction mixture was hydrolyzed with a saturated aqueous solution of NH_4Cl and diluted with ethyl acetate. An aliquot of the organic phase was filtered over a pad of silica, which was washed with ethyl acetate. The solution was analyzed by GC-FID and GC-MS. After the end of the reaction the crude mixture was filtered over silica and the product isolated by solvent evaporation.

5.5.3.2 Optimization Reactions

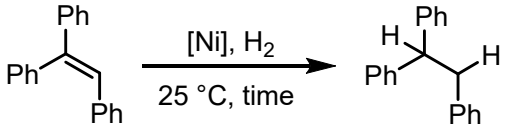

Table S1. Optimization of reaction conditions.

Entry	Catalyst[a]	Solvent [mL]	p (H_2) [bar]	T [°C]	T [h]	Yield (Conversion) [%][d]
1	**1**[b]	THF (1 mL)	10	25	5	97 (100)
2	**1**	THF (0.5 mL)	5	25	15	81 (82)
3	**1**	DME (0.5 mL)	5	25	15	97 (98)
4	**1**	DME (0.25 mL)	5	25	15	99 (100)
5	**1**	DME (0.25 mL)	1.9	25	15	72 (74)
6	[Ni(η^4-cod)$_2$]	THF (0.5 mL)	5	25	15	22 (26)
7	[Ni(η^4-cod)$_2$]	DME (0.5 mL)	5	25	15	36 (38)
8	**1** + Hg[c]	DME (0.5 mL)	5	25	15	2 (5)

[a] 1 mol%, if not stated otherwise. [b] 5 mol%. [c] Addition of an excess mercury (50 mg, 0.025 mmol, 125 equiv.) before the hydrogenation was started. [d] Yields and conversions determined by quantitative GC-FID vs. internal *n*-pentadecane.

5.5.3.3 Comparative Experiments

a) P. J. Chirik and co-workers.[16]

Hydrogenation with $Ni(OAc)_2$ (1 equiv.) and HBPin (4 equiv.)

Table S2. Hydrogenation of 1-Ph-1-cycloxhexene. Yields were determined by GC-FID analysis.

Entry	Substrate	Conditions	Yield (Lit.) [%]	Yield (1) [%]
1	1-Ph-1-cyclohexene	4 bar H_2, 0.4 mol%, 50 °C, 3 h	>98	>99 (after 2h)

Determination of the turnover frequency (TOF):

1-Phenyl-1-cyclohexene (catalyst **1**): t = 2 h, 0.4 mol% Ni, 4 bar H_2, 50°C; TOF = 125 h^{-1};

1-Phenyl-1-cyclohexene (catalyst **D**, ref. [16]): t = 3 h, 0.4 mol% Ni, 4 bar H_2, 50°C; TOF = 82.5 h^{-1}

b) M. Driess and co-workers.[4]

Hydrogenation with a nickel-silylene complex

Table S3. Hydrogenation of 1-octene. Yields were determined by GC-FID analysis.

Entry	Substrate	Conditions	Yield (Lit.) [%]	Yield (Using 1) [%]
1	1-octene	1 bar H_2, 1.5 mol%, 25 °C, 24 h	>99	86 [a]

[a]: Full conversion using catalyst **1**.

c) Unsupported $[Ni(\eta^4\text{-cod})_2]$

Table S4. Hydrogenation of several C=C bonds. Yields were determined by GC-FID analysis.

Entry	Substrate	Conditions[a]	Yield ($[Ni(\eta^4\text{-cod})_2]$) [%]	Yield (Using 1) [%]
1	triphenylethylene	15 h	36	99
2	1-dodecene	30 min	90	90
3	1-Ph-1-cyclohexene	4 h	0	74

[a] 5 bar H_2, 1 mol%, 25 °C

5.5.3.4 Isolated Hydrogenation Products

1,2-diphenylpropane

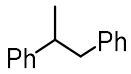

$C_{15}H_{16}$ 196.29 g mol^{-1}

colorless liquid

Yield 191.8 mg (0.97 mmol, 97%)

^{1}H NMR (400.13 MHz, 300 K, $CDCl_3$) δ[ppm]: 7.36–7.21 (m, 8H, CH_{Ar}), 7.16–7.14 (m, 2H, CH_{Ar}), 3.10 – 2.99 (m, 2H, CH_2), 2.86 – 2.81 (m, 1H, CH), 1.31 (d, J = 6.8 Hz, 3H, CH_3)

^{13}C{^{1}H}-NMR (100.6 MHz, 300 K, $CDCl_3$) δ[ppm]: 147.1, 140.9, 129.3, 128.4, 128.2, 127.1, 126.1, 125.9, 45.2, 42.0, 21.2

GC-MS t_R = 9.46 min, (EI, 70 eV): m/z = 196.1 [M$^+$]

Analytical data were in full agreement with those published by *Pilkington* and co-workers.[5]

1,4-diphenylbutane

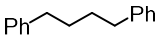

$C_{16}H_{18}$ 210.32 g mol^{-1}

colorless liquid

Yield 208 mg (0.99 mmol, 99%)

^{1}H NMR (400.13 MHz, 300 K, $CDCl_3$) δ[ppm]: 7.48 – 7.26 (m, 10H, CH_{Ar}), 2.76 (br s, 4H, CH_2), 1.80 (br s, 4H, CH_2)

^{13}C{^{1}H} NMR (100.6 MHz, 300 K, $CDCl_3$) δ[ppm]: 142.7, 128.6, 128.5, 128.4, 128.4, 125.8, 35.9, 31.2

GC-MS t_R = 11.00 min, (EI, 70 eV): m/z = 210.2 [M$^+$]

Analytical data were in full agreement with those published by *Weix* and co-workers.[6]

pinane

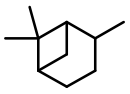

$C_{10}H_{18}$ 138.25 g mol^{-1}

colorless liquid

Yield 107 mg (0.77 mmol, 79%)

^{1}H NMR (400.13 MHz, 300 K, $CDCl_3$) δ[ppm]: 2.31 (m, 1H), 2.13 (1H), 2.00 – 1.60 (m, 5H), 1.47 – 1.30 (m, 1H), 1.19 (br s, 3H), 1.01 (m, 2H), 0.88 – 0.82 (m, 2H)

^{13}C{^{1}H} NMR (100.6 MHz, 300 K, $CDCl_3$) δ[ppm]: main isomer: 48.1, 41.4, 38.8, 36.0, 34.0, 28.3, 26.6, 23.9, 23.2, 22.9; minor isomer: 47.7, 40.9, 39.5, 29.4, 26.9, 26.7, 24.6, 24.0, 23.0, 21.6, 20.1

GC-MS t_R = two isomers 3.87 min (16.5%), 4.00 min (83.5%) (EI, 70 eV): m/z = 138.1 [M$^+$]

Analytical data were in full agreement with a sample obtained from *Sigma-Aldrich*.

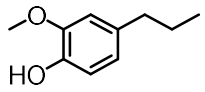

2-methoxy-4-propylphenol (from eugenol)

$C_{10}H_{14}O_2$ 166.22 g mol^{-1}

colorless liquid

Yield 163 mg (0.99 mmol, 99%)

^{1}H NMR (400.13 MHz, 300 K, $CDCl_3$) δ[ppm]: 6.86 (d, J = 7.8 Hz, 1H, CH_{Ar}), 6.70 (d, J = 7.9 Hz, 2H, CH_{Ar}), 5.58 (br s, 1H, OH), 3.89 (s, 3H, O-CH_3), 2.55 (t, 7.6 Hz, 2H, CH_2), 1.65 (m, 2H, CH_2), 0.97 (m, 3H, CH_3)

^{13}C{^{1}H} NMR (100.6 MHz, 300 K, $CDCl_3$) δ[ppm]: 146.4, 143.6, 134.7, 121.0, 114.2, 111.1, 55.9, 37.8, 24.9, 13.8

GC-MS t_R = 7.86 min, (EI, 70 eV): m/z = 166.1 [M$^+$]

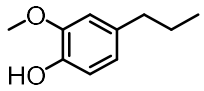

2-methoxy-4-propylphenol (from isoeugenol)

$C_{10}H_{14}O_2$ 166.22 g mol^{-1}

colorless liquid

Yield 136 mg (0.83 mmol, 83%)

^{1}H NMR (400.13 MHz, 300 K, $CDCl_3$) δ[ppm]: 6.85 (d, J = 7.8 Hz, 1H, CH_{Ar}), 6.69 (d, J = 7.9 Hz, 2H, CH_{Ar}), 5.52 (br s, 1H, OH), 3.89 (s, 3H, O-CH_3), 2.54 (t, 7.6 Hz, 2H, CH_2), 1.65 (m, 2H, CH_2), 0.96 ((t, 7.3 Hz, 3H, CH_3)

^{13}C{^{1}H}-NMR (100.6 MHz, 300 K, $CDCl_3$) δ[ppm]: 146.3, 143.6, 134.7, 121.0, 114.1, 111.1, 55.9, 37.8, 24.9, 13.8

GC-MS t_R = 7.86 min, (EI, 70 eV): *m*/*z* = 166.1 [M$^+$]

Analytical data were in full agreement with those published by *Minnaard* and co-workers.[7]

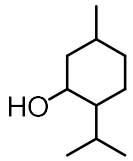

2-isopropyl-5-methylcyclohexan-1-ol

$C_{10}H_{20}O$ 156.27 g mol^{-1}

colorless liquid

Yield 155.5 mg (0.99 mmol, 99%)

^{1}H NMR (400.13 MHz, 300 K, $CDCl_3$) δ[ppm]: 3.36 (s, 1H, OH), 2.16 (m, 1H), 1.93 (m, 1H), 1.70 – 1.47 (m, 4H), 1.39 (m, br s, 1H), 1.11 (m, 1H), 1.00 – 0.75 (m, 13H)

^{13}C{^{1}H} NMR (100.6 MHz, 300 K, $CDCl_3$) δ[ppm]: mixture of isomers: 71.8, 71.5, 67.9, 67.7, 50.1, 48.0, 45.1, 42.6, 40.1, 39.1, 35.1, 34.6, 31.7, 30.5, 29.2, 27.6, 25.8, 25.8, 24.2, 23.2, 22.4, 22.2, 21.2, 21.1, 21.0, 20.8, 20.0, 19.6, 18.1, 16.1

GC-MS t_R = four isomers: 5.93 min (24%), 6.01 min (64%), 6.12 min (4%), 6.17 min (8%), (EI, 70 eV): *m*/*z* = 154.2 [M$^+$]

Analytical data were in agreement with those published by *Krempner* and co-workers.[8]

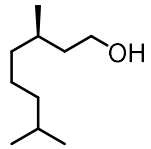

(*R*)-3,7-dimethyloctan-1-ol

$C_{10}H_{22}O$ 158.29 g mol^{-1}

colorless liquid

Yield 153.3 mg (0.97 mmol, 97%)

^{1}H NMR (400.13 MHz, 300 K, $CDCl_3$) δ[ppm]: 3.71 – 3.60 (m, 2H), 1.71 (br s, 1H, OH), 1.64 – 1.45 (m, 3H), 1.40 – 1.20 (m , 4H), 1.18 – 1.05 (m, 3H), 0.89 – 0.82 (m, 9H)

^{13}C{^{1}H} NMR (100.6 MHz, 300 K, $CDCl_3$) δ[ppm]: 61.1, 40.0, 39.3, 37.4, 29.5, 28.0, 24.7, 22.7, 22.6, 19.6

GC-MS t_R = 6.19 min, (EI, 70 eV): *m*/*z* = 140.1 [M$^+$]

Analytical data were in full agreement with those published by *Pilkington* and co-workers.[5]

5.5.3.5 NMR spectra

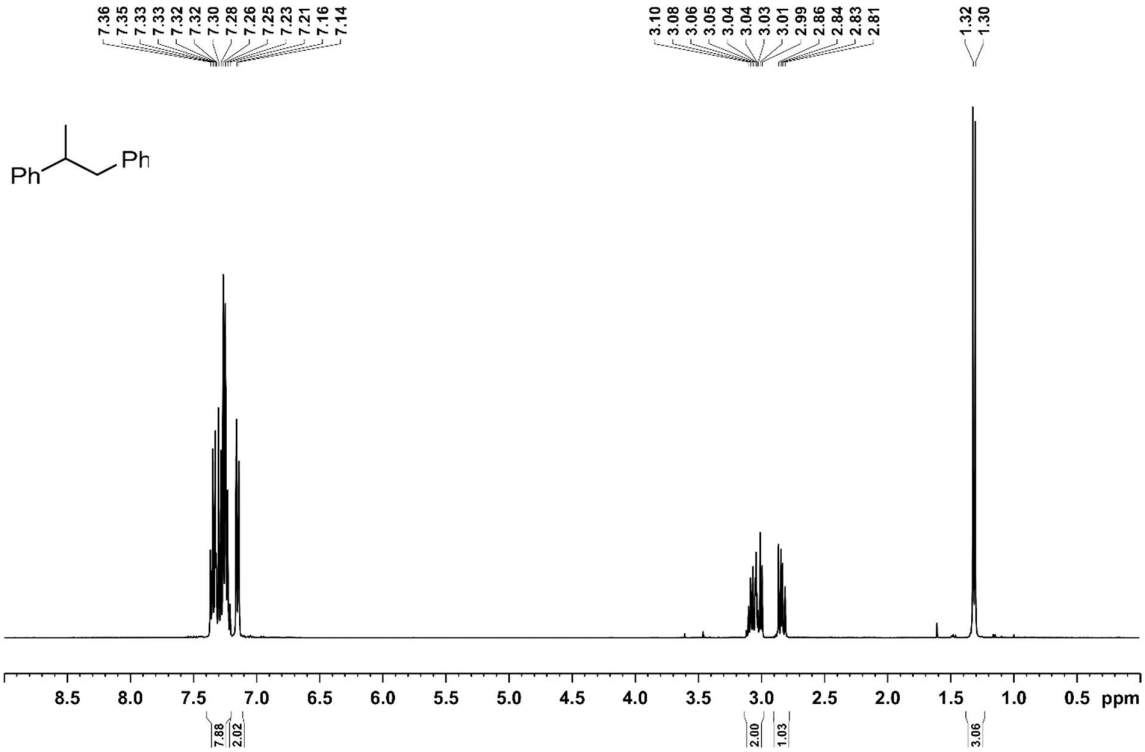

Figure S2. ^{1}H NMR spectrum (400.13 MHz, 300 K, $CDCl_3$) of 1,2-diphenylbutane.

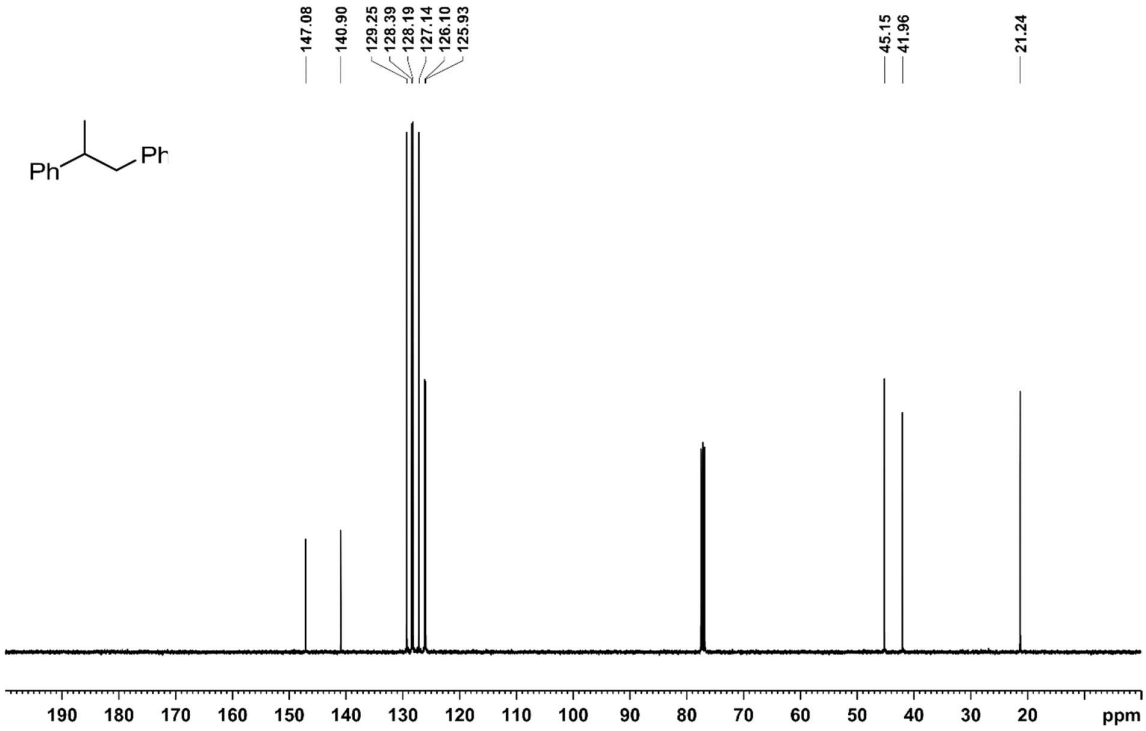

Figure S3. $^{13}C\{^{1}H\}$ NMR spectrum (100.6 MHz, 300 K, $CDCl_3$) of 1,2-diphenylbutane.

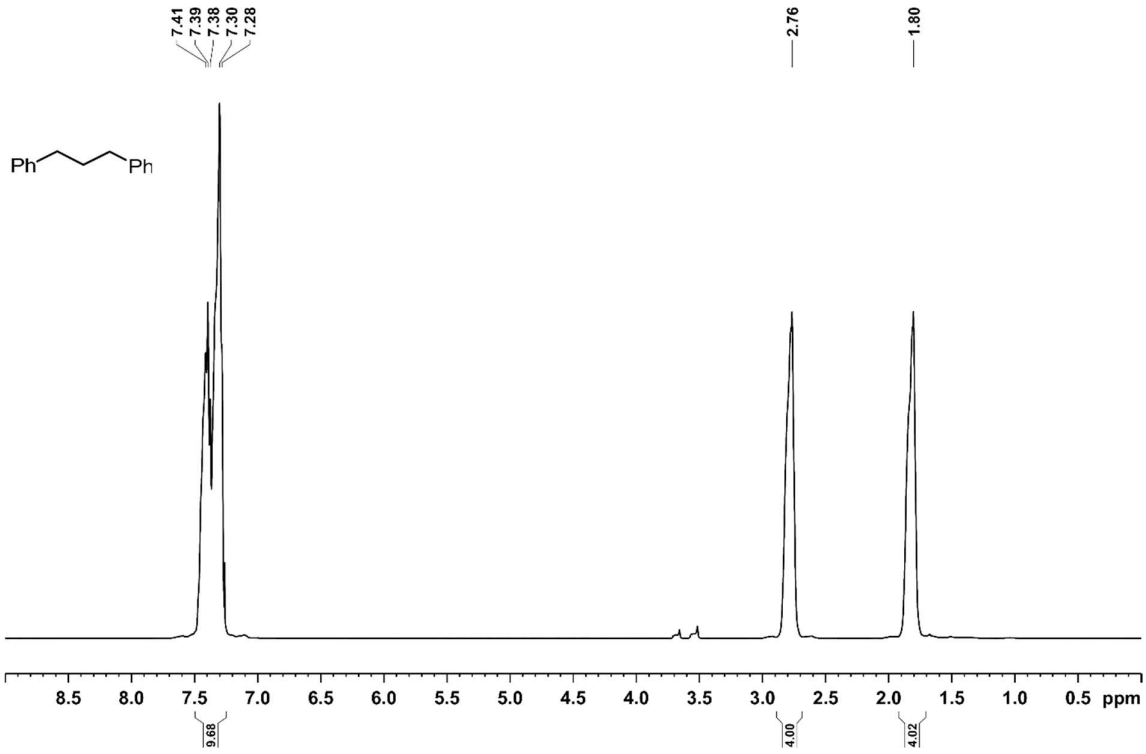

Figure S4. ^{1}H NMR spectrum (400.13 MHz, 300 K, $CDCl_3$) of 1,4-diphenylbutane.

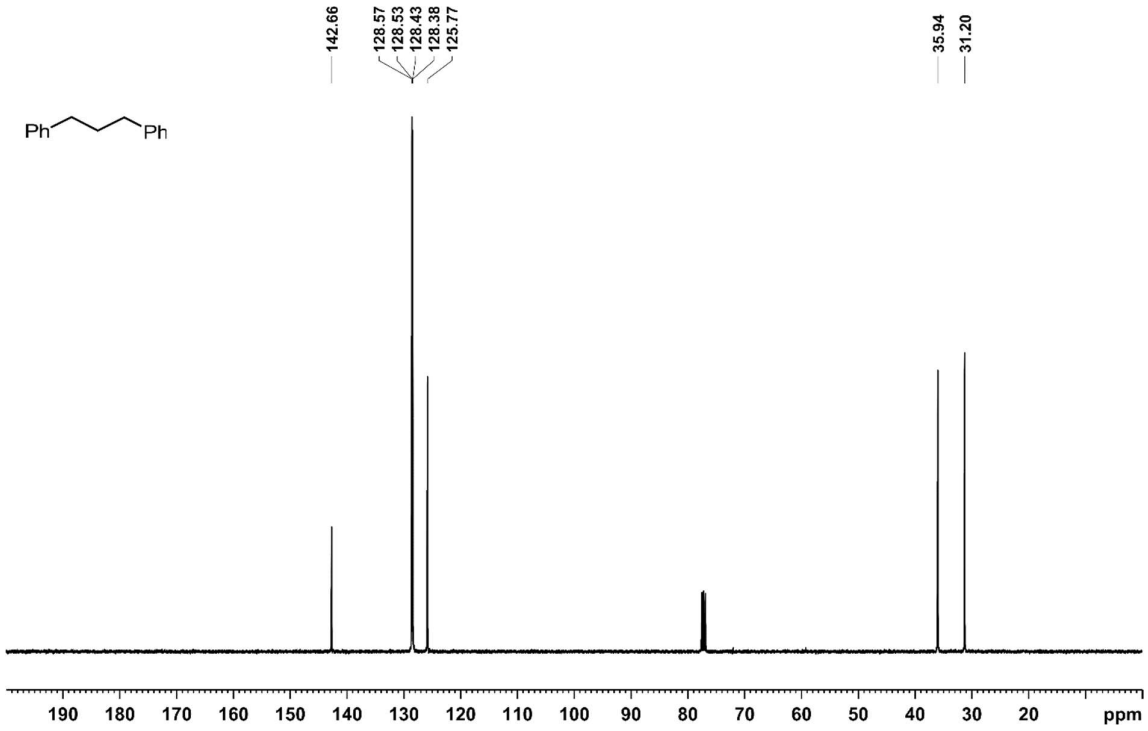

Figure S5. $^{13}C\{^{1}H\}$ NMR spectrum (100.6 MHz, 300 K, $CDCl_3$) of 1,4-diphenylbutane.

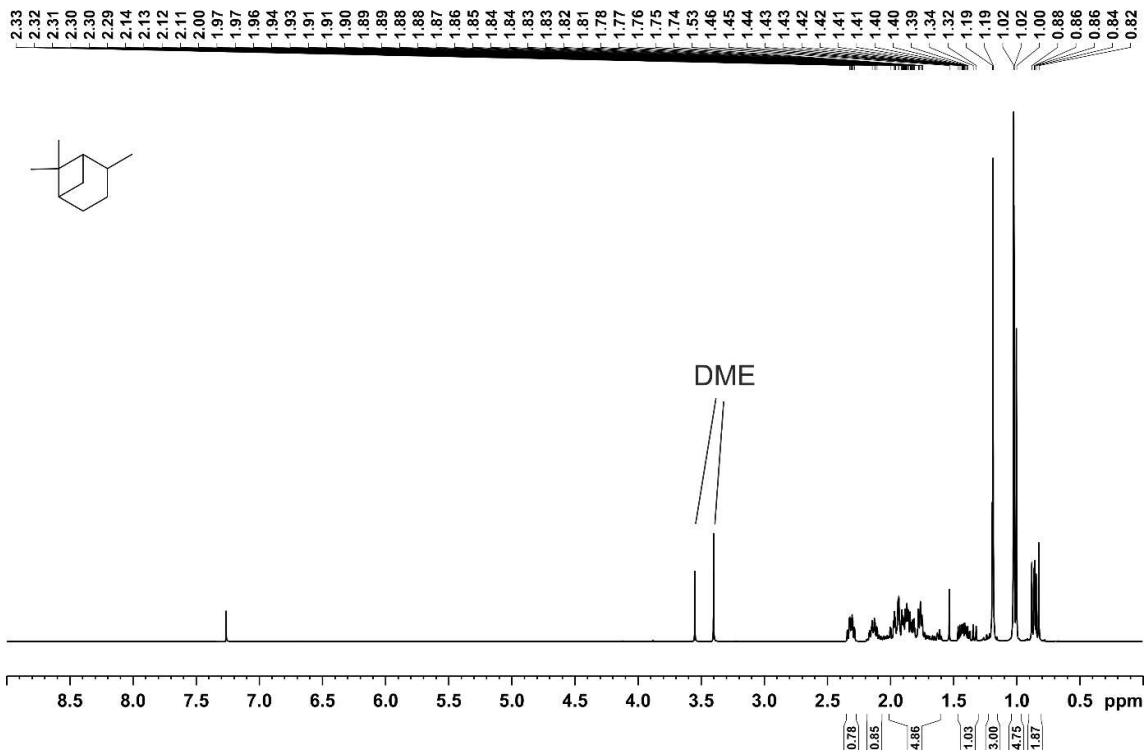

Figure S6. ^{1}H NMR spectrum (400.13 MHz, 300 K, $CDCl_3$) of pinane; small signals of residual solvent: 3.55, 3.40 (DME).

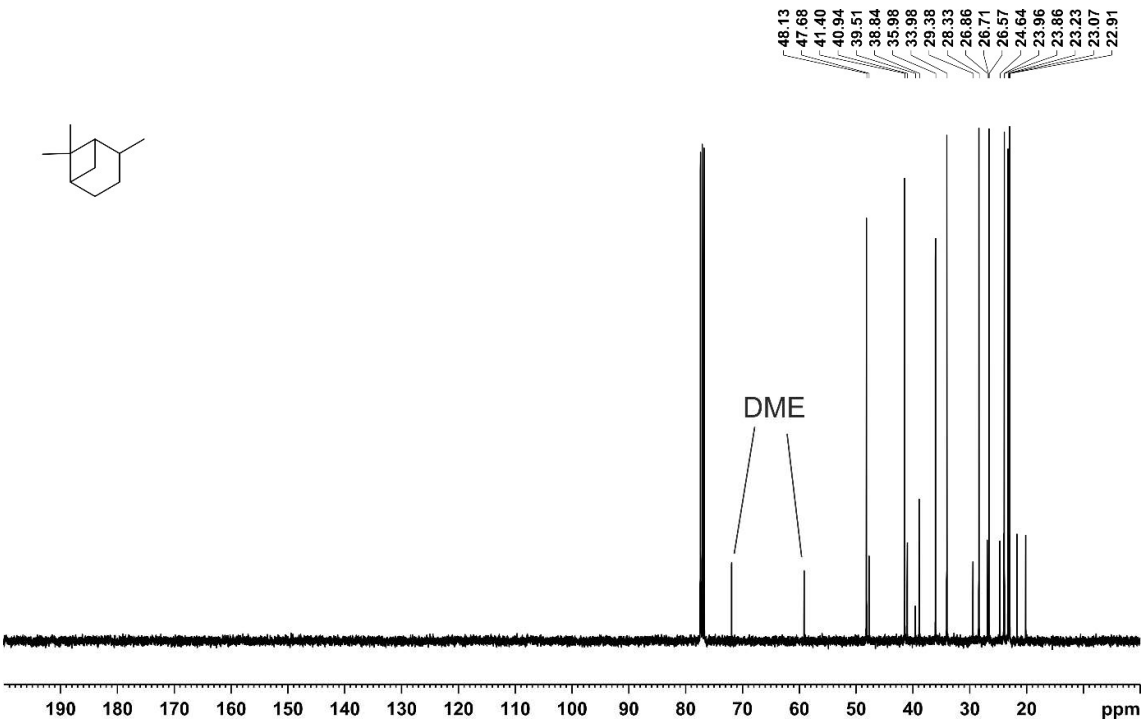

Figure S7. $^{13}C\{^{1}H\}$ NMR spectrum (100.6 MHz, 300 K, $CDCl_3$) of pinane; small signals of residual solvent: 72.6, 58.7 (DME).

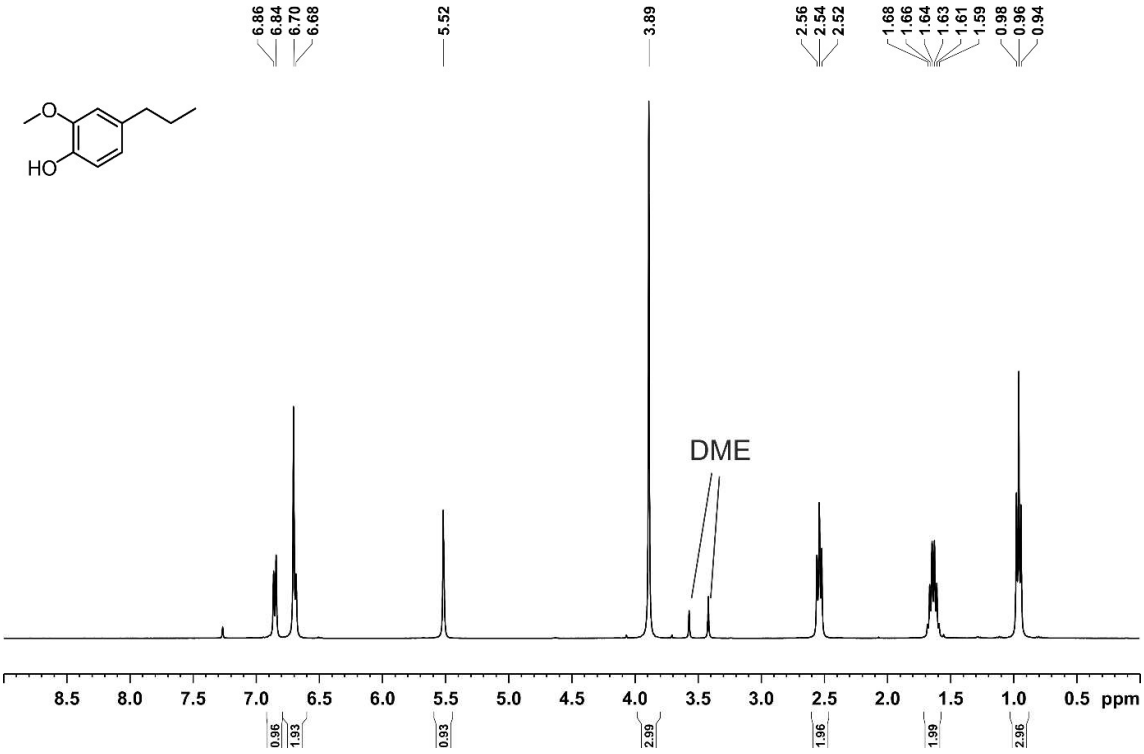

Figure S8. ^{1}H NMR spectrum (400.13 MHz, 300 K, $CDCl_3$) of 2-methoxy-4-propylphenol; small signals of residual solvent: 3.55, 3.40 (DME).

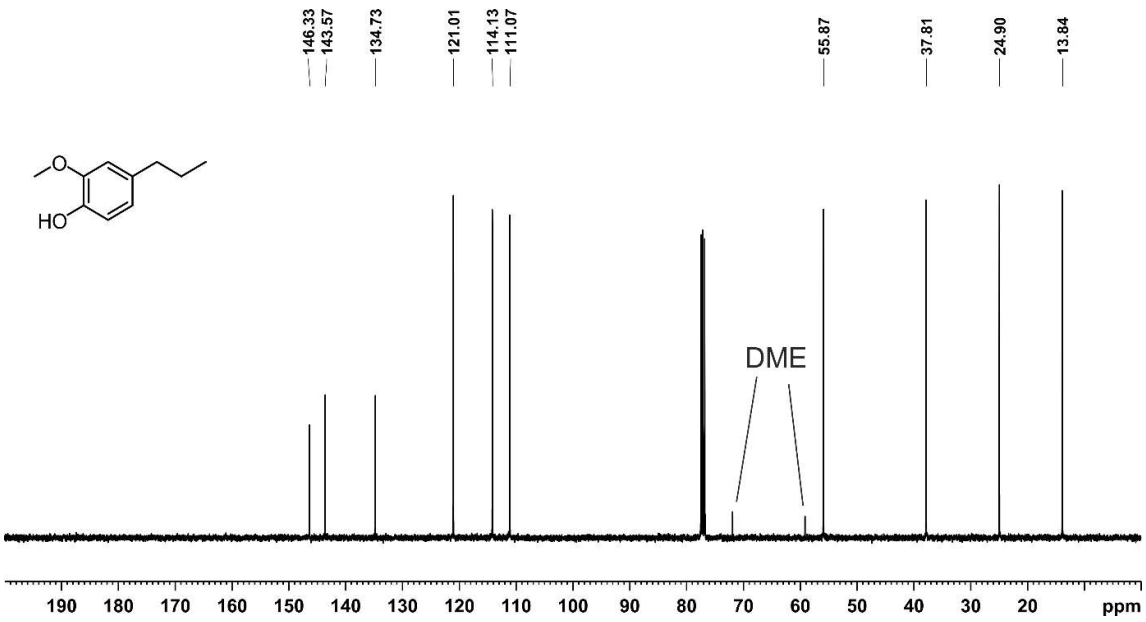

Figure S9. $^{13}C\{^{1}H\}$ NMR spectrum (100.6 MHz, 300 K, $CDCl_3$) of 2-methoxy-4-propylphenol; small signals of residual solvent: 72.6, 58.7 (DME).

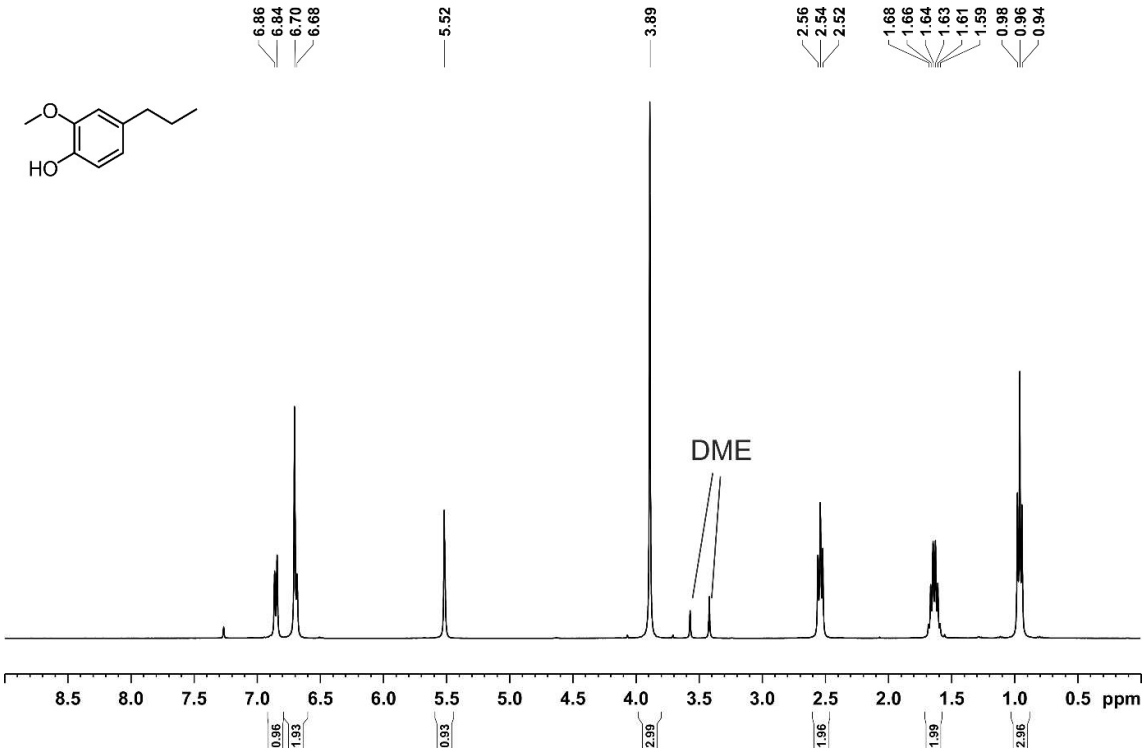

Figure S10. ^{1}H NMR spectrum (400.13 MHz, 300 K, $CDCl_3$) of 2-methoxy-4-propylphenol; small signals of residual solvent: 3.55, 3.40 (DME).

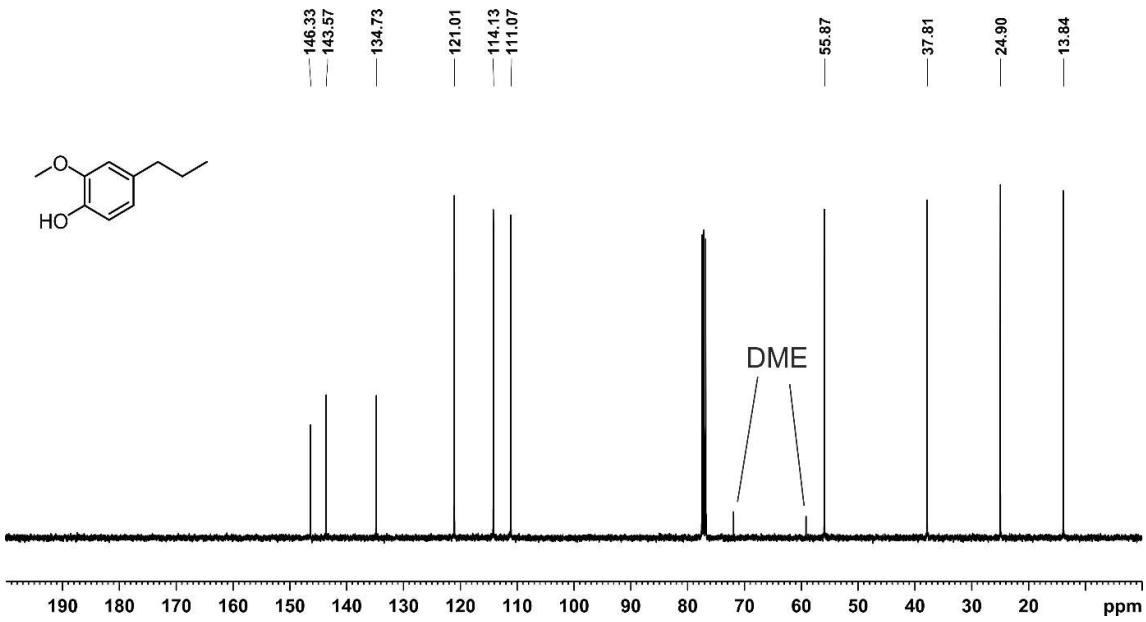

Figure S11. $^{13}C\{^{1}H\}$ NMR spectrum (100.6 MHz, 300 K, $CDCl_3$) of 2-methoxy-4-propylphenol; small signals of residual solvent: 72.6, 58.7 (DME).

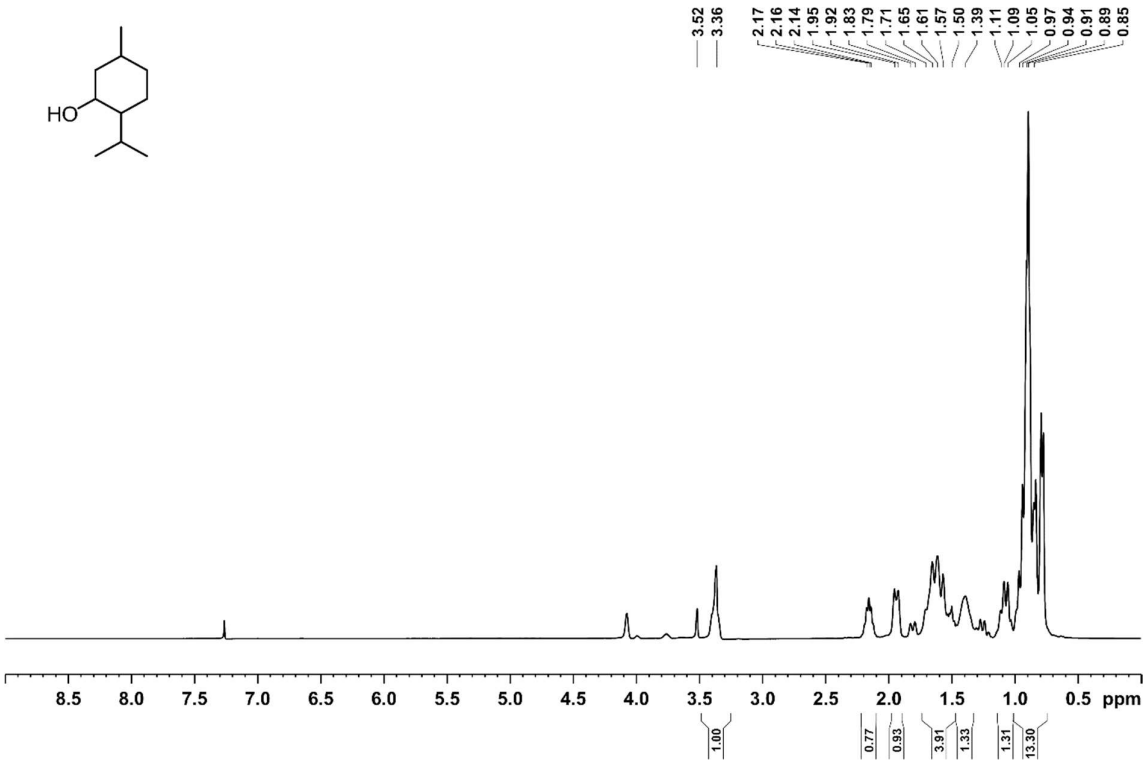

Figure S12. ^{1}H NMR spectrum (400.13 MHz, 300 K, $CDCl_3$) of 2-isopropyl-5-methylcyclohexan-1-ol; small signals of residual solvent: 3.55, 3.40 (DME).

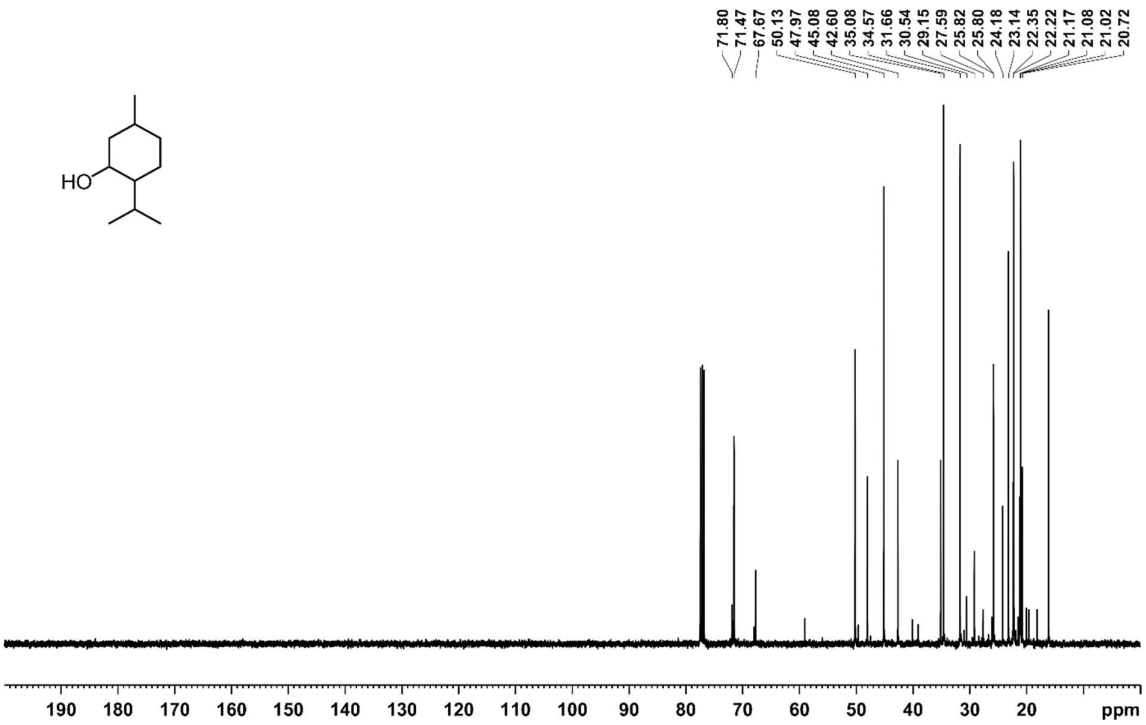

Figure S13. $^{13}C\{^{1}H\}$ NMR spectrum (100.6 MHz, 300 K, $CDCl_3$) of 2-isopropyl-5-methylcyclohexan-1-ol; small signals of residual solvent: 72.6, 58.7 (DME).

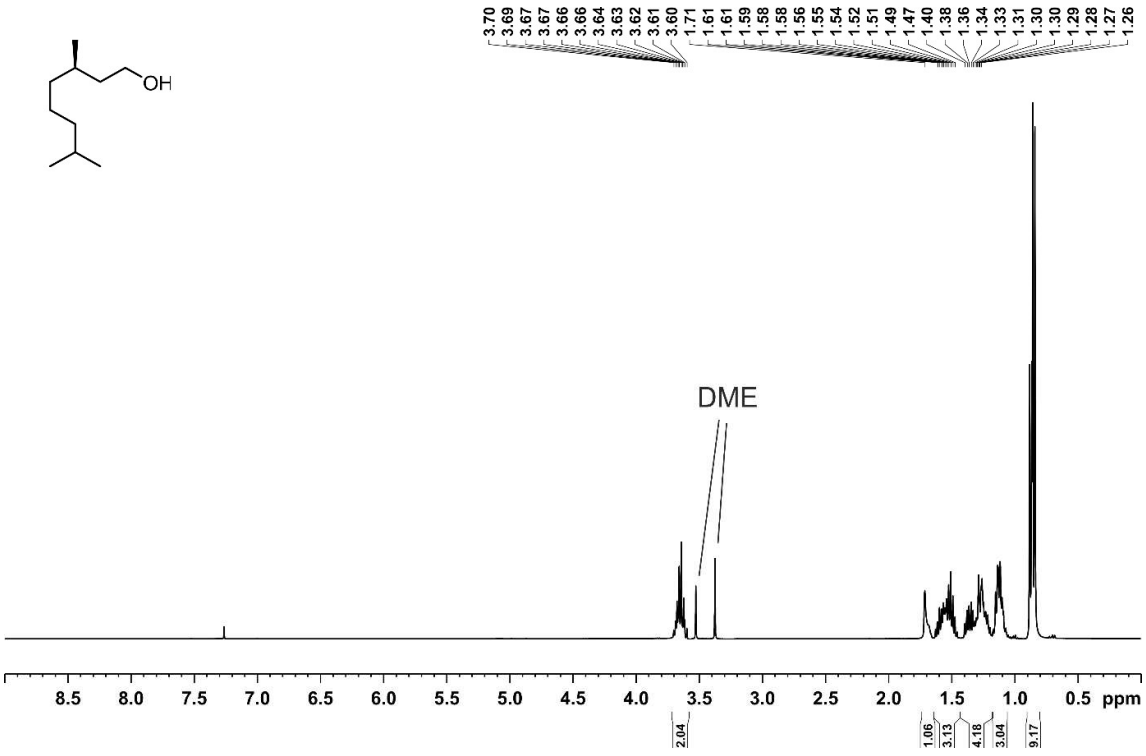

Figure S14. ^{1}H NMR spectrum (400.13 MHz, 300 K, $CDCl_3$) of 3,7-dimethyloctan-1-ol; small signals of residual solvent: 3.55, 3.40 (DME).

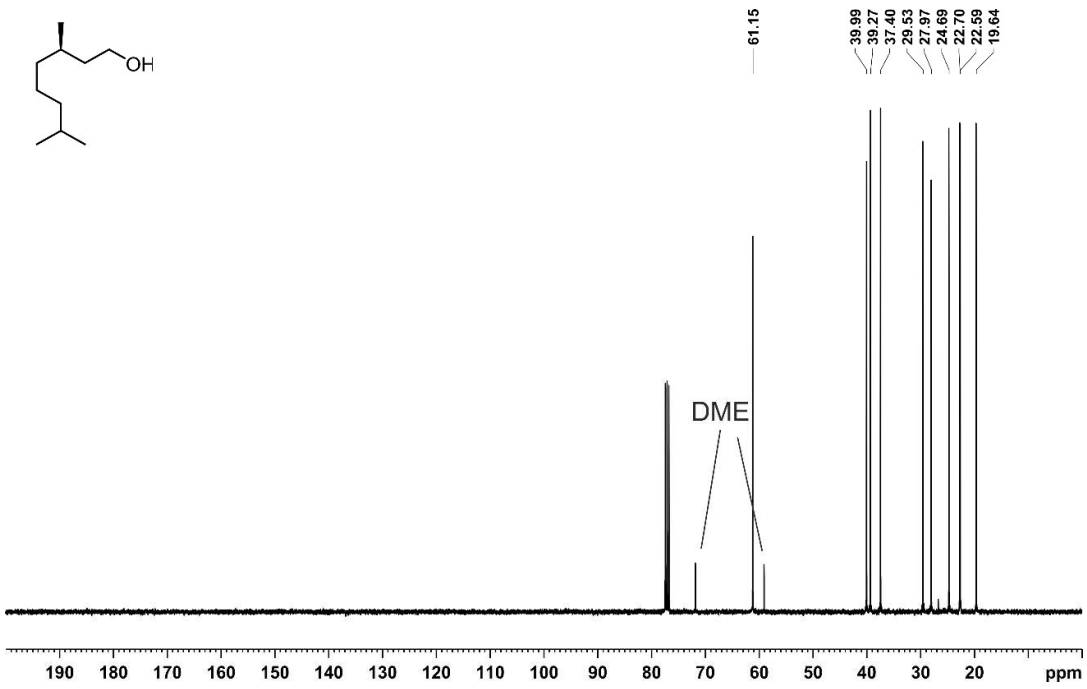

Figure S15. $^{13}C\{^{1}H\}$ NMR spectrum (100.6 MHz, 300 K, $CDCl_3$) of 3,7-dimethyloctan-1-ol; small signals of residual solvent: 72.6, 58.7 (DME).

5.5.3.6 GC-FID Analyses

For the substrates myrcene, *α*-pinene, and (*R*)-limonene the peak area of the substrate and the corresponding products in the chromatogram (GC-FID) were compared in order to estimate the yield and conversion. Peak at 5.82 min corresponds to the internal standard *n*-pentadecane.

a) Myrcene

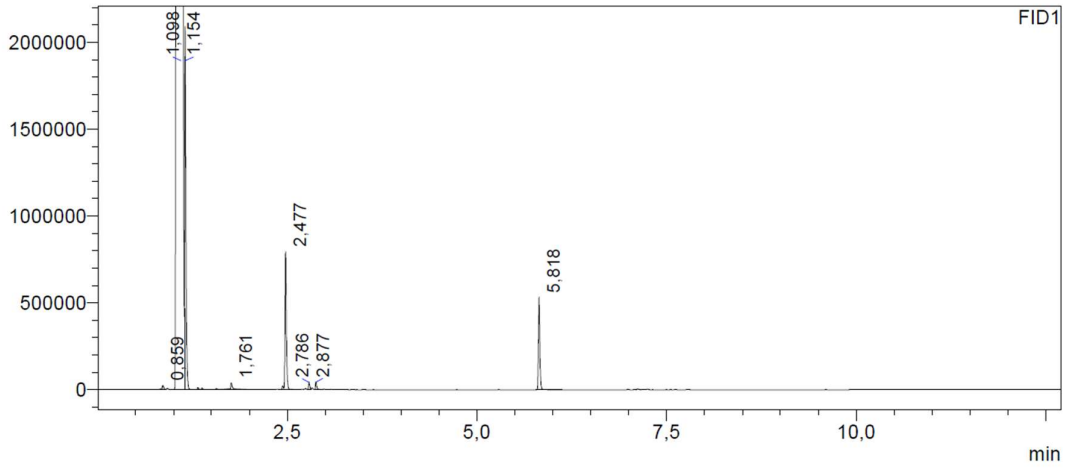

Figure S16. GC-FID chromatogram of the hydrogenation of myrcene using catalyst **1**.

Table S5. Analysis of the GC-FID chromatogram of the hydrogenation of myrcene.

Retention time [min]	Assignment	Peak area	Relative peak area [%]
2.477	2,6-dimethyloctane	972490	91
2.786	Isomer with one C=C bond	48166	4
2.877	Isomer with one C=C bond	51724	5

b) α-Pinene

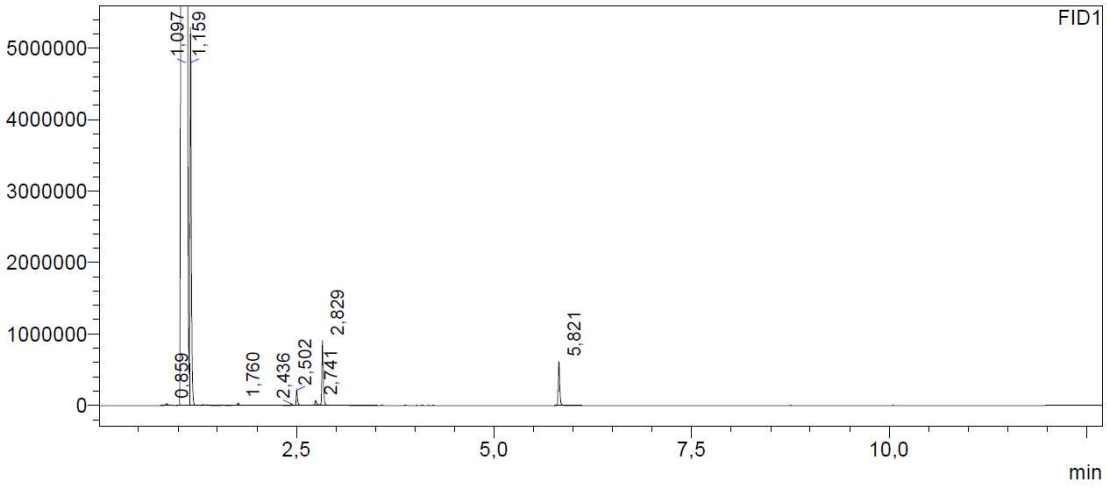

Figure S17. GC-FID chromatogram of the hydrogenation of α-pinene using catalyst **1**.

Table S6. Analysis of the GC-FID chromatogram of the hydrogenation of α-pinene.

Retention time [min]	Assignment	Peak area	Relative peak area [%]
2.791	α-pinene	240603	16
2.882	pinane	75076	5
3.076	pinane	1152099	79

c) (*R*)-Limonene

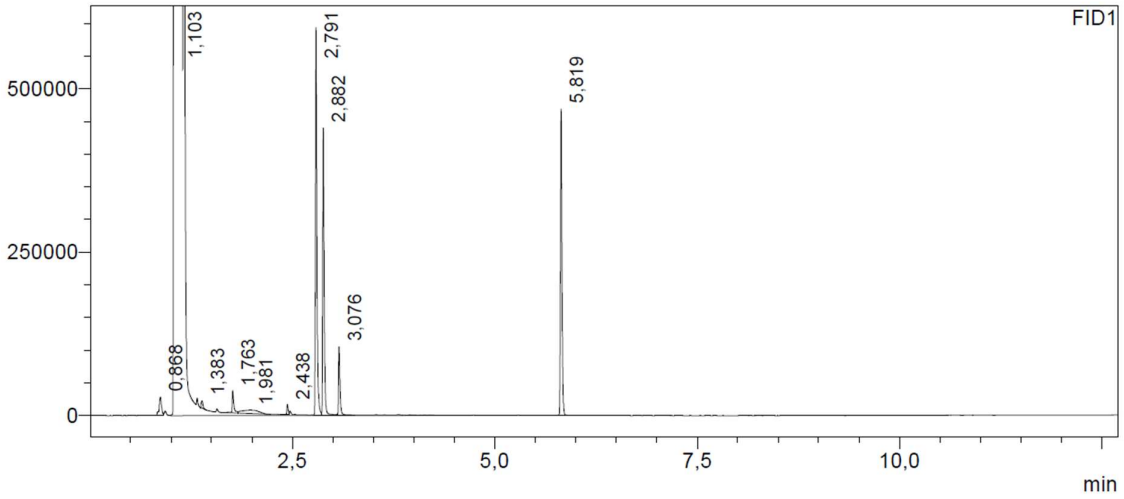

Figure S18. GC-FID chromatogram of the hydrogenation of (*R*)-limonene using catalyst **1**.

Table S7. Analysis of the GC-FID chromatogram of the hydrogenation of (*R*)-limonene..

Retention time [min]	Assignment	Peak area	Relative peak area [%]
2.502	1-isopropyl-4-methylcyclohexane	732649	54
2.741	1-isopropyl-4-methylcyclohexane	535522	38
3.076	Isomer with one C=C bond	129610	9

5.5.4 Mechanistic Investigations

5.5.4.1 Catalytic Experiments

5.5.4.1.1 Isomerization of Olefins

a) Isomerization of allylbenzene

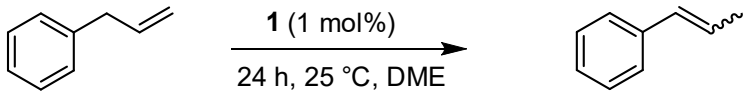

55%

Allylbenzene (26.5 µL, 0.2 mmol, 1.0 equiv.) was stirred for one day with a solution of **1** (1.2 mg, 0.002 mmol, 0.01 equiv.) in 0.25 mL DME and 20 L *n*-pentadecane as internal reference and analyzed by GC-FID and GC-MS after work-up (see the general information, chapter 3.1). According to GC-FID, 55% of allylbenzene isomerized to 1-propenylbenzene.

b) Isomerization of 1-octene

1-Octene (31.5 µL, 0.2 mmol, 1.0 equiv.) was stirred for one day with a solution of **1** (1.2 mg, 0.002 mmol, 0.01 equiv.) in 0.2 mL DME and 20 L *n*-pentadecane as internal reference and analyzed by GC-FID and GC-MS after work-up (see the general information, chapter 3.1). 1-Octene, as well as 2-,3-, and 4-octene were observed.

The GC-FID spectrum and the corresponding peak table are depicted in Figure S19 and Table S8. The assignment of to the signals from 1.945 – 2.067 min being internal octenes was proven by GC-MS (m/z = 112) as well.

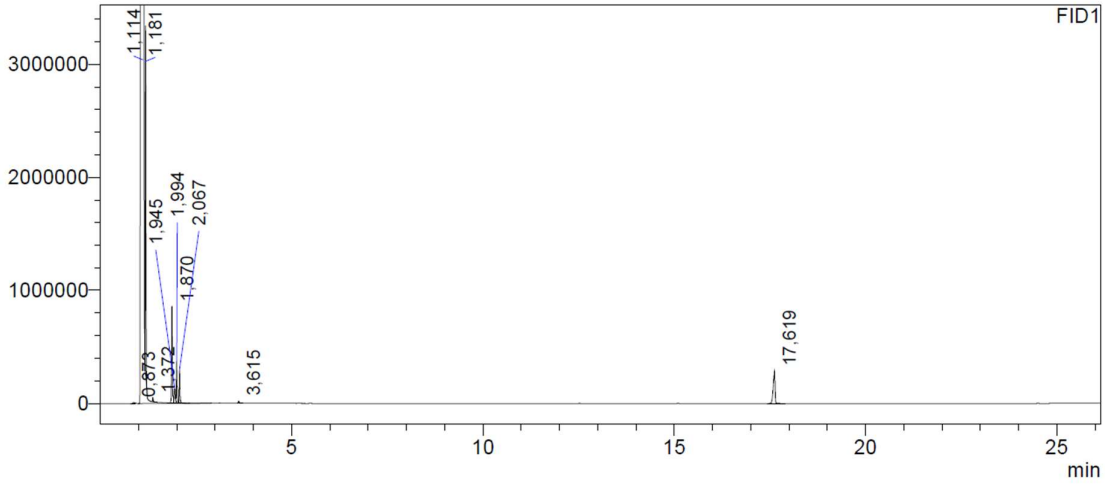

Figure S19. GC-FID chromatogram of the isomerization of 1-octene using catalyst **1**.

Table S8. Analysis of the GC-FID chromatogram of the isomerization of 1-octene.

Retention time [min]	Assignment	Peak area
1.870	1-octene	1188125
1.945	Internal octene	249948
1.994	Internal octene	494294
2.067	Internal octene	402791
17.619	*n*-pentadecane	906465

5.5.4.1.2 Ring-Opening Experiment with α-Cyclopropylstyrene

The hydrogenation reaction was performed according to the general procedure (chapter 3.1).

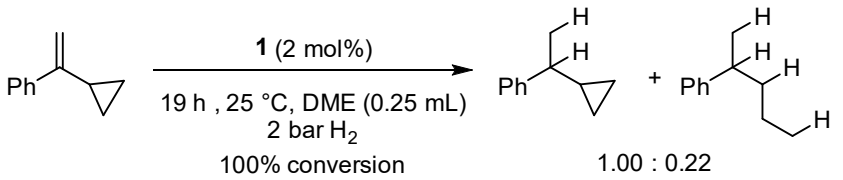

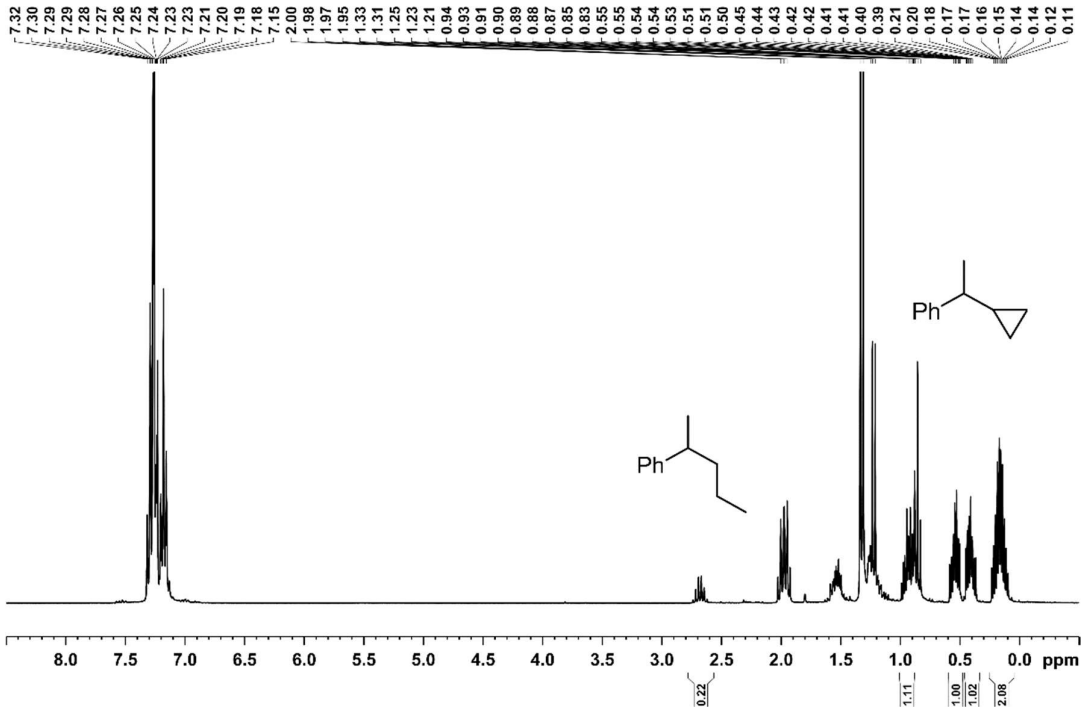

Figure S20. ^{1}H NMR spectrum (300 MHz, 300 K, $CDCl_3$) of the product mixture from the hydrogenation of α-cyclopropylstyrene using catalyst **1**.

5.5.4.1.3 Kinetic Investigations

Catalyst **1** (5.8 mg, 10 μmol, 3 mol%) was dissolved in DME (0.25 mL) and the alkene (0.2 mmol, 1.0 equiv.) was added, during which the color changed from orange to red in case of α-methylstyrene (no color change was observed for the octenes). The mixture was injected by syringe to a flame-dried 10 mL two-necked flask, which was connected to a *Man on the Moon X201 gas uptake* system (9 bar H_2, reservoir pressure 1.9 bar H_2 pressure). The hydrogen uptake started with the addition of catalyst/substrate. After the reaction, the mixture was treated with a saturated aqueous solution of NH_4Cl and ethyl acetate. The organic phases were dried over $MgSO_4$ and analyzed by quantitative GC-FID analysis vs. internal standard

(*n*-pentadecane). The monitored hydrogen consumption is related to the yield of product, which was determined by GC FID.

During the reaction, the dark red color slowly changed to black accompanied by formation of a black precipitate in case of α-methylstyrene. The color of the related octene/catalyst mixture immediately changed to black accompanied by formation of a black precipitate. This observation further supports an electron transfer to styrenic substrates, which is not observed for octenes (see main text, Figure 5, III). The formation of the precipitate under hydrogen atmosphere presumably accounts for the formation of nanoparticles.

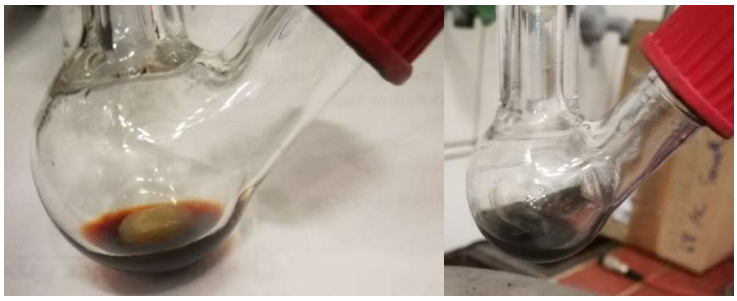

Figure S21. Selected pictures from the reaction mixture after addition of the catalyst to the flask. Left: 1-octene as substrate. Right: α-methylstyrene as substrate

Determination of turnover frequencies (TOFs) for selected reactions:

General procedure: The TOFs were determined from reaction progress analyses (see Figure 4 of the manuscript) by analysing the slope of a selected part of the reaction time profile showing a linear ascent. Note that that the resulting TOF values are necessarily approximate due to the presence of an induction period..

1-octene: t = 4.18 min to 4.51 min; TOF = 601 h^{-1};

2-octene: t = 60.8 min to 65.9 min; TOF = 103 h^{-1};

α-methylstyrene: t = 31.2 min to 34.3 min; TOF = 287 h^{-1};

5.5.4.1.4 Poisoning Experiments

Poisoning experiments were performed with catalyst **1**, triphenylethylene as substrate and Hg, dct (dibenzo[*a,e*]cyclooctatetraene), benzonitrile, and naphthalene as poisoning agents.

General procedure:

A solution of **1** (1.2 mg, 0.002 mmol) in 0.25 mL DME was added to the catalyst poison. The resulting solution was stirred for one minute and added to triphenylethylene and *n*-pentadecane. The hydrogenation reaction and work-up was performed according to the general procedure described in chapter 3.1.

Table S9. Hydrogenation of triphenylethylene in presence of selected poisoning agents.[a]

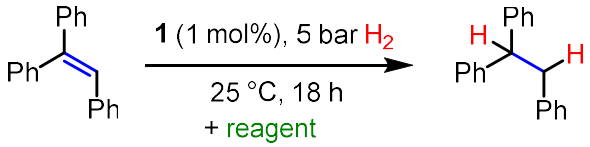

Entry	Reagent / equiv. per [Ni]	Yield (Conversion)[b] / %
1	Hg (50 mg, 0.025 mmol, 125 equiv.)	2 (5)
2	Dct (0.8 mg, 0.004 mmol, 2.0 equiv.)	92 (>99)[c]
3	Benzonitrile (1 µL, 0.01 mmol, 5.0 equiv.)	1 (11)[c]
4	Naphthalene (0.5 mg, 0.004 mmol, 2.0 equiv.)	82 (82)[c]

[a] Standard conditions: substrate (0.2 mmol), 25 °C, 5 bar H_2, 18 h. [b] Yields and conversions were determined by quantitative GC-FID vs. internal *n*-pentadecane. [c] 21 h.

5.5.4.2 Stoichiometric Reactions

5.5.4.2.1 Deuterium Experiments

a) Triphenylethylene: deuterated solvent

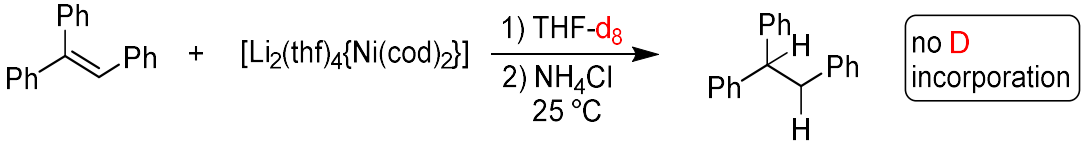

Triphenylethylene (25.8 mg 0.1 mmol, 1.0 equiv.) and **1** (58.1 mg, 0.1 mmol, 1.0 equiv.) were dissolved in 1 mL THF-d_8. The solution immediately turned deep purple upon addition of **1** to the organic substrate and was subsequently quenched with an aqueous NH_4Cl solution. After addition of *n*-pentane the organic phase was filtered over a pad of silica and dried *in vacuo*. The residue was dissolved in *n*-pentane, filtered over a pad of silica and analyzed by GC-MS. The *n*-pentane solution was dried in *vacuo* and the residue dissolved in $CDCl_3$ and analyzed by ^1H NMR and ^2H NMR spectroscopy.

According to GC-FID peak area comparison 55% of triphenylethylene was reduced to the corresponding alkane.

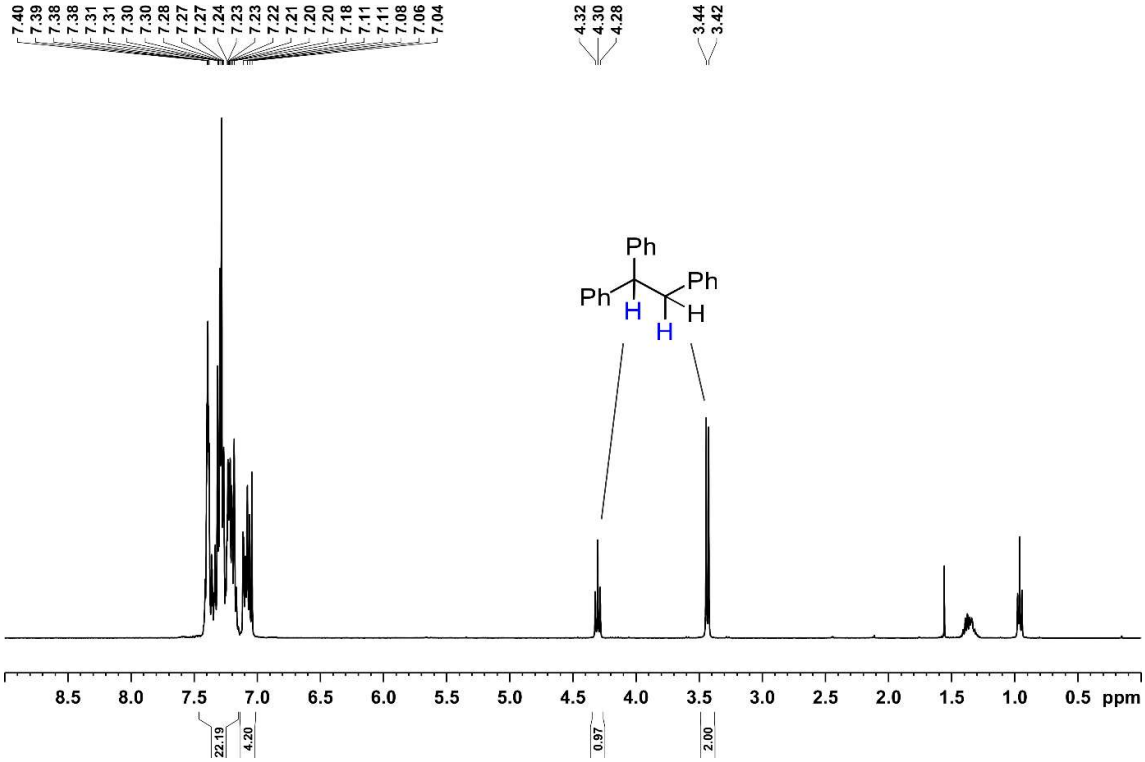

Figure S22. ^{1}H NMR spectrum (400.13 MHz, 300 K, $CDCl_3$) of reaction 5.5.4.2.1 a.

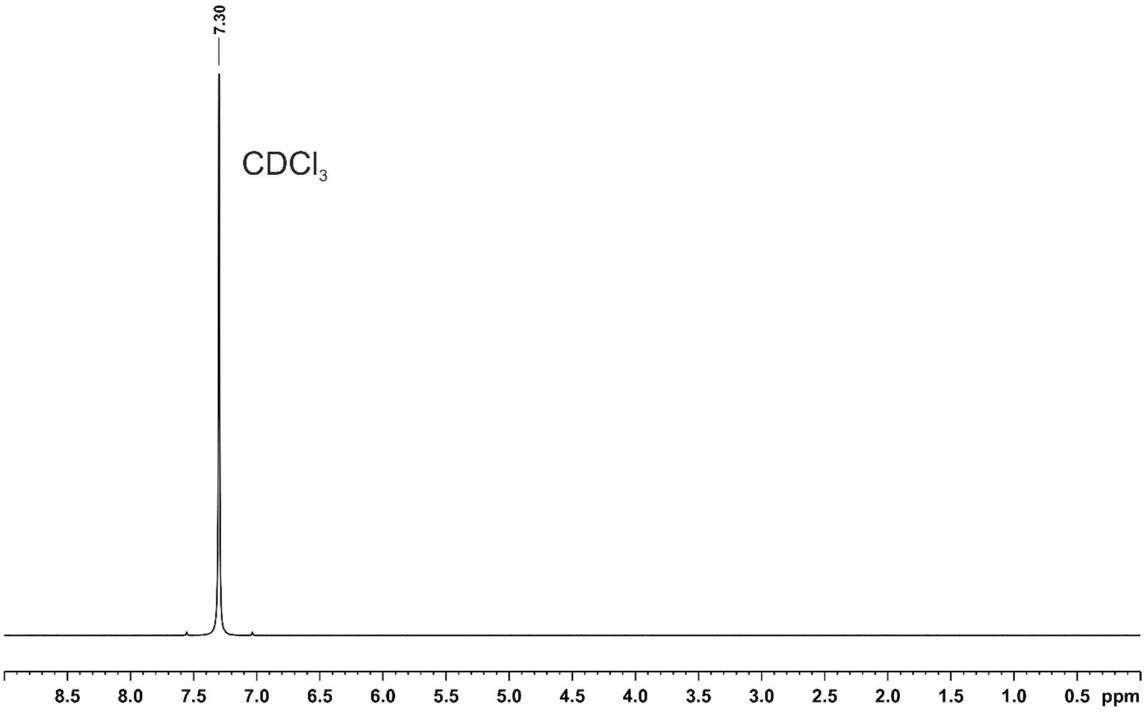

Figure S23. ^{2}H NMR spectrum (61.4 MHz, 300 K, $CDCl_3$) of reaction 5.5.4.2.1 a.

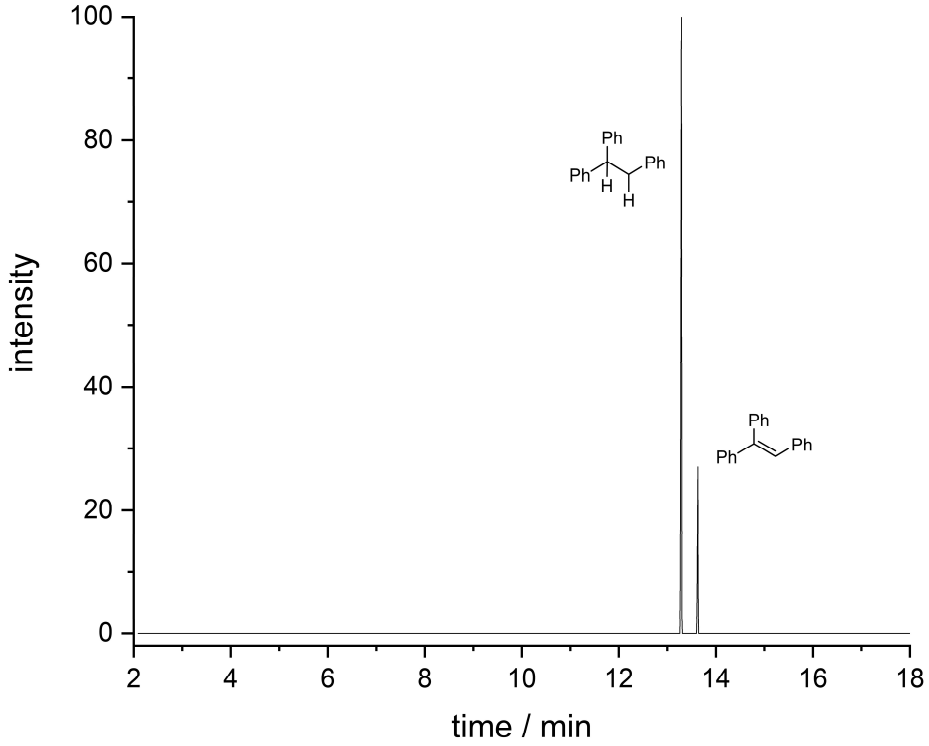

Figure S24. GC-MS chromatogram of reaction 5.5.4.2.1 a.

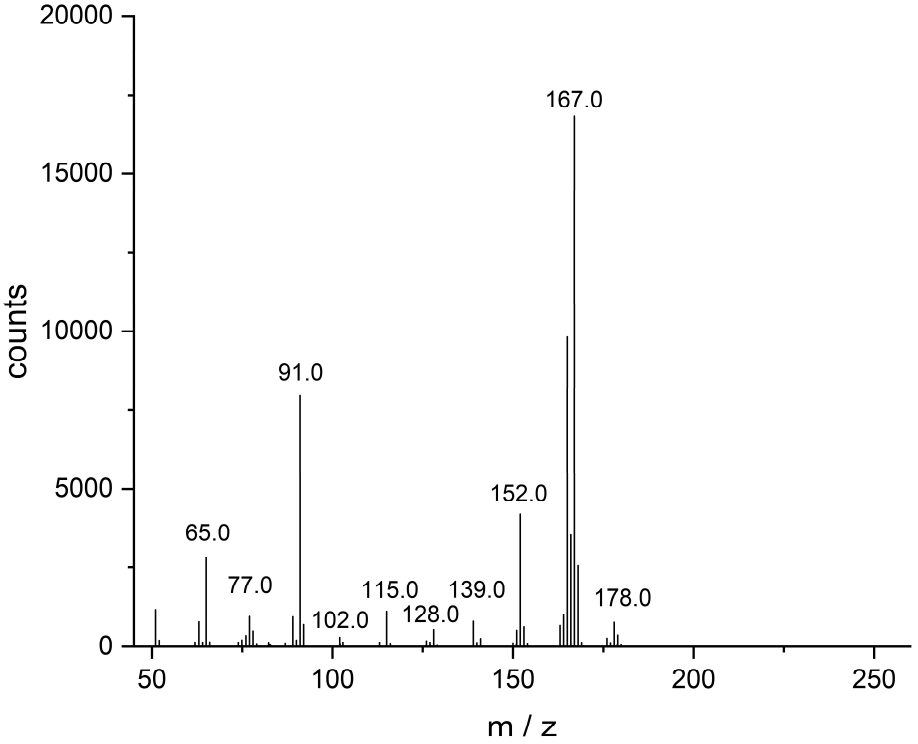

Figure S25. m/z data of peak 13.274 – 13.297 min.

b) Triphenylethylene: quench with D_2O

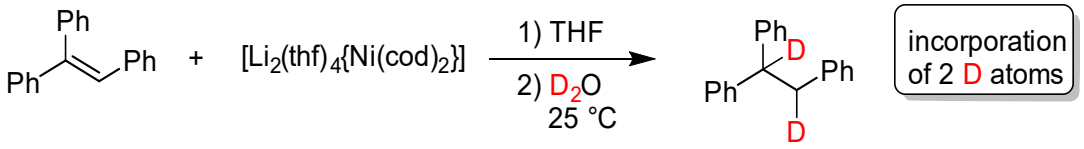

Triphenylethylene (27.0 mg 0.105 mmol, 1.0 equiv.) and **1** (60.8 mg, 0.105 mmol, 1.0 equiv.) were dissolved in 2 mL THF. The solution immediately turned deep purple upon addition of **1** to the organic substrate and was subsequently quenched with 1 mL D_2O. After addition of *n*-pentane the organic phase was filtered over a pad of silica and dried *in vacuo*. The residue was dissolved in *n*-pentane, filtered over a pad of silica and analyzed by GC-MS. The *n*-pentane solution was dried in *vacuo* and the residue dissolved in $CDCl_3$ and analyzed by ^1H NMR and ^2H NMR spectroscopy.

According to GC-FID peak area comparison 80% of triphenylethylene was reduced to the corresponding alkane. The value is significantly higher compared to 4.2.1a) which can be explained by the higher water content of THF-d_8 compared to THF.

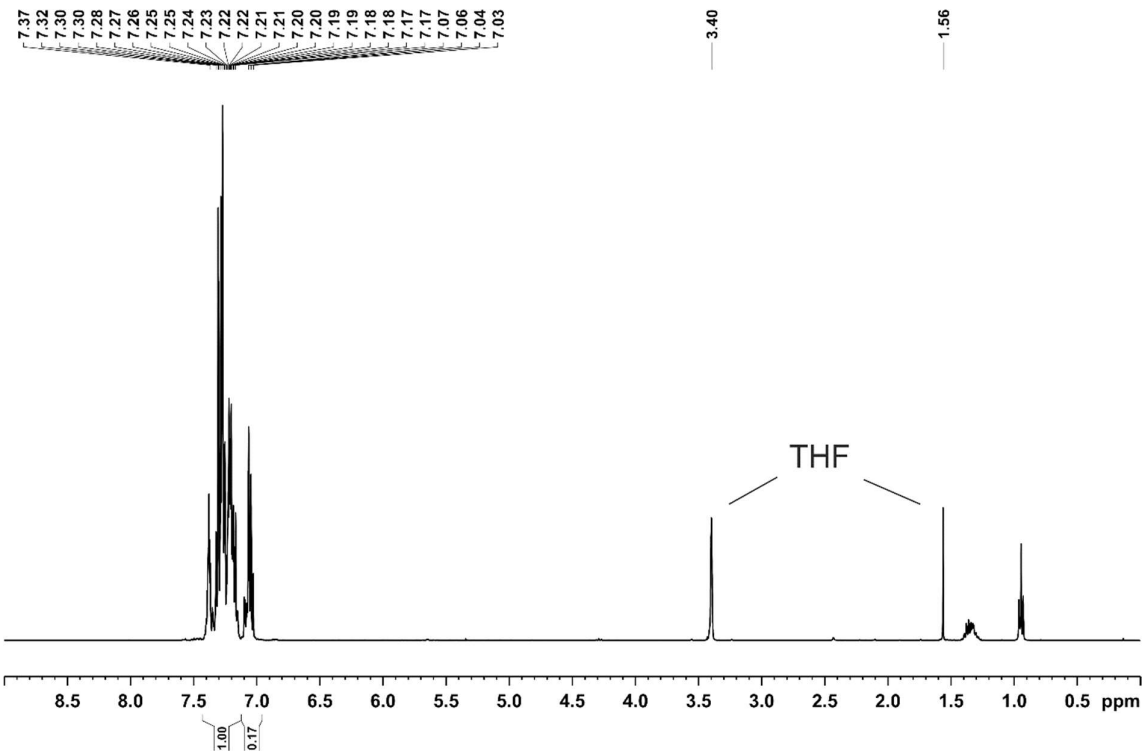

Figure S26. ^1H NMR spectrum (400.13 MHz, 300 K, $CDCl_3$) of reaction 5.5.4.2.1 b.

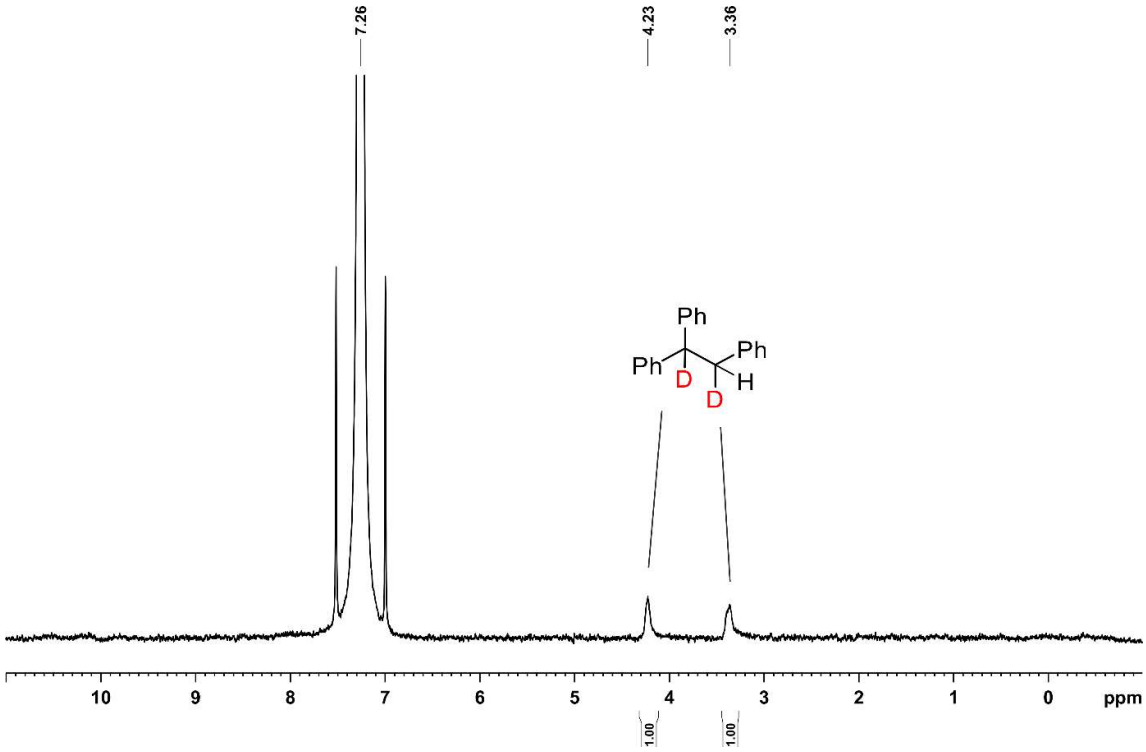

Figure S27. ^{2}H NMR spectrum (61.4 MHz, 300 K, $CDCl_3$) of reaction 5.5.4.2.1 b.

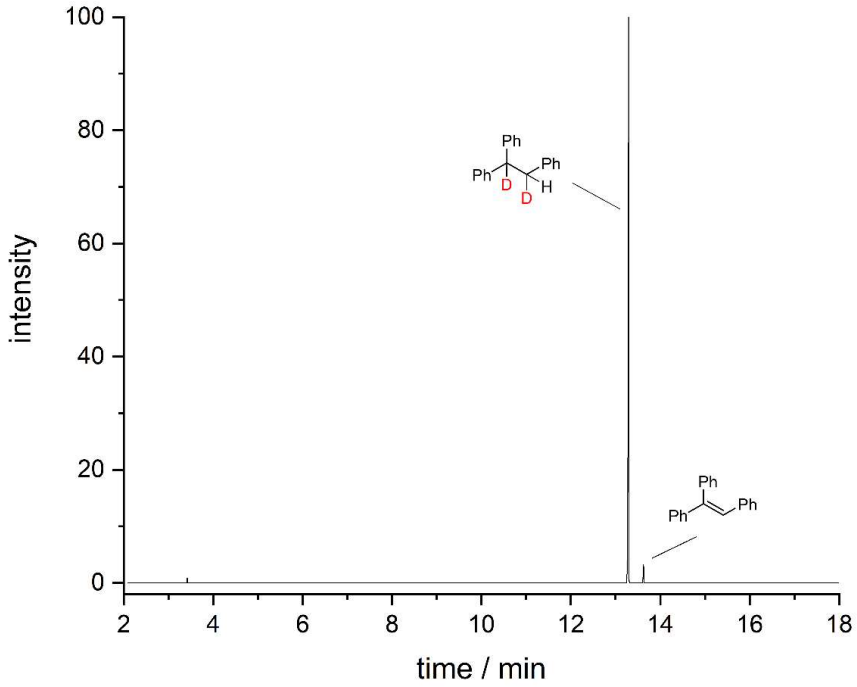

Figure S28. GC-MS chromatogram of reaction 5.5.4.2.1 b.

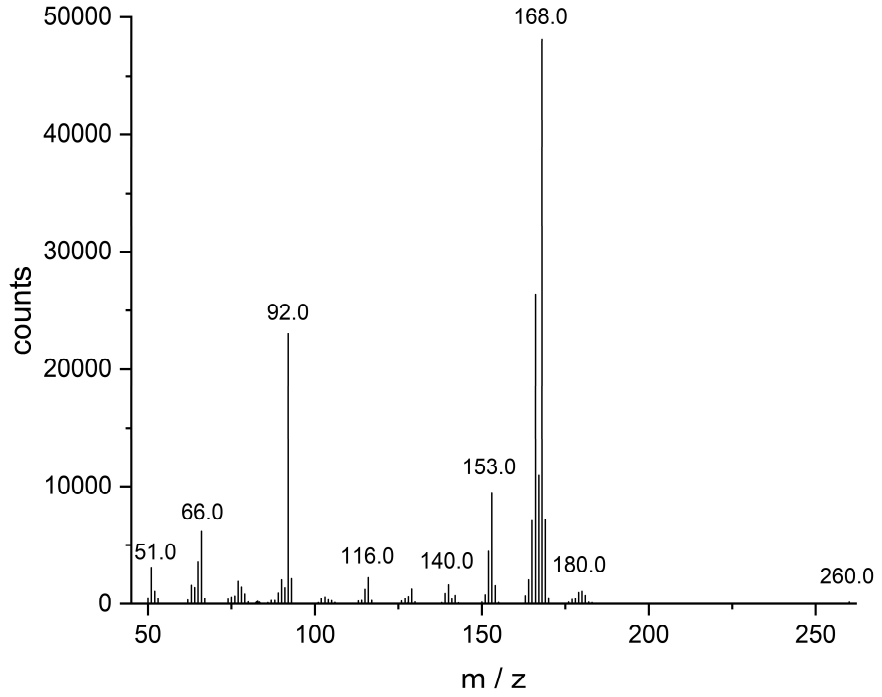

Figure S29. m/z data of peak 13.268 – 13.297 min.

5.5.4.2.2 NMR Experiments

a) Triphenylethylene (2:1 reaction)

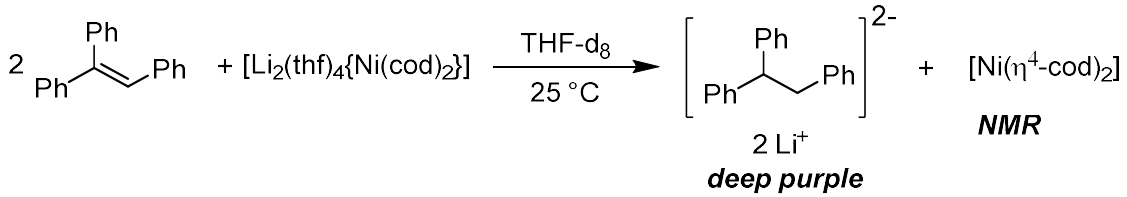

Triphenylethylene (6.9 mg 0.027 mmol, 2.0 equiv.) and **1** (7.8 mg, 0.0135 mmol, 1.0 equiv.) were dissolved in 0.6 mL THF-d_8. The solution immediately turned purple from red and was analyzed by ^{1}H NMR spectroscopy.

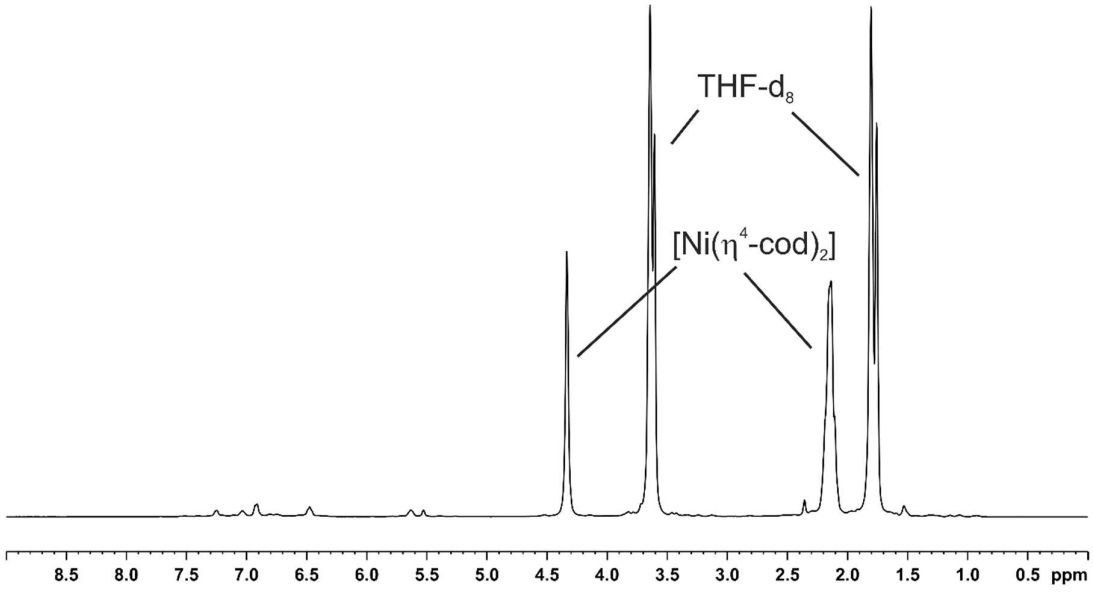

Figure S30. ^{1}H NMR spectrum (400.13 MHz, 300K, THF-d$_8$) of **1** and triphenylethylene (2 equiv.).

b) Triphenylethylene (1:1 reaction)

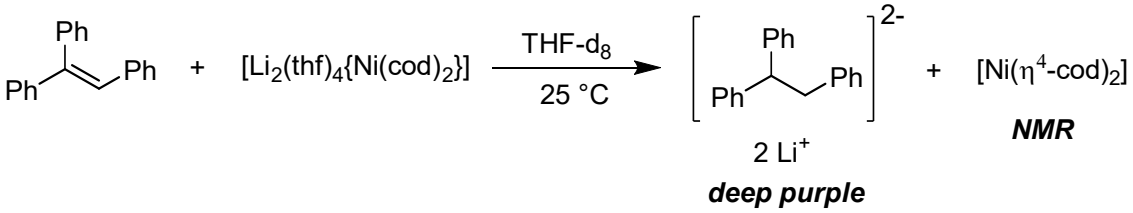

Triphenylethylene (5.3 mg 0.021 mmol, 1.0 equiv.) and **1** (12.1 mg, 0.021 mmol, 1.0 equiv.) were dissolved in 0.6 mL THF-d$_8$. The solution immediately turned deep purple and was analyzed by ^{1}H NMR spectroscopy.

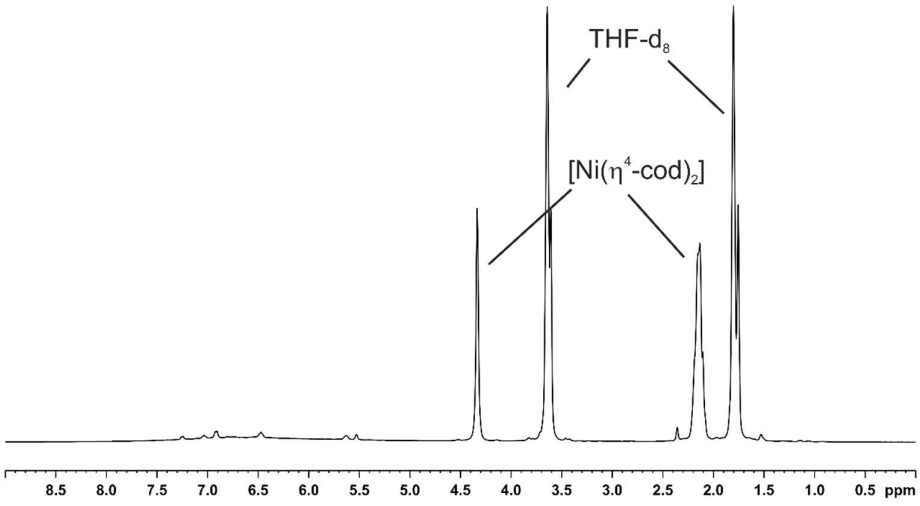

Figure S31. ^{1}H NMR spectrum (400.13 MHz, 300K, THF-d$_8$) of **1** and triphenylethylene (1 equiv.).

c) 1-Dodecene (1:1 reaction)

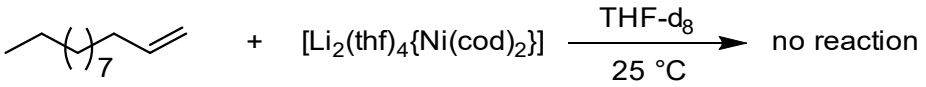

1-Dodecene (5 µL, 0.023 mmol, 1.0 equiv.) and **1** (13.3 mg, 0.022 mmol, 1.0 equiv.) were dissolved in 0.6 mL THF-d_8. The solution did not change the color and was analyzed by ^{1}H NMR spectroscopy.

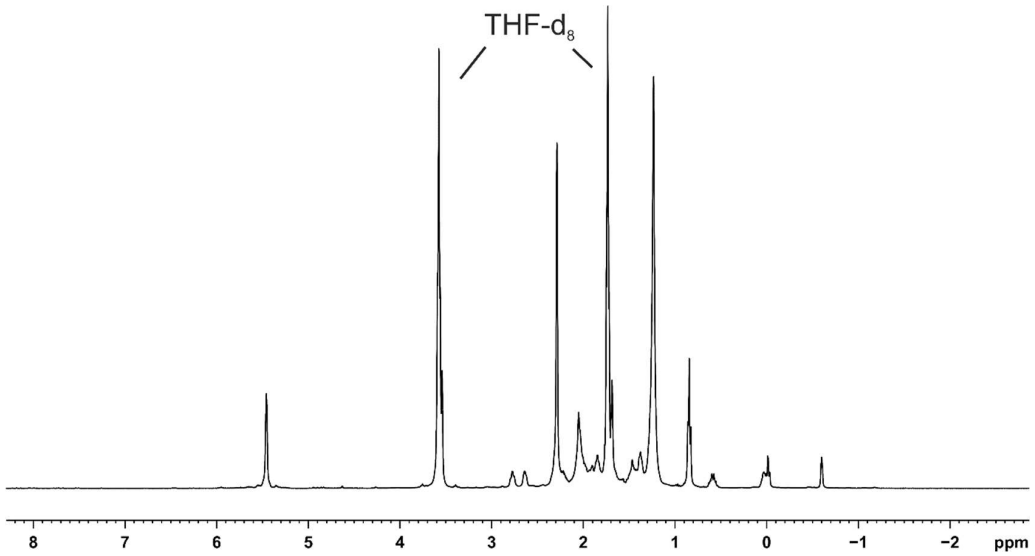

Figure S32. ^{1}H NMR spectrum (400.13 MHz, 300K, THF-d_8) of **1** and 1-dodecene.

5.5.4.2.3 GC Analyses

a) Triphenylethylene (1:2 reaction)

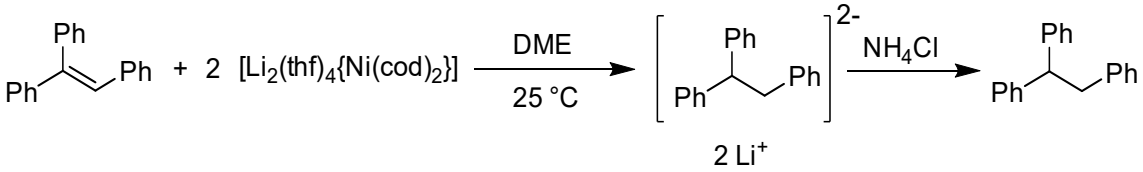

Triphenylethylene (0.8 mg 0.0031 mmol, 1.0 equiv.) and **1** (3.6 mg, 0.0062 mmol, 2.0 equiv.) were dissolved in 0.5 mL DME. The solution immediately turned from red to purple and was quenched after five minutes with a saturated NH_4Cl solution and ethyl acetate. An aliquot of the organic phase was analyzed by GC-MS. A significant amount of triphenylethane was formed.

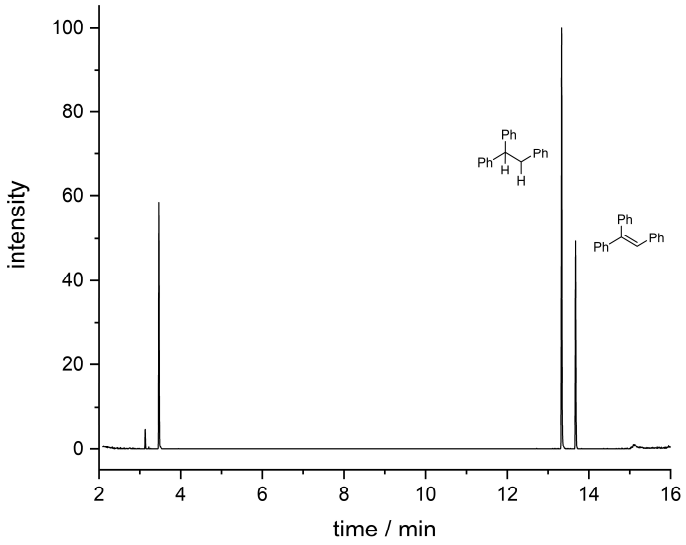

Figure S33. Chromatogram (GC-MS) from the reaction of 1,1',2-triphenyethylene with 2.0 equiv. **1**.

b) Triphenylethylene (1:1 reaction)

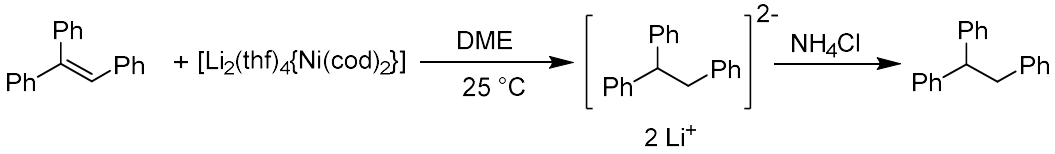

Triphenylethylene (1.6 mg 0.0062 mmol, 1.0 equiv.) and **1** (3.6 mg, 0.0062 mmol, 1.0 equiv.) were dissolved in 0.5 mL DME. The solution immediately turned purple from red and was quenched after five minutes with a saturated NH_4Cl solution and ethyl acetate. An aliquot of the organic phase was analyzed by GC-MS. A significant amount of triphenylethane was formed.

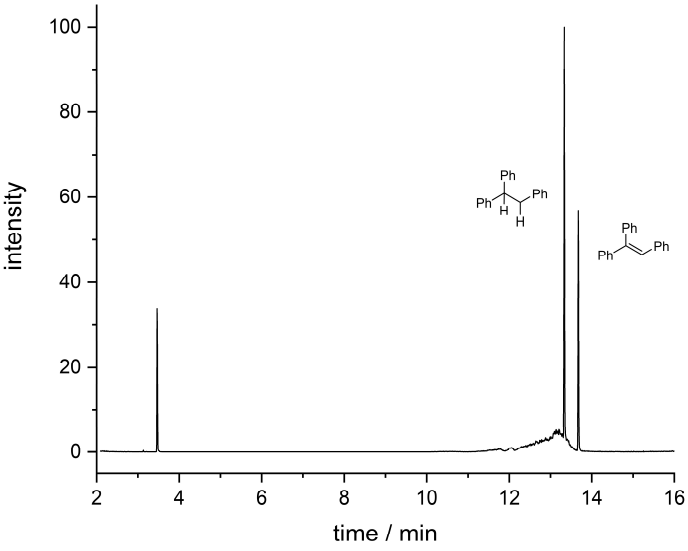

Figure S34. Chromatogram (GC-MS) from the reaction of triphenylethylene with **1**.

c) 1-Dodecene (1:1 reaction)

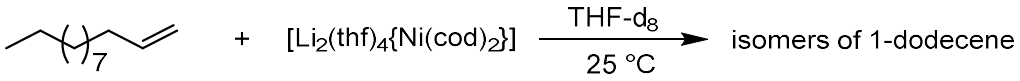

The reaction of 4.1.1 c) was quenched after NMR spectroscopic analysis with saturated aqueous NH_4Cl solution and ethyl acetate. An aliquot of the organic phase was analyzed by GC-MS. No dodecane was observed. Instead, a significant amount of 1-dodecene isomers were detected.

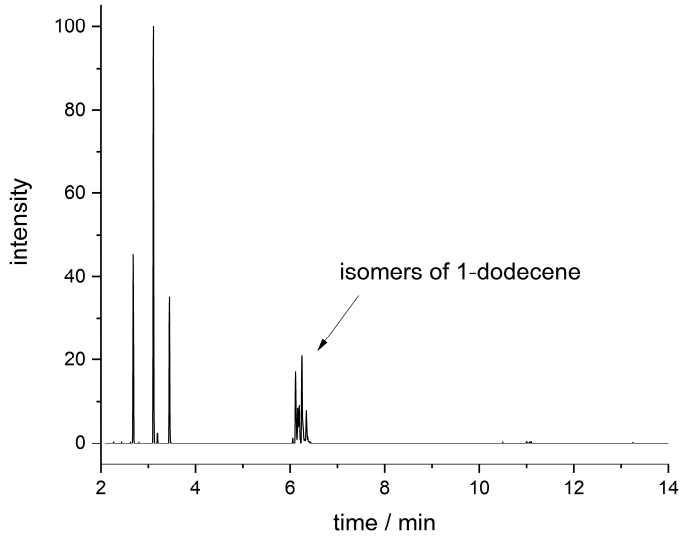

Figure S35. Chromatogram (GC-MS) from the reaction of 1-dodecene with **1**.

d) Benzaldehyde

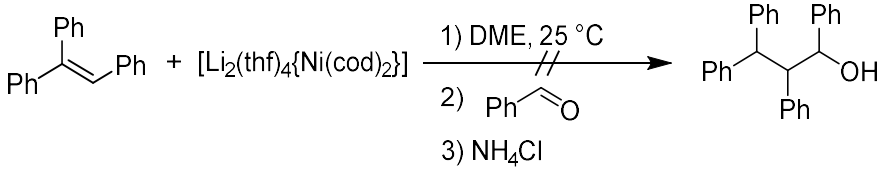

Triphenylethylene (4.5 mg 0.018 mmol, 1.0 equiv.) and **1** (10.4 mg, 0.018 mmol, 1.0 equiv.) were dissolved in 0.25 mL DME each. The solution turned deep-purple upon addition of **1** to 1,1',2-triphenyethylene. The reaction was quenched with benzaldehyde (8.8 µL, 0.087 mmol, 5.0 equiv.) and became colorless. Aqueous NH_4Cl and ethylacetate was added and an aliquot of the organic phase was filtered and subsequently analzyed by GC-MS. No formation of the proposed product was observed.

This experiment supports the hypothesis that a dianionic intermediate is formed and not a monoanionic one.

5.5.5 Cyclic Voltammetry

The electrochemical properties of triphenylethylene (TPE) were investigated by cyclic voltammetry in DME/^{n}Bu$_4$NPF$_6$ and THF/ ^{n}Bu$_4$NPF$_6$. The CV of complex **1** was recorded in THF/^{n}Bu$_4$NPF$_6$.

a) Triphenylethylene

Triphenylethylene (2.5 mg, 0.010 mmol) was dissolved in a solution of ^{n}Bu$_4$NPF$_6$ (375 mg, 0.97 mmol) in 10 mL THF.

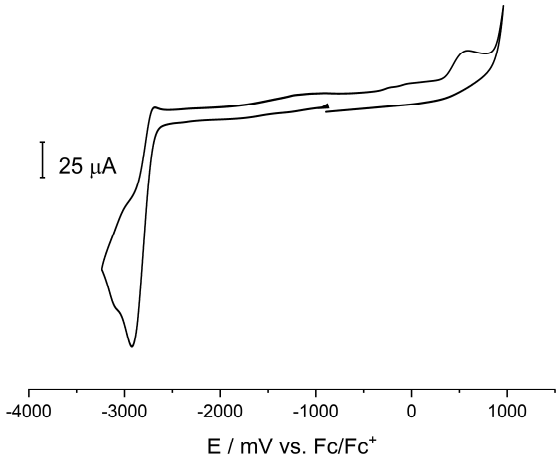

Figure S36. Cyclic voltammogram of TPE in THF/^{n}Bu$_4$NPF$_6$. Scan rate = 100 mV s^{-1}.

b) DME

Triphenylethylene (3.3 mg, 0.013 mmol) was dissolved in a solution of ^{n}Bu$_4$NPF$_6$ (378 mg, 0.98 mmol) in 10 mL DME.

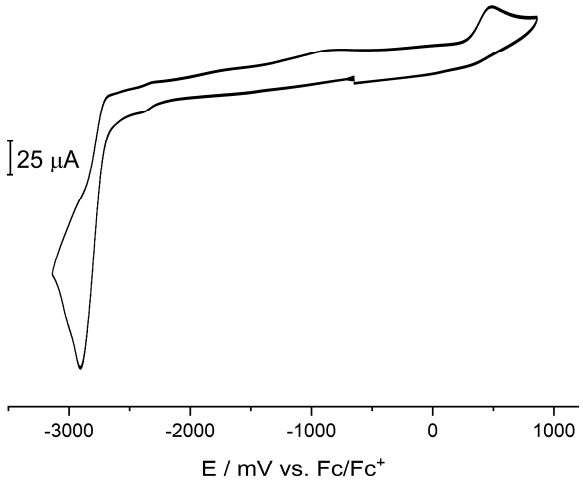

Figure S37. Cyclic voltammogram of TPE in DME. Scan rate = 200 mV s^{-1}.

c) Complex **1**

Complex **1** (11.3 mg, 0.02 mmol) was dissolved in a solution of $^{n}Bu_4NPF_6$ (380 mg, 0.98 mmol) in 10 mL THF.

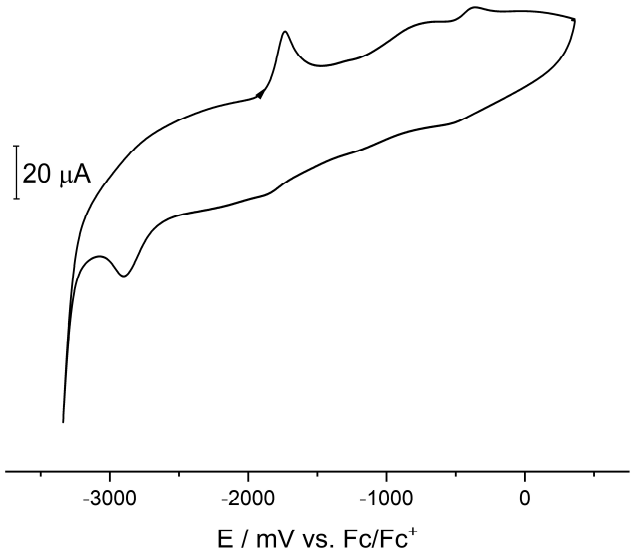

Figure S38. Cyclic voltammogram of complex **1** in THF. Scan rate = 200 mV s^{-1}.

5.5.6 UV-vis Spectroscopy

a) Triphenylethylene

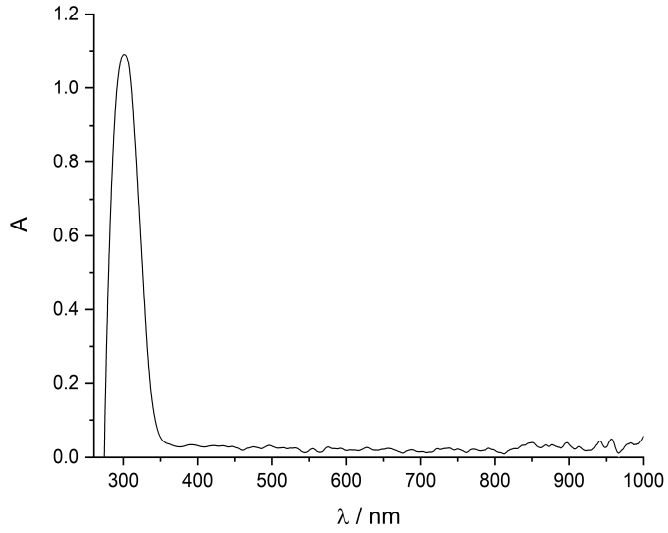

Figure S39. UV-vis spectrum of TPE with λ_{max} = 301 nm.

b) Reaction of triphenylethylene with **1**

Triphenylethylene (2.0 mg, 0.078 mmol) and **1** (4.3 mg, 0.0074 mmol) were both dissolved in 0.2 mL THF. The nickel complex **1** was added to the olefin solution upon color change to deep purple was observed. So much THF has been added to the solution that the absorbance was between 0 and 1.

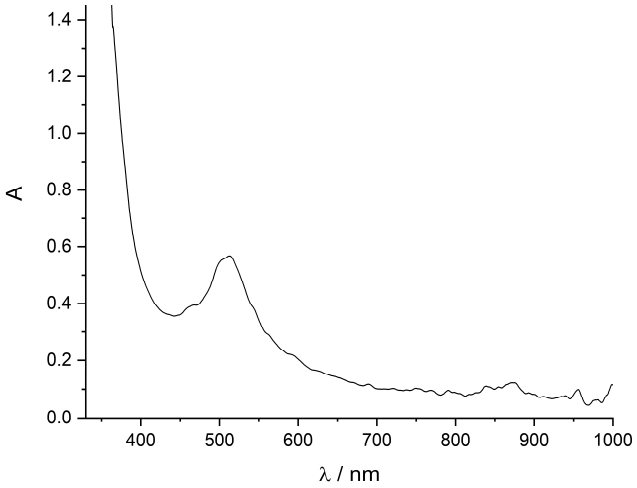

Figure S40. UV-vis spectrum of reaction of TPE and **1** with λ_{max} = 511 nm.

5.5.7 TEM Analyses

Complex **1** (1.2 mg, 0.002 mmol, 1.0 equiv.) and 1-phenyl-1-cyclohexene (31.5 μL, 0.2 mmol, 100 equiv.) were dissolved in 0.25 mL DME. The solution was saturated with 1 bar H_2 by freeze-pump-thaw (3 times). Further preparation work was carried out in a Glove Box under argon to prevent any alteration of the particles. A droplet of the DME solution was transferred onto a regular, commercially available holey carbon grid. The holey carbon grid was then transferred into a special vacuum transfer holder (*Gatan Inc*), where the specimen can be retracted into the holder casing for protection against the atmosphere. Additionally, the holder was flooded with the inert gas form the Glove Box. After transfer of the holder, containing the sealed specimen, into the microscope, the vacuum holder was first pumped to remove the inert gas, afterwards the specimen cartridge was moved out of the sealed area, now ready for inspection by the microscope. The images were then recorded using a 1k x 1k CCD camera.

5.5.8 References

[1] K. Jonas, *Angew. Chem. Int. Ed.* **1975**, *14*, 752-753; *Angew. Chem.* **1975**, *87*, 809–810.

[2] L. Nattmann, S. Lutz, P. Ortsack, R. Goddard, J. Cornella, *J. Am. Chem. Soc.* **2018**, *140*, 13628–13633.

[3] N. G. Léonard, P. J. Chirik, *ACS Catal.* **2018**, *8*, 342–348.

[4] Y. Wang, A. Kostenko, S. Yao, M. Driess, *J. Am. Chem. Soc.* **2017**, *139*, 13499–13506.

[5] C. Metallinos, J. Zaifman, L. Van Belle, L. Dodge, M. Pilkington, *Organometallics* **2009**, *28*, 4534-4543

[6] M. R. Prinsell, D. A. Everson, D. J. Weix, *Chem.Commun.* **2010**, *46*, 5743-5745.

[7] C. Smit, W. Fraaije, A. J. Minnaard, *J. Org. Chem.* **2008**, *73*, 9482.

[8] S. Mummadi, A. Brar, G. Wang, D. Kenefake, R. Diaz, D. K. Unruh, S. Li, C. Krempner, *Chem. Eur. J.* **2018**, *24*, 16526-16531.

6 Highly-Reduced α-Diimine Ferrates: Electronic Structure and Catalysis

Thomas M. Maier, Nicolaas P. van Leest, Serhiy Demeshko, Michael Bodensteiner, Bas de Bruin, Franc Meyer, and Robert Wolf

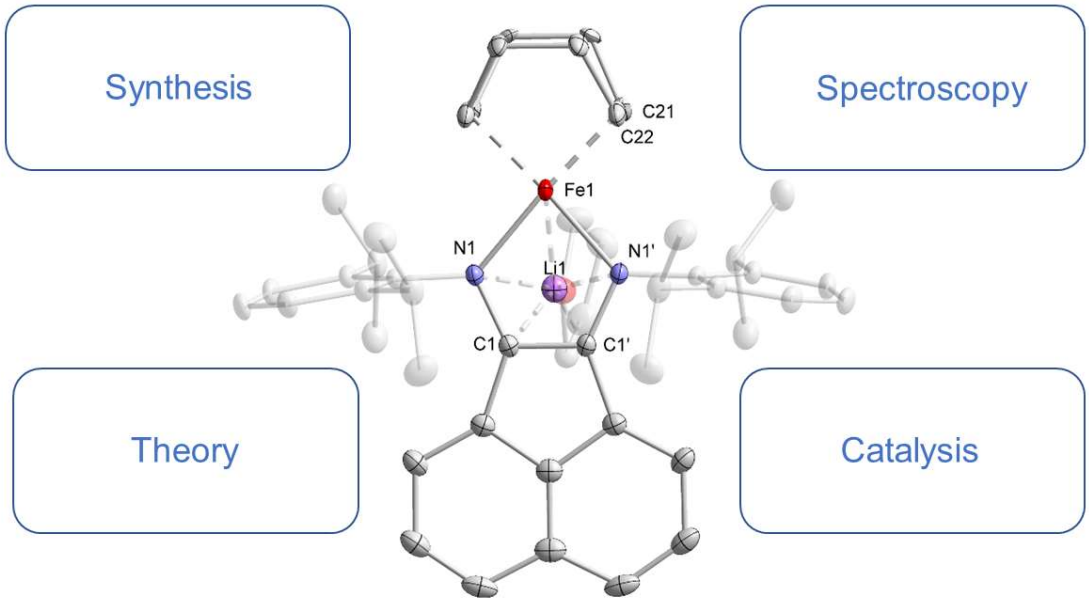

T. M. Maier performed the experimental work and wrote the chapter. N. P. van Leest and B. de Bruin recorded and analyzed EPR data (Figures 8 and 15). M. Bodensteiner assisted with the refinement of single-crystal X-ray crystallography data. S. Demeshko and F. Meyer conducted and interpreted ^{57}Fe Mößbauer spectra and SQUID magnetization measurements (Figures 9, 10 and 16). P. Coburger assisted with quantum-chemical calculations. R. Wolf supervised and directed the project.

6.1 Introduction

Organometallic and coordination chemistry can have a huge impact on a sustainable future by supporting the development of efficient catalysts based on earth-abundant metals.[1] These complexes can both replace precious metals in existing reactions and potentially mediate entirely new reactions, which are not yet accessible. One of the most important earth-abundant metals is iron which is cheap, non-toxic, and shows a high synthetic versatility due to its formal oxidation states ranging formally from –II to +VI. Meanwhile, some of the most important classes of large-scale chemical reactions are catalytic reductions (hydrogenations, hydroborations, hydrosilylations) which play crucial roles in the synthesis of numerous fine chemicals, agrochemicals, fragrances, and food additives.[2] In this context, low-valent highly-reducing iron species became unsurprisingly compounds of special interest, which can be used as efficient catalysts.[3]

Metal-mediated catalytic cycles typically consist of elementary two-electron processes such as oxidative addition or reductive elimination. Precious metals such as rhodium [Rh(I)/Rh(III)] or palladium [Pd(0)/Pd(II)] easily undergo such redox reactions and hence are typically favored from this point of view. In contrast, first-row transition metal complexes one-electron reactions are often observed. To overcome this problem and to mimic the behavior of precious metals, the concept of using redox-active ligands was introduced for first-row transition metal catalysis.[4] A redox-active ligand is capable of storing and releasing electrons and can therefore be directly involved in catalytic reactions by facilitating net $2e^-$ processes that would otherwise be disfavored.[5] A prominent class of redox-active ligands is the α-diimine family, members of which are almost always good π-acceptors and so well able to stabilize electron rich metal centers. Thus, low-valent iron complexes with redox-active α-diimine ligands provide an attractive motif for applications in sustainable catalysis.

As a result, the synthesis of low-valent α-diimine iron complexes bearing an unsaturated hydrocarbon as second ligand has attracted significant interest over the last two decades (Figure 1).[7]-[19] In these complexes the hydrocarbon is supposed to act as "placeholder" which can easily be replaced by substrates to initiate the catalytic cycle. These hydrocarbons are typically simple arenes as used for example in complexes **A** – **E** shown in Figure 1. The first example was reported by *Zenneck* and co-workers in 1998, who described the synthesis of a family of 1,4-diaza-1,3-diene iron toluene complexes with numerous slightly different α-diimines.[6] Complexes of type **A** are efficient pre-catalysts for the dimerization of

1,3-butadiene to 1,5-cyclooctadiene and 4-vinyl-cyclohex-1-ene after activation with $(Et_2AlOEt)_2$. In these complexes the C–C bond of the α-diimine unit is significantly shortened relative to the free ligand, whereas the C–N bonds were stretched, which can be explained by an electron transfer from the metal center to the now formally anionic ligand.

Similar net-neutral α-diimine iron arene complexes with varying α-diimine and arene ligands were synthesized by the groups of *Chirik*, *Song*, and *Findlater*.[7]-[10] Of particular interest are the complexes **D** and **E** by *Findlater* and co-workers, who chose a bis(aryl)iminoacenaphthene (BIAN) ligand with a polyarene backbone instead of a simple α-diimine ligand with a saturated backbone.[8],[9] BIAN ligands are known since the 1960s and were established in coordination chemistry by *Elsevier* and co-workers.[11],[12] This ligand class benefits from a rigid backbone which ensures that the donor nitrogen atoms are fixed in the *cis* orientation that is required for metal coordination. *Fedushkin* and co-workers intensively studied the redox behavior of the ^{Dipp}BIAN (Dipp = 2,6-diisopropylphenyl) ligand. Remarkably, it is possible to reduce ^{Dipp}BIAN to its tetraanionic state using sodium metal.[13] However, such an extreme formal charge is rather unusual in transition metal complexes and usually neutral, monoanionic or dianionic BIAN ligands are observed. *Findlater* and co-workers synthesized the [(^{Dipp}BIAN)Fe(arene)] (arene = benzene, toluene) complexes **D** and **E** by reduction of [(^{Dipp}BIAN)$FeCl_2$] with Na/Hg in presence of the corresponding arene. The benzene complex acts as active pre-catalyst for the polymerization of L-lactide, whereas the toluene adduct can be used as a pre-catalyst in the hydrosilylation of ketones and aldehydes under solvent-free conditions. Metrical data taken from single-crystal X-ray crystallography support the hypothesis of a monoanionic α-diimine ligand in those complexes. Independently, the group of *Jacobi von Wangelin* studied the hydrogenation of olefins mediated by an *in situ* catalyst formed from [(^{Dipp}BIAN)$FeCl_2$] and *n*-butyllithium in toluene.[14]

Chelating olefins such as 1,5-cyclooctadiene (cod) can also be used as labile hydrocarbon ligands. Such complexes have been reported by the groups of *Chirik*, *Ritter*, and *Findlater*.[7],[15],[16] *Chirik* and co-workers synthesized the neutral tetrahedral iron complex **F** which contains cod and an α-diimine unit based on biacetyl.[7] This complex is an efficient pre-catalyst for the hydrogenation of simple olefins under mild conditions [0.3 mol [Fe], 4 bar H_2, r.t. (r.t = room temperature)], although the formation of the catalytically inactive benzene complex **B** was observed for some styrenic substrates. *Ritter* and co-workers observed the catalytic dimerization of 1,3-butadiene to cod on a >100 g scale using the similar complex **G**.[15]

In the same report, the electronic structure of this complex was investigated with various techniques (SQUID magnetization measurements, ^{57}Fe Mößbauer spectroscopy, and DFT calculations), suggesting the presence of a high-spin Fe(I) ($S = 3/2$) center which is antiferromagnetically coupled to an α-diimine radical anion. *Findlater* and co-workers introduced the BIAN ligand in this class of complexes, resulting in the formation of complex [(^{Dipp}BIAN)Fe(η^4-cod)] (**H**).[16] The group of *Chirik* further contributed the neutral heteroleptic iron α-diimine complexes **J** and **K**.[18] Both complexes are coordinated by an α-diimine ligand based on biacetyl with a ligand-sphere completed either by two –CH_2SiMe_3 ligands (**J**) or by isoprene (**K**).

In contrast to the research on neutral heteroleptic iron α-diimine complexes, there are only three reports about anionic complexes, coming from the groups of *Lichtenberg*, *de Bruin*, *Grützmacher* (**L** – **N**). In these complexes the olefin and α-diimine ligands were combined in one framework using a trop$_2$dad ligand (trop = 5*H*-dibenzo[*a*,*d*]cycloheptene-5-yl, dad = diazadiene).[19] The central iron atom of complex **L** adopts an almost square-planar geometry. The electronic structures of these complexes were studied by various experimental techniques and DFT calculations using the broken-symmetry approach. Single-crystal X-ray crystallography on the $[Na(thf)_3]^+$ salt **L** suggested the presence of a dianionic diazadiene bound to Fe(I). The low-spin d^7 electronic configuration was further confirmed by SQUID analysis, ^{57}Fe Mößbauer spectroscopy, and EPR studies. Analogous complexes **M** and **N** featuring a saturated backbone were also prepared and fully characterized. These complexes were used for the efficient dehydrogenation of dimethylamine-borane and the dehydrogenative coupling of silanes and 1,4-dibenzenemethanol.

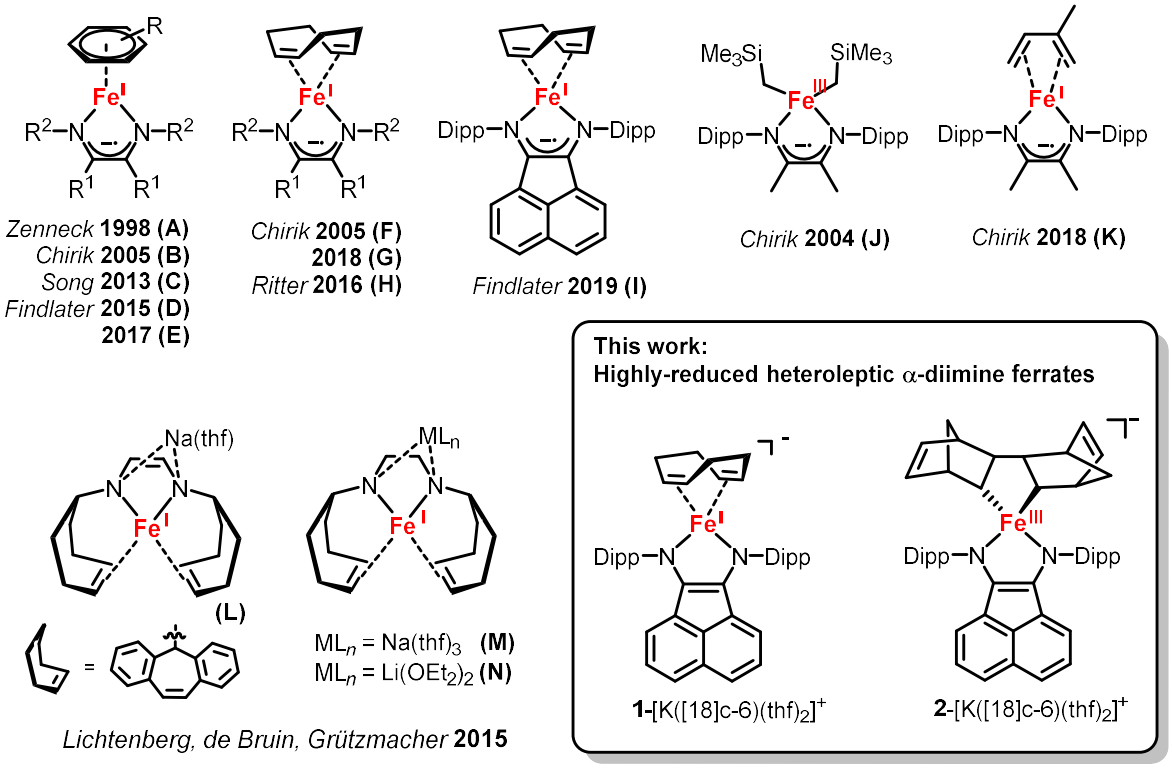

Figure 1. Previously reported low-valent α-diimine iron complexes with hydrocarbon ligands, and the new complexes presented in this work. R = H, Me; R^1 = H, Me (**A**, **B**, **C**) BIAN (**D**, **E**); R^2 = aryl, alkyl; Dipp = 2,6-diisopropylphenyl.

Although there are several reports on heteroleptic α-diimine complexes, the corresponding homoleptic counterparts remain scarce (Figure 2).[7],[20]-[23] These complexes have limited potential for applications in catalysis due to their limited capability to generate vacant coordination sites. Thus, such species have mainly served as subjects for electronic structure analysis. The group of *tom Dieck* synthesized the first low-valent bis(α-diimine) iron species **O** by the reduction of bis(α-diimine) iron(II) chloride salts with sodium metal.[20] The investigated α-diimines investigated were all 1,4-diaza-1,3-dienes derived from biacetyl and the resulting complexes were only analyzed by elemental analysis. Later on, *Walther* and co-workers investigated the chemistry of benzil dianil and electron rich metal centers **P**.[21] The iron complex was investigated by magnetic methods (μ_{eff} = 3.23 μB at r.t.), as well as spectroscopic techniques (IR, UV-vis). *Chirik* and co-workers synthesized the neutral bis(α-diimine) iron complex **Q** by reduction of the corresponding α-diimine iron(II) chloride precursor with Na/Hg.[7] This was the first compound of this type that was structurally characterized by single-crystal X-ray crystallography, revealing a tetrahedral geometry at iron. The metrical

data, in particular the relatively long C–C bond and short C–N bond, in combination with magnetic susceptibility measurements, suggested a significant degree of α-diimine ligand reduction. *Wieghardt* and co-workers subsequently provided a detailed analysis of the electronic structure of the species **R** by a combination of ^{57}Fe Mößbauer spectroscopy, magnetic susceptibility measurements, single-crystal X-ray crystallography, and density-functional theory using the broken-symmetry approach.[22] It was concluded that the commonly used description of the electron structure with a central Fe(0) atom is in fact not correct. Instead, the complexes each contain two monoanionic α-diimine ligands (S = 1/2) with a high-spin Fe(II) (S = 2) center. Due to antiferromagnetic coupling between the α-diimine ligands and the iron atom, an overall spin of S = 1 is observed for the ground state. This work established the fact that α-diimines are redox-active ligands. Later, a similar outcome was reported by *Fedushkin* and co-workers, who synthesized neutral [(^{Dipp}BIAN)$_2$Fe] (**S**) by the reaction of K[^{Dipp}BIAN] with FeI_2.[23] The C–C and C–N bond lengths of the BIAN ligand have been very well investigated as a function of the oxidation state of the ligand. In the case of [(^{Dipp}BIAN)$_2$Fe] the structural data suggest the formation of a monoanionic ligand and consequently an Fe(II) center. Magnetic measurements and theoretical calculations also support the presence of antiferromagnetic coupling.

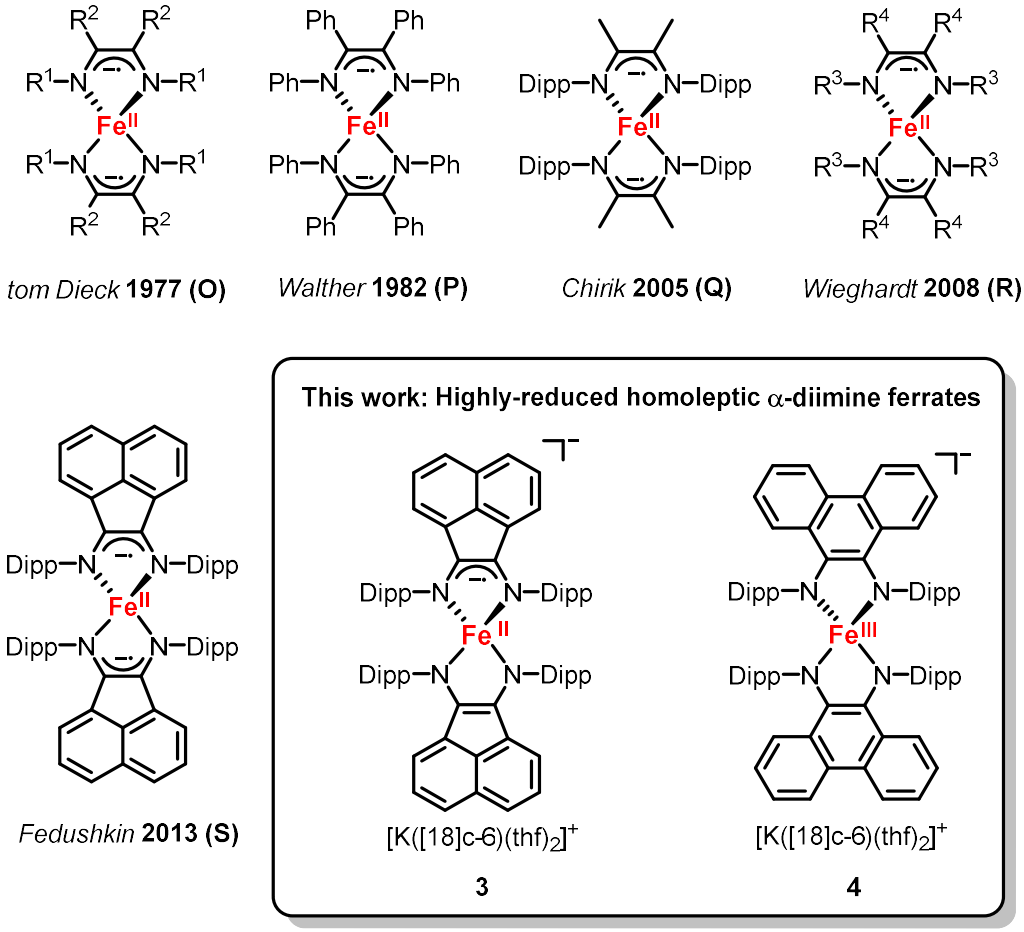

Figure 2. Previously reported homoleptic low-valent α-diimine iron complexes and new anionic complexes presented in this work.

Interestingly, there are currently no reports on anionic bis(α-diimine) iron complexes. It is of obvious interest to compare these highly-reduced species with the neutral complexes described in literature. Recently, we reported amine-borane dehydrogenation and transfer hydrogenation catalyzed by the α-diimine cobaltates [K(thf)$_x${(^{Ar}BIAN)Co(η^4-cod)}] [Ar = Mes (2,4,6-trimethylphenyl), Dipp (2,6-diisopropylphenyl)].[24] This work showed that such highly reduced α-diimine metal anions can be effectively used in reductive catalysis. This suggested that an analogous *Fe* complex should be a promising pre-catalyst for similar reactions. Herein, we report the synthesis, characterization, and catalytic applications of highly-reduced anionic heteroleptic and homoleptic α-diimine iron complexes.

6.2 Results and Discussion

6.2.1 Heteroleptic α-Diimine Iron Complexes

As [K(thf)$_x${(^{Ar}BIAN)Co(η^4-cod)}] is synthesized from the cobalt(1–) source [Co(η^4-cod)$_2$]$^-$ by simple ligand exchange, it was sought out to synthesize the analogous iron complex in the same manner starting from dianionic bis(cylooctadiene) ferrate(2–) [Li$_2$(dme)$_4${Fe(η^4-cod)$_2$}].[25] Surprisingly, the reaction of this ferrate with ^{Dipp}BIAN gave exclusively the monoanionic complex [Li(thf){(^{Dipp}BIAN)Fe(η^4-cod)}] (**1**-[Li(thf)]) and not the expected dianion. A plausible explanation for this observation is that LiBIAN is formed as a side product by an outer-sphere redox process, although this has not been confirmed experimentally. A ligand to metal [^{Dipp}BIAN:Fe(2–)] ratio of 1.5:1 seemed to be ideal after optimization of the reaction conditions, although it is formally a 2:1 reaction (see the SI for details). Complex **1-Li** was isolated as dark black crystals after work-up and crystallization from *n*-hexane in 55% yield (41 mg). Unfortunately, scale up of this reaction proved to be difficult. Therefore, a second approach involving reduction of the Fe(II) precursor [(^{Dipp}BIAN)FeBr$_2$] using strong reductants such as alkali metals was investigated. [(^{Dipp}BIAN)FeBr$_2$] can be prepared in large scale (> 20 g) scale in a single step from ^{Dipp}BIAN and FeBr$_2$. Reduction of this complex using potassium graphite (KC$_8$, three equivalents) in the presence of excess 1,5-cyclooctadiene was found to be more efficient than with lithium or potassium metal. Thus, [{(^{Dipp}BIAN)Fe(η^4-cod)}]$^-$ (**1**) was isolated as **1**-[K([18]c-6)(thf)$_{0.5}$] in good yield (78%) and at multi-gram scale (> 7g) after crystallization from THF/ *n*-hexane.

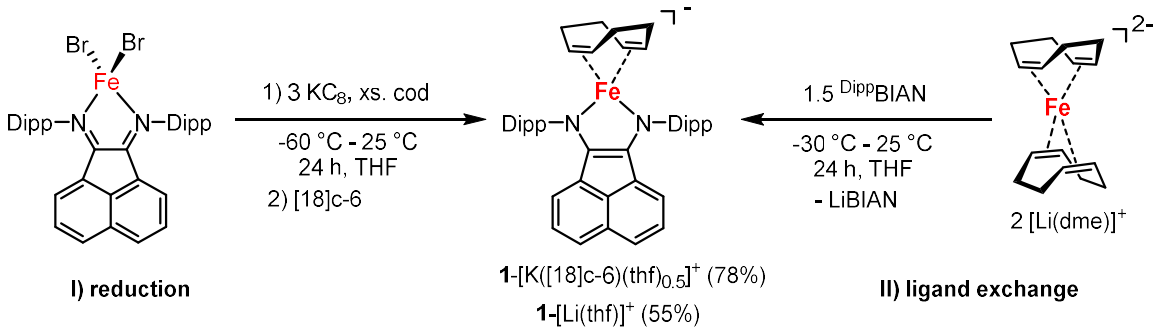

Scheme 1. Synthesis of the anion [{(^{Dipp}BIAN)Fe(η^4-cod)}]$^-$ (**1**) by reduction of an Fe(II) precursor (left) or ligand exchange of an Fe(–II) source (right).

Both complexes **1**-[K([18]c-6)(thf)$_{0.5}$] and **1**-[Li(thf)] were structurally characterized by single-crystal X-ray crystallography. Unfortunately, the structure of **1**-[K([18]c-6)(thf)$_{0.5}$] was

highly disordered and it was impossible to determine reliable bond distances. However, the connectivity and overall structure were confirmed. In contrast, the crystal structure of **1**-[Li(thf)] gave good values (R_1 = 0.0383; wR_2 = 0.0929) and is shown in Figure 3. The complex crystallizes in the orthorhombic space group $Pmn2_1$ with two molecules per formula unit. The central iron atom Fe1 is coordinated in an almost perfect square-planar environment (twist angle of 0.5°) by two nitrogen atoms and two C=C double bonds. The elongated C1–N1 (1.385(4) Å) and shortened C1–C1' (1.388(5) Å) bond lengths are in the range of dianionic BIAN ligands (*c.f.* 1.40 Å (C–C bond) and 1.39 Å (C–N bond) for Na_2[^{Dipp}BIAN]).[23] Consequently, an oxidation state of +I with a d^7 configuration for iron can be assigned. The lithium cation is η^4-coordinated to the dianionic moiety of the BIAN framework as well as by one THF molecule. Compound **1**-[Li(thf)] is therefore a contact-ion pair. It is worth noting that the recently published cobaltate [Li(thf){(^{Dipp}BIAN)Co(η^4-cod)}] is isostructural to this compound (see chapter 4.5.4)

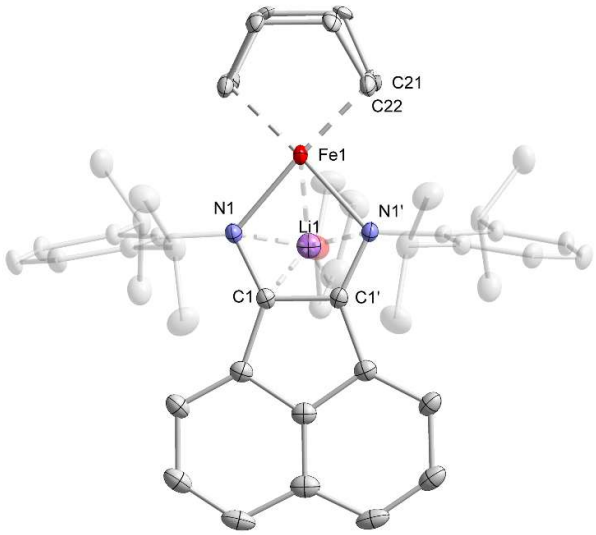

Figure 3. Solid-state structure of **1**-[Li(thf)] with thermal ellipsoids drawn at the 40% probability level. Selected bond lengths [Å] and angles [°]: N1–C1 1.385(4), C1–C1' 1.388(5), C21–C22 1.409(5), Fe1–N1 1.971(2), Fe1–C21 2.045(3), N1–Fe1–N1' 82.1(1) Hydrogen atoms are omitted for clarity.

It is of further interest to investigate the influence of the bis(olefin) ligand with respect to the structure and reactivity. The replacement of the 1,5-cyclooctadiene (cod) ligand in our proposed ferrate pre-catalyst by 2,5-norbornadiene (nbd) was attempted. Therefore, the same reductive approach was pursued: reaction of [(^{Dipp}BIAN)$FeBr_2$] with potassium graphite and

an excess of 2,5-norbornadiene followed by the addition of 18-crown-6 ([18]c-6) to facilitate crystallization from THF/*n*-hexane. Unexpectedly, a salt of the complex [{(DippBIAN)Fe(η⁴-nbd)}]⁻ was not obtained under the reaction conditions. Instead, single-crystal X-ray crystallography revealed that two nbd ligands underwent C–C coupling to form a bis(norbornyl) ligand, resulting in a new complex **2**-[K([18]c-6)(thf)$_2$], which was isolated in high yield (83%) as deep green crystals.

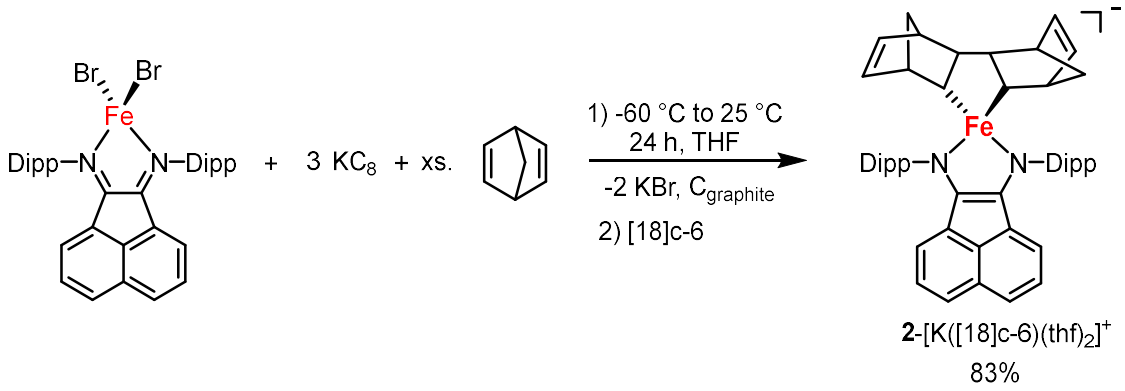

Scheme 2. Synthesis of complex **2**-[K([18]c-6)(thf)$_2$].

While crystallographic analysis of **2**-[K([18]c-6)(thf)$_2$] allowed to determine the connectivity of the ferrate anion, significant disorder prevented a more detailed structural analysis. Fortunately, the [2.2.2]cryptand complex **2**-[K([2.2.2]cryptand)] prepared in an analogous manner provided a structure which could be refined to a much more satisfactory degree of accuracy. The complex crystallizes in the non-centrosymmetric space group $P2_1$ with one molecule per asymmetric unit, which is shown in Figure 4. Here the central iron atom Fe1 is coordinated by the two nitrogen atoms of BIAN (N1, N2) and two carbon atoms (C3, C4) of the bis(norbornyl) ligand in a distorted tetrahedral structure with a twist angle of 53.4°. Analysis of the C–C (C1–C2 1.385(6) Å) and C–N (C1–N1 1.382(6) Å, C2–N2 1.371(6) Å) bonds indicated a dianionic BIAN ligand.[23] In combination with the dianionic bis(norbornyl) ligand an oxidation state of +III for iron can be assumed. Two molecules of norbornadiene have clearly dimerized through formation of a C–C bond (olefin coupling) to give a bis(norbornyl) ligand and a five-membered, perfectly planar ferracycle. Stereochemically, the ligand exists in an *exo-trans-exo* conformation. Such a norbornadiene dimerization at the metal center is rare and only known for three other systems two based on iridium and one on zirconium. For the latter, *Rosenthal* and co-workers used a zirconocene alkyne complex as starting material and observed a twisted and not perfectly planar five-membered zirconacycle.[26] In 1980, *Osborn*,

Fraser and co-workers reported on an octahedral iridium complex bearing a dimerized norbornadiene ligand, one acetylacetonate ligand, and an additional single η^4-norbornadiene ligand.[27] In there, the iridacycle is also nonplanar, being folded with one carbon atom displaced 0.24 Å out of the plane of the ring atoms. Recently, *Oro* and co-workers also synthesized iridium complexes containing this structural motif.[28] All are octahedral iridium complexes with five-membered, nonplanar iridacycles.

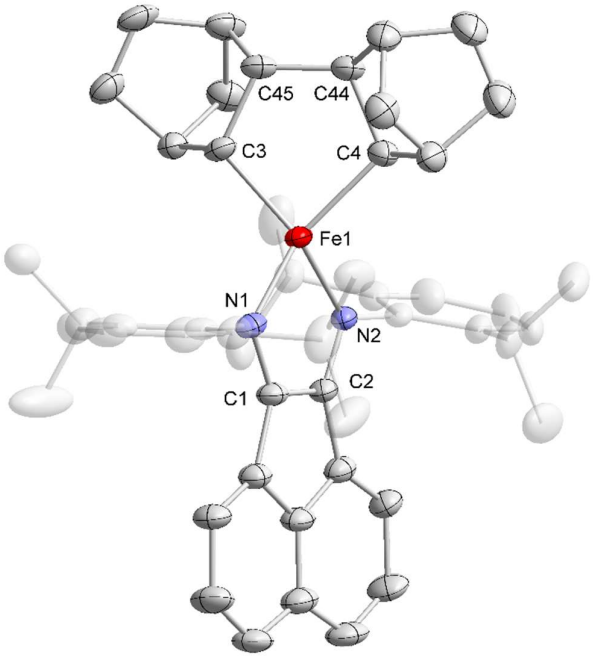

Figure 4. Solid-state structure of **2**-[K([2.2.2]cryptand)] with thermal ellipsoids drawn at the 40% probability level. Selected bond lengths [Å] and angles [°]: C1–C2 1.385(6) Å, C1–N1 1.382(6) Å, C2–N2 1.371(6) Å, Fe1–N1 1.961(4) Å, Fe1–N2 2.001(3) Å, Fe1–C3 2.023(4) Å, Fe1–C4 2.042(5) Å, C3–C44 1.562(6) Å, C4–C44 1.585(6) Å, N1–Fe1–N2 84.8(2), C3-Fe-C4 86.7(2). Hydrogen atoms, solvent molecules (three THF molecules) and cation **2**-[K([2.2.2]cryptand)]$^+$ are omitted for clarity.

1-[K([18]c-6)(thf)$_{0.5}$] and **2**-[K([18]c-6)(thf)$_2$] are paramagnetic according to ^{1}H NMR spectroscopy. **1**-[K([18]c-6)(thf)$_{0.5}$] showed broad resonances from 9 to –16 ppm in THF-d$_8$, whereas **2**-[K([18]c-6)(thf)$_2$] exhibits sharper signals in a range of 70 to –55 ppm (see the SI, Figures S1, S2). Both complexes also investigated by EPR spectroscopy in a frozen 2-methyltetrahydrofurane (^{Me}THF) solution at 20 K (Figure 5). **1**-[K([18]c-6)(thf)$_{0.5}$] shows a rhombic signal with $g_{11} = 2.22$, $g_{22} = 2.10$ and $g_{33} = 2.01$. No hyperfine interaction to nitrogen is observed, which is consistent with the proposed Fe(I) structure from single-crystal X-ray crystallography. Calculation of the EPR parameters at the B3LYP[29]/def2-TZVP[30] level of theory gave g values of 2.13, 2.08, and 2.01, which are close to the experimentally observed g

values. Hyperfine coupling constants were predicted to be small for all protons ($A^{H} \leq 1$ MHz) and nitrogen atoms (A^{N}_{11} = –4.73, A^{N}_{22} = –5.69 and A^{N}_{33} = -7.61). In all cases these coupling constants were too small to be observed in the obtained experimental spectrum. Moreover, the small A^{N} confirms the proposed spin density on the iron center and a dianionic closed-shell BIAN ligand. **2**-[K([18]c-6)(thf)$_2$] shows a completely different EPR spectrum. Only a broad signal at half field was observed, which indicated the presence of an intermediate or high-spin iron complex. The experimental spectrum of **2**-[K([18]c-6)(thf)$_2$] as approximated by simulation using the same approach as for complex **1** with an S= 3/2 system and g_{11} = 2.25, g_{22} = 2.25, g_{33} = 1.90, D = 15 cm^{-1}, E = 0.8 cm^{-1} (E/D = 0.05). Herein, D and E describe the axial and rhombic extent of the zero field splitting, respectively. Notably, we were not able to satisfactorily simulate the experimental spectrum by consideration of an S = 5/2 system.

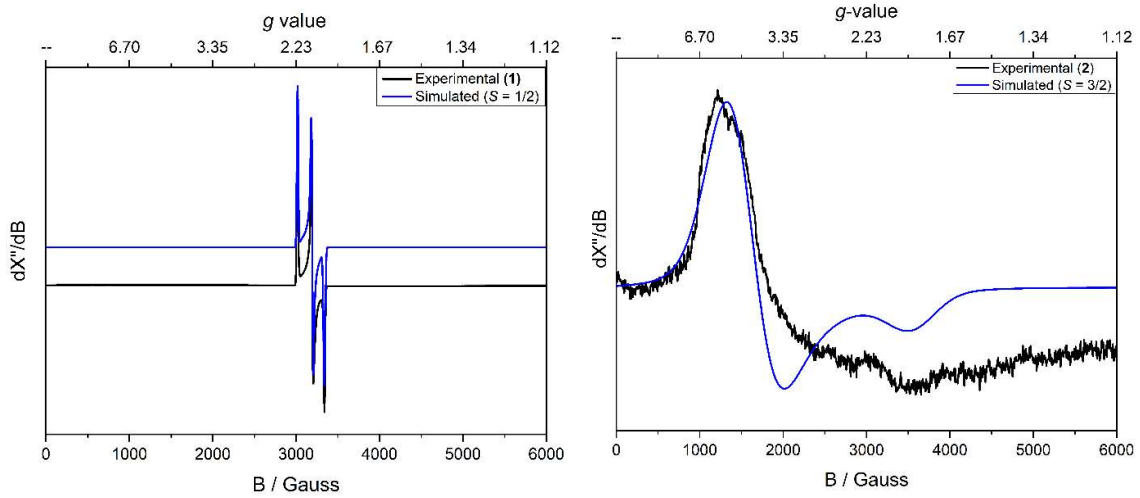

Figure 5. Experimental and simulated X-band EPR spectra of **1**-[K([18]c-6)(thf)$_{0.5}$] and **2**-[K([18]c-6)(thf)$_2$] recorded in a frozen ^{Me}THF solution at 20 K. Experimental parameters: Microwave frequency: 9.37466 GHz (**1**-[K([18]c-6)(thf)$_{0.5}$]), 9.376835 GHz (**2**-[K([18]c-6)(thf)$_2$]); Modulation amplitude: 4.000 G; Power: 0.6325 mW. The experimental spectrum of **1**-[K([18]c-6)(thf)$_{0.5}$] could be fitted with the following parameters for an S =1/2 system on a nucleus with a nuclear spin of 0, which we attribute to iron. g_{11} = 2.217, g_{22} = 2.095, g_{33} = 2.005, W_{11} = 10, W_{22} = 11 and W_{33} = 13. The experimental spectrum of **2**-[K([18]c-6)(thf)$_2$] can be fitted using the following parameters for an S = 3/2 system. g_{11} = 2.25, g_{22} = 2.25, g_{33} = 1.90, D = 15 cm^{-1}, E = 0.8 cm^{-1}, E/D = 0.05.

1-[K([18]c-6)(thf)$_{0.5}$] and **2**-[K([18]c-6)(thf)$_2$] were further investigated by ^{57}Fe Mößbauer spectroscopy at 80 K. A polycrystalline sample of **1**-[K([18]c-6)(thf)$_{0.5}$] showed an asymmetric spectrum with an isomer shift of δ = 0.23 mm s^{-1} and a quadrupole splitting of $|\Delta E_Q|$ = 2.26 mm s^{-1} (Figure 6, left). The quadrupole splitting is in accordance with the calculated $|\Delta E_Q|$ = 2.50 mm s^{-1} value determined using DFT methods (CP(PPP) basis set for Fe). The asymmetry of the spectrum is typical for an iron species with an odd number of unpaired

electrons with slow paramagnetic relaxation and is consequently in line with the result of EPR spectroscopy. **2**-[K([18]c-6)(thf)$_2$] also gave a doublet with a similar isomer shift of δ = 0.17 mm s^{-1}, but significantly smaller quadrupole splitting of $|\Delta E_Q|$ = 1.32 mm s^{-1} (Figure 9, right). Similar values (δ = 0.43 mm s^{-1}, ΔE_Q = 1.37 mm s^{-1}) were observed in the five coordinated pyridine-diimine iron tetrazene complex [(^{iPr}PDI)Fe{(NR)NN(NR)}] (^{iPr}PDI = 2,6-(ArN=CMe)$_2$C$_5$H$_3$N; Ar = Dipp, R = 3,5-Me$_2$C$_6$H$_3$) prepared by *Chirik* and co-workers, who proposed an intermediate-spin Fe(III) center.[31]

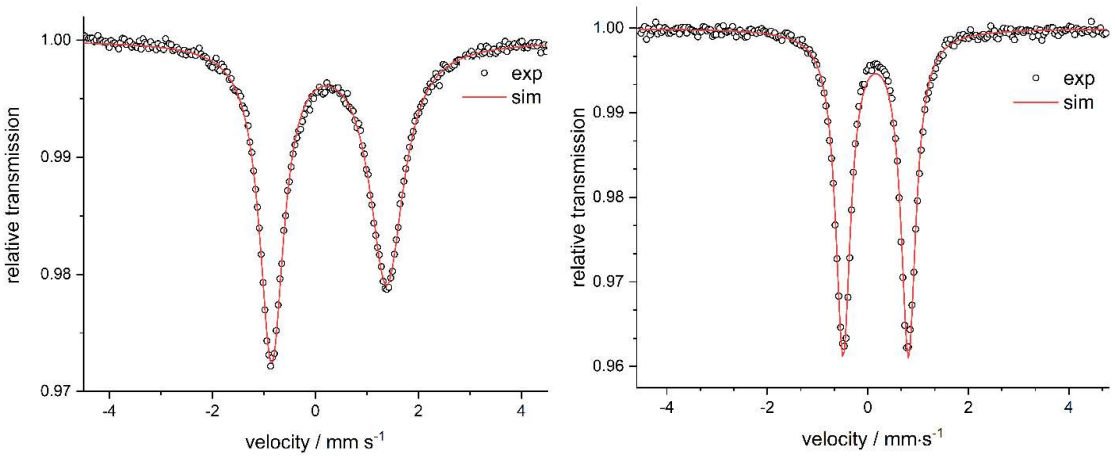

Figure 6. ^{57}Fe Mößbauer spectra of **1**-[K([18]c-6)(thf)0.5] (left) and **2**-[K([18]c-6)(thf)$_2$] (right); exp = experimental, sim = simulated.

The ^{57}Fe Mößbauer data for complex **1**-[K([18]c-6)(thf)$_{0.5}$] are also in agreement with the magnetic moment μ_{eff} = 2.0(1) μ_B determined in solution (THF-d$_8$) at ambient temperature by the Evans method[32], which corresponds to one unpaired electron (spin-only value: 1.73 μ_B). Magnetic susceptibility measurements confirm that **2**-[K([18]c-6)(thf)$_2$] is paramagnetic in the solid-state (SQUID magnetization measurement in the temperature range 2–295 K) with $\chi_M T$ = 2.03 cm^3 mol^{-1} K (corresponds to μ_{eff} = 4.0 μ_B) at 295 K (Figure 7). The measurement can be simulated with a spin of 3/2 (g = 2.08, D =17.0 cm^{-1}), which is in agreement with the experimental data (Figure 7). The magnetic moment determined in solution (THF-d$_8$) by Evans method is μ_{eff} = 3.9(1) μ_B at ambient temperature, which is almost identical to the spin-only value for three unpaired electrons (3.87 μ_B). Thus, these experiments further support the assignment of an Fe(III) center with an intermediate spin of S = 3/2.

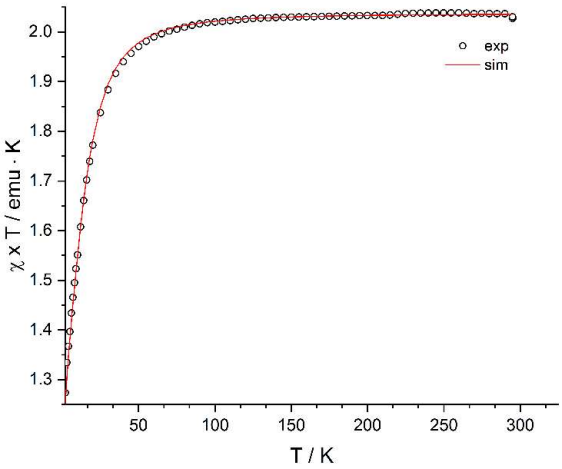

Figure 7. SQUID magnetization measurement of **2**-[K([18]c-6)(thf)$_2$]; exp = experimental, sim = simulated.

Theoretical investigations using the DFT and CASSCF methods were used to analyze the electronic structures of the anions of **1**-[K([18]c-6)(thf)$_{0.5}$] and **2**-[K([18]c-6)(thf)$_2$] in comparison with experimental results. Geometries were optimized at the OPBE-D3BJ/def2-TVZP[29],[30],[33] level of theory in the gas phase. In the case of **1**-[K([18]c-6)(thf)$_{0.5}$], the diisopropyl groups were replaced by methyl groups to minimize computational cost and a doublet state was assumed according to all experimental data. The optimized geometry is in good agreement with the structure determined by single-crystal X-ray crystallography. DFT calculations confirmed that spin density is localized at the metal center, as shown in Figure 8 (left). Analysis of the orbitals showed that the highest occupied orbital is a singly-occupied molecular orbital (SOMO) with high d character. Thus, a d^7 electronic configuration with a Fe(I) species is plausible and consistent with experimental and theoretical data.

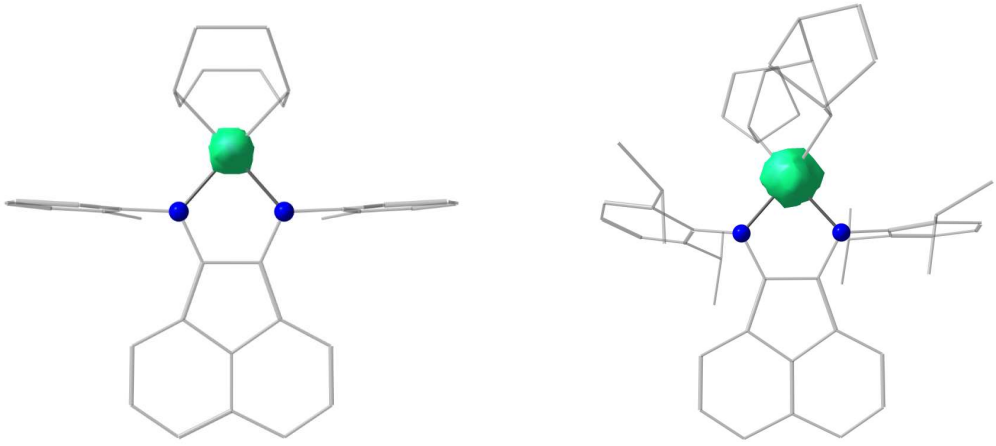

Figure 8. Spin-density plots according to Mulliken population analysis of **1**-[K([18]c-6)(thf)$_{0.5}$] (left) and **2**-[K([18]c-6)(thf)$_2$] (right); isosurface value = 0.05.

State-averaged CASSCF-DLPNO-NEVPT2/def2-mTZVP def2-TZVP/C[36] calculations were conducted including three different ground state multiplicities (S = 2, 4, 6) to get an insight into the electronic structure of the anion of **2**-[K([18]c-6)(thf)$_2$]. The quartet state was energetically most favored while the sextet (ΔE = +39.9 kcal mol^{-1}) and doublet state (ΔE = +26.6 kcal mol^{-1}) are significantly higher in energy. The quartet state corresponds to an Fe(III) intermediate spin system (S = 3/2) with d^5 configuration at iron. Moreover, the spin-density obtained from a single-point DFT calculation is mainly localized on the metal center (Figure 8, right). Thus, the theoretical data are therefore consistent with the experimental data. Complexes **1**-[K([18]c-6)(thf)$_{0.5}$] and **2**-[K([18]c-6)(thf)$_2$] both possess two potentially redox-active sites: the central iron atom and the redox-active BIAN ligand. The redox properties of **1**-[K([18]c-6)(thf)$_{0.5}$] and **2**-[K([18]c-6)(thf)$_2$] are therefore of interest and were studied by cyclic voltammetry (Figures 9 and 10). Both heteroleptic complexes are similar in their redox properties according to their cyclic voltammograms. One reversible and at least one irreversible oxidation is observed. In the case of complex **1** the chemically reversible wave at $E_{1/2}$ = –1.98 V vs. Fc/Fc$^+$ is consistent with previous results by *Findlater* and co-workers, who prepared the neutral complex [(^{Dipp}BIAN)Fe(η^4-cod)] by Na/Hg reduction of [(^{Dipp}BIAN)FeCl$_2$] and cod.[16] Complex **2**-[K([18]c-6)(thf)$_2$] can also be reversibly oxidized by one electron at a similar, but slightly less negative potential ($E_{1/2}$ = –1.71 V vs. Fc/Fc$^+$). Both complexes are further irreversibly oxidized at much less negative potentials (–0.85 V for **1**-[K([18]c-6)(thf)$_{0.5}$] and –0.8 V for **2**-[K([18]c-6)(thf)$_2$]).

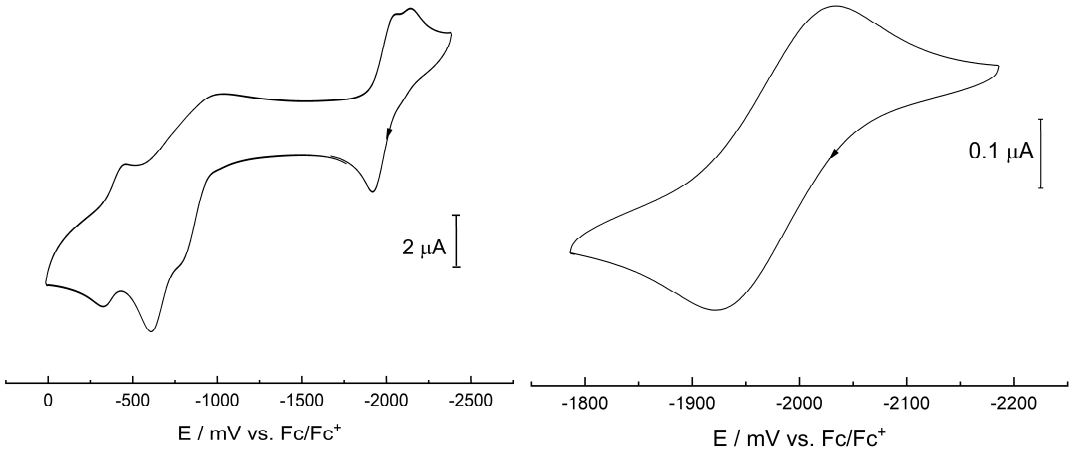

Figure 9. Cyclic voltammograms of **1**-[K([18]c-6)(thf)$_{0.5}$] in THF/^{n}Bu$_4$NPF$_6$, scan rate: 100 mV s^{-1} (left) and 50 mV s^{-1} (right).

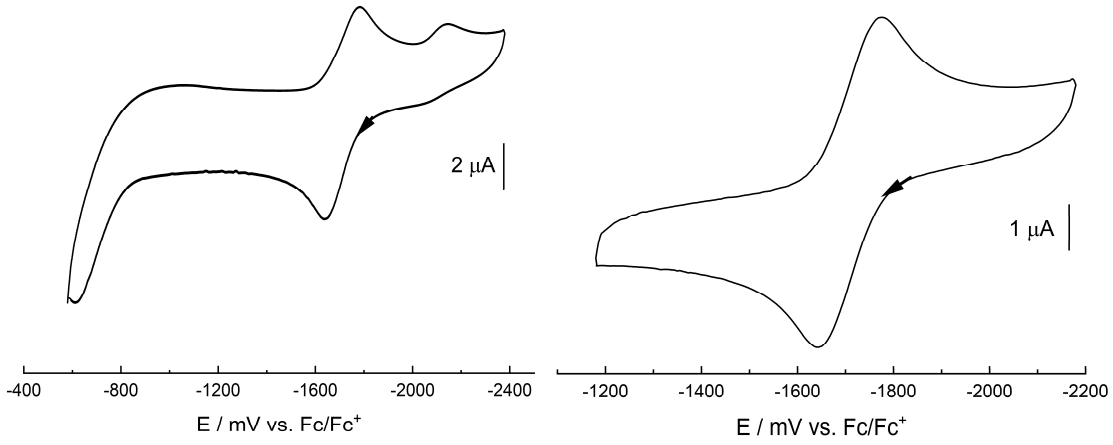

Figure 10. Cyclic voltammograms of **2**-[K([18]c-6)(thf)$_2$] in THF/^{n}Bu$_4$NPF$_6$, scan rate: 100 mV s^{-1} (left) and 50 mV s^{-1} (right).

Complexes **1**-[K([18]c-6)(thf)$_{0.5}$] and **2**-[K([18]c-6)(thf)$_2$] were also investigated by UV-vis spectroscopy. The UV-vis spectra in THF are shown in Figure 11. **1**-[K([18]c-6)(thf)$_{0.5}$] absorbs at 294 nm (ε = 21000 L mol^{-1} cm^{-1}), 408 nm (ε = 12000 L mol^{-1} cm^{-1}), and shows a broad shoulder at 697 nm (ε = 5000 L mol^{-1} cm^{-1}), whereas for **2**-[K([18]c-6)(thf)$_2$] absorptions at 298 nm (ε = 22000 L mol^{-1} cm^{-1}), 366 nm (ε = 13500 L mol^{-1} cm^{-1}), 418 nm (ε = 8000 L mol^{-1} cm^{-1}), and a broad shoulder at 740 nm (ε = 5000 L mol^{-1} cm^{-1}) are observed.

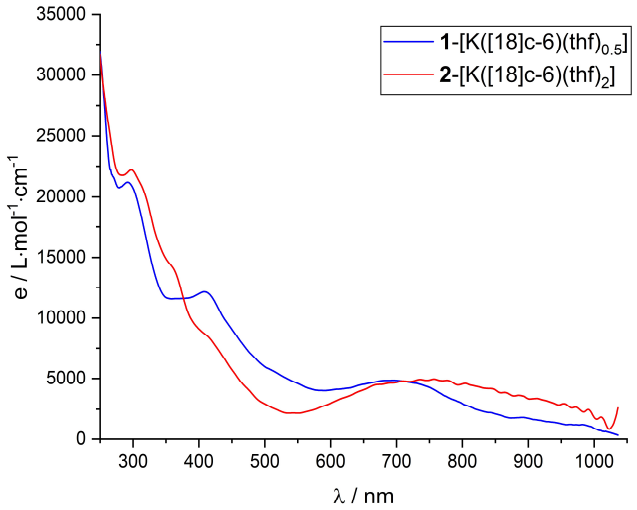

Figure 11. UV-vis spectra of **1**-[K([18]c-6)(thf)$_{0.5}$] and **2**-[K([18]c-6)(thf)$_2$] in THF.

6.2.2 Homoleptic α-Diimine Iron Complexes

For the synthesis of homoleptic anionic bis(α-diimine) iron complexes, the bis(anthracene) ferrate(1–) anion served as an available source for an iron anion.[34] First, the reactivity of the α-diimines ^{Dipp}BIAN and ^{Dipp}PhDi towards this anion was investigated. Regardless if one or two equivalents of the α-diimine were added, only homoleptic and no heteroleptic complexes were isolated. Thus, the replacement of both anthracene ligands furnished the homoleptic bis α-diimine ferrate complexes **3** and **4**. Complex **3** was isolated in 46% crude yield and was recrystallized from THF/*n*-hexane in 15% (sample **3-1**) yield. Sample **3-1** was recrystallized one more time to obtain sample **3-2** (7%). Complex **4** was also obtained after extraction and crystallization from THF/*n*-hexane in 19% yield. These complexes represent the first anionic iron bis(α-diimine) complexes known in literature.

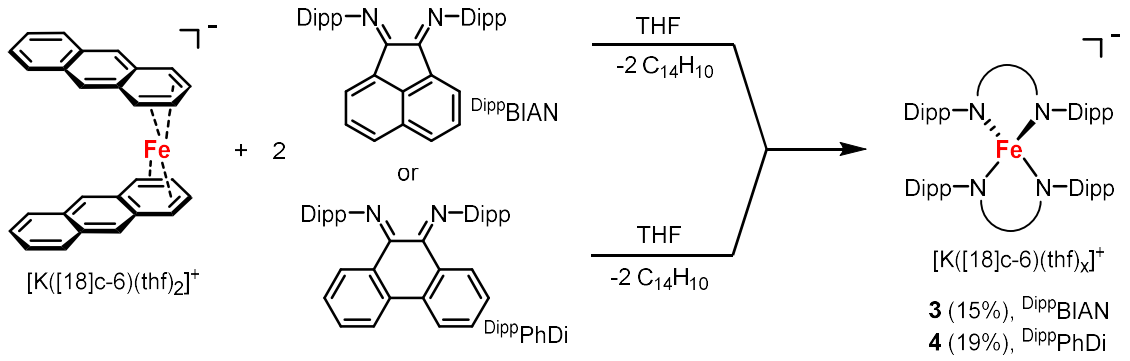

Scheme 3. Synthesis of homoleptic bis(α-diimine) ferrate anions.

Crystals of **3** suitable for single-crystal X-ray diffraction were obtained by slow diffusion of *n*-hexane into a THF solution. More than 10 crystals were examined. It is noteworthy, that all of these had the same space group and cell parameters. A full single crystal X-ray structure analysis on one of the crystals revealed that complex **3** crystallizes in the monoclinic space group $P2_1/n$ with four molecules of **3** per formula unit. The molecular structure is shown in Figure 12. There is no close interaction between the cation $[K([18]c\text{-}6)(thf)_2]^+$ and the anion $[(^{Dipp}BIAN)_2Fe]^-$. The central iron atom is coordinated via four nitrogen atoms. The dihedral angle between the two BIAN ligands is 42.2° and the coordination geometry can therefore be described as neither square planar nor tetrahedral, but rather as a distorted structure that lies somewhere between these two extremes. The C–C bond lengths of the α-diimine fragment (C1–C2 1.411(3) Å, C3–C4 1.406(3) Å) are similar to those observed in $Na_2[^{Dipp}BIAN]$ (C1–C2

1.402(4) Å) suggesting a dianionic BIAN ligand. It has to be mentioned though that the experimentally observed C–N bond lengths (C1–N1 1.351(3) Å, C2–N2 1.359(2) Å, C3–N3 1.362(3) Å, C4–N4 1.364(2) Å) are in between the values for the dianionic BIAN ligand in Na_2[^{Dipp}BIAN] (C1–N1 1.387(4) Å, C2–N2 1.386(4) Å), and the monoanionic BIAN ligand (C1–N1 1.336(3) Å, C1–N1 1.325(3) Å) in [(^{Dipp}BIAN)Ni(η^4-cod)].[13],[35] Consequently, a clear assignment from metrical data is not feasible.

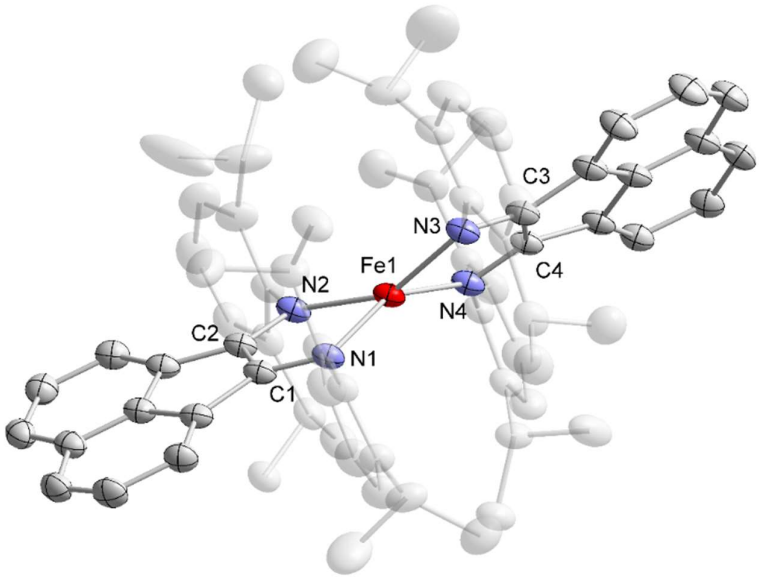

Figure 12. Solid-state structure of **3** with thermal ellipsoids drawn at the 40% probability level. Selected bond lengths [Å] and angles [°]: N1–C1 1.351(3), N2–C2 1.359(2), N3–C3 1.362(3), N4-C4 1.364(2), C1–C2 1.411(3), C3–C4 1.406(3), Fe1–N1 2.090(1), Fe1–N2 1.976(1), Fe1–N3 2.048(1), Fe1–N4 2.072(1), N1–Fe1–N2 81.58(1), N3–Fe1–N4 82.56(6). Hydrogen atoms and [K([18]c-6)(thf)$_2$]$^+$ cation are omitted for clarity.

Crystals of **4** suitable for single-crystal X-ray diffraction were grown in the same manner as for **3** from THF/*n*-hexane. Complex **4** crystallizes in the monoclinic space group *P*2/*n* with two molecules of **4** per formula unit and the iron atom located on an inversion center. The molecular structure is superficially very similar to that of **3**. However, in contrast to **3**, the coordination geometry around iron is almost perfectly tetrahedral (dihedral angle determined for **4** is 89.0°). The C–C and C–N bond lengths of the α-diimine fragment (C1–C2 1.417(3) Å, C1–N1 1.396(3) Å, C2–N2 1.390(3) Å) again indicate a dianionic ligand (*c.f.* the dianionic ligand in [Mg(OEt$_2$)$_3$][^{Dipp}PhDi] (C–C 1.409(4) Å, C–N 1.384(4) Å).[38] Hence, the oxidation state of iron can be assigned as +III.

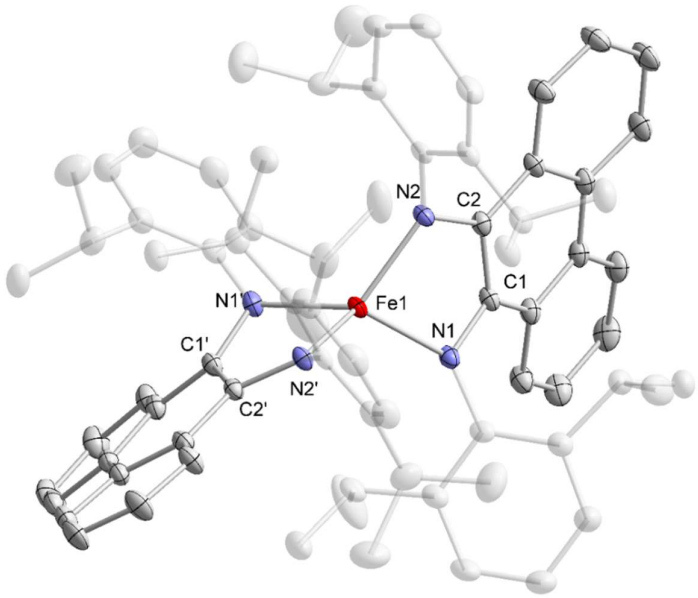

Figure 13. Solid-state structure of **4** with thermal ellipsoids drawn at the 40% probability level. Selected bond lengths [Å] and angles [°]: N1–C1 1.396(3), N2–C2 1.390(3), C1–C2 1.417(3), Fe1–N1 2.013(1), Fe1–N2 1.976(1), N1–Fe1–N2 82.91(7). Hydrogen atoms and $[K([18]c\text{-}6)(thf)_2]^+$ are omitted for clarity.

In order to confirm the electronic structures of **3** and **4** derived from single-crystal X-ray crystallography and to gain further insight, various spectroscopic techniques (^{1}H NMR, EPR, ^{57}Fe Mößbauer, UV-vis), magnetic measurements, elemental analyses, and theoretical methods (DFT, CASSCF) were employed. For the spectroscopic and analytical data different batches of **3** were used. In order to determine the presence of minor impurities both the recrystallized bulk material (**3**-**1**) and additional samples (**3**-**2**) that were recrystallized one more time from THF/*n*-hexane were analyzed.

Both samples were subjected to CHN analysis. For sample **3**-**1** the carbon value does not perfectly match the calculated value for **3** bearing one THF molecule (calcd.: 73.77; found: 72.03). However, the experimentally obtained values for hydrogen (calcd.: 7.88; found: 7.57) and nitrogen (calcd.: 3.91; found: 3.88) are close to the calculated values within the range of 0.4%. For sample **3**-**2**, the CHN calculated values are in agreement with the experimentally determined values (C 73.30, H 7.76, N 3.81). The same applies for complex **4** assuming the presence of two THF molecules (calcd.: C 74.06, H 8.03, N 3.59; found: C 74.18, H 7.82, N 3.54). Both complexes **3** and **4** are paramagnetic in solution according to ^{1}H NMR spectroscopy in THF-d_8. Complex **3** shows 14 resonances between +50 and –50 ppm. This is almost in accordance with the expected number of resonances (15) for two chemically non-equivalent

^{Dipp}BIAN ligands and one 18-crown-6 molecule. Another possibility is the presence of two isomeric complexes. Variable-temperature (VT) ^{1}H NMR spectra of sample **3**-**2** in the range from 298 K to 328 K showed that no resonances appear or disappear upon heating and only minor shifts of the signals are observed (Figure 14). Note that the ^{1}H NMR spectra of **3**-**1** and **3**-**2** are identical. In contrast, complex **4** is completely NMR silent in the range of +100 to –100 ppm (see the SI).

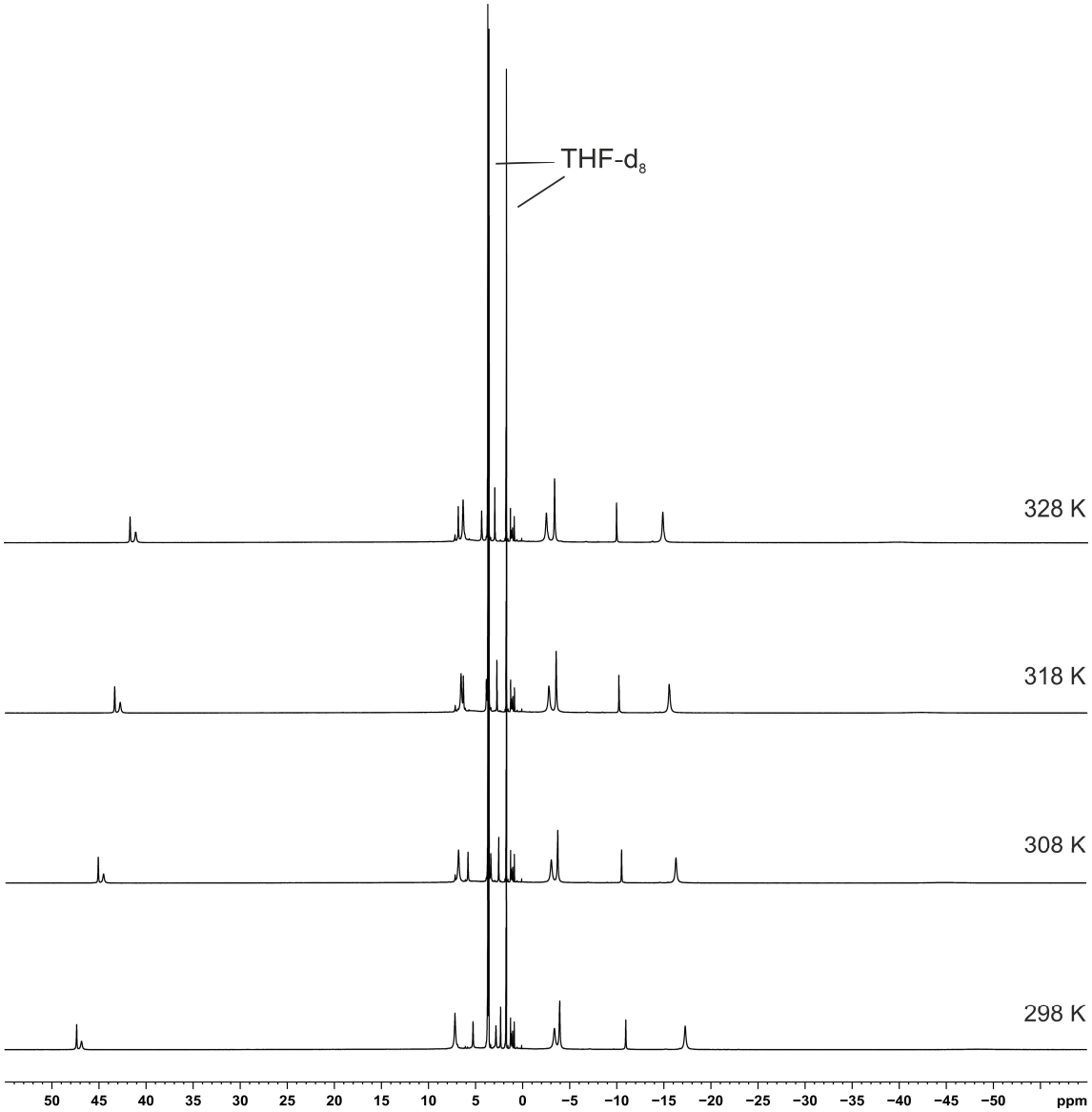

Figure 14. VT-^{1}H NMR spectra (400 MHz, THF-d$_8$) of **3**-**2** in the range from 298 K to 328 K.

Due to the paramagnetism of both complexes, **3** and **4** were analyzed by EPR spectroscopy. Both sample **3**-**1** and sample **3**-**2** were analyzed in a 2-methyltetrahydrofurane (^{Me}THF) glass

at 20 K. The resulting spectrum of sample **3-2** shows a rhombic signal with simulated g-values (g_{11} = 2.13, g_{22} = 2.10, g_{33} = 2.06) consistent with an S = 3/2 ground state with large zero-field splitting and rhombicity (D = 20 cm^{-1}, E = 4.1 cm^{-1}, E/D = 0.20). Notably, no hyperfine interaction (HFI) to nitrogen is observed. The spectrum for **3-1** can also be simulated as an S = 3/2 species with the same parameters as for **3-2**. However, the spectrum of **3-1** shows additional signals at 1550 Gauss and 3350 Gauss (see the SI, Figure S5). Although these additional signals could not be simulated, these signals clearly suggest the presence of a second species, which appears to be absent in the spectrum of sample **3-2**.

The EPR spectrum of complex **4** was also measured in a ^{Me}THF glass at 20 K and shows a rhombic signal as well. The experimental spectrum can be simulated as an S = 5/2 system with g_{11} = 2.03, g_{22} = 2.03, g_{33} = 2.03. The zero field splitting of **4** (D = 7 cm^{-1}, E = 2.2 cm^{-1}, E/D = 0.31) is smaller compared to **3**. It is noteworthy that it is also possible to simulate the spectrum using two components with S = 3/2 (see the SI, Figure S6).

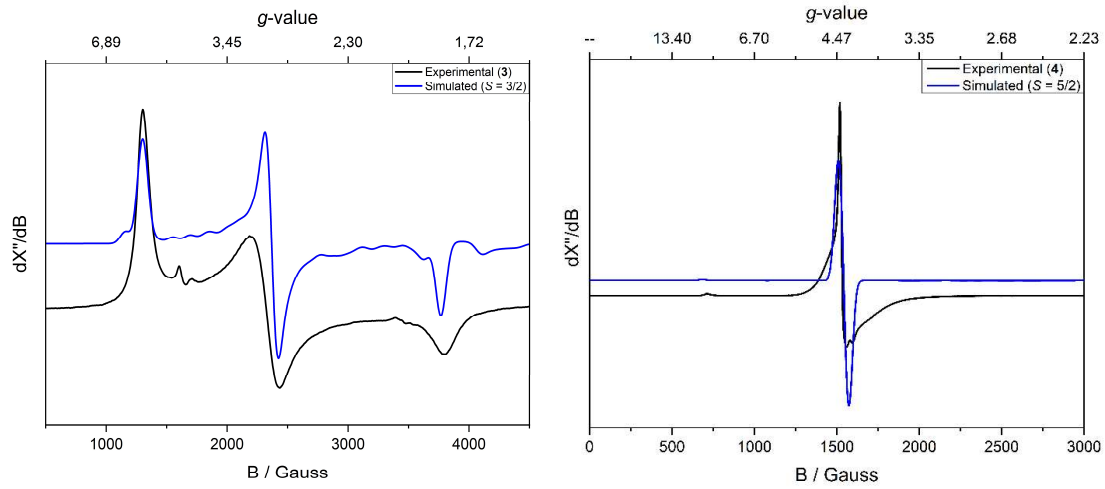

Figure 15. Experimental X-band EPR spectra of sample **3-2** and **4** recorded in ^{Me}THF glass at 20 K. Experimental parameters: Microwave frequency: 9.375682 GHz (**3-2**), 9.378092 GHz (**4**); Modulation amplitude: 4.000 G; Power: 0.6325 mW. Sample **3-2** can be simulated as an S = 3/2 species: g_{11} = 2.13, g_{22} = 2.10, g_{33} = 2.06, D = 20 cm^{-1}, E = 4.1 cm^{-1}, E/D = 0.20. Complex **4** can be simulated as an S = 5/2 system using the following parameters: g_{11} = 2.03, g_{22} = 2.03, g_{33} = 2.03, D = 7 cm^{-1}, E = 2.2 cm^{-1}, E/D = 0.31.

Complex **3** was further investigated by ^{57}Fe Mößbauer spectroscopy at 80 K. As shown in Figure 16, this polycrystalline sample of **3-1** gave rise to a slightly asymmetric spectrum with an apparent isomer shift δ = 0.76 mm s^{-1} and an apparent quadrupole splitting $|\Delta E_Q|$ = 1.63 mm s^{-1}. A fitting procedure revealed that the simulated spectrum can be divided into two subunits. A doublet with an isomer shift of δ = 0.75 mm s^{-1} and a quadrupole splitting

$|\Delta E_Q|$ = 1.60 mm s^{-1} corresponds to 75% of the sample (see Figure 16, sub1). A second quadrupole doublet with δ = 0.78 mm s^{-1} and and $|\Delta E_Q|$ = 2.17 mm s^{-1} accounts for 25% of the total spectrum (see Figure 16, sub2). The observation of two quadrupole doublets is presently unclear and suggests the presence of two species or isomers investigated sample. The isomer shifts and quadrupole splittings of the two quadrupole doublets observed for **3-1** are consistent with those of related high-spin Fe(II) complexes. For example, *Holland* and co-workers reported ^{57}Fe Mößbauer data for a neutral tetra-coordinated iron complex with a tetrazene and a β-diketiminato ligand.[37] This compound shows a similar ^{57}Fe Mößbauer isomer shift (δ = 0.69(2) mm s^{-1}) and a smaller quadrupole splitting ($|\Delta E_Q|$ = 1.32(4) mm s^{-1}) as the two species observed for **3-1.** Comparable ^{57}Fe Mößbauer data have also been reported for the anionic reduction product of *Holland's* complex (δ = 0.81(2) mm s^{-1}, $|\Delta E_Q|$ = 1.40(2) mm s^{-1}). [37] Nonetheless, the observed ^{57}Fe Mößbauer data are clearly in line with the presence of a high-spin Fe(II) species. Further ^{57}Fe Mößbauer investigations on an additionally recrystallized sample **3-2** are currently underway.

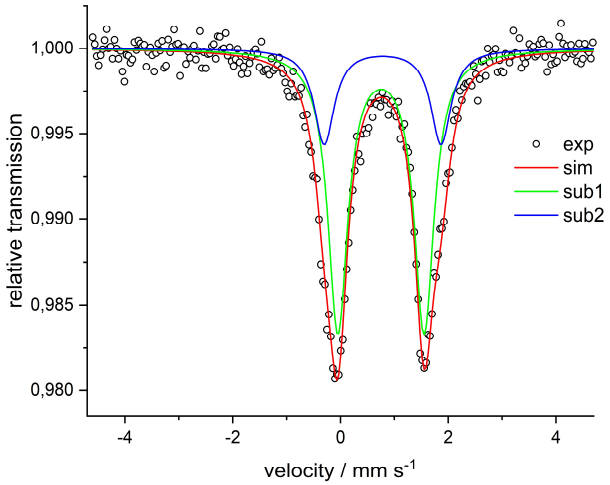

Figure 16. ^{57}Fe Mößbauer spectrum of complex **3** (sample **3-1**); exp = experimental, sim = simulated, sub1 = subunit 1, sub2 = subunit 2.

The magnetic moment was determined for samples **3-1** and **3-2** by the Evans NMR method in THF-d_8 solution.[32] For both samples, the observed magnetic moment was μ_{eff} = 4.7(1) μ_B at ambient temperature. This value is between the calculated spin-only values for three unpaired electrons (3.3 μ_B; quartet state) and for five unpaired electrons (5.9 μ_B; sextet state). A similar result was obtained for complex **4**, which shows an experimental moment of μ_{eff} = 5.1(1) μ_B at room temperature. SQUID magnetization measurements on complexes **3** and **4** are in progress.

State-averaged CASSCF-DLPNO-NEVPT2/def2-mTZVP def2-TZVP/C[36] calculations were conducted for three different ground state multiplicities (S = 2, 4, 6) to get an insight into the electronic structures of the anions of **3** and **4** (see the SI for details). For both complexes, the doublet states are significantly higher in energy (+21 kcal mol^{-1}) compared to the most stable high-spin configuration. The quartet and sextet configurations are very similar in energy. While the quartet state is preferred by 1.7 kcal mol^{-1} for complex **3**, the sextet state is 3.0 kcal mol^{-1} more stable in complex **4**. Based on an analysis of the orbital occupations resulting from the CASSCF-DLPNO-NEVPT2 calculations, a high-spin Fe(II) center with one monoanionic and one dianionic BIAN ligand is conceivable for complex **3**, whereas a high-spin Fe(III) center with two doubly-reduced PhDi ligands can be proposed for complex **4**. The change from an acenaphthene to a phenanthrene backbone in homoleptic bis(α-diimine) iron complexes thus has an impact on the electronic structure of the complexes (see the Supporting Information for a detailed discussion of the quantum chemical calculations).

Similar to **1**-[K([18]c-6)(thf)$_{0.5}$] and **2**-[K([18]c-6)(thf)$_2$] the presence of three potentially redox-active sites (one iron atom and two α-diimine ligands) renders the redox properties of **3** and **4** of interest. In case of complex **3**, cyclic voltammograms (CVs) of sample **3**-**1** and sample **3**-**2** were recorded. The CV of **3**-**1** in THF/^{n}Bu$_4$NPF$_6$ shows two quasi-reversible processes with waves at $E_{1/2}$ = –1.6 V and –2.2 V vs. Fc/Fc$^+$ and waves assigned to quasi-reversible or irreversible processes at –0.4 V and –0.2 V (Figure 17). There is an additional wave at –1.8 V which might arise from a secondary redox process or an impurity. Moreover, the CV of sample **3**-**2** shows an irreversible reduction at –2.7 V. The CV of sample **3**-**1** measured under identical conditions is similar to that of **3**-**2** (see the SI, Figure S8). Compared to the CV of **4** (*vide infra*), there is an apparent doubling of redox processes (–1.6 V/–2.2 V and –0.2 V/–0.4 V). This may indicate the possible presence of isomers, which is also the case in ^{57}Fe Mößbauer spectra.

The cyclic voltammogram of complex **4** shows two reversible waves at $E_{1/2}$ = –0.1 V and –1.2 V vs. Fc/Fc$^+$, which may be assigned to the oxidation of **4** by one electron to a presumably neutral complex and one further electron to a cationic one, respectively (Figure 18). In contrast to complex **3**, no doubling of redox processes is observed. Furthermore, the comparison of these CVs shows that the diimine ligand has a significant impact on the observed redox potentials.

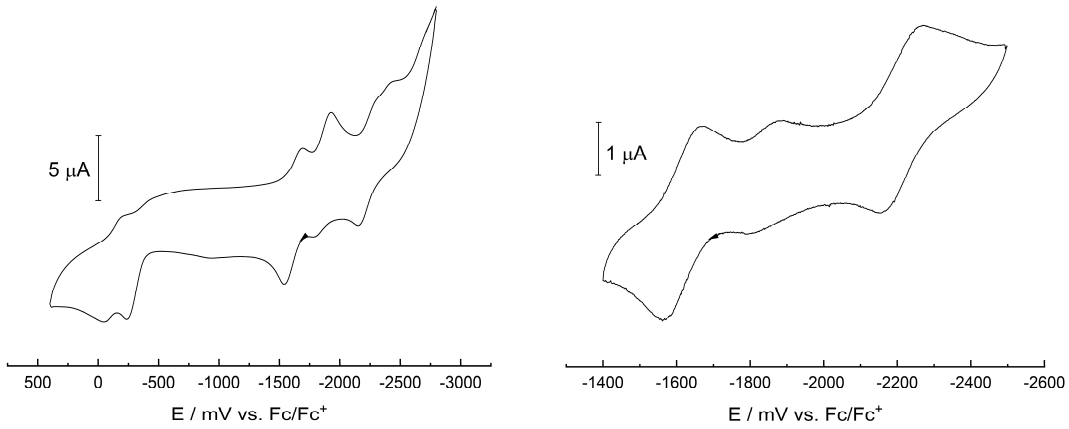

Figure 17. Cyclic voltammogram of **3-2** in THF/^{n}Bu$_4$NPF$_6$ in the range –2750 to 500 mV (left, scan rate: 100 mV s^{-1}) and −2500 to −1400 mV (right, 50 mV s^{-1}).

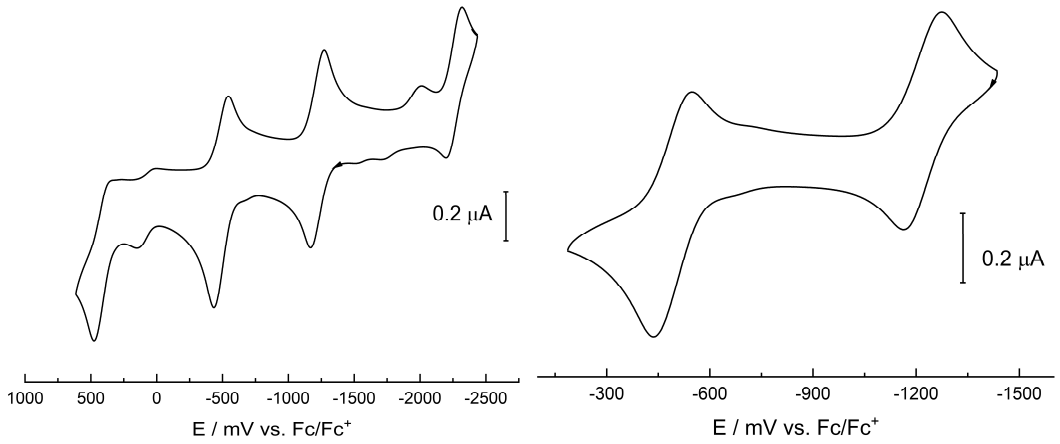

Figure 18. Cyclic voltammogram of **4** in THF/^{n}Bu$_4$NPF$_6$ in the range −2500 to 750 mV (left, scan rate: 100 mV s^{-1}) and −1500 to 250 mV (right, 50 mV s^{-1}).

The UV-vis spectra of complexes **3** (sample **3-2**) and **4** were recorded in THF are shown in Figure 19. Complex **3**, which shows a brown color in solution, displays a broad shoulder at 360 nm (ε = 18000 L mol^{-1} cm^{-1}). Additional bands are found at 435 nm (ε = 8500 L mol^{-1} cm^{-1}), 505 nm (ε = 8000 L mol^{-1} cm^{-1}), and 588 nm (ε = 4000 L mol^{-1} cm^{-1}). The UV-vis spectra of sample **3-1** and sample **3-2** are identical (see the SI, Figure S7). Complex **4** is deep green in solution and shows intense absorptions at 590 nm and 398 nm (ε = 28500 L mol^{-1} cm^{-1}) and a shoulder at 306 nm. The absorption at 590 nm is relatively broad and intense with an extinction coefficient of ε = 11500 L mol^{-1} cm^{-1}.

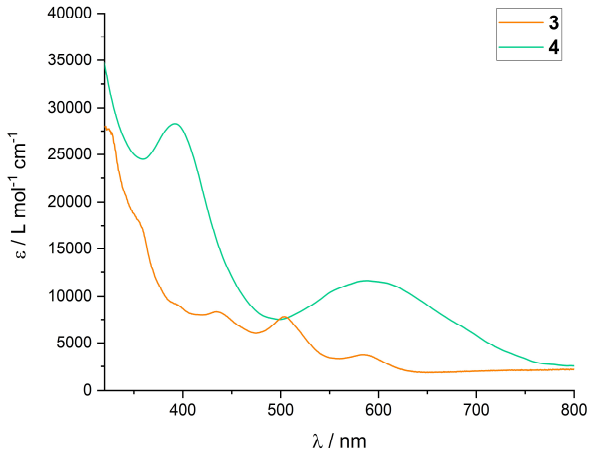

Figure 19. UV-vis spectra of complex **3** (sample **3-2**) and **4** in THF.

6.2.3 Catalytic Hydroboration

We were interested in investigating the further reactivity of the newly synthesized low-valent hetero- and homoleptic α-diimine ferrate complexes. Due to their high reduction potential, it was anticipated that complexes **1 – 4** should be excellent candidates as catalysts for reductive transformations such as hydrogenation, hydroboration, and hydrosilylation. As already mentioned in the introduction it is a key challenge to develop earth-abundant transition metal catalysts.[39] As a proof of principle the catalytic hydroboration of carbonyls using HBpin was chosen, which is an important organic reaction and affords widely used borate esters and the corresponding alcohols by facile hydrolysis. [40],[41] This catalytic reaction has been intensively studied using precious metal catalysts, but there has also been recent progress in using 3d metal complexes based on Mn,[42] Co,[43] Ni,[44] and Fe.[45]-[50] Although a number of reports on iron-catalyzed alkene hydroborations are known, only a few examples for the hydroboration of carbonyl compounds are described in literature. *Findlater* and co-workers reported the hydroboration of ketones and aldehydes with HBpin (1.5 equiv.) using catalytic amounts of $Fe(acac)_3$ (10 mol%) and $NaBEt_3H$ (10 mol%) in THF. The reaction proceeds to completion at ambient temperature within one day.[45] Subsequently, *Bai* and co-workers described a more efficient system suitable for various ketones and aldehydes using a lower catalyst loading (2.5 mol%) based on a low-coordinate tri-*tert*-butylphosphoranimido-iron(II) dimer.[46] An iron(II) hydride complex was also developed by *Tong*, *Wang* and co-workers used for the exclusive hydroboration of aldehydes at low catalyst loading (0.1 mol%).[47] One of the most active systems for aldehydes so far is an imine coupled $[Fe\text{-}N_2S_2]_2$ complex (0.1 mol%) reported

by *Baker* and co-workers, which is capable of reducing aldehydes to primary borate esters with HBpin within 30 min at ambient temperature.[48] Two systems based on the cooperation of iron and silicon were reported by *Fenske* and co-workers and *So* and co-workers. Both systems were applied in the hydroboration of ketones at ambient temperature with HBpin and catalyst loadings of 1 mol% (*Fenske*) or 10 mol% (*So*).[49] Recently, *Gade* and co-workers showed that a chiral bis(oxazolinyl-methylidene)isoindoline iron alkyl complex is able to catalyze the hydroboration of various functionalized ketones, which led to chiral halohydrines, oxaheterocycles and amino-alcohols after work-up. These reactions were performed at –30°C and achieved remarkable turnover frequencies of more than 40000 h^{-1}.[50]

We decided to investigate the hydroboration of acetophenone using **1** – **4** and pinacolborane (HBpin) as a model reaction. Optimization of the reaction conditions was performed using α-diimine ferrate **1**-[K([18]c-6)(thf)$_{0.5}$]. Best activity and full conversion were first obtained using 0.1 mol% catalyst loading and a small excess of HBpin (1.03 equiv.) at 25 °C in THF. Under these optimized conditions, the complexes **2**-[K([18]c-6)(thf)$_2$], **3**, and **4** were tested as well. While the homoleptic complexes **3** and **4** were significantly less active than **1**-[K([18]c-6)(thf)$_{0.5}$], the heteroleptic complex **2**-[K([18]c-6)(thf)$_2$] displayed similar activity. A plausible reason for the different reactivities of **1**-[K([18]c-6)(thf)$_{0.5}$]/**2**-[K([18]c-6)(thf)$_2$] and **3**/**4** is the absence of a vacant coordination site. However, the activation processes for **1**-[K([18]c-6)(thf)$_{0.5}$] and **2**-[K([18]c-6)(thf)$_2$] must be different due to the fact that **2**-[K([18]c-6)(thf)$_2$] is coordinated by two alkyl ligands.

Table 1. Hydroboration of acetophenone with HBPin using Fe pre-catalysts **1** – **4**.

Entry	Catalyst [mol%]	HBpin [equiv.]	Solvent [mL]	Time [min]	Yield[a] (Conversion)[a]
1	**1**-[K([18]c-6)(thf)$_{0.5}$] (0.1)	1.03	THF (0.1)	10	>99
2	**2**-[K([18]c-6)(thf)$_2$] (0.1)	1.03	THF (0.1)	10	>99
3	**3** (0.1)	1.03	THF (0.1)	10	67 (67)
4	**4** (0.1)	1.03	THF (0.1)	10	55 (55)

[a] Yields and conversions were determined by quantitative GC vs. internal *n*-pentadecane.

Complex **1**-[K([18]c-6)(thf)$_{0.5}$] was selected for further investigations. The optimized reaction conditions described above using 0.1 mol% of catalyst were applied to various *para*-substituted acetophenone derivatives, in order to investigate functional group tolerance. Gratifyingly, the

system was found to be compatible with electron-donating (OMe, Me), as well as electron-withdrawing groups (CF_3). Furthermore, halogenated (F, Cl, Br, I) acetophenones were cleanly hydroborated with no observable dehydrohalogenation, a problem sometimes observed for other highly-reduced metalates.[24] Pendant amine (NMe_2) and carboxylic ester (COOMe) were also tolerated. Furthermore, efficient hydroboration was observed for 3-methylacetophenone, propiophenone, the aliphatic substrate 2-octanone, and 2-acetyl pyridine. More sterically hindered substrates such as 2-methylacetophenone or benzophenone were also viable substrates, although slightly extended reaction times were required to achieve full conversion. Prolonged reaction times were also necessary for substrates such as 1-cylohexylethan-1-one, benzaldehyde, and α,β-unsaturated ketones. The hydroboration of 4-nitroacetophenone was not selective as nitro reduction was observed as well. 4-Acetylphenol was not hydroborated at all. Notably, no C=C bond reduction was observed for α,β-unsaturated ketone substrates. Moreover, the aldehyde group in 4-acetaldehyde was hydroborated more rapidly than the ketone moiety as proven by GC-MS, despite benzaldehyde itself requiring a longer reaction time for conversion than acetophenone.

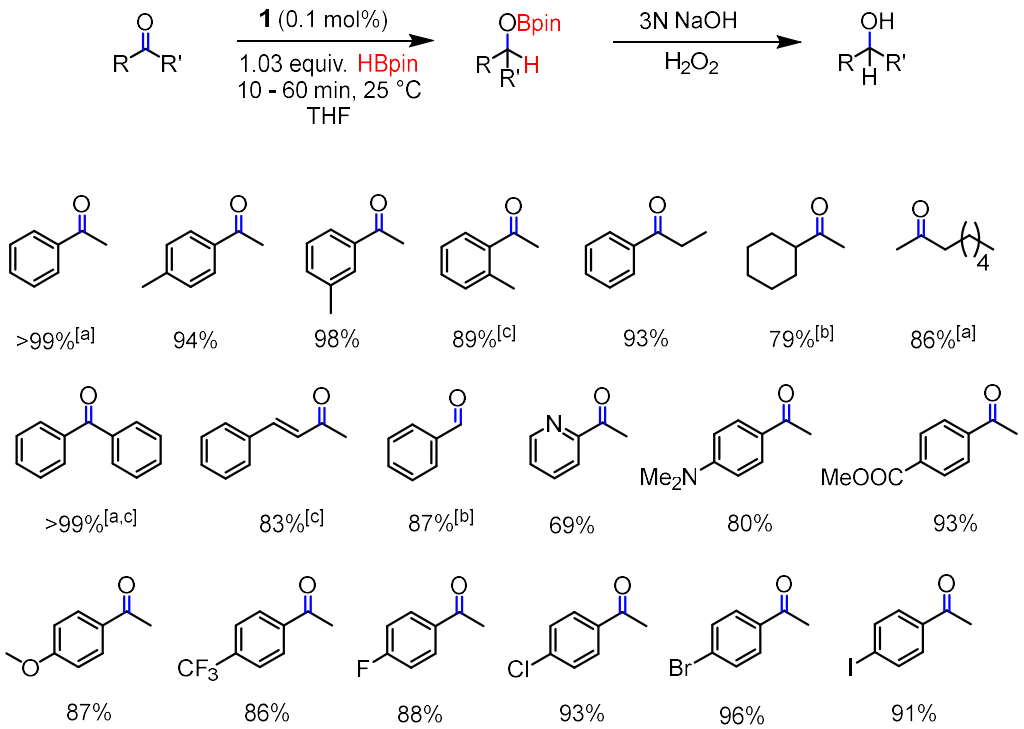

Scheme 4. Substrate scope for the hydroboration of carbonyls catalyzed by **1**-[K([18]c-6)(thf)$_{0.5}$]. Yields correspond to isolated alcohols. Reaction conditions: Substrate (1 mmol), HBpin (1.03 mmol), 1 (0.001 mmol), THF (0.5 mL), 25 °C. [a] = yield determined by quantitative GC-FID vs. internal *n*-pentadecane; [b] 30 min; [c] 1 h.

In order to gain more insight into the reaction mechanism, the model hydroboration reaction of acetophenone, the decrease of the C=O stretching band ($\nu_{(C=O)}$ = 1689 cm^{-1}) was monitored by *in situ* IR spectroscopy. Full consumption of acetophenone was achieved within 30 seconds at 25 °C with a catalyst loading of 0.05 mol% (**1**-[K([18]c-6)(thf)$_{0.5}$]); this corresponds to a turnover frequency of 220000 h^{-1}. Catalyst **1**-[K([18]c-6)(thf)$_{0.5}$] therefore represents one of the most active iron catalysts for the hydroboration of ketones reported to date. For comparison, a turnover frequency of 43500 h^{-1} at –30 °C was reported by *Gade* and co-workers for 4'-fluoroacetophenone hydroboration of HBPin using the current state-of-the-art bis(oxazolinyl-methylidene)isoindoline iron catalyst.[50]

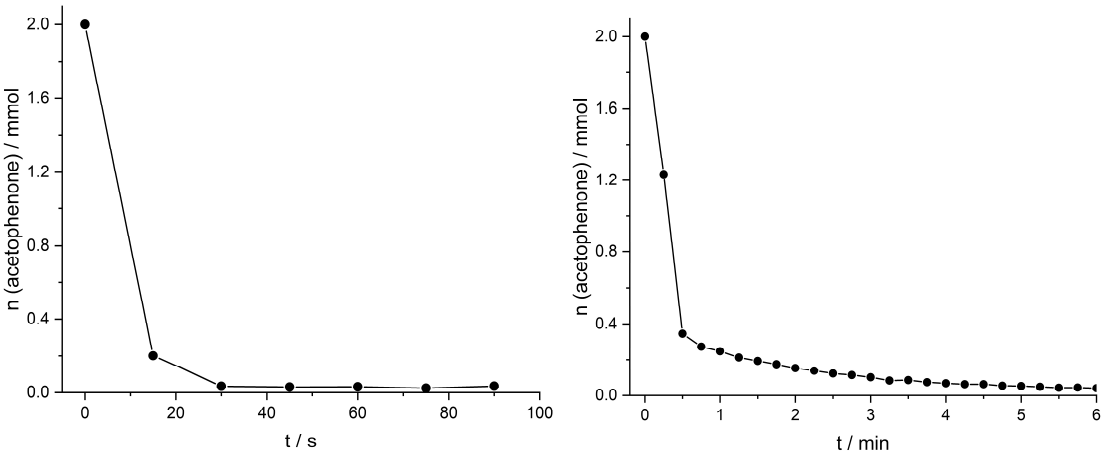

Figure 19. Reaction profile for of the hydroboration of acetophenone by HBpin catalyzed by **1**-[K([18]c-6)(thf)$_{0.5}$]. Reaction conditions: Acetophenone (2 mmol), HBpin (2 mmol), **1**-[K([18]c-6)(thf)$_{0.5}$] (0.05 mol% (left), 0.036 mol% (right)), THF (4 mL), 25 °C. Data points were obtained from time-resolved FT-IR spectra (see the SI for details).

In addition to this monitoring study, we also conducted a poisoning experiment using mercury, which is known to selectively inhibit the catalytic activity of heterogeneous catalysts. The hydroboration of acetophenone by **1**-[K([18]c-6)(thf)$_{0.5}$] was not negatively influenced by the presence of mercury (one drop).[51] Several illustrative stoichiometric reactions were also carried out. The reaction of a molar 1:1 ratio of **1**-[K([18]c-6)(thf)$_{0.5}$] and HBPin did not lead to any new signal in the ^{11}B NMR spectrum, suggesting a lack of any direct, productive reaction between these two components. Conversely, a brown solution of **1**-[K([18]c-6)(thf)$_{0.5}$] turned immediately green upon addition of one equivalent of acetophenone. Moreover, the $\nu_{(C=O)}$ stretching band of acetophenone disappeared from the IR spectrum of the resulting mixture,

indicating a direct reaction between **1**-[K([18]c-6)(thf)$_{0.5}$] and the substrate. Unfortunately, several attempts to crystallize or isolate the resulting species have so far been unsuccessful.

6.3 Conclusion

Two anionic α-diimine iron complexes **1**-[K([18]c-6)(thf)$_{0.5}$] and **2**-[K([18]c-6)(thf)$_2$] were synthesized by reduction of α-diimine iron(II) dibromide salts with potassium graphite. The iron atoms are tetracoordinated and feature a heteroleptic environment containing a BIAN ligand and an additional cod ligand for **1**-[K([18]c-6)(thf)$_{0.5}$], while a PhDi ligand and a dimerization product of norbornadiene are present in the structure of **2**-[K([18]c-6)(thf)$_2$]. The electronic structures of the ferrate anions in these complexes were analyzed by various experimental techniques (^{1}H NMR and EPR spectroscopy, single-crystal X-ray crystallography, ^{57}Fe Mößbauer spectroscopy, SQUID magnetization measurement) as well as theoretical calculations at the DFT and CASSCF level. The resulting data revealed an Fe(I) center with S =1/2 for **1**-[K([18]c-6)(thf)$_{0.5}$] and an Fe(III) center with rare intermediate spin S =3/2 for **2**-[K([18]c-6)(thf)$_2$]. Both complexes were successfully applied in the catalytic hydroboration of carbonyls with HBpin at ambient temperature. In particular complex **1**-[K([18]c-6)(thf)$_{0.5}$] showed high activity with a TOF = 220000 h^{-1} for reduction of acetophenone and a broad functional group tolerance.

The homoleptic complexes **3** and **4** are accessible by ligand exchange of the bis(anthracene)ferrate(1−) with α-diimine ligands. Compounds **3** and **4** exhibited significant lower activity in catalytic hydroboration, but showed interesting molecular properties. CASSCF calculations revealed that the quartet (S = 3/2) and sextet (S = 5/2) states are very close in energy. While the quartet state is favored for complex **3** with a small energy difference of 1.7 kcal mol^{-1}, the sextet state for complex **4** is more stable by 3.0 kcal mol^{-1}. The theoretical data are in agreement with EPR spectroscopic investigations and metrical data from single-crystal X-ray crystallography. In case of complex **3** ^{57}Fe Mößbauer data and cyclic voltammetry indicate the presence of isomers or a second unknown species. Further experiments (e.g. additional ^{57}Fe Mößbauer spectra and SQUID magnetization measurements) are needed to explain this observation.

6.4 References

[1] R. H. Crabtree, *Organometallics* **2011**, *30*, 17–19.

[2] C. Bolm, J. Legros, J. Le Paih, L. Zani, *Chem. Rev.* **2004**, *104*, 6217–6254. I. Bauer, H.-J. Knölker, *Chem. Rev.* **2015**, *115*, 3170–3387.

[3] D.Wei, C. Darcel, *Chem. Rev.* **2019**, *119*, 2550–2610.

[4] a) P. J.Chirik, K. Wieghardt, *Science* **2010**, *327*, 794–795. b) V. K. K. Praneeth, M. R. Ringenberg, *Angew. Chem. Int. Ed.* **2012**, *51*, 10228–10234; *Angew. Chem.* **2012**, *124*, 10374–10380. c) O. R.Luca, R. H. Crabtree, *Chem. Soc. Rev.* **2013**, *42*, 1440–1459.

[5] J. I. van der Vlugt, *Chem. Eur. J.* **2019**, *25*, 2651–2662.

[6] P. Le Floch, F. Knoch, F. Kremer, F. Mathey, J. Scholz, W. Scholz, K.-H. Thiele, U. Zenneck, *Eur. J. Inorg. Chem.* **1998**, *1998*, 119–126.

[7] a) S. C. Bart, E. J. Hawrelak, E. Lobkovsky, P. J. Chirik, *Organometallics* **2005**, *24*, 5518–5527. b) V. A. Schmidt, C. R. Kennedy, M. J. Bezdek, P. J. Chirik, *J. Am. Chem. Soc.* **2018**, *140*, 3443–3453.

[8] T. Janes, J. M. Rawson, D. Song, *Dalton Trans*. **2013**, *42*, 10640–10648.

[9] F. S. Wekesa, R. Arias-Ugarte, L. Kong, Z. Sumner, G. P. McGovern, M. Findlater, *Organometallics* **2015**, *34*, 5051–5056.

[10] L. A. Brown, F. S. Wekesa, D. K. Unruh, M. Findlater, B. K. Long, *J. Polym. Sci. Part A: Polym. Chem.* **2017**, *55*, 2824–2830.

[11] a) I. Matei, T. Lixandru *Bul. Inst. Politeh. Iasi* **1967**, *13*, 245. b) M. Dvolaitzky *C. R. Acad. Sci. Prais, Ser. C.* **1969**, *268*, 1811.

[12] a) R. van Asselt, J. C. Elsevier, *J. Mol. Catal.* **1991**, *65*, L13-L19. b) R. van Asselt, E. E. C. G. Gielens, R. E. Rülke, C. J. Elsevier, *J. Chem. Soc., Chem. Commun.* **1993**, *102*, 1203–1205. c) R. van Asselt, E. E. C. G. Gielens, R. E. Rulke, K. Vrieze, C. J. Elsevier, *J. Am. Chem. Soc.* **1994**, *116*, 977–985.

[13] I. L. Fedushkin, A. A. Skatova, V. A. Chudakova, G. K. Fukin, *Angew. Chem. Int. Ed.* **2003**, *42*, 3294–3298; *Angew. Chem.* **2003**, *115*, 3416-3420.

[14] M. Villa, D. Miesel, A. Hildebrandt, F. Ragaini, D. Schaarschmidt, A. Jacobi von Wangelin, *ChemCatChem* **2017**, *9*, 3203–3209.

[15] H. Lee, M. G. Campbell, R. Hernández Sánchez, J. Börgel, J. Raynaud, S: E. Parker, T. Ritter, *Organometallics* **2016**, *35*, 2923–2929.

[16] P. J. Larson, F. S. Wekesa, A. Singh, C. R. Smith, A. Rajput, G. P. McGovern, D. K. Unruh, A. F. Cozzolino, M. Findlater, *Polyhedron* **2019**, *159*, 365–374.

[17] A. C. Bowman, A. M. Tondreau, E. Lobkovsky, G. W. Margulieux, P. J. Chirik, *Inorg. Chem.* **2018**, *57*, 9634-9643.

[18] S. C. Bart, E. J. Hawrelak, A. K. Schmisseur, E. Lobkovsky, P. J. Chirik, *Organometallics* **2004**, *23*, 237–246.

[19] a) C. Lichtenberg, M. Adelhardt, T. L. Gianetti, K. Meyer, B. de Bruin, H. Grützmacher, *ACS Catalysis* **2015**, *5*, 6230-6240. b) C. Lichtenberg, L. Viciu, M. Adelhardt, J. Sutter, K. Meyer, B. de Bruin, H. Grützmacher, *Angew. Chem. Int. Ed.* **2015**, *54*, 5766–5771; *Angew. Chem.* **2015**, *127*, 5858–5863.

[20] H. tom Dieck, H. Bruder, *J. Chem. Soc., Chem. Commun.* **1977**, 24–25.

[21] D. Walther, G. Kreisel, R. Kirmse, *Z. Anorg. Allg. Chem.* **1982**, *487*, 149–160.

[22] N. Muresan, C. C. Lu, M. Ghosh, M.; J. C. Peters, M. Abe, L. M. Henling, T. Weyhermöller, E. Bill, K. Wieghardt, *Inorg. Chem.* **2008**, *47*, 4579–4590.

[23] I. L. Fedushkin, A. A. Skatova, N. M. Khvoinova, A. N. Lukoyanov, G. K. Fukin, S. Y. Ketkov, M. O. Maslov, A. S. Bogomyakov, V. M. Makarov, *Russ Chem Bull* **2013**, *62*, 2122–2131.

[24] T. M. Maier, S. Sandl, I. G. Shenderovich, J. J. Weigand, A. Jacobi von Wangelin, R. Wolf, *Chem. Eur. J.* **2018**., *25*, 238-245

[25] K. Jonas, L. Schieferstein, C. Krüger, Y.-H. Tsay, *Angew. Chem. Int. Ed.* **1979**, *18*, 550-551; *Angew. Chem.* **1979**, *91*, 590–591.

[26] H. Sun, V. Burlakov, A. Spannenberg, W. Baumann, P. Arndt, U. Rosenthal, *Organometallics* **2001**, *20*, 5472-5477.

[27] S. A. Bezman, P. H. Bird, A.R. Fraser, J. A. Osborn, *Inorg. Chem.* **1980**, *19*, 3755–3763.

[28] M. P. Betoré, M. A. Casado, P. García-Orduña, F. J. Lahoz, V. Polo, L. A. Oro, *Eur. J. Inorg. Chem.* **2016**, *2016*, 3489-3499.

[29] P. J. Stephens, F. J. Devlin, C. F. Chabalowski, M. J. Frisch, *J. Phys. Chem.* **1994**, *98*, 11623–11627.

[30] F. Weigend, R. Ahlrichs, *Phys. Chem. Chem. Phys.* **2005**, *7*, 3297–3305.

[31] A. C. Bowman, A. M. Tondreau, E. Lobkovsky, G. W. Margulieux, P. J. Chirik, *Inorg. Chem*. **2018**, *57*, 9634-9643.

[32] D. F. Evans, *J. Chem. Soc.* **1959**, 2003.

[33] M. Swart, A. W. Ehlers, K. Lammertsma, *Mol. Phys.* **2004**, *102*, 2467–2474.

[34] W. W. Brennessel, R. E. Jilek, J.E. Ellis, *Angew. Chem. Int. Ed.* **2007**, *46*, 6132–6136; *Angew. Chem.* **2007**, *119*, 6244–6248.

[35] M. J. Srgo, D. W. Stephan, *Dalton Trans.* **2010**, *39*, 5786-5794.

[36] A. Hellweg, C. Hattig, S. Hofener, W. Klopper, *Theor. Chem. Acc.* **2007**, *117*, 587.

[37] R. E. Cowley, E. Bill, F. Neese, W. W. Brennessel, P. L. Holland, *Inorg. Chem.* **2009**, *48*, 4828-4836.

[38] B. Gao, D. Zhao, X. Li, Y. Cui, R. Duan, X. Pang, *RSC Adv.* **2015**, *5*, 440–447.

[39] R. Morris Bullock *Catalysis without precious metals* **2010**, Wiley-VCH

[40] M. Sittig, *Metal-Organic Compounds; Advances in Chemistry* Ser No. 23; ACS **1959**.

[41] C. C. Chong, R. Kinjo, *ACS Catal.* **2015**, *5*, 3238–3259.

[42] a) G. Zhang, H. Zeng, J. Wu, Z. Yin, S. Zheng, J. C. Fettinger, *Angew. Chem. Int. Ed.* **2016**, *55*, 14369–14372; *Angew. Chem.* **2016**, *128*, 14581–14584. b) V. Vasilenko, C. K. Blasius, H. Wadepohl, L. H. Gade, *Angew. Chem. Int. Ed.* **2017**, *56*, 8393–8397; *Angew. Chem.* **2017**, *129*, 8513–8517. c) V. Vasilenko, C. K. Blasius, L. H. Gade, *J. Am. Chem. Soc.* **2018**, *140*, 9244–9254.

[43] a) J. Guo, J. Chen, Z. Lu, *Chem. Commun.* **2015**, *51*, 5725–5727. b) J. H. Docherty, J. Peng, A. P. Dominey, S. P. Thomas, *Nat. Chem.* **2017**, *9*, 595–600. c) S. R. Tamang, D. Bedi, S. Shafiei-Haghighi, C. R. Smith, C. Crawford, M. Findlater, *Org. Lett.* **2018**, *20*, 6695–6700.d) J. Wu, H. Zeng, J. Cheng, S. Zheng, J. A. Golen, D. R. Manke, G. Zhang, *J. Org. Chem.* **2018**, *83*, 9442–9448.

[44] A. E. King, S. C. E. Stieber, N. J. Henson, S. A. Kozimor, B. L. Scott, N. C. Smythe, A. D. Sutton, J. C. Gordon, *Eur. J. Inorg. Chem.* **2016**, *2016*, 1635–1640.

[45] S. R. Tamang, M. Findlater, *J. Org. Chem.* **2017**, *82*, 12857–12862.

[46] T. Bai, T. Janes, D. Song, *Dalton Trans.* **2017**, *46*, 12408–12412.

[47] J. Liu, A. Zhang. H. Song, Q. Tong, C.-H. Tung, W. Wang, *Chin. Chem. Lett.* **2018**, *29*, 949-953.

[48] U. K. Das, C. S. Higman, B. Gabidullin, J. E. Hein, R. T. Baker, *ACS Catal.* **2018**, *8*, 1076–1081.

[49] a) S. Khoo, J. Cao, F. Ng, C.-W. So, *Inorg. Chem.* **2018**, *57*, 12452–12455. b) X. Qi, T. Zheng, J. Zhou, Y. Dong, X. Zuo, X. Li, H. Sun, O. Fuhr, D. Fenske, *Organometallics* **2019**, *38*, 268–277.

[50] C. K. Blasius, V. Vasilenko, L. H. Gade, *Angew. Chem. Int. Ed.* **2018**, *57*, 10231–10235; *Angew. Chem*. **2018**, *130*, 10388–10392.

[51] a) R. H. Crabtree, *Chem. Rev.* **2012**, *112*, 1536–1554. b) V. Artero, M. Fontecave, *Chem. Soc. Rev.* **2013**, *42*, 2338–2356. c) D. Gärtner, A. Welther, B. Razaei Rad, R. Wolf, A. Jacobi v. Wangelin, *Angew. Chem. Int. Ed.* **2014**, *53*, 3722–3726; *Angew. Chem.* **2014**, *126*, 3796–3800. d) J. F. Sonnenberg, R. H. Morris, *Catal. Sci. Technol.* **2014**, *4*, 3426–3438.

6.5 Supporting Information

6.5.1 General Procedures

All experiments were performed under an atmosphere of dry Argon (Argon 4.6, Linde) using standard Schlenk techniques or a MBraun UniLab Glovebox.

***Chemicals and Solvents**:* Solvents were dried and degassed with an MBraun SPS800 solvent-purification system. THF, diethylether were stored over molecular sieves (3 Å). *n*-hexane was stored over a potassium mirror. 1,2-dimethoxyethane was stirred over K/benzophenone, distilled and stored over molecular sieves (3 Å). All chemicals were purchased from commercial suppliers and used as received, if not stated otherwise. $[Li_2(dme)_2\{Fe(\eta^4\text{-}cod)_2\}]$ was synthesized by *Julia Märsch* according to a protocol of Fürstner and co-workers.[1]

Cyclic Voltammetry: Cyclic Voltammetry experiments were performed in a single-compartment cell inside a nitrogen-filled glovebox using a CH Instruments CH1600E potentiostat. The cell was equipped with a platinum disc working electrode (2 mm diameter) polished with 0.05 μm alumina paste, a platinum wire counter electrode and an $Ag/AgNO_3$ reference electrode. The supporting electrolyte, tetra-*n*-butylammonium hexafluorophosphate, was dried *in vacuo* at 110°C for three days. All redox potentials are reported vs. the ferrocenium/ferrocene (Fc^+/Fc) couple.

Elemental Analyses: CHN analyses were recorded by the analytical department of the University of Regensburg with a Micro Vario Cube (Elementar)

ESI-MS: ESI-MS spectra carried out by the analytical department of the University of Regensburg, Agilent Q-TOF 6549 UHD

EPR spectroscopy: The experimental X-band EPR spectra was recorded on a Bruker EMX spectrometer (Bruker BioSpin Rheinstetten) equipped with a He temperature-control cryostat system (Oxford Instruments). The *g* values were calculated with the ORCA software package[2] at the B3LYP[3]/def2-TZVP[4] level of theory. The spectra of **1–4** were analyzed and simulated using the W95EPR program of Prof. Frank Neese or the Simultispin extension to EasySpin (easyspin.org).

NMR spectroscopy: ^{1}H NMR spectra in solutions were recorded on *Bruker Avance 300* (300 MHz) and *BrukerAvance 400* (400 MHz) if not stated otherwise. These chemical shifts are given relative to solvents resonances in the tetramethylsilane scale. The following abbreviations have been used for multiplicities: s = singlet, d = doublet, t = triplet, q = quartet, sept = septet, m = multiplet, dd = doublet of doublet, dt = doublet of triplet.

Melting point: Melting points were measured on samples in sealed capillaries on a Stuart SMP10 melting point apparatus.

^{57}***Fe Mößbauer spectroscopy***: ^{57}Fe Mößbauer spectra were recorded with a ^{57}Co source in a Rh matrix using an alternating constant acceleration Wissel Mößbauer spectrometer operated in the transmission mode and equipped with a Janis closed cycle helium cryostat. Isomer shifts are given relative to Fe metal at ambient temperature. Simulation of the experimental data was performed with the Mfit program using *Lorentzian* line doublets.[5]

Single-crystal X-ray crystallography: The single crystal X-ray diffraction (XRD) data were recorded on an Agilent Super Nova diffractometer with an Atlas CCD detector. Microfocus Cu K_α radiation (λ = 1.54184 Å) was used in each measurement. Empirical multi-scan[6] and analytical absorption corrections[7] were applied to the data. The structures were solved with SHELXT[8] and least-square refinements on F^2 were carried out with SHELXL.[9] The program package Olex2 was used.[10] Crystal data for **1**-[Li(thf)], **2**-[K([2.2.2]cryptand)(thf)$_3$], **3** and **4** are given in section 6.5.4. below.

Magnetic susceptibility measurements: Temperature-dependent magnetic susceptibility measurements were carried out with a Quantum-Design MPMS-XL-5 SQUID magnetometer equipped with a 5 Tesla magnet in the range from 200 (or 295) to 2.0 K at a magnetic field of 0.5 T. The powdered sample was contained in a gelatin capsule or polypropylene bucket and fixed in a non-magnetic straw. Each raw data file for the measured magnetic moment was corrected for the diamagnetic contribution of the sample holder. The molar susceptibility data were corrected for the diamagnetic contribution.

Experimental data for complex **1** were modelled by using a fitting procedure to the appropriate Heisenberg-Dirac-van-Vleck (HDvV) spin Hamiltonian for Zeeman splitting and zero-field splitting, equation (1).

$$\hat{H} = \mu_B \vec{B}\vec{S} + D\left[\hat{S}_z^2 - \frac{1}{3}S(S+1)\right] \qquad (1)$$

Temperature-independent paramagnetism (*TIP*) and a Curie-behaved paramagnetic impurity (*PI*) with spin $S = ½$ were included according to $X_{calc} = (1 - PI) \cdot X_c + PI \cdot X_{cmono} + TIP$

UV-vis spectra: UV-vis spectra were recorded on an Ocean Optics Flame spectrometer (Varian Cary 50 Spectrophometer) in a Quartz cuvette with a layer thickness of 1 cm at room temperature with a concentration of 10^{-4} to 10^{-6} M.

6.5.2 Syntheses of Starting Materials

^{Dipp}BIAN was synthesized according to *Chapter 2*.

6.5.2.1 Synthesis of [(^{Dipp}BIAN)FeBr$_2$]

[(^{Dipp}BIAN)FeBr$_2$] was synthetized according to an adapted protocol of *Hoyt* and co-workers.[12]

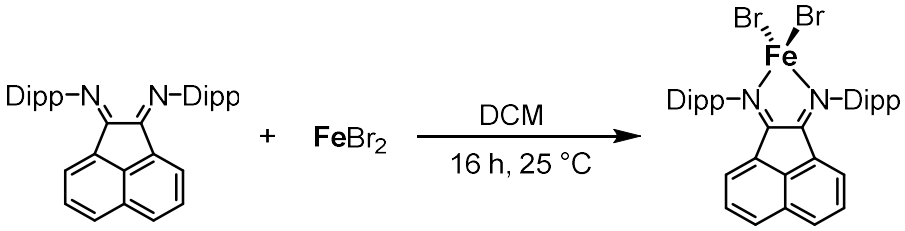

Anhydrous FeBr$_2$ (1.05 g, 4.85 mmol, 1.0 equiv.) and ^{Dipp}BIAN (2.42 g, 4.85 mmol, 1.0 equiv.) were dissolved in 60 mL DCM. The reaction mixture turned green within few minutes and was stirred for 16 h. The solution was filtered, the solvent reduced to 40 mL and layered with 100 mL *n*-hexane. Dark green needles of [(^{Dipp}BIAN)FeBr$_2$] were formed within few days and dried *in vacuo* after isolation.

Yield: 2.5 g (34.0 mmol, 83%)

Chemical formula: $C_{36}H_{40}N_2FeBr_2$ (M = 716.38 g mol^{-1})

^{1}H NMR (400.13 MHz, 300 K, THF-d$_8$) δ[ppm]: 11.6 (2H), 8.9 (4H), 6.5 (2H), 5.0 (2H), 1.7 (12H), –3.3 (12H), –15.0 (2H)

6.5.2.1 Synthesis of [K([18]c-6)(thf)$_2$][Fe(η^4-C$_{14}$H$_{10}$)$_2$]

[K([18]c-6)(thf)$_2$][Fe(η^4-C$_{14}$H$_{10}$)$_2$] was synthesized according to a protocol of *Ellis* and co-workers.[13]

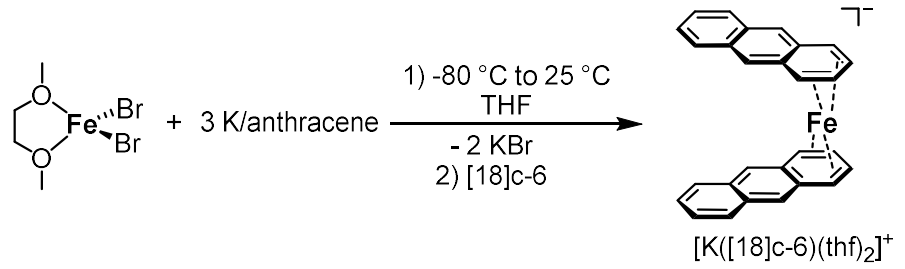

FeBr$_2$(dme) (4.59 g, 15.0 mmol, 1.0 equiv.) was dissolved in 150 mL THF and freshly cut potassium metal (1.76 g, 45.0 mmol, 3.0 equiv.) as well as anthracene (8.03 g, 45.0 mmol, 3.0 equiv.) in 200 mL THF. Both solutions were stirred for one day. The FeBr$_2$(dme) solution

was cooled to –40 °C and added to the –80 °C cooled K/anthracene solution with a canula. The reaction mixture was slowly warmed to room temperature, stirred for one day and filtered. 18-crown-6 ([18]c-6) was dissolved in 150 mL THF and added to the red-brown filtrate and 300 mL *n*-heptane was added. A brown precipitate appeared. Precipitation of $[K([18]c\text{-}6)(thf)_2][Fe(\eta^4\text{-}C_{14}H_{10})_2]$ was completed by reducing the solvent to 350 mL and subsequent addition of 60 mL diethylether. The red-brown solid was collected on a frit, washed with 600 mL diethylether and dried *in vacuo*.

Yield: 6.51 g (7.6 mmol, 51%)

Chemical formula: $C_{40}H_{44}FeKO_6 \cdot (C_4H_8O)_2$ ($M = 859.94$ g mol^{-1})

Elemental analysis calcd. for $C_{40}H_{44}FeKO_6 \cdot (C_4H_8O)_2$: C 67.04, H 7.03; found: C 65.72, H 6.33. The combustion analysis gave significantly lower C and H values presumably due to the presence of residual KBr as an impurity.

6.5.3 Syntheses of Anionic α-Diimine Iron Complexes

6.5.3.1 Synthesis of $[K([18]c\text{-}6)(thf)_2][(^{Dipp}BIAN)Fe(\eta^4\text{-}cod)]$ (**1**-$[K([18]c\text{-}6)(thf)_{0.5}]$)

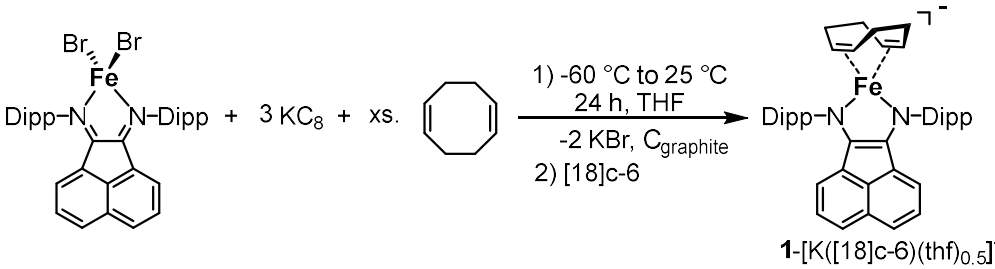

1,5-cyclooctadiene (1.0 mL, 8.1 mmol, 5.8 equiv.) was added to a solution of $[(^{Dipp}BIAN)FeBr_2]$ (1.0 g, 1.4 mmol, 1.0 equiv.) in 100 mL THF. The solution was cooled to –60 °C and KC_8 (0.6 g, 4.4 mmol, 3.15 equiv.) was added in portions over five minutes and then slowly warmed to ambient temperature. Meanwhile, the solution turned yellow-brownish. After stirring overnight at ambient temperature, the resulting suspension was filtered and [18]c-6 (0.37 g, 1.4 mmol, 1.0 equiv.) in 15 mL THF was added. The solution was concentrated to 80 mL THF, layered with 80 mL *n*-hexane and stored at –10 °C. Brown-green block shaped crystals were formed within a few days. $[K([18]c\text{-}6)(thf)_2][(^{Dipp}BIAN)Fe(\eta^4\text{-}cod)]$ (**1**-$[K([18]c\text{-}6)(thf)_{0.5}]$) was isolated in 65% yield by decanting the solvent and drying the remaining crystalline solid in

vacuo. Crystals suitable for single-crystal X-ray crystallography were obtained by recrystallization from THF/*n*-hexane.

Formula: $C_{56}H_{76}N_2KFeO_6 \cdot (C_4H_8O)_{0.5}$ (M = 1004 g mol^{-1})

Yield: 1.09 g (1.086 mmol, 78%)

^{1}H NMR (400.13 MHz, 300 K, THF-d_8): δ [ppm]: 8.63 (m, Int 1), 4.77 (br s, Int 0.7), 4.35 (br s, Int 1), 3.51 (br s, overlap with THF-d_8, Int 12.5), 2.18 (br s, Int 3.3), 1.29 (br s, Int 1.7), 0.89 (br s, Int 1), 0.43 (br s, Int 2.5), –16.2 (br s)

Elemental analysis calcd. for $C_{56}H_{76}N_2KFeO_6 \cdot (C_4H_8O)_{0.5}$: C 69.37, H 8.03, N 2.79; found: C 69.78, H 7.82, N 2.47

EPR spectroscopy: Measured in ^{Me}THF glass at 20 K. Microwave frequency: 9.37466 GHz, Modulation amplitude: 4.000 G, Power: 0.6325 mV. The experimental spectrum could be fitted with the following parameters for an S =1/2 system on a nucleus with a nuclear spin of 0. g_1 = 2.217, g_2 = 2.095, g_3 = 2.005, W_1 = 10, W_2 = 11 and W_3 = 13.

Magnetic moment (Evans method in THF-d_8 at ambient temperature.): μ_{eff} = 2.0(1) μ_B

Melting point: T > 70°C: decomposition to a black oil

^{57}Fe Mößbauer spectroscopy: Isomer shift δ = 0.23 mm s^{-1}; quadrupole splitting |ΔE$_Q$| = 2.26 mm s^{-1}. Calculated |ΔE$_Q$| value for [($^{2,6\text{-dimethylphenyl}}$BIAN)Fe(η^4-cod)]$^-$: 2.50 mm s^{-1} at the OPBE D3BJ def2TZVP def2/J level of theory using the CP(PPP) basis set for Fe.[4],[14]-[16]

UV-vis (THF): λ_{max}/nm (ε/L mol^{-1} cm^{-1}) = 294 (21000), 408 (12000), 697 (5000)

6.5.3.2 Synthesis of [Li)(thf){(^{Dipp}BIAN)Fe(η^4-cod)}] (1-[Li(thf)])

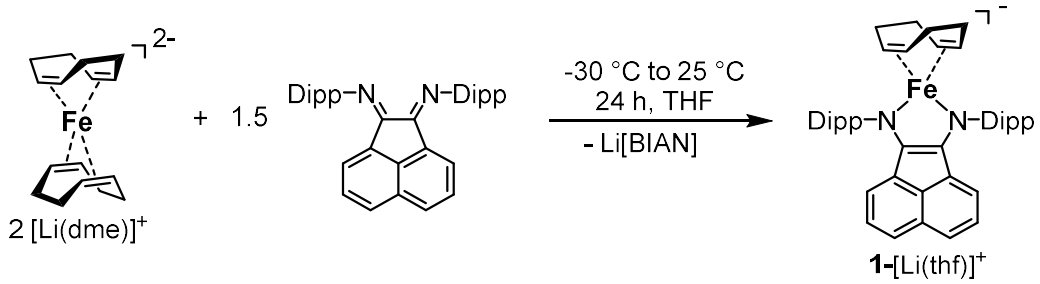

^{Dipp}BIAN (75.2 mg, 0.15 mmol, 1.5 equiv.) was dissolved in 2 mL THF and added dropwise as cooled (–30°C) solution to a –30°C cold solution of [Li$_2$(dme)$_2${Fe(η^4-cod)$_2$] (46.7 mg, 0.10 mmol, 1.0 equiv.) in 2 mL THF (Note: the dissolved ferrate contains some black particles). The olive-green solution turned dark brown and was warmed up to room temperature and stirred

for 24 hours. The solvent was evaporated and residue extracted with 20 mL *n*-hexane and filtered. Dark green-brown crystals were obtained by slow evaporation at room temperature and isolated by decanting the mother liquor and dried *in vacuo*.

Formula: $C_{48}H_{60}N_2LiFeO$ ($M = 743.81\ g{\cdot}mol^{-1}$)

Yield: 40.8 mg (0.055 mmol, 55%)

^{1}H NMR (400.13 MHz, 300 K, THF-d_8): δ [ppm]: 8.73 (br s), 7.20 (br s), 6.92 (br s), 6.07 (br s), 5.82 (br s), 5.50 (br s), 5.17 – 4.04 (m), 3.04 – 2.02 (m), 1.39 – 0.82 (m), 0.41 (br s), –0.98 (br s)

Elemental analysis calcd. for $C_{48}H_{60}N_2LiFeO$: C 77.51, H 8.13, N 3.77; found: C 76.57, H 7.88, N 3.55

6.5.3.3 Synthesis of [K([18]c-6)(thf)$_2$][(^{Dipp}BIAN)Fe($C_{14}H_{16}$)] (2-[K([18]c-6)(thf)$_2$])

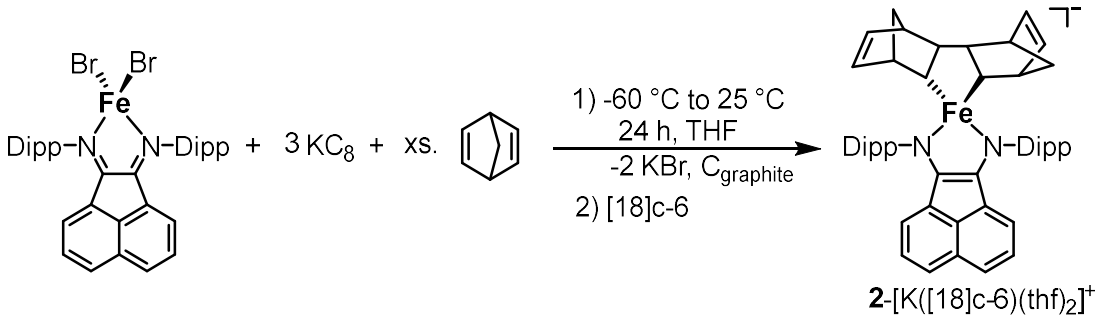

[(^{Dipp}BIAN)FeBr$_2$] (506 mg, 0.71 mmol, 1.0 equiv.) and 2,5-norbornadiene (1.4 mL, 13.8 mmol, 19.4 equiv.) were dissolved in 10 mL THF and cooled to –70°C. Potassium graphite (KC_8, 304 mg, 2.25 mmol, 3.2 equiv.) was added in small portions. The color changed over orange-brown to deep green. The reaction mixture was warmed to room temperature and stirred overnight. The suspension was filtered and [18]c-6 (187 mg, 0.71 mmol, 1.0 equiv.) in 5 mL THF was added to the filtrate. The solution was reduced to 10 mL and layered with 25 mL *n*-hexane. Dark green crystals of [K([18]c-6)(thf)$_2$][(^{Dipp}BIAN)Fe($C_{14}H_{16}$)] (**2**-[K([18]c-6)(thf)$_2$]) were formed within one day, were isolated and dried *in vacuo.* Recrystallization from THF/*n*-hexane afforded crystals which were suitable for single-crystal X-ray crystallography. The same reaction was conducted with [2.2.2]cryptand instead of [18]c-6 to obtain crystals of the [2.2.2]cryptand complex **2**-[K([2.2.2]cryptand)] suitable for single-crystal X-ray crystallography, which was not further characterized.

Characterization data for 2-[K([18]c-6)(thf)$_2$]:

Formula: $C_{62}H_{76}N_2KFeO_6 \cdot (C_4H_8O)_2$ (M = 1187 g mol^{-1})

Yield: 0.7 g (0.59 mmol, 83%)

^{1}H NMR (400.13 MHz, 300 K, THF-d$_8$): δ [ppm]: 69.2 (s, Int 1.5), 44.0 (s, Int 1), 30.5 (s, Int 1.2), 23.4 (s, Int 2), 14.6 (br s, Int 1.7), 14.4 (s, Int 2), 11.6 (s, Int 1.8), 4.9 (br s, Int 6), 4.8 (s, Int 3.5), 3.4 (s, Int 24, 18[c]-6), –7.9 (m, Int 7.4), –10.2 (s, Int 1,5), –15.6 (s, Int 4.7), –55.4 (br s, Int 0.06)

Elemental analysis calcd. for $C_{62}H_{76}N_2KFeO_6 \cdot (C_4H_8O)_2$: C 70.74, H 8.14, N 2.36; found: C 70.57, H 7.84, N 2.13

EPR spectroscopy: Measured in ^{Me}THF glass at 20 K. Microwave frequency: 9.376835 GHz, Modulation amplitude: 4.000 G, Power: 0.6325 mV. The experimental spectrum of **2** can be fitted using the following parameters for an $S = 3/2$ system. $g_{11} = 2.25$, $g_{22} = 2.25$, $g_{33} = 1.90$, D = 15 cm^{-1}, E = 0.8 cm^{-1}, E/D = 0.05.

Magnetic moment (Evans method in THF-d$_8$ at ambient temperature): $\mu_{eff} = 3.9(1)\ \mu_B$. SQUID magnetization measurement on the solid: χ x T = 2.03 (20 °C)

Melting point: T > 200°C: decomposition to a black oil

^{57}Fe Mößbauer spectroscopy: Isomer shift $\delta = 0.17$ mm s^{-1}; quadrupole splitting $|\Delta E_Q| = 1.32$ mm s^{-1}.

UV-vis (THF): λ_{max}/nm (ε/L·mol^{-1}·cm^{-1}) = 298 (22000), 366 (13500), 418 (8000), 740 (5000)

6.5.3.4 Synthesis of [K([18]c-6)(thf)$_{0.5}$][(^{Dipp}BIAN)$_2$Fe] (3)

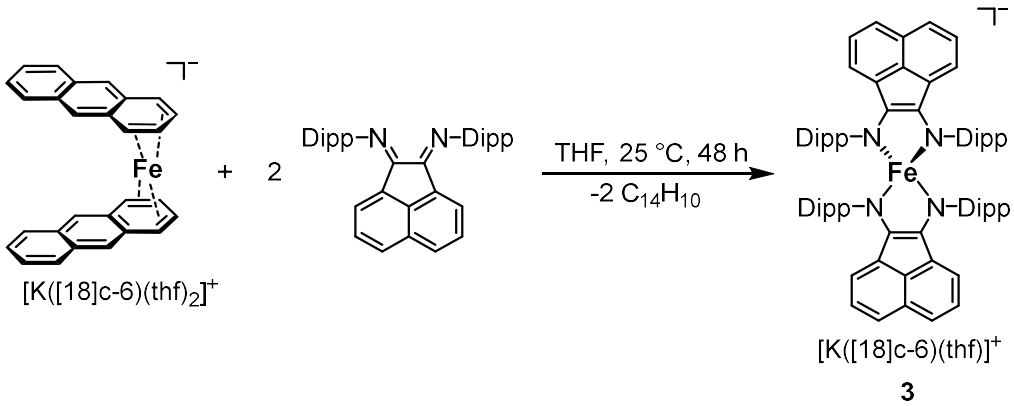

3

[K([18]c-6)(thf)$_2$][Fe(η^4-C$_{14}$H$_{10}$)$_2$] (653 mg, 0.76 mmol, 1.0 equiv.) was dissolved in 60 mL THF and ^{Dipp}BIAN (761 mg, 1.52 mmol, 2.0 equiv.) was added as solid to the solution. The color immediately changed from green to orange and the reaction mixture was stirred for 48 h The solvent was removed and the residue washed with 20 mL *n*-hexane. The residue was extracted

with 40 mL THF and filtered. The solution was layered with 50 mL of *n*-hexane and stored at room temperature. After a few days, black crystals of **3** were isolated (490 mg, 0.35 mmol, 46%) and dried *in vacuo*. Several samples were used for elemental analysis and spectroscopic characterization. These samples were obtained by two different methods:

Samples **3-1**: Samples labelled **3-1** were obtained by recrystallizing the crude product from THF/*n*-hexane.

Samples **3-2**: This sample was obtained by recrystallization of a sample **3-1** from THF/*n*-hexane.

For both types of samples, crystals suitable for single-crystal X-ray crystallography were obtained by diffusion of *n*-hexane into a concentrated THF solution. Several crystalline samples were examined by X-ray crystallography. All examined crystals hat the same unit cell parameters as reported in section 6.5.4. (*vide infra*).

Formula: $C_{84}H_{104}N_2KFeO_6 \cdot (C_4H_8O)$ ($M = 1432.8$ g mol^{-1})

Yield: crude product 490 mg (0.35 mmol, 46%); sample **3-1**: 163 mg (0.11 mmol, 15%); sample **3-2**: 82 mg (0.06 mmol, 7%).

^{1}H NMR (400.13 MHz, 300 K, THF-d_8) of sample **3-2**: δ [ppm]: 47.3 (s, Int: 1.0), 46.8 (br s, Int: 0.8), 7.1 (br s, Int: 3.5), 5.2 (s, Int: 1.5), 3.7 (br s, Int: 6.5), 3.58 ($THF_{coordinated}$), 2.8 (br s, Int: 1), 2.3 (br s, Int: 1), 1.74 ($THF_{coordinated}$), 1.29 (*n*-hexane), 1.2 (br s, Int: 0.4), 1.0 (br s, Int: 0.5), 0.89 (*n*-hexane), –3.4 (br s, Int: 2.6), –3.4 (s, Int: 2.8), –11.0 (br s, Int: 1.0), -17.3 (br s, Int: 2.8), –48.3 (br s, Int: 0.4)

Elemental analysis calcd. for $C_{84}H_{104}N_4KFeO_6 \cdot (C_4H_8O)$: C 73.77, H 7.88, N 3.91; results for sample **3-1**: C 72.03, H 7.57, N 3.88; results for sample **3-2**: C 73.30, H 7.76, N 3.81.

EPR spectroscopy: Samples **3-1** and **3-2** were measured in a frozen ^{Me}THF glass at 20 K. Sample **3-2**: Microwave frequency: 9.375682 GHz, Modulation amplitude: 4.000 G, Power: 0.6325 mV. Sample **3-2** can be simulated as a $S = 3/2$ species: $g_{11} = 2.13$, $g_{22} = 2.10$, $g_{33} = 2.06$, D = 20 cm^{-1}, E = 4.1 cm^{-1}, E/D = 0.20. Sample **3-1**: Microwave frequency: 9.375682 GHz; Modulation amplitude: 4.000 G; Power: 0.6325 mW. Sample **3-1** can be simulated as an $S = 3/2$ species: $g_{11} = 2.20$, $g_{22} = 2.12$, $g_{33} = 2.06$, D = 20 cm^{-1}, E = 4.1 cm^{-1}, E/D = 0.20.

Magnetic moment (Evans method in THF-d_8 at ambient temperature): Sample **3-1**: $\mu_{eff} = 4.7(1)\ \mu_B$; sample **3-2**: $\mu_{eff} = 4.7(1)\ \mu_B$

Melting point (sample **3-1**): T > 200°C: decomposition to a black oil.

^{57}Fe Mößbauer spectroscopy (sample **3-1**): Isomer shift $\delta = 0.76$ mm s^{-1}; quadrupole splitting $|\Delta E_Q| = 1.63$mm s^{-1}. A fitting procedure revealed that the simulated spectrum can be divided into two subunits with isomer shifts of $\delta = 0.75$ mm s^{-1} (share of 75%, sub1) and $\delta = 0.78$ mm s^{-1} (share of 25%, sub2). The corresponding quadrupole splitting values are $|\Delta E_Q| = 1.60$ mm s^{-1} (sub1) and $|\Delta E_Q| = 2.17$ mm s^{-1} (sub2).

UV-vis (THF): λ_{max}/nm (ε/L·mol^{-1}·cm^{-1}) = for sample **3-1**: 360 (20000, shoulder), 435 (7000), 505 (6500), 588 (3500); for sample **3-2:** 360 (18000, shoulder), 435 (8500), 505 (8000), 588 (4000);

6.5.3.5 Synthesis of [K([18]c-6)(thf)$_2$][(^{Dipp}PhDi)$_2$Fe] (4)

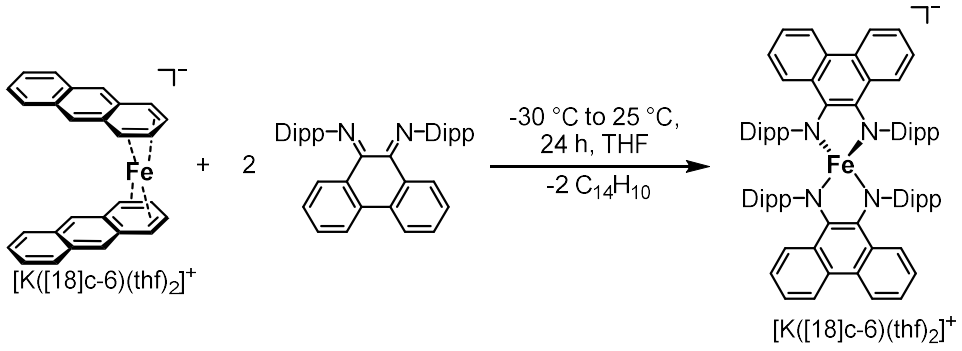

^{Dipp}PhDi (92.2 mg, 0.176 mmol, 2.0 equiv.) was dissolved in 2 mL THF, cooled to –30°C and added dropwise to a –30°C cold solution of [K([18]c-6)(thf)$_2$][Fe(η^4-C$_{14}$H$_{10}$)$_2$] (75.5 mg, 0.03 mmol, 1.0 equiv.) in 2 mL THF. The color immediately changed over brown to green and the reaction mixture was stirred for one day. The solvent was removed and the residue washed with 8 mL *n*-hexane. The residue was extracted with 4 mL THF and layered with 1 mL *n*-hexane. Crystals suitable for single-crystal X-ray crystallography were obtained by diffusion of *n*-hexane into a concentrated THF solution.

Formula: C$_{96}$H$_{124}$N$_2$KFeO$_6$ · (C$_4$H$_8$O)$_2$ (M = 1557 g·mol^{-1})

Yield: 25.4 mg (0.0163 mmol, 19%)

^{1}H NMR (400.13 MHz, 300 K, THF-d$_8$): δ [ppm]: only solvent signals observed

Elemental analysis calcd. C$_{96}$H$_{124}$N$_2$KFeO$_6$ · (C$_4$H$_8$O)$_2$: C 74.06, H 8.03, N 3.59; found: C 74.18, H 7.82, N 3.54

EPR spectroscopy: Measured in ^{Me}THF glass at 20 K. Microwave frequency: 9.378092 GHz, Modulation amplitude: 4.000 G, Power: 0.6325 mV. The spectrum can be simulated as an *S* = 5/2 system using the following parameters: $g_{11} = 2.03$, $g_{22} = 2.03$, $g_{33} = 2.03$, D = 7 cm^{-1}, E = 2.2

cm^{-1}, E/D = 0.31. The spectrum can also be simulated as a mixture of two components which are both S = 3/2 systems. Component 1: Weight 66.7%, g_{11} = 2.19, g_{22} = 2.19, g_{33} = 2.19, D = 10 cm^{-1}, E = 0.25 cm^{-1}, E/D = 0.03. Component 2: Weight: 33.3%. g_{11} = 2.20, g_{22} = 2.20, g_{33} = 2.20, D = 10 cm^{-1}, E = 0.002 cm^{-1}, E/D = 0.00.

Magnetic moment (Evans method in THF-d_8 at ambient temperature): μ_{eff} = 5.1(1) μ_B

Melting point: no decomposition up to 300 °C

UV-vis (THF): λ_{max}/nm (ε/L·mol^{-1}·cm^{-1}) = 310 (40000, shoulder), 398 (28500), 590 (11500)

6.5.4 Single-Crystal X-ray Crystallography

	1-[Li(thf)]	**2**-[K([2.2.2]cryptand)$(thf)_3$]
Empirical formula	$C_{48}H_{60}FeLiN_2O$	$C_{88}FeH_{132}KN_4O_{11}$
Formula weight	743.77	1516.92
Temperature/K	123(1)	123(1)
Crystal system	orthorhombic	monoclinic
Space group	$Pmn2_1$	$P2_1$
a/Å	17.5096(3)	13.9042(3)
b/Å	10.5351(2)	14.0644(2)
c/Å	10.9916(2)	20.0255(4)
α/°	90	90
β/°	90	107.389(2)
γ/°	90	90
Volume/$Å^3$	2027.57(6)	3737.10(13)
Z	2	2
$\varrho_{calc}g/cm^3$	1.218	1.348
μ/mm^{-1}	3.256	2.646
F(000)	798.0	1642.0
Crystal size/mm^3	0.209 × 0.165 × 0.142	0.291 × 0.2 × 0.158
Radiation	CuK_α (λ = 1.54184)	CuK_α (λ = 1.54184)
2Θ range for data collection/°	8.392 to 147.262	6.882 to 152.086
Index ranges	-21 ≤ h ≤ 18, -12 ≤ k ≤ 12, -13 ≤ l ≤ 13	-17 ≤ h ≤ 16, -17 ≤ k ≤ 17, -25 ≤ l ≤ 24
Reflections collected	14765	31924
Independent reflections	3970 [R_{int} = 0.0379, R_{sigma} = 0.0308]	14978 [R_{int} = 0.0242, R_{sigma} = 0.0313]
Data/restraints/parameters	3970/2/286	14978/343/800
Goodness-of-fit on F^2	1.043	1.019
Final R indexes [I>=2σ (I)]	R_1 = 0.0359, wR_2 = 0.0910	R_1 = 0.0586, wR_2 = 0.1564
Final R indexes [all data]	R_1 = 0.0383, wR_2 = 0.0929	R_1 = 0.0603, wR_2 = 0.1586
Largest diff. peak/hole / e $Å^{-3}$	0.26/-0.38	0.51/-0.53
Flack parameter	-0.007(5)	0.262(5)

	3	**4**
Empirical formula	$C_{92}H_{120}FeKN_4O_8$	$C_{96}H_{124}FeKN_4O_8$
Formula weight	1504.86	1556.93
Temperature/K	123.(1)	123(1)
Crystal system	monoclinic	Monoclinic
Space group	$P2_1/n$	$P2/n$
a/Å	25.3585(5)	18.7236(2)
b/Å	13.6726(2)	11.7866(2)
c/Å	26.9463(5)	19.1757(3)
α/°	90	90
β/°	93.452(2)	94.1230(10)
γ/°	90	90
Volume/Å^3	9325.8(3)	4220.89(11)
Z	4	2
ρ_{calc}g/cm^3	1.072	1.225
μ/mm^{-1}	2.096	2.333
F(000)	3236.0	1674.0
Crystal size/mm^3	0.595 × 0.492 × 0.327	0.659 × 0.237 × 0.128
Radiation	CuK_α (λ = 1.54184)	CuK_α (λ = 1.54184)
2Θ range for data collection/°	7.348 to 147.542	6.848 to 147.39
Index ranges	$-18 \le h \le 31$, $-16 \le k \le 15$, $-33 \le l \le 30$	$-23 \le h \le 21$, $-14 \le k \le 10$, $-23 \le l \le 23$
Reflections collected	33019	15447
Independent reflections	18024 [R_{int} = 0.0256, R_{sigma} = 0.0355]	8156 [R_{int} = 0.0207, R_{sigma} = 0.0271]
Data/restraints/parameters	18024/198/1017	8156/31/515
Goodness-of-fit on F^2	1.017	1.078
Final R indexes [I>=2σ (I)]	R_1 = 0.0548, wR_2 = 0.1458	R_1 = 0.0612, wR_2 = 0.1757
Final R indexes [all data]	R_1 = 0.0642, wR_2 = 0.1542	R_1 = 0.0636, wR_2 = 0.1792
Largest diff. peak/hole / e Å^{-3}	0.72/-0.64	1.39/-0.66

6.5.5 ^{1}H NMR Spectra

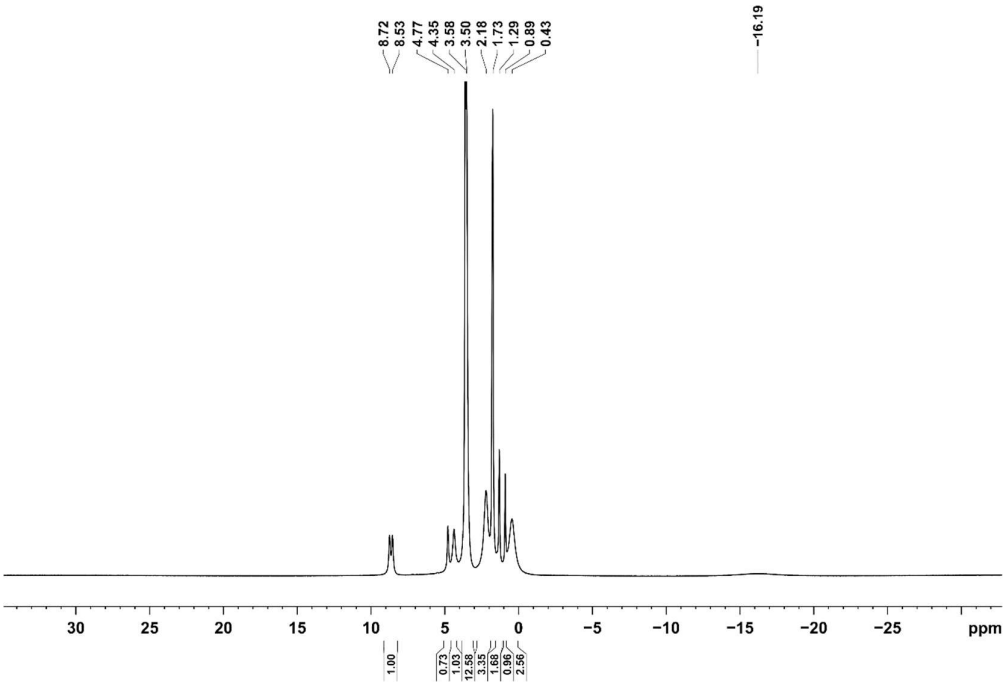

Figure S1. ^{1}H NMR spectrum (400.13 MHz, 300 K, THF-d_8) of **1**-[K([18]c-6)(thf)$_{0.5}$].

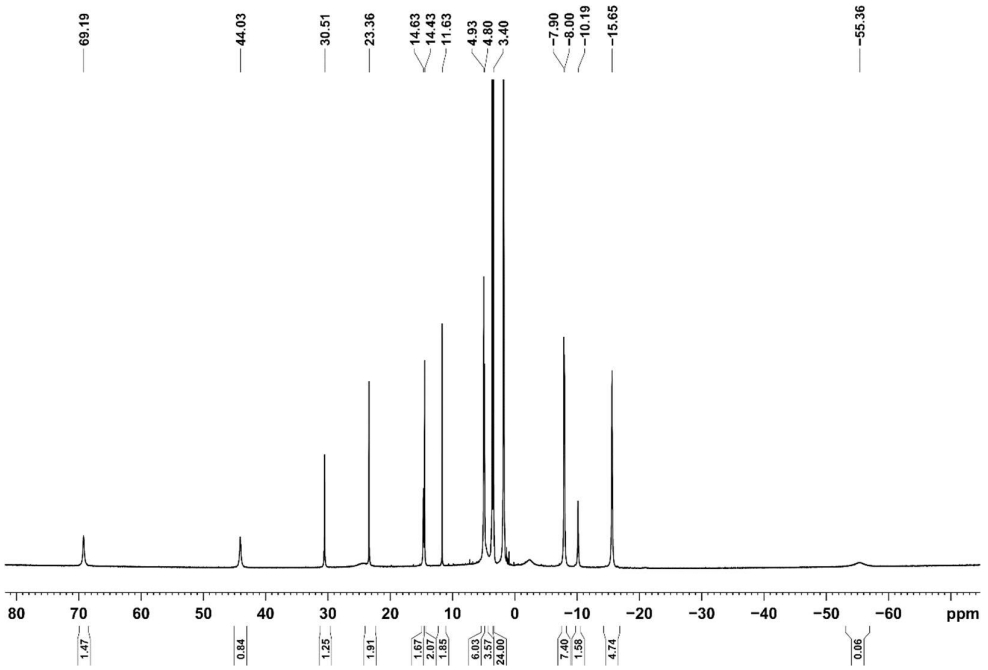

Figure S2. ^{1}H NMR spectrum (400.13 MHz, 300 K, THF-d_8) of **2**-[K([18]c-6)(thf)$_2$].

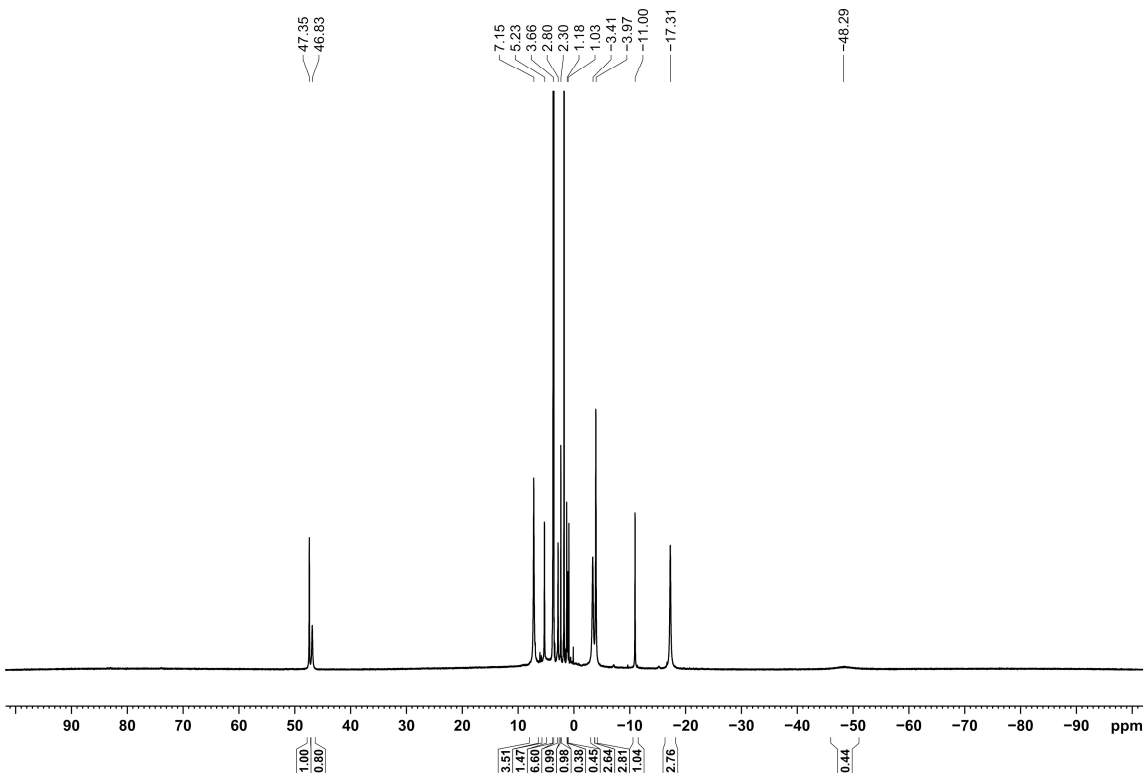

Figure S3. ^{1}H NMR spectrum (400.13 MHz, 300 K, THF-d$_8$) of **3**.

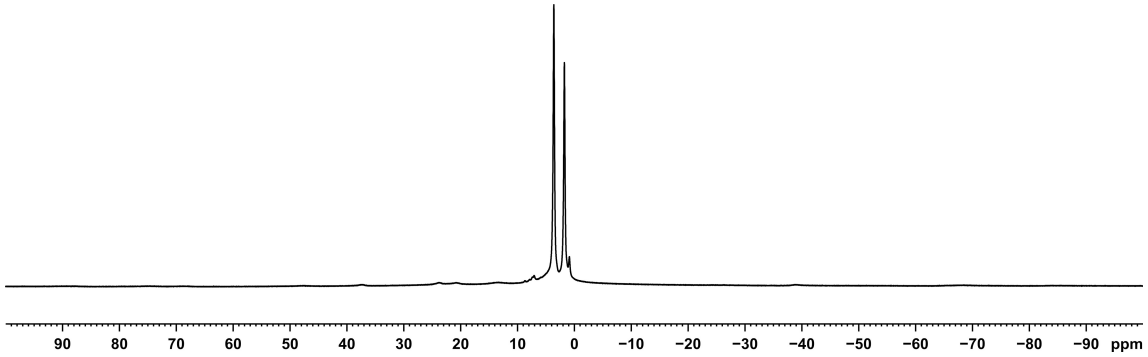

Figure S4. ^{1}H NMR spectrum (400.13 MHz, 300 K, THF-d$_8$) of **4**.

6.5.6 EPR Spectra

a) Sample **3-1**

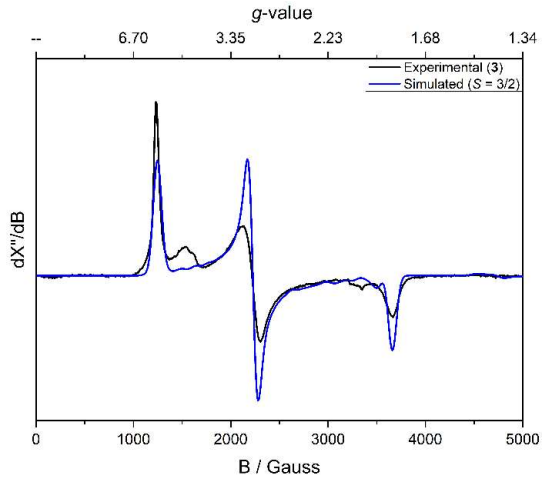

Figure S5. Experimental X-band EPR spectra of sample **3-1** ^{Me}THF glass at 20 K. Experimental parameters: Microwave frequency: 9.375682 GHz; Modulation amplitude: 4.000 G; Power: 0.6325 mW. Sample **3-1** can be simulated as a S = 3/2 species: g_{11} = 2.20, g_{22} = 2.12, g_{33} = 2.06, D = 20 cm^{-1}, E = 4.1 cm^{-1}, E/D = 0.20.

b) Complex **4**

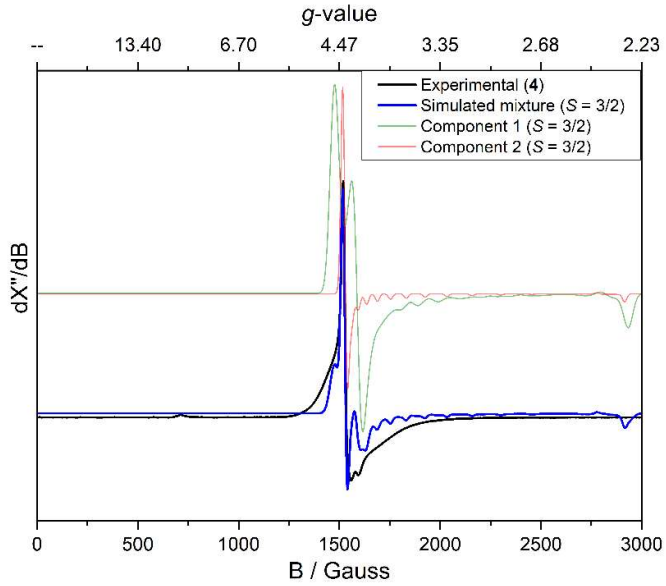

Figure S6. Experimental and simulated EPR spectrum (^{Me}THF, 80 K) of complex **4** using a S = 3/2 system.

6.5.7 UV-vis spectroscopy

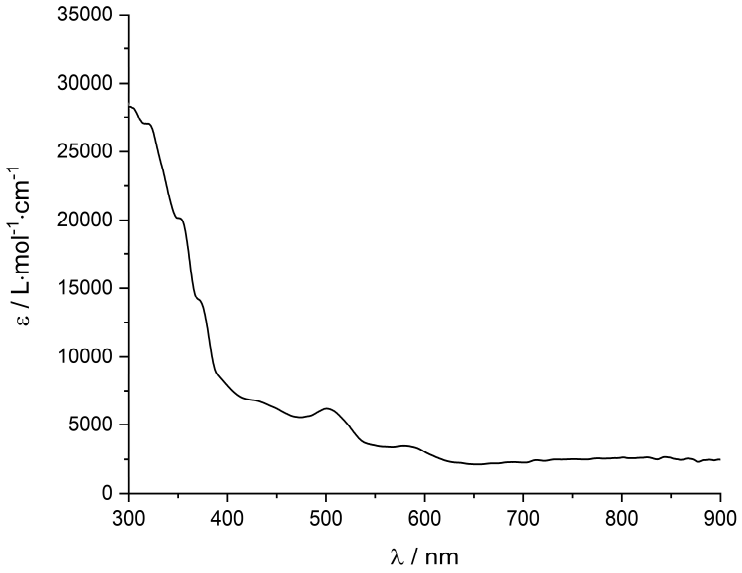

Figure S7. UV-vis spectrum of sample **3-1**.

6.5.8 Cyclic Voltammetry

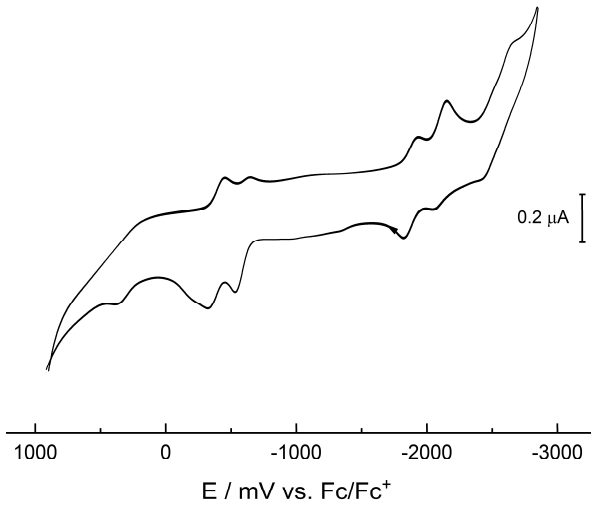

Figure S8. Cyclic voltammogram of sample **3-1** in THF/^{n}Bu$_4$NPF$_6$, scan rate: 100 mV s^{-1}

6.5.9 Catalytic Hydroboration

6.5.9.1 General Procedure

Under an atmosphere of argon, a 5 mL screw cap vial with a PTFE septum and magnetic stirrer was charged with the substrate (1.0 mmol). The iron catalyst was added as solution in 0.5 mL

THF, before HBpin (1.03 mmol) was added dropwise with a Hamilton syringe. The reaction mixture was stirred for 10 min and subsequently quenched with 10 mL diethylether in air. The formed boronic ester was hydrolyzed by addition of 1 mL 3 M NaOH and 1 mL 30% H_2O_2. The organic phase was separated and the aqueous phase extracted three times with diethylether. The collected organic phases were dried over Na_2SO_4, filtered and the solvent was removed. The crude products were purified by column chromatography on silica gel.

The alcohols of acetophenone, benzophenone and 2-octanol were not isolated, but quantified with GC-FID. Hence, the reduction was performed on a 0.2 mmol scale and with 20 µL *n*-pentadecane as internal standard.

6.5.9.2 Optimization of Reaction Conditions

Entry	Catalyst (mol%)	HBpin (equiv.)	Solvent (mL)	Time [min]	Yield (Conversion)
1	-	1.03	THF (0.1)	10	14 (14)
2	**1** (0.5)	-	THF (0.1)	10	0 (3)
3	**1** (0.5)	1.03	THF (0.1)	10	>99
4	***1 (0.1)***	***1.03***	***THF (0.1)***	***10***	***>99***
5	**1** (0.05)	1.03	THF (0.1)	10	71 (70)
6	**1** (0.01)	1.03	THF (0.1)	10	22 (21)
7	**1** (0.05)	1.38	THF (0.1)	10	38 (37)
8	**1** (0.05)	1.03	THF (0.1)	30	82 (81)
9	**1** (0.05)	1.03	THF (0.05)	10	75 (76)
10	**1** (0.05)	1.03	THF (0.05)	120	87 (89)
11	**1** (0.05)	1.03	THF (0.3)	10	25 (26)
12	**1** (0.05)	1.03	DME (0.1)	10	33 (34)
13	**2** (0.1)	1.03	THF (0.1)	10	>99
14	**3** (0.1)	1.03	THF (0.1)	10	68 (67)
15	**4** (0.1)	1.03	THF (0.1)	10	57 (55)

6.5.9.3 Isolated Hydroboration Products

6.5.9.3.1 Characterization

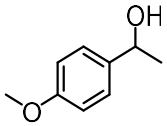

4-methoxy-α-methylbenzyl alcohol

$C_9H_{12}O_2$ 152.19 g mol^{-1}

almost colorless liquid

Yield 132.7 mg (0.87 mmol, 87%)

Solvent *n*-hexane/ethylacetate 5:1; R_f = 0.2

Column SiO_2, l=18cm, ⌀=2.5cm

^{1}H NMR (400.13 MHz, 300 K, $CDCl_3$) δ[ppm]: 7.27 (d, J = 8.5 Hz, 2H, CH_{Ar}), 6.87 (d, J = 8.7 Hz, 2H, CH_{Ar}), 4.82 (q, J = 6.4 Hz, 1H, CH), 3.79 (s, 3H, O-CH_3), 2.19 (br s, 1H, OH), 1.46 (d, J = 6.4 Hz, 3H, CH_3)

^{13}C{^{1}H}-NMR (100.6 MHz, 300 K, $CDCl_3$) δ[ppm]: 159.0, 138.2, 126.7, 113.9, 70.0, 55.3, 25.1

GC-MS t_R = 7.37 min, (EI, 70 eV): *m*/*z* = 152.1 [M$^+$]

HR-MS found: 152.08348 (calcd.: 152.08318)

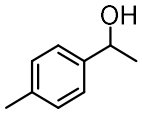

1-(*p*-tolyl)ethanol

$C_9H_{10}O$ 136.19 g mol^{-1}

colorless liquid

Yield 128.5 mg (0.96 mmol, 94%)

Solvent *n*-hexane/ethylacetate 5:1; R_f = 0.3

Column SiO_2, l=18cm, ⌀=2.5cm

^{1}H NMR (400.13 MHz, 300 K, $CDCl_3$) δ[ppm]: 7.27 (d, J = 8.1 Hz, 2H, CH_{Ar}), 7.17 (d, d, J = 8.0 Hz, 2H, CH_{Ar}), 4.84 (q, J = 6.4 Hz, 1H, CH), 2.51 (br s, 1H, OH), 2.38 (s, 3H, Ar-CH_3), 1.49 (d, J = 6.4 Hz, 3H, CH_3)

^{13}C{^{1}H}-NMR (100.6 MHz, 300 K, $CDCl_3$) δ[ppm]: 143.0, 137.0, 129.2, 125.4, 70.2, 25.1, 21.1

GC-MS t_R = 5.90 min, (EI, 70 eV): *m*/*z* = 136.1 [M$^+$]

HR-MS found: 136.0881 (calcd.: 136.08827)

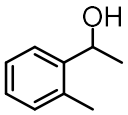

2-methyl-α-methylbenzyl alcohol

$C_9H_{12}O$ 136.19 g mol^{-1}

colorless liquid

Yield 120.0 mg (0.88 mmol, 89%)

Solvent *n*-hexane/ethylacetate 5:1; R_f = 0.25

Column SiO_2, l=18cm, ⌀=2.5cm

^{1}H NMR (400.13 MHz, 300 K, $CDCl_3$) δ[ppm]: 7.51 (d, J = 7.9 Hz, 1H, CH_{Ar}), 7.25 (ps t, J = 7.9 Hz, 1H, CH_{Ar}), 7.5 (ps t, J = 7.5 Hz, 1H, CH_{Ar}), 7.25 (d, J = 7.0 Hz, 1H, CH_{Ar}),), 5.09 (q, J = 6.4 Hz, 1H, CH), 2.52 (br s, 1H, OH), 2.35 (s, 3H, Ar-CH_3), 1.46 (d, J = 6.4 Hz, 3H, CH_3)

^{13}C{^{1}H}-NMR (100.6 MHz, 300 K, $CDCl_3$) δ[ppm]: 144.0, 134.2, 130.4, 127.1, 126.4, 124.6, 66.7, 23.9, 18.9

GC-MS t_R = 6.07 min, (EI, 70 eV): *m*/*z* = 136.1 [M^+]

HR-MS found: 136.08858 (calcd.: 136.08827)

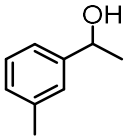

3-methyl-α-methylbenzyl alcohol

$C_9H_{12}O$ 136.19 g mol^{-1}

colorless liquid

Yield 133.2 mg (0.98 mmol, 98%)

Solvent *n*-hexane/ethylacetate 5:1; R_f = 0.18

Column SiO_2, l=20cm, ⌀=2.5cm

^{1}H NMR (400.13 MHz, 300 K, $CDCl_3$) δ[ppm]: 7.26 (t, J = 7.5 Hz, 1H, CH_{Ar}), 7.18 (t, J = 7.5 Hz, 2H, CH_{Ar}), 7.11 (d, J = 7.4 Hz, 1H, CH_{Ar}), 4.84 (q, J = 6.5 Hz, 1H, CH), 2.37 (s, 3H, Ar-CH_3), 2.36 (br s, 1H, OH), 1.49 (d, J = 6.5 Hz, 3H, CH_3)

^{13}C{^{1}H}-NMR (100.6 MHz, 300 K, $CDCl_3$) δ[ppm]: 145.9, 138.1, 128.4, 126.2, 122.5, 70.4, 25.2, 21.5

GC-MS t_R = 5.887 min, (EI, 70 eV): m/z = 136.1 [M^+]

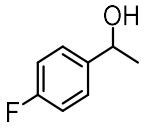

4-fluoro-α-methylbenzyl alcohol

C_8H_9OF 140.16 g mol^{-1}

colorless liquid

Yield 124.0 mg (0.89 mmol, 88%)

Solvent n-hexane/ethylacetate 5:1; R_f = 0.1

Column SiO_2, l=18cm, ⌀=2.5cm

^{1}H NMR (400.13 MHz, 300 K, $CDCl_3$) δ[ppm]: 7.26 (m, 2H, CH_{Ar}), 6.97 (m, 2H, CH_{Ar}), 4.78 (q, J = 6.4 Hz, 1H, CH), 2.64 (br s, 1H, OH), 1.40 (d, J = 6.7 Hz, 3H, CH_3)

^{13}C{^{1}H}-NMR (100.6 MHz, 300 K, $CDCl_3$) δ[ppm]: 162.1 (d, $^1J_{C-F}$ = 245 Hz), 141.6 (d, $^2J_{C-F}$ = 21.3 Hz), 127.1 (d, $^3J_{C-F}$ = 8.1 Hz), 115.2 (d, $^4J_{C-F}$ = 3.1 Hz), 69.7, 25.3

^{19}F-NMR (376.7 MHz, 300 K, $CDCl_3$) δ[ppm]: -116 (m)

GC-MS t_R = 5.03 min, (EI, 70 eV): m/z = 140.1 [M^+]

HR-MS found: 1.40.06300 (calcd.: 140.06319)

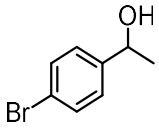

4-bromo-α-methylbenzyl alcohol

C_8H_9BrO 201.06 g mol^{-1}

colorless liquid

Yield 192.3 mg (0.96 mmol, 96%)

Solvent N-hexane/ethylacetate 5:1; R_f = 0.25

Column SiO_2, l=18cm, ⌀=2.5cm

^{1}H NMR (400.13 MHz, 300 K, $CDCl_3$) δ[ppm]: 7.45 (d, J = 8.4 Hz, 2H, CH_{Ar}), 7.22 (d, J = 8.4 Hz, 2H, CH_{Ar}), 4.81 (q, J = 6.6 Hz, 1H, CH), 2.17 (br s, 1H, OH), 1.45 (d, J = 6.5 Hz, 3H, CH_3)

^{13}C{^{1}H}-NMR (100.6 MHz, 300 K, $CDCl_3$) δ[ppm]: 144.9, 131.6, 127.3, 121.2, 69.8, 25.3

GC-MS t_R = 7.72 min, (EI, 70 eV): m/z = 200.0 [M^+]

HR-MS found: 199.98351 (calcd.: 199.98313)

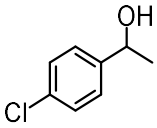

4-chloro-α-methylbenzyl alcohol

C_8H_9ClO 156.61 g mol^{-1}

colorless liquid

Yield 145.0 mg (0.93 mmol, 93%)

Solvent *n*-hexane/ethylacetate 5:1; R_f = 0.18

Column SiO_2, l=18cm, ⌀=2.5cm

^{1}H NMR (400.13 MHz, 300 K, $CDCl_3$) δ[ppm]: 7.28 (m, 4H, CH_{Ar}), 4.83 (q, J = 6.6 Hz, 1H, CH), 2.28 (br s, 1H, OH), 1.44 (d, J = 6.5 Hz, 3H, CH_3)

^{13}C{^{1}H}-NMR (100.6 MHz, 300 K, $CDCl_3$) δ[ppm]: 144.3, 133.1, 128.7, 126.9, 69.8, 25.3

GC-MS t_R = 6.871 min, (EI, 70 eV): *m*/*z* = 156.0 [M^+]

HR-MS found: 156.03373 (calcd.: 156.03364)

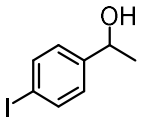

4-iodo-α-methylbenzyl alcohol

C_8H_9IO 248.06 g mol^{-1}

colorless liquid

Yield 225.5 mg (0.91 mmol, 91%)

Solvent *n*-hexane/ethylacetate 5:2; R_f = 0.4

Column SiO_2, l=27cm, ⌀=2.5cm

^{1}H NMR (400.13 MHz, 300 K, $CDCl_3$) δ[ppm]: 7.63 (d, J = 8.1 Hz, 2H, CH_{Ar}), 7.06 (d, J = 8.3 Hz, 2H, CH_{Ar}), 4.76 (q, J = 6.4 Hz, 1H, CH), 2.66 (br s, 1H, OH), 1.41 (d, J = 6.5 Hz, 3H, CH_3)

^{13}C{^{1}H}-NMR (100.6 MHz, 300 K, $CDCl_3$) δ[ppm]: 145.5, 137.5, 127.5, 92.7, 69.7, 25.2

GC-MS t_R = 8.70 min, (EI, 70 eV): *m*/*z* = 248.0 [M^+]

HR-MS found: 247.96902 (calcd.: 247.96926)

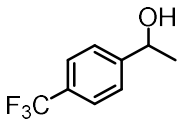

4-trifluoromethyl-α-methylbenzyl alcohol

$C_9H_9F_3O$ 190.17 g mol^{-1}

colorless liquid

Yield 162.0 mg (0.85 mmol, 86%)

Solvent *n*-hexane/ethylacetate 5:1; R_f = 0.25

Column SiO_2, l=18cm, ⌀=2.5cm

^{1}H NMR (400.13 MHz, 300 K, $CDCl_3$) δ[ppm]: 7.58 (d, J = 8.2 Hz, 2H, CH_{Ar}), 7.45 (d, J = 8.0 Hz, 2H, CH_{Ar}), 4.92 (q, J = 6.4 Hz, 1H, CH), 2.43 (br s, 1H, OH), 1.47 (d, J = 6.4 Hz, 3H, CH_3)

^{13}C{^{1}H}-NMR (100.6 MHz, 300 K, $CDCl_3$) δ[ppm]: 149.9, 129.7 (q, $^1J_{C-F}$ = 33 Hz), 125.8, 125.5 (q, $^2J_{C-F}$ = 4 Hz), 122.9, 69.9, 25.4

^{19}F-NMR (376.7 MHz, 300 K, $CDCl_3$) δ[ppm]: -63.0 (s, CF_3)

GC-MS t_R = 5.36 min, (EI, 70 eV): *m*/*z* = 190.1 [M$^+$]

HR-MS found: 190.06024 (calcd.: 190.0600)

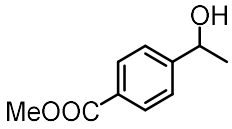

4-methylbenzoate-α-methylbenzyl alcohol

$C_{10}H_{12}O_3$ 180.20 g mol^{-1}

colorless liquid

Yield 168.1 mg (0.93 mmol, 93%)

Solvent *n*-hexane/ethylacetate 5:1; R_f = 0.13

Column SiO_2, l=13cm, ⌀=3cm

^{1}H NMR (400.13 MHz, 300 K, $CDCl_3$) δ[ppm]: 7.94 (d, J = 8.3 Hz, 2H, CH_{Ar}), 7.38 (d, J = 8.2 Hz, 2H, CH_{Ar}), 4.8 (q, J = 6.5 Hz, 1H, CH), 2.16 (br m, 1H, OH), 1.49 (d, J = 6.5 Hz, 3H, CH_3)

^{13}C{^{1}H}-NMR (100.6 MHz, 300 K, $CDCl_3$) δ[ppm]: 150.2, 134.0, 126.5, 112.7, 70.0, 40.8, 24.8

GC-MS t_R = 9.13 min, (EI, 70 eV): *m*/*z* = 180.1 [M$^+$]

HR-MS found: 180.07777 (calcd.:180.07810)

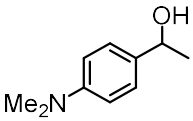

4-dimethylamino-α-methylbenzyl alcohol

$C_{10}H_{15}NO$ 165.24 g mol^{-1}

colorless liquid

Yield 135.0 mg (0.82 mmol, 80%)

Solvent *n*-hexane/ethylacetate 5:1; R_f = 0.15

Column SiO_2, l=14cm, ⌀=3cm

^{1}H NMR (400.13 MHz, 300 K, $CDCl_3$) δ[ppm]: 7.26 (d, J = 8.7 Hz, 2H, CH_{Ar}), 6.74 (d, J = 8.7 Hz, 2H, CH_{Ar}), 4.80 (q, J = 6.5 Hz, 1H, CH), 2.16 (br m, 1H, OH), 1.49 (d, J = 6.5 Hz, 3H, CH_3)

^{13}C{^{1}H}-NMR (100.6 MHz, 300 K, $CDCl_3$) δ[ppm]: 150.2, 134.0, 126.5, 112.7, 70.0, 40.8, 24.8

GC-MS t_R = 7.68 min, (EI, 70 eV)

HR-MS found: 166.1227 $(M+H)^+$ (calcd.: 166.1226 $(M+H)^+$)

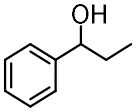

1-phenylpropran-1-ol

$C_9H_{12}O$ 136.19 g mol^{-1}

colorless liquid

Yield 145.0 mg (0.93 mmol, 93%)

Solvent *n*-hexane/ethylacetate 5:1; R_f = 0.3

Column SiO_2, l=20cm, ⌀=2.5cm

^{1}H NMR (400.13 MHz, 300 K, $CDCl_3$) δ[ppm]: 7.35 (m, 4H, CH_{Ar}), 7.28 (m, 1H, CH_{Ar}), 4.83 (m, 1H, CH), 2.26 (br s, 1H, OH), 1.78 (m, 2H, CH_2), 0.92 (t, J = 7.4 Hz, 3H, CH_3)

^{13}C{^{1}H}-NMR (100.6 MHz, 300 K, $CDCl_3$) δ[ppm]: 144.7, 128.4, 127.5, 126.1, 76.0, 31.9, 10.2

GC-MS t_R = 5.81 min, (EI, 70 eV): *m*/*z* = 136.1 $[M^+]$

HR-MS found: 136.08835 (calcd.: 136.08827)

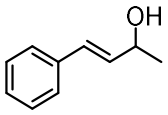

4-phenyl-but-3-en-2-ol

$C_{10}H_{12}O$ 148.18 g mol^{-1}

colorless liquid

Yield 122.2 mg (0.83 mmol, 83%)

Solvent *n* -hexane/ethylacetate 5:1; R_f = 0.18

Column SiO_2, l=20cm, ⌀=2.5cm

^{1}H NMR (400.13 MHz, 300 K, $CDCl_3$) δ[ppm]: 7.39 (m, 2H, CH_{Ar}), 7.33 (m, 2H, CH_{Ar}), 7.25 (m, 2H, CH_{Ar}), 6.57 (d, J = 16 Hz, 1H, CH_{Alkene}), 6.57 (dd, J = 6.6 Hz, 16 Hz, 1H, CH_{Alkene}), 4.49 (ps pent, J = 6.4 Hz, 1H, CH), 2.09 (br s, 1H, OH), 1.38 (d, J = 6.4 Hz, 3H, CH_3)

^{13}C{^{1}H}-NMR (100.6 MHz, 300 K, $CDCl_3$) δ[ppm]: 136.8, 133.7, 129.4, 128.7, 127.7, 126.5, 68.9, 23.5

GC-MS t_R = 7.47 min, (EI, 70 eV): *m*/*z* = 148.1 [M^+]

HR-MS found: 148.08862 (calcd.: 148.08827)

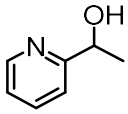

1-(pyridin-2-yl)-ethan-1-ol

C_7H_9NO 123.16 g mol^{-1}

colorless liquid

Yield 85.3 mg (0.69 mmol, 69%)

Solvent *n*-hexane/ethylacetate 5:2; R_f = 0.08

Column SiO_2, l=20cm, ⌀=2.5cm

^{1}H NMR (400.13 MHz, 300 K, $CDCl_3$) δ[ppm]: 8.45 (m, 1H, CH_{Ar}), 7.62 (t, J = 7.8 Hz, 1H, CH_{Ar}), 7.25 (t, J = 8.2 Hz, 2H, CH_{Ar}), 7.12 (m, J = 7.4 Hz, 1H, CH_{Ar}), 4.83 (q, J = 6.6 Hz, 1H, CH), 4.37 (br s, 1H, OH), 1.44 (d, J = 6.5 Hz, 3H, CH_3)

^{13}C{^{1}H}-NMR (100.6 MHz, 300 K, $CDCl_3$) δ[ppm]: 163.4, 148.2, 136.9, 122.2, 119.9, 69.1, 24.3

GC-MS t_R = 4.965 min, (EI, 70 eV)

HR-MS found: 123.06769 (calcd.: 123.06787)

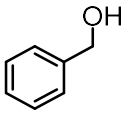

Benzyl alcohol

C_7H_8O 108.14 g mol^{-1}

colorless liquid

Yield 94.1 mg (0.87 mmol, 87%)

Solvent *n*-hexane/ethylacetate 5:1; R_f = 0.15

Column SiO_2, l=13cm, ⌀=3cm

^{1}H NMR (400.13 MHz, 300 K, $CDCl_3$) δ[ppm]: 7.4-7.28 (m, 5H, CH_{Ar}), 4.63 (s, 2H, CH_2), 2.47 (br s, 1H, OH)

^{13}C{^{1}H}-NMR (100.6 MHz, 300 K, $CDCl_3$) δ[ppm]: 141.0, 128.6, 127.6, 127.1, 65.2

GC-MS t_R = 4.58 min, (EI, 70 eV): *m*/*z* = 108.1 [M$^+$]

HR-MS found: 108.05666 (calcd.: 108.05697)

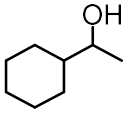

1-cyclohexylethan-1-ol

$C_8H_{16}O$ 128.22 g mol^{-1}

colorless liquid

Yield 99.0 mg (0.77 mmol, 79%)

Solvent *n*-hexane/ethylacetate 10:1;

Column SiO_2, l=12cm, ⌀=3cm

^{1}H NMR (400.13 MHz, 300 K, $CDCl_3$) δ[ppm]: 3.51 (quint, J = 6.2 Hz, 1H, CH), 2.16 (m, 1H), 1.73 (m, 2H), 1.64 (m, 3H), 1.23 (m, 3H), 1.12 (d, J = 6.5 Hz, 3H, CH_3), 0.97 (m, 2H)

^{13}C{^{1}H}-NMR (100.6 MHz, 300 K, $CDCl_3$) δ[ppm]: 72.3, 45.2, 28.7, 28.5, 26.6, 26.3, 26.3, 26.2, 20.4

GC-MS t_R = 4.72 min, (EI, 70 eV): *m*/*z* = 127.1 [M$^+$]

6.5.8.3.2 NMR spectra

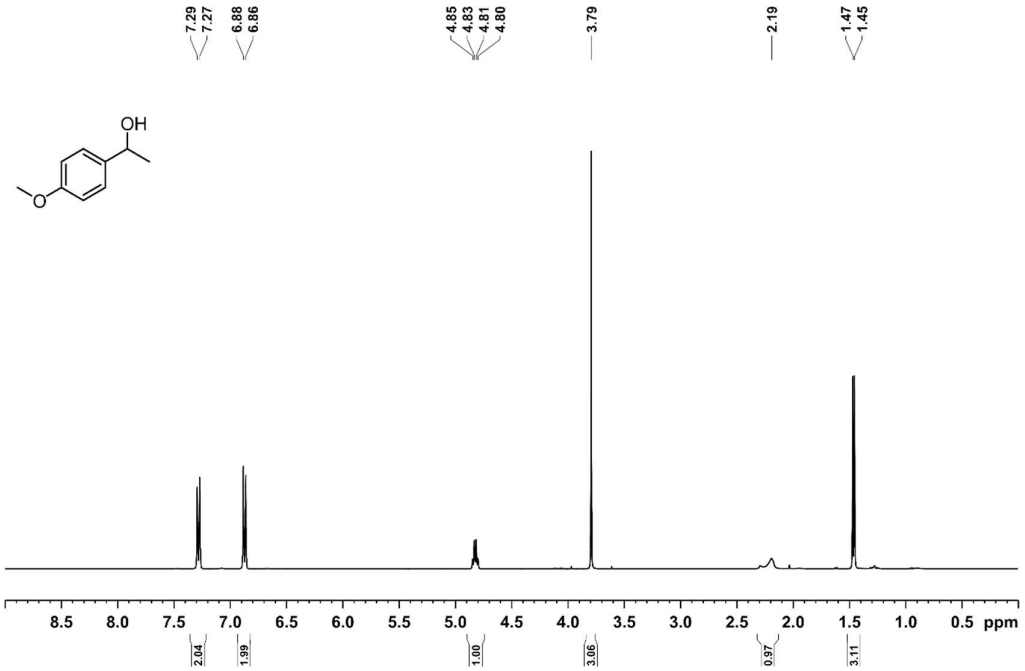

Figure S9. ^{1}H NMR spectrum (400.13 MHz, 300 K, $CDCl_3$) of 4-methoxy-α-methylbenzyl alcohol.

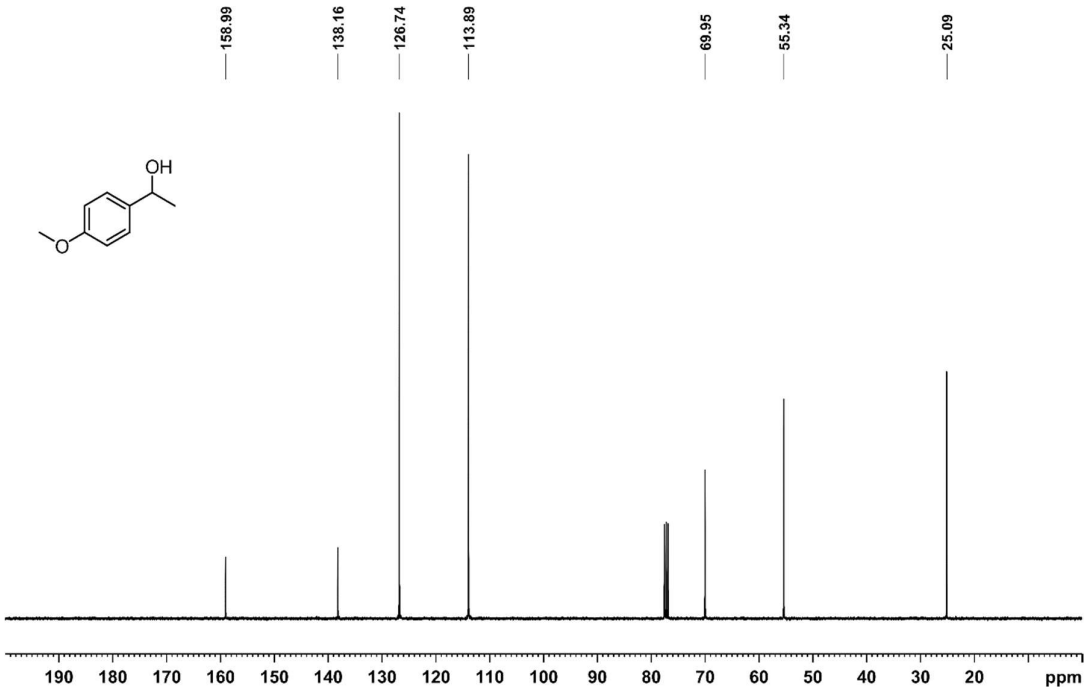

Figure S10. $^{13}C\{^{1}H\}$ NMR spectrum (100.6 MHz, 300 K, $CDCl_3$) of 4-methoxy-α-methylbenzyl alcohol.

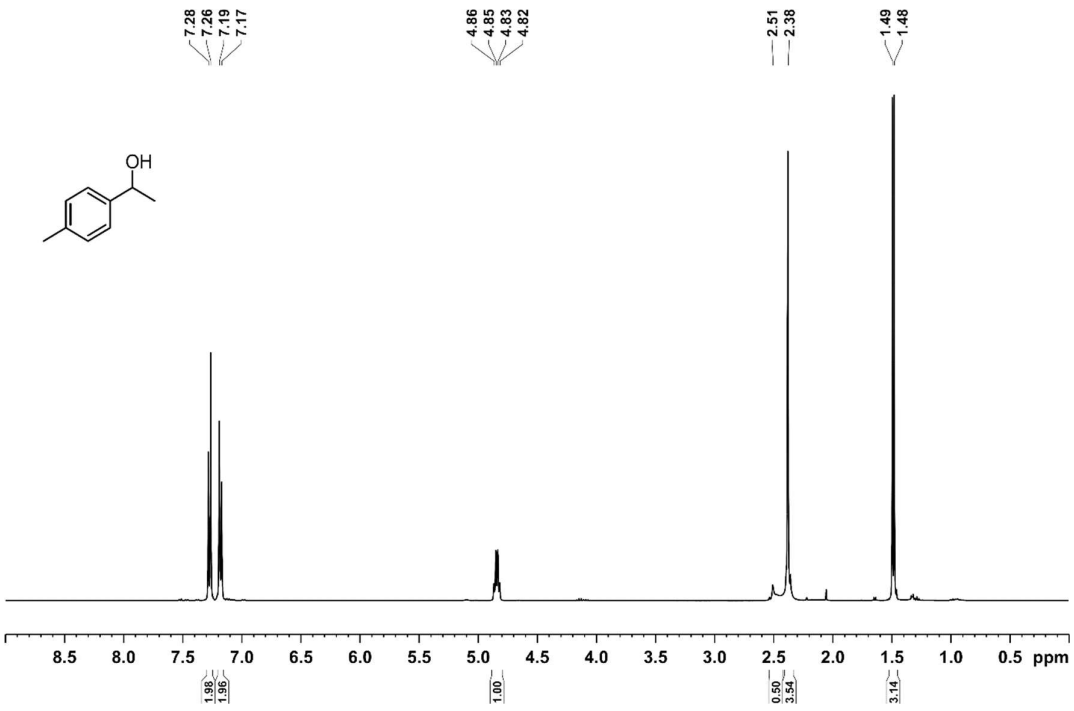

Figure S11. ^{1}H NMR spectrum (400.13 MHz, 300 K, $CDCl_3$) of 4-methyl-α-methylbenzyl alcohol.

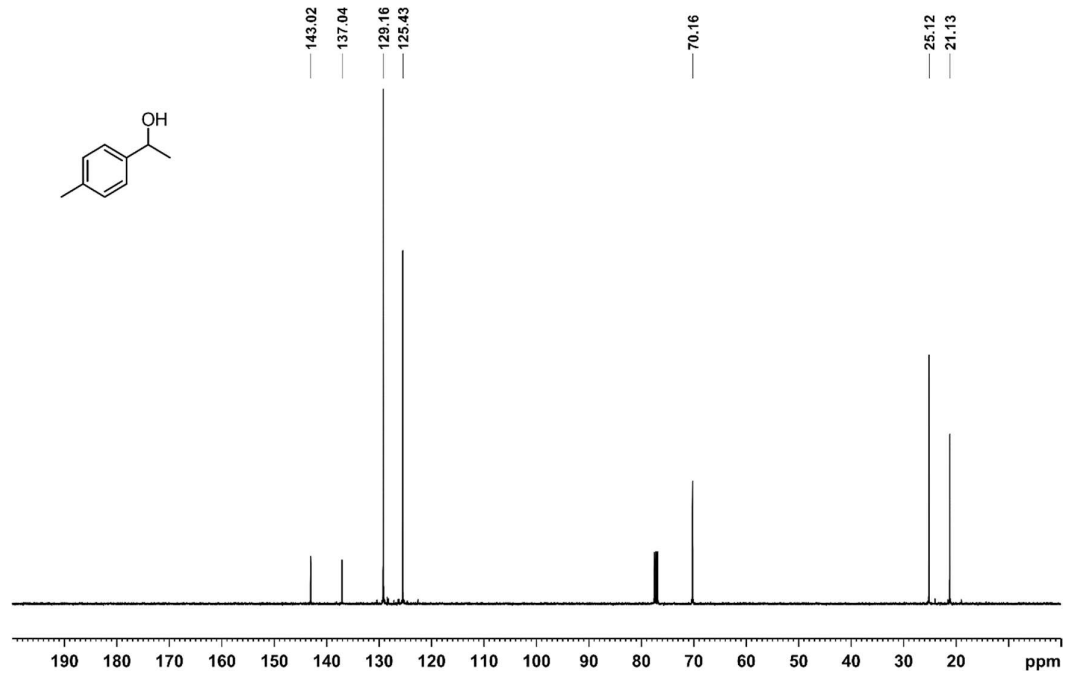

Figure S12. $^{13}C\{^{1}H\}$ NMR spectrum (100.6 MHz, 300 K, $CDCl_3$) of 4-methyl-α-methylbenzyl alcohol.

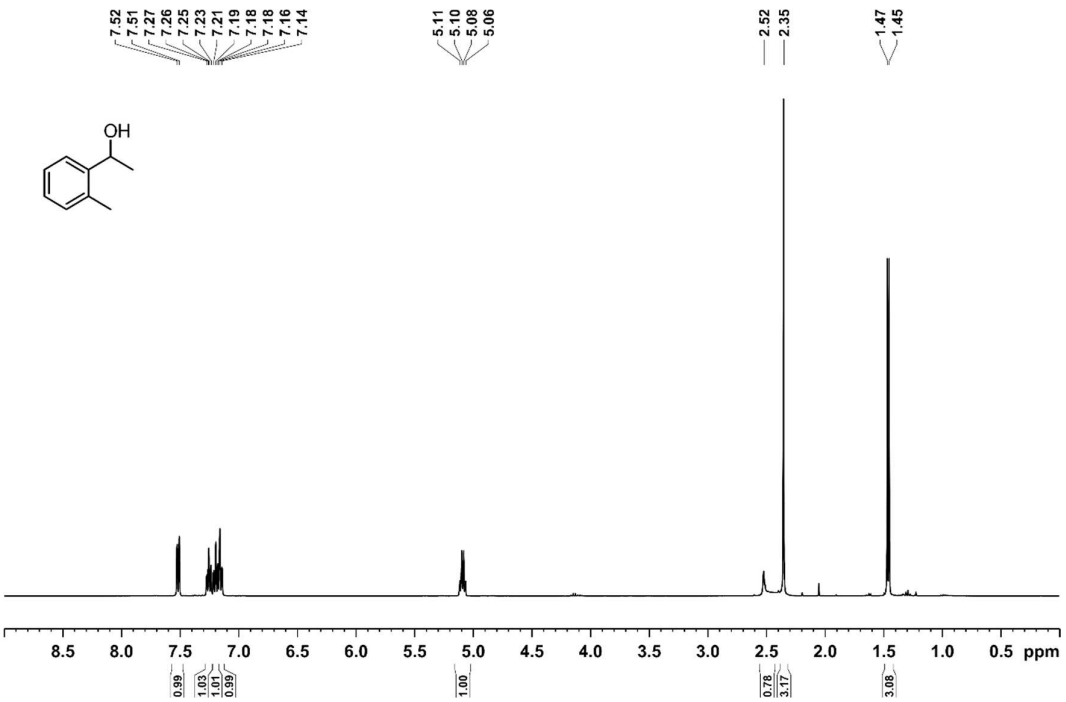

Figure S13. ^{1}H NMR spectrum (400.13 MHz, 300 K, $CDCl_3$) of 2-methyl-α-methylbenzyl alcohol.

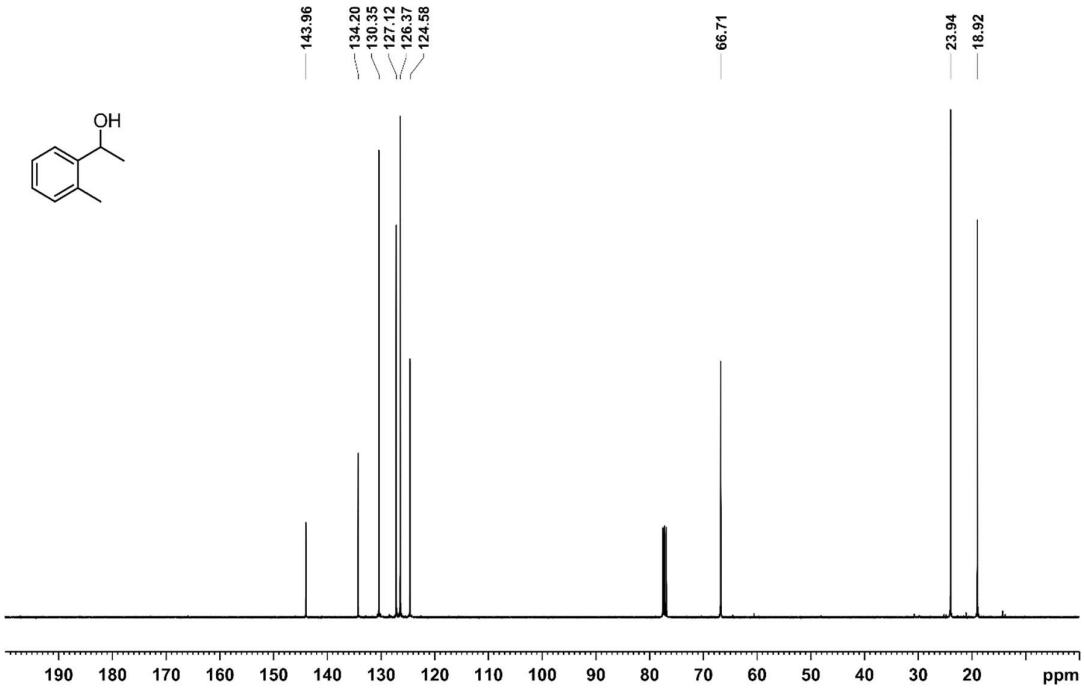

Figure S14. $^{13}C\{^{1}H\}$-NMR spectrum (100.6 MHz, 300 K, $CDCl_3$) of 2-methyl-α-methylbenzyl alcohol.

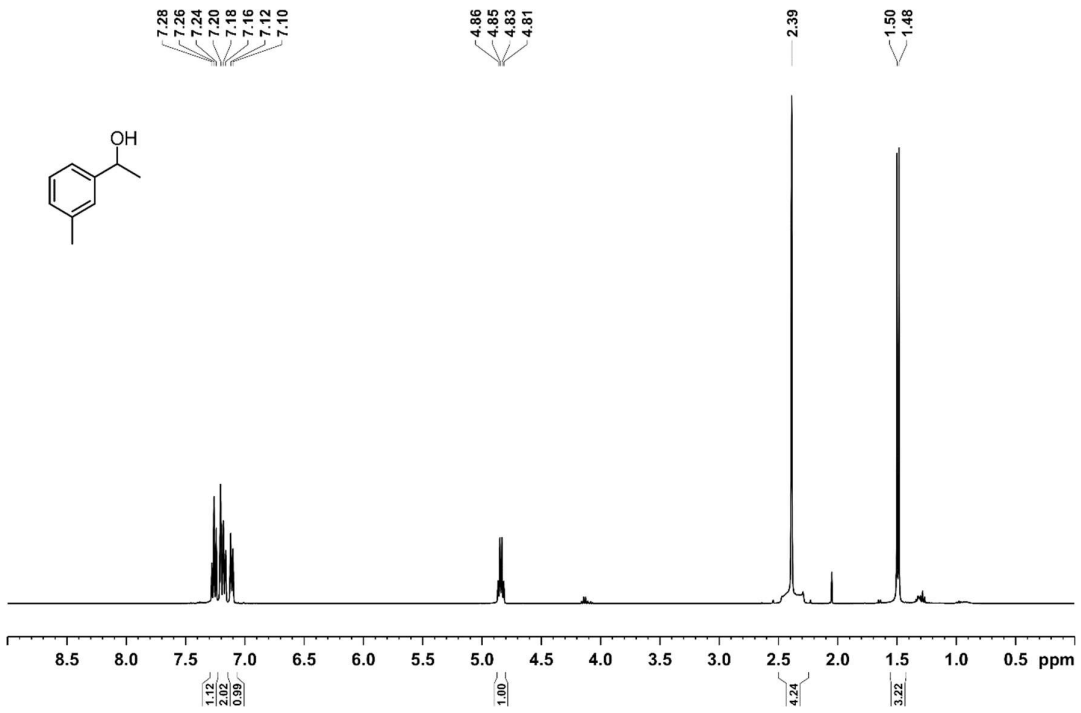

Figure S15. ^{1}H NMR spectrum (400.13 MHz, 300 K, $CDCl_3$) of 3-methyl-α-methylbenzyl alcohol.

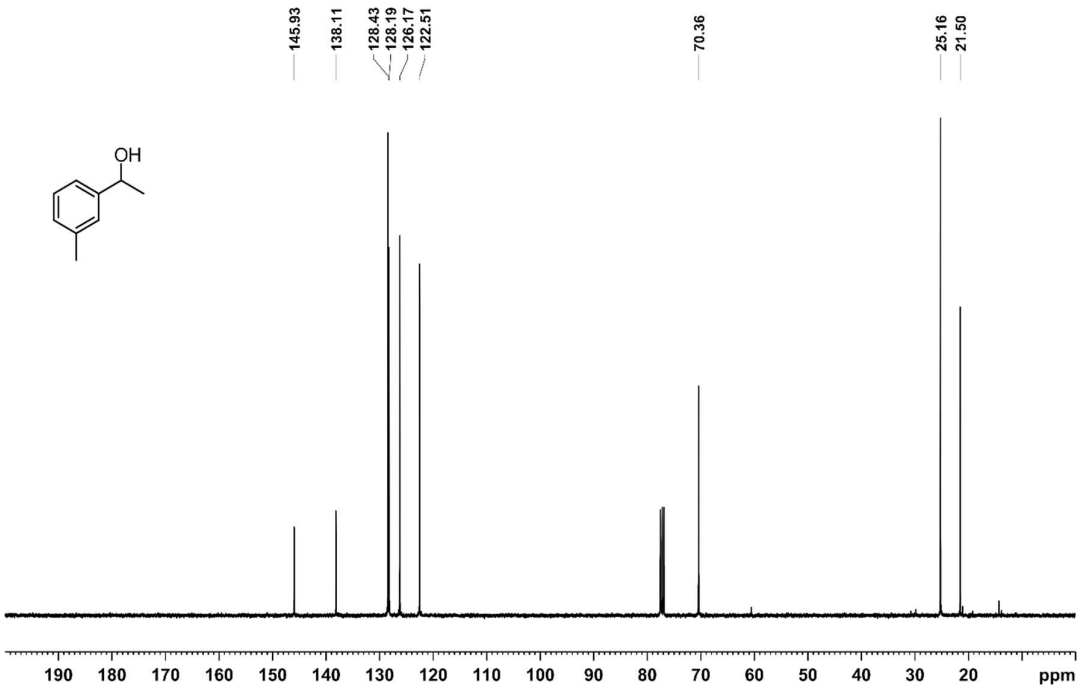

Figure S16. $^{13}C\{^{1}H\}$ NMR spectrum (100.6 MHz, 300 K, $CDCl_3$) of 3-methyl-α-methylbenzyl alcohol.

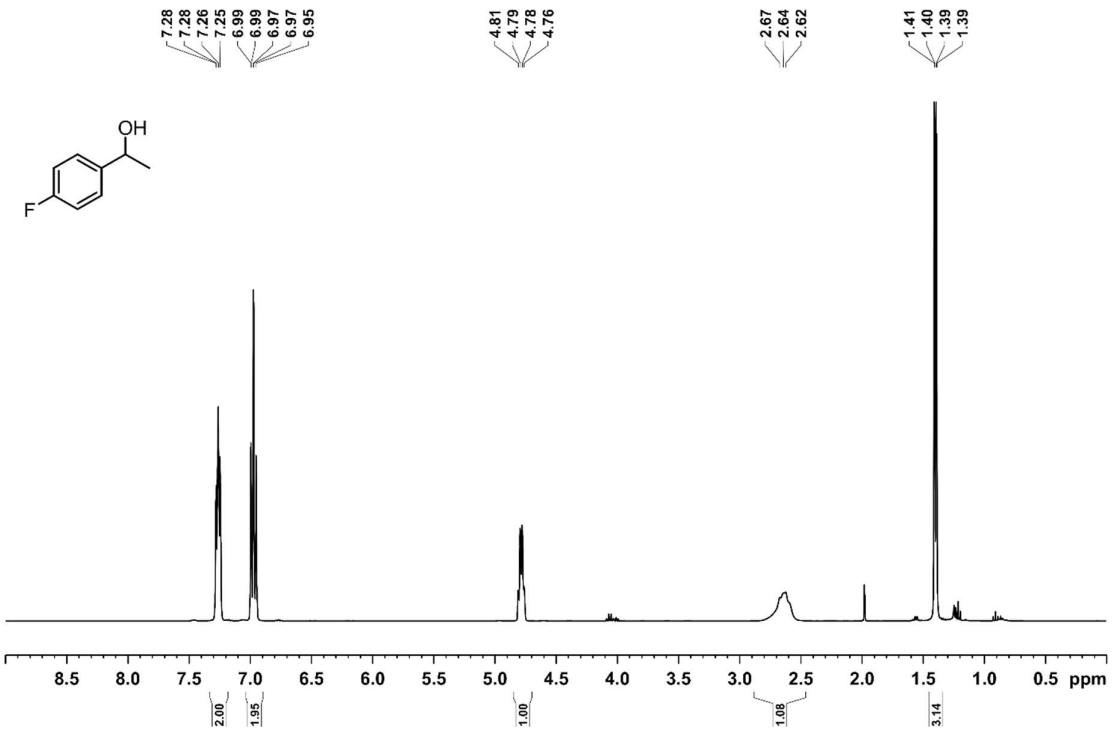

Figure S17. ^{1}H NMR spectrum (400.13 MHz, 300 K, $CDCl_3$) of 4-fluoro-α-methylbenzyl alcohol.

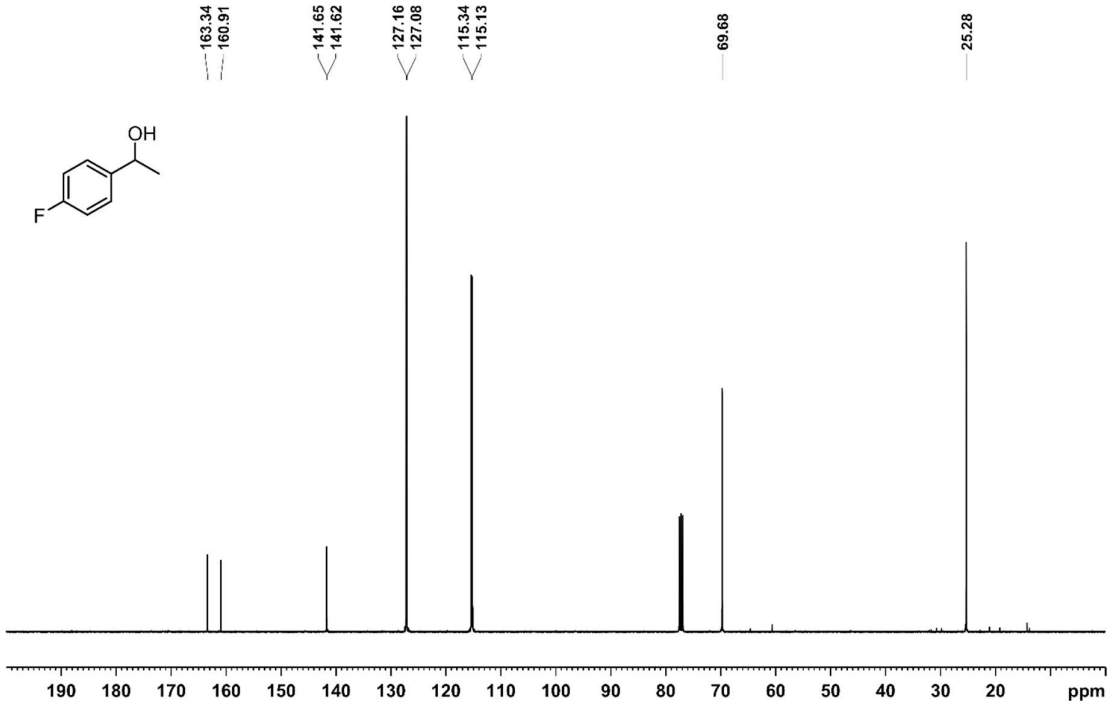

Figure S18. $^{13}C\{^{1}H\}$ NMR spectrum (100.6 MHz, 300 K, $CDCl_3$) of 4-fluoro-α-methylbenzyl alcohol.

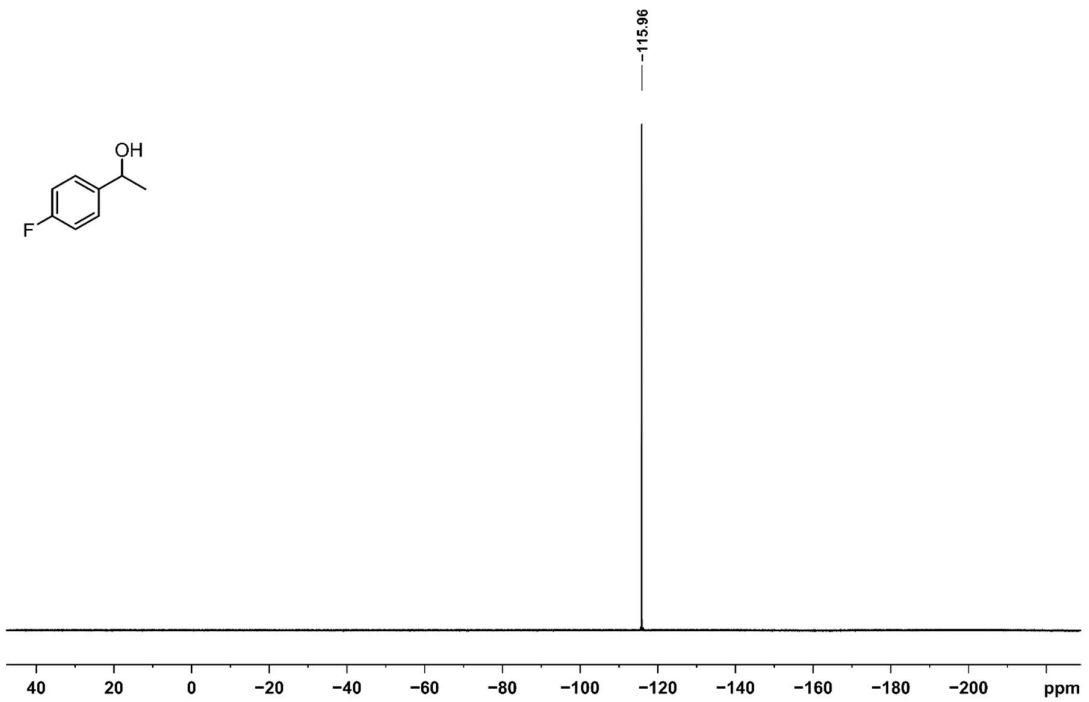

Figure S19. ^{19}F NMR spectrum (376.7 MHz, 300 K, $CDCl_3$) of 4-fluoro-α-methylbenzyl alcohol.

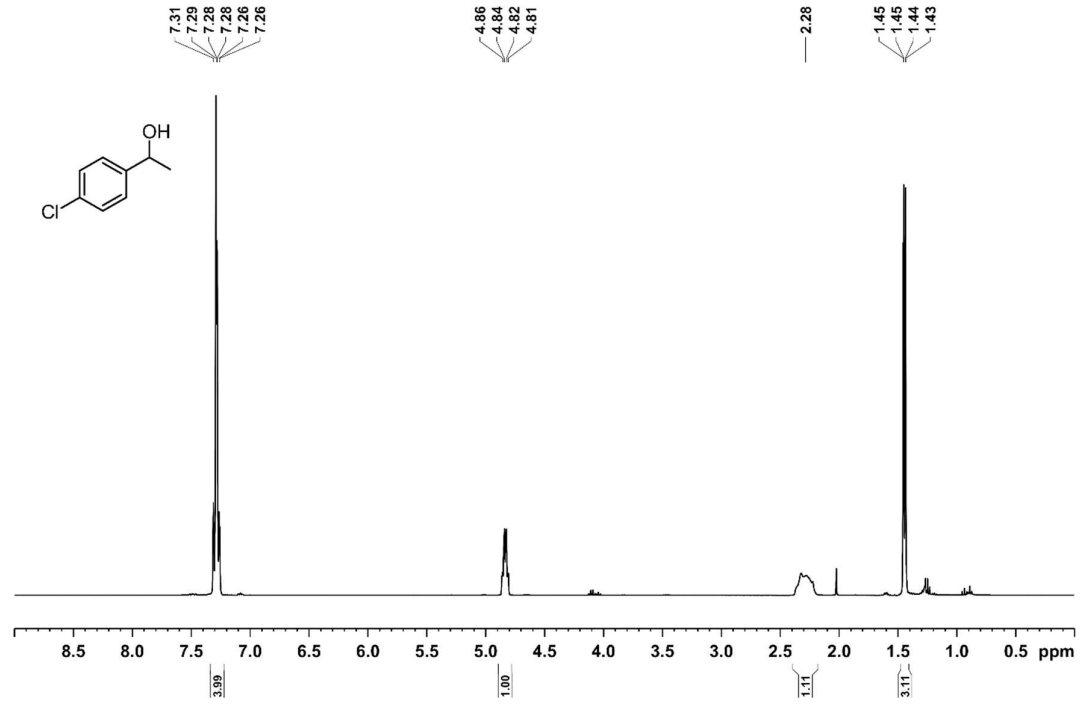

Figure S20. ^{1}H NMR spectrum (400.13 MHz, 300 K, $CDCl_3$) of 4-chloro-α-methylbenzyl alcohol.

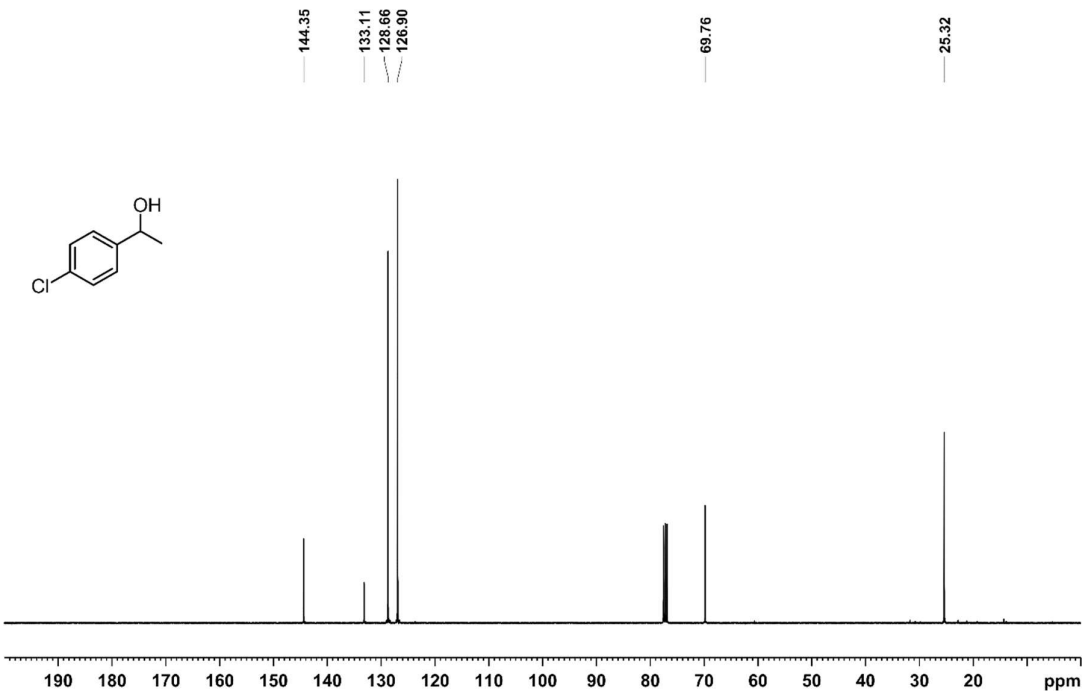

Figure S21. $^{13}C\{^{1}H\}$ NMR spectrum (100.6 MHz, 300 K, $CDCl_3$) of 4-chloro-α-methylbenzyl alcohol.

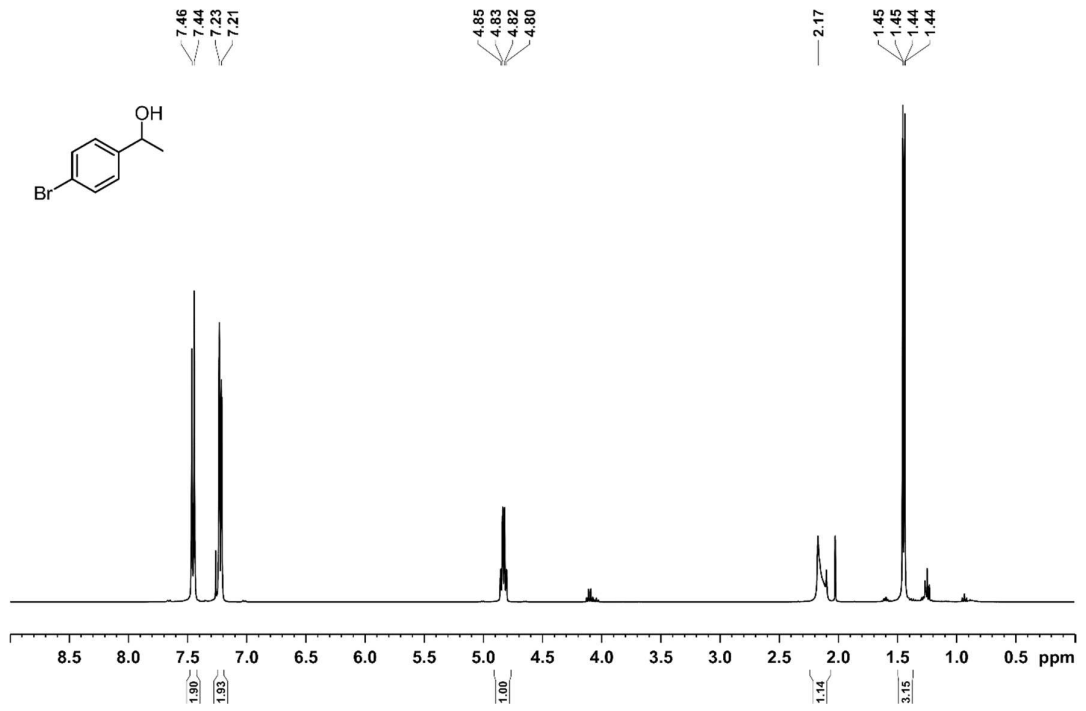

Figure S22. ^{1}H NMR spectrum (400.13 MHz, 300 K, $CDCl_3$) of 4-bromo-α-methylbenzyl alcohol.

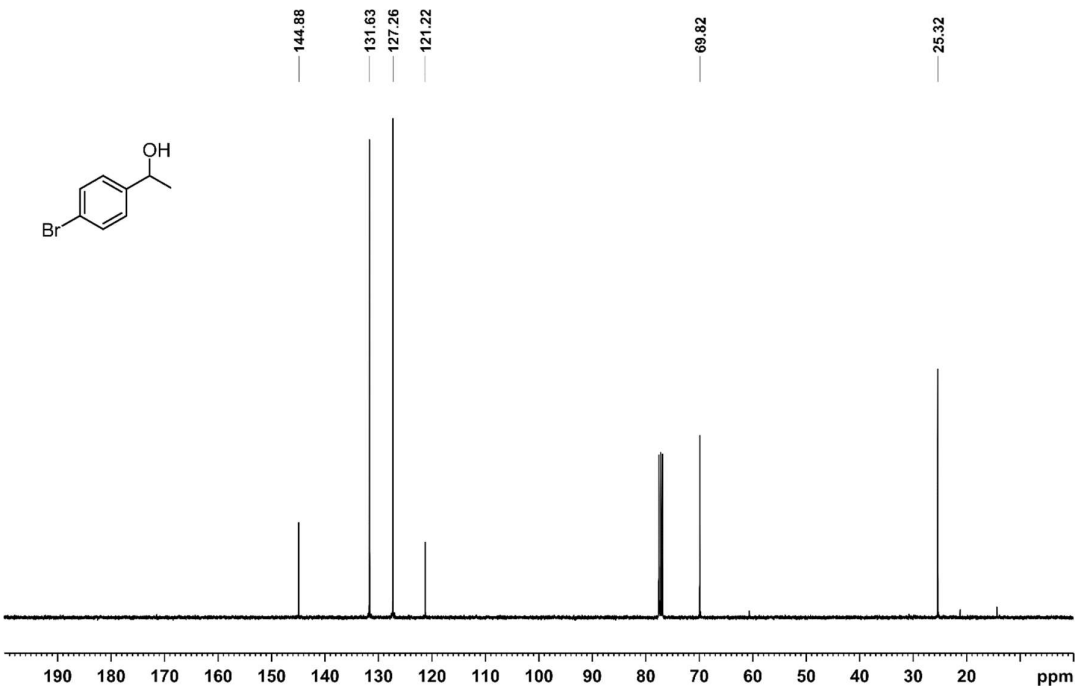

Figure S23. $^{13}C\{^{1}H\}$ NMR spectrum (100.6 MHz, 300 K, $CDCl_3$) of 4-bromo-α-methylbenzyl alcohol.

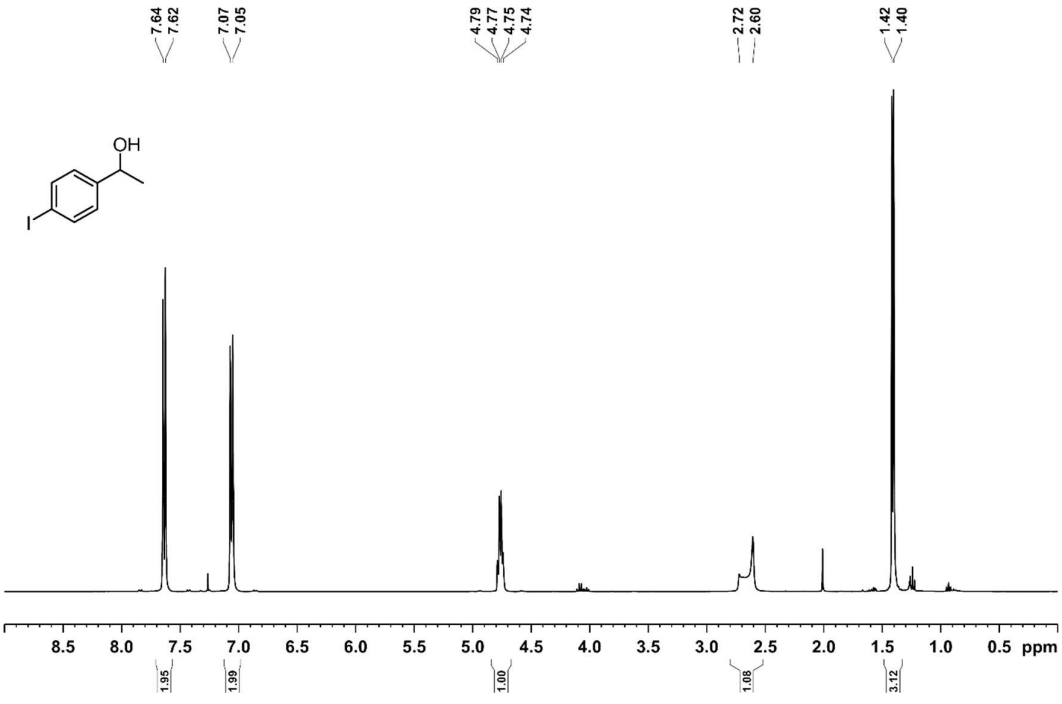

Figure S24. ^{1}H NMR spectrum (400.13 MHz, 300 K, $CDCl_3$) of 4-iodo-α-methylbenzyl alcohol.

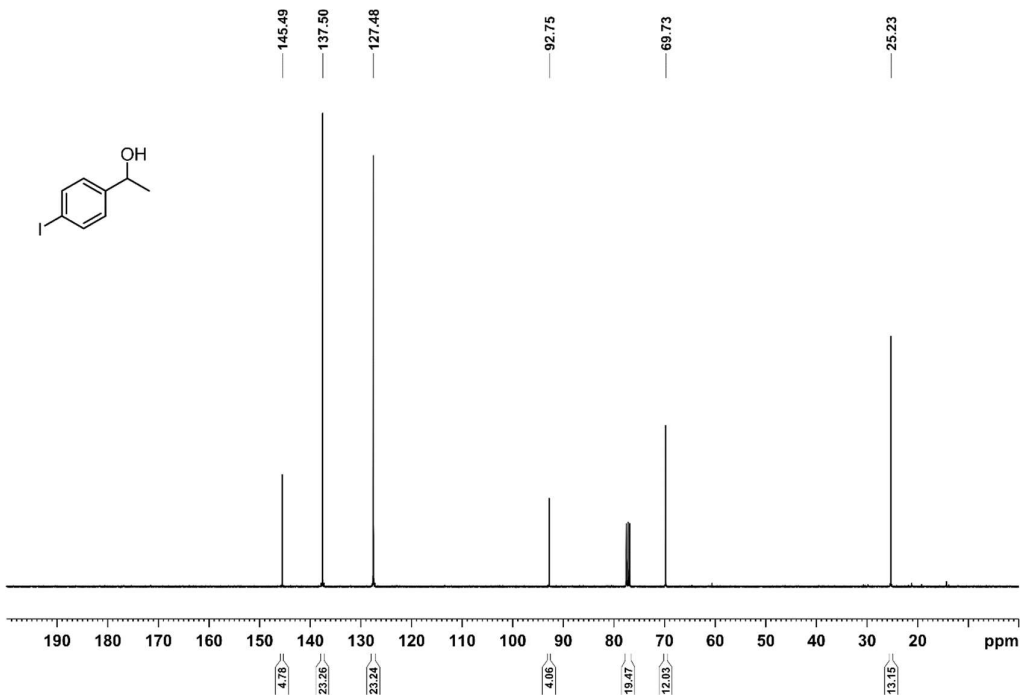

Figure S25. $^{13}C\{^{1}H\}$ NMR spectrum (100.6 MHz, 300 K, $CDCl_3$) of 4-iodo-α-methylbenzyl alcohol.

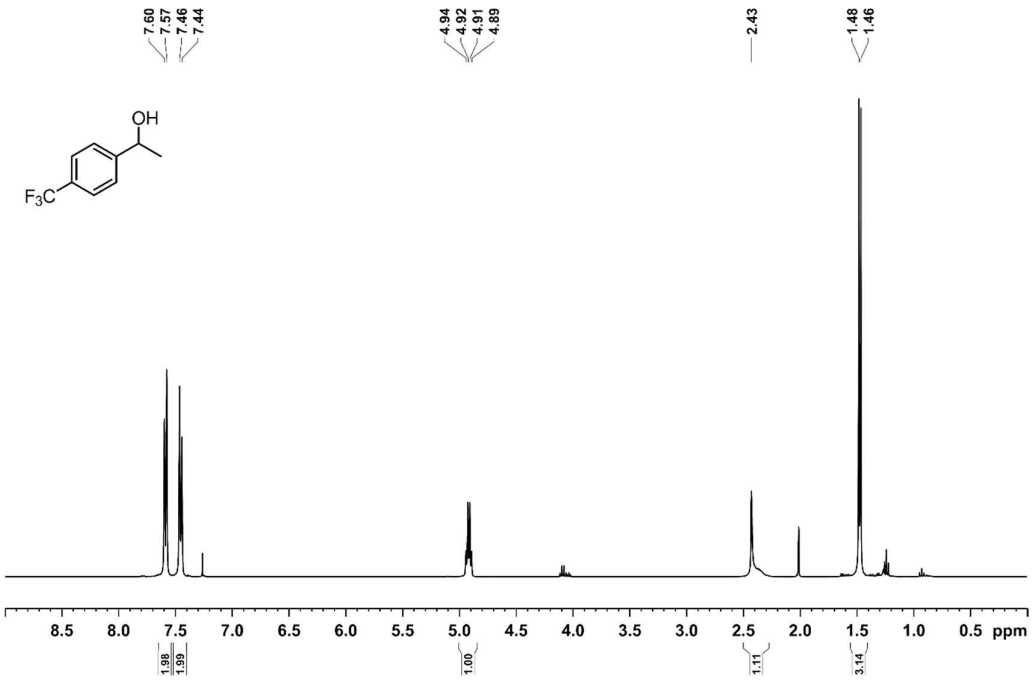

Figure S26. ^{1}H NMR spectrum (400.13 MHz, 300 K, $CDCl_3$) of 4-trifluoromethyl-α-methylbenzyl alcohol.

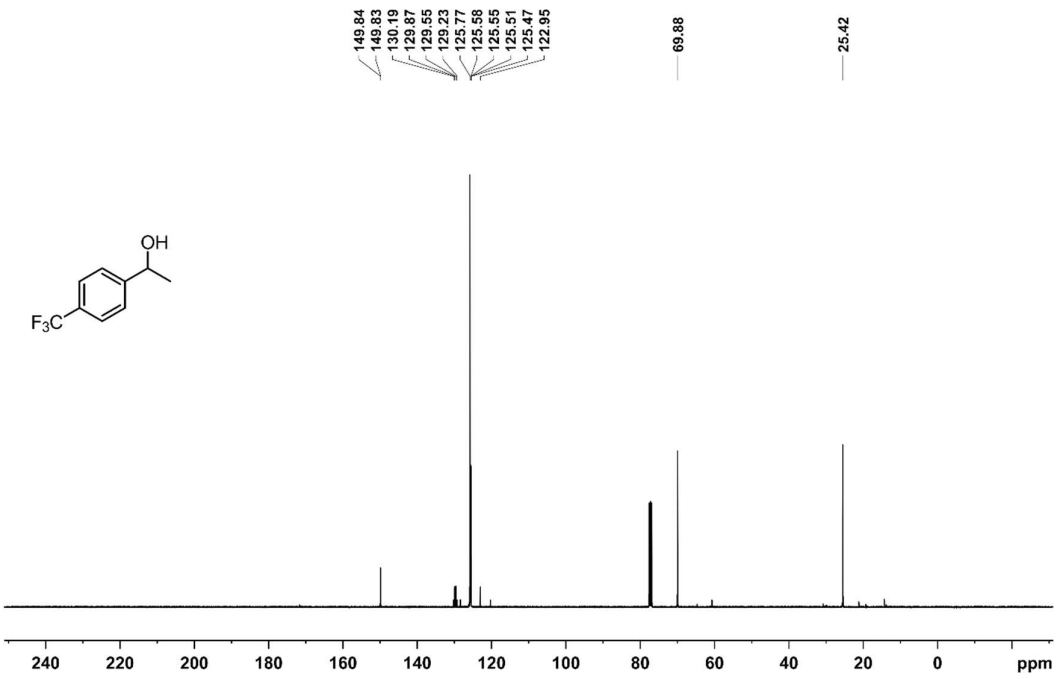

Figure S27. $^{13}C\{^{1}H\}$ NMR spectrum (100.6 MHz, 300 K, $CDCl_3$) of 4-trifluoromethyl-α-methylbenzyl alcohol.

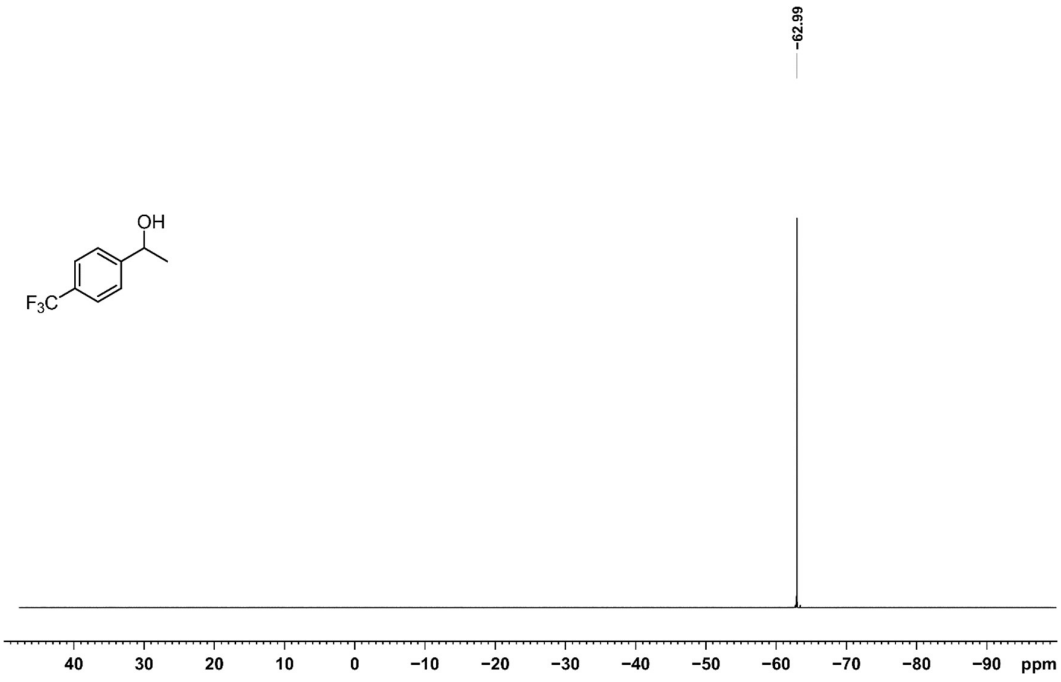

Figure S28. ^{19}F NMR spectrum (376.7 MHz, 300 K, $CDCl_3$) of 4-trifluoromethyl-α-methylbenzyl alcohol.

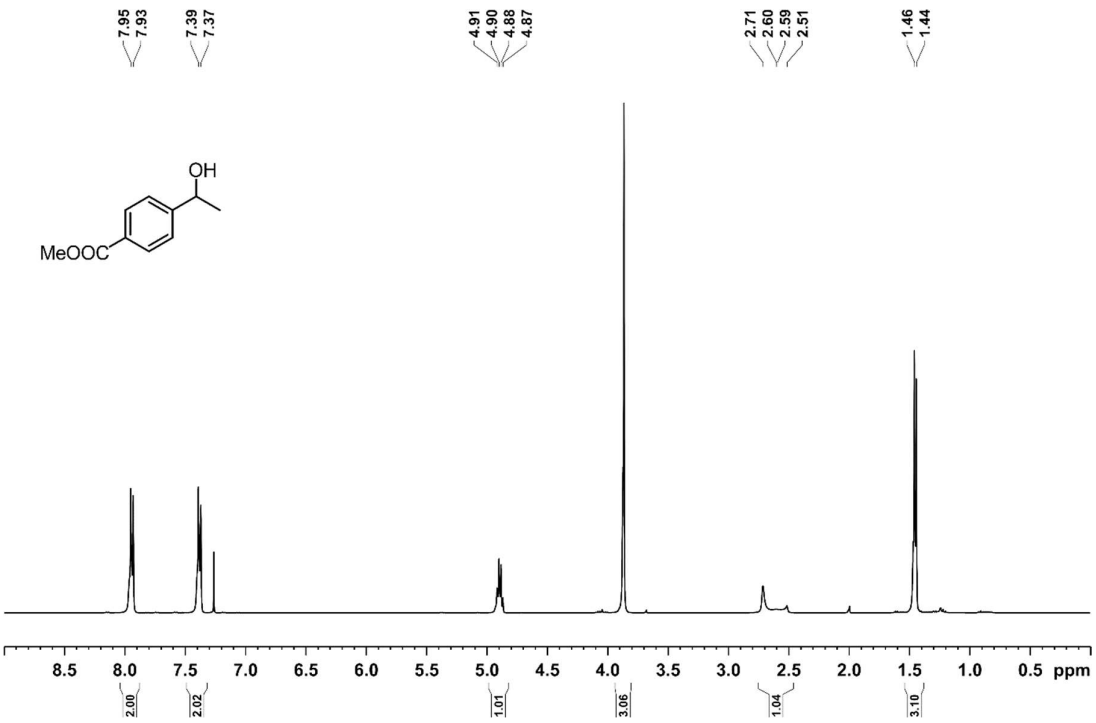

Figure S29. ^{1}H NMR spectrum (400.13 MHz, 300 K, $CDCl_3$) of 4-methylbenzoate-α-methylbenzyl alcohol

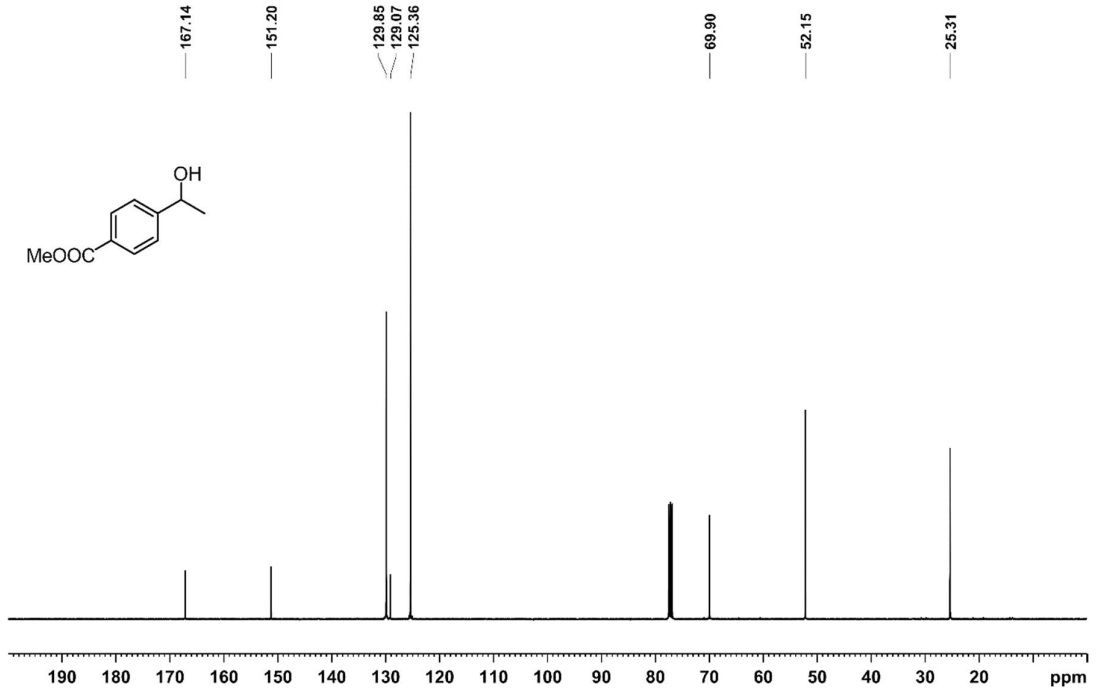

Figure S30. $^{13}C\{^{1}H\}$ NMR spectrum (100.6 MHz, 300 K, $CDCl_3$) of 4-methylbenzoate-α-methylbenzyl alcohol.

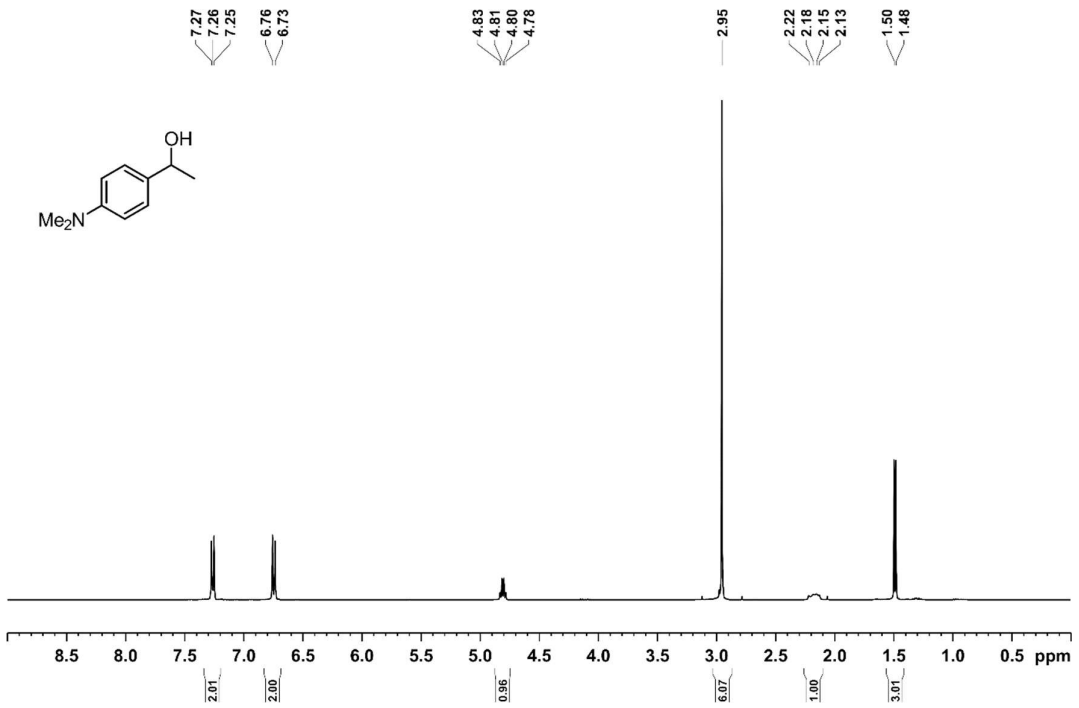

Figure S31. ^{1}H NMR spectrum (400.13 MHz, 300 K, $CDCl_3$) of 4-dimethylamino-α-methylbenzyl alcohol.

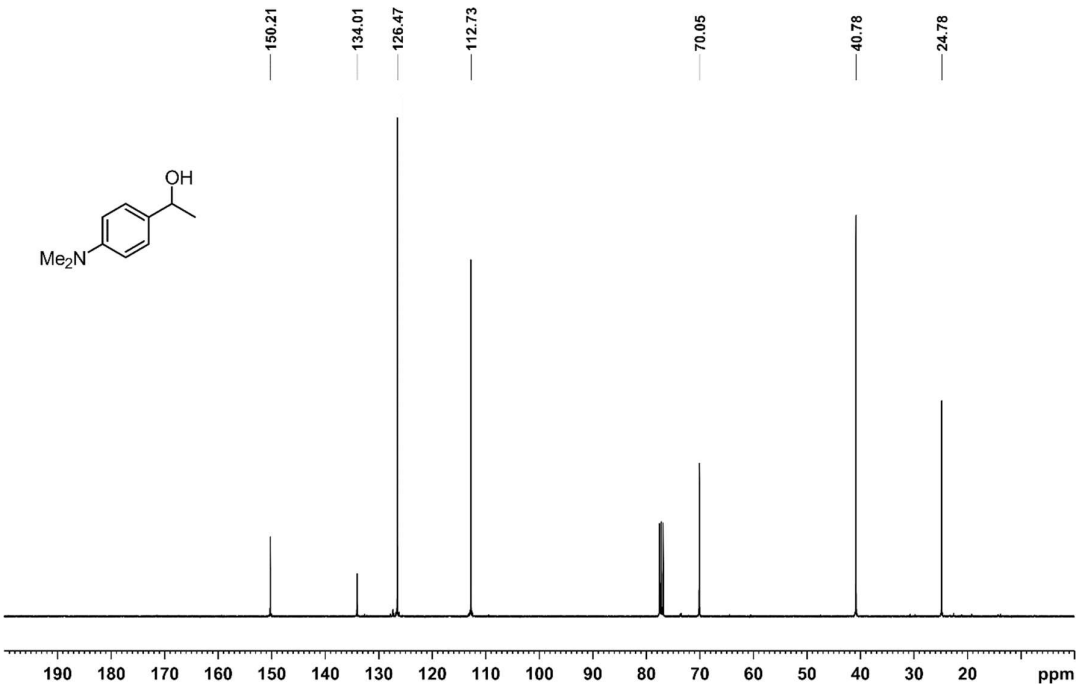

Figure S32. $^{13}C\{^{1}H\}$ NMR spectrum (100.6 MHz, 300 K, $CDCl_3$) of 4-dimethylamino-α-methylbenzyl alcohol.

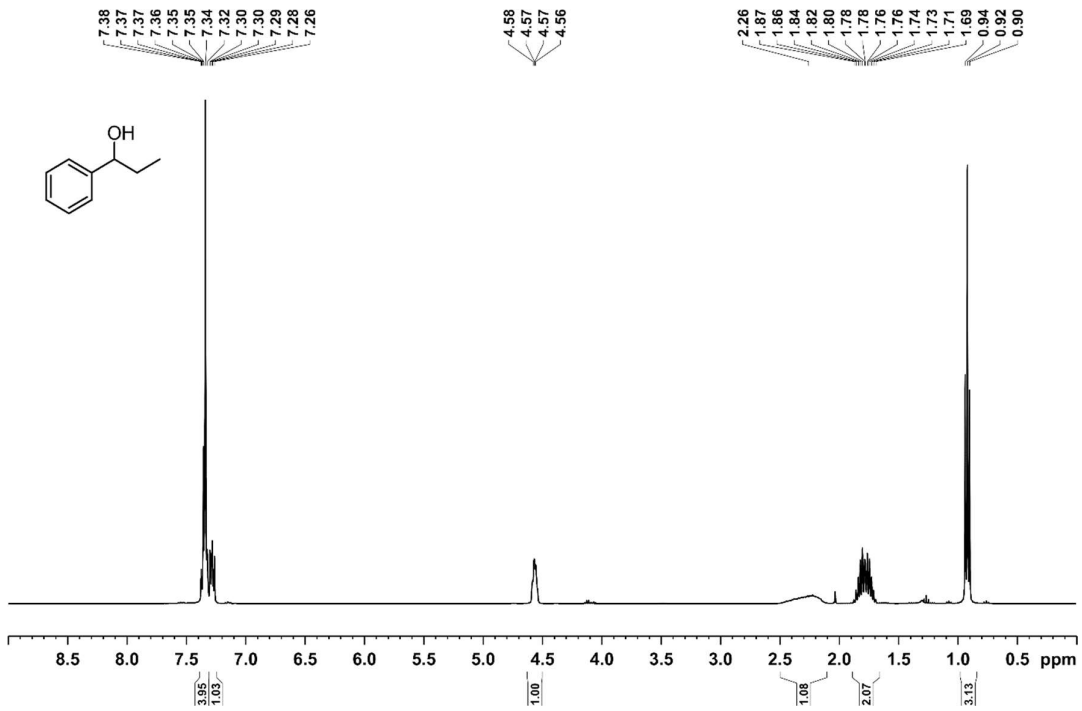

Figure S33. ^{1}H NMR spectrum (400.13 MHz, 300 K, $CDCl_3$) of 1-phenylpropran-1-ol.

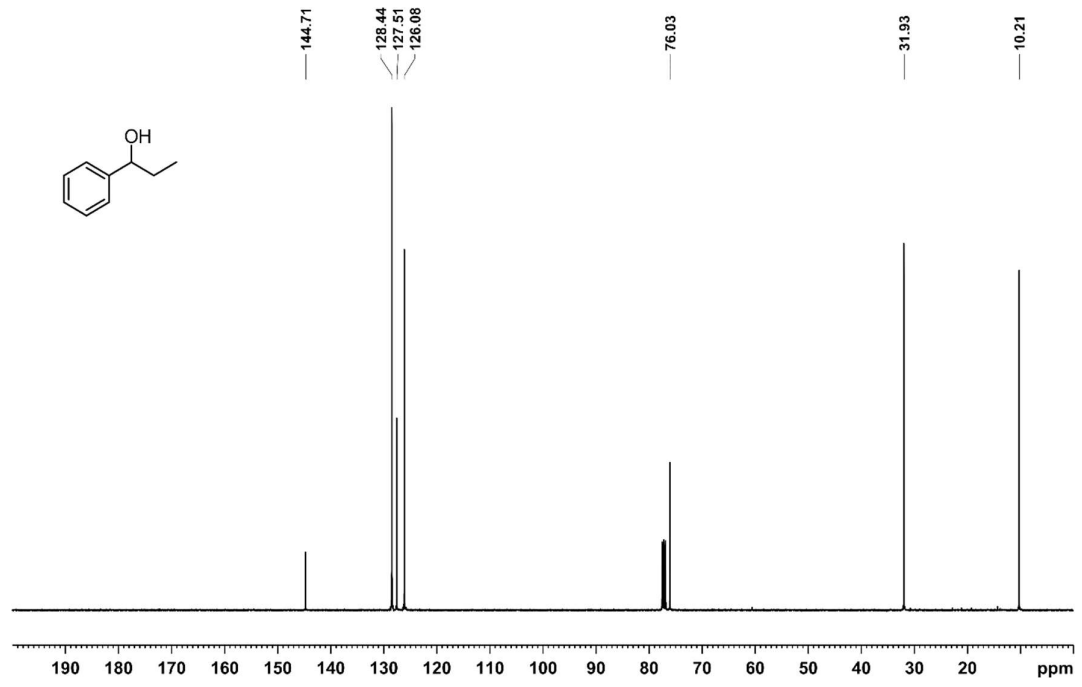

Figure S34. $^{13}C\{^{1}H\}$ NMR spectrum (100.6 MHz, 300 K, $CDCl_3$) of 1-phenylpropran-1-ol.

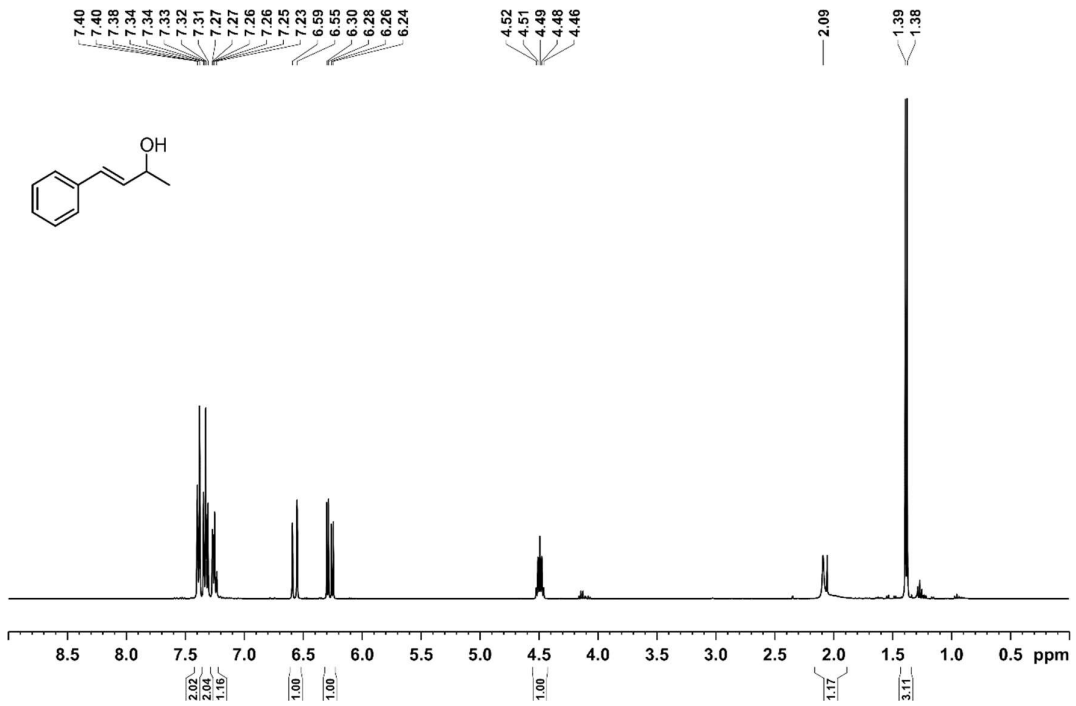

Figure S35. ^{1}H NMR spectrum (400.13 MHz, 300 K, $CDCl_3$) of 4-phenyl-but-3-en-2-ol.

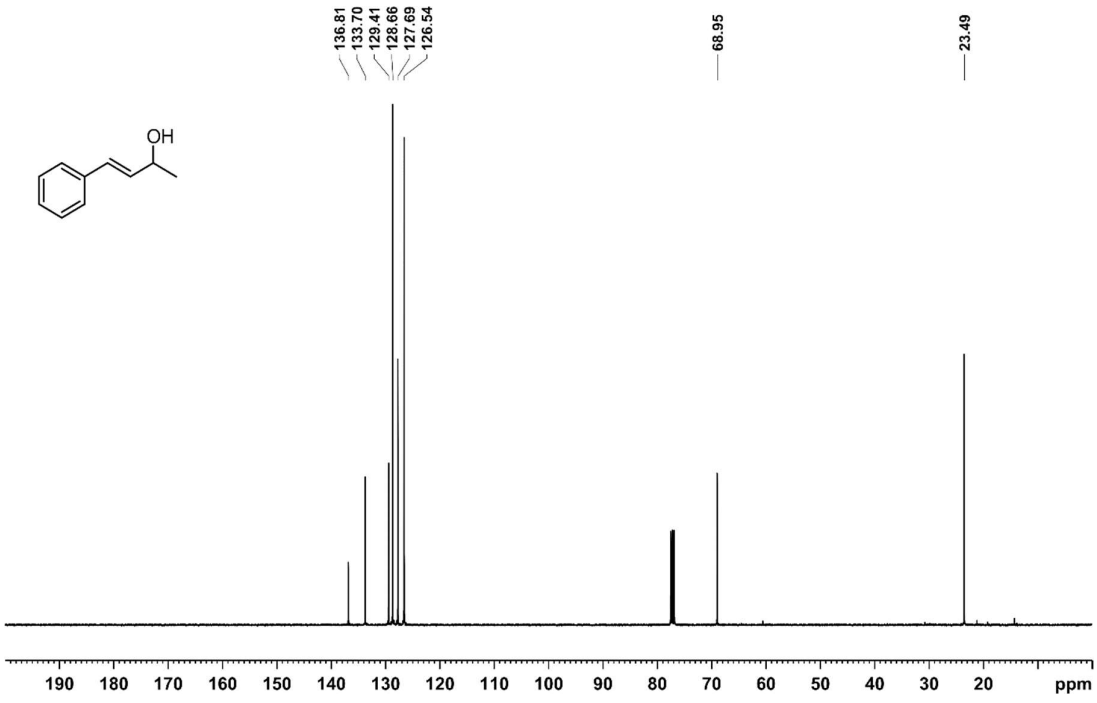

Figure S36. $^{13}C\{^{1}H\}$ NMR spectrum (100.6 MHz, 300 K, $CDCl_3$) of 4-phenyl-but-3-en-2-ol.

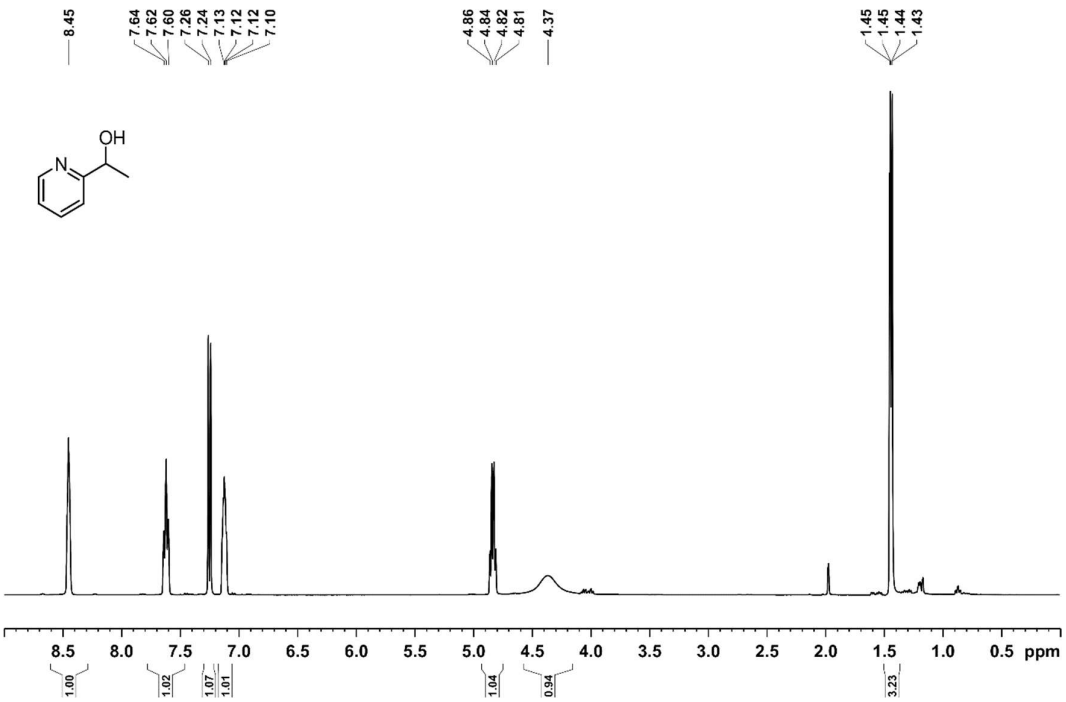

Figure S37. ^{1}H NMR spectrum (400.13 MHz, 300 K, $CDCl_3$) of 4-1-(pyridin-2-yl)-ethan-1-ol.

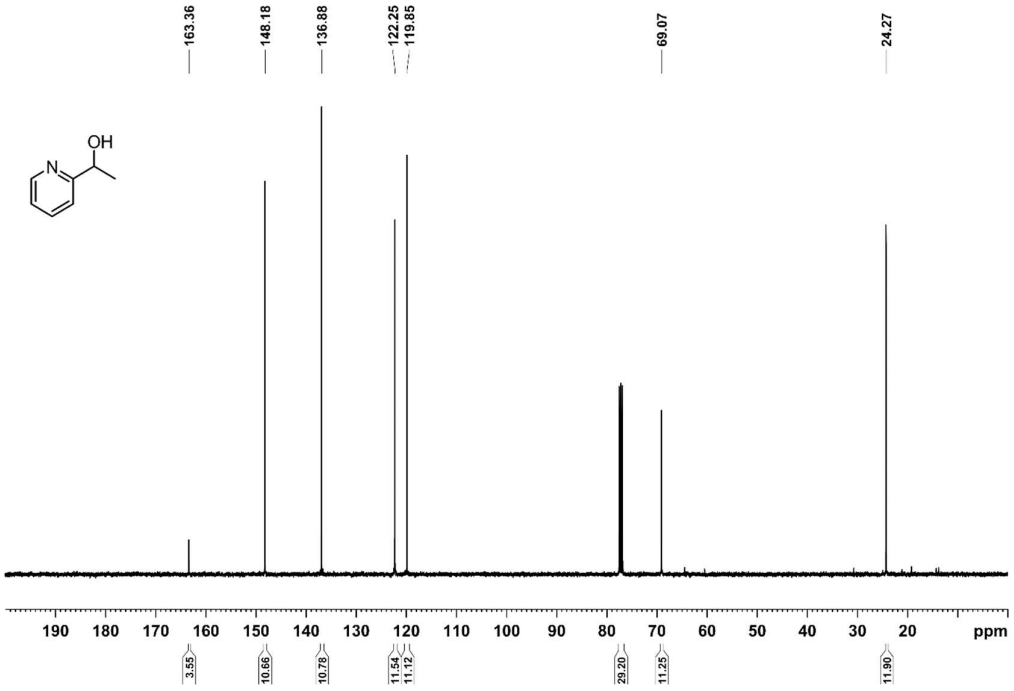

Figure S38. $^{13}C\{^{1}H\}$ NMR spectrum (100.6 MHz, 300 K, $CDCl_3$) of 1-(pyridin-2-yl)-ethan-1-ol.

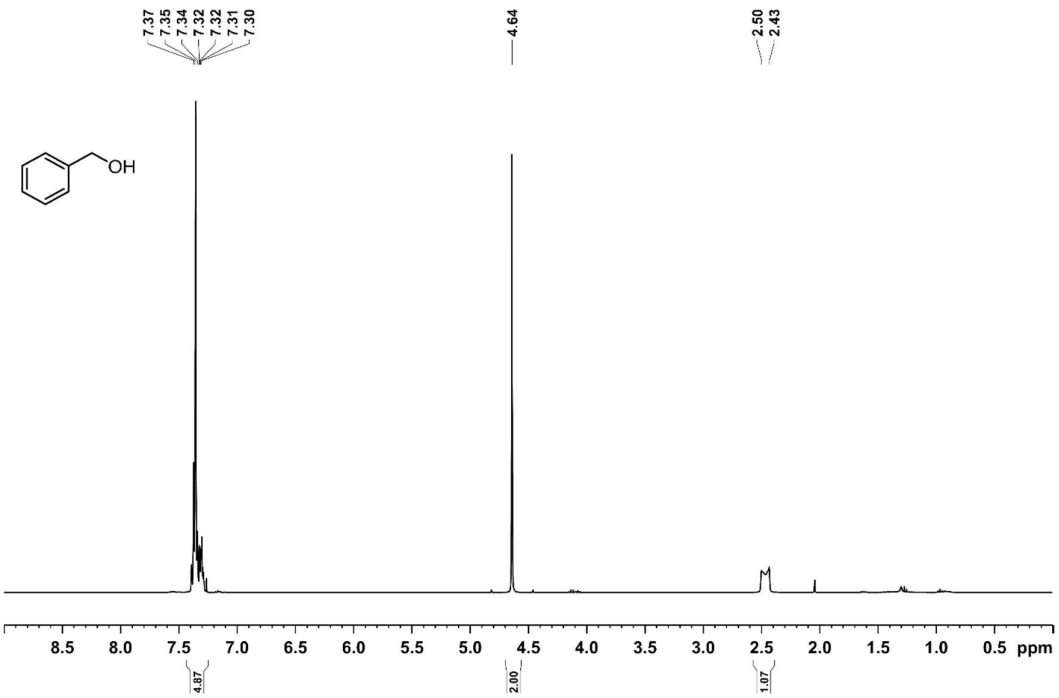

Figure S39. ^{1}H NMR spectrum (400.13 MHz, 300 K, $CDCl_3$) of benzyl alcohol.

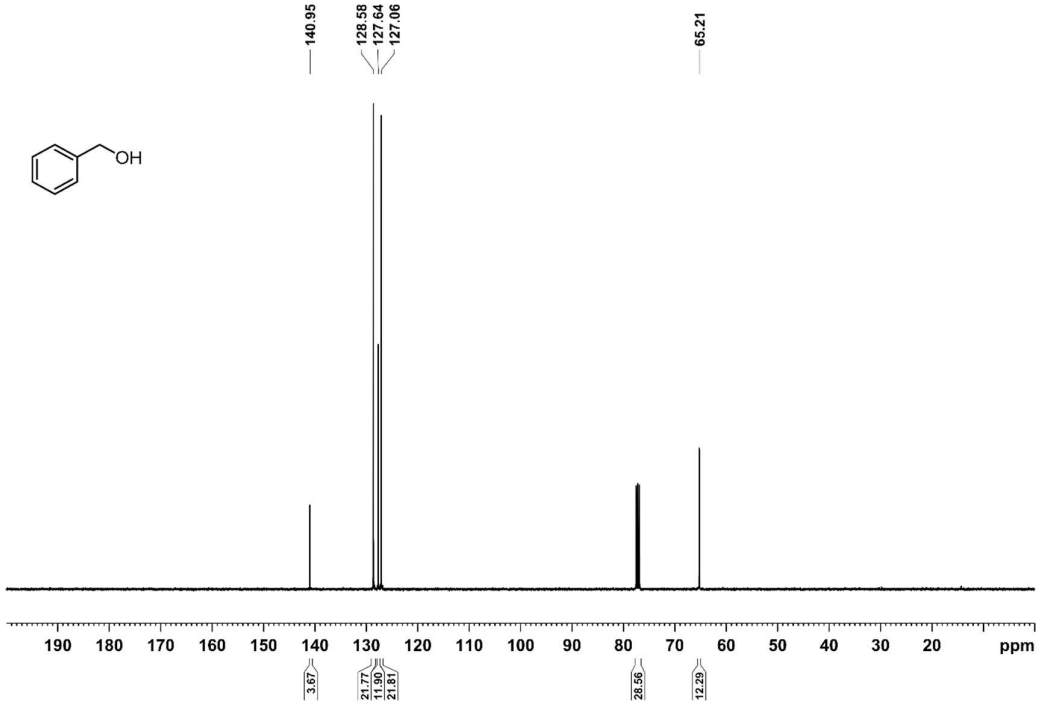

Figure S40. $^{13}C\{^{1}H\}$ NMR spectrum (100.6 MHz, 300 K, $CDCl_3$) of benzyl alcohol.

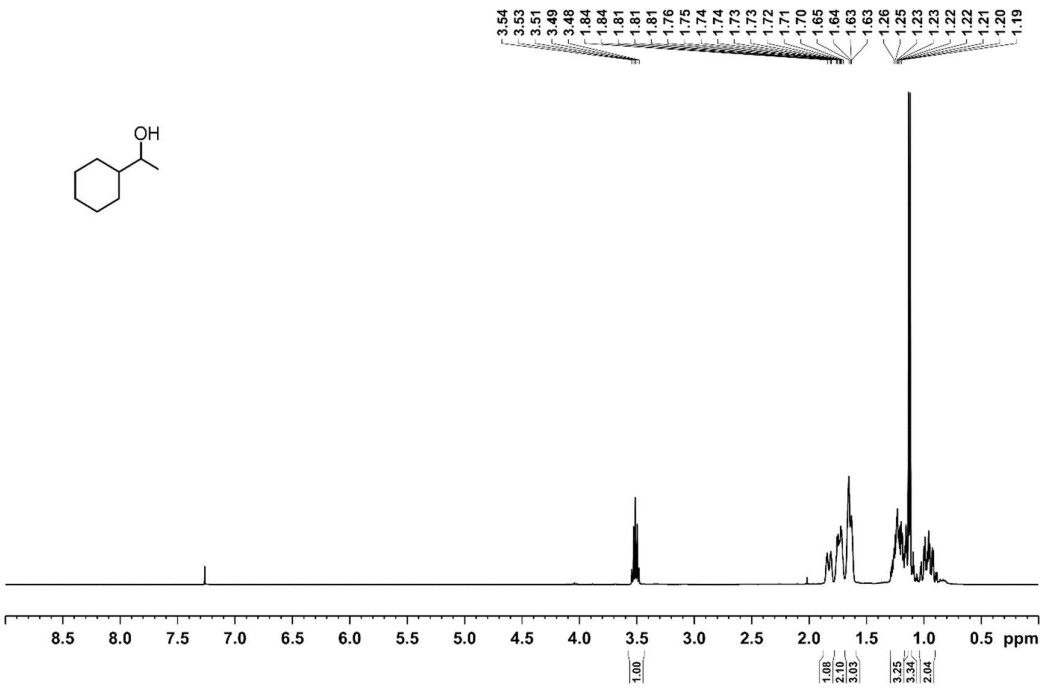

Figure S41. ^{1}H NMR spectrum (400.13 MHz, 300 K, $CDCl_3$) of 1-cyclohexylethan-1-ol

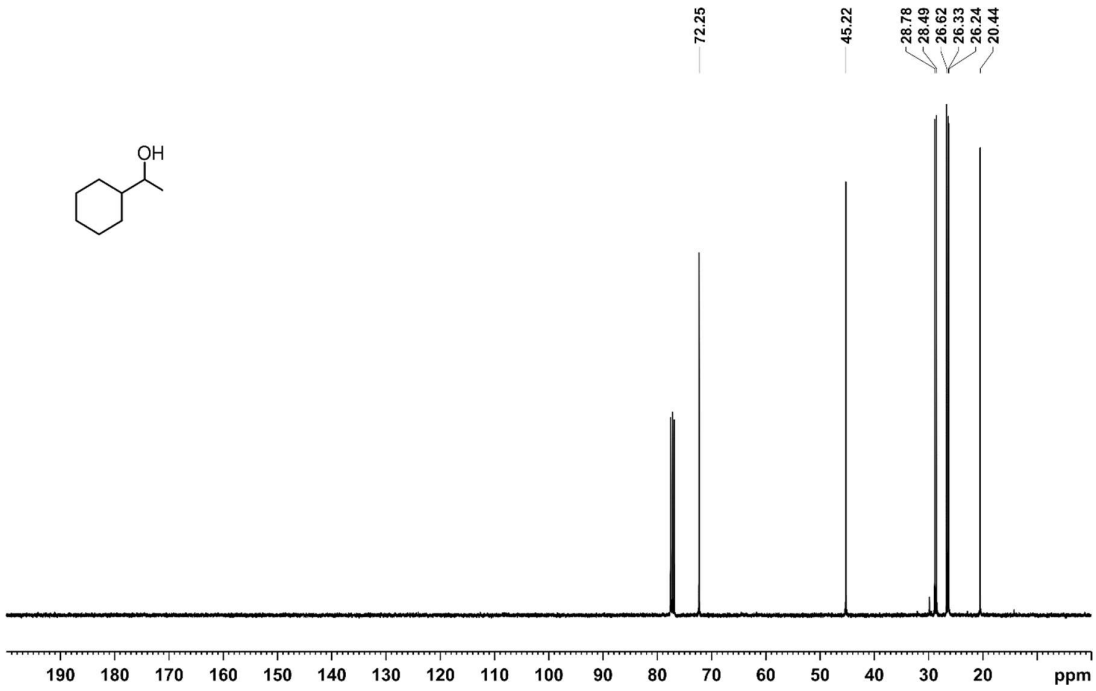

Figure S42. $^{13}C\{^{1}H\}$ NMR spectrum (100.6 MHz, 300 K, $CDCl_3$) of 1-cyclohexylethan-1-ol

6.5.9.4 IR Spectroscopy

Measurement of turnover frequency

1-[K([18]c-6)(thf)$_{0.5}$] (1.2 mg, 0.1 mol, 0.05 mol%) and acetophenone (235 µL, 2 mmol) were dissolved in 2 mL THF in a 10 mL Schlenk tube and stirred at 25 °C under an atmosphere of nitrogen. HBpin (300 µL, 2 mmol) was dissolved in 2 mL THF and added with a syringe. Decrease of ν (CO) = 1689 cm^{-1} stretching vibration was monitored with a ReactIR machine. In order to determine the dilution effect an experiment without catalyst was conducted. With this information it was possible to convert the peak height into the amount of substrate (mmol).

Turnover frequency (TOF) was calculated with the slope between the first two data points.

Catalyst loading: 0.05 mol%: turnover = 0.12 mmol/s. TOF = 220000 h^{-1}

Catalyst loading: 0.036 mol%: turnover = 0.055 mmol/s. TOF = 140000 h^{-1}

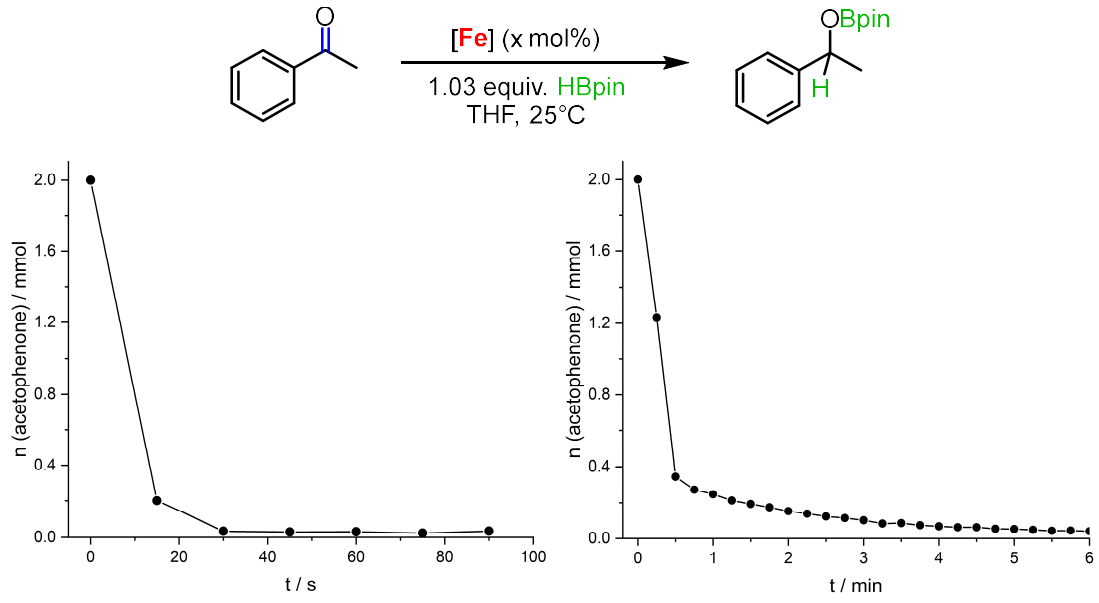

Figure S43. Hydroboration of acetophenone using 0.05 mol% (left), respectively 0.036 mol% (right) of **1**-[K([18]c-6)(thf)$_{0.5}$].

Poisoning experiment:

1-[K([18]c-6)(thf)$_{0.5}$] (1.4 mg, 0.1 mol, 0.063 mol%), acetophenone (235 µL, 2 mmol) and Hg (one drop) were dissolved in 2 mL THF in a 10 mL Schlenk tube and stirred at 25 °C under an

atmosphere of nitrogen. HBpin (300 µL, 2 mmol) was dissolved in 2 mL THF and added with a syringe.

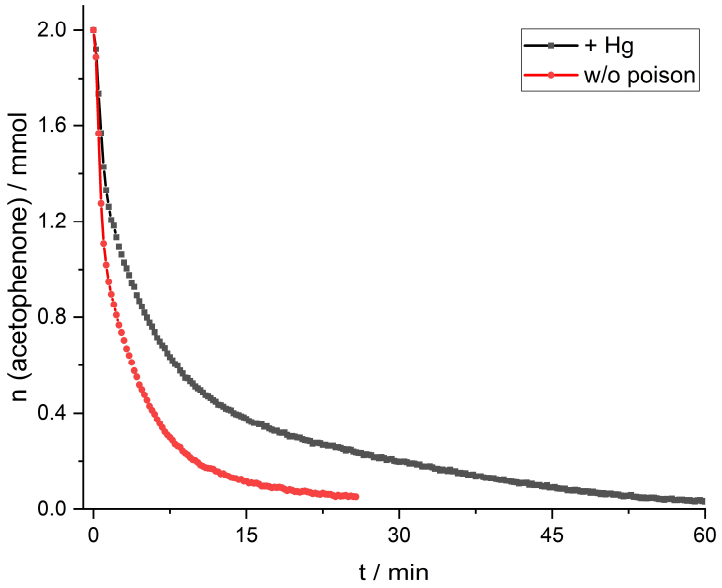

Figure S44. Hydroboration of acetophenone using catalyst **1**-[K([18]c-6)(thf)$_{0.5}$] (0.063 mol%) without poison (red curve) and with addition of one drop of mercury (black curve).

6.5.10 Computational Details

6.5.10.1 [K([18]c-6)(thf)$_2$][(^{Dipp}BIAN)Fe(η^4-cod)] (1-[K([18]c-6)(thf)$_{0.5}$])

To save computational cost [K([18]c-6)(thf)$_2$][(^{Dipp}BIAN)Fe(η^4-cod)] (**1**-[K([18]c-6)(thf)$_{0.5}$]) was simplified by omitting the cation and replacing diisopropyl groups by methyl groups. Geometry optimization for this truncated complex was performed at the OPBE/def2-TZVP level of theory in gas phase. Frequency calculations were carried out to confirm the nature of stationary points found by geometry optimisations Population analysis was conducted using Löwdin reduced orbital populations per unrestricted natural orbitals (UNO).

The doubly occupied orbitals with the highest energy are the orbitals **141**-**145**. Here, especially **142** (3, and 3) **144** ($3d_{xy}$), and **145** ($3d_{xz}$) exhibit a high d-orbital character. Together with the SOMO **146**, which is also d-orbital centered (3 and 3), a d^7-configuration can be assumed. The orbitals **143**-**145** possess bonding character from iron to the C–C double bond (**143**, **144**), and to the diimine ligand (**144**, **145**). In contrast, the unoccupied orbitals **147**-**149** show antibonding character. The orbitals are displayed with an isosurface value = 0.08. The spin density is mainly located on the iron atom with a spin population for iron of 1.42 according to Mulliken population analysis.

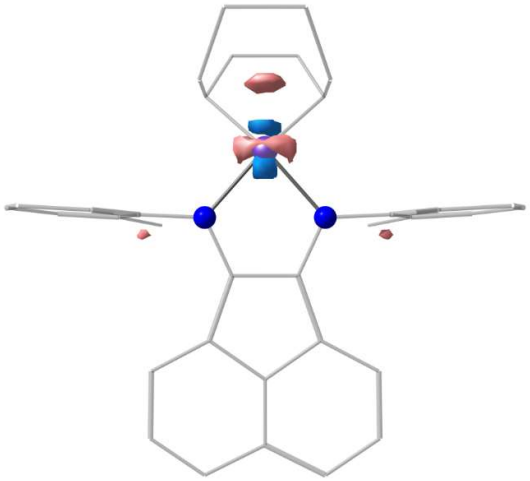

150 (occ.: 0.001, 18% 3, 6% 3,); E = 1.86 eV

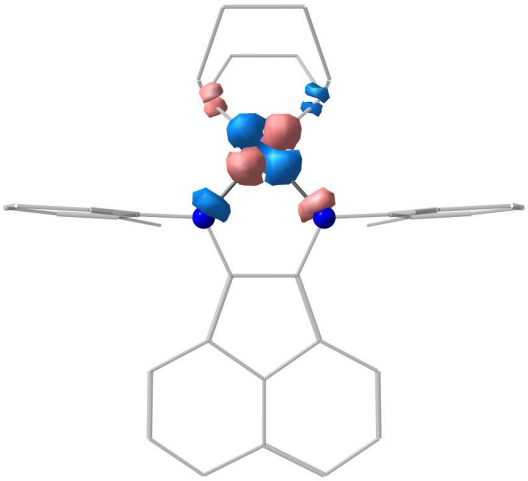

149 (occ.: 0.0003, 64% $3d_{yz}$) ; E = 1.77 eV

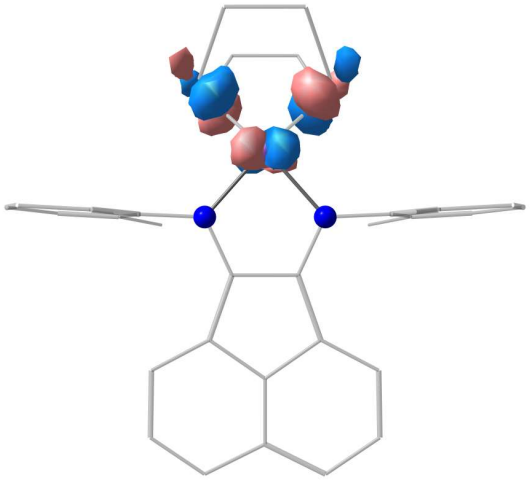

148 (occ.: 0.004, 31% $3d_{xy}$); E = 1.62 eV

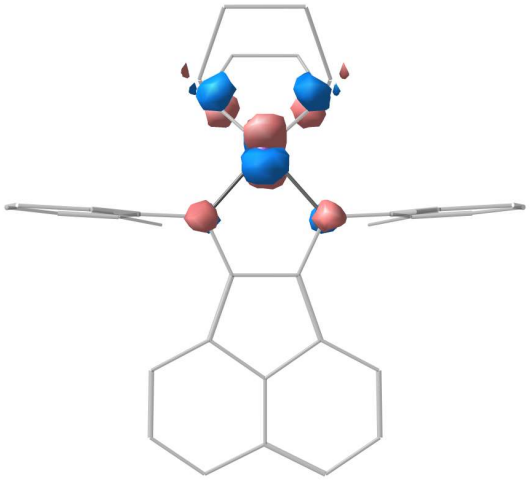

147 (occ.: 0.009, 31% $3d_{xz}$); E = 0.74 eV

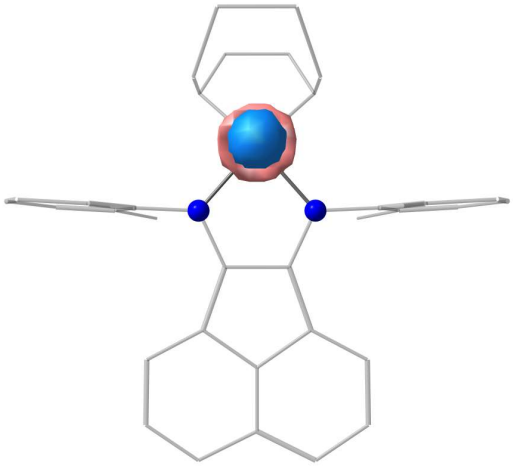

146 (occ.: 1.000, 20% 3, 67% 3,); E = –0.16 eV

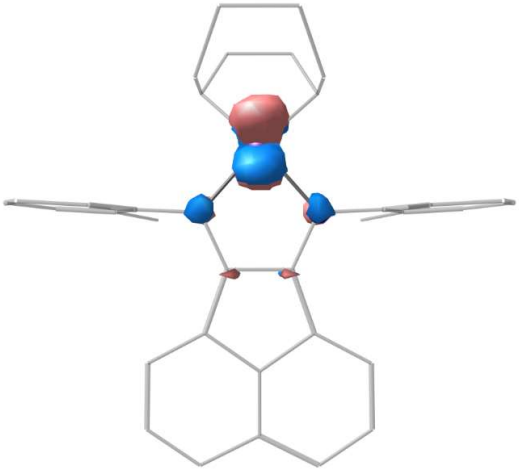

145 (occ.: 1.991, 58% $3d_{xz}$) ; E = –1.11 eV

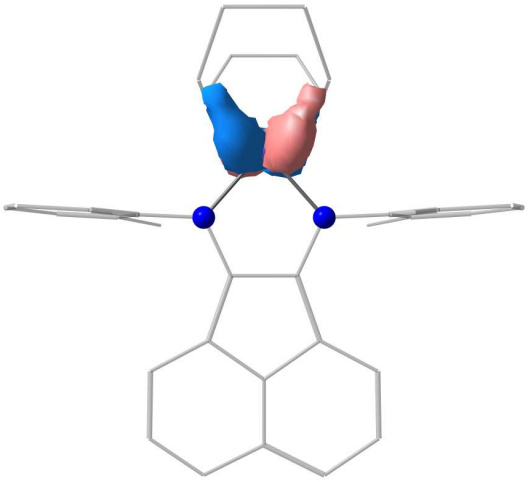

144 (occ.: 1.995, 73% $3d_{xy}$) ; E = –1.58 eV

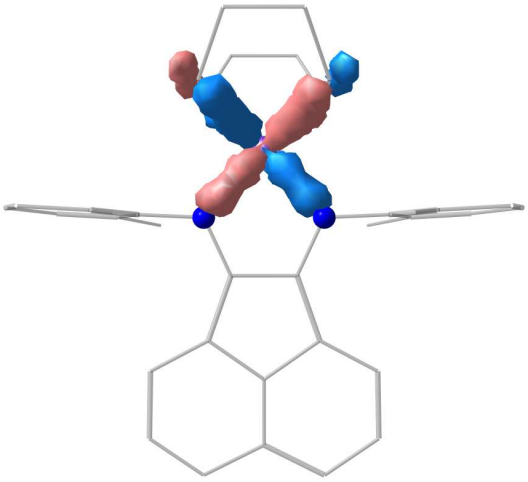

143 (occ.: 1.997, 38% $3d_{yz}$); E = –1.61 eV

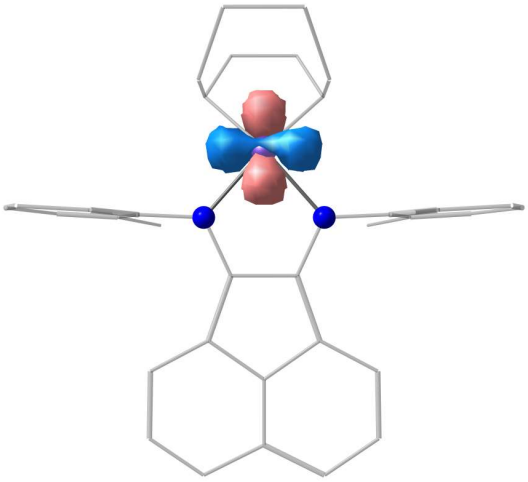

142 (occ.: 1.999, 67% 3, 21% 3,); E = –2.19 eV

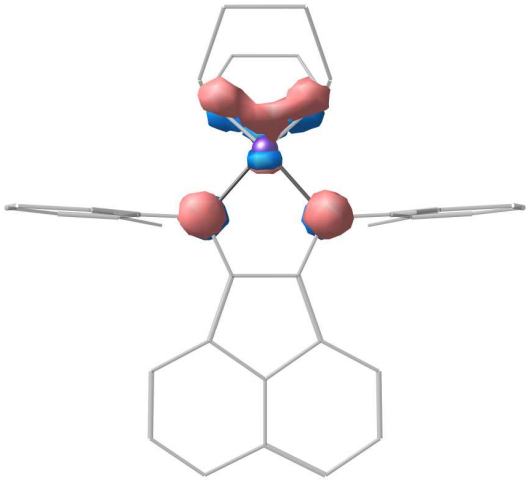

141 (occ.: 1.999) ; E = –2.45 eV

Figure S45. Löwdin reduced orbital populations per unrestricted natural orbitals (UNO) of [($^{2,6\text{-dimethylphenyl}}$BIAN)Fe($\eta^4$-cod)]$^-$ with an isosurface value of 0.08.

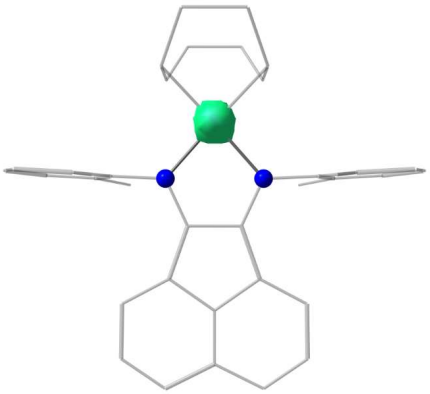

Figure S46. Spin density plot of [($^{2,6\text{-dimethylphenyl}}$BIAN)Fe($\eta^4$-cod)]$^-$ according to Mulliken population analysis with an isosurface value of 0.05

6.5.10.2 [K([18]c-6)(thf)$_2$][(^{Dipp}BIAN)Fe($C_{14}H_{16}$] (2-[K([18]c-6)(thf)$_2$])

State-averaged CASSCF-DLPNO-NEVPT2/def2-mTZVP def2-TZVP/C calculations were conducted for three different ground state multiplicities (S = 2, 4, 6) to get an insight into the electronic structure of the anion of **2**-[K([18]c-6)(thf)$_2$]. The initial guess orbitals were chosen from a BP86 def2-SV(P) def2/J calculation. Thereby, the active space was constructed to contain the 3d orbitals on iron as well as the bonding interaction between iron and the ligands (**194**-**199**). Additionally, five orbitals (**201**-**205**) of the second d-shell (containing the 4d orbitals on iron) were included to aid convergence and to obtain reliable energies. In total, this led to an active space of 9 electrons in 12 orbitals. The orbitals are displayed in Figure S44.

Analysis of the natural orbitals of the active space reveals two metal-ligand bonding orbitals (**194**, **195**) and the correlating antibonding orbitals (**199**, **200**), whereas orbital **199** exhibits significant 3d orbital character. The orbitals **196**, **197**, and **198** are almost pure 3d orbitals.

Analysis of the total energy of the different multiplicities (2, 4, 6) showed that the quartet state is energetically most favored and the sextet state (ΔE = +39.9 kcal mol^{-1}) and the doublet state (ΔE = +26.6 kcal mol^{-1}) are significantly higher in energy. For the quartet state the contribution of the ground-state configuration is 87% (22**2111**00000), which is an Fe(III) intermediate spin system with the five 3d orbitals (**196**-**200**). Based on these orbitals a d^5 configuration on iron can be proposed with doubly occupied **196**, singly occupied orbitals **197**, **198**, **199** and unoccupied orbital **200**. The obtained spin-density from a DFT calculation is in agreement with the CASSCF results and is mainly located on the iron atom with a spin population of 2.91 for Fe according to Mulliken population analysis, see Figure S45.

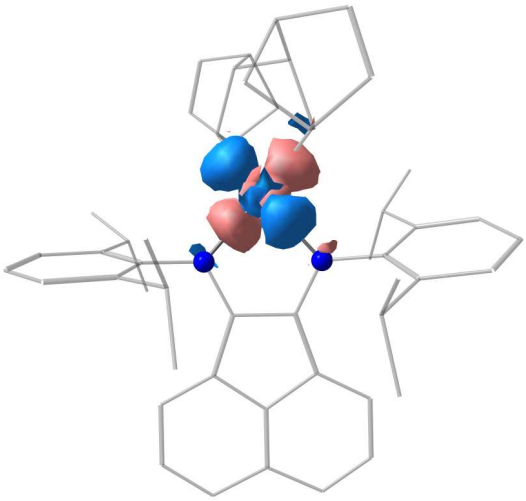

205 (occ.: 0.004, 28% 4d$_{yz}$, 26% 4d$_{xz}$, 11% 4, 10% 4)

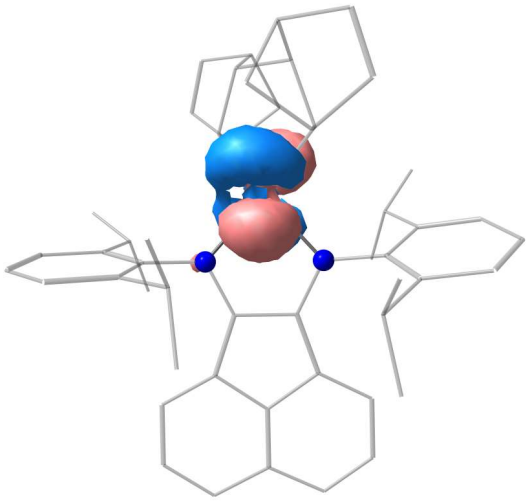

204 (occ.: 0.006, 30% 4d$_{yz}$, 13% 4)

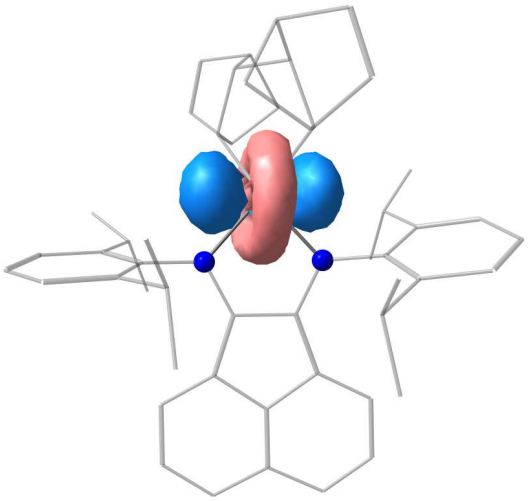

203 (occ.: 0.007, 41% 4, 23% $4d_{xy}$, 18% $4d_{xz}$)

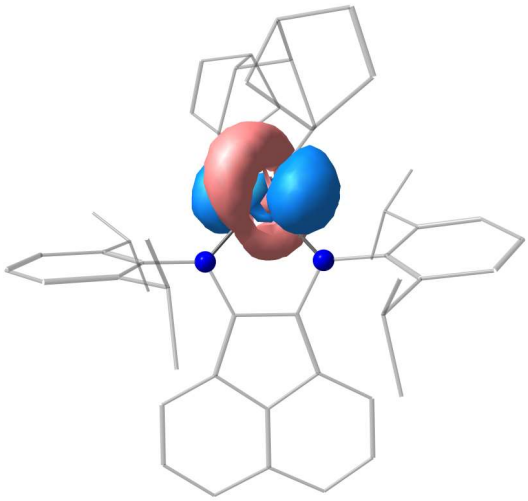

202 (occ.: 0.012, 51% 4, 26% $4d_{xz}$)

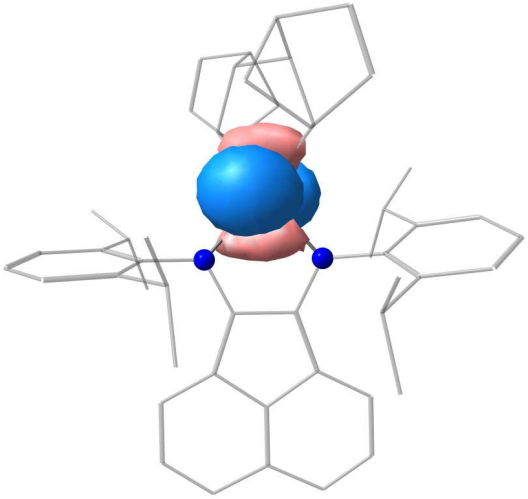

201 (occ.: 0.017, 30% 4, 28% $4d_{xy}$, 20% $4d_{yz}$)

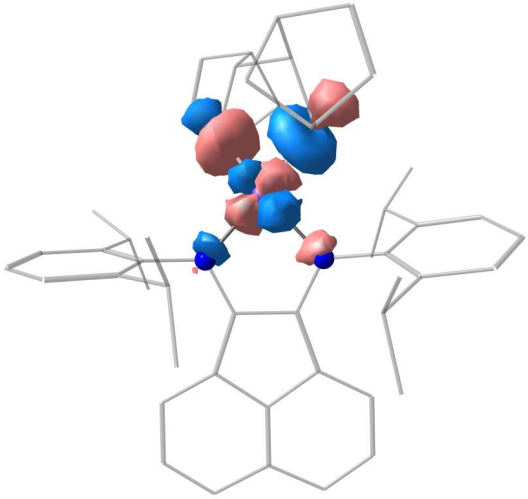

200 (occ.: 0.419, 26% $3d_{xz}$, 13% 3)

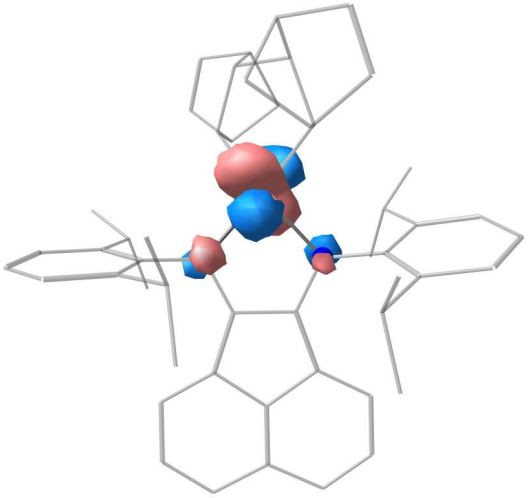

199 (occ.: 0.739, 52% $3d_{yz}$, 23% $3d_{xy}$)

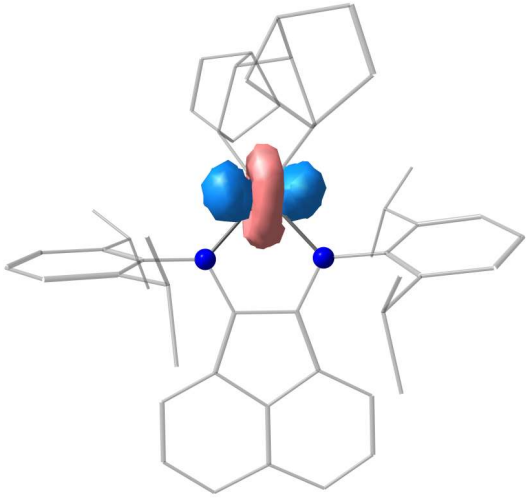

198 (occ.: 0.995, 47% 3, 30% $3d_{xy}$, 17% $3d_{xz}$)

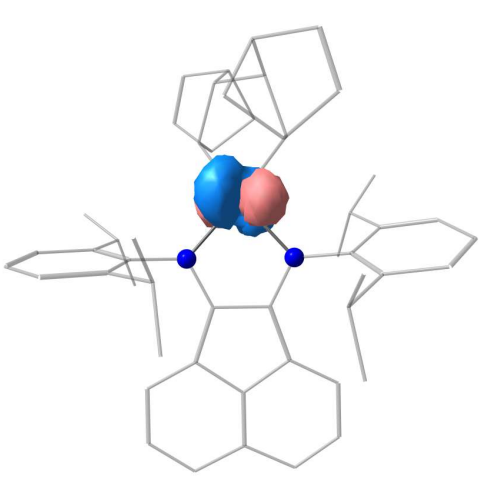

197 (occ.: 1.302, 64% 3, 29% $3d_{xz}$)

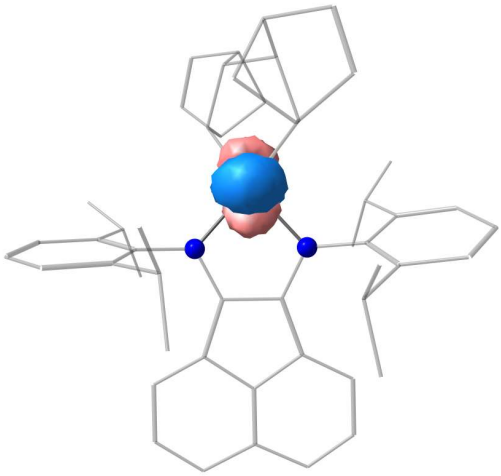

196 (occ.: 1.626, 38% $3d_{xy}$, 35% 3, 22% $3d_{yz}$)

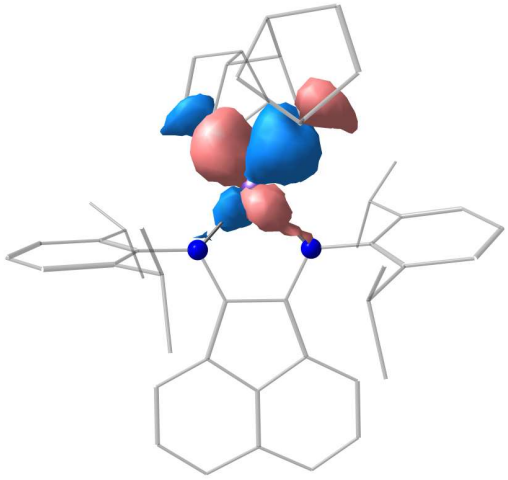

195 (occ.: 1.909, 26% $3d_{xz}$, 15% 3)

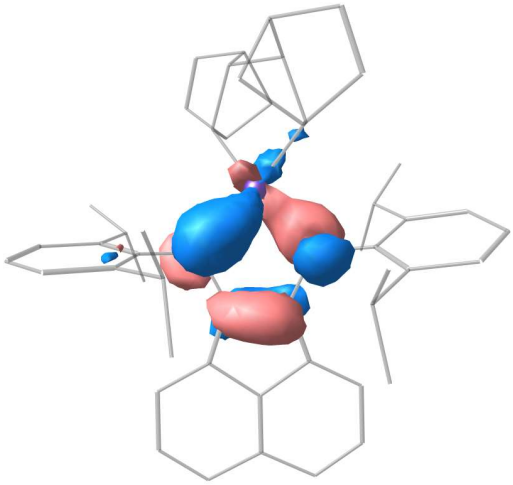

194 (occ.: 1.965, 12% $3d_{yz}$)

Figure S44. Orbitals of **2** obtained from CASSCF calculation. The orbitals are displayed with an isosurface value of 0.05. The occupancies are state-averaged occupancies.

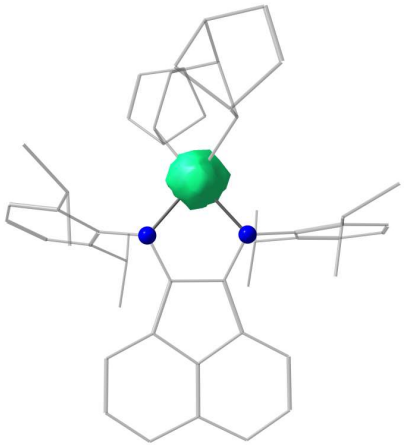

Figure S45. Spin density plot of **2** according to Mulliken population analysis (isosurface value = 0.02).

6.5.10.3 [K([18]c-6)(thf)$_2$][(^{Dipp}BIAN)$_2$Fe] (3)

State-averaged CASSCF-DLPNO-NEVPT2/def2-mTZVP def2-SVP/C calculations were conducted for three different ground state multiplicities (S = 2, 4, 6) to get an insight into the electronic structure of the anion of **3**. The initial guess orbitals were chosen from an OPBE def2-SV(P) calculation. Thereby, the active space was constructed to contain the 3d orbitals on iron (**279**, **280**, **281**, **283-285**) as well as the bonding interaction between iron and the ligands (**279**, **282**). Additionally, five orbitals (**286-290**) of the second d-shell (containing the 4d orbital on iron) were included to aid convergence and reliable energies. In total, this led to an active space of 9 electrons in 12 orbitals. The orbitals are displayed in Figure S46.

Analysis of the natural orbitals of the active space reveals one double-occupied metal-ligand bonding orbital (**279**). Orbital **282** is singly-occupied and shows strong ligand character, thus indicating the presence of a ligand-centered radical. The orbitals **280**, **281**, **283**, **284**, and **285** represent the five 3d orbitals. The latter is the correlating antibonding orbital to **279**.

Analysis of the total energy of the different multiplicities (2, 4, 6) showed that the quartet state is favored, but the sextet state is very close in energy (ΔE = +1.7 kcal mol^{-1}). The doublet state (ΔE = +21.2 kcal mol^{-1}) is significantly higher in energy. For the quartet state the contribution of the ground-state configuration is 75% (22**11111**00000) where two of the electrons are coupled. One further state correlating with the composition (22**1211**00000) contributes significantly (16%) to the wave function. For the sextet state the contribution of the ground-state configuration is 98% (22**11111**00000) Based on these results a high-spin Fe(II) species is conceivable as there is one electron in orbital **282**, which exhibits high ligand character. This would result in two BIAN ligands with an averaged formal charge of −1.5 and consequently a formal charge of +2 for iron.

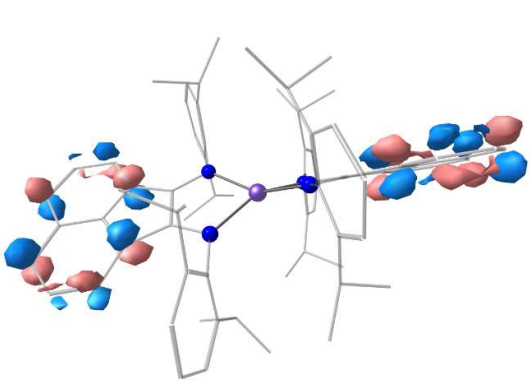

291 (occ.: 0.000)

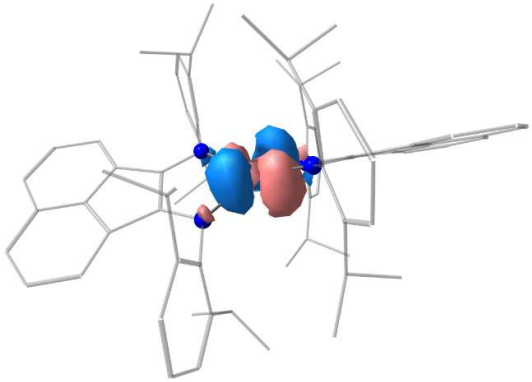

290 (occ.: 0.004 4d$_{yz}$)

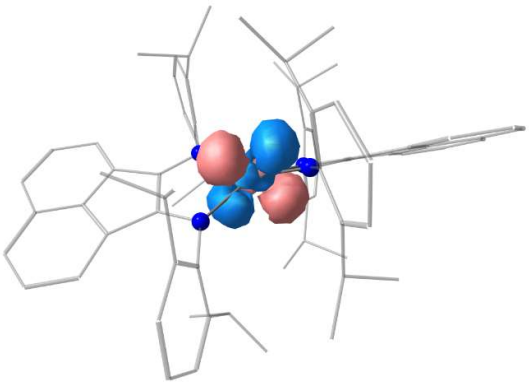

289 (occ.: 0.005, 87% $4d_{xz}$)

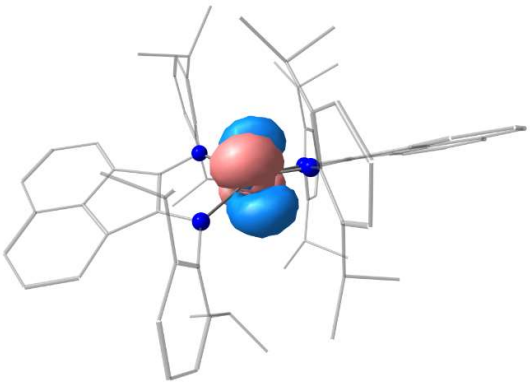

288 (occ.: 0.006, $4d_{xy}$)

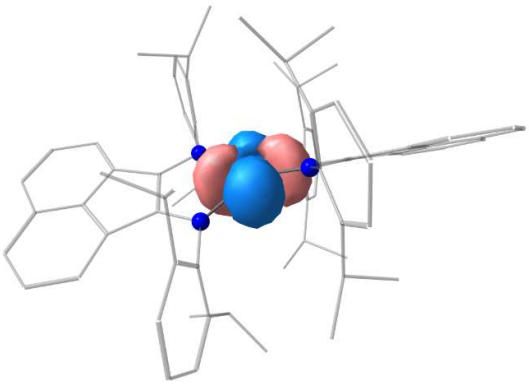

287 (occ.: 0.008, 51% 4, 38% 4)

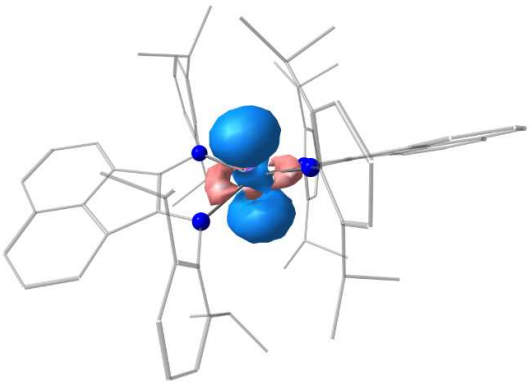

286 (occ.: 0.018, 48% 4, 31% 4, 4% $4d_{xz}$)

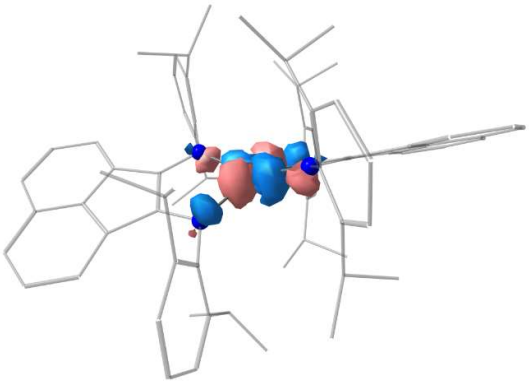

285 (occ.: 0.660, 79% $3d_{yz}$)

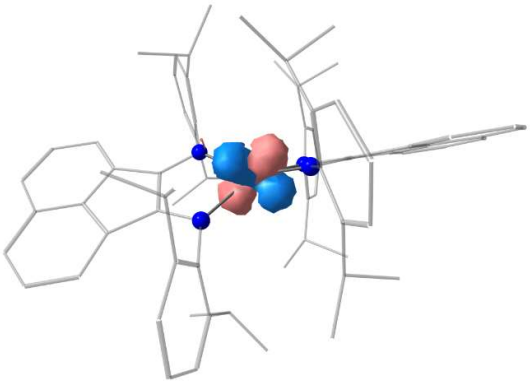

284 (occ.: 0.994, 90% $3d_{xz}$, 4% 3,)

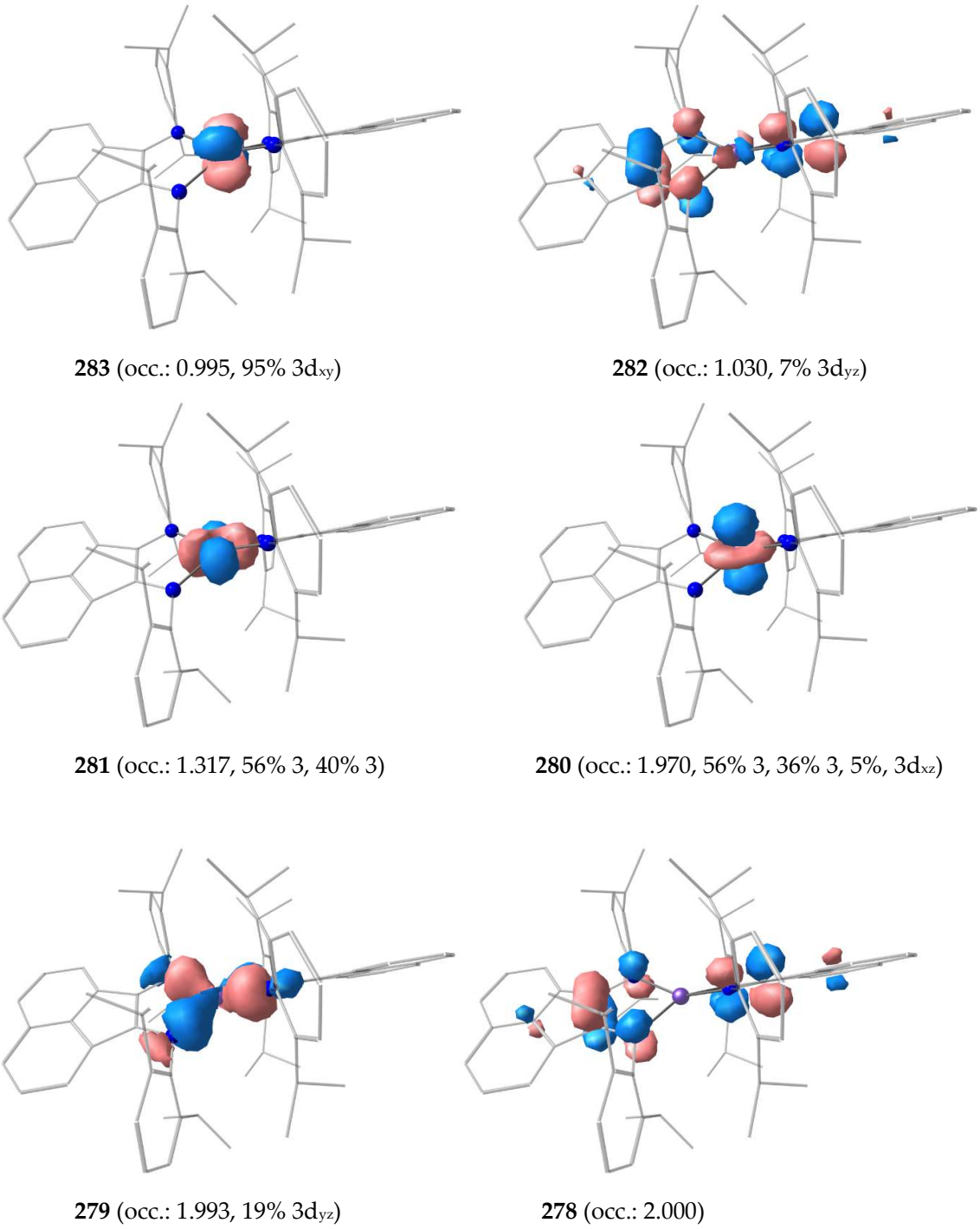

Figure S46. Orbitals of **3** obtained from CASSCF calculation. The orbitals are displayed with an isosurface value of 0.05.

6.5.10.4 [K([18]c-6)(thf)$_2$][(^{Dipp}PhDi)$_2$Fe] (4)

State-averaged CASSCF-DLPNO-NEVPT2/def2-mTZVP def2-TZVP/C calculations were conducted for three different ground state multiplicities (S = 2, 4, 6) to get an insight into the

electronic structure of the anion of **4**. The initial guess orbitals were chosen from an OPBE D3BJ def2-TZVP def2/J calculation. Thereby, the active space was constructed to contain the 3d orbitals on iron (**295-299**) as well as the bonding interaction between iron and the ligands (**292-294**, **298**, and **299**). Additionally, five orbitals (**300-304**) of the second d-shell (containing the 4d orbital on iron) were included to aid convergence and reliable energies. In total, this led to an active space of 9 electrons in 12 orbitals.

Analysis of the natural orbitals of the active space reveals two metal-ligand bonding orbitals (**293**, **294**) and the correlating antibonding orbitals (**298**, **299**), whereas **298** exhibits significant 3d orbital character. The orbitals **295**, **296**, **297**, and **298** are 3d orbitals. Orbital **299** also consist of high 3d-orbital character (55% $3d_{yz}$). Analysis of the total energy of the different multiplicities (2, 4, 6) showed that the sextet state is energetically most favored but the quartet state (ΔE = +3.0 kcal mol^{-1}) is close in energy. The doublet state (ΔE = +21.0 kcal mol^{-1}) is significantly higher in energy For the sextet state the contribution of the ground-state configuration is 94% (22**11111**00000), which is consistent with a high-spin Fe(III) center. In contrast, for the quartet state the contribution of the ground state is 66% (22**21110**00000). Two excited states contribute significantly to the wave function and are d-d transitions. 18% of the wave function correlate with the composition (21**2111**100000), whereas 11% represent the composition (20**2111**200000). The orbitals are displayed with an isosurface value = 0.05. The occupancies are state-averaged occupancies.

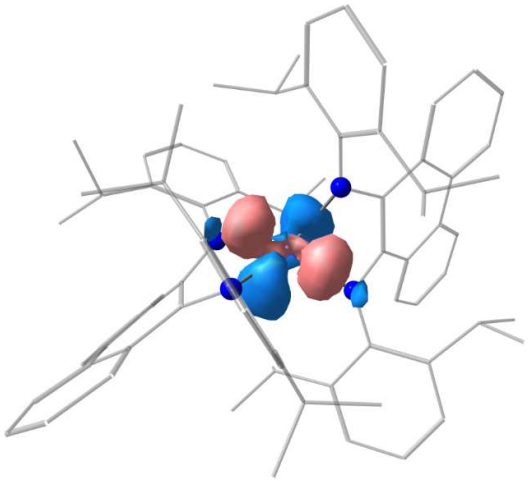

304 (occ.: 0.005, 61% 4, 14% 4, 6% $4d_{xz}$)

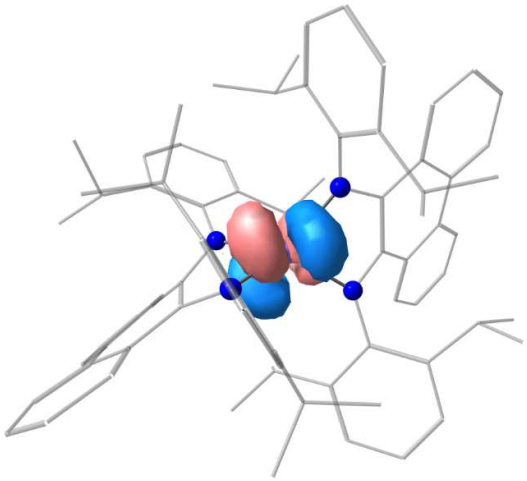

303 (occ.: 0.006, 45% $4d_{yz}$, 39% $4d_{xy}$)

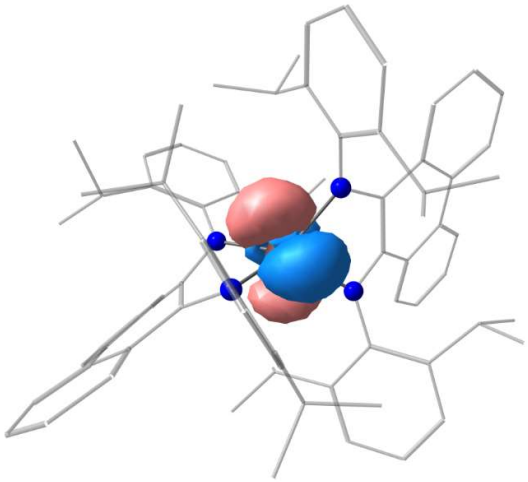

302 (occ.: 0.007, 48% $4d_{xz}$, 42% $4d_{yz}$)

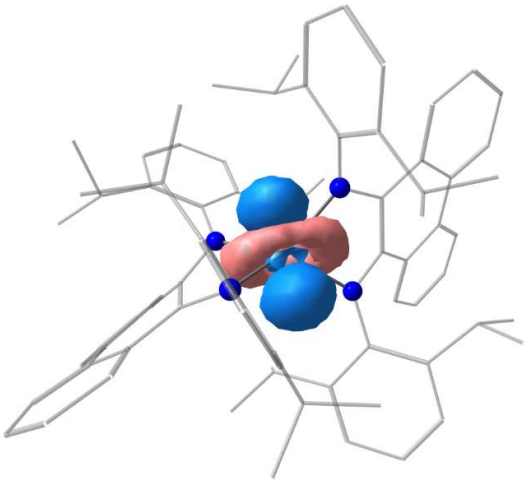

301 (occ.: 0.009, 70% $4d_{xy}$, 19% 4)

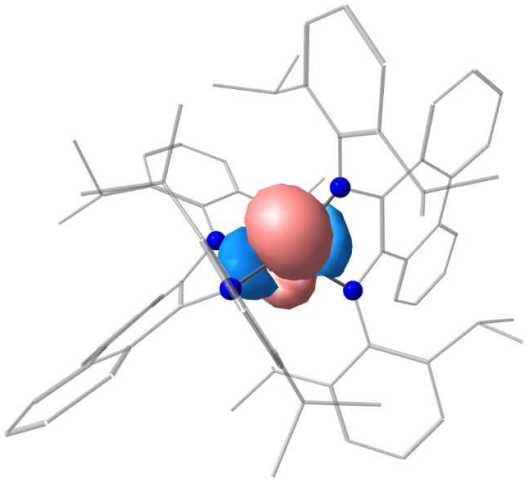

300 (occ.: 0.015, 53% 4, 21% 4, 10% $4d_{xz}$)

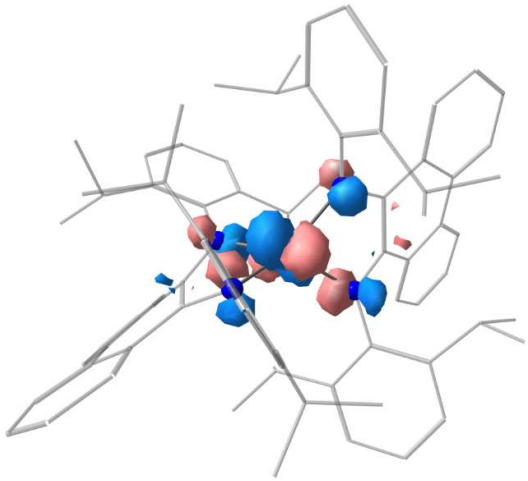

299 (occ.: 0.579, 55% $3d_{yz}$)

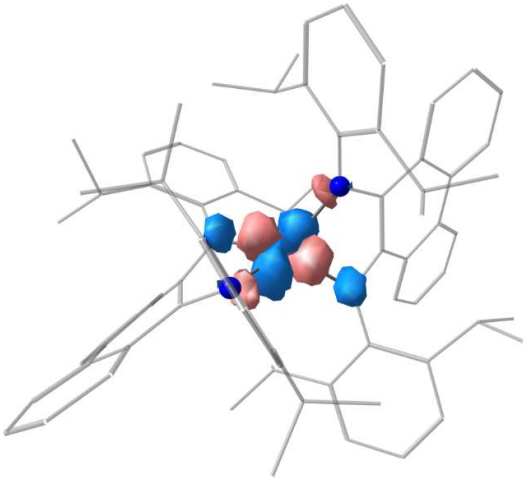

298 (occ.: 0.714, 62% 3, 16% 3, 6% $3d_{xz}$)

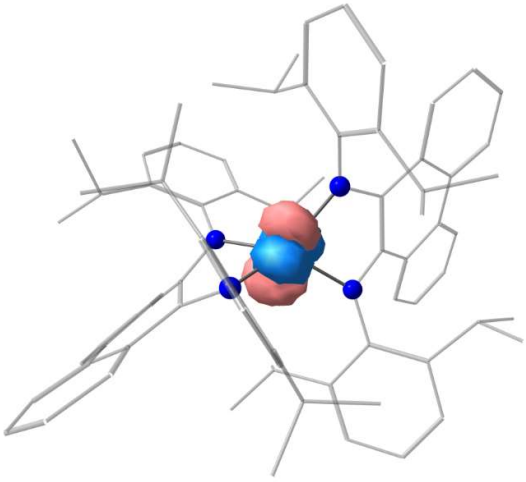

297 (occ.: 0.998, 94% $3d_{xy}$)

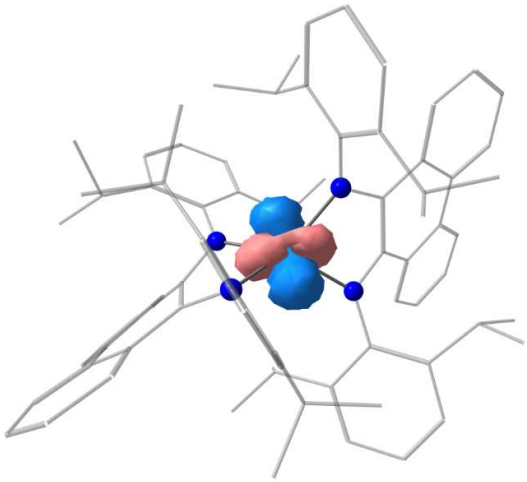

296 (occ.: 1.314, 83% $3d_{xz}$, 12% 3)

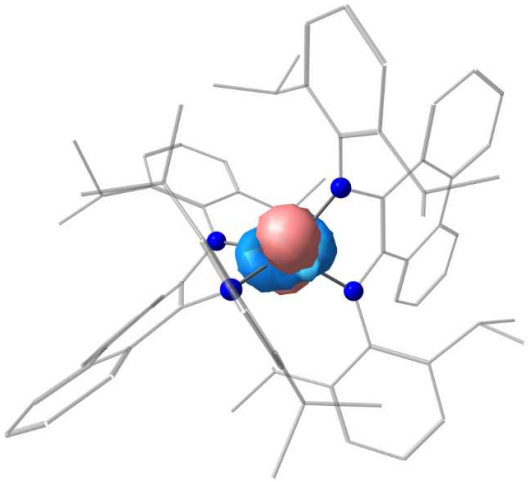

295 (occ.: 1.635, 66% 3, 24% 3, 6% d_{xz})

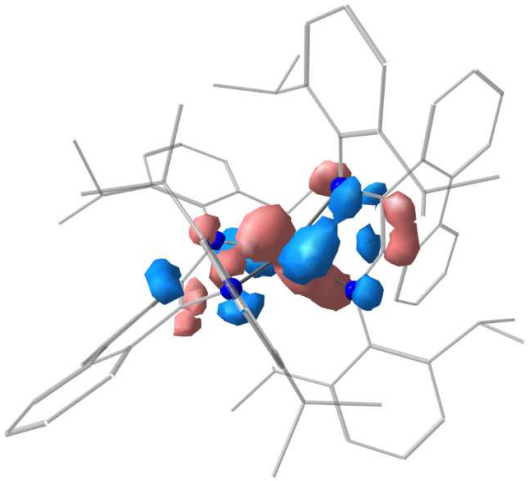

294 (occ.: 1.750, 44% $3d_{yz}$)

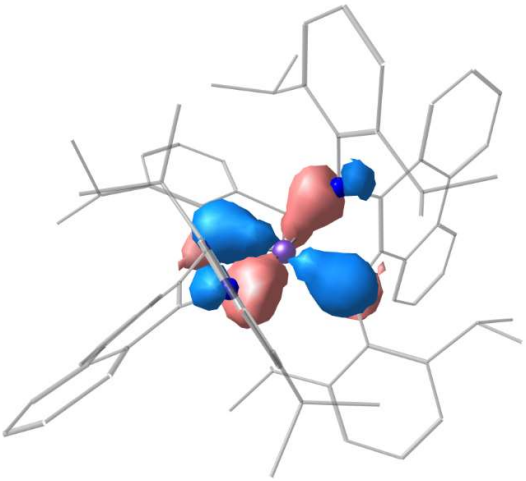

293 (occ.: 1.969, 16% 3, 3% 3)

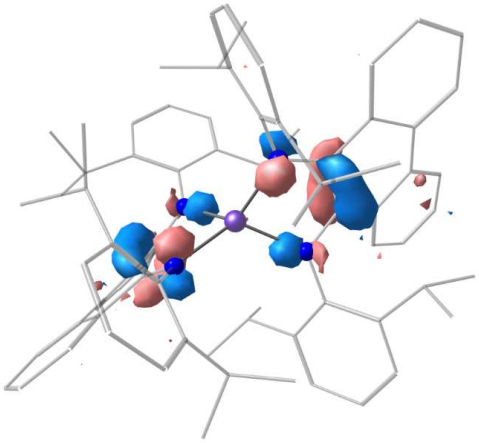

292 (occ.: 2.000)

Figure S47. Orbitals of **3** obtained from CASSCF calculation with an isosurface value of 0.05.

6.5.11 References

[1] A. Fürstner, R. Martin, H. Krause, G. Seidel, R. Goddard, C. W. Lehmann, *J. Am. Chem. Soc.* **2008**, *130*, 8773-8787.

[2] F. Neese Software update: the ORCA program system, version 4.0, *Interdiscip. Rev. Comput. Mol. Sci.*, **2012**, *2*, 73-78.

[3] P. J. Stephens, F. J. Devlin, C.F. Chabalowski, M. J. Frisch, *J. Phys. Chem.* **1994**, *98*, 11623–11627.

[4] F. Weigend, R. Ahlrichs, *Phys. Chem. Chem. Phys.* **2005**, *7*, 3297–3305.

[5] E. Bill, Max-Planck Institute for Chemical Energy Conversion, Mühlheim/Ruhr, Germany.

[6] a) SCALE3ABS, CrysAlisPro, Agilent Technologies Inc. Oxford, GB; b) Sheldrick, G. M. SADABS, Bruker AXS, Madison USA 2007

[7] a) R. C. Clark, J. S. Reid, *Acta Cryst. Section A* **1995**, *51*, 887–897. b) CrysAlisPRo, version 40_64.18, Agilent Technologies Inc. Oxford, GB

[8] G. M. Sheldrick, *Acta Cryst. Section A* **2015**, *71*, 3–8.

[9] G. M. Sheldrick, *Acta Cryst. Section C* **2015**, *71*, 3–8.

[10] O. V. Dolomanov, L. J. Bourhis, R. J. Gildea, J. A. K. Howard, H. Puschmann, *J. Appl. Cryst.* **2009**, *42*, 339–341.

[11] A. Paulovicova, U. El-Ayaan, K. Shibayama, T. Morita, Y. Fukuda, *Eur. J. Inorg. Chem.* **2001**, *2001*, 2641–2646.

[12] M. J. Supej, A. Volkov, L. Darko, R. A. West, J. M. Darmon, C. E. Schulz, K. A. Wheeler, H. M. Hoyt, *Polyhedron* **2016**, *114*, 403–414.

[13] W. W. Brennessel, R. E. Jilek, J. E. Ellis, *Angew. Chem. Int. Ed.* **2007**, *46*, 6132–6136; *Angew. Chem.* **2007**, *119*, 6244–6248.

[14] M. Swart, A. W. Ehlers, K. Lammertsma, *Mol. Phys.* **2004**, *102*, 2467–2474.

[15] P. J. Stephens, F. J. Devlin, C. F. Chabalowski, M. J. Frisch, *J. Phys. Chem.* **1994**, *98*, 11623–11627.

[16] F. Weigend, *Phys. Chem. Chem. Phys.* **2006**, *8*, 1057.

[17] A. Hellweg, C. Hattig, S. Hofener, W. Klopper, *Theor. Chem. Acc.* **2007**, *117*, 587.

7 Direct Synthesis of an Anionic 13-Vertex *closo*-Cobaltacarborane Cluster

Thomas M. Maier, Peter Coburger, Nicolaas P. van Leest, Evamarie Hey-Hawkins, and Robert Wolf

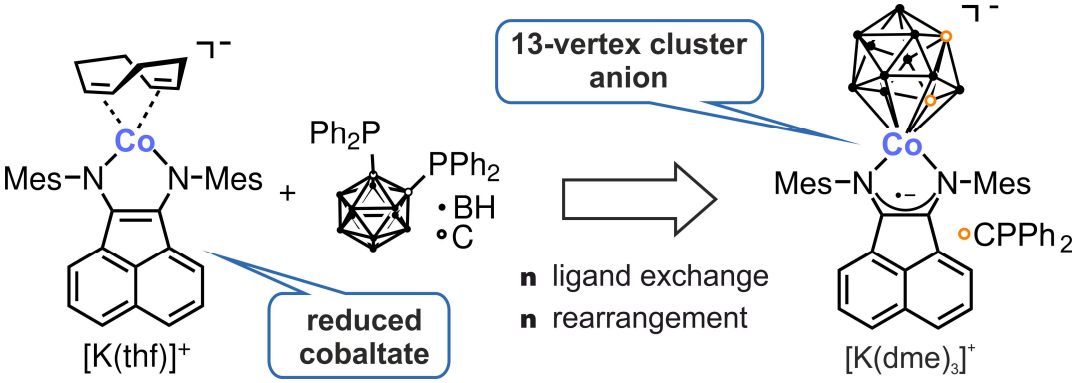

T. M. Maier performed the experimental work and wrote the manuscript. P. Coburger performed and interpreted the quantum chemical calculations. A. Straube (University of Leipzig) measured $^{13}C\{^{1}H, ^{31}P\}$ NMR spectra. N. P. van Leest recorded the EPR spectra and analyzed the results. R. Wolf and E. Hey-Hawkins supervised and directed the project.

This chapter was published in *Dalton Transactions* as a communication: T. M. Maier, P. Coburger, N. P. van Leest, E. Hey-Hawkins, R. Wolf, *Dalton Trans.* **2019**, 48, 15772-15777. Reproduced with permission from Royal Society of Chemistry. Schemes, Figures, and text may differ from published version.

7.1 Introduction

Supraicosahedral metallacarboranes are of interest due to various applications in catalysis, materials science, and biomedicine.[1] 13-Vertex metallacarboranes (MC_2B_{10}) dominate this area. The first member of this class of compounds [$CpCo(C_2B_{10}H_{12})$] (Cp = cyclopentadienide), was reported by *Hawthorne* and co-workers in 1971.[2] In this seminal work, the synthesis of the 13-vertex cobaltacarborane was achieved by reduction of the parent 1,2-dicarba-*closo*-dodecaborane ($C_2B_{10}H_{12}$) with elemental sodium and subsequent treatment with NaCp, $CoCl_2$ and air. This synthetic scheme was called "polyhedral expansion", a term coined by *Hawthorne*. Subsequently, a large variety of 13-vertex cobaltacarborane derivatives was synthesized following this approach in the next decades.[3]-[13] Notably, *Stone*, *Welch* and co-workers established another synthetic route towards such species in 1984 by treating the parent 12-vertex carborane with the low-valent cobalt complex [$Co(PEt_3)_4$]. Here a $Co(PEt_3)_2$ fragment was directly inserted into the cluster with the cobalt phosphane complex simultaneously acting as the reducing agent and metal source.[14]

As shown by several groups in electrochemical investigations, neutral 13-vertex cobaltacarboranes can be reduced reversibly.[3],[8],[9],[15] Such reduced species were used *in situ* as nucleophilic intermediates for the synthesis of 14-vertex bimetallacarboranes.[12],[16]-[18] Despite their synthetic value, only a few anionic 13-vertex cobaltacarboranes have been well characterized. One important example is the homoleptic complex anion [4,4'-Co-(1,6-*closo*-$C_2B_{10}H_{12})_2$]$^-$ **A** reported as its tetraethylammonium salt by *Hawthorne* in 1973.[3] Shortly afterwards, *Hawthorne* published the fascinating complex **B**, where the B–H moieties in the 5-position of both clusters units in **A** were formally substituted by cyclopentadienyl cobalt fragments.[19] Homoleptic complex **C** shown in Figure 1, an isomer of **A**, was synthesized and characterized by X-ray crystallography by *Welch* and co-workers.[8]

Further detailed electrochemical and spectroscopic studies have shown that a series of anionic 13-vertex indenyl cobaltacarboranes with 4,1,6-, 4,1,8-, 4,1,10- and 4,1,12-CoC_2B_{10} architectures, e.g. **D**, are accessible by the reduction of neutral precursors.[9] These anions were characterized *in situ* by UV-vis and EPR spectroscopy.

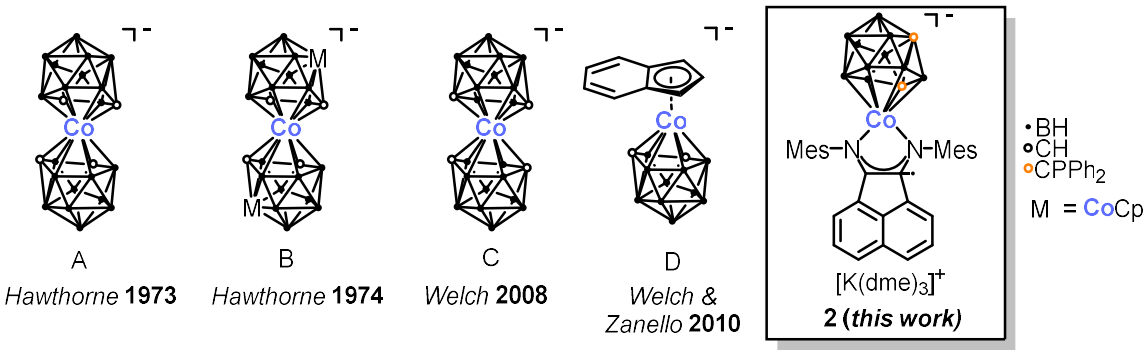

Figure 1. Examples of anionic 13-vertex cobaltacarboranes. For clarity, only the 4,1,6-isomer of **D** is shown, the respective 4,1,8-, 4,1,10-, and 4,1,12-isomers were described in the same work.[9]

7.2 Results and Discussion

Here we report the synthesis and characterization of a new anionic 13-vertex cobaltacarborane, **2**, which contains a redox-active bis(iminoacenapthene) (BIAN) ligand at cobalt and two phosphanyl moieties attached to the cluster carbon atoms. Similar to *Stone's* approach, this complex is obtained in a facile one-pot procedure from 1,2-bis(diphenylphosphino)-*closo*-carborane **L** and a highly reduced cobaltate anion **1** (Scheme 1).[20],[21] We describe the structural and spectroscopic characteristics of **2**, and we propose a mechanism for its formation based on model reactions, NMR spectroscopic monitoring and quantum chemical calculations.

As part of a research program studying the chemistry of phosphanyl-substituted carborane compounds,[22] it was presumed that bis(phosphane) **L** might be a suitable chelate ligand for the $[Co(BIAN)]^-$ fragment due to the strongly electron-withdrawing properties of **L**. [20],[21] In order to test this hypothesis, the 1:1 reaction of **1** with **L** was performed in THF as shown in Scheme 1. Upon mixing **1** and **L** in THF, a deep purple reaction mixture is formed immediately. In contrast to initial expectations, the desired adduct **2'** is not observed at any stage of the reaction; instead, a polyhedral ring expansion occurs, resulting in a 13-vertex cluster anion. The deep purple crystalline potassium salt **2** can be isolated in 59% yield after work-up and crystallisation of the crude product from DME/*n*-hexane. $^{31}P\{^1H\}$ NMR spectroscopic monitoring shows that the reaction takes approximately 40 h at 50 °C to go to completion. Several reaction intermediates can be observed (*vide infra*), yet the formation of the final product is very selective when the reaction is finished.

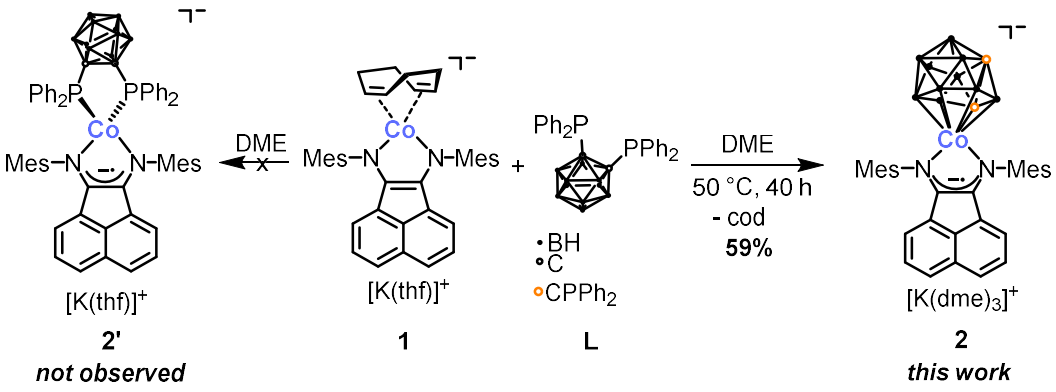

Scheme 1. Synthesis of **2** and initially attempted synthesis of **2'**.

Crystals of **2** suitable for single-crystal X-ray diffraction (XRD) were obtained by slow diffusion of *n*-hexane into a DME solution. The molecular structure is shown in Figure 2. A contact ion pair between $[K(dme)_3]^+$ and a 13-vertex cobaltacarborane cluster anion is observed, in which the cobalt atom caps a six-membered CB_5 ring with typical Co–B distances of 2.149(2) – 2.197(2) Å and Co1–C3 of 2.090(1) Å.[4],[5],[7],[22] During the course of the reaction an isomerization takes place, and in the final 13-vertex cluster, the carbon atoms occupy the positions 1 and 8. Thus, **2** can be classified as a 4,1,8-cobaltacarborane according to common numbering schemes of such clusters.[5] Such an isomerization is frequently observed for related 13-vertex metallacarboranes.[1],[24] The potassium cation K1 interacts with two B–H moieties (K1–B5/B6 3.409(1) Å) of the carborane cluster. Cobalt is additionally coordinated by the ^{Mes}BIAN ligand with unexceptional Co–N distances of 1.960(1) Å and 1.935(1) Å. Key bond lengths within the ^{Mes}BIAN framework of this α-diimine ligand suggest that it is present in its monoanionic form. In particular, the C1–C2 bond (1.420(2) Å) is slightly longer than in the structures of closely related dianionic BIAN ligands (1.40 Å for $Na_2[^{Dipp}BIAN]$, ^{Dipp}BIAN = bis(2,6-diisopropylphenyliminoacenaphthene)diimine), and the N1–C1 (1.332(2) Å), and N2–C2 bonds (1.325(2) Å) are also shorter than expected for a dianionic ligand (1.39 Å for $Na_2[^{Dipp}BIAN]$).[25]

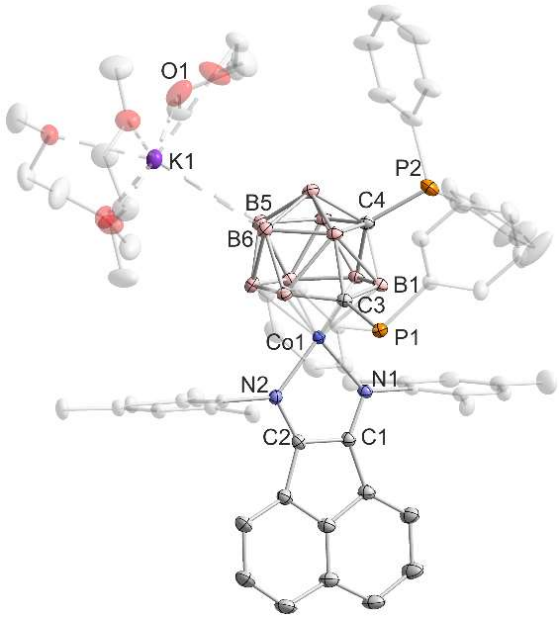

Figure 2. Solid-state structure of **2** with thermal ellipsoids drawn at the 40% probability level. Selected bond lengths [Å] and angles [°]: N1–C1 1.332(2), N2–C2 1.325(2), C1–C2 1.420(2), N1–Co1 1.960(1), N2–Co1 1.935(1), Co1–C3 2.090(1), C3–B1 1.549(2), K1···B5 3.409(1), K1···B6 3.409(1), C3–P1 1.837(1), C4–P2 1.867(1), N1–Co1–N2 82.20(5). Hydrogen atoms are omitted for clarity.

Multinuclear NMR spectra of **2** in THF-d_8 are consistent with the crystallographically determined molecular structure. The $^{31}P\{^1H\}$ NMR spectrum shows two singlets at 28.9 ppm and 24.1 ppm (*cf.* a shift of 7.8 ppm for the starting material **L**), while the ^1H and $^{13}C\{^1H\}$ NMR data show that the *ortho*-methyl substituents of the mesityl groups are diastereotopic presumably due to hindered rotation around the $C_{(mesityl)}$–N bond. These methyl groups show four resonances in the $^{13}C\{^1H\}$ NMR spectrum. Two of them split into a doublet due to through-space coupling to the phosphorus atom P1, proven by a $^{13}C\{^1H,^{31}P\}$ NMR experiment. The hydrogen atoms of the carborane unit give rise to a very broad signal from 4.0 to 0.0 ppm. The ^{11}B and $^{11}B\{^1H\}$ NMR spectra are typical for a metallacarborane framework and show four broad signals in the range of 13.3 to –20.9 ppm.

Due to the presence of three potentially redox-active sites (cobalt atom, ^{Mes}BIAN, and carborane ligand), the redox properties of **2** were of interest. A cyclic voltammogram recorded in THF/^{n}Bu$_4$NPF$_6$ shows a reversible wave at $E_{1/2}$ = –0.6 V vs. Fc/Fc$^+$, which may be assigned to the oxidation of anion **2** by one electron to a neutral compound (Figure 3). In addition, two irreversible waves are observed at +0.5 V and –2.5 V vs.

Fc/Fc^+, which can be assigned to a second oxidation and a reduction process, respectively.

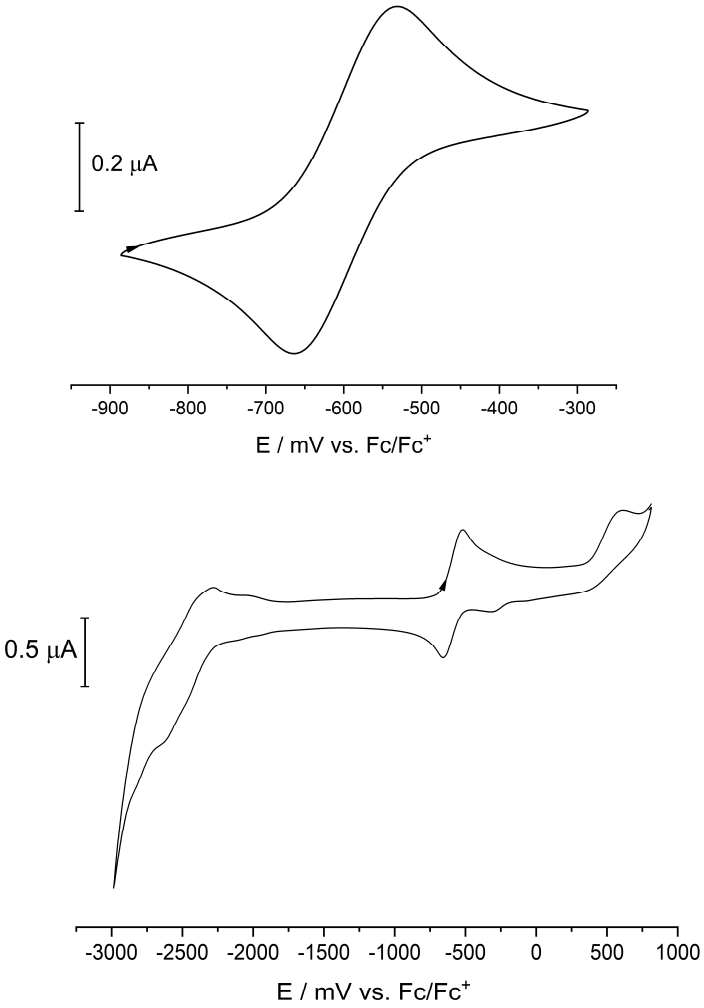

Figure 3. Cyclic voltammograms of **2** in THF/^{n}Bu$_4$NPF$_6$. Scan rate: 50 mV s^{-1}.

The UV-vis spectrum of deep purple **2** shows intense absorptions at 320 nm and 504 nm (ε = 51000 L mol^{-1} cm^{-1}) with a shoulder at 605 nm. A calculated spectrum obtained with TD-DFT methods qualitatively confirms the experimental spectrum (Figure 4) and shows that the intense absorptions observed in the visible region arise from MLCT transitions involving cobalt and the ^{Mes}BIAN ligand (see the SI, Figure S18) as observed in other main group and transition metal BIAN complexes.[25]

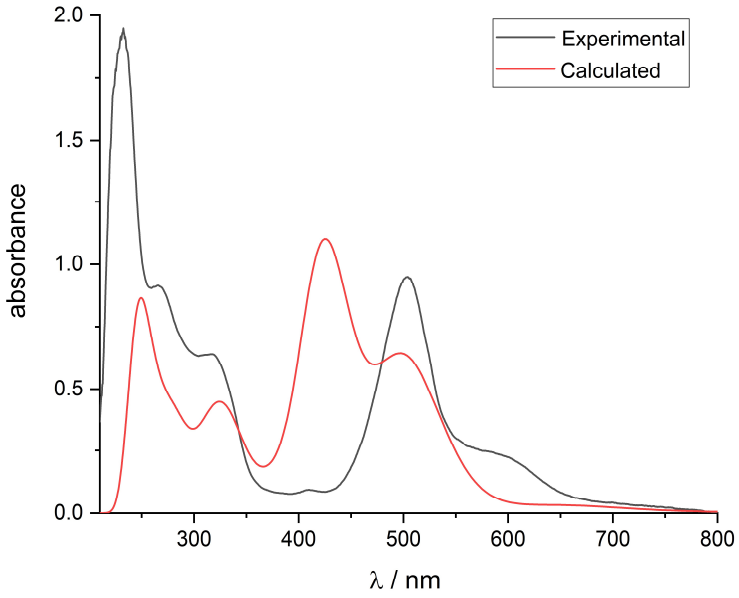

Figure 4: Calculated (red) and measured UV-vis spectrum of **2**.

The electronic structure of **2** was additionally probed by CASSCF calculations (see the SI for details). These calculations reveal the strongly covalent nature of the bonding between cobalt and the BIAN ligand, making the assignment of an oxidation state to the cobalt center somewhat ambiguous. An MO analysis clearly shows that a BIAN-centerd π*-orbital is partially occupied and thus indicates a redox-noninnocent behaviour of the ligand (see the SI for details). This is in line with the solid-state molecular structure of **2**, which suggests that a monoanionic BIAN ligand is present (*vide supra*).

To gain insight into the reaction mechanism, a 1:1 reaction between cobaltate **1** and **L** was monitored by $^{31}P\{^{1}H\}$ NMR spectroscopy at room temperature, where the rate of the reaction was slow enough to detect reaction intermediates (Figure 5). After 30 min, a signal at 17.9 ppm was observed (see Figure 5a), which can presumably be assigned to 1,2-bis(diphenylphosphanyl)-1,2-dicarba-*nido*-dodecaborate(12) (***nido*-L**$^{2-}$) as independently confirmed by the detection of the protonated derivative (***nido*-HL**$^{-}$) in electrospray ionisation mass spectra (*vide infra*).§ After work-up and crystallization of the crude product from *n*-hexane, a mixture of dark orange crystals of [(^{Mes}BIAN)Co(η^4-cod)] (**Int-A**) and a few crystals of a second complex [(^{Mes}BIAN)Co(**L**)] (**3**) were isolated.‡ **3** is likely formed by reaction of **Int-A** and remaining **L**. An isolated yield of 17% can be estimated for **Int-A** assuming that it is by far the major species in

this mixture. Complex **3** was not detected by $^{31}P\{^{1}H\}$ NMR spectroscopy due to its paramagnetic nature.

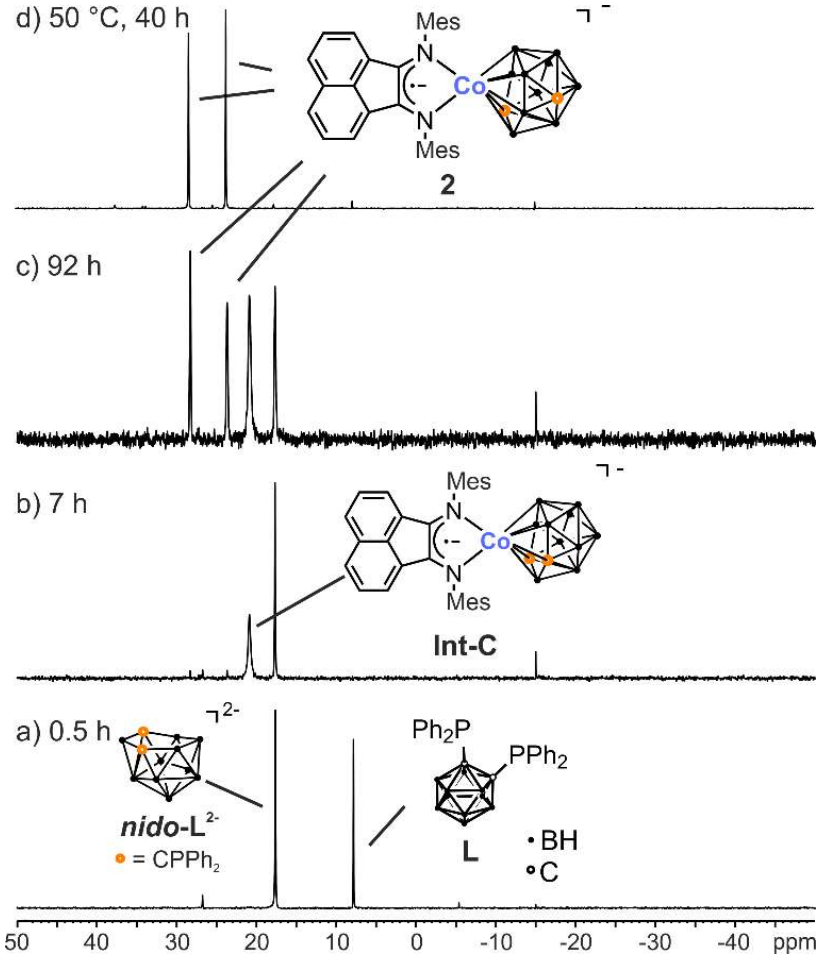

Figure 5. $^{31}P\{^{1}H\}$ NMR spectra (161 MHz, 300 K, C_6D_6) of a 1:1 reaction of **1** and **L** in THF at 25 °C (a-c); Reaction NMR at 50 °C in THF (d); Signal at –15.1 ppm = P_2Ph_4

The molecular structure of **Int-A** was determined by single-crystal XRD and is shown in Figure 6a. A square-planar cobalt(I) complex is observed, which contains an η^4-coordinated 1,5-cyclooctadiene molecule. In addition, a ^{Mes}BIAN ligand binds via the two nitrogen atoms. Using the midpoints of the C=C bonds of cod, the dihedral angle between the planar ^{Mes}BIAN moiety and the cod ligand was determined to be 5.3°, which shows that the coordination geometry for cobalt is essentially square planar. The C–C and C–N bond lengths of the diimine fragment (C1–C2 1.428(5) Å, C1–N1 1.316(5) Å, and C2–N2 1.332(5) Å) are similar to those in the closely related Ni complex

[(DippBIAN)Ni(η⁴-cod)].[26] These values suggest the presence of a monoanionic diimine ligand and, consequently, a +I oxidation state for cobalt.[26]

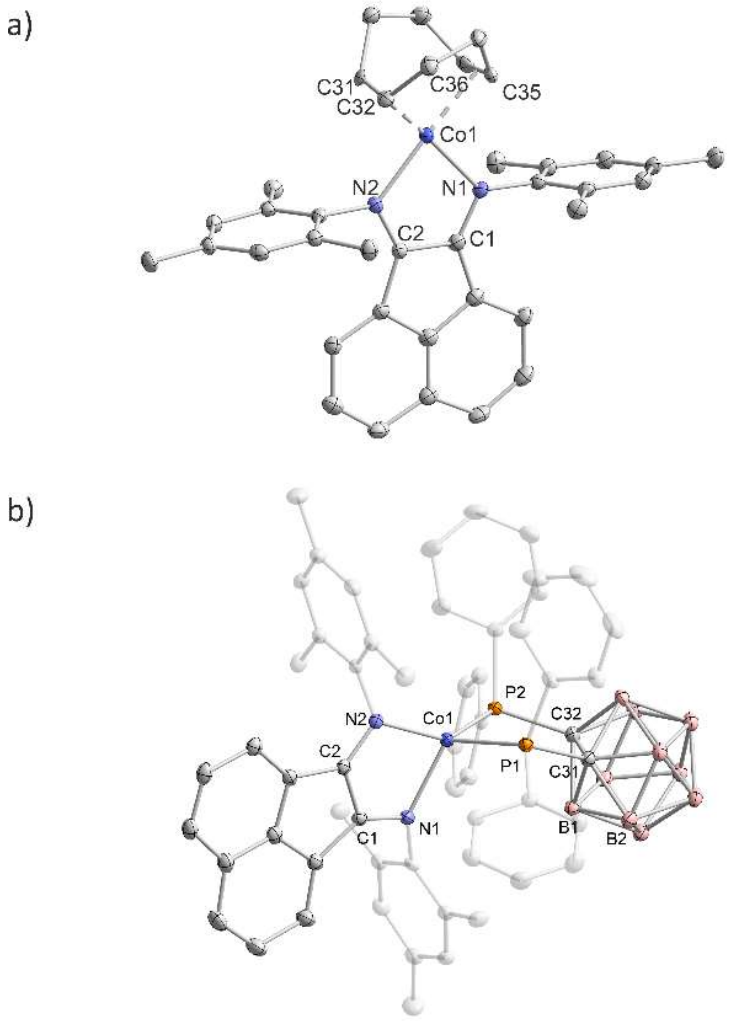

Figure 6. Solid-state structures of a) [(MesBIAN)Co(η⁴-cod)] (**Int-A**) and b) [(MesBIAN)Co(**L**)] (**3**) with thermal ellipsoids drawn at the 40% probability level. Selected bond lengths [Å] and angles [°]: For **Int-A**: N1–C1 1.316(5), N2–C2 1.332(5), C1–C2 1.428(5), N1–Co1 1.963(3), N2–Co1 1.976(3), C31–C32 1.391(6), N1–Co1–N2 83.0(1); For **3**: N1–C1 1.340(3), N2–C2 1.322(3), C1–C2 1.432(3), N1–Co1 2.042(2), Co1–P1 2.169(6), Co1–P2 2.198(1), P1–C31 1.902(2), P2–C32 1.908(2), C31–C32 1.697(3). P1–Co1–P2 90.08(2), N1–Co1–N2 83.16(8). Hydrogen atoms are omitted for clarity.

[(MesBIAN)Co(η⁴-cod)] (**Int-A**) is paramagnetic with a magnetic moment of μ_{eff} = 1.8(1) μ_B determined by the Evans NMR method in C_6D_6 solution. An EPR spectrum of **Int-A** in toluene glass at 20 K is slightly axial (nearly isotropic) with simulated g values of 2.01 ($g_{\parallel}$) and 2.00 ($g_{\perp}$) (Figure 7, left) indicating a ligand-centered

radical. This is also supported by DFT calculations, which show that the spin density mainly resides on the ^{Mes}BIAN ligand (Figure 7, right).

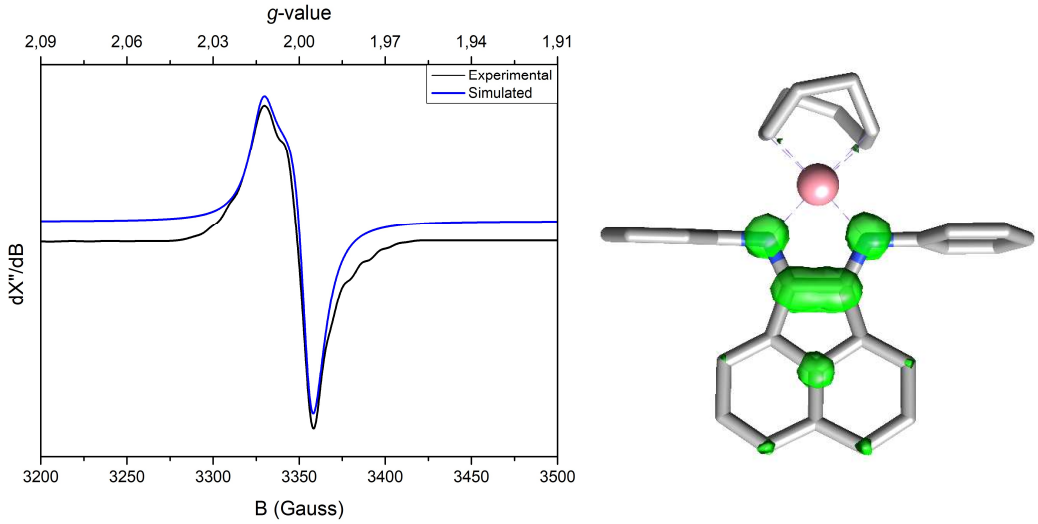

Figure 7. Experimental (black) and simulated (blue) X-band EPR spectrum of **3** at 20 K (Microwave frequency: 9.370555 GHz, power: 0.6325 mW, modulation amplitude: 1.000 G) (left); Spin density plot of **3**; M06-D3(0)-def2-TZVP CPCM(THF); Isosurface value: 0.05 (right).

Figure 6b shows the single-crystal XRD structure of **3**. Both the ^{Mes}BIAN ligand and the *ortho*-carboranyl bis(phosphane) **L** act as bidentate chelate ligands, while the cobalt atom shows a distorted tetrahedral coordination environment (83.7° between the planes P1–Co1–P2 and N1–Co1–N2) (Figure 6b). The bite angle of the bis(phosphane) P1–Co1–P2 (90.1°) is similar to our previously reported cobalt(III)-phosphanido (90.7°) complex.[28] The C–N and C–C distances in the diimine unit of the ^{Mes}BIAN framework (C1–N1 1.340(3) Å, C2–N2 1.322(3) Å, and C1–C2 1.432(3) Å) indicate the presence of a ^{Mes}BIAN^{-} monoanion similar to **Int-A**.[25] Assuming that the bis(phosphane) ligand **L** remains neutral, this would result in the +I oxidation state for cobalt, for which a square-planar coordination is normally preferred. A tetrahedral structure is probably observed due to steric repulsion between the bulky mesityl groups and the phenyl substituents on **L**. Further spectroscopic characterization of **3** was unfortunately not possible due to the small amount of isolated crystalline material, which could not be successfully separated from the major species **Int-A**.

When the 1:1 reaction between cobaltate **1** and **L** is carried out for a longer reaction time, the formation of additional intermediates can be observed. As shown in Figures 5b and

5c, a new, broad singlet (20.9 ppm, $\Delta\nu_{1/2}$= 74 Hz) was detected by $^{31}P\{^{1}H\}$ NMR spectroscopy after several hours. The chemical shift is very similar to the final product **2**, thus, this signal can likely be assigned to the symmetric 13-vertex cobaltacarborane **Int-C** shown in Scheme 3. After four days at room temperature, the signals of ***nido*-L**$^{2-}$ and **Int-C** are still present, while significant quantities of **2** are formed at this point. As shown by Figure 5d, **2** is by far the dominant species observed by $^{31}P\{^{1}H\}$ NMR spectroscopy after heating at 50 °C for 40 h, showing that the reaction is eventually very selective towards the formation of the final product **2**. The mechanism shown in Scheme 3 can be proposed based on the experimental observations discussed above in conjunction with quantum chemical calculations. According to DFT calculations at the M06-D3(0)/def2-TZVP CPCM(THF) level of theory (see the SI),[29] it is conceivable that the *ortho*-carboranyl bis(phosphane) ligand **L** is reduced by **1** in the first step of the reaction, forming ***ortho*-L**$^{2-}$ and **Int-A**. The calculations suggest that this step is exothermic by –8.4 kcal mol^{-1}. In addition, such a redox reaction is in agreement with the reduction and oxidation potentials determined by cyclic voltammetry for **1** ($E_{1/2}$ = –1.72 V vs. Fc/Fc^{+} in THF) and for **L** ($E_{1/2}$ = –1.9 V vs. Fc/Fc^{+} in MeCN).[30] O***rtho*-L**$^{2-}$ was not directly observed, because it rapidly isomerises to ***nido*-L**$^{2-}$ (step 2) in an exothermic process (–7.7 kcal mol^{-1}). The latter species was detected by $^{31}P\{^{1}H\}$ NMR spectroscopy (*vide supra*). Moreover, the protonated species ***nido*-HL**$^{-}$ was also detected in electrospray ionisation mass spectra of the reaction mixture (see the SI). A substitution of 1,5-cyclooctadiene in **3** by ***nido*-L**$^{2-}$ (step 3) followed by concomitant oxidation of the resulting intermediate **Int-B** yields the symmetric 13-vertex metallacarborane **Int-C**, also detected by $^{31}P\{^{1}H\}$ NMR spectroscopy. Taken together, steps 3 and 4 are exothermic by –7.4 kcal mol^{-1}. An isomerization to the unsymmetrical complex **2** is the final step of this sequence (step 5, again exothermic by –13.3 kcal mol^{1}). Such an isomerization is commonly observed for related 13-vertex metallacarboranes.[1],[24] The mechanism proposed in Scheme 3 is thus in line with all NMR spectroscopic and crystallographic observations. The proposed intermediates **Int-A** – **Int-C** are viable species based on the DFT calculations, and the (mostly exothermic) reaction steps add up to a total reaction energy of −36.8 kcal mol^{-1}.§§

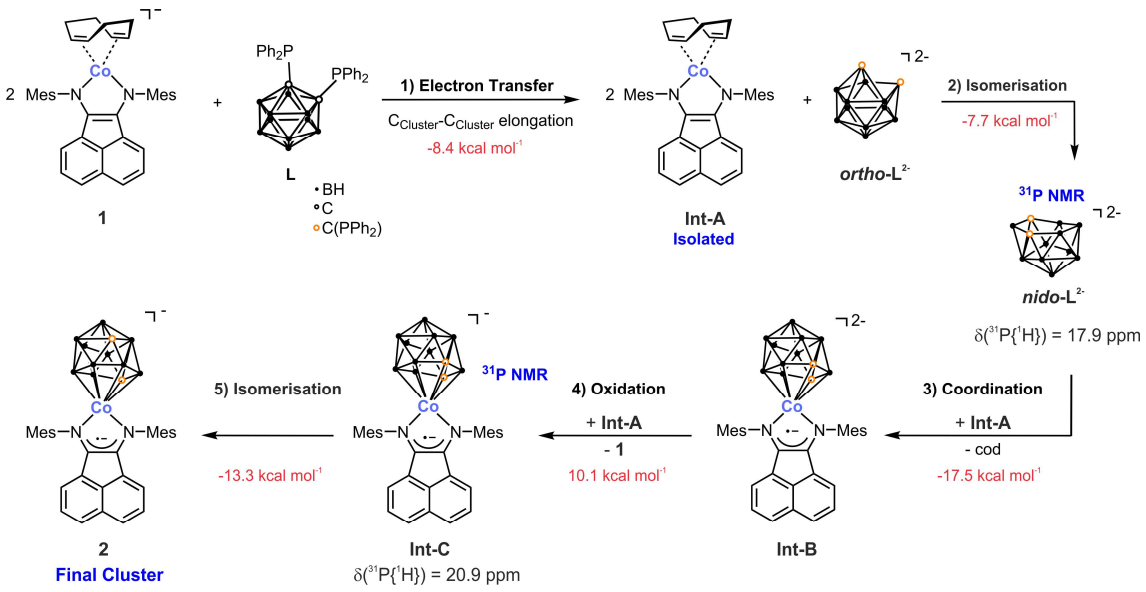

Scheme 3. Proposed mechanism based on experimental and quantum mechanical methods. Cations are omitted for clarity. Reaction energies were calculated on the M06-D3(0)def2-TZVP CPCM(THF) level of theory.

7.3 Conclusion

The anionic 13-vertex *closo*-cobaltacarborane cluster was synthesized by a direct route using α-diimine cobaltate [K(thf){(^{Mes}BIAN)Co(η^4-cod)}] (**1**) and isolated in a high yield of 59%. The mechanism of this transformation was studied by experimental techniques (single-crystal XRD, multinuclear NMR spectroscopy and ESI-MS) and through DFT calculations. An intermediate [(^{Mes}BIAN)Co(η^4-cod)] (**Int-A**) was isolated, while ESI-MS data and DFT investigations hint at the formation of a dianionic *nido*-carborane ***nido*-L^{2-}** as a key intermediate *en route* to the final cluster **2**. These results suggest a redox mechanism that is initiated by an electron transfer from **1** to the 1,2-bis(diphenylphosphino)-*ortho*-carborane ligand **L**. Based on the work presented here, the synthesis of new anionic, metallacarborane derivatives by reaction of further carborane derivatives with low-valent metalate anions[31] should be an appealing subject for future investigations.

7.4 Notes and References

Note that the CHN analysis for **Int-A** is not in agreement with the calculated values for $C_{38}H_{40}N_2Co$ [found (calc.): C: 76.26 (78.20) H: 6.95 (6.91) N: 4.09 (4.80)]. The observed discrepancies are likely due to the contamination of **Int-A** with a minor amount of **3.**

§ The possible formation of ***nido*-L**$^{2-}$ as a reaction intermediate is additionally corroborated by an independent experiment, where bis(phosphane) **L** was reduced with two equivalents of potassium graphite (KC_8, see the SI).

§§ The chelate complex **2′** was not observed in any of our NMR spectroscopic investigations. In fact, this complex lies higher in energy than **2** by 5.7 kcal mol^{-1} at the M06-D3(0)/def2-TZVP CPCM(THF) level of theory.

[1] a) R. N. Grimes, *Coord. Chem. Rev.* **2000**, *200-202*, 773-811; b) R. N. Grimes, *Carboranes*, Elsevier, Saint Louis, 3rd edition, **2016**; c) V. I. Bregadze, *Chem. Rev.* **1992**, *92*, 209-223.

[2] M. F. Hawthorne, G. B. Dunks, M. M. McKown, *J. Am. Chem. Soc.* **1971**, *93*, 2541–2543.

[3] D. F. Dustin, G. B. Dunks, M. F. Hawthorne, *J. Am. Chem. Soc.* **1973**, *95*, 1109–1115.

[4] M. R. Churchill, B. G. DeBoer, *Inorg. Chem.* **1974**, *13*, 1411–1418.

[5] D. Ellis, M. E. Lopez, R. McIntosh, G. M. Rosair, A. J. Welch, R. Quenardelle, *Chem. Commun.* **2005**, 1348–1350.

[6] S. Zlatogorsky, D. Ellis, G. M. Rosair, A. J. Welch, *Chem. Commun.* **2007**, 2178–2180.

[7] L. Deng, H.-S. Chan, Z. Xie, *Inorg. Chem.* **2007**, *46*, 2716–2724.

[8] D. Ellis, R. D. McIntosh, S. Esquirolea, C. Viñas, G. M. Rosair, F. Teixidor, A. J. Welch, *Dalton Trans.* **2008**, 1009–1017.

[9] G. Scott, A. McAnaw, D. McKay, A. S. F. Boyd, D. Ellis, G. M. Rosair, S. A. Macgregor, A. J. Welch, F. Laschi, F. Rossi, P. Zanello, *Dalton Trans.* **2010**, *39*, 5286–5300.

[10] D. Ellis, G. M. Rosair, A. J. Welch, *Chem. Commun.* **2010**, *46*, 7394–7396.

[11] A. McAnaw, M. E. Lopez, G. Scott, D. Ellis, D. McKay, G. M. Rosair, A. J. Welch, *Dalton Trans.* **2012**, *41*, 10957–10969.

[12] A. McAnaw, M. E. Lopez, D. Ellis, G. M. Rosair, A. J. Welch, *Dalton Trans.* **2012**, *42*, 671–679.

[13] D. Mandal, W. Y. Man, G. M. Rosair, A. J. Welch, *Acta Crystallogr. Sect. C Struct. Chem.* **2015**, *71*, 793–798.

[14] G. K. Barker, M. P. Garcia, M. Green, F. G. A. Stone, A. J. Welch, *J. Chem. Soc. Chem. Commun.* **1983**, 137–139.

[15] Z. Qiu, K.-H. Wong, Z. Xie, *J. Organomet. Chem.* **2012**, *721–722*, 97–103.

[16] J. S. Ward, H. Tricas, G. Scott, D. Ellis, G. M. Rosair, A. J. Welch, *Organometallics* **2012**, *31*, 2523–2525.

[17] W. J. Evans, M. F. Hawthorne, *J. Chem. Soc. Chem. Commun.* **1974**, 38–39.

[18] A. McAnaw, M. Elena Lopez, D. Ellis, G. M. Rosair, A. J. Welch, *Dalton Trans.* **2014**, *43*, 5095–5105.

[19] D. F. Dustin, M. F. Hawthorne, *J. Am. Chem. Soc.* **1974**, *96*, 3462–3467.

[20] a) R. P. Alexander, H. Schroeder, *Inorg. Chem.* **1963**, *2*, 1107–1110; b) A. R. Popescu, F. Teixidor, C. Viñas, *Coord. Chem. Rev.* **2014**, *269*, 54–84.

[21] a) S. Pelties, T. Maier, D. Herrmann, B. de Bruin, C. Rebreyend, S. Gärtner, I. G. Shenderovich, R. Wolf, *Chem. Eur. J.* **2017**, *23*, 6094–6102; b). C. P. G. Ziegler, T. M. Maier, S. Pelties, C. Taube, F. Hennersdorf, A. W. Ehlers, J. J. Weigand, R. Wolf, *Chem. Sci.* **2019**, *10*, 1302-1308; c) T. M. Maier, S. Sandl, I. G. Shenderovich, A. Jacobi von Wangelin, J. J. Weigand, R. Wolf, *Chem. Eur. J.* **2019**, *25*, 238-245.

[22] Selected examples: a) S. Stadlbauer, R. Frank, I. Maulana, P. Lönnecke, B. Kirchner, E. Hey-Hawkins, *Inorg. Chem.* **2009**, *48*, 6072–6082; b) S. E. Lyubimov, V. A. Davankov, K. N. Gavrilov, T. B. Grishina, E. A. Rastorguev, A. A. Tyutyunov, T. A. Verbitskaya, V. N. Kalinin, E. Hey-Hawkins, *Tetrahedron Lett.* **2010**, *51*, 1682–1684; c) A. Kreienbrink, P. Lönnecke, M. Findeisen, E. Hey-Hawkins, *Chem. Commun.* **2012**, *48*, 9385–9387; d) P. Coburger, J. Schulz, J. Klose, B. Schwarze, M. B. Sárosi; E. Hey-Hawkins, *Inorg. Chem.* **2017**, *56*, 292–304; e) P. Coburger, G. Kahraman, A. Straube; E. Hey-Hawkins, *Dalton Trans.* **2019**, *48*, 9625–9630.; and references therein.

[23] a) M. R. Churchill, B. G. DeBoer, *J. Chem. Soc., Chem. Commun.* **1972**, *24*, 1326–1327. b) K. J. Donaghy, P. J. Carroll, L. G. Sneddon, *J. Organomet. Chem.* **1998**, *550*, 77. c) A. Burke, R. McIntosh, D. Ellis, G. M. Rosair, A. J. Welch, *Collect. Czech. Chem. Commun.*, **2002**, *67(7),* 991. d) R. McIntosh, D. Ellis, J. Gil-Lostes, K. J. Dalby, G. M. Rosair, A. J. Welch, *Dalton Trans.* **2005**, *10*, 1842–1846. e) L. Deng, H.-S. Chan, Z. Xie, *J. Am. Chem. Soc.* **2006**, *128*, 5219-5230.

[24] J. A. Doi, E. A. Mizusawa, C. B. Knobler, M. F. Hawthorne, *Inorg. Chem.* **1984**, *23*, 1482-1484.

[25] a) J. Wang, R. Gaguly, L. Yongxin, J. Diaz, H.S. Soo, F. Garcia, *Inorg. Chem.* **2017**, *56*, 7811-7820; b) P. A. Papanikolaou, N. V. Tkachenko, *Phys. Chem. Chem. Phys.*, **2013**, *15*, 13128-13136.

[26] M. J. Srgo, D. W. Stephan, *Dalton Trans.* **2010**, *39*, 5786–5794.

[27] For characteristic C-C and C-N bond lengths see e.g. I. L. Fedushkin, A. A. Skatova, V. A. Chudakova, G. K. Fukin, *Angew. Chem. Int. Ed.* **2003**, *42*, 3294–3298; *Angew. Chem.* **2003**, *115*, 3416-3420.

[28] P. Coburger, S. Demeshko, C. Rödl, E. Hey-Hawkins, R. Wolf, *Angew. Chem. Int. Ed.* **2017**, *56*, 15871–15875.; *Angew. Chem.* **2017**, *129*, 16087–16091.

[29] a) S. Grimme, J. Antony, S. Ehrlich, H. Krieg, *J. Chem. Phys.* **2010**, *132*, 154104; b) F. Weigend, R. Ahlrichs, *Phys. Chem. Chem. Phys.* **2005**, *7*, 3297–3305; c) Y. Zhao, D. G. Truhlar, *Theor. Chem. Acc.* **2008**, *120*, 215–241; d) Y. Zhao, D. G. Truhlar, *Chem. Phys. Lett.* **2011**, *502*, 1–13; e) M. Cossi, N. Rega, G. Scalmani, V. Barone, *J. Comput. Chem.*, **2003**, *24*, 669–681; f) A. V. Marenich, C. J. Cramer, D. G. Truhlar, *J. Phys. Chem. B* **2009**, *113*, 6378–6396.

[30] R. Núñez, M. Tarrés, A. Ferrer-Ugalde, F. F. de Biani, F. Teixidor, *Chem. Rev.* **2016**, *116*, 14307–14378.

[31] a) J. E. Ellis, *Inorg. Chem.* **2006**, *45*, 3167-3186; b) W. W. Brennessel, J. E. Ellis, *Inorg. Chem.* **2012**, *51*, 9076-9094.

7.5 Supporting Information

7.5.1 General Procedures

All experiments were performed under an atmosphere of dry Argon (Argon 4.6, Linde) using standard Schlenk techniques or a MBraun UniLab Glovebox.

Chemicals and Solvents: Solvents were dried and degassed with an MBraun SPS800 solvent-purification system. THF, diethyl ether were stored over molecular sieves (3 Å). *n*-hexane was stored over a potassium mirror. 1,2-Dimethoxyethane was stirred over K/benzophenone, distilled and stored over molecular sieves (3 Å). All chemicals were purchased from commercial suppliers and used as received, if not stated otherwise.

Cyclic Voltammetry: Cyclic voltammetry experiments were performed in a single-compartment cell inside a nitrogen-filled glovebox using a CH Instruments CH1600E potentiostat. The cell was equipped with a platinum disc working electrode (2 mm diameter) polished with 0.05 μm alumina paste, a platinum wire counter electrode and an $Ag/AgNO_3$ reference electrode. The supporting electrolyte, tetra-*n*-butylammonium hexafluorophosphate, was dried *in vacuo* at 110 °C for three days. All redox potentials are reported vs. the ferrocenium/ferrocene (Fc^+/Fc) couple.

Elemental Analyses: CHN analyses were recorded by the analytical department of the University of Regensburg with a Micro Vario Cube (Elementar).

ESI-MS: Electron spray ionisation mass spectra were carried out by the analytical department of the University of Regensburg, Agilent Q-TOF 6549 UHD.

EPR spectroscopy: The experimental X-band EPR spectrum of **Int-A** was recorded on a Bruker EMX spectrometer (Bruker BioSpin Rheinstetten) equipped with a He temperature-control cryostat system (Oxford Instruments). The *g* values were calculated with the ORCA software package[1],[2] at the B3LYP[3]/def2-TZVP[4] level of theory. The spectrum was analyzed and simulated using the W95EPR program of Prof. Frank Neese.

NMR spectroscopy: ^{1}H, $^{13}C\{^{1}H\}$, $^{13}C\{^{1}H,^{31}P\}$, $^{11}B\{^{1}H\}$, ^{11}B, $^{31}P\{^{1}H\}$, and ^{31}P NMR spectra in solutions were recorded on Bruker Avance 300 (300 MHz) and Bruker Avance 400 (400 MHz) if not stated otherwise. These chemical shifts are given relative to solvents resonances on the tetramethylsilane (^{1}H, $^{13}C\{^{1}H\}$), 15% BF_3 OEt_2 ($^{11}B\{^{1}H\}$, ^{11}B), 85% H_3PO_4 in H_2O ($^{31}P\{^{1}H\}$, ^{31}P)

scale. The following abbreviations have been used for multiplicities: s = singlet, d = doublet, t = triplet, q = quartet, sept = septet, m = multiplet, dd = doublet of doublets, dt = doublet of triplets.

Melting point: Melting points were measured on samples in sealed capillaries on a Stuart SMP10 melting point apparatus.

UV-vis spectra: UV-vis spectra were recorded on an Ocean Optics Flame spectrometer (Varian Cary 50 spectrometer) in a Quartz cuvette with a layer thickness of 1 cm at room temperature with a concentration of 10^{-4} to 10^{-6} M.

Single-crystal X-ray crystallography: The single crystal X-ray diffraction (XRD) data were recorded on an Agilent GV1000 with a Titan S2 CCD detector (for **2**) and an Agilent Super Nova diffractometer with an Atlas CCD detector (for **Int-A** and **3**). Microfocus Cu K_α radiation (λ = 1.54184 Å) was used in each measurement. Empirical multi-scan[9] and analytical absorption corrections[10] were applied to the data. The structures were solved with SHELXT[11] and least-square refinements on F^2 were carried out with SHELXL[12].

7.5.2 Synthesis of Starting Materials

^{Mes}BIAN,[9] Cp_2Co,[10] [K(thf){Co(η^4-cod)}],[13] [K(thf){(^{Mes}BIAN)Co(η^4-cod)}][12],[13] were synthesized according to Chapters 2 and 3.

7.5.2.1 Synthesis of 1,2-Bis(diphenylphosphino)carborane

1,2-bis(diphenylphosphino)-*ortho*-carborane was synthesized by an adapted procedure of *Schröder* and co-workers.[14]

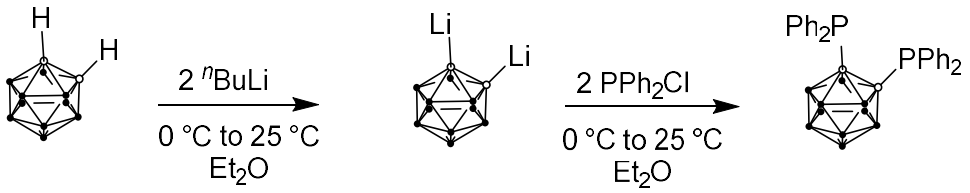

o-Carborane (2.54 g, 17.6 mmol, 1.0 equiv.) was dissolved in 100 mL Et_2O and cooled to 0 °C. *n*-BuLi (15.0 mL, 37.5 mmol, 2.1 equiv., 2.5 M in *n*-hexane) was added dropwise within 5 minutes. A colorless precipitate was formed, and the solution was stirred at 0 °C for 30 min and 2 h at room temperature. Freshly distilled PPh_2Cl (6.8 mL, 37.5 mmol, 2.1 equiv.) in 10 mL Et_2O was added dropwise again at 0 °C. The resulting reaction mixture was stirred overnight and the bright yellow solution was filtered over a pad of silica. The solvent was removed from the clear filtrate and the raw material recrystallized from high-boiling petroleum ether (b.p. 130 °C). 1,2-Bis(diphenylphosphino)-*ortho*-carborane (**L**) was obtained as white crystalline solid.

Yield: 1.10 g (2.15 mmol, 12.2%)

Chemical formula: $C_{26}H_{30}P_2B_{10}$ ($M = 512.57$ g mol^{-1})

^{1}H NMR (400.13 MHz, 300 K, THF-d_8) δ[ppm]: 7.90 (m, 8H, CH_{Ar}), 7.46 (m, 10H, CH_{Ar}), 2.17 (br s, 10H, $B_{10}H_{10}$)

^{11}B{^{1}H} NMR (128.4 MHz, 300 K, THF-d_8) δ[ppm]: 1.16 (br s), –5.72 (br s), –8.12 (br s), –10.33 (br s)

^{31}P{^{1}H} NMR (162 MHz, 300 K, THF-d_8) δ[ppm]: 10.1 ppm

7.5.2 Synthesis of Anionic 13-vertex-*closo*-Cobaltacarborane Cluster

7.5.2.1 Synthesis

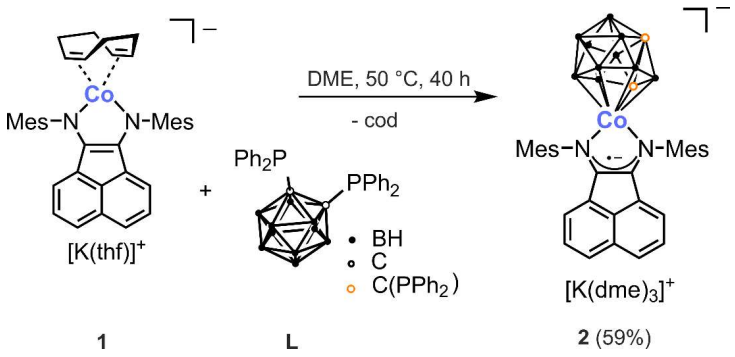

[K(thf){(MesBIAN)Co(η⁴-cod)}] (274 mg, 0.39 mmol, 1.0 equiv.) (**1**) was dissolved in 10 mL THF and added dropwise to a solution of 1,2-bis(diphenylphosphino)-*ortho*-carborane (200 mg, 0.39 mmol, 1.0 equiv.) (**L**) in 10 mL THF. The solution immediately turned red-orange and was stirred for 40 h at 50 °C. During that time the color of the reaction mixture became dark violet. After the reaction the solvent was removed and the residue dissolved in 15 mL DME. The solution was filtered, and the solid residue washed with 3 mL DME. The filtrate was layered with 30 mL *n*-hexane and stored at –35 °C. Dark violet microcrystals were obtained upon storing for one week and isolated by decanting the mother liquor. The crystals still contained three molecules of DME after drying the powder *in vacuo* according to ^{1}H NMR spectroscopy. Analytically pure, crystalline samples suitable for single-crystal X-ray crystallography were obtained by diffusion of *n*-hexane into a concentrated DME solution.

Yield: 286 mg (0.23 mmol, 59%)

Chemical formula: $C_{56}H_{70}KCoN_2P_2B_{10}\cdot(C_4H_8O_2)_3$ (M = 1244.5 g mol^{-1})

^{1}H NMR (400.13 MHz, 300 K, THF-d$_8$) δ[ppm]: 7.90 (m, 2H, $CH_{Ar(Phosphine)}$) 7.69 (m, 2H, $CH_{Ar(Phosphine)}$), 7.50 (m, 4H, $CH_{Ar(Phosphine)}$), 7.10 (m, 4H, $CH_{Ar(Phosphine)}$), 7.10 (m, 2H, CH_{BIAN}), 7.05 (m, 8H, $CH_{Ar(Phosphine)}$), 6.83 (m, 2H, $CH_{Ar(BIAN)}$), 6.80 (s, 1H, $CH_{Ar(Mes)}$), 6.75 (s, 1H, $CH_{Ar(Mes)}$),6.71 (s, 1H, $CH_{Ar(Mes)}$), 6.65 (s, 1H, $CH_{Ar(Mes)}$), 5.73 (d, J = 7.2 Hz), 1H, CH_{BIAN}), 5.64 (d, J = 7.2 Hz, 1H, CH_{BIAN}), 3.43 (DME, CH_2), 3.27 (DME, CH_3) 2.40 (two overlapping singlets, 6H, *o*-CH_3), 2.32 (s, 3H, *p*-CH_3), 2.19 (s, 3H, *p*-CH_3), 1.90 (s, 3H, *o*-CH_3), 1.88 (s, 3H, *o*-CH_3)

^{11}B NMR (128.4 MHz, 300 K, THF-d$_8$) δ[ppm]: 13.3 (br s), 0.4 (br s), –9.6 (br d), –20.9 (br d)

^{11}B{^{1}H} NMR (128.4 MHz, 300 K, THF-d$_8$) δ[ppm]: 13.3 (br s), 0.4 (br s), –9.6 (br s), –20.9 (br s)

$^{13}C\{^{1}H\}$ NMR (100.6 MHz, 300 K, THF-d_8) δ[ppm]: 153.5, 152.0, 151.4, 145.1 (d, J_{CP} = 21.3 Hz), 143.9 (d, J_{CP} = 21.0 Hz), 139.8 (d, J_{CP} = 25.3 Hz), 137.8 (dd, J_{CP} = 7.0 Hz, 7.8 Hz), 136.5 (d, J_{CP} = 5.5 Hz), 136.4 (d, J_{CP} = 5.8 Hz), 135.8 (dd, J_{CP} = 3.8 Hz, 25.3 Hz), 135.0(d, J_{CP} = 22.6 Hz), 134.4, 134.2, 133.8, 133.6, 132.8, 132.3, 131.6, 130.8 (d, J_{CP} = 2.6 Hz), 130.5 (d, J_{CP} = 2.5 Hz), 129.1, 128.9, 128.7, 128.4, 128.3, 128.1, 128.0, 127.9 (d, J_{CP} = 8.0 Hz), 127.6, 127.4 (d, J_{CP} = 3.2 Hz), 127.3(d, J_{CP} = 2.6 Hz), 124.2, 124.0, 118.2, 118.0, 72.5 (DME), 58.7 (DME), 21.5 (CH_3), 21.1 (CH_3), 20.7 (d, J_{CP} = 12.1 Hz, CH_3), 20.2 (d, J_{CP} = 9.4 Hz, CH_3), 19.5 (CH_3), 19.2 (CH_3)

$^{13}C\{^{1}H,^{31}P\}$ NMR (100.6 MHz, 300 K, THF-d_8) δ[ppm]:153.5, 152.0, 151.4, 145.1, 143.9, 139.8, 137.8, 136.5, 136.4, 135.8, 135.0, 134.4, 134.2, 133.8, 133.6, 132.8, 132.3, 131.6, 130.8, 130.5, 129.1, 128.9, 128.7, 128.4, 128.3, 128.1, 128.0, 127.9, 127.6, 127.4, 127.3, 124.2, 124.0, 118.2, 118.0, 72.5 (DME), 58.7 (DME), 21.5 (CH_3), 21.1 (CH_3), 20.7 (CH_3), 20.2 (CH_3), 19.5 (CH_3), 19.2 (CH_3)

$^{31}P\{^{1}H\}$ NMR (162 MHz, 300 K, THF-d_8) δ[ppm]: 28.9 (s, 1P), 24.2 (s, 1P)

Cyclic voltammogram (CV): The CV of complex **2** (13.5 mg) was recorded in 10 mL THF and with the addition of 380 mg $^{n}Bu_4NPF_6$ as electrolyte.

Elemental analysis: calcd. For $C_{68}H_{88}B_{10}CoKN_2O_6P_2$: found (calc.): C: 63.20 (62.95) H: 6.70 (6.84) N: 2.02 (2.16)

Melting point: T > 285 °C: decomposition to a black oil

UV-vis (THF): λ_{max} (nm) / ε ($L \cdot mol^{-1} \cdot cm^{-1}$): 320 (34000), 504 (51000), 605 (11000)

7.5.2.2 NMR spectra

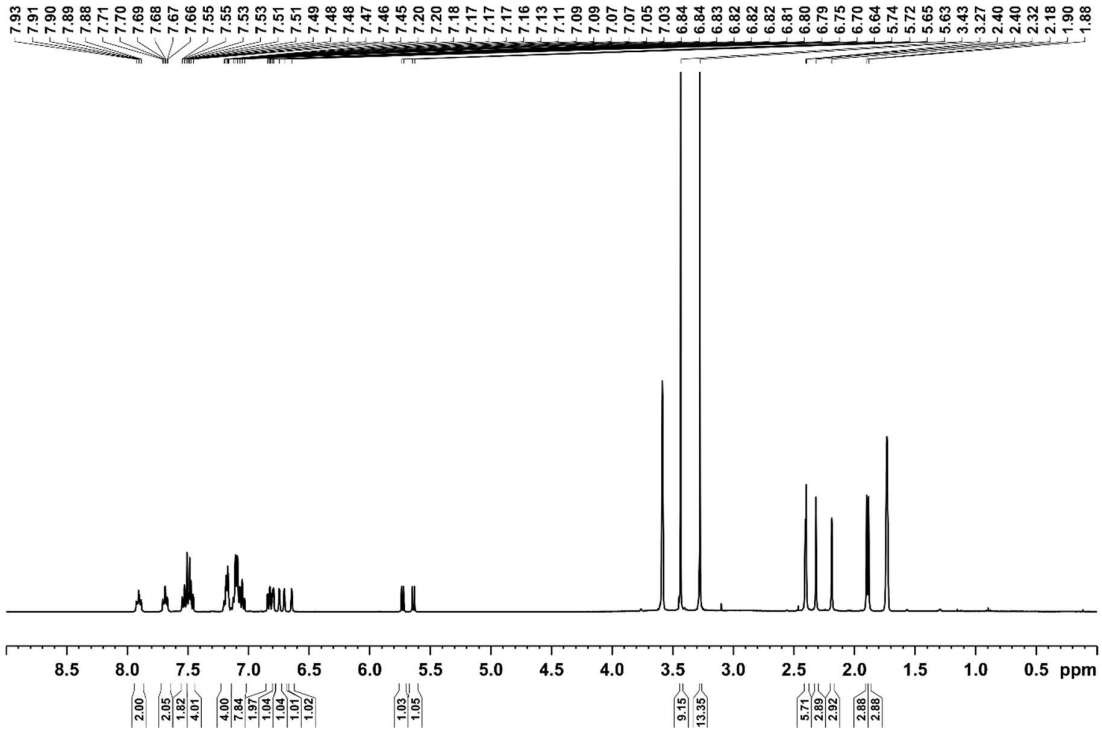

Figure S1. ^{1}H NMR spectrum (400.13 MHz, 300 K, THF-d$_8$) of **2**.

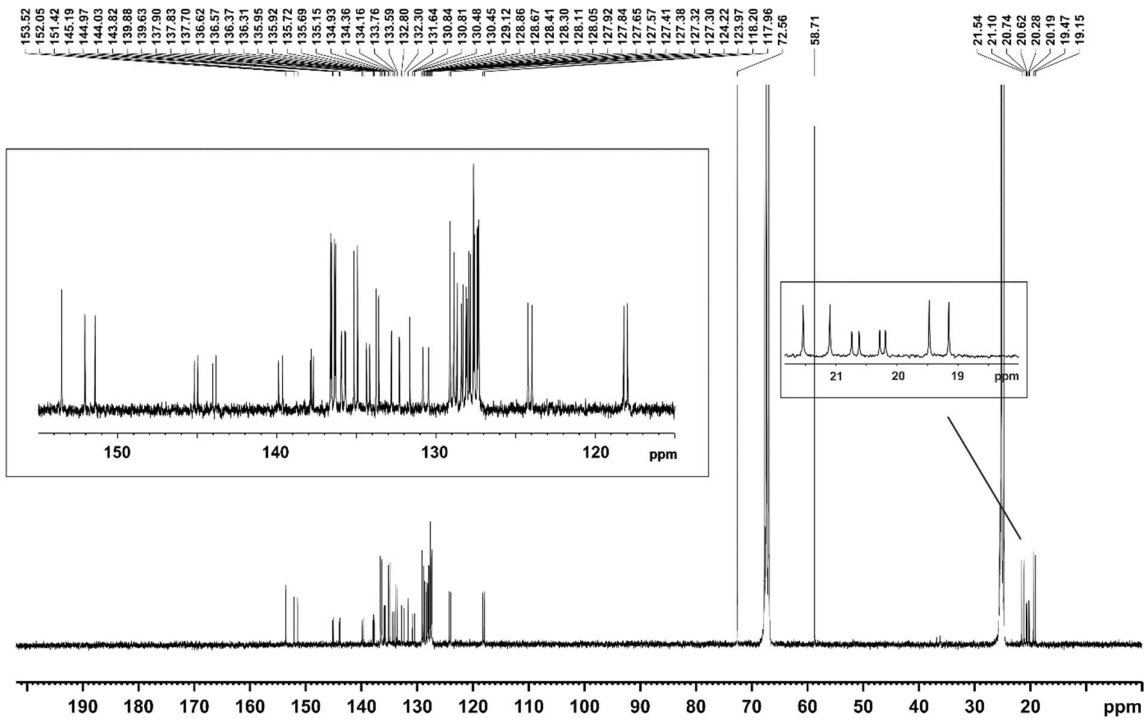

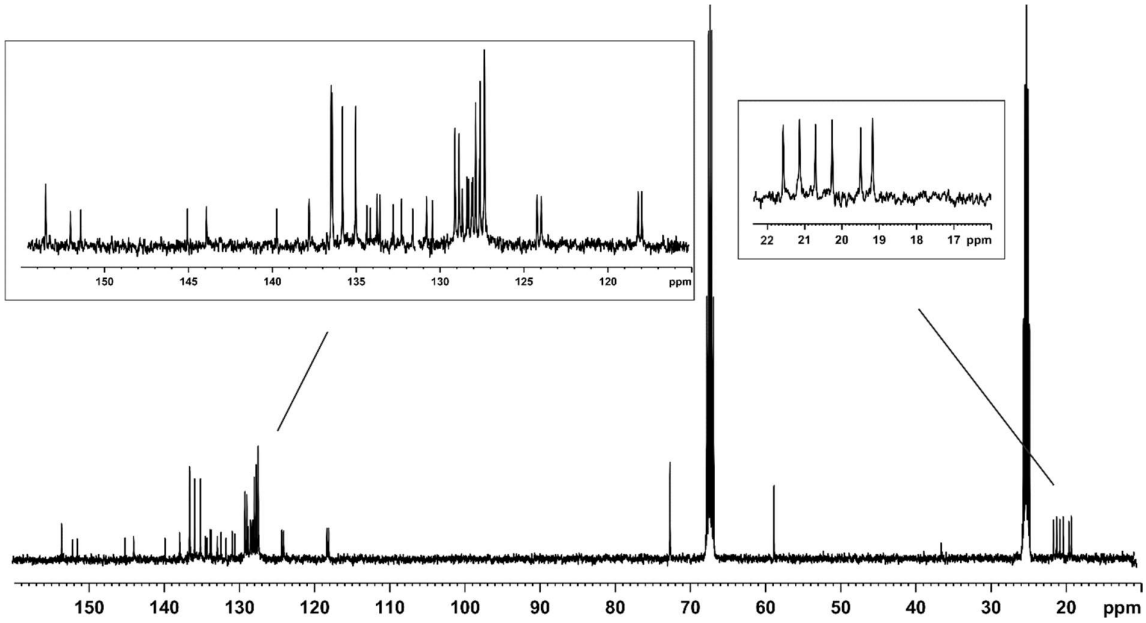

Figure S2. $^{13}C\{^{1}H\}$ and $^{13}C\{^{1}H,^{31}P\}$ NMR spectra (100.6 MHz, 300 K, THF-d_8) of **2**.

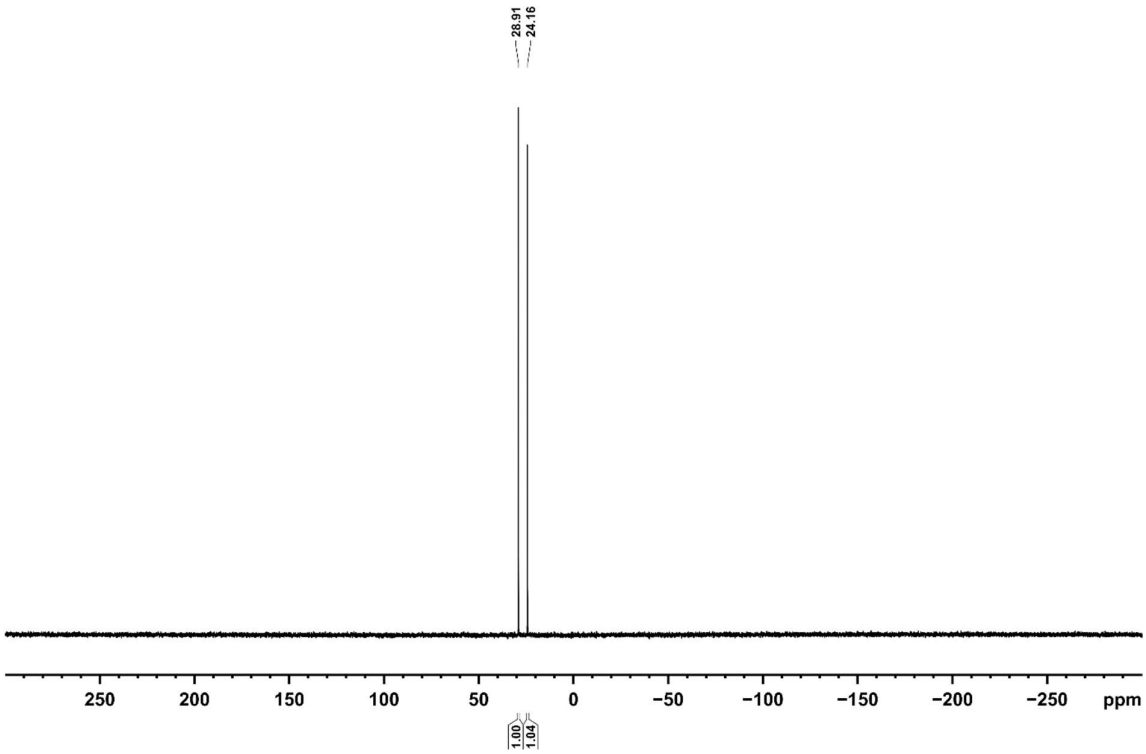

Figure S3. $^{31}P\{^{1}H\}$ NMR spectrum (161 MHz, 300 K, THF-d_8) of **2**.

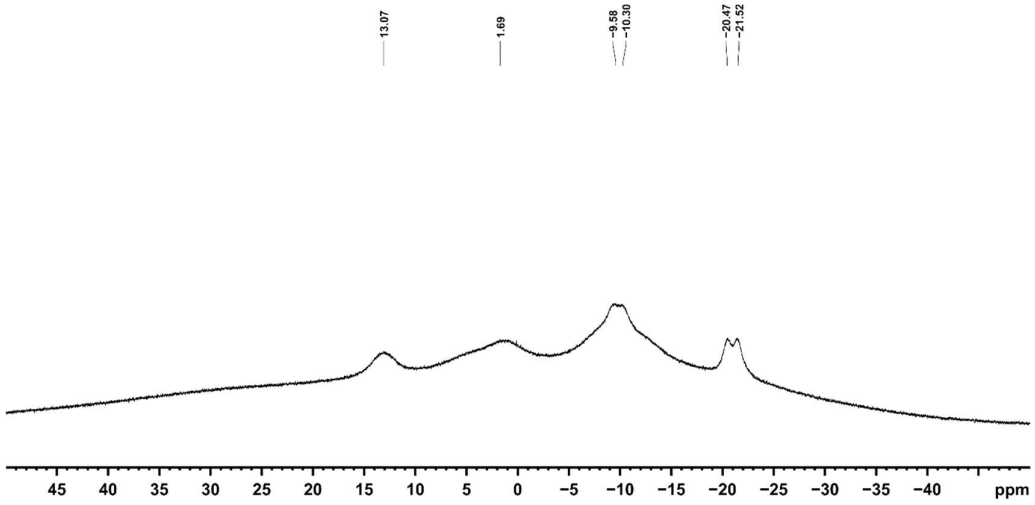

Figure S4. ^{11}B NMR spectrum (128.4 MHz, 300 K, THF-d$_8$) of **2**.

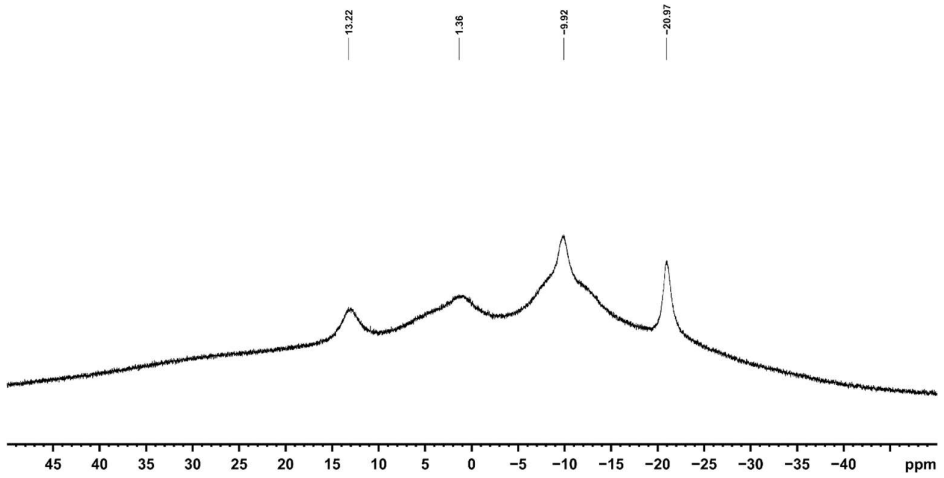

Figure S5. ^{11}B{^{1}H} NMR spectrum (128.4 MHz, 300 K, THF-d$_8$) of **2**.

7.5.2.3 UV-vis spectra

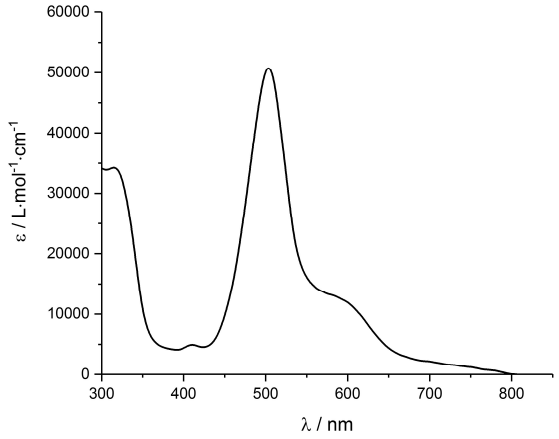

Figure S6. UV-vis spectrum of **2** in THF.

7.5.2.4 Single-crystal X-ray crystallography

Table S1. Crystallographic data of **2**

Compound	**2**
Empirical formula	$C_{68}H_{88}B_{10}CoKN_2O_6P_2$
Formula weight	1297.47
Temperature [K]	123.(1)
Crystal system	monoclinic
Space group	$P2_1/c$
a [Å]	13.9629(1)
b [Å]	13.7270(2)
c [Å]	36.1365(4)
α [°]	90
β [°]	95.597(1)
γ [°]	90
Volume [Å^3]	6893.2(1)
Z	4
ρ_{calc} [g/cm^3]	1.250
μ [mm^{-1}]	3.326
F(000)	2736.0
Crystal size [mm^3]	0.526 × 0.294 × 0.161
2Θ range for data	6.892 to 147.778
Index ranges	-17 ≤ h ≤ 13, -16 ≤ k ≤ 16, -44 ≤ l ≤ 39
Reflections collected	32794
Independent reflections	13569 [R_{int} = 0.0282, R_{sigma} = 0.0332]]
Data / restraints /	13569/49/858
Goodness-of-fit on F^2	1.031
Final R indexes [I>=2σ (I)]	R_1 = 0.0365, wR_2 = 0.0892
Final R indexes [all data]	R_1 = 0.0423, wR_2 = 0.0926
Largest diff. peak/hole [e	0.28/-0.30
Flack parameter	
CCDC-	1943845

7.5.3 Characterization of Intermediate Species

7.5.3.1 Synthesis

[K(thf){(^{Mes}BIAN)Co(η^4-cod)] (**1**) (126 mg, 0.179 mmol, 1.0 equiv.) was dissolved in 3 mL THF and added to a solution of 1,2-bis(diphenylphosphino)-*ortho*-carborane (**L**) (93 mg, 0.181 mmol, 1.01 equiv.) in 3 mL THF. The solution turned orange immediately upon addition and was stirred for 30 min. After solvent evaporation, the dark orange residue was dried *in vacuo* and was subsequently extracted with *n*-hexane (8 mL). Storage of the solution at room temperature afforded dark orange crystals of [(^{Mes}BIAN)Co(η^4-cod)] (**3**) as the major

component and a minor amount of dark orange, almost black crystals of [(^{Mes}BIAN)Co(**L**)] (**3**), which were both characterized by single-crystal X-ray crystallography. **3** could not be further characterized due to the small amount of isolated compound, which is formed as a mixture with **Int-A** and **L**. **3** is presumably formed by reaction of ligand **L** and **3**.

Characterization data for Int-A:

Yield: 20.3 mg (0.031 mmol, 17%)

Chemical formula: $C_{38}H_{40}N_2Co$ ($M = 583.69$ g mol^{-1})

^{1}H NMR (400.13 MHz, 300 K, THF-d_8) δ[ppm]: Paramagnetic compound with broad signals at 10.5, 7.8, 0.7 and -2 ppm (see Figure S7). An assignment of these signals was not possible and no other resonances were observed from –100 to +100 ppm.

Elemental analysis: calcd. For $C_{38}H_{40}N_2Co$: found (calc.): C: 76.26 (78.20) H: 6.95 (6.91) N: 4.09 (4.80). The found CHN values are not consistent with the calculated CHN values. This is likely due to contamination of the major species **Int-A** with complex **3** and ligand **L** as shown by single-crystal X-ray crystallography.

EPR spectroscopy: The sample was prepared in a nitrogen-filled glovebox in degassed, dry toluene and measured in a glass at 20 K. The signal shows very slightly axial symmetry (nearly isotropic) with calculated g values: $g_x = 1.998$, $g_y = 1.994$, $g_z = 2.003$ and simulated g values: $g_{\parallel} = 2.011$, $g_{\perp} = 1.996$ (see Figure S10)

Magnetic moment (Evans method in THF-d_8 at ambient temperature): $\mu_{eff} = 1.8(1)\ \mu_B$

Melting point: > 210 °C: decomposition to a black oil

7.5.3.2 ^{1}H NMR spectra

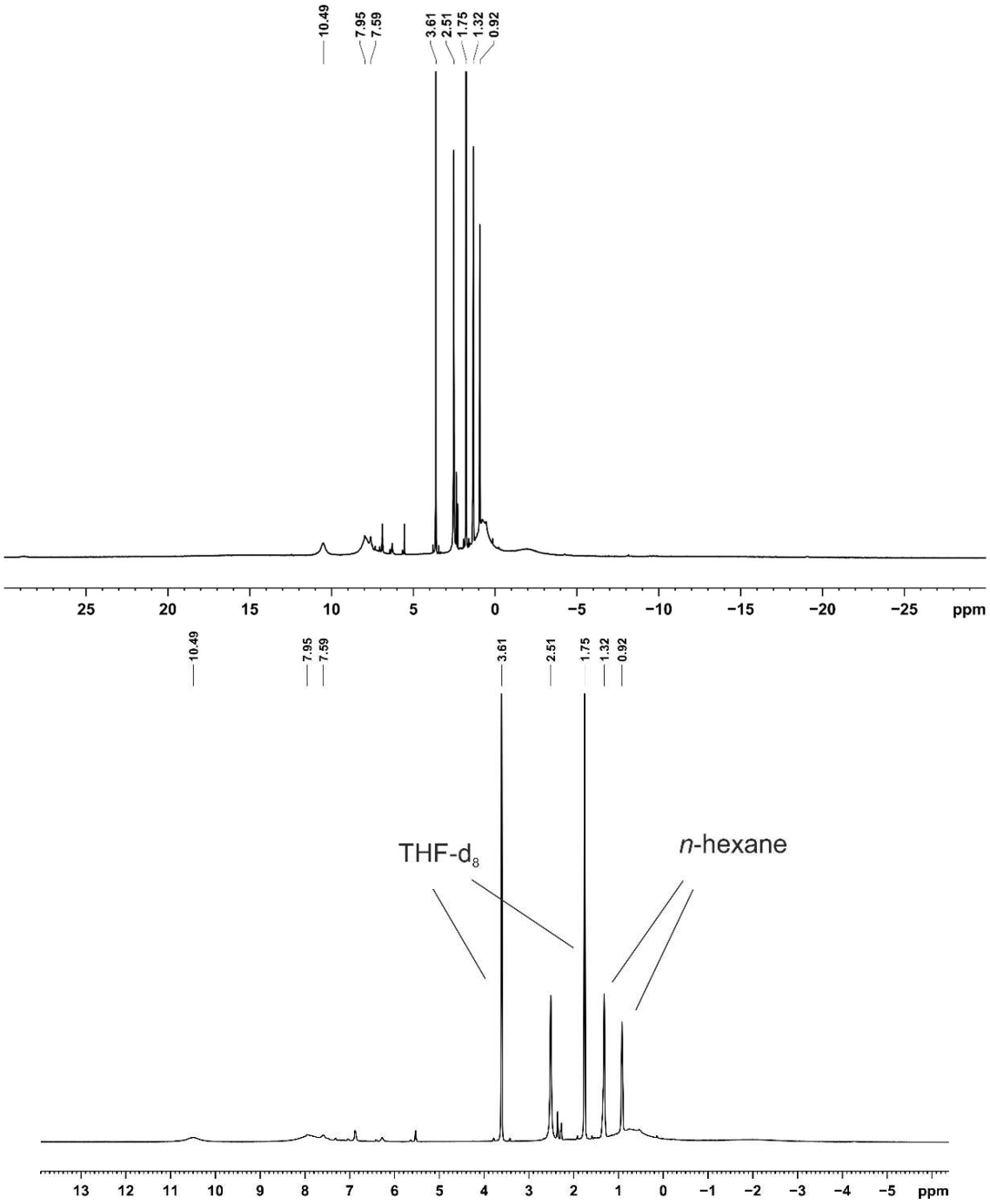

Figure S7. ^{1}H NMR spectrum (400.13 MHz, 300 K, THF-d$_8$) of **Int-A**; top: complete, bottom: zoom..

7.5.3.3 Single-crystal X-ray crystallography

Table S2. Crystallographic data of **Int-A** and **3**

Compound	**Int-A**	**3**
Empirical formula	$C_{41}H_{47}CoN_2$	$C_{56}H_{58}B_{10}CoN_2P_2$
Formula weight	626.73	988.01
Temperature [K]	123.(1)	123(1)
Crystal system	triclinic	monoclinic
Space group	*P*-1	$P2_1/c$
a [Å]	8.1878(9)	11.2578(2)
b [Å]	10.6068(9)	24.1038(4)
c [Å]	19.841(1)	19.6169(3)
α [°]	102.644(6)	90
β [°]	95.457(7)	96.950(2)
γ [°]	97.860(8)	90
Volume [Å^3]	1651.5(3)	5284.0(2)
Z	2	4
ρ_{calc} [g/cm^3]	1.260	1.242
μ [mm^{-1}]	4.294	3.406
F(000)	668.0	2060.0
Crystal size [mm^3]	0.423 × 0.216 × 0.135	0.292 × 0.259 × 0.176
2Θ range for data	8.658 to 148.162	7.336 to 147.688
Index ranges	-10 ≤ h ≤ 9, -12 ≤ k ≤ 12, -18 ≤ l ≤ 24	-13 ≤ h ≤ 13, -29 ≤ k ≤ 28, -24 ≤ l ≤ 24
Reflections collected	9999	20536
Independent reflections	6275 [R_{int} = 0.0618, R_{sigma} = 0.0826]	10282 [R_{int} = 0.0325, R_{sigma} = 0.0418]
Data / restraints /	6275/0/404	10282/0/646
Goodness-of-fit on F^2	1.098	1.060
Final R indexes [I>=2σ (I)]	R_1 = 0.0683, wR_2 = 0.1661	R_1 = 0.0459, wR_2 =
Final R indexes [all data]	R_1 = 0.0790, wR_2 = 0.1728	R_1 = 0.0524, wR_2 =
Largest diff. peak/hole [e	0.98/-0.85	0.58/-0.54
CCDC-	1943847	1943848

7.5.4 Mechanistic Investigations

7.5.4.1 $^{31}P\{^1H\}$ NMR monitoring

K(thf){(^{Mes}BIAN)Co(η^4-cod)] (15 mg, 0.021 mmol, 1.0 equiv.) (**1**) and 1,2-bis(diphenylphosphino)-*ortho*-carborane (10.8 mg, 0.021 mmol, 1.0 equiv.) (**L**) were dissolved in THF (0.7 mL) in a *J. Young* NMR tube and a few drops of C_6D_6 were added.

7.5.4.2 Stoichiometric reductions with potassium graphite

a) 1:1 reaction

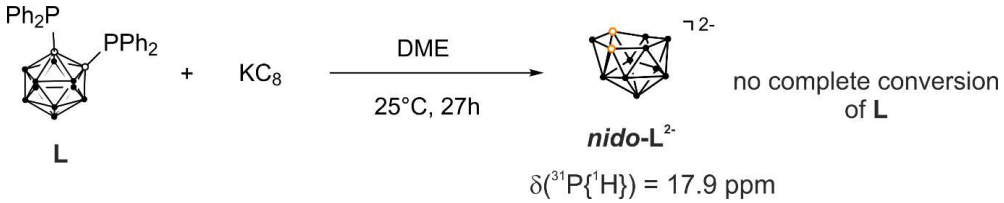

Potassium graphite (KC_8, 5.3 mg, 0.039 mmol, 1.0 equiv.) was added to a solution of 1,2-bis(diphenylphosphino)-*ortho*-carborane (**L**) (19.2 mg, 0.037 mmol, 1.0 equiv.) in 1.0 mL DME at ambient temperature. The solution turned light yellow and was stirred for 27 h. After addition of a few drops C_6D_6 the reaction mixture was analyzed by ^{11}B and ^{31}P NMR spectroscopy.

$^{31}P\{^1H\}$ NMR (162 MHz, 300 K, C_6D_6 in DME) δ[ppm]: main signals at: 17.8 (***nido*-L^{2-}**, integral: 1), 8.0 (**L**, integral 0.94), –15.1 (P_2Ph_4)

^{11}B NMR (128.4 MHz, 300 K, C_6D_6 in DME) δ[ppm]: 20.8 (br s), –1.5 (m), –9.4 (m), –18.5 (m), -22.0 (m)

$^{11}B\{^1H\}$ NMR (128.4 MHz, 300 K, C_6D_6 in DME) δ[ppm]: 20.1 (br s), –0.9 (s), –2.2 (s), –7.7 (s), –9.9 (s), –18.4 (s), –21.9 (s)

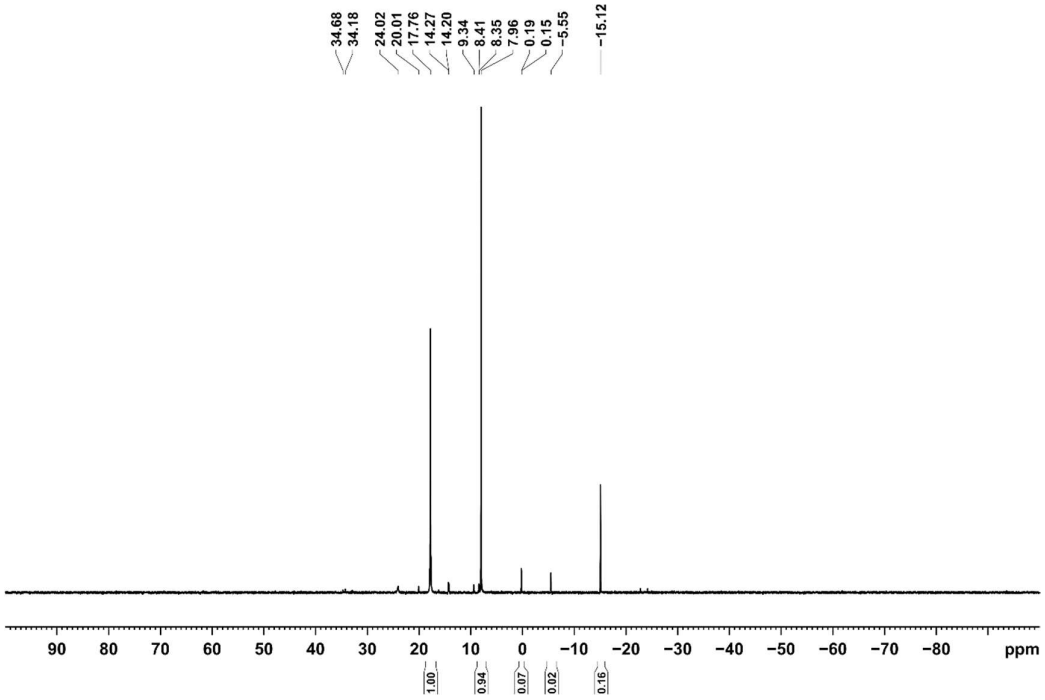

Figure S8. $^{31}P\{^1H\}$ NMR spectrum (161 MHz, 300 K, C_6D_6) of **L** and 1.0 equiv. KC_8 in DME.

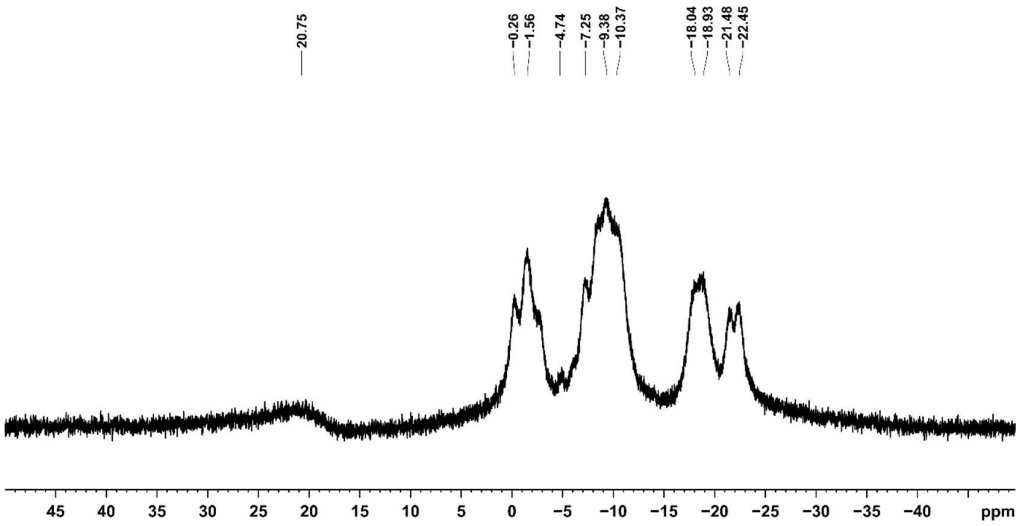

Figure S9. ^{11}B NMR spectrum (128.4 MHz, 300 K, C_6D_6) of **L** and 1.0 equiv. KC_8 in DME.

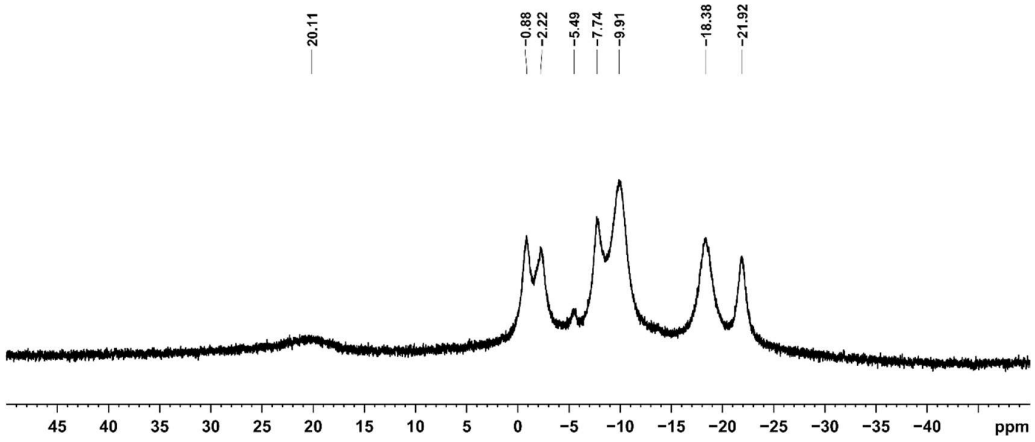

Figure S10. $^{11}B\{^1H\}$ NMR spectrum (128.4 MHz, 300 K, C_6D_6) of **L** and 1.0 equiv. KC_8 in DME.

b) 2:1 reaction

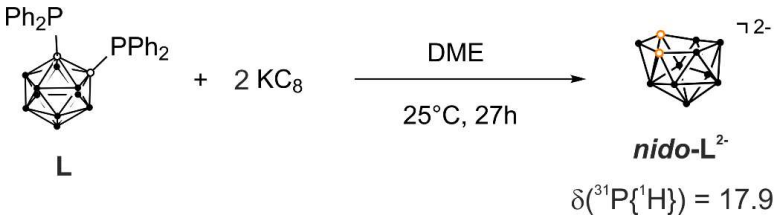

Potassium graphite (KC_8, 10.7 mg, 0.079 mmol, 2.0 equiv.) was added to a solution of 1,2-bis(diphenylphosphino)-*ortho*-carborane (**L**) (20.2 mg, 0.04 mmol, 1.0 equiv.) in 1.5 mL DME at ambient temperature. The solution turned yellowish and was stirred for 16 h. After addition of a few drops C_6D_6 the reaction mixture was analyzed by ^{11}B and ^{31}P NMR spectroscopy.

^{31}P{^{1}H} NMR (162 MHz, 300 K, C_6D_6 in DME) δ[ppm]: main signals at: 17.8 (*nido*-L^{2-}, integral: 1), -15.2 (P_2Ph_4, integral 0.05)

^{11}B NMR (128.4 MHz, 300 K, C_6D_6 in DME) δ[ppm]: 20.9 (br s), –2.4 (m), –18.5 (m), –22.0 (m)

^{11}B{^{1}H} NMR (128.4 MHz, 300 K, C_6D_6 in DME) δ[ppm]: 20.9 (br s), –2.4 (s), –18.5 (s), –22.0 (s)

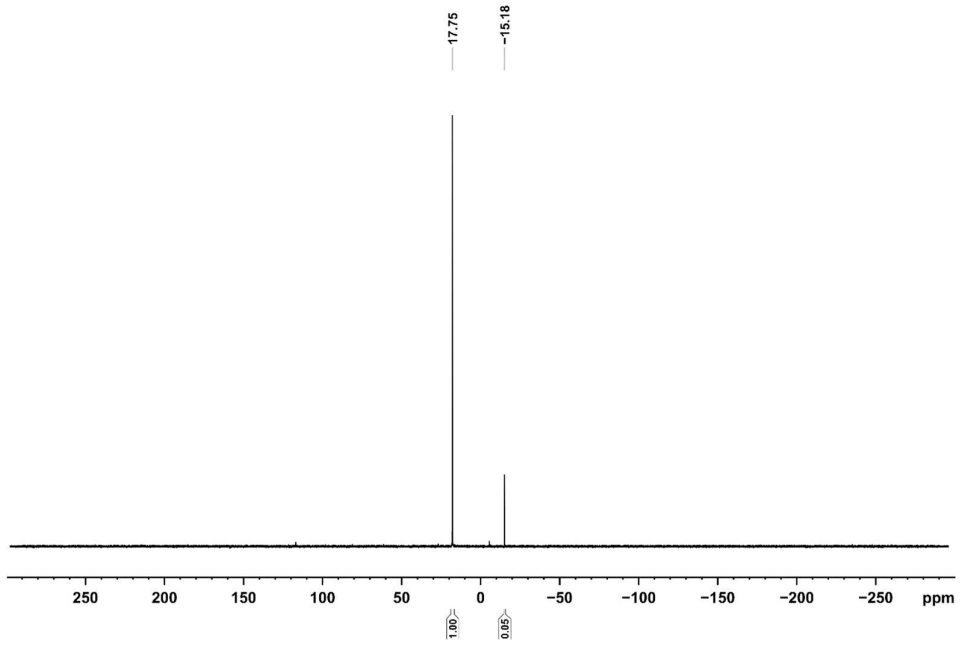

Figure S11. ^{31}P{^{1}H} NMR spectrum (161 MHz, 300 K, C_6D_6) of **L** and 2.0 equiv. KC_8 in DME.

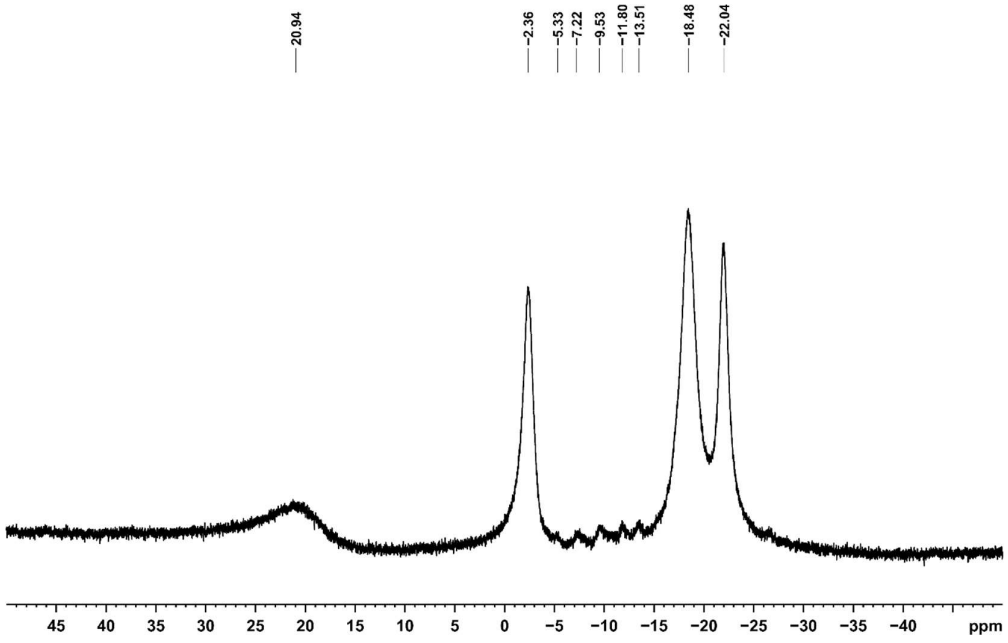

Figure S12. ^{11}B{^{1}H} NMR spectrum (128.4 MHz, 300 K, C_6D_6) of **L** and 2.0 equiv. KC_8 in DME.

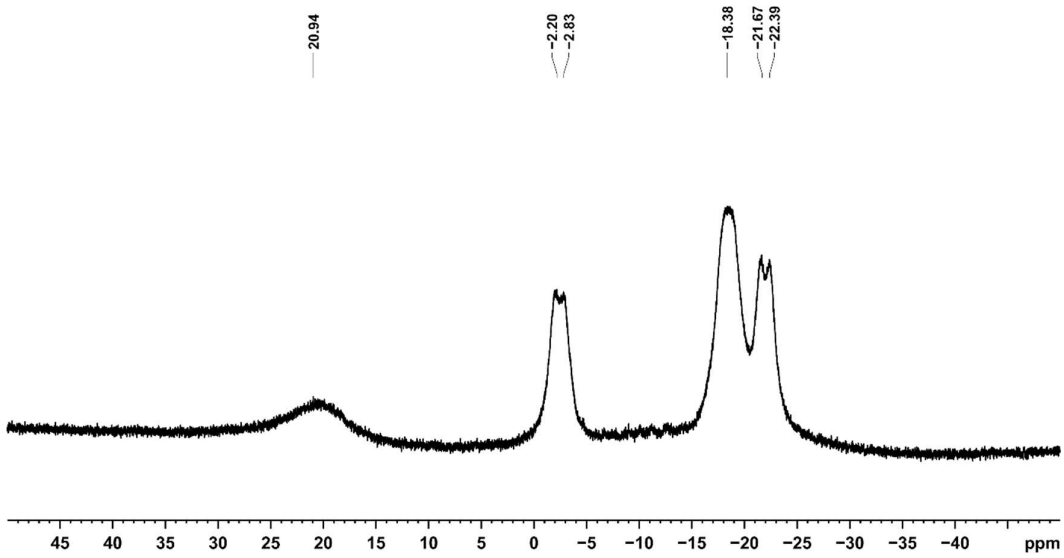

Figure S13. ^{11}B NMR spectrum (128.4 MHz, 300 K, C_6D_6) of **L** and 2.0 equiv. KC_8 in DME.

7. 5.4.3 ESI-MS analysis

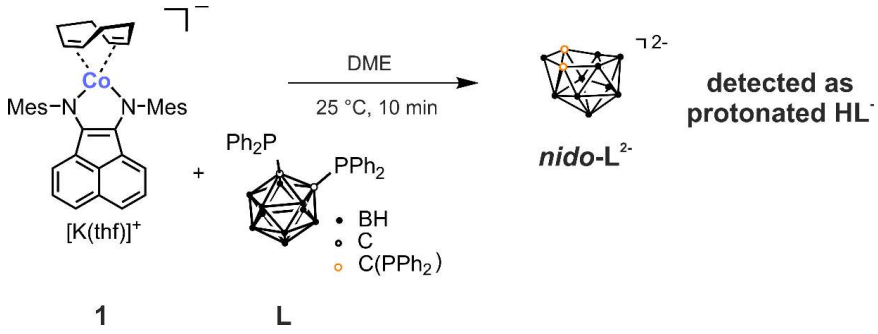

In an inert atmosphere, [K(thf){(^{Mes}BIAN)Co(η^4-cod)] (**1**) (5 mg, 0.0071 mmol, 1.0 equiv.) and 1,2-bis(diphenylphosphino)-*ortho*-carborane (**L**) (3.6 mg, 0.0071 mmol, 1.0 equiv.) were dissolved in DME (1 mL). The solution was added dropwise to the cobaltate solution. The solution immediately turned orange and was diluted to a concentration of around 10^{-4} mol·L^{-1}. The solution was injected into the ESI-MS spectrometer with a Hamilton syringe. The sample was analyzed using a negative fragmentator potential (–120 V). The simulation suggests that the observed species has the molecular formula $B_{10}C_{26}H_{31}P_2$ (***nido*-HL$^-$**) This means that ligand **L** was reduced by two electrons and subsequently protonated, which underlines the hypothesis that a dianionic *nido*-carborane (***nido*-L^{2-}**) is initially formed.

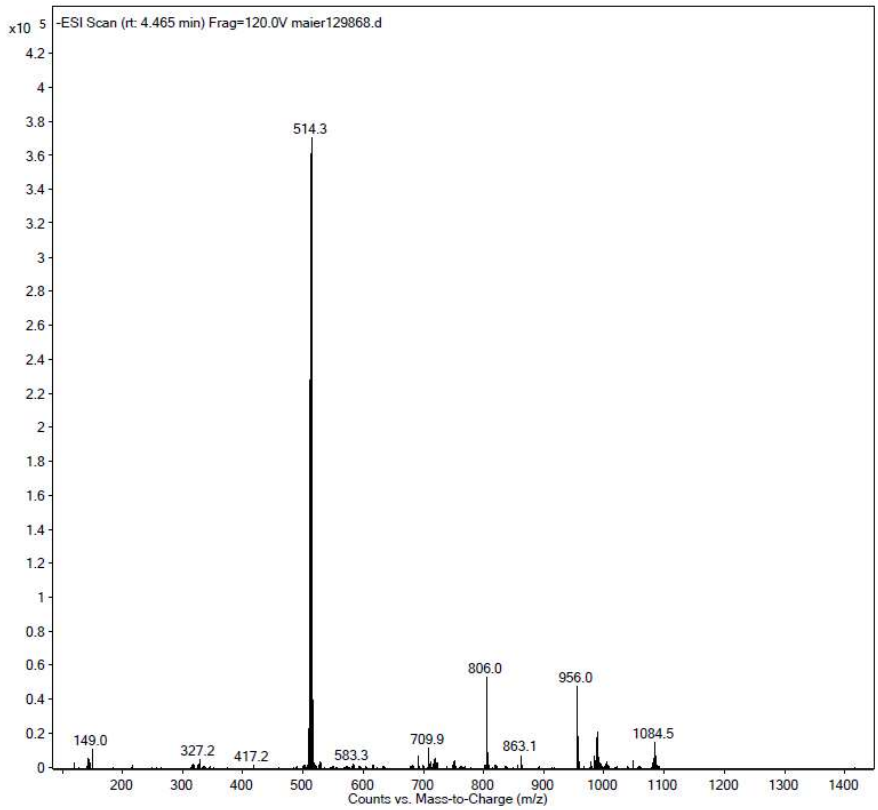

Figure S14. ESI Scan (4.465 min) Frag = –120.0 V.

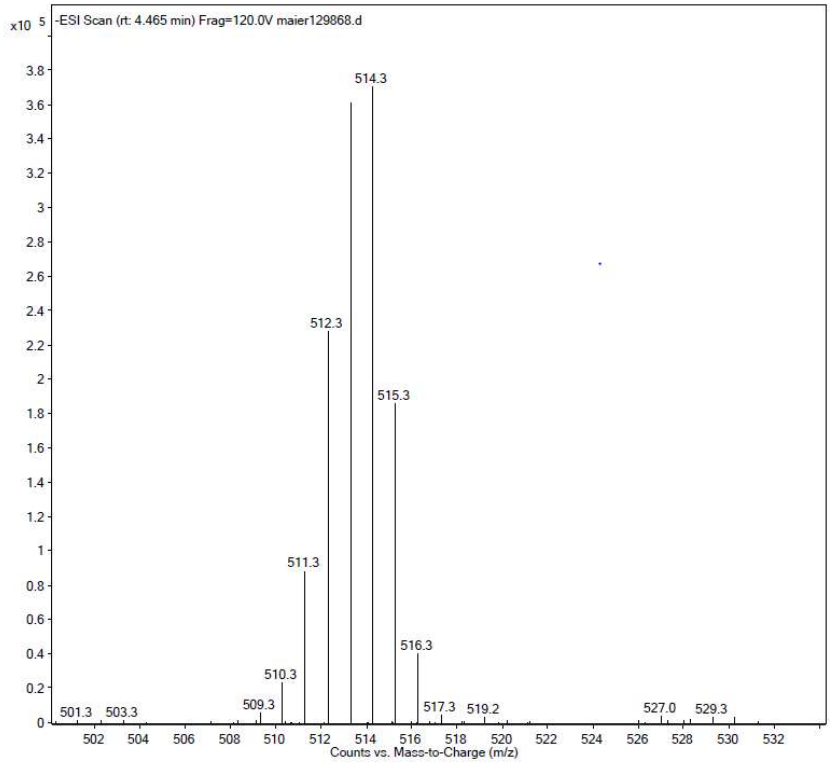

Figure S15. ESI Scan (4.465 min) Frag = –120.0 V (zoom).

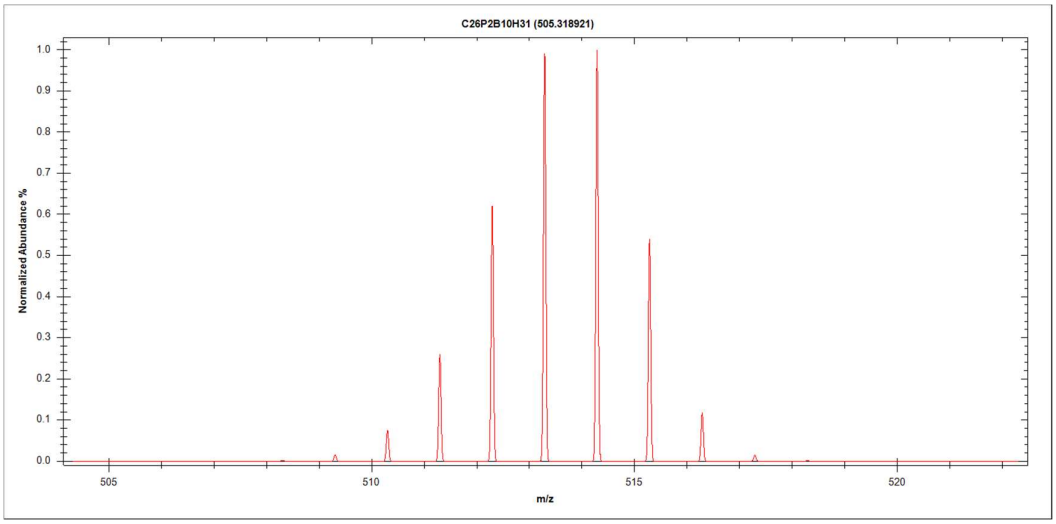

Figure S16. Simulation of mass spectrum of $C_{26}P_2B_{10}H_{31}$.

7.5.5 Computational Details

General Methods

All calculations were carried out with the ORCA program package.[1],[2] All geometry optimisations were performed at the BP86-D3BJ/def2-TZVP[4],[15]-[18] level of theory in the gas phase. Frequency calculations were carried out to confirm the nature of stationary points found by geometry optimisations. Density fitting techniques, also called resolution-of-identity approximation (RI),[19] were used for GGA calculations, whereas the RIJCOSX[20] approximation was used for all other calculations. To save computational cost, all mesityl groups on the BIAN ligand were replaced by phenyl groups, except for the calculations presented in the CASSCF and TD-DFT sections where only the methyl groups in the *para*-position were replaced by hydrogen atoms. Final-single point energies for the mechanistic investigations have been obtained at the M06-D3(0)/def2-TZVP[4],[16],[21],[22] CPCM(THF)[23],[24] level of theory.

CASSCF calculations

α-Diimine complexes potentially exhibit open-shell singlet character (or broken-symmetry character in the framework of density functional theory) due to the non-innocent ligand system.[25] This behaviour imposes challenges to single-reference methods. Therefore, we conducted CASSCF-DLPNO-NEVPT2/cc-pVTZ [26]-[28] calculations to get an insight into the electronic structure of **2**. The initial guess orbitals were chosen from a PBE/def2-SVP

calculation. Thereby, the active-space was constructed to contain the 3d orbitals on cobalt as well as the bonding-interaction between cobalt and the ligands. Additionally, three orbitals of the second d-shell (containing the 4d orbital on cobalt) were included to aid convergence. In total, this led to an active space of 10 electrons in 10 orbitals. Analysis of the natural orbitals of the active space reveals six 3d electrons on cobalt (**245**, **246**, **248**), two metal–ligand bonding orbitals (**247**, **249**) and their correlating antibonding orbitals (**251**, **250**) and finally three 4d orbitals on cobalt (**252**, **253**, **254**), which present the above-mentioned double-shell of the occupied 3d orbitals on Co. The orbitals **247** and **250** are almost equally distributed over the metal atom and the BIAN ligand framework, which indicates a strong covalent interaction between the metal atom and the ligand. For this reason, an assignment of an oxidation state to Co remains ambiguous (see the main text). As discussed in the main text, partial reduction of the BIAN ligand can be deduced from the orbitals **249** and **250**, which resemble the Co-BIAN π-bonding and π-antibonding orbitals. Their respective occupations, 1.776 and 0.231, indicate dominant closed-shell character of **2** (occupations of 2.00 and 0.00 would account for an ideal closed-shell compound, whilst equal occupations of 1.000 would account for an ideal open-shell singlet species). This can also be deduced by looking at the composition of the CASSCF wave function: The contribution of the ground state configuration state function is 80%, whilst higher configuration state functions (corresponding to excited states in a single-reference framework) contribute the remaining 20%, indicating some multi-reference character of **2.** The configuration state function where **250** is doubly occupied and **249** is empty shows the most significant contribution of all higher configuration state functions to the overall wave function (8%, a contribution of 50% would indicate an ideal open-shell singlet species).

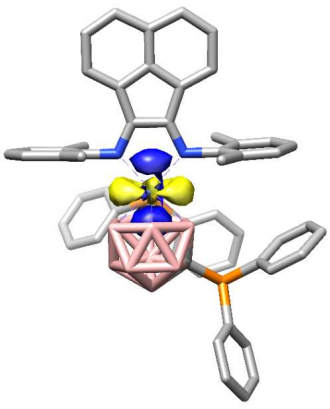

254 (occ.: 0.025, 47% 4)

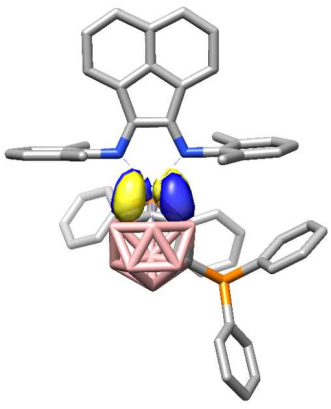

253 (occ.: 0.035, 10% 4, 37% $4d_{xz}$)

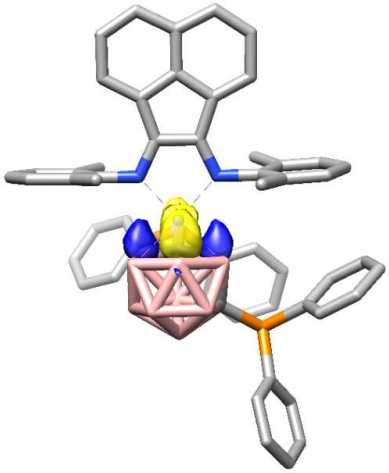

252 (occ.: 0.063, 30% 4, 12% $4d_{xz}$)

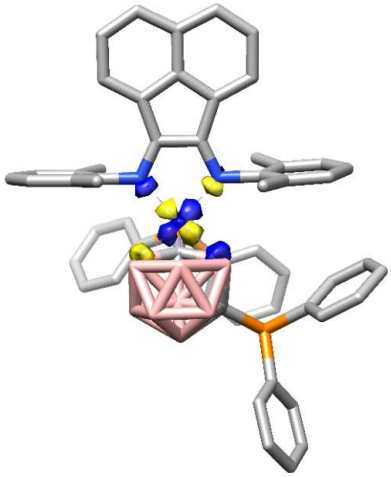

251 (occ.: 0.087, 59% $3d_{xy}$)

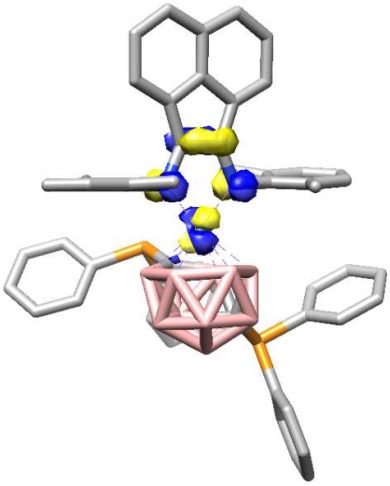

250 (occ.: 0.231, 37% $3d_{yz}$)

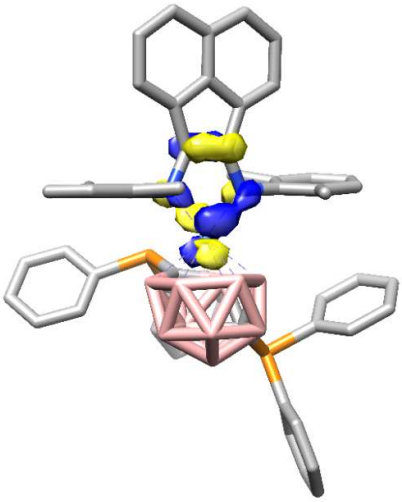

249 (occ.: 1.776, 42% $3d_{yz}$)

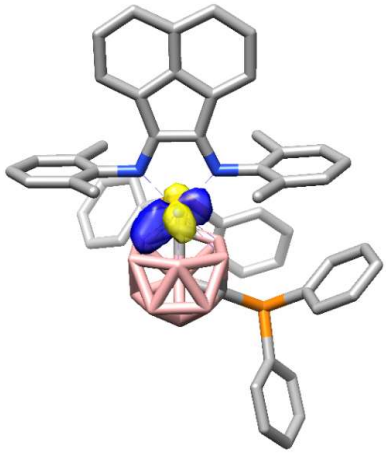

248 (occ.: 1.928, 47% 3, 13% d_{xz}, 10% d_{xy})

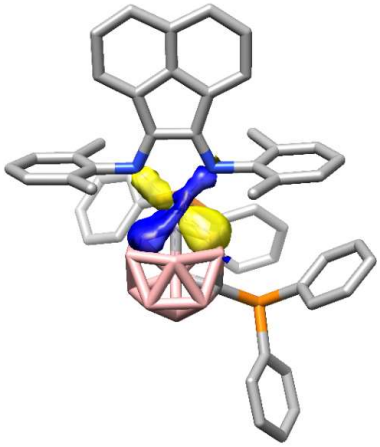

247 (occ.: 1.930, 41% 3d)

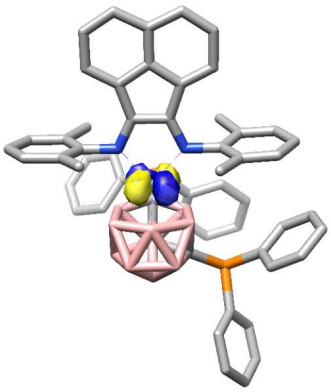

246 (occ.: 1.954, 58% $3d_{xz}$, 16% 3)

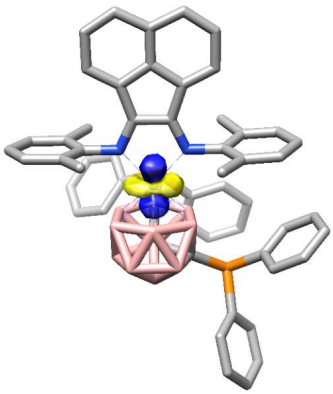

245 (occ.: 1.971, 69% 3, 12% $3d_{yz}$)

Figure S17: CASSCF natural orbitals of **2**. For each orbital, the occupation (occ.) and the highest contribution of d orbitals on cobalt as derived from Löwdin population analysis are given. For orbital **247**, the sum of all contributions is given, since all 3d orbitals atomic orbitals of Co contribute significantly to this orbital. Surface isovalue = 0.06.

TD-DFT calculations on 2

TD-DFT calculations on **2** have been conducted at the M06/def2-TZVP level in the gas phase. Compared to the experimental absorption spectrum, the calculated absorption spectrum is blue-shifted, however, the overall shape agrees reasonably well (Figure S24). Looking at the difference densities of the most intense transitions (as judged by the calculated oscillator strengths f_{osc}) in the visible region of the spectrum allowed for the assignment of these transitions as MLCT (d−π*) bands (Figure S18).

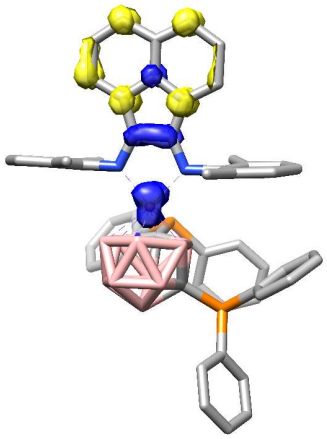

3 (652 nm, f_{osc} = 0.016355562)

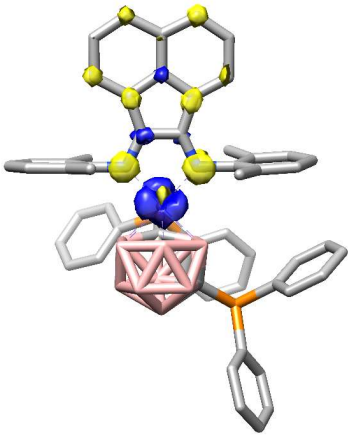

6 (502 nm, f_{osc} = 0.314564984)

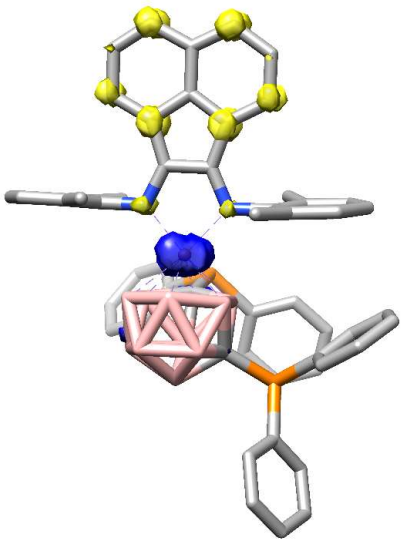

10 (428 nm, f_{osc} = 0.412937032)

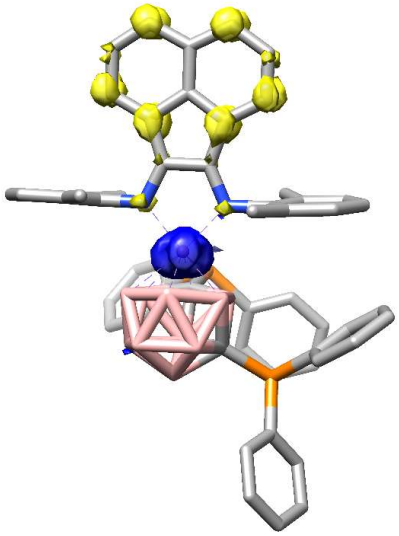

12 (417 nm, f_{osc} = 0.173695227)

Figure S18: Difference densities for selected excited states of **2** (transitions proceed from blue to yellow). Surface isovalue = 0.004 (0.002 for state 6) together with calculated wavelengths of the transitions and oscillator strengths.

Cartesian Coordinates of optimized structures

1,2-bis(diphenylphosphino)-*ortho*-carborane (**L**)

P	2.65421812827846	7.37367936317896	2.78173969969008
P	3.53792233623493	6.82168171269276	5.86861568339196
C	1.62794338499846	5.86772146188883	0.71383297497796
H	1.25145405334320	5.25661069314031	1.53582479807679
C	3.50482871751196	4.61880010358639	7.52445185444037
H	2.70869167948196	4.30149714390811	6.84747205798437
C	4.13646668442575	5.85537221217030	7.31088996442934
C	5.13979060170252	6.27190645772864	8.19565343200451
H	5.61755173831239	7.24188826194006	8.06470385563254
C	3.94880568920122	8.55409006036635	6.30887974614204
C	2.37880505817515	7.02004766272085	1.00021236831990
C	4.00710841794903	9.91173258793522	2.30532494622536
H	4.83969251743492	9.39001749138482	1.83831269554040
C	2.58791468138369	7.44249763635032	-1.37852499764891
H	2.95878805797633	8.06389929989575	-2.19472720134997
C	2.82268562654551	9.35719401229529	6.55245250444069
H	1.82752654515217	8.92213273346985	6.44052786829250
C	1.85964628262676	9.89728874656466	3.41286269852417
H	1.01369266398171	9.34033209857496	3.82113407570257
C	2.91601762544916	9.18936839332278	2.81569832749948
C	4.04293104474799	11.30253597161177	2.40761516506161
H	4.90316240445037	11.84863313275646	2.01761096514557
C	5.22464466757606	9.12802423405939	6.43473060839706
H	6.11476218122891	8.53134478833964	6.24464536624530
C	4.23512728705153	11.25811732210594	7.02737298154846
H	4.34946539494722	12.30837341432243	7.29852571156967
C	4.36810584592864	6.60120533681744	2.97794624626085
C	4.82882851304501	6.30042952179625	4.59220173402316
C	1.88685635067438	11.28958098855894	3.49852826036296

H	1.05776735617714	11.82096018978326	3.96744615268843
C	2.84544070445746	7.81191704895525	-0.05741707025910
H	3.40672771117707	8.72302603678663	0.14602564361602
C	1.86099334174220	6.28149652367122	-1.65623364028814
H	1.66468616083083	5.99380525530339	-2.68993712095068
B	6.63900717404658	5.30621247165283	2.05237475543443
H	7.28165522171954	4.95474078105675	1.11242145350078
C	4.91056343265526	4.21062854196673	9.44717184417400
H	5.21641642084850	3.57100218917654	10.27625287597001
C	3.89529126879862	3.79656096366799	8.58137156161590
H	3.40413475001513	2.83440938063756	8.73046168245222
B	7.14057075431222	6.66052359873432	3.09713554700303
H	8.13509176578877	7.29596883249055	2.93267305199981
B	7.12049400522332	4.99361588991841	3.73227626836761
H	8.11884292123169	4.41509886132926	4.03072964337238
C	5.52536681530506	5.45108229207229	9.25642985211772
H	6.31135685320181	5.78108821888734	9.93762162454328
C	1.37814948207683	5.49526586872721	-0.60699283661161
H	0.80369593543358	4.59222046437131	-0.81739878087299
C	2.98490643040274	11.99476386967591	3.00384974921794
H	3.01969810588065	13.08241006627796	3.08443822067002
B	5.67574737158347	7.47185836106992	3.66810644342107
H	5.53013513110651	8.61342107736588	3.92640718274682
B	5.64816669037003	4.79852520954694	4.69947746568914
H	5.50827516224039	4.15638102704097	5.68571765154592
C	5.36430538707936	10.47050947597156	6.78510760198997
H	6.36187291447794	10.90418975734894	6.86931247162482
B	6.52549895626849	6.33272689941659	4.72972564417357
H	6.99233237374000	6.73869017527642	5.74440428837198
B	4.86893000655181	5.30264371207403	1.97844379907883
H	4.19086738326003	5.00851391532215	1.05227693166114
B	5.74649307202835	6.83880637081438	2.01124452741327
H	5.65922598667361	7.60145731725574	1.10265428959927
C	2.96257344054461	10.69690899655798	6.91655775239368
H	2.07577368293290	11.30481429693753	7.09838106678239
B	5.69518629969760	4.16194388156621	3.04846628578558
H	5.65089244946001	2.98915377401615	2.84332318938023
B	4.25283926862194	5.00124948977591	3.61715176051994
H	3.16478764392036	4.58527666617886	3.85281601118934

Dianionic ligand $\mathbf{L^{2-}}$ (***ortho*-$\mathbf{L^{2-}}$**)

P	2.270395	6.978628	1.786529
P	3.608758	7.161786	6.189151
C	3.140017	6.393960	-0.816587
H	3.451494	5.444613	-0.379637
C	5.648195	6.678135	8.179240
H	6.295119	7.327864	7.589320
C	4.317608	6.480288	7.769185
C	3.509778	5.625167	8.537710
H	2.482348	5.445917	8.210254
C	4.427781	8.813825	6.311435
C	2.610883	7.394299	0.027545
C	3.410954	9.589848	2.237792
H	4.077680	9.383722	1.399803
C	2.354386	8.825931	-1.939552
H	2.044728	9.782852	-2.369882
C	3.820881	9.742957	7.176439
H	2.922356	9.439428	7.721494
C	1.627480	8.900248	3.704113
H	0.897545	8.148550	4.011554
C	2.436069	8.639585	2.588329
C	3.558220	10.767778	2.970137
B	5.641750	4.176388	2.361604
H	6.200093	3.391843	1.636272
C	5.325533	5.212259	10.085838
H	5.718992	4.718213	10.977793
C	6.146375	6.050562	9.321908
H	7.187050	6.210723	9.616689
B	6.404191	5.690579	3.032615
H	7.507001	6.035022	2.688784
B	6.126825	4.224667	4.065215
H	6.995093	3.470481	4.424583
C	4.001792	4.999246	9.684993
H	3.353113	4.337884	10.266003
C	3.280080	6.612192	-2.187152
H	3.709464	5.825305	-2.812732
C	2.744626	11.014220	4.080939
H	2.898112	11.909217	4.686001
B	4.941020	6.794487	3.389845
H	5.123572	7.967863	3.251461
B	4.766959	4.625436	5.102295
H	4.567002	4.144943	6.183222
C	6.073602	10.516279	5.747555

H	4.344205	11.478243	2.703481
C	5.570908	9.218319	5.605221
H	6.060715	8.513548	4.937021
C	5.462796	11.427609	6.612249
H	5.857176	12.441661	6.716536
C	3.686689	6.109255	2.452788
C	4.435961	6.235273	4.891635
C	1.781980	10.073762	4.448338
H	1.174173	10.233485	5.341151
C	2.219112	8.611326	-0.566111
H	1.806299	9.402490	0.062950
C	2.889310	7.827979	-2.762292
H	3.003511	7.996503	-3.835999
H	6.955288	10.813755	5.174309
B	6.020174	5.829153	4.758224
H	6.816868	6.256587	5.551045
B	3.938957	4.516317	2.143306
H	3.254333	3.968270	1.317079
B	5.156951	5.769693	1.790375
H	5.414209	6.217846	0.706422
C	4.333842	11.029222	7.339657
H	3.843043	11.730870	8.019748
B	4.441681	3.709754	3.633364
H	4.084054	2.569458	3.788670
B	3.428641	5.273763	3.881880
H	2.282399	5.162543	4.235641

Dianionic *nido*-ligand (***nido*-L^{2-}**)

P	12.767632	8.993113	21.032991
P	9.283148	7.258670	24.682926
C	9.385112	7.505835	22.879073
B	9.993972	10.002890	21.606907
C	13.411655	7.263132	20.996019
C	14.803199	7.078520	21.091924
H	15.448013	7.958213	21.174361
C	15.367163	5.802186	21.076116
H	16.451947	5.684155	21.144226
C	14.541808	4.674936	20.982304
H	14.976618	3.672235	20.975980
C	13.156087	4.845308	20.909958
H	12.498287	3.975433	20.848028
C	12.592458	6.124997	20.918083
H	11.509352	6.252254	20.834791
C	13.249175	9.513451	19.325112
C	13.596745	8.637610	18.284022
H	13.575611	7.562662	18.463182
C	13.949322	9.127167	17.023772
H	14.205796	8.426417	16.224864
C	13.949757	10.502881	16.773599
H	14.218141	10.883903	15.785089
C	13.592054	11.386230	17.798017
H	13.573316	12.463051	17.611826
C	13.251978	10.894246	19.058875
H	12.965720	11.582086	19.857719
C	10.640150	6.081787	25.068976
C	11.520003	5.613195	24.082156
H	11.336353	5.894767	23.046469
C	12.621157	4.822562	24.417999
H	13.301491	4.497420	23.628222
C	12.850861	4.460920	25.749038
H	13.712799	3.842657	26.012024
C	11.977969	4.915602	26.745622
H	12.153496	4.649618	27.791763
C	10.896936	5.732009	26.408985
H	10.241840	6.119891	27.193916
C	7.791752	6.213498	24.968819
C	7.780544	4.958736	25.599164
H	8.725556	4.485290	25.869907
C	6.578477	4.293368	25.863488
H	6.601337	3.313117	26.348276
C	5.357687	4.862526	25.493713
H	4.418899	4.339287	25.691182
C	5.355834	6.106727	24.848278
H	4.412916	6.555822	24.527010
C	6.551742	6.773230	24.593851
H	6.541786	7.732812	24.073101
B	10.464582	8.562324	22.550155
B	8.632712	9.012829	22.385971
B	8.507004	6.823179	21.847438
H	7.730008	5.960075	22.192813
B	7.704087	8.218120	20.845866
B	8.460132	9.790958	20.787596
H	7.755724	10.765920	20.740399
B	10.016854	9.641761	19.893148
H	10.504440	10.462924	19.166883
B	8.660612	8.618764	19.427437
B	8.758443	7.031433	20.134759
H	8.291855	6.111441	19.495716
B	10.245989	7.855251	19.786089
H	10.983375	7.488207	18.899088
C	10.961652	8.757285	20.979427
H	7.990544	9.532959	23.263080
H	8.181464	8.809203	18.336295
H	6.498803	8.164520	20.904149
H	10.445317	11.051945	21.981633
H	11.199492	8.934331	23.438572

1,5-Cyclooctadiene

C	-0.41185212371428	3.41590588214800	10.31328503005713
H	-0.44136709306268	2.33414663681654	10.47962611323184
C	-1.39608204280898	4.13019745659533	10.87830844435137
H	-2.15020447798168	3.56072998925915	11.43240906101921
C	-1.64539244085067	5.61402026003244	10.87918515304142
H	-1.98000271498881	5.89392818306824	11.89348479818368
H	-2.51115693392225	5.83047534803359	10.22533583318824

C	-0.47638422186483	6.53824937958188	10.48044803200364
H	-0.20871935036117	6.37652281925826	9.42964577987667
H	-0.84011057324584	7.57577430564365	10.53800811817250
C	0.72502592392791	6.40267634731401	11.38360769428802
H	0.76830652815249	7.12630871605275	12.20409951787104
C	1.71582044873241	5.50038728670505	11.33567902015101
H	2.48765385793220	5.58821061462692	12.10807748072953
C	1.95224064928247	4.36339303363498	10.37905677353430
H	2.30556438514229	3.50027526950277	10.97017175693717
H	2.80230440076682	4.62276433336367	9.72026836618447
C	0.76687236327611	3.90230481398781	9.50623678118875
H	0.47594259093813	4.69954435897611	8.81218153347965
H	1.12280082465037	3.07366496539885	8.87478471251035

[(^{Ph}BIAN)Co(η^4-cod)]$^-$ (phenyl substituted **1**)

Co	0.176648	4.284464	12.571629
N	0.370934	5.004246	14.367305
N	0.038557	2.582977	13.505580
C	0.341899	4.037148	15.326803
C	0.113474	2.720427	14.858617
C	0.089903	1.806819	16.003703
C	-0.024527	0.436191	16.212321
H	-0.148265	-0.256419	15.380156
C	0.014046	-0.067349	17.543247
H	-0.078729	-1.146562	17.688390
C	0.156273	0.750595	18.653271
H	0.171835	0.323289	19.658638
C	0.288363	2.163747	18.477181
C	0.441250	3.143723	19.507577
H	0.461410	2.833975	20.555055
C	0.557137	4.482390	19.167054
H	0.665753	5.224044	19.962377
C	0.548470	4.940773	17.819364
H	0.653122	6.006017	17.614797
C	0.413005	4.014627	16.789991
C	0.265192	2.636552	17.160500
C	-0.397320	1.368541	12.958797
C	0.328511	0.775072	11.909390
C	-0.116351	-0.401027	11.308634
H	0.466097	-0.844394	10.497804
C	-1.299709	-1.015107	11.736160
C	-2.034649	-0.427413	12.772247
H	-2.967999	-0.885858	13.107263
C	-1.591860	0.748548	13.376996
C	0.809019	6.292868	14.701021
C	2.020096	6.515388	15.386601
C	2.461922	7.811335	15.651293
H	3.407982	7.959772	16.177143
C	1.710022	8.917594	15.239594
C	0.510350	8.705593	14.549546
H	-0.085501	9.558439	14.216562
C	0.066356	7.412149	14.281586
C	-0.879665	3.745299	10.948157
H	-1.436468	2.831964	11.174892
C	-1.375612	4.955488	11.522885
H	-2.276148	4.874479	12.144786
C	-1.147973	6.326335	10.910866
H	-1.530042	7.083201	11.613767
H	-1.730077	6.458859	9.974540
C	0.357334	6.576867	10.668503
H	0.621146	6.349536	9.621416
H	0.588597	7.643812	10.814253
C	1.195643	5.735314	11.624071
H	1.768299	6.308940	12.357897
C	1.694896	4.437551	11.295503
H	2.611154	4.116695	11.807056
C	1.439742	3.758209	9.961763
H	1.836101	2.732264	10.017052
H	1.994222	4.254153	9.137313
C	-0.073701	3.699874	9.655063
H	-0.363185	4.532368	8.991242
H	-0.309617	2.776172	9.103566
H	-2.168122	1.216056	14.176315
H	-0.859154	7.230919	13.735311
H	1.242146	1.270161	11.580933
H	2.609644	5.651338	15.695406
H	-1.650300	-1.932901	11.260828
H	2.059435	9.931084	15.444463

[(^{Ph}BIAN)Co(η^4-cod)] (phenyl-substituted **Int-A**)

Co	0.18285955827941	4.31353830856844	12.48400949294306
N	0.64304127283696	4.97528732521083	14.26705170195598
N	-0.21345791092416	2.65684841178506	13.45135985702927
C	0.47246677938101	4.04978981907910	15.21454756227334
C	-0.02036228046401	2.77715135960982	14.76713293123919
C	-0.16222723348218	1.89576063937059	15.92509587762773
C	-0.56473406915622	0.58724907112282	16.15082049836386
H	-0.88938040025102	-0.05821320823595	15.33528690402214
C	-0.54960583513698	0.09115116973782	17.48282266149153

H	-0.86809171284365	-0.93838436534259	17.65441356267927
C	-0.15000947745287	0.86008286309496	18.56624503599226
H	-0.15742197912351	0.43583597452148	19.57191670531862
C	0.27280639187216	2.20801170447731	18.36928257169851
C	0.71393642622374	3.13015871030810	19.36405230547119
H	0.75069209854887	2.82187492207879	20.41049001287893
C	1.09504045342654	4.41419808308601	19.00233534586036
H	1.42883239251808	5.10467654129941	19.77862179472549
C	1.07226679794204	4.87350862439494	17.65726306622047
H	1.38506528643674	5.89129503294531	17.42604623814524
C	0.64959579406278	4.00068244944625	16.66502346763956
C	0.25351498142721	2.67968371228733	17.04831389160800
C	-0.72910670971158	1.42236607450045	12.97702368425796
C	0.13889928101701	0.44115792572239	12.47831883016970
C	-0.36751047028289	-0.77893329416623	12.02766644742722
H	0.31601563039786	-1.54016296711673	11.64875400145441
C	-1.74266414388429	-1.02763267013066	12.06286455071641
C	-2.61035581931896	-0.04842133847022	12.55456184338694
H	-3.68455274370907	-0.23632773145751	12.58744677257603
C	-2.10828217272429	1.17224674434333	13.00877666942359
C	1.15820794853336	6.23533831127372	14.66962707321876
C	2.54075986472687	6.42376000648573	14.80466809570596
C	3.04300233844939	7.65970792888806	15.21578713827699
H	4.12005604044563	7.79610756104926	15.32340723695535
C	2.17163280154443	8.71701231294791	15.49200655754089
C	0.79285172405264	8.53221839249395	15.35398173509995
H	0.10681974966379	9.35222293564822	15.57113302665510
C	0.28637780816273	7.29886138468740	14.94104103460431
C	0.07780265336987	3.39344656269370	10.65150233178091
H	0.22995487746577	2.32921120050151	10.84391146677669
C	-1.16777162767248	3.93215476782562	11.02767220009760
H	-1.89189122677556	3.23696270802969	11.46419951274763
C	-1.76625105027712	5.21238184788388	10.49313033707520
H	-2.61167775669957	5.48725636392438	11.14199088310176
H	-2.19051560855283	5.06033166188026	9.48205980686384
C	-0.73357775900261	6.35847553575714	10.49434694395549
H	-0.19314446694396	6.39651280660899	9.53767579985075
H	-1.25024744873941	7.32452963630956	10.59130591271625
C	0.23961119873092	6.18511032604204	11.64560550136428
H	0.11038927701512	6.88837091325286	12.47137058131714
C	1.49029217102554	5.54428266706735	11.55230012923716
H	2.23714752278466	5.81624643426717	12.30483878354901
C	2.05500436842108	4.89829695394555	10.30891705997910
H	2.91685453066401	4.28315444549957	10.60912310229711
H	2.44876461568135	5.66103784642882	9.60990322113183
C	1.00787215130517	4.00076269164751	9.61817999756741
H	0.43370551061841	4.57326570740982	8.87580397749187
H	1.51385369021823	3.19875285313607	9.06107107265581
H	-2.77236015145866	1.93885991418967	13.41001670064790
H	-0.78702520023346	7.13559452705273	14.83784870461569
H	1.21000434274223	0.64639717573102	12.46641661869242
H	3.20807483222581	5.58532194600151	14.60127451364636
H	-2.13643863412404	-1.98102178824957	11.70915286917690
H	2.56560072672795	9.68180556961827	15.81322578901032

Int-B (with phenyl groups)

Co	8.271950	5.415248	22.056285
P	11.837756	6.613412	21.091105
P	8.346178	6.746012	25.104822
N	9.228333	3.760836	21.590980
N	7.065914	4.085439	23.066844
C	8.656477	2.644929	22.098302
H	14.136769	11.016131	20.277529
C	14.225157	10.417624	22.355265
H	14.757921	11.316007	22.676097
C	13.876239	9.436072	23.286672
H	14.121493	9.563690	24.342867
C	13.193976	8.290196	22.873039

C	7.544556	2.828038	22.969825
C	7.092792	1.513545	23.431272
C	6.075995	1.016476	24.242473
H	5.386215	1.684968	24.756914
C	5.948711	-0.391132	24.405146
H	5.147907	-0.763871	25.049719
C	6.792784	-1.302645	23.786996
H	6.659219	-2.376524	23.941132
C	7.839400	-0.829088	22.934225
C	8.773308	-1.625974	22.199371
H	8.736603	-2.715890	22.274720
C	9.712156	-1.006850	21.387109
H	10.417150	-1.625646	20.825390
C	9.801058	0.406127	21.242464
H	10.554075	0.834367	20.581579
C	8.911703	1.211521	21.948719
C	7.948911	0.558381	22.787539
C	6.102451	4.365613	24.045904
C	4.897403	4.993963	23.685488
C	3.956259	5.330629	24.658508
H	3.036040	5.838239	24.361654
C	4.196087	5.051959	26.007475
C	5.389914	4.421222	26.374181
H	5.599354	4.219397	27.426912
C	6.336189	4.086629	25.407748
C	10.247833	3.528315	20.635491
C	11.578903	3.358310	21.045697
C	12.570423	3.050220	20.113536
H	13.603757	2.932458	20.445762
C	12.253976	2.926677	18.757481
C	10.933617	3.119720	18.342295
H	10.680426	3.053717	17.282265
C	9.936492	3.418202	19.271459
C	8.335110	7.097007	23.317033
B	9.824273	8.860642	21.632255
C	12.430775	6.419530	19.355110
C	11.653425	6.437861	18.188463
H	10.591662	6.660421	18.255675
C	12.226245	6.153545	16.944928
H	11.594786	6.166798	16.053456
C	13.584333	5.851334	16.834880
H	14.025626	5.627133	15.860947
C	14.372956	5.830044	17.991741
H	15.436823	5.588181	17.927928
C	13.797899	6.098139	19.231261
H	14.414577	6.058904	20.133072
C	12.823091	8.118230	21.529977
C	13.179284	9.111125	20.602877
H	12.882607	8.996953	19.559830
C	13.879213	10.247234	21.010119
H	12.910209	7.532862	23.605081
C	6.947846	7.622134	25.931516
C	6.048529	8.519522	25.336728
H	6.164957	8.782251	24.288147
C	4.998876	9.069152	26.078615
H	4.304674	9.757488	25.590952
C	4.832944	8.746715	27.427787
H	4.006834	9.174413	28.000813
C	5.730343	7.861750	28.035001
H	5.609006	7.590845	29.086718
C	6.764751	7.299951	27.288563
H	7.445526	6.582357	27.753998
C	9.726596	7.797739	25.758491
C	9.664453	9.196206	25.854302
H	8.745662	9.709842	25.570566
C	10.775271	9.930218	26.272399
H	10.718541	11.020263	26.315082
C	11.964425	9.278434	26.615822
H	12.835133	9.856235	26.933834
C	12.033132	7.884519	26.542215
H	12.959220	7.366117	26.801428
C	10.920331	7.153293	26.119506
H	10.974568	6.065715	26.034808
B	9.732955	7.433810	22.715780
B	8.233126	8.718170	22.580122
B	7.006330	7.173845	22.484686
H	5.974276	7.085318	23.077642
B	6.916470	8.437586	21.235739
B	8.345441	9.355056	20.867113
H	8.227108	10.533897	20.668742
B	9.519376	8.345533	19.990694
H	10.233063	8.719783	19.104142
B	7.796196	8.061141	19.763429
B	7.140813	6.748301	20.742740
H	6.218346	6.143763	20.252196
B	8.844475	6.638970	20.169710
H	9.148829	5.884848	19.293245
C	10.103186	7.270833	21.110797
H	10.678503	7.435036	23.449303
H	8.062899	9.562677	23.413473
H	7.337564	8.295132	18.676225
H	5.859714	9.014097	21.227658
H	13.037215	2.725113	18.025453
H	3.474800	5.351012	26.769898
H	8.902022	3.568245	18.965097
H	4.732946	5.219190	22.632888
H	7.284125	3.627365	25.686500
H	11.813493	3.471200	22.103199
H	10.716375	9.609347	21.888431

Int-C (with phenyl groups)

Co	8.529797	5.480325	22.136027
P	11.922576	6.386787	21.207813
P	8.455798	6.922082	25.275686
N	9.285363	3.852807	21.438623
N	7.499853	4.272710	23.206958
C	8.707186	2.748011	21.936575
C	7.705819	2.981590	22.906552
C	7.111074	1.701096	23.300884
C	6.103712	1.269817	24.151085
H	5.523425	1.972174	24.748413
C	5.833307	-0.124658	24.237562
H	13.879060	10.941957	20.408864
C	14.087467	10.312189	22.467894
H	14.571894	11.237077	22.786801
C	13.848459	9.291237	23.390299
H	14.136923	9.415450	24.434788
C	13.224162	8.111794	22.981224
H	13.024773	7.321145	23.705486
C	6.955971	7.681739	26.027832
C	5.943782	8.402828	25.378230
H	6.019693	8.609522	24.314360
C	4.829153	8.857880	26.088980

H	5.038156	-0.454050	24.909507
C	6.534030	-1.073338	23.508762
H	6.291542	-2.133633	23.607343
C	7.572794	-0.663339	22.620060
C	8.376130	-1.500963	21.789439
H	8.226686	-2.582737	21.803808
C	9.338530	-0.938518	20.965077
H	9.944181	-1.592802	20.334696
C	9.574570	0.463287	20.898174
H	10.342161	0.850586	20.229102
C	8.811882	1.305188	21.694112
C	7.823376	0.714006	22.545592
C	6.484304	4.498324	24.181309
C	5.189071	4.861489	23.794374
C	4.199194	5.040227	24.761519
H	3.196800	5.342626	24.455106
C	4.491053	4.847473	26.114688
C	5.776125	4.456748	26.496885
H	6.011618	4.303974	27.550723
C	6.773728	4.285677	25.535457
C	10.277841	3.571112	20.451361
C	11.594985	3.318785	20.851107
C	12.548015	2.930228	19.906479
H	13.575950	2.748539	20.222429
C	12.192712	2.791104	18.563803
C	10.874339	3.033170	18.168075
H	10.590318	2.931627	17.119740
C	9.917886	3.420717	19.106358
C	8.437110	7.096493	23.454179
B	9.807955	8.564645	21.882640
C	12.478521	6.259944	19.452989
C	11.709296	6.289358	18.283073
H	10.641989	6.479441	18.340157
C	12.300892	6.062075	17.036231
H	11.677037	6.086209	16.140512
C	13.667278	5.804702	16.929810
H	14.122900	5.627747	15.953711
C	14.447551	5.770223	18.091044
H	15.518480	5.566303	18.028974
C	13.856269	5.985488	19.333046
H	14.470000	5.943142	20.236755
C	12.810962	7.944798	21.651188
C	13.065697	8.971925	20.728933
H	12.745206	8.854082	19.694017
C	13.700483	10.145601	21.134126
H	4.048286	9.408221	25.560441
C	4.711767	8.618780	27.459445
H	3.838032	8.975039	28.008554
C	5.723297	7.916445	28.122288
H	5.645542	7.720427	29.193689
C	6.823651	7.445365	27.408730
H	7.599307	6.871360	27.922560
C	9.707529	8.196571	25.759541
C	9.442602	9.573161	25.792761
H	8.447907	9.934115	25.533015
C	10.444401	10.479912	26.143303
H	10.227581	11.549840	26.146861
C	11.721959	10.023744	26.479809
H	12.504565	10.735341	26.749392
C	11.990863	8.652852	26.471688
H	12.983377	8.285899	26.740970
C	10.989016	7.748138	26.116439
H	11.195651	6.676329	26.103430
B	9.861413	6.929201	22.908089
B	8.095636	8.625603	22.651379
B	7.114402	7.069979	22.556034
H	6.111031	6.921931	23.175552
B	6.940742	8.272569	21.288594
B	8.445474	9.155414	21.006198
H	8.422467	10.334734	20.799360
B	9.622989	8.098440	20.199830
H	10.390886	8.426107	19.348568
B	7.899666	7.891156	19.868867
B	7.219391	6.567374	20.834461
H	6.334354	5.909185	20.355341
B	8.880486	6.454547	20.246711
H	9.198760	5.725098	19.366378
C	10.129116	6.967779	21.313116
H	10.816359	6.741919	23.603218
H	7.860923	9.485061	23.447529
H	7.514431	8.124817	18.758436
H	5.873455	8.811605	21.196079
H	12.944799	2.515029	17.824192
H	3.722177	5.013120	26.870294
H	8.883199	3.598301	18.817620
H	4.979513	5.002181	22.735151
H	7.782235	3.988093	25.815495
H	11.852304	3.421212	21.903283
H	10.687600	9.231799	22.322982

2 (isolated product, phenyl groups)

Co	8.46119589552652	6.51288929634681	22.64612951951804
P	11.68172684778420	9.86536941398784	21.81008856361535
P	9.62624701327115	7.50954746765845	25.62987656509710
N	9.57663035402917	4.94355042262857	22.70479901498552
N	7.17567467808002	5.34866401233725	23.48237330344316
C	8.97170185465215	3.88413186888978	23.25431103751334
C	7.63911339715784	4.11369704097667	23.69504677038575
C	7.12685515957183	2.89030993496038	24.31824206184539
C	5.94992737840818	2.48678562171859	24.93021365911822
H	5.10754838640964	3.16857268480313	25.04487769381391
C	5.85874622875903	1.15295078348454	25.41685501314555
H	4.92935989118421	0.84193401149513	25.89829057287804
C	6.89659081855407	0.23940812906813	25.30610904716688
H	6.78084659591039	-0.77431099828163	25.69571650422868
C	8.12207239517547	0.62349514828185	24.68368768889464
C	9.28400016824333	-0.18272098572330	24.49210812208554

H	9.28930226167054	-1.21806176428840	24.83967259978656
C	10.40181007153299	0.35047528162902	23.86753358129354
H	11.28208103588895	-0.28075885061724	23.72966211684260
C	10.45727795220694	1.69222578561349	23.39769222720893
H	11.36315827380147	2.06407917680258	22.91948908857892
C	9.34461553033313	2.50244840997865	23.56847278655664
C	8.19360937981659	1.94178127131310	24.21037694703269
C	5.92536574476201	5.65042505944599	24.09325946641508
C	4.73312139603695	5.58513290438317	23.36726120827191
C	3.51987742050511	5.85491124571354	24.00501513433504
H	2.59041554383656	5.80476150549948	23.43519488312220
C	3.49353804799465	6.20151515208396	25.35910651043601
C	4.68988955153655	6.27357976456609	26.08022708611487
H	4.68771265708612	6.56208428658258	27.13253161783165
C	5.90108992113057	5.99449342437132	25.45039645086107
C	10.96500260515224	4.78343785963663	22.44334748525456
C	11.86256336879691	4.82113159622652	23.51782381347581
C	13.22102143879918	4.59286207455724	23.30094122137074
H	13.91534708555460	4.62123134781744	24.14277532369106
C	13.68947155996465	4.32766005531142	22.01126297466294
C	12.79432974300027	4.30747375857350	20.93889827536734
H	13.15841758868669	4.12320505119122	19.92764065493672
C	11.43458999230314	4.53869180934685	21.14901884996088
C	9.04090288882167	7.93251715978453	23.95525155748876
C	10.01169321848482	9.06564390123286	21.65694201698312
C	12.79850279651695	8.66503138972535	20.96165684438403
C	13.86865269160615	8.15087718572521	21.70527068849804
H	13.95017766396069	8.41615408801336	22.76074436403041
C	14.81716971704957	7.31875296710468	21.10535382035674
H	15.64587868752652	6.92494725468403	21.69615645209779
C	14.69520406973219	6.98288910583222	19.75675127382754
H	15.43285907715998	6.33030283290019	19.28551178996649
C	13.61470897147316	7.47052820354970	19.01322226198674
H	13.50766538912888	7.19833256518398	17.96129660378267
C	12.67443075595934	8.30937529268002	19.61024764558463
H	11.83701709779279	8.69383770115909	19.02732920114804
C	11.80945531308009	11.23624594949493	20.57217621761392
C	12.88448666499712	12.11078422306602	20.81420649690446
H	13.51358997695336	11.94361685358720	21.69254797106967
C	13.15458310179623	13.17778137455628	19.95645818826181
H	13.99992568440306	13.83821047887351	20.16038971623705
C	12.33282879005237	13.40784739197486	18.84922960629994
H	12.53146889087580	14.24832415619614	18.18143949203820
C	11.24894296778495	12.55890043670355	18.61099680181428
H	10.59567543984531	12.73394644529144	17.75368438607550
C	10.99023005107867	11.48040573707198	19.46052621085970
H	10.14537509070371	10.82680894833392	19.25752160843987
C	8.42629970191180	8.30812474231134	26.77749782533106
C	7.74505172707529	9.50951635375401	26.51901851495994
H	7.92549402802394	10.04664933255403	25.58825443400893
C	6.81510008513111	10.00826549323170	27.43152156150542
H	6.28602901576027	10.93633884252397	27.20805009182637
C	6.54845222221781	9.31664789134061	28.61754757329831
H	5.81167548681688	9.70422423968161	29.32368397625974
C	7.22100876481343	8.12297489502416	28.88905784629801
H	7.01440423221817	7.57233821216483	29.80882191312221
C	8.14933527318535	7.62386066856106	27.97142585772194
H	8.66050839090181	6.67841325365249	28.16882367424201
C	11.10581124526334	8.60776209176947	25.79987952196089
C	11.05338846294090	9.96047784583433	26.16529509993736
H	10.09788292086854	10.41396687077675	26.42790038105986
C	12.21278874648545	10.73810010939282	26.18718557630257
H	12.14858229822267	11.79443139055620	26.45507626705727
C	13.44631737688236	10.17470235456399	25.85234643008309
H	14.34992581166594	10.78671563239105	25.85962051575518
C	13.51483368365495	8.82258760889851	25.50845272828305

H	14.47433308193343	8.36864026735830	25.25289345543625
C	12.35524973392751	8.04701242791311	25.48686122936373
H	12.41222596779995	6.99621559356910	25.20180332649902
B	10.11778624464870	7.83403097062410	22.85316363928589
H	11.25180260477478	7.57030094231107	23.13200905131359
B	8.97683872202614	9.47792134640698	23.16027072267393
B	7.55362779368944	8.24499957936339	23.60055543167434
H	6.75851554094457	8.25123721567326	24.49080276000148
B	7.30344495892929	9.55427933399473	22.42970378415554
B	8.67326638337771	10.05278406224548	21.47341935965521
H	8.88506196576570	11.20533694531105	21.24936808283584
B	9.06480373017470	8.76279369649725	20.28390546466881
H	9.51329615567817	9.00486226607746	19.20401679355892
B	7.39077656710727	9.05379300878055	20.74642697746996
B	6.91619345035390	7.87665641061845	21.96241546251299
H	5.77686870851001	7.50927141509630	22.00217358104795
B	8.02553404626636	7.36685027399384	20.69886772744063
H	7.69448657175108	6.62587751119808	19.81165115529177
B	9.70614140632453	7.41813490434217	21.17770960347779
H	10.63585634070439	6.86359078688499	20.67912369343134
H	9.45013674732668	10.34093434892348	23.83894935662612
H	6.61722584557451	9.49849755379928	19.94683625789483
H	6.50808836262548	10.38007013323554	22.78107838189348
H	14.75231867857076	4.15430552734939	21.83852552266736
H	2.54384770900754	6.42446389771188	25.84841831965016
H	10.72220668082793	4.52431655023180	20.32553286617642
H	4.77403900021851	5.32687627622496	22.31013261820588
H	6.84296902795680	6.05342596870893	25.99472565296800
H	11.46702026926670	5.01444325547677	24.51619027621696

2 (isolated product, xylyl groups)

Co	8.55402005041267	6.50379886662418	22.93752156382546
P	11.71468501726361	9.87963003565017	21.95005077633607
P	9.74928698259570	7.88415686442691	25.91723311061255
N	9.64993658002357	4.90550197424760	22.89418636372034
N	7.23284856762310	5.28962959104242	23.65170643942589
C	9.00558265100712	3.81648483520941	23.32374334470085
C	7.66753901790400	4.03317884387735	23.75382228965612
C	7.09853739474372	2.75952527702883	24.20081871844968
C	5.88781642879089	2.32237342167190	24.71652757443925
H	5.05812041847286	3.01090590952521	24.87693714361505
C	5.74376050301381	0.94268251680965	25.03320920050695
H	4.78848090737625	0.60388809001126	25.43915358328038
C	6.76054210631011	0.01754897973531	24.84674259090685
H	6.60218909941494	-1.03209490084857	25.10349747841046
C	8.01816719097182	0.43507464691736	24.31647654646765
C	9.16260864511553	-0.37809974544420	24.05870208363809
H	9.12748579641760	-1.44803065617903	24.27484149835506
C	10.31364045665944	0.19085719493567	23.53374480412329
H	11.17861473313041	-0.44724186310264	23.34178916601703
C	10.42200629586712	1.57701454238868	23.23109119569428
H	11.34944983656105	1.97441176676891	22.81872103825800
C	9.32793356991765	2.39514141280518	23.47250812776291
C	8.14258233225663	1.79816515938236	24.01186998418532
C	5.87904149353510	5.50176976261481	24.05104561104078
C	4.85408809832489	5.27811533923792	23.10943244962341
C	3.53006909063182	5.46997340743974	23.51797469419192
H	2.72735417661370	5.31371770095906	22.79394325287999
C	3.23034037246685	5.86385674984373	24.82380671068132
C	4.25860862951154	6.04714881066499	25.74681250719198
H	4.03010904303398	6.34139632576933	26.77361890919916
C	5.59819827521230	5.85645059643939	25.38140866304869

C	10.99635611166465	4.67193492257264	22.47812148340867
C	12.01078750656953	4.65469467983371	23.45354975351269
C	13.31759942919646	4.35492927076120	23.04939389986044
H	14.11204354262275	4.34448501004842	23.79921266340689
C	13.60432849482801	4.05734364986942	21.71831527440279
C	12.57928391334697	4.04699643357332	20.77332506754993
H	12.79775277370151	3.80544205287873	19.73123972503642
C	11.25913104888786	4.34030832951006	21.13437082030240
C	9.11815672808459	8.02748455948058	24.20709684807370
C	10.04852399527144	9.05807981904914	21.85042709451296
C	12.78802819445770	8.67529407058802	21.05554526070927
C	13.78369190794826	8.02791565309683	21.79942460817366
H	13.85966479524908	8.23282882062777	22.86845205140463
C	14.66236605022361	7.13403960150453	21.18380345645977
H	15.42727963874139	6.63022594226449	21.77621103249498
C	14.54872976090942	6.87377014671501	19.81779656885405
H	15.22851088397911	6.16825132505361	19.33643596519818
C	13.54950817089092	7.50516855208097	19.07013996852012
H	13.44854422903583	7.29427184962315	18.00367750370054
C	12.67689707405670	8.40271356218139	19.68412811561353
H	11.89806176323710	8.89155916186347	19.09871147330454
C	11.76400558680965	11.26213107830670	20.72264710232185
C	12.76804738909179	12.21042356401702	20.98905099108176
H	13.38538264483219	12.08656221910456	21.88259109589820
C	12.98061337492649	13.29588294732426	20.13761318809735
H	13.77092031135921	14.01545605440319	20.36107854788534
C	12.17056306054802	13.46756909094867	19.01176489663125
H	12.32356988732192	14.32124434998498	18.34871740334404
C	11.15578310059436	12.54357798033161	18.74789264517789
H	10.51177998068121	12.67339063108106	17.87569763762859
C	10.95514145940176	11.44878351488117	19.59168724075225
H	10.16163390155013	10.73810189285251	19.37066468093654
C	8.61750774382911	8.87681765957076	26.97925481225714
C	7.82826789908428	9.95677436190170	26.55292094235508
H	7.84595076851784	10.26897188632892	25.51004041094566
C	7.00337541893967	10.63197780078180	27.45453906074156
H	6.38988250933122	11.46275713710376	27.10129828484593
C	6.95661504789117	10.24575430207567	28.79724950736995
H	6.30582834490650	10.77280352143547	29.49753162268300
C	7.74108227554454	9.17557850089519	29.23536878453365
H	7.70740949272561	8.86109946196447	30.28033615645063
C	8.55759023976540	8.49522813395649	28.32959119806759
H	9.15334380413221	7.64227954731199	28.66356404337167
C	11.22868989159750	8.99463568062213	25.86828180392369
C	11.16779910138725	10.38670868521220	26.02788909547680
H	10.21221619251720	10.86508843449783	26.24144425723816
C	12.31729736539137	11.16940504895636	25.90584221374764
H	12.24443389285168	12.25347182451773	26.01119299699562
C	13.55025656780050	10.57360706373563	25.63225752909387
H	14.44599872733256	11.18779957105118	25.52496390912518
C	13.62879976237722	9.18570946667150	25.49735265777289
H	14.58898892102735	8.70798719854601	25.29280343571319
C	12.47896356550554	8.40463759695168	25.61827934555031
H	12.54428927313673	7.32355867313185	25.49993111723006
B	10.18397569342984	7.86183464226534	23.10119389152743
H	11.32553830580784	7.63236123060234	23.38038190041868
B	9.02804735132275	9.51225476361154	23.32592627758613
B	7.61673990587371	8.24622122923757	23.84804284703781
H	6.82234594971201	8.25946161304173	24.74272507339137
B	7.33941926022794	9.52247164771580	22.62370254971636
B	8.68878636224601	10.01223382956314	21.63636519387455
H	8.87550133940371	11.15982273937641	21.37108109378067
B	9.10185279665473	8.68609249378035	20.49584876513706
H	9.54280777206276	8.88916483176201	19.40504740566551
B	7.42342583415877	8.96086108352867	20.95947679447345
B	6.98241181601860	7.83099444272475	22.22815749806323

H	5.84776572068600	7.46084719613432	22.29313821315720
B	8.09377653396491	7.29198574861251	20.97523199891409
H	7.76463522942529	6.51563656604400	20.11591517988122
B	9.78022679587593	7.39764659955114	21.44462302282020
H	10.72174868173919	6.84586525449143	20.96606461015953
H	9.48879977701681	10.42004438751803	23.95002242963374
H	6.63502914456624	9.35126785301472	20.14657491312649
H	6.53193516199040	10.34485675267990	22.95561496354518
H	14.62839030593767	3.83334096477192	21.41537226599243
H	2.19244054720789	6.02393085606839	25.12183629849044
C	10.13862387553447	4.22777191759316	20.14076857641371
C	5.18762265819948	4.81062599265772	21.72129196219080
C	6.69606690622788	5.94981227197529	26.40195742157355
C	11.67152766161434	4.83452754656401	24.90480379145436
H	7.64742173447162	6.24414120896892	25.94420601271541
H	6.86347019858163	4.96984171179200	26.87942696662594
H	6.44819676024705	6.67342008765885	27.18869273250071
H	4.29478184065796	4.82420245720305	21.08231087944663
H	5.58304911135438	3.78228482853761	21.73788940584435
H	5.96163118000788	5.44614499192893	21.26905269435062
H	10.53350606621564	4.07256034078786	19.12804960122819
H	9.50418294983684	5.12363076720234	20.14409260494506
H	9.48489483813692	3.37644226818303	20.38983911235799
H	10.96733204258192	5.66089557908234	25.07321556312111
H	12.57707602900740	5.00958807700315	25.50158464372476
H	11.18037858520366	3.93037947668021	25.30063017512510

2′ (phenyl groups)

P	7.59460311913128	9.87609398730674	22.42242501946684
P	9.26022405683305	9.92403436299470	24.89350130863415
C	9.67015920150671	9.35433874776162	20.65034198319102
H	9.98279775591025	8.71918112247367	21.48299891124839
C	11.71661726540650	10.11402985092210	23.60267083507738
H	11.09552621627008	9.94233850465588	22.72639412010197
C	11.10089354926025	10.18595050115767	24.86444844899168
C	11.92572514074284	10.28945767763731	25.99442887453143
H	11.49118978975879	10.28581750174927	26.99196272250661
C	8.93862371883380	9.77376442374709	26.71164857759584
C	8.47652083474809	10.06871579739727	20.79909057263153
C	5.66193192867910	8.91499942178598	20.65949659632957
H	6.52098701537740	8.52878674015942	20.11026307555174
C	8.75799190172246	10.94382520797989	18.55246588790838
H	8.39417962655103	11.56217017873427	17.72939267284712
C	8.31959393959274	8.57963337357445	27.11252999194645
H	8.04946831520289	7.85492210684606	26.33884715123048
C	4.74336536135491	10.14024716126552	22.52264277847605
H	4.86530604761365	10.68924455237690	23.45109073896509
C	5.86947207135570	9.70866255761587	21.80378268810446
C	4.37318540445646	8.61580885924438	20.21745678521081
H	4.23965454366102	7.99928844997648	19.32631934011762
C	9.28504480050414	10.71590653983855	27.69447026763901
H	9.78377243691610	11.64118126153661	27.41185616425112
C	8.36701020205109	9.29084413560837	29.42534688677562
H	8.13771301142770	9.10960936506541	30.47725183778246
C	7.70680615499569	11.68081498517259	23.07084826845837
C	8.64425245382617	11.69446162341311	24.48370027995871
C	3.45579533073375	9.85771112331356	22.06806393683000
H	2.59876369114171	10.21059908802399	22.64274952171197
C	8.01398197978889	10.85054407973071	19.73027590042309
H	7.06256455897197	11.37541223697677	19.81472066541880
C	9.96530136334848	10.24836558311715	18.42483971271852
H	10.54541524032303	10.32686775839893	17.50321642403983

B	7.35065984199304	14.42689804688182	23.24405444676552
H	6.86798753281141	15.41219838289256	22.77265209520472
C	13.90626540329187	10.34603243409030	24.59817207343768
H	14.99158740957029	10.40130601782135	24.49666085196226
C	13.09800474700556	10.21033248663048	23.46611802228661
H	13.54603874585095	10.14292392095856	22.47397504043908
B	6.70699784751388	13.66596654152378	24.72247694689515
H	5.77595223650201	14.09058530908545	25.33694448903794
B	8.32168073278426	14.43475114660396	24.72585240114625
H	8.55290436650744	15.42730708557991	25.34834263173144
C	13.31486117207953	10.36936434558364	25.86179092652792
H	13.93637580840302	10.44367508650936	26.75666989859063
C	10.41700546022295	9.44326275337378	19.47435471199421
H	11.34859782337669	8.88198424958851	19.37995254134018
C	3.26182830746925	9.10423940303171	20.90878471748058
B	6.94893670750194	11.91060961792649	24.58452635200452
B	9.53255140468671	13.13479594592304	24.60008612270058
H	10.60956573146800	13.07574447072891	25.10289468486140
C	8.99156744710982	10.48034219642041	29.03959106532845
H	9.25231086255588	11.23075355263292	29.78863799663863
B	8.06105642731563	12.89277869595727	25.55365802277889
H	8.08809137675392	12.70027434022784	26.72119500288315
B	7.95492177277555	13.13088594950030	22.19943261981491
B	6.49395201068369	12.87447295238705	23.15236168333466
H	5.45635325900915	12.67281979339399	22.61374554842739
C	8.03938302481686	8.33610051907961	28.45846529161851
H	7.55704461792412	7.40085130389425	28.74762463609980
B	9.10033462323197	14.08712800465526	23.16183484910734
H	9.88746402097238	14.81438299626155	22.63702981294241
B	9.29195231772959	12.33255923064949	23.03314300317635
H	10.13272208593571	11.74208841344876	22.45234482098884
Co	8.34771862247364	8.48996253223950	23.73879209737904
N	9.49543424771891	6.95683528084383	23.57159634625062
N	6.98882300356240	7.17311568141082	24.15133574971635
C	8.84939810821567	5.79606148845744	23.81526152969419
C	7.45270063865953	5.89932932637506	24.07171610267318
C	6.93571767774693	4.55796015574624	24.36598579735185
C	5.72338995988226	3.99064766052669	24.74545151684249
H	4.82544399327923	4.59603371978412	24.86326814640297
C	5.65776668391394	2.58973579219000	24.98367125936295
H	4.69593290954624	2.16318602336198	25.27796010851932
C	6.75487717560668	1.75100148725588	24.85921109486879
H	6.65857408057958	0.68024033060642	25.05215462033509
C	8.02217820575550	2.29770149133946	24.49135577668552
C	9.25541459892124	1.58811950551631	24.35680184117972
H	9.27977830776027	0.50800836996293	24.51801890939592
C	10.41599225753265	2.27502457771011	24.03304049286173
H	11.35185263734093	1.71931488593634	23.93934472208102
C	10.44507271344545	3.68160428041304	23.82265528915347
H	11.38730992698993	4.17538904718778	23.58509166477144
C	9.26037661887188	4.39867733435277	23.93656683981314
C	8.06649464310015	3.67895379291802	24.26203526735953
C	5.61192306073371	7.40832675117262	24.29070240680795
C	4.65572088200102	6.76354565663784	23.48505210046880
C	3.29600498259085	6.99806070001936	23.67808039182277
H	2.56828047517816	6.50106417078521	23.03395344228723
C	2.86151356782231	7.87930814632129	24.67384114162746
C	3.80845207122909	8.55300635086564	25.45217741765526
H	3.48552437998061	9.26199229862051	26.21708565821361
C	5.17071557262235	8.33243472867628	25.25376743983192
C	10.90385760844997	6.91110506968661	23.48951278475533
C	11.68667839046999	7.02493423841663	24.65077347709190
C	13.07624911822008	6.98013487018008	24.57259049112541
H	13.66909238626421	7.08607692009297	25.48219816277964
C	13.71120358884001	6.81948758094535	23.33627981710024
C	12.93760921495667	6.70397475985311	22.17737202817823

H	13.42227236695280	6.57480716197422	21.20732183121669
C	11.54403565506832	6.74829096721488	22.25069418653409
H	14.80028059670047	6.79725792777932	23.27606893701403
H	1.79555469607783	8.05944763891224	24.82266432956675
H	10.92958188132573	6.63637675268265	21.35666739111758
H	5.00036751840472	6.08633172847473	22.70368527941417
H	5.92217408449474	8.85461305714814	25.84515225925263
H	11.17958071643828	7.15354851045145	25.60715975671206
H	2.25234536590507	8.87558283714881	20.56282855616372
H	7.93312208533856	13.09245025005794	21.01470617107769
H	6.30299856918055	11.02654510094670	25.03956611526838

7.5.6 References

[1] F. Neese, *Wiley Interdiscip. Rev. Comput. Mol. Sci.* **2018**, *8*, e1327.

[2] F. Neese, *Wiley Interdiscip. Rev. Comput. Mol. Sci.* **2012**, *2*, 73–78.

[3] P. J. Stephens, F. J. Devlin, C. F. Chabalowski, M. J. Frisch, *J. Phys. Chem.* **1994**, *98*, 11623–11627.

[4] F. Weigend, R. Ahlrichs, *Phys. Chem. Chem. Phys.* **2005**, *7*, 3297–3305.

[5] a) SCALE3ABS, CrysAlisPro, Agilent Technologies Inc. Oxford, GB; b) G. M. Sheldrick, SADABS, Bruker AXS, Madison, USA, **2007**.

[6] a) R. C. Clark and J. S. Reid, *Acta Cryst. A.* **1995**, *51*, 887–597 b) CrysAlisPro, version 40_64.18, Agilent Technologies Inc. Oxford, GB.

[7] G. M. Sheldrick, *Acta Cryst.* **2015**, *A71*, 3–8.

[8] G. M. Sheldrick, *Acta Cryst.* **2015**, *C71*, 3–8.

[9] M. Gasperini, F. Ragaini, S. Cenini, *Organometallics* **2002**, *21*, 2950–2957.

[10] R. B. King, M. B. Bisnette, *J. Organomet. Chem.* **1967**, *8*, 287–297.

[11] a) K. Jonas, R. Mynott, C. Krüger, J. C. Sekutowski, Y.-H. Tsay, *Angew. Chem. Int. Ed. Engl.*, **1976**, *15*, 767–768; *Angew. Chem.* **1976**, *88*, 808–809; b) K. Jonas, US Patent 4169845 **1979**.

[12] S. Pelties, T. Maier, D. Herrmann, B. de Bruin, C. Rebreyend, S. Gärtner, I. G. Shenderovich R. Wolf, *Chem. Eur. J.* **2017**, *23*, 6094–6102.

[13] T. M. Maier, S. Sandl, I. G. Shenderovich, A. Jacobi v. Wangelin, J. J. Weigand, R. Wolf, *Chem. Eur. J.* **2019**, *1*, 238–245.

[14] R. P. Alexander, H. Schroeder, *Inorg. Chem.* **1963**, *2*, 1107–1110.

[15] S. Grimme, S. Ehrlich, L. Goerigk, *J. Comput. Chem.* **2011**, *32*, 1456–1465

[16] S. Grimme, J. Antony, S. Ehrlich, H. Krieg, *J. Chem. Phys.* **2010**, *132*, 154104, 1-19.

[17] A. D. Becke, *Phys. Rev. A* **1988**, *38*, 3098–3100.

[18] J. P. Perdew, *Phys. Rev. B*, **1986**, *33*, 8822–8824.

[19] J. L. Whitten, *J. Chem. Phys.* **1973**, *58*, 4496–4501.

[20] F. Neese, F. Wennmohs, A. Hansen, U. Becker, *Chem. Phys.* **2009**, *356*, 98–109.

[21] Y. Zhao, D. G. Truhlar, *Theor. Chem. Acc.* **2008**, *120*, 215–241.

[22] Y. Zhao, D. G. Truhlar, *Chem. Phys. Lett.* **2011**, *502*, 1–13.

[23] M. Cossi, N. Rega, G. Scalmani, V. Barone, *J. Comput. Chem.* **2003**, *24*, 669–681.

[24] A. V. Marenich, C. J. Cramer, D. G. Truhlar, *J. Phys. Chem. B* **2009**, *113*, 6378–6396.

[25] N. Muresan, C. C. Lu, M. Ghosh, J. C. Peters, M. Abe, L. M. Henling, T. Weyhermöller, E. Bill, K. Wieghardt, *Inorg. Chem.* **2008**, *47*, 4579–4590.

[26] Y. Guo, K. Sivalingam, E. F. Valeev, F. Neese, *J. Chem. Phys.* **2016**, *144*, 094111.

[27] T. H. Dunning, *J. Chem. Phys.* **1989**, *90*, 1007–1023.

[28] N. B. Balabanov, K. A. Peterson, *J. Chem. Phys.* **2005**, *123*, 064107.

8 Summary

Chapter 1. *α-Diimine Complexes of Fe and Co in Catalysis*

The introductory chapter of this thesis reviews the relevance of Fe and Co diimine complexes in reductive transformations. Remarkable catalysts have already been discovered based on neutral heteroleptic 1,3-diiminopyridine and BIAN (bis(aryl)iminoacenapthene) complexes. Furthermore, this chapter describes how the synthesis of heteroleptic low-valent Fe and Co complexes with redox-active α-diimine ligands provides a platform for highly reactive complex fragments. In particular, anionic complexes with high reduction power and an arene or olefin molecule as second "placeholder" ligand – while rare – show impressive catalytic activity as was reported by the groups of *Lichtenberg*, *Grützmacher*, and *de Bruin*. Finally, the contribution of our group to this field is discussed with the synthesis of [K(thf){(^{Dipp}BIAN)Co(η^4-cod)}] (Dipp = 2,6-diisopropylphenyl; cod = 1,5-cyclooctadiene).

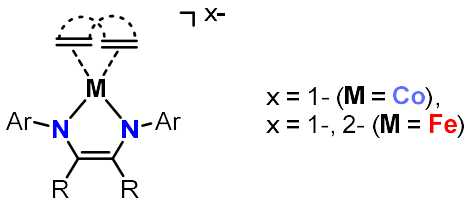

Figure 1. Heteroleptic α-diimine Co and Fe complexes with labile arene or olefin ligands as a key structural motif in this thesis.

Chapter 2. *Acenaphthene- and Phenanthrenediimine Ligands in Low-Valent Cobalt Complexes*

Chapter 2 starts with theoretical investigations using DFT methods on the α-diimines ^{Ar}BIAN and ^{Ar}PhDi (bis(aryl)phenanthrenediimine), which revealed that ^{Ar}PhDi is a better two-electron acceptor than ^{Ar}BIAN. Three heteroleptic ^{Ar}PhDi cobaltates **2-3**, **2-4**, and **2-5** were subsequently synthesized in a series of ligand exchange reactions starting from "quasi-naked" cobaltates, and thoroughly characterized. The reactivity differences between **2-4** and its BIAN-based counterpart **2-2** were rationalized using single-crystal X-ray crystallography, which illustrated the increased steric hindrance of PhDi. This hypothesis was further confirmed in the activation of white phosphorus and the formation of dinuclear $[Co_2P_4]^{2-}$ complexes in the case of ^{Dipp}BIAN and in contrast an end-deck $[CoP_4]^-$ complex in the case of ^{Dipp}PhDi. The chapter ends with quantum chemical calculations on the anion $[(^{Dipp}PhDi)Co(P_4)]^-$, which

showed the aromaticity of the tetraphosphido ligand alongside an electronic structure analysis.

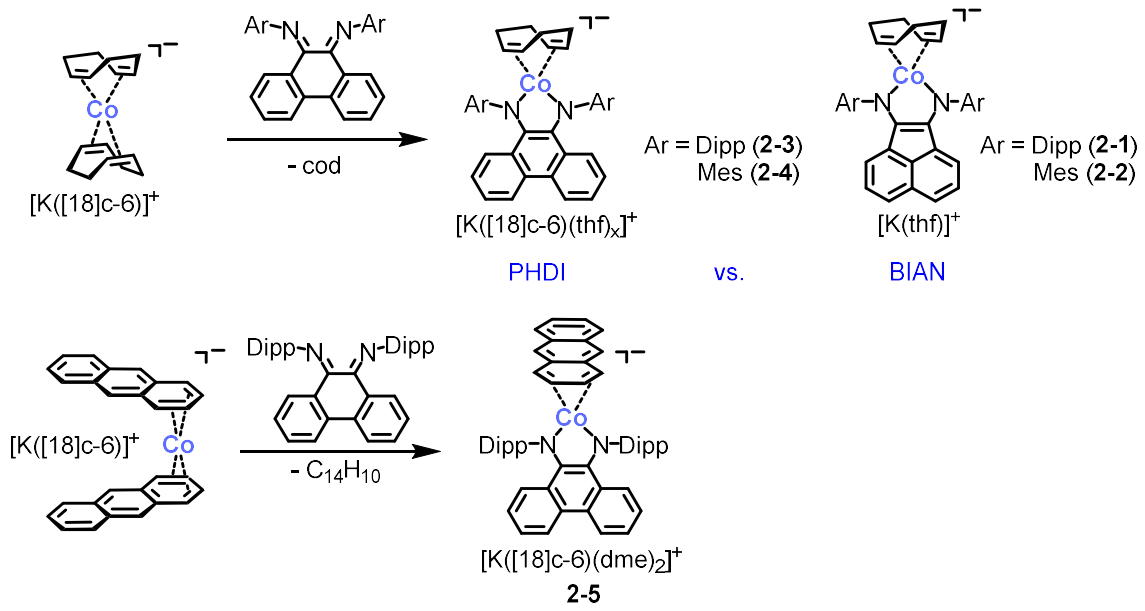

Scheme 1. Synthesis of heteroleptic ^{Ar}PhDi cobaltates **2-3**, **2-4**, and **2-5** and their comparison with heteroleptic BIAN cobaltates **2-1** and **2-2**.

Chapter 3. *Amine-Borane Dehydrogenation and Transfer Hydrogenation Catalyzed by α-Diimine Cobaltates*

Chapter 3 describes the application of the BIAN cobaltates **3-1** and **3-2** in catalytic dehydrogenation and transfer hydrogenation reactions. [K(thf){(^{Dipp}BIAN)Co(η^4-cod)}] (**3-1**) is a highly active catalyst for the dehydrogenation of alkyl-substituted amine-boranes NR_2HBH_3 (R_2 = ^{i}Pr$_2$, Me$_2$, MeH) and ammonia borane under mild conditions (5 mol%, 25 °C, 24 – 72 h). The dehydrogenation of NH_3BH_3 led to the formation of a mixture of polyaminoborane, borazine, and polyborazine as proven by ^{11}B NMR spectra in solution and the solid state. Kinetic analysis using the *Man on the Moon* setup demonstrated that more than one equivalent of H_2 were released per NH_3BH_3. Reaction monitoring indicated the formation of a dinuclear species as the active catalyst. Poisoning experiments with homogeneous (dct = dibenzo[*a*,*e*]cyclooctatetraene) and heterogeneous [Hg, $P(OMe)_3$] catalyst poison indicated that a homogeneous catalyst is present. Experiments using deuterated ammonia boranes (NH_3BD_3, ND_3BH_3, ND_3BD_3) showed that the protic N–H bond participates in the rate-determining step. Catalyst **3-1** was also able to transfer the hydrogen from NH_3BH_3 to

unsaturated molecules such as olefins, imines, and quinolines. The latter molecule was effectively hydrogenated (C=C and C=N bond) with only one equivalent of NH_3BH_3, and must therefore lose two equiv. H_2. Poisoning experiments again supported a homogeneous mechanism and experiments with deuterium gas suggested a direct transfer of H_2. Complex **3-2** showed similar results for the transfer hydrogenation. A related protocol was developed for the hydrogenation of sterically hindered tri-substituted olefins which involved first an initial activation step by catalytic amounts of NH_3BH_3, and subsequent hydrogenation under 10 bar H_2. An overall mechanism is depicted in Scheme 2.

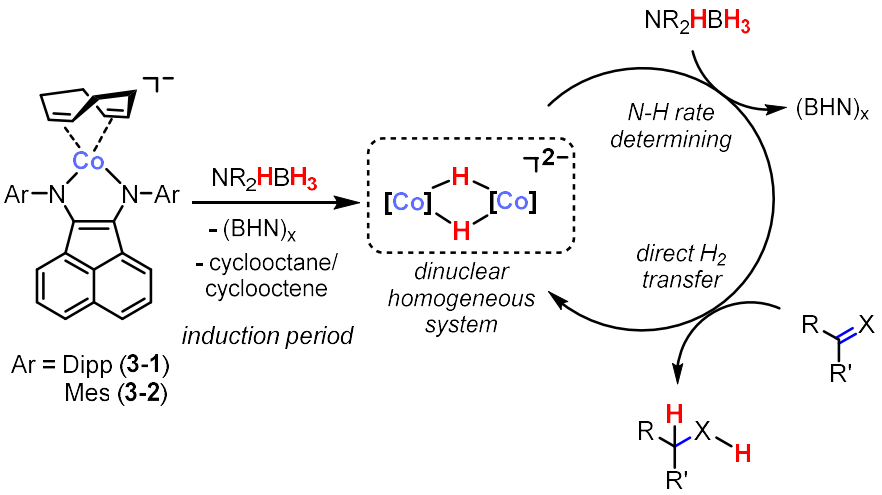

Scheme 2. Summary of the mechanistic information gained for amine-borane dehydrogenation and transfer hydrogenation (X = CR_2; NHR"); Ar = Dipp, Mes.

Chapter 4. *Cobalt-Catalyzed Hydrogenations via Cobaltate Intermediates*

Chapter 4 illustrates the application of an *in situ* catalytic system formed by reduction of [(^{Dipp}BIAN)$CoBr_2$] with three equivalents of $LiBEt_3H$ in the hydrogenation of sterically hindered olefins under mild conditions (Scheme 3).

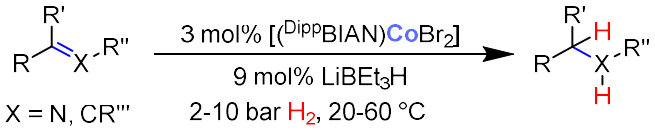

Scheme 3. Hydrogenation of olefins and imines catalyzed by an *in situ* mixture of [(^{Dipp}BIAN)$CoBr_2$] and three equivalents of lithium superhydride.

Particular emphasis was placed on poisoning experiments to distinguish between heterogeneous and homogeneous catalysis using dct, $P(OMe)_3$, and mercury (Figure 2,

left). Finally, the chapter ends with computational studies on [(^{Dipp}BIAN)Co(η^6-C_6H_6)] (**4-3**). DFT calculations using the broken-symmetry approach revealed a Co(I) center, which is antiferromagnetically coupled to a monoanionic BIAN ligand, which results in an overall S = 1/2 spin state (Figure 2, right).

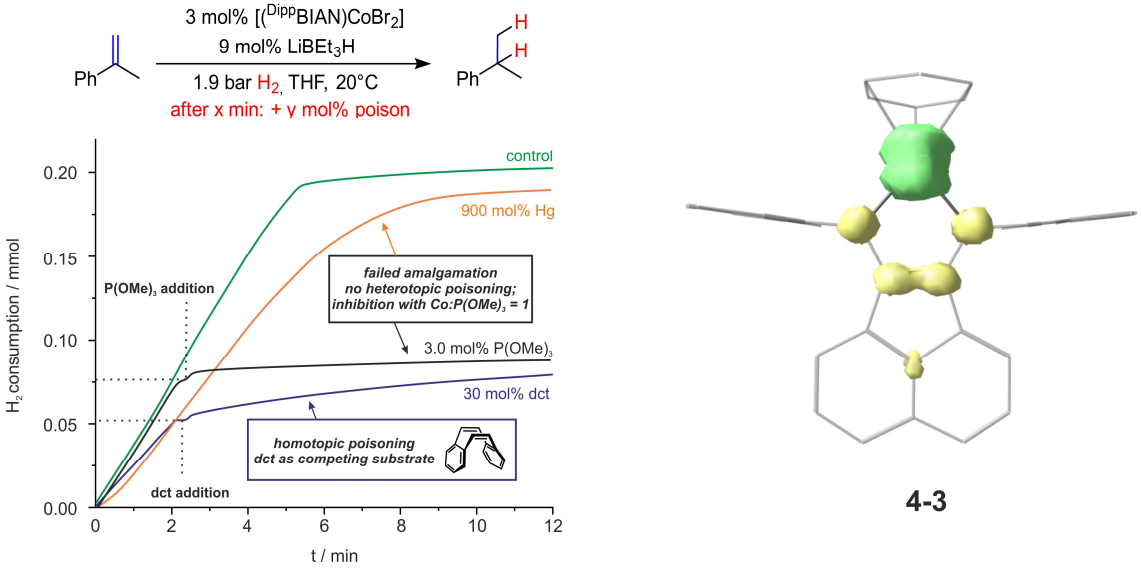

Figure 2. Kinetic data including poisoning experiments of the hydrogenation of α-methylstyrene catalyzed by an *in situ* mixture of [(^{Dipp}BIAN)CoBr$_2$] and LiBEt$_3$H (left). Spin distribution from DFT calculations of [(^{Dipp}BIAN)Co(η^6-C_6H_6)] (**4-3**) (right).

Chapter 5. *Heterogeneous Olefin Hydrogenation Enabled by a Nickel(-II) Pre-Catalyst*

In chapter 5 the application of highly-reduced [Li$_2$(thf)$_4${Ni(η^4-cod)(η^2-cod)] (**5-1**) in the hydrogenation of sterically hindered olefins under mild conditions (5 bar H_2, DME, 24 h) is reported. The main goal of this work was a comparison of performance in catalytic hydrogenation reactions with other base metalate anions such as bis(anthracene) ferrate(1−), bis(anthracene) cobaltate(1−) and bis(cyclooctadiene) cobaltate(1−). The nickelate generates a more active catalyst in the hydrogenation of olefins and is also compatible with several functional groups not tolerated by other metals (OH, esters, halides). In contrast to the homogeneous system proposed for the base metalate anions of iron and cobalt, the active species in the nickelate system are found to be nickel nanoparticles. This has been demonstrated with the use of reaction progress analyses, stoichiometric reactions, poisoning experiments, and transmission electron microscopy.

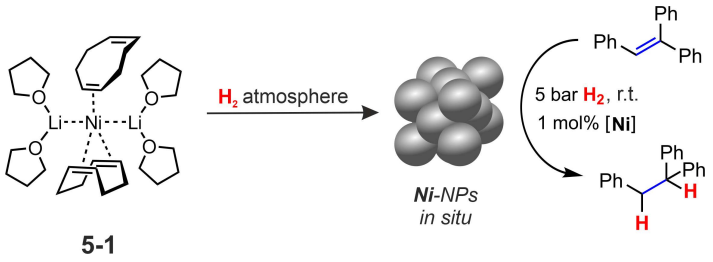

Figure 3. *In situ* formation of catalytically-active nickel nanoparticles from the pre-catalyst $[Li_2(thf)_4\{Ni(cod)_2\}]$ **5-1** and subsequent hydrogenation of triphenylethylene to triphenylethane.

Chapter 6. *Highly-Reduced α-Diimine Ferrates: Electronic Structure and Catalysis*

In an extension of the work on anionic α-diimine cobaltate complexes described in chapters 2 - 4 , it was a major goal to synthesize analogous iron complexes and investigate their reactivity in catalysis. Two different synthetic routes were applied to get access to such species: i) reduction of α-diimine iron(II) dihalide complexes and ii) ligand exchange reaction with anionic iron species (Scheme 4). Both routes were suitable for the synthesis of **6-1**-[K([18]c-6)$(thf)_{0.5}$] and **6-1**-[Li(thf)].

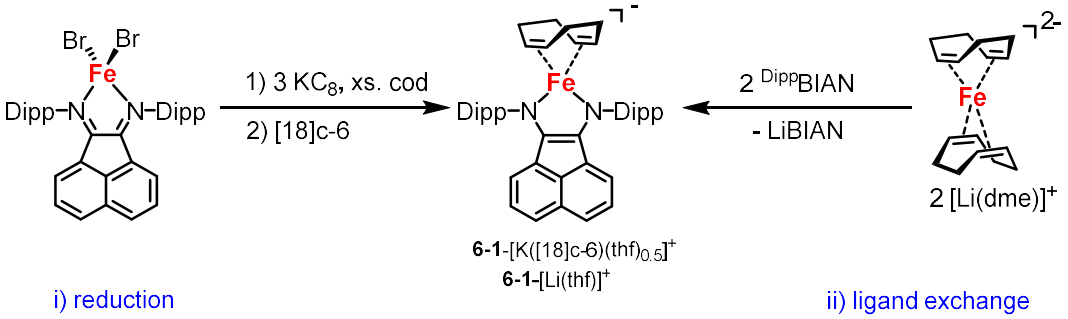

Scheme 4. Synthesis of **6-1**-[K([18]c-6)$(thf)_{0.5}$] and **6-1**-[Li(thf)]. by reduction of [(^{Dipp}BIAN)$FeBr_2$] (left) or ligand exchange with $[Li_2(dme)_2\{Fe(\eta^4\text{-}cod)_2\}]$ (right).

An unusual bis(alkyl) complex **6-2** was obtained using 2,5-norbornadiene instead of cod in analogous reactions. In this case, norbornadiene underwent C–C coupling to form a five-membered ferracycle. Meanwhile, starting from bis(anthracene) ferrate(1–), the reaction with the α-diimines ^{Dipp}BIAN and ^{Dipp}PhDi led to the formation of homoleptic bis(α-diimine) ferrates **6-3** and **6-4** (Figure 3). The characterization of these iron species was done using spectroscopy (^{1}H NMR, EPR, ^{57}Fe Mößbauer), theory (DFT, CASSCF), and magnetic measurements (Evans NMR, SQUID magnetization measurement). The experimental and theoretical data support

the presence of a d^7 configuration (S = 1/2) for complex **6-1** and a d^5 configuration (S = 3/2) for complex **6-2**. The electronic configuration of the homoleptic bis(α-diimine) ferrates **6-3** and **6-4** is more complicated and not fully understood. Both complexes are inbetween a square-planar and a tetrahedral coordination environment. Theoretical investigations (CASSCF) showed that in both complexes the quartet (S = 3/2) and the sextet state (S = 5/2) are close in energy, differing just by 1.7 kcal mol^{-1} in favor of the quartet state for **6-3** and to 3.0 kcal mol^{-1} in favor of the sextet state for **6-4**. The EPR spectra can be simulated using the spin states provided by theory. Magnetic susceptibility measurements and ^{57}Fe Mößbauer investigations are in progress for these complexes.

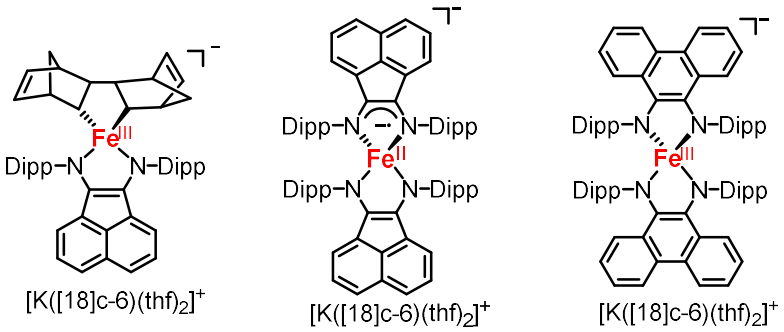

Figure 3. Chemical structures of the heteroleptic α-diimine bis(alkyl) iron complex **6-2** and the two homoleptic bis(α-diimine) iron complexes **6-3** and **6-4**.

The reactivity of the four complexes **6-1** – **6-4** was further investigated in the catalytic hydroboration of carbonyl compounds with pinacolborane. As expected, the heteroleptic complexes **6-1** and **6-2** with potentially vacant coordination sites are far more active compared to the homoleptic complexes **6-3** and **6-4**. Pre-catalyst **6-1**-[K([18]c-6)$(thf)_{0.5}$] showed a broad functional group tolerance for halogen, ether, amine, and ester functionalities and exhibits a high TOF of 22000 h^{-1} for the hydroboration of acetophenone with HBPin, which is one of the highest TOFs for Fe catalyzed hydroboration of carbonyl compounds (Scheme 5). Mechanistic experiments suggest a homogeneous system (Hg poisoning test) and an activation step initiated by acetophenone. Further studies should focus on the asymmetric hydroboration of carbonyl compounds using chiral α-diimine ligands.

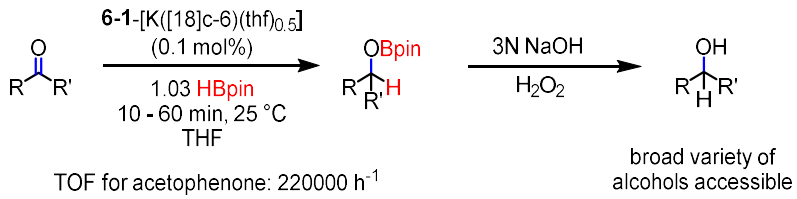

Scheme 5. Generic scheme for the catalytic hydroboration of carbonyls with pinacolborane catalyzed by pre-catalyst **6-1**-[K([18]c-6)(thf)$_{0.5}$] and subsequent work-up with aqueous NaOH/H_2O_2.

Chapter 7. *Direct Synthesis of an Anionic 13-Vertex closo-Cobaltacarborane Cluster*

The reaction of the α-diimine cobaltate [K(thf){(^{Mes}BIAN)Co(η^4-cod)}] (**7-1**) and 1,2-bis(diphenylphosphino)-*closo*-carborane **7-L** led to the anionic 13-vertex *closo*-cobalta-carborane cluster (**7-2**) and not to the expected bis(phosphane) complex. This unexpected transformation was investigated by synthetic, spectroscopic , and computational methods. The first step of this reaction is an one-electron oxidation of **7-1** to [(^{Mes}BIAN)Co(η^4-cod)] (**7-1-Int A**) as proven by isolation of this compound and subsequent reduction of the bis(phosphane) ligand to an dianionic *ortho*-carborane **7-*ortho*-L**$^{2-}$ which isomerizes to a *nido*-carborane **7-*nido*-L**$^{2-}$. This is consistent with ESI-MS data and DFT calculations. The anionic 13-vertex *closo*-cobalta-carborane cluster **7-2** is formed after further outer-sphere electron transfer and isomerization reactions.

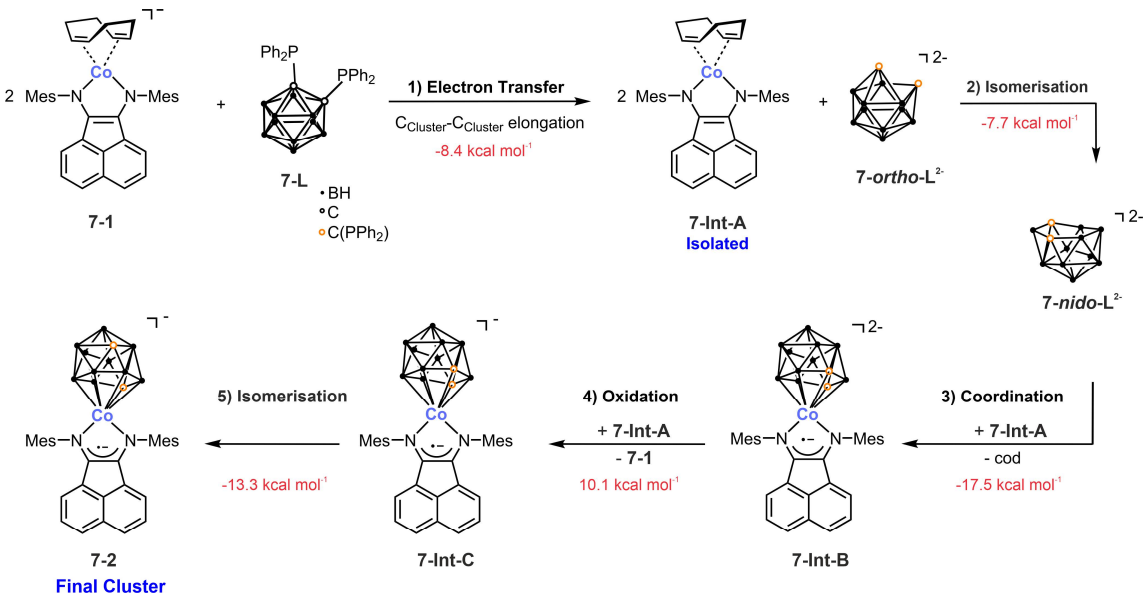

Scheme 6. Proposed mechanism based on experimental and quantum mechanical methods. Cations are omitted for clarity. Reaction energies were calculated on the M06-D3(0)def2-TZVP CPCM(THF) level of theory.

References

Chapter 2 C. M. Hoidn, **T. M. Maier**, K. Trabitsch, R. Wolf, *Angew. Chem.* **2019**, *131*, 19107-19112; *Angew. Chem. Int. Ed.* **2019**, *58*, 18931-18936.

Chapter 3 **T. M. Maier**, S. Sandl, I. G. Shenderovich, J. J. Weigand, A. Jacobi v. Wangelin, R. Wolf, *Chem. Eur. J.* **2019**, *2*, 238-245.

Chapter 4 S. Sandl, **T. M. Maier**, N. P. van Leest, S. Kröncke, U. Chakraborty, S. Demeshko, K. Koszinowski, B. de Bruin, F. Meyer, M. Bodensteiner, C. Herrmann, R. Wolf, A. Jacobi v. Wangelin, *ACS Catal.* **2019**, *9*, 7596-7606.

Chapter 5 **T. M. Maier**, S. Sandl, P. Melzl, J. Zweck, A. Jacobi v. Wangelin, R. Wolf, *Chem. Eur. J.* **2020**, *26*, 6113-6117.

Chapter 6 **T. M. Maier**, N. P. van Leest, S. Demeshko, M. Bodensteiner, B. de Bruin, F. Meyer, R. Wolf, *manuscript in preparation*

Chapter 7 **T. M. Maier**, P. Coburger, N. P. van Leest, E. Hey-Hawkins, R. Wolf, *Dalton Trans.* **2019**, 48, 15772-15777.

9 Acknowledgement

Zu guter Letzt möchte ich mich bei folgenden Personen und Organisationen bedanken:

Prof. Dr. Robert Wolf für die hervorragende Betreuung, die interessante Aufgabenstellung, tollen Arbeitsbedingungen und die Möglichkeit in seiner Arbeitsgruppe meine Dissertation anzufertigen. Weiterhin bedanke ich mich bei ihm für die Unterstützung bei meinem Stipendienantrag und dem Fonds der Chemischen Industrie für die Gewährung dessen.
Prof. Dr Axel Jacobi von Wangelin (Zweitgutachter), Prof. Dr. Manfred Scheer und Prof. Dr. Alkwin Slenczka für die Bereitschaft an meinem Prüfungskomitee mitzuwirken.

Den Mitarbeitern der Analytik-Einrichtungen und Werkstätten: Der Kristallographie-Abteilung (Dr. Michael Bodensteiner, Dr. Stefanie Gärtner, Sabine Stempfhuber und Birgit Hischa), der NMR-Abteilung (Fritz Kastner, Veronica Scheidler, Annette Schramm, Georgine Stühler), der Elementaranalyse-Abteilung (Barbara Baumann, Helmut Schüller), der Massenspektrometrie (Josef Kiermaier, Wolfgang Söllner), der Feinmechanik (stellvertretend Herbert Tischhöfer und Andreas Graf), der Elektronikwerkstatt (stellvertretend Peter Fuchs und Andreas Gruber) und der Glasbläserei (Markus Lindner, Carl-Heinz Hierl, Romy Knop, Helena Ackermann) – sie alle haben maßgeblichen Anteil am Erfolg meiner Promotion mitgewirkt.

Meinen Kooperationspartnern, insbesondere Sebastian Sandl und Prof. Dr. Axel Jacobi von Wangelin für die vielen durchgeführten Projekte und die gute Zusammenarbeit in den letzten Jahren. Klaas van Leest und Prof. Dr. Bas de Bruin für die Aufnahme und Interpretation der EPR Spektren. Dr. Ilya G. Shenderovich für die Durchführung und Interpretation der Festkörper NMR Spektren. Dr. Serhiy Demeshko und Prof. Dr. Franc Meyer für die Aufnahme und Auswertung der SQUID Analysen und ^{57}Fe Mößbauer Daten. Prof. Dr. Jan J. Weigand für die Bereitstellung seines NMR Spektrometers für kinetische Studien. Dr. Peter Coburger und Prof. Dr. Evamarie Hey-Hawkins für die Unterstützung und Mitarbeit am Cobaltacarboran Projekt. Andreas Rösch und Prof. Dr. Robert Kretschmer danke ich für den Zugang zu ihrem ReactIR.

Dr. Andreas Ehlers und Prof. Dr. Moniek Tromp für die Betreuung während meines Aufenthalts in Amsterdam.

Meinen Bachelorstudenten Felix Seeberger, Martin Gawron und Marcel Fischer, sowie den Forschungspraktikanten Matthias Ackermann und Matthew Margeson für die Mitarbeit an meinen Projekten.

Den ehemaligen und aktuellen Mitgliedern des AKs Wolf.

Der Generation Stefan Pelties, Bernd Mühldorf, Christian Rödl und Philipp Büschelberger für die lehrreiche Anfangszeit und den vielen hilfreichen Diskussion. Dem Labor 23.2.23 (1st Generation: Stefan, Christian, Philipp; 2nd Generation: Christoph, Christian, Philipp; 3rd Generation: Christoph, Marion, Julia M.) für die tolle musikalische Untermalung des Arbeitsalltages und die kollegiale Arbeitsatmosphäre im Labor.

Meiner zweiten Familie, dem Freien TuS Regensburg, für den Ausgleich zum Studium bzw. der Promotion und die fußballerischen Höhe- und Tiefpunkte. Wir sind der Freier!

Meinen Freunden, vor allem Philipp Paintner, Christian Preischl und Peter Kleiner für Ihre Unterstützung und ihr stets offenes Ohr.

Meiner Familie, namentlich hervorzuheben meiner Schwester Kerstin, meiner Oma Eleonora, meinem Patenonkel Markus und meinen Eltern Roland und Klaudia für den bedingungslosen Rückhalt in meinem Leben, während des Studiums und der Promotion. Ihr habt mir ein in aller Hinsicht sorgenfreies Studium ermöglicht und wart immer da, als es drauf ankam. Den Dank, zu dem ich euch verpflichtet bin, kann ich nur schwer in Worte fassen.

Zu guter Letzt Danke ich Karin, die mir all die Jahre während meines Studiums und meiner Promotion zur Seite stand und alle Momente mit mir geteilt hat. Ich bin dir unendlich dankbar für die schöne Zeit.

„Die Wissenschaft fängt eigentlich erst da an interessant zu werden, wo sie aufhört." ***Justus von Liebig***

10 Curriculum Vitae

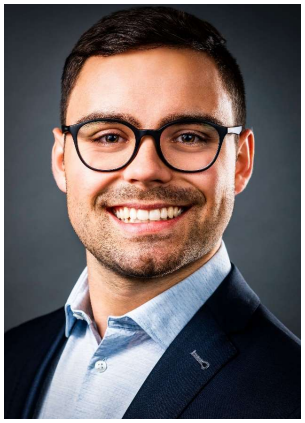

PERSÖNLICHE DATEN

Name:	Thomas Markus Maier
Geboren am:	22.01.1993 in Amberg/Oberpfalz
Nationalität:	Deutsch
Adresse:	Leobschützer Str. 10 92245 Kümmersbruck

AUSBILDUNG

11/2016 – 05/2020	**Promotion** am Arbeitskreis von Prof. R. Wolf, Institut für Anorganische Chemie, Universität Regensburg
10/2014 – 02/2015	**Forschungsaufenthalt** am Arbeitskreis von Prof. M. Tromp. Betreuer: Assist. Prof. A. W. Ehlers (Universiteit van Amsterdam)
10/2014 – 09/2016	**Master of Science** in **Chemie** an der Universität Regensburg mit den Schwerpunkten anorganische, organische, physikalische und nachhaltige Chemie, **Gesamtnote 1.0**
	Masterarbeit: *"Synthese und Reaktivitätsstudien hochreaktiver, anionischer Cobalt-Diimin Komplexe"* am Institut für Anorganische Chemie, Betreuer: Prof. R. Wolf, **Note 1.0**
06/2016	**Forschungsaufenthalt** am Arbeitskreis von Prof. J. J. Weigand, Technische Universität Dresden
10/2011 – 09/2014	**Bachelor of Science** in **Chemie** an der Universität Regensburg, **Gesamtnote 1.5**
	Bachelorarbeit: *"Photokatalytische C–H Oxidation mit Hilfe von biomimetischen Eisenkatalysatoren"* am Institut für Anorganische Chemie, Betreuer: Prof. R. Wolf, **Note 1.0**
09/2003 – 07/2011	**Abitur** am Gregor-Mendel-Gymnasium Amberg. Abiturfächer: Deutsch, Englisch, Mathematik, Sport, Wirtschaft & Recht, **Gesamtnote 1.9**

WISSENSCHAFTLICHE KONFERENZEN

03/2020	16tes Koordinationschemie-Treffen in Freiburg, Posterpräsentation: *"Highly–Reduced Anionic α-Diimine Co and Fe Complexes as Catalysts in (De)Hydrogenation Reactions"*
09/2018	19te Vortragstagung für Anorganische Chemie der Fachgruppen Wöhler-Vereinigung und Festkörperchemie und Materialforschung in Regensburg, Posterpräsentation: *"α-Diimine Cobaltates as (De-)Hydrogenation Catalysts"*
07/2018	International Conference on Organometallic Chemistry in Florenz (Italien), Posterpräsentation: *" α-Diimine Cobaltates as (De-) Hydrogenation Catalysts"*
03/2018	Regionales Stipendiatentreffen des Fonds der Chemischen Industrie in Regensburg, Vortrag: *" α-Diimine Cobaltates as (De-)Hydrogenation Catalysts"*
08/2017	133rd International Summer Course 2017 der BASF in Ludwigshafen, Vortrag und Poster: *"α-Diimine Ferrates and Cobaltates as Sources for Highly-Reactive Complex Fragments"*
07/2017	22nd European Conference on Organometallic Chemistry in Amsterdam (Niederlande), Posterpräsentation: *"α-Diimine Cobaltates as (De-)Hydrogenation Catalysts"*
03/2017	14th European Conference on Phosphorus Chemistry in Cluj-Napoca (Rumänien), Posterpräsentation: "*Novel Anionic Cobalt Tetraphosphido Complexes*"

PREISE UND STIPENDIEN

03/2017 – 03/2019	**Doktoranden-Stipendium** des Fonds der Chemischen Industrie
06/2017	**Studienabschlusspreis** für M. Sc. mit Bestnote der Dr. Alfons Paulus Stiftung der Universität Regensburg

MITGLIEDSCHAFTEN

Freier TuS Regensburg e.V., Gesellschaft Deutscher Chemiker e.V., ChemPharm Graduate School Regensburg

11 List of Publications

1. **T. M. Maier**, S. Sandl, P. Melzl, J. Zweck, A. Jacobi v. Wangelin, R. Wolf, *Chem. Eur. J.* **2020**, *26*, 6113-6117. „*Heterogeneous Olefin Hydrogenation Enabled by a Highly-Reduced Nickel(-II) Catalyst Precursor*"

2. **T. M. Maier**, P. Coburger, N. P. van Leest, E. Hey-Hawkins, R. Wolf, *Dalton Trans.* **2019**, 48, 15772-15777. "*Direct synthesis of an anionic 13-vertex closo-cobaltacarborane"*

3. **T. M. Maier**, S. Sandl, I. G. Shenderovich, J. J. Weigand, A. Jacobi v. Wangelin, R. Wolf, *Chem. Eur. J.* **2019**, *2*, 238-245. "*Amine-Borane Dehydrogenation and Transfer Hydrogenation Catalyzed by α-Diimine Cobaltates*"

4. C. M. Hoidn, **T. M. Maier**, K. Trabitsch, R. Wolf, *Angew. Chem.* **2019** *131*, 19107-19112; *Angew. Chem. Int. Ed.* **2019**, *58*, 1302-1308. "*[3+2] Fragmentation of a Pentaphosphido Ligand by Cyanide*"

5. S. Sandl, **T. M. Maier**, N. P. van Leest, S. Kröncke, U. Chakraborty, S. Demeshko, K. Koszinowski, B. de Bruin, F. Meyer, M. Bodensteiner, C. Herrmann, R. Wolf, A. J. v. Wangelin, *ACS Catal.* **2019**, *9*, 7596-7606. "*Cobalt-Catalyzed Hydrogenations via Olefin Cobaltate and Hydride Intermediates*"

6. C. P. G. Ziegler, **T. M. Maier**, S. Pelties, C. Taube, F. Hennersdorf, A. W. Ehlers, J. J. Weigand, R. Wolf, *Chem. Sci.* **2019**, *10*, 1302-1308. "*Construction of Alkyl-Substituted Pentaphosphido Ligands in the Coordination Sphere of Cobalt*"

7. S. Pelties, **T. M. Maier**, D. Herrmann, B. de Bruin, C. Rebreyend, S. Gärtner, I. G. Shenderovich, R. Wolf, *Chem. Eur. J.* **2017**, *23*, 6094-6100. "*Selective P_4-Activation by a Highly-Reduced Cobaltate: Synthesis of Dicobalt Tetraphosphido Complexes*"

12 Eidesstattliche Erklärung

Ich erkläre hiermit an Eides statt, dass ich die vorliegende Arbeit ohne unzulässige Hilfe Dritter und ohne Benutzung anderer als der angegeben Hilfsmittel angefertigt habe, die aus anderen Quellen direkt oder indirekt übernommenen Daten und Konzepte sind unter Angabe des Literaturzitats gekennzeichnet. Die Arbeit wurde bisher weder im In- noch im Ausland in gleicher oder ähnlicher Form einer anderen Prüfungsbehörde vorgelegt.

Regensburg, den 28.05.2020